2013 Volume 4

The Journal on Advanced Studies in Theoretical and Experimental Physics, including Related Themes from Mathematics

PROGRESS IN PHYSICS

"All scientists shall have the right to present their scientific research results, in whole or in part, at relevant scientific conferences, and to publish the same in printed scientific journals, electronic archives, and any other media."
— Declaration of Academic Freedom, Article 8

ISSN 1555-5534

The Journal on Advanced Studies in Theoretical and Experimental Physics, including Related Themes from Mathematics

PROGRESS IN PHYSICS

A quarterly issue scientific journal, registered with the Library of Congress (DC, USA). This journal is peer reviewed and included in the abstracting and indexing coverage of: Mathematical Reviews and MathSciNet (AMS, USA), DOAJ of Lund University (Sweden), Zentralblatt MATH (Germany), Scientific Commons of the University of St. Gallen (Switzerland), Open-J-Gate (India), Referativnyi Zhurnal VINITI (Russia), etc.

Electronic version of this journal:
http://www.ptep-online.com

Postal Address

Department of Mathematics and Science,
University of New Mexico,
705 Gurley Ave., Gallup, NM 87301, USA

ISSN: 1555-5534 (print)
ISSN: 1555-5615 (online)

Standard Address Number: 297-5092
Printed in the United States of America

OCTOBER 2013 **VOLUME 4**

CONTENTS

Information for Authors and Subscribers

Progress in Physics has been created for publications on advanced studies in theoretical and experimental physics, including related themes from mathematics and astronomy. All submitted papers should be professional, in good English, containing a brief review of a problem and obtained results.

All submissions should be designed in LaTeX format using *Progress in Physics* template. This template can be downloaded from *Progress in Physics* home page http://www.ptep-online.com. Abstract and the necessary information about author(s) should be included into the papers. To submit a paper, mail the file(s) to the Editor-in-Chief.

All submitted papers should be as brief as possible. We accept brief papers, no larger than 8 typeset journal pages. Short articles are preferable. Large papers can be considered in exceptional cases to the section *Special Reports* intended for such publications in the journal. Letters related to the publications in the journal or to the events among the science community can be applied to the section *Letters to Progress in Physics*.

All that has been accepted for the online issue of *Progress in Physics* is printed in the paper version of the journal. To order printed issues, contact the Editors.

This journal is non-commercial, academic edition. It is printed from private donations. (Look for the current author fee in the online version of the journal.)

Space-Time Uncertainty and Cosmology: a Proposed Quantum Model of the Universe

Sebastiano Tosto

Italy, E-mail: stosto@inwind.it, stosto44@gmail.com

The paper introduces a cosmological model of the quantum universe. The aim of the model is (i) to identify the possible mechanism that governs the matter/antimatter ratio existing in the universe and concurrently to propose (ii) a reasonable growth mechanism of the universe and (iii) a possible explanation of the dark energy. The concept of time-space uncertainty, on which is based the present quantum approach, has been proven able to bridge quantum mechanics and relativity.

1 Introduction

Physical cosmology is the science of the most fundamental questions about past, present and future of the universe. Born in the modern form with the early Einstein general relativity (1916), it involves today all branches of the theoretical physics. The conceptual basis of cosmology relies not only on the theories of gravity field, but also on the fundamental interactions between elementary particles. Likely the first attempt of extending the achievements of general relativity to propose a model of universe based on a physical theory was made by Einstein himself with the introduction of the cosmological constant Λ. At that time the quantum theory was at its very early beginning, while the gravitational interaction seemed the most general physical law governing the dynamics of celestial bodies; so the relativity, with or without Λ, soon appeared as the most valuable resource to proceed beyond the Newton physics.

The first milestone of the modern cosmology is due to Friedmann (1922) and (1924); the hypothesis of universe homogeneous and isotropic allowed inferring the equations that describe shape and expansion/contraction propensity of the universe depending on the value of the density parameter Ω. After these early contributions, have been proposed several models of universe, e.g. by Lemaitre (1929) and Eddington (1930).

The first experimental milestone of cosmology is due to Hubble, who measured the Doppler shift of light emitted by far galaxies (1929): the experimental data revealed the recession velocity law of galaxies with respect to earth. Since then, any model of universe should allow for this experimental evidence. The second experimental landmark was the discovery of the cosmic microwave background radiation (Penzias and Wilson, 1965).

An essential added value to the theoretical cosmology came from the almost simultaneous development of quantum mechanics. Without this physical background and the recent Standard Model, the modern cosmology would be inconceivable. The cosmic abundance of elements has been investigated by Weizsacker (1938) and then by Gamow et al (1948); Chandrasekhar (1942) and more recently Fowler et al [1] pointed out several processes in the stars that concurrently account for the formation of heavy elements in the universe.

On the one hand, the understanding of the nuclear processes explains the existence of stars and other objects (quasars, white dwarf and so on); on the other hand, however, is the general relativity that explains the existence and features of the black holes. The crucial point of the modern physics and cosmology is the difficulty of merging relativistic and quantum theories. Several papers have been published on quantum gravity, e.g. [2,3]. Today the string theory is deemed to be a step towards the unification of both theories [4,5]; unavoidably the string theory has been also implemented by cosmologists to investigate problems of mere quantum nature, like for instance the vacuum energy and the dark energy [6], and the cosmological constant as well [7,8,9]. However, the mathematical difficulties of these theories are daunting, and their previsions hardly testable.

Yet to shed light on fundamental issues of cosmology are also useful plain models that exploiting simple assumptions allow reliable order of magnitude estimates; simplified models are functional to focus essential but even so significant information.

The present paper aims to infer the order of magnitude estimates starting from a quantum standpoint. The input values implemented in this paper are the literature estimates of the universe diameter $d_u = 8.7\times10^{26}$ m and age $t_u = 4.3\times10^{17}$ s. The total mass of the universe reported in the literature is estimated to be about $m_u = 3\times10^{52}$ kg, counting however the stars only. Thus it is reasonable to expect that the effective value M_u of total mass should actually be considerably greater than m_u. Indeed this latter does not include contributions like the dark mass or the total mass of all black holes possible existing in our universe, which instead should be also taken into account when correlating these three main features of the universe; this reasonably suggests $M_u > m_u$. The fourth key value to be introduced is the expansion rate on the universe, usually expressed through the Hubble constant $H_0 = 2.3\times10^{-18}$ s^{-1}; this number, which presumably averages the value of a true function of time, has been object of great debate because of its importance in cosmology.

2 Quantum background

Physicists believe unsatisfactory a theory based on the wave function ψ without direct physical meaning, e.g. [10]; indeed $\psi^*\psi$ only has the statistical meaning of probability density and contains the maximum information obtainable about a physical system. Moreover also the Wigner function [11], although providing significant information about the quantum states, presents conceptual difficulties: it cannot be really regarded as a probability distribution in the classical sense, it is a quasi-probability that can take negative values; moreover it can represent the average value of an observable but not, in general, also its higher power moments. These difficulties, both inherent the wave formalism, are overcome in a model that exploits directly the statistical formulation of the quantum uncertainty, which becomes itself a fundamental assumption of the model and reads in one space dimension

$$\Delta x\, \Delta p_x = n\hbar = \Delta\varepsilon\, \Delta t. \qquad (2,1)$$

The second equality is formally obtained from the former rewritten $(\Delta x/\mathrm{v}_x)(\mathrm{v}_x \Delta p_x) = n\hbar$ with the same number n of states and defining $\mathrm{v}_x = \Delta x/\Delta t$ and $\Delta\varepsilon = \mathrm{v}_x \Delta p_x$; these definition hold because n and the uncertainty ranges are arbitrary. (2,1) compel the positions

$$x \to \Delta x; \qquad p_x \to \Delta p_x; \qquad t \to \Delta t; \qquad \varepsilon \to \Delta\varepsilon. \qquad (2,2)$$

No further hypothesis is necessary besides that of waiving the random local values of the dynamical variables, considered random, unknown and unpredictable. To clarify the kind of quantum approach required by the positions (2,2) and highlight why (2,1) have prospective interest also in cosmology, are useful two examples shortly sketched below. The quantum properties are inferred implementing directly the physical definitions of the observable of interest, without solving the pertinent wave equations; note however that the operator formalism of wave mechanics is also obtained as a corollary of these equations [12], which explains why the results are anyway the same.

The first example concerns the angular momentum $\mathbf{M} = \mathbf{r} \times \mathbf{p}$ whose component along the arbitrary unit vector $\mathbf{w}$ is $M_w = \mathbf{r} \times \mathbf{p} \cdot \mathbf{w}$; the vectors are defined in a reference system R. The positions (2,2) compel $\mathbf{r} \to \Delta\mathbf{r}$ and $\mathbf{p} \to \Delta\mathbf{p}$ to calculate the number l of states consistent with the ranges $\Delta\mathbf{r}$ and $\Delta\mathbf{p}$ physically allowed to the particle. Thus $M_w = (\Delta\mathbf{r} \times \Delta\mathbf{p}) \cdot \mathbf{w} = (\mathbf{w} \times \Delta\mathbf{r}) \cdot \Delta\mathbf{p}$ yields $M_w = \Delta\mathbf{W} \cdot \Delta\mathbf{p}$, where $\Delta\mathbf{W} = \mathbf{w} \times \Delta\mathbf{r}$. So $M_w = 0$ if $\Delta\mathbf{p}$ and $\Delta\mathbf{W}$ are orthogonal; else, rewriting $\Delta\mathbf{W} \cdot \Delta\mathbf{p} = (\Delta\mathbf{p} \cdot \Delta\mathbf{W}/|\Delta\mathbf{W}|)\,|\Delta\mathbf{W}|$ one finds $\pm\Delta p_W = \Delta\mathbf{p} \cdot \Delta\mathbf{W}/|\Delta\mathbf{W}|$ and thus $M_w = \pm\Delta W \Delta p_W$, i.e. $M_w = \pm l\hbar$ according to (2,1). One component of $\mathbf{M}$ only is knowable; repeating the same approach for another component trivially means changing $\mathbf{w}$. Therefore the average values $< M_x^2 >$, $< M_y^2 >$ and $< M_z^2 >$ calculated in the same way should be equal. The components are averaged over the possible states summing $(l\hbar)^2$ from $-L$ to $+L$, where L is an arbitrary maximum value of l; so $< M_i^2 > = \sum_{l_i=-L}^{l_i=L} (\hbar l)^2/(2L+1)$ i.e. $M^2 = \sum_{i=1}^{3} < M_i^2 > = L(L+1)\hbar^2$. The mere physical definition of angular momentum is enough to find quantum results completely analogous to that of the wave mechanics without any hypothesis on the angular motion. The same holds for the energy levels of hydrogenlike atoms. The concerned definitions are now the energy $\varepsilon = p^2/2m - Ze^2/r$, being m the electron mass, and the momentum $p^2 = p_r^2 + M^2/r^2$. The positions (2,2) $p_r \to \Delta p_r$ and $r \to \Delta r$ yield $\Delta\varepsilon = \Delta p_r^2/2m + M^2/2m\Delta r^2 - Ze^2/\Delta r$. Two numbers of states are expected because of the radial and angular uncertainties. The positions (2,2) and the previous result yield $\Delta\varepsilon = n^2\hbar^2/2m\Delta r^2 + l(l+1)\hbar^2/2m\Delta r^2 - Ze^2/\Delta r$ that reads also $\Delta\varepsilon = \varepsilon_o + l(l+1)\hbar^2/2m\Delta r^2 - E_{el}$ with $E_{el} = Z^2e^4m/2n\hbar^2$ and $\varepsilon_o = (n\hbar/\Delta r - Ze^2m/n\hbar)^2/2m$. Minimizing $\Delta\varepsilon$ with $\varepsilon_o = 0$ yields $\Delta r = n^2\hbar^2/Ze^2m$; so $l \le n-1$ in order to get $\varepsilon < 0$, i.e. a bound state; $\varepsilon_{rot} = l(l+1)E_o/n^4$ yields the rotational energy of the atom as a whole. Also here appears that the range sizes do not play any role in determining the energy levels. The physical meaning of Δr, the early Bohr radius, appears noting that actually $E_{el} = -Ze^2/2\Delta r$, i.e. E_{el} is the energy of two charges of opposite sign delocalized within a diametric distance $2\Delta r$ apart. It appears now that the quantum numbers of the eigenvalues are actually numbers of allowed states of quantum systems.

The key point of this introduction is not the chance of having found well known results, but the fact of having extended this kind of approach to the special and general relativity [13,14]; selected results of interest for the purposes of the present paper are reported in the appendix. In this respect, some relevant features of this approach will be exploited later and thus deserve attention.

- Both time and space coordinates are by definition inherent any model based on (2,1).
- Any uncertainty range is defined by two boundary values, e.g. $\Delta x = x_1 - x_0$; either of them is necessarily defined with respect to the origin of a reference system, the other one controls the range size. Since both x_0 and x_1 are arbitrary, unknown and unknowable by assumption, neither size nor reference system are specified or specifiable. Any result obtained from $\mathbf{M} = \mathbf{r} \times \mathbf{p}$ depends on the particular R where are defined $\mathbf{r}$ and $\mathbf{p}$. Yet, once having introduced the positions (2,2), any reference to the initial R is lost, whereas the eigenvalues are correctly inferred from $\Delta\mathbf{r}$ and $\Delta\mathbf{p}$ only; indeed $\Delta\mathbf{M} = \Delta\mathbf{r} \times \Delta\mathbf{p}$ yields a range $\Delta\mathbf{M}$ of angular momenta corresponding to all values of the arbitrary number n of states concurrently introduced via (2,1). Otherwise stated, the previous examples have shown that the boundary values r_0 and r_1 of each i-th component Δr_i are unnecessary and do not play any role to find the eigenvalues; so, since the same holds also for the momentum range, once disregarding both coordinates

neither the range sizes nor the reference system are in fact specifiable. Hence, in general, privileged reference systems are inherently excluded by the agnostic form of space-time uncertainty of (2,1), i.e. the results hold in any four dimensional reference system.

- These examples emphasize that both boundary coordinates could even be time dependent without changing approach or result: once ignoring the local dynamical variables, conceptually and not to simplify or approximate some calculation, no information on the ranges is actually required.
- The positions (2,2) skip the necessity of solving the pertinent wave equations and allow working directly on the physical definitions of the observables; (2,1) extract the allowed quantum information from the analytical form itself of the equation defining the observable.
- The concept of delocalization resulting from (2,1) has more agnostic meaning than that of the wave formalism: here is waived even the concept of probability density.
- (2,1) and the positions (2,2) rule out the classical concept of distance, because the local coordinates that define the distance are disregarded themselves "a priori"; this means that comoving and proper distances cannot in fact be calculated, while saving however their conceptual physical meaning.

Two questions arise at this point: are (2,1) usefully applicable also in cosmology? If they really do, why not think that even the physical dimensions of G could be regarded like that of the angular momentum previously sketched? Nothing excludes "a priori" positive answers, which however imply clearly that the universe is understandable like a quantum object. In fact is just this the crucial point that justifies the present model. These quantum examples have been shortly introduced to highlight the strategy of the present paper, i.e. to emphasize the role of the space-time quantum uncertainty in cosmology. The same kind of approach will be extended to the physics of the universe exploiting both (2,1) to implement G via its physical dimensions: the idea is to regard the physical definition of G likewise as done with the angular momentum. Accordingly the gravity constant is not a mere numerical value, but a physical amount defined by its dimensional factors. In effect, at least in principle, nothing prevents regarding the numerical value of G as that resulting from a combination of mass and time and space uncertainties; so these factors can be replaced by the respective time-space ranges that characterize the properties of the universe and handled exactly as done previously. Three examples useful in the following are highlighted below.

Write $G = \Delta r^3 m^{-1} \Delta t^{-2}$ and calculate

$$\delta G = (dG/d\Delta r)_0 \, \delta\Delta r + (dG/d\Delta t)_0 \, \delta\Delta t + (dG/dm)_0 \, \delta m$$

in an arbitrary reference system R; the subscript emphasizes that the derivatives are calculated at arbitrary Δr_0, m_0 and Δt_0. Apparently a well defined value of gravity constant seems inconsistent with the arbitrariness of Δt, Δr and m inherent its physical dimensions and required by the positions (2,2). Yet the chance of compelling $\delta G = 0$ establishes a constrain on the variability of the constituent factors that makes the definition of G compatible even with a constant value; moreover this constrain is ensured at any age of the universe just because of the arbitrary values of Δr_0 and m_0 that represent its size and total mass at any age Δt_0. So the problem is not the constancy of G, but that of demonstrating a sensible physical meaning of the constrain itself. Divide both sides of the previous expression by $\Delta r_0^3/(m_0 \Delta t_0^2)$ and put $\delta G = 0$; this is not necessarily true because some theories regard G as time dependent function [15, 16], yet let us implement for simplicity this usual position. Here $\delta m \neq 0$ because some models of universe, the so called self-creation cosmology models [17], introduce mass production as a function of time. One finds thus $3\delta\Delta r/\Delta r_0 - \delta m/m_0 - 2\delta\Delta t/\Delta t_0 = 0$. Exploit the fact that the range sizes are arbitrary and that the increments $\delta\Delta r$, δm and $\delta\Delta t$ are arbitrary as well and of course defined independently of Δr_0, m_0 and Δt_0; then regard

$$\left(\frac{3}{2} - \frac{\Delta r_0}{2m_0}\frac{\delta m}{\delta\Delta r}\right)\delta\Delta r = \frac{\Delta r_0}{\Delta t_0}\,\delta\Delta t$$

in order that this equation has in particular a physical meaning of specific interest for the present model. So let us write

$$a(t) = \frac{3}{2} - \frac{\Delta r_0}{2m_0}\frac{\delta m}{\delta\Delta r}; \qquad c = \frac{\Delta r_0}{\Delta t_0}; \qquad \delta\Delta r = \frac{c}{a(t)}\,\delta\Delta t$$

where $a(t)$ is a dimensionless arbitrary function of time. Consider now the particular case of very small range size increments via the positions $\delta\Delta r \to dr$ and $\delta\Delta t \to dt$, possible just because of their arbitrariness, and integrate both sides of the former equation between two arbitrary r_1 and r_2 to which correspond the respective times t_1 and t_2 necessary for a photon to travel the space range $\chi = r_2 - r_1$. Of course the integration reads $\chi = \int_{t_1}^{t_2} a(t)^{-1} c dt$. Therefore with these integration limits and this definition of the constant ratio $\Delta r_0/\Delta t_0$, the resulting equation has the well known physical meaning of particle horizon distance and introduces the concept of scale function $a(t)$.

To complete this analysis on the physical dimensions of G, put $\delta m \to dm$ consistently with dr and dt and consider that the equation of $a(t)$ takes the form $dm = \alpha(3/2 - a(t))dr$, where $\alpha = 2m_0/\Delta r_0$; having defined $dr = cdt/a(t)$, one finds $dm/\alpha = 3ca(t)^{-1}dt/2 - cdt$. The integral of this equation between the fixed times t_1 and t_2 arbitrarily defined and the corresponding m_1 and m_2 yields $(m_2 - m_1)/\alpha = 3(r_2 - r_1)/2 - c(t_2 - t_1)$. In general an equation having the form $\alpha^{-1}\delta m = 3\delta r/2 - c\delta t$ does not have specific physical meaning, because the quantities at right hand side are arbitrary; for instance

$\delta m = 0$ if in particular $\delta r = 2c\delta t/3$, whereas any other value of $\delta m \neq 0$ would be in principle allowed as well. This simply emphasizes that the physical meaning of $a(t)$ is not hampered by constrains on the values of δm or $\delta\Delta t$ or χ. Yet it is also possible to split the equation into $m_2/\alpha - 3r_2/2 + ct_2 = r_0$ and $m_1/\alpha - 3r_1/2 + ct_1 = r_0$, with r_0 arbitrary, which read thus $m_2/\alpha = \delta r_2^*$ and $m_1/\alpha = \delta r_1^*$ with $\delta r_2^* = r_0 + 3r_2/2 - ct_2$ and $\delta r_1^* = r_0 + 3r_1/2 - ct_1$. These equations have in effect a well defined physical meaning, because they read $m_2/\delta r_2^* = m_1/\delta r_1^* = const$. The chance of having inferred from G an equation having the form $m/\delta r^* = const$ is important because it links uniquely any mass m to a corresponding range δr^* via a proportionality factor *const*; as this link must necessarily involve G via a constant term, one expects by dimensional reasons that necessarily $const \propto G/c^2$. Before concerning this point, note that these results have been obtained simply defining $G = \Delta r^3 m^{-1}\Delta t^{-2}$, rather than by implementing additional hypotheses; thus this way of regarding G contains inherently concepts essential to describe an expanding universe.

To better understand the last result, let us consider a further way to exploit the physical dimensions of G via (2,1). Rewrite $G = \Delta r^3/(m\Delta t^2)$ as $\Delta r = Gm/\mathrm{v}^2$ with $\mathrm{v} = \pm\Delta r/\Delta t$; so v is the average velocity necessary for a particle to travel Δr during a time range Δt in any R, as stressed before. The maximum value allowed to v, defined along one coordinate axis for simplicity, introduces a minimum range size Δr_0 of Δr given by $\Delta r_0 = Gm/c^2$. By definition Δr_0 is the distance traveled by a photon starting from an arbitrary point, defined without loss of generality as the origin of R. Since the photon can move around the origin towards the negative or positive side of the reference axis with equal probability, as indeed either sign of v is identically admissible, Δr_0 is one half of a total uncertainty range Δr_s where the photon is certainly enclosed; so $\Delta r_s = 2\Delta r_0$ yields

$$\Delta r_s = 2Gm/c^2 \qquad (2,3)$$

that defines therefore the boundary of the space range outside which the photon cannot escape. This range size has a general physical meaning characterized by the ratio $m/\Delta r_s$ only; also, the same holds of course for a massive particle having $\mathrm{v} < c$. This equation, already inferred in a more general way still via (2,1) only [18], has the same form just found examining $a(t)$: here we simply acknowledge that $const = 2G/c^2$.

Consider eventually that (2,1) read $\Delta x = (\Delta\varepsilon/\Delta p_x)\Delta t$; moreover it is shown in the appendix that $\Delta p_x = \mathrm{v}_x\Delta\varepsilon/c^2$, so that $\Delta x^3 = (c^2/\mathrm{v}_x)^3\Delta t^3$. Dividing both sides of this equation by $m\Delta t^2$ one finds $\Delta x^3/(m\Delta t^2) = (c^2/\mathrm{v}_x)^3\Delta t/m$. Hence

$$\frac{\Delta x^3}{m\Delta t^2} = \frac{c^3}{\xi^3}\frac{\Delta t}{m}; \qquad \mathrm{v_x} = \frac{\mathrm{c^2\Delta t}}{\Delta \mathrm{x}}; \qquad \xi = \frac{\mathrm{v_x}}{\mathrm{c}}; \qquad \xi < 1. \quad (2,4)$$

Define $\xi = \xi_G\,\xi_c$, so that the right hand side of the first (2,4) reads $(c/\xi_c)^3\Delta t/m$ and the left hand side $\xi_G^3\Delta x^3/(m\Delta t^2)$. Moreover regard in particular $\Delta t \equiv \Delta t_u$ and $\Delta x \equiv \Delta r_u$; this is certainly possible because all range sizes of (2,1) are arbitrary, so they can be regarded with reference to any specific case of interest. It is also possible to define ξ_G in order that the left hand side term corresponds to the value of G with the known values of Δr_u and Δt_u, so that (2,4) yields also the value of ξ_c; in other words (2,4) splits as follows

$$G = \xi_G^3\,\frac{\Delta r_u^3}{m\Delta t_u^2}; \qquad G = \frac{c^3}{\xi_c^3}\,\frac{\Delta t_u}{m}; \qquad \xi = \xi_G\,\xi_c < 1. \qquad (2,5)$$

The previous considerations have evidenced that both expressions are compatible with a constant value of G. The problem is to show that in this way ξ effectively verifies the required inequality. The numerical results for $m \equiv m_u$ yield $\xi_G = 0.17$ and $\xi_c = 1.79$, i.e. $\xi = 0.3$. According to (2,4) ξ does not depend directly on m, whereas (2,5) show that ξ_G and ξ_c do. For instance, repeating the calculation with $m \equiv 10m_u$ at the same Δt_u one would find $\xi_G = 0.36$ and $\xi_c = 0.84$, of course still consistent with the same ξ. In both cases ξ_G and ξ_c have reasonable values, as in general a proportionality constant between two correlated quantities is expected to be of the order of unity; if not, then some physical reason hidden in the concerned correlation should account for its actual order of magnitude. Actually the factor ten just introduced is not accidental, although it appears at the moment arbitrary and unjustified; its physical meaning will be highlighted in the next section. So are of interest the following values

$$M_u = 10m_u; \quad \xi_G = 0.36; \quad \xi_c = 0.84; \quad \mathrm{v}_u = 0.3c. \qquad (2,6)$$

These estimates imply that v_x of (2,4) takes the meaning of recession velocity v_u of today's universe boundary, being specifically calculated via Δr_u at our current time Δt_u. Yet there is no reason to think that the ratio $\Delta r/\Delta t$ is necessarily constant; so (2,4) prospects in general a variable expansion rate controlled by this ratio at different ages of the universe. Moreover, since v_u should reasonably depend also on the amount of mass within the universe, one expects a link between Δr_u and m_u or more likely M_u; in effect this conclusion will be confirmed in the next section.

At this point, therefore, the first target of the present model is to highlight how $\mathrm{v_u}$ is related to M_u via Δr_u, see in particular the next equation (3,3) that is the key together with (2,5) to link Δr_u and Δt_u to M_u. The model is described implementing first these today data, useful to assess the results, then it is also extended to past times when necessary. For reasons that will be clear soon, it is useful to begin with the matter era. The starting points of the present paper are not the general relativity and the Friedmann equations, but the quantum equations (2,1). The paper aims to check the effectiveness of this approach to formulate a possible model of universe. The worth of the present approach relies in particular on the fact that just (2,1) have been proven suitable to link the roots of the quantum mechanics to that of the special and general relativity [13,14].

3 Physical background of a possible model of the universe

According to (2,1) and positions (2,2), the key quantities of the present paper are not r_u and t_u, but the ranges $\Delta r_u = r_u - r_0$ and $\Delta t_u = t_u - t_0$. Let r_u be the current coordinate of the boundary of the universe at the time t_u, respectively defined with respect to an arbitrary initial value r_0 at the arbitrary time t_0. As previously emphasized, these latter coordinates are in turn fixed in an arbitrary space-time reference system R. Once accepting the quantum approach shortly introduced in section 2 to describe the universe as a quantum system, however, both r_0 and t_0 are deemed unknown and unnecessary to infer the eigenvalues of the physical observables, described instead by Δr_u and Δt_u only; moreover no particular R is specifiable, in agreement with one of the basic hypotheses of the relativity according which all reference systems are equivalent to describe the physical systems. If the uncertainty ranges only have physical meaning to define the quantum eigenvalues describing the observables, as shortly sketched in section 2, then this kind of universe has no defined center; this latter should be determined with respect to the origin of R, which however is undefined and indefinable itself like r_0 and t_0. Hence the physical universe is a space-time shell between the radii r_0 and r_u that define Δr_u. As the same holds for the time, the beginning of time defining the cosmological space-time is conceptually unidentifiable; it could be $t = 0$ or $t = t_0$ or any intermediate time. Strictly speaking, Δr_u and Δt_u only characterize the actual physical features of today's quantum universe. It means that r_0 and t_0, and in an analogous way ε_0 and p_0 of the respective ranges, characterize a pre-universe only; i.e. they are precursors of the space-time quantum ranges of (2,1) to which are actually related the physical observables of the universe. In fact, the following considerations will confirm the idea that trying to determine the initial values r_0 and t_0 is in fact inessential. The starting point of the present model is introduced as follows. Consider $\Delta p_r = n\hbar/\Delta r$ putting $\Delta p_r = h/\lambda_r - p_0$: coherently with Δr, also Δp_r defines an allowed range of local radial momenta falling between h/λ_r and p_0, both arbitrary. This equation yields in particular, specifying $\Delta r = \Delta r_u$,

$$n\lambda_u = 2\pi\Delta r_u; \quad \lambda_u = \lambda_r\lambda_0/(\lambda_0 - \lambda_r); \quad \lambda_0 = h/p_0. \qquad (3,1)$$

Whatever λ_0 might be, λ_r introduces a new wavelength λ_u; this result has in principle general valence because of the fundamental character of (2,1). For instance (3,1) imply a condition well known in quantum mechanics: an integer number n of wavelengths λ_u around a circumference corresponds to steady electron waves around a nucleus, in agreement with the quantization here introduced just by n. As λ_u has been defined without specifying the nature of the wave it characterizes, let us concern the particular case of a steady electromagnetic wave of wavelength λ_u traveling on the surface of a sphere. The assumption $r_0 \ll r_u$ brings thus to mind a hyperspherical four dimensional closed universe of radius Δr_u surrounded by a light wave running around any diametric circumference. This preliminary standpoint suggests in turn a possible hypothesis about its hypervolume and hypersurface

$$V_u = (4\pi/3)\,\Delta r_u^3; \qquad A_u = 4\pi\Delta r_u^2 \qquad (3,2)$$

filled with an amount of matter such to fulfill both (2,3) and (3,1). This also suggests regarding the universe consistent with the condition of "maximum growth efficiency", i.e. like a supermassive black hole; in effect, the previous considerations show that this conclusion is compatible with the analysis of the physical dimensions of G. Usually a black hole is allowed to form when any system, e.g. a star of sufficient mass at the end of its life cycle, collapses down to a critical radius fulfilling (2,3); so is seemingly surprising an expanding universe regarded as a supermassive black hole. Yet there is no physical reason to think that in general the shrinking process is the distinctive condition allowing a black hole; this usual idea implemented to explain observable events occurring inside the universe cannot be extrapolated to the behavior of the whole universe itself. Indeed Δr_s has been inferred via the physical definition of G simply exploiting (2,1), regardless of any specific reference to collapse events. Actually the present hypothesis seems reasonable for a growing universe, whose main requirement is to prevent mass and radiation energy losses outside it that could avert its possible evolution. According to the Hawking mechanism based on the vacuum polarization in the presence of a strong gravity field, a black hole inside the universe is able to split a couple of virtual particles generated by vacuum quantum fluctuation; it captures one of them, while releasing the other that thus appears as an ordinary particle. Outside the universe however this mechanism does not hold, as the concept of vacuum is replaced by that of "nothing". So no energy can escape outside Δr_u. The universe is thus a closed box unobservable from an external observer possibly existing. This point of view is assessed preliminarily by introducing the Schwarzschild range (2,3) and identifying $\Delta r_s \equiv \Delta r_u$ and $m \equiv m_u$; this position yields $\Delta r_s = 4.5 \times 10^{25}$ m, which is not very far from the estimated literature radius of the universe. Considering however that m_u quoted above is surely underestimated, as already emphasized, it is not surprising a value of Δr_s smaller than the expected Δr_u consistent with (2,3). Trust thus to the size of Δr_u and try to replace m_u with a value $M_u > m_u$ defined by

$$\Delta r_u = 2M_uG/c^2; \qquad (3,3)$$

one finds

$$M_u = 3 \times 10^{53}\ \text{kg}; \qquad M_u = m_u + m_? \approx 10m_u \qquad (3,4)$$

i.e. a total mass higher than the literature estimate of the visible m_u, as anticipated in section 2. This equation includes both the visible mass m_u plus a further contribution $m_?$ to be

explained next. Actually nothing excludes in principle the hypothesis (3,3), which in fact can be checked in several ways. So in the following M_u only, and not m_u, will be implemented. Estimate with the help of (3,2) and (3,3) the average density of the universe

$$\rho_u = \frac{3c^6}{32\pi M_u^2 G^3} = \frac{3}{8\pi G}\left(\frac{c}{\Delta r_u}\right)^2 \qquad (3,5)$$

which justifies why this paper starts just from the so called matter controlled era.

The most direct consequence of (3,3) is the Hawking entropy. Define first the circular frequencies of a light wave trapped by gravity around the border of the universe as

$$\omega_n = n\omega_u; \qquad \omega_u = c/(2\pi\Delta r_u)$$

in agreement with (3,1); so the boundary layer of the universe is marked out by the allowed frequencies of the electromagnetic field surrounding the total mass M_u, whose energy ε_ω is given by

$$\begin{aligned} \omega_n &= 1.1n \times 10^{-19}\ \mathrm{s}^{-1} \\ \varepsilon_\omega &= \frac{n\hbar c}{2\pi\Delta r_u} = 1.2n \times 10^{-53}\ \mathrm{J}. \end{aligned} \qquad (3,6)$$

Then let us concern also the total energy $\varepsilon_u = M_u c^2$ due to the whole amount of mass present in the universe. Since one expects that bulk energy ε_u and surface energy ε_ω should be someway correlated, the simplest hypothesis is to introduce a dimensionless proportionality factor σ_{H} such that $\varepsilon_u = \sigma_{\mathrm{H}}\varepsilon_\omega$. To infer the physical meaning of σ_{H}, calculate the mean values of this equation, which reads $<\varepsilon_u> = \sigma_{\mathrm{H}} <\varepsilon_\omega>$. Clearly $<\varepsilon_u> \equiv \varepsilon_u$. The standard way to calculate $<n\hbar\omega_u>$ via the partition function is well known; noting that $\hbar\omega_u \ll k_B T$ is verified for T down to values of the order of 10^{-28} K, one finds $<n\hbar\omega_u> \approx k_B T$. So $k_B\sigma_{\mathrm{H}}$ defined by an energy over a temperature can be nothing else but entropy. With the help of the Plank length $l_P = \sqrt{\hbar G/c^3}$, one finds indeed thanks to (3,2) and (3,3)

$$\sigma_{\mathrm{H}} = \frac{<\varepsilon_u>}{<n\hbar\omega_u>} = \frac{A_u}{4l_P^2}; \quad \hbar\omega_u = \frac{\hbar c}{2\pi\Delta r_u}; \quad \varepsilon_u = \frac{c^4}{G}\frac{\Delta r_u}{2}.$$

In effect, σ_{H} coincides just with the well known Hawking surface entropy in Boltzmann's units.

Before discussing further evidences to support the idea of black hole-like universe, as concerns in particular the value of M_u hypothesized here, let us implement the right hand side of (2,1): one finds $\Delta\varepsilon_u = \hbar/\Delta t_u$, whose physical meaning is clearly that of energy uncertainty range within which is defined the energy ε_u of the universe. Moreover, multiplying both sides by M_u, one finds

$$\Delta\varepsilon_u = \frac{\hbar}{\Delta t_u} = 2.4 \times 10^{-52}\ \mathrm{J}; \quad \Delta p_u = \sqrt{M_u \Delta\varepsilon_u} = 9\ \mathrm{kg\ m/s}.$$

So the uncertainty range of the momentum p_u of the universe has size of the order of the Planck momentum. The fact that the size of $\Delta\varepsilon_u$ is very narrow means of course that ε_u, whatever its value might be, is defined almost exactly. It is interesting to implement this result via the definition of G. Replace m with M_u and $\Delta t_u = \hbar/\Delta\varepsilon_u$ in the second (2,5); one finds thus $\Delta\varepsilon_u = \hbar c^3/(\xi_c^3 G M_u) = 1.4\xi_c^{-3} \times 10^{-52}$ J. Therefore $\Delta\varepsilon_u$ here calculated with $\xi_c = 0.84$, i.e. with the same value of (2,6), agrees with that obtained here directly from (2,1) via the age of the universe only. So this result on the one hand supports the value of M_u previously found, on the other hand it also confirms that the physical dimensions of G actually summarize the quantum features of the universe.

Owing to (3,3), the second (2,4) reads

$$\mathrm{v}_u = c^2\frac{\Delta t_u}{\Delta r_u} = \frac{c^4}{G}\frac{\Delta t_u}{2M_u} \qquad (3,7)$$

whose numerical value coincides of course with that of (2,6). According to (2,5), an increasing ratio $\Delta t_u/M_u$ means a smaller mass at Δt_u and thus a greater $\mathrm{v_u}$, as it is natural to expect.

To implement further these considerations, note that $\sqrt{\rho G}$ yields a frequency; so, replacing ρ with ρ_u of (3,5), one finds

$$\sqrt{\rho_u G} = 2.4 \times 10^{-19}\ \mathrm{s}^{-1}. \qquad (3,8)$$

This value is nicely twice the ground value of (3,6), even though calculated via G only and regardless of the condition (3,1); i.e. it requires $n = 2$. This result has a remarkable physical meaning that will be highlighted later. After having examined the physical meaning of the ratio $\hbar\omega_n/\varepsilon_u$ let us consider now the ratio $\hbar\omega_n/\Delta\varepsilon_u$: we emphasize that the deviation of M_u from the visible mass m_u is controlled by the constrain between (3,6) and (2,4), i.e. between the surface energy $\hbar\omega_{n=2} = \hbar c/(\pi\Delta r_u)$ of the electromagnetic wave surrounding the universe and the uncertainty energy range $\Delta\varepsilon_u = \hbar c^3/(\xi_c^3 G M_u) = \hbar/\Delta t_u$ of the bulk universe; indeed with the help of (3,3) and (3,6) we obtain

$$\omega_n \Delta t_u = \frac{nc\Delta t_u}{2\pi\Delta r_u} = \frac{n\mathrm{v}_u}{2\pi c}; \qquad \frac{\hbar\omega_n}{\hbar/\Delta t_u} = \frac{n}{2}\frac{\xi_c^3}{2\pi} \approx 0.05n \qquad (3,9)$$

according to the values (2,6), which yields $\hbar\omega_{n=2}/(\hbar/\Delta t_u) \approx 0.1 = m_u/M_u$. This result is crucial to understand the physical meaning of $m_?$, as highlighted in section 4.

Consider now that the ratio $c/\Delta r_u$ of (3,5) has physical dimensions time^{-1}; thus it is definable in general as $\dot{a}/a$, being a a function of coordinate and time. It is known that Δr_u^{-1} describes the local curvature of a surface; so $c/\Delta r_u$ must be actually expressed as $(\dot{a}+b)/a$ via an additive constant b, without which the curvature of the universe would tend to zero merely for a tending to a constant. Instead it seems more sensible to think that even for constant Δr_u the curvature becomes con-

stant itself, but not necessarily equal to zero. So (3,5) reads

$$\begin{aligned}\frac{8\pi\rho_u G}{3} &= \left(\frac{\dot a}{a}\right)^2 + \left(\frac{b}{a}\right)^2 + \frac{2\dot a b}{a^2}\\ \frac{c}{\Delta r_u} &= \frac{\dot a}{a}\left(1+\frac{b}{\dot a}\right)\end{aligned} \tag{3,10}$$

i.e., more expressively,

$$\frac{8\pi\rho_u G}{3H^2} = \frac{\rho_u}{\rho_c} = 1 + \frac{b}{\dot a}\left(2+\frac{b}{\dot a}\right);\quad \rho_c = \frac{3H^2}{8\pi G};\quad H = \frac{\dot a}{a}.$$

Despite the quantum approach has been carried out regardless of the general relativity, the conclusion is that $b/\dot a < 0$ or $b/\dot a = 0$ or $b/\dot a > 0$ depending on the ratio ρ_u/ρ_c; either sign of $b/\dot a$ depends on that of $\dot a$ and b controlling the curvature according to (3,10). Calling $b = \pm c$ and $\Lambda = \mp 6H/(ac)$ the right hand side reads $H^2 + (c/a)^2 - \Lambda c^2/3$, i.e. this equation reduces to the Friedmann equation; H is the Hubble parameter and Λ the cosmological constant. The implications of the Friedmann equation, as concerns in particular the parameter k, are so well known that a detailed discussion of (3,10) is superfluous. We emphasize the crucial role of (3,3) to obtain directly from (3,5) this result, which however compels automatically accepting here $\rho_u/\rho_c > 1$ once having hypothesized since the beginning a closed universe with hyperspherical geometry. If this inequality is such that $\rho_u/\rho_c \gtrsim 1$, then the previous considerations are consistent with an almost Euclidean closed universe, in which case

$$\frac{b}{\dot a}\left(2+\frac{b}{\dot a}\right) \gtrsim 0. \tag{3,11}$$

This is verified by $0 < b \ll \dot a$ and $b/\dot a \gtrsim -2$. Now, after having preliminarily verified the hypothesis (3,3) suggested by (3,1), let us check also the self-consistency of the considerations hitherto exposed examining once more $c/\Delta r_u$.

It is reasonable to think Δr_u proportional to the age Δt_u of the universe; so it is possible to write a series expansion defining Δr_u as $\Delta r_u = \sum_{j=1} a_j (cf)^j$, where $f = f(\Delta t)$ is an appropriate function of time to be defined and a_j are constant coefficients of the series. Rewriting more conveniently this series as $\Delta r_u = a_1 cf\varphi$, where $\varphi = 1 + a_2 cf/a_1 + a_3 (cf)^2/a_1 + \cdots$, one expects that a_1 of the first order term should be close to the unity for the aforesaid reasons. Implement once again the physical dimensions of G similarly as done before and put in particular $f(\Delta t) \equiv \Delta t_u$; if this position is correct, then $\Delta r_u = a_1 c\varphi\Delta t_u$ with $\varphi \approx 1$ yields $a_1 \approx 2c/\xi_c^3$. On the other hand ξ_c of (2,6) has been calculated in order to fit the numerical value of $G = c^3\Delta t_u/(\xi_c^3 M_u)$ of (2,5), which results also in agreement with that of (3,9); as this equation of G reads $\Delta r_u = (2c/\xi_c^3)\Delta t_u$ with the help of (3,3), one finds at the first order $a_1 \approx 2c/\xi_c^3$ and thus $\Delta r_u \approx (2c/\xi_c^3)\varphi\Delta t_u$. Also this result agrees with the previous estimate of ξ_c defining $\Delta r_u/\Delta t_u$: in effect from (2,4) and (2,6), $\Delta r_u = (c/\xi)\Delta t_u$ compares well with $\Delta r_u = (2c/\xi_c^3)\Delta t_u$ because the values (2,6) verify $\xi^{-1} = 2/\xi_c^{-3}$. This confirms that effectively $\varphi \approx 1$. Hence defining

$$H_0 = \frac{1}{\varphi\Delta t_u}$$

one finds with $a_1 \approx 2c/\xi_c^3$ and once more the given value of ξ_c

$$H_0 = \frac{2c}{\xi_c^3\Delta r_u} = 2.4\times 10^{-18}\ \mathrm{s}^{-1}.$$

So at the first order H_0 coincides with Δt_u^{-1}; moreover the second (3,10) yields $H(1+b/\dot a) = \xi/(\varphi\Delta t_u)$, i.e. $1+b/\dot a \approx \xi H_0/H$ and thus $1 + b/\dot a \approx 1$ in agreement with (3,11). The present estimate of H_0 fits well the average value of the Hubble constant, which according to recent measurements falls in the range $(2.2 \div 2.6)\times 10^{-18}\ \mathrm{s}^{-1}$.

These results justify the advantage of introducing the present quantum model with the matter era; once having estimated H_0 and inferred the Friedmann equation, it is easy to describe also the radiation controlled era as shown below.

It is worth emphasizing the strategy of the present approach. The standard way to infer cosmological information is to find the solution of the gravity field equations and next to implement the Friedmann solutions: these equations provide information about the open or closed geometry of the universe. Here a different approach has been followed. The quantum equations (2,1) have been implemented since the beginning to introduce the wavelength λ_u and formulate by consequence the concurrent hypothesis (3,3) about a possible geometry of closed universe; thereafter this preliminary idea has been checked to infer (i) the Hawking entropy, (ii) the link between mass density and curvature radius of the universe, (iii) to obtain a Friedmann-like equation and (iv) to estimate the Hubble constant. Moreover, exploiting the same approach outlined in section 2 for the angular momentum, the factors that define the physical dimensions of G allowed to correlate correctly size, age and mass of the universe. The remainders of this paper aim to implement these preliminary ideas to show that further reasonable results are inferred hereafter.

3.1 The matter era

Let us estimate the average mass and energy densities ρ_u and $\eta_{in} = \rho_u c^2$ of the universe, which result to be with the help of (3,2) and (3,5) of the order of

$$\begin{aligned}\rho_u &= \frac{M_u}{V_u} = \frac{3c^2}{2A_u G} = 8.7\times 10^{-28}\ \mathrm{kg/m^3}\\ \eta_{in} &= \frac{M_u c^2}{V_u} = \frac{3c^4}{2A_u G} = 7.8\times 10^{-11}\ \mathrm{J/m^3}.\end{aligned} \tag{3,12}$$

These values reasonably agree with that calculated in a very different way in [18]; the corresponding "non-visible" energy density is instead of the order of

$$\eta_? = 3m_? c^2/(4\pi\Delta r_u^3) = 7\times 10^{-11}\ \mathrm{J/m^3};\qquad m_? \approx 9m_u.$$

The ordinary visible mass of the universe is about 10% of the total mass only, whereas the remainder mass $m_?$ accounts for the 90% gravitational effect responsible of the black hole-like behavior of the whole universe. The average density ρ_u hides the physical nature of the actual total mass. Moreover, besides m_u of visible stars, M_u consists of a preponderant contribution $m_?$ of different physical nature: for instance all black holes possibly existing in the universe, or interstellar gas and dust, or free elementary particles, and so on including also the so called dark mass. A complex system of particles contributes to M_u, whose actual nature is however not explicitly concerned in neither of (3,12). According to some theories the elements were formed inside the stars by neutron bombardment of light nuclei and subsequent β decay, e.g. [19], other authors believed instead that elements were formed during the early stages after the big bang, e.g. [20]; more recently other authors returned to their formation inside the star by virtue of several nuclear processes [1]. Despite (3,12) waive specific information about the actual composition of M_u, the assumption of large scale homogeneity and isotropy of the universe supports the effective physical meaning of average ρ_u. Moreover the concept of quantum delocalization introduced by (2,1) stimulates itself the idea of average mass spreading uniformly throughout the universe likewise as the energy field of light radiation. This idea is useful to link the matter era to the earlier radiation era. It will be emphasized in the next subsection 3.2 that the radiation field, almost mono-chromatic at the beginning of the radiation era, turned into a more complex spectrum of wavelengths because of the concurrent expansion of the universe; so quantum fluctuations and possible events of constructive interference, statistically allowed to occur anywhere in the radiation field, promoted favorable conditions to form local couples of virtual particles uniformly distributed in the available volume of the early universe. It is known indeed that proton and antiproton virtual couples are formed by vacuum fluctuations and high order two-photon interactions during photon fluctuations able to generate fermion-antifermion pairs [21]. So it seems reasonable to guess that this mechanism triggered the evolution of the early radiation field to couples of virtual particles continuously annihilating and re-materializing up to the later formation of colder real matter. Some considerations on this point will be shortly sketched in the appendix. For the purposes of the present paper, however, it is enough to acknowledge that today's ρ_u corresponds on average to about one half proton mass per cubic meter of universe and that (3,12) hold identically while considering the mass of antiprotons. Despite this idea is mere statistical abstraction, (3,12) are useful for the purposes of the present model; they implement the assumed homogeneity and isotropy of the universe in its strongest form possible. Even with such information only, i.e. whatever the actual abundances of the j-th elements of mass m_j might be today within each unit volume of universe, it is possible to introduce: (i) an elementary volume V_0 physically located anywhere and defined as that containing on average one proton or one antiproton and (ii) a linear combination $m_p = \sum_j a_{ij} m_j$ that accounts via the local coefficients $a_{ij} = a_{ij}(x_i, y_i, z_i, t, m_j)$ for the actual composition of real matter progressively formed everywhere after the radiation era. These coefficients weight the time profile of the local effective abundances, e.g.: they are null if the pertinent coordinates of a_{ij} correspond to an empty volume of universe where $m_j = 0$, moreover all a_{ij} were equal to zero during the early radiation era, and so on. Since the local coordinates are conceptually disregarded by (2,1) and positions (2,2), however, let the indexes i and j number respectively the N_{in} elementary volumes V_{0i} of the universe and the various elements therein formed a time range Δt after its birth. The abundances are subjected to the boundary condition of the first (3,12); for instance, at today's Δt_u this point of view is summarized by the sums

$$\begin{aligned} \rho_u &= \frac{1}{V_u} \sum_{i,j} a_{ij} m_j \\ a_{ij} &= a_{ij}(V_{0i}, \Delta t, m_j) \\ \sum_{i,j} a_{ij} m_j &= N_{in} m_p . \end{aligned} \qquad (3,13)$$

The first two equations emphasize the local composition of ρ_u, the last one fits in particular the condition of today's average density. In fact (3,13) regard the universe as a lattice, whose elementary cells are the volumes V_{0i} uniformly occupied by one proton or one antiproton of every virtual couple with equal probability. Each cell is therefore a possible allowed state for either of them, i.e. the universe is statistically described by a total number $N_{in} = V_u/V_0 \approx 1.7 \times 10^{80}$ of degenerate states corresponding to η_{in}; also, since by definition each V_0 contains on average one proton mass, $m_p N_{in} = M_u$. So according to (3,12) the energy levels ε_{V_0} of one proton or one antiproton in the respective V_0 states are $m_p c^2/2$ and $m_{\bar{p}} c^2/2$, i.e.

$$\varepsilon_{V_0} = 7.8 \times 10^{-11} \text{ J}; \qquad V_0 \approx 2 \text{ m}^3 \qquad (3,14)$$

in order that effectively $M_u/V_u = m_p/V_0$, in agreement with (3,12). Of course ε_{V_0} includes also the interaction energy between charges in different cells, e.g. that of couples of all virtual particles possibly generated together with energetic protons and antiprotons; this is possible because $M_u c^2$ involves the visible mass energy $m_u c^2$ plus the contribution of $m_? c^2$. Note eventually that despite $M_u c^2$ results statistically equivalent to the sums

$$\sum_i (\varepsilon_{V_0 prot} + \varepsilon_{V_0 antiprot}) = N_{in} m_p c^2/2 + N_{in} m_{\bar{p}} c^2/2 \qquad (3,15)$$

over all the elementary volumes V_0, it will be shown later that an effective entropy driven mechanism in fact marked the transition from the radiation era to the matter era; so the sum

of (3,15) reads actually

$$\sum_i (\varepsilon_{V_0\,prot} + \varepsilon_{V_0\,antiprot}) = N_{in} m_p c^2. \qquad (3,16)$$

Before describing this mechanism, the results so far obtained are summarized as follows: (i) each cell is in fact an allowed state for one proton or one antiproton; (ii) (3,14) represents the excitation energy necessary to remove either of them from its own V_0 and leave behind an empty cell; (iii) the latter represents a vacuum state, whereas either particle present in V_0 defines an occupied state.

To highlight the physical meaning of these points, consider an arbitrary mass m at the boundary of the universe. The shell theorem shows that the gravity force acting on m is that due to M_u regarded in the ideal center of a spherical body; so is accordingly calculated for a radius Δr_u its energy $\varepsilon = GM_u m/\Delta r_u$ that, exploiting once again (3,3), reads also $\varepsilon = mc^2/2$. If for instance m represents the mass of one proton or one electron, $m_p = 1.7 \times 10^{-27}$ kg and $m_e = 9.1 \times 10^{-31}$ kg, then one finds

$$\begin{aligned} \varepsilon_p &= G\frac{M_u m_p}{\Delta r_u} = \frac{m_p c^2}{2} = 1.0 \times 10^{-10}\ \text{J} \\ \varepsilon_e &= G\frac{M_u m_e}{\Delta r_u} = \frac{m_e c^2}{2} = 5.4 \times 10^{-14}\ \text{J}. \end{aligned} \qquad (3,17)$$

The second (3,17) emphasizes that if the volume V_0 would be occupied by one electron with its own energy level $m_e c^2/2$, then V_0 would represent a possible state for this electron. To clarify where anyway does m come from, note that at today's Δt_u the proton energy level ε_{V_0} inside any state V_0 of the bulk universe, (3,14), is equal to the energy ε_p, (3,17), of one proton at the boundary of the universe. So

$$\varepsilon_p = \varepsilon_{V_0}. \qquad (3,18)$$

This equation in fact reads $c^2/2 = M_u G/\Delta r_u$, which is nothing else but (3,3). Thus (3,18) and the first (3,17) do not depend on the proton mass, and hold whatever else m_p might represent. Moreover neither the analytical form of ρ_u nor that of η_{in} introduce explicitly m_p. Rather, the latter introduces the mere Planck force c^4/G acting on the total surface A_u of the universe. There are two reasons why the average values defined by (3,12) and (3,13) have importance for the following discussion: on the one hand, the right side of (3,12) links correctly energy density and pressure; on the other hand, being known that the pressure of a perfect gas is 2/3 of its energy density, the second (3,12) suggests regarding η_{in} in each volume V_0 as due to a proton/antiproton gas occupying uniformly all bulk states of the universe. As this average pressure appears to be a physical property of all elementary volumes V_0, then the internal pressure that characterizes the whole universe results to be, again via (3,3),

$$P_{in} = \frac{2}{3}\frac{M_u c^2}{V_u} = \frac{c^4}{A_u G} = 5.6 \times 10^{-11}\ \text{Pa}. \qquad (3,19)$$

The fact that even P_{in} does not depend explicitly on m_p suggests that (3,12) have actual physical meaning. The factor 2/3, numerically irrelevant in the frame of the order of magnitude estimates proposed here, is however conceptually significant to check the physical meaning of (3,12). Taking into account (3,16), (3,19) reads

$$P_{in} V_u = \frac{2}{3} E; \qquad M_u c^2 = E = N_{in} m_p c^2.$$

The surprising fact is that the mere definition of energy density, without any additional hypothesis, portrays the whole universe as a container full of quantum or classical gas, whose mass M_u exerts Planck force against its inner boundary; indeed the first equation holds for Boltzmann, Bose and Fermi statistics, which confirms that effectively any kind of quantum or classical particle, thus why not the proton, is compatible with M_u without affecting the validity of (3,19). Furthermore this picture holds at any time, because the surface A_u can be replaced by any A likewise related to the pertinent M/V whatever the numerical value of the ratio might be. Formally this is justified by the second equation, where E resulting from $M_u c^2$ is also associated to a number N_{in} of proton masses fulfilling the global energy conservation. Yet the simple equivalence matter/energy does not seem enough to explain why chunks of matter like asteroids or stars or cosmic powder could mimic the pressure of a proton gas of equivalent total mass filling uniformly the universe. This is however a classical way to think the universe. More stimulating appears in this respect the quantum character of the present model. First of all, the couples proton/antiprotons have been guessed as mere numerical hint due to the average value of the mass resulting in (3,12); but in fact any gas could be consistent with (3,19), which indeed does not make explicit reference to m_p. The chance that any gas mixture could contribute to E is a step towards introducing the actual existence of chemical abundances symbolized by various m_j; the first (3,13) merely means that the degenerate proton or antiproton energy levels $m_p c^2/2$ split into a complex system of non-degenerate energy levels describing the local bound states of cosmic matter. From this point of view, the energy conservation between two different systems of quantum energy levels appears more pertinent: since in principle one level could split into several non-degenerate levels in an infinite number of ways, the energy conservation appears as essential boundary condition to calculate the latter from the former, rather than a mere statistical abstraction. More significant is however the dual wave/corpuscle behaviour of matter. A body of real matter is superposition of waves to form a group in principle spreading from minus infinity to infinity but with a maximum probability of being somewhere: the amplitude of the wave packet rapidly decreases at the edge of a region that determines the most probable position and the finite extent of the body, whose possible motion is nothing else but the group velocity of the wave packet. It is known that the electromag-

netic waves exert a pressure, whence the photon gas physics: why not to think the same about delocalized matter waves, according to (2,1)? If so, then the matter era began when matter waves started to appear in the pre-existing field of electromagnetic radiation according to the mechanism [21]. The appendix gives some more hints on this topic.

On the one hand these considerations are interesting because P_{in} controls the expansion of the universe, as it will be shown below; on the other hand the idea of V_0 bulk states allowed to protons and antiprotons, although suggested by the numerical values of (3,12) only, is attracting because it links radiation era and matter era, at the beginning of which couples of matter/antimatter particles were in fact formed. Anyway the significant conclusion is that (3,17) to (3,19) skip m_p and thus can be further implemented in the following regardless of whether the volumes V_0 are really occupied by protons or any other mass.

Exploit (3,19) to infer the average temperature T related to P_{in} in V_0. Here $T \approx E/(N_{in}k_B) = m_pc^2/k_B$ helps to estimate the average temperature in each elementary volume V_0; one finds $T \approx 10^{13}$ K. This estimate fulfills the usual statistical meaning of temperature, as the proton here concerned has a statistical meaning itself. To better assess this result consider the pressure P of an ideal gas of molecular weight M_{mol} and average density ρ in the volume V_0, so that $\rho = PM_{mol}/RT$. Exploiting (3,12) and (3,19) at the time Δt_u to express $\rho \equiv \rho_u$ and $P \equiv P_{in}$, one finds $M_u/V_u = (2M_uc^2/3V_u)M_{mol}/RT$, i.e. $T = 2c^2M_{mol}/3R$. Hence T is explicitly related to the specific M_{mol} only, regardless of the time Δt_u and related universe volume V_u. A uniform distribution of hydrogen in each V_0, i.e. $M_{mol} = 10^{-3}$ kg, estimates again $T \approx 10^{13}$ K, in agreement with that inferred directly from m_pc^2/k_B. Even the formation of hydrogen will be justified in the subsection 3.4 as a consequence of the step from (3,15) to (3,16). This large value is enough for protons to form further couples of virtual photons and fermions/antifer-mions; this supports the idea that effectively the protons early formed trigger the successive energy balance in V_0 qualitatively indicated in (3,13).

The previous ways to estimate T refer to the time where early hadrons began to form everywhere in the radiation field of such universe and indicate a temperature corresponding to a uniform distribution of virtual couples occupying the available states at the end of the radiation era. The same equations could in principle estimate the local T even during the subsequent matter era, when the bombardment with energetic neutrons allowed forming heavy elements; yet the concurrent clustering of matter determined a structure of the universe locally inhomogeneous, so at that later time a unique average T does no longer make sense. Actually both time and volume of the universe determine the value of M_{mol}. In particular, the expansion of the universe is crucial to determine the time profile of T after the radiation era: the hypothesis (3,3) requires $M/\Delta r = const$, which also compels that $M/\Delta r^3$ is a decreasing function of time for increasing Δr. So an increasing fraction of empty zones of the universe corresponds in principle to a global decreasing value of T; the calculation of the respective temperatures is not as immediate and straightforward as in the previous case, characterized by a uniform distribution of a unique kind of early particles. In this case both local coefficients a_{ij} and atomic weights of the elements m_j must be known: the sums of (3,13) are related to the abundances within the various volumes V_{0i} of cosmic objects, characterized by the different kinds of elements and local coefficients a_{ij}, and to empty parts of the universe.

A question arises now: did (3,3) and (3,18) hold even in the past? In fact there is no reason to suspect that this condition is an exclusive feature of the today space-time coordinates Δr_u and Δt_u, which indeed have nothing special with respect to any past or future Δr and Δt. The only necessary hypothesis to answer affirmatively is that the current V_0 grows together with the size of the universe, which is possible if its sizes are comoving distances. Otherwise stated, let V_0' be the past value of V_0 at any $\Delta r < \Delta r_u$ and $\Delta t < \Delta t_u$; we require $m_pc^2/2 = Mm_pG/\Delta r$, being M the past total mass. This requirement emphasizes the previous remarks: the actual nature of proton mass m_p is irrelevant as concerns (3,18), which holds thus whatever m_p stands for, i.e. whatever the relative element abundance of (3,11) in V_0 might have been at Δt. On the one hand $c^2/2G = M_u/\Delta r_u$ requires $M_u/\Delta r_u = M/\Delta r$ and thus $M = c^2\Delta r/2G$, i.e. the black hole condition held also in the past. On the other hand one expects that V_0' scales with $\propto \Delta r^3$, in order that it be definable even for the smaller universe sizes of the early matter era; so $V_0' = (\Delta r/\Delta r_u)^3V_0$, i.e. V_0' was reasonably much smaller than today's V_0. In this way multiplying both sides by N_{in} one finds $N_{in}V_0' = (\Delta r/\Delta r_u)^3N_{in}V_0$; since by definition $N_{in}V_0 = V_u$, (3,2) yield $N_{in}V_0' = (4\pi/3)\Delta r^3$, i.e. in the early hypersphere volume defined by Δr the number of elementary volumes and thus of states allowed to the new born matter was the same as today's N_{in}. In summary

$$M = \frac{\Delta r}{\Delta r_u}\, M_u; \quad V_0' = \left(\frac{\Delta r}{\Delta r_u}\right)^3 V_0; \quad N_{in} = const. \qquad (3,20)$$

What is important for the following discussion is that under reasonable assumptions the condition (3,18) could hold also in the past and that N_{in} was since the beginning fingerprint of our universe. (3,20) help to guess the size of the universe at the beginning of the matter era. It is instructive to proceed stepwise calculating Δr and V_0' by trial and error, i.e. assessing these quantities as a function of sensible values of M. If M would be the mass of one couple proton/antiproton only, then $\Delta r \approx 4.9 \times 10^{-54}$ m, which would mean a volume $V_0' \approx 2.9 \times 10^{-240}$ m^3, unrealistically smaller than the expected order of magnitude of Planck volume. This value of V_0' suggests an early number of virtual couples much higher than this. More reasonable results are obtained putting $V_0' \approx 4.2 \times 10^{-105}$ m^3 to estimate via the second equation the

order of magnitude of Δr, which results $\Delta r = 5.5 \times 10^{-9}$ m; with this range the first equation yields $M = 3.8 \times 10^{18}$ kg corresponding to about 2.2×10^{45} protons, i.e. about 10^{45} virtual couples proton/antiproton at the beginning of the matter era. Note that $Mc^2 = 3.4 \times 10^{35}$ J corresponds to an average fluctuation energy $\varepsilon_{fl} = 3.4 \times 10^{-10}$ J, i.e. 2.1 GeV, per virtual couple of matter particles newly created: this is the fluctuation energy of the radiation field able to create matter. It is interesting the fact that with the given choice of V_0' this result fits well the energy of a couple of protons, despite it has been calculated implementing M_u and Δr_u via (3,20) only; this supports the interpretation of (3,12). Supposing that on average each couple of photons generates one virtual couple of matter/antimatter, the fluctuation extra energy of radiation field increases the early Planck frequency of each couple of photons by about $\delta\omega = 3.4 \times 10^{-10}/\hbar = 3 \times 10^{24}$ s^{-1} to produce matter. The obvious conclusion of this section is to admit that before the time of mass production there was an earlier massless era, i.e. the radiation era.

3.2 The radiation era

Consider the density ρ corresponding to M and Δr of (3,20) by replacing M with $h/(\lambda c)$; in this way the total mass of the universe is expressed via the momentum h/λ of an electromagnetic wave propagating with velocity c. For simplicity we have assumed that the refractive index of the medium where the wave propagates is 1, although in principle this is an approximation only; the aforesaid gamma-gamma physics [21] predicts photon fluctuations resulting in charged fermion -antifermion pairs, leptons or quarks, which couple with the photons themselves. In the presence of electron-positron and proton-antiproton couples of particles that typically also form as a consequence of this kind of interaction, a refraction index equal to 1 is certainly an approximation; yet this is acceptable for the following reasoning and order of magnitude estimates. So the late $\rho_u = 3M_u/(4\pi\Delta r_u^3)$ of matter era reads $\rho^r = 3h/(4\pi\lambda c\Delta r^3)$ at the time Δt. A boundary condition for λ comes from the fact that the early electromagnetic radiation waves bounced between diametric distances $2\Delta r$ inside a sphere, i.e. still $\lambda = 2\Delta r/n$ with n integer according to eq (3,1); in this way steady waves were allowed to fill the universe at any time Δt. The internal bouncing of radiation is justified even admitting that the early stages of growth were allowed in non-equilibrium condition, owing to the rapid growth of the universe size, and without radiation energy loss unfavorable for the subsequent growth and evolution of the new-born universe. So λ was a function of time like Δr, i.e. the number n of allowed frequencies increased along with Δr; it seems reasonable to guess that an initial field almost monochromatic evolved towards a complex spectrum of steady wavelengths. Anyway the density of the universe in the radiation era reads

$$\rho^r = \frac{3nh}{8\pi c\Delta r^4} = \frac{3n\hbar}{4c\Delta r^4}.$$

while (3,3) reads $\Delta r = 2hG/(\lambda c^3)$; so the condition $\lambda = 2\Delta r/n$ yields $\Delta r = \sqrt{nhG/c^3}$. Hence increasing n means increasing Δr and the number of states allowed for the radiation field. So radiation density, radiation energy density and pressure during the radiation era read

$$\rho^r = \frac{3c^5}{4n\hbar G^2}; \qquad \eta_{in}^r = \frac{3c^7}{4n\hbar G^2}; \qquad P_{in}^r = \frac{c^7}{4n\hbar G^2}.$$

At the beginning of the radiation era, therefore, $\Delta r = \sqrt{hG/c^3}$ with $\lambda = \Delta r$ and $n = 1$ has the expected order of the Planck length with which in effect has been calculated the Planck volume V_0'. Moreover estimating hc/λ with λ of the order of the Planck length, $\approx 10^{-35}$ m, yields a temperature $T \approx hc/k_B\lambda$ of the order of 10^{33} K. The fact that this characteristic temperature is much higher than that estimated for the proton in today's V_0, confirms that actually the radiation era precedes the matter era. Putting Δr of the order of the Planck length, with $n = 1$ one finds $\rho^r \approx 4 \times 10^{96}$ kg/m^3 and $P_{in}^r \approx 10^{113}$ Pa and $\eta_{in}^r = 3.5 \times 10^{113}$ J/m^3; at this stage of evolution of the universe the energy $\varepsilon_{in}^r = (4\pi/3)\Delta r^3 P_{in}^r$ results about $\varepsilon_{in}^r \approx 1.7 \times 10^9$ J, to which corresponds a temperature of the order of $\varepsilon_{in}/k_B \approx 10^{32}$ K in agreement with that already estimated. Estimating an energy $k_B T \approx 1.3 \times 10^9$ J of the radiation field corresponding to this temperature, one finds $\omega^r = 1.6 \times 10^9/\hbar \approx 1.6 \times 10^{43}$ s^{-1} i.e. a radiation field with Planck frequency. These values correspond well therefore to the Planck pressure, energy, frequency and temperature.

So, trying to understand the physical meaning of these results beyond the numerical estimates, the radiation era was just after the very early time step of the creation of radiation just concerned; this initial step can be therefore nothing else but the Planck era. The huge internal pressure accounts for the rapid volume of the universe. Note that the value of ε_{in}^r is large, but not spectacularly high like P_{in}^r and η_{in}^r; these latter are due to the extremely small values of Planck volume. These ideas explain thus the subsequent beginning of the matter era, during which however the expansion mechanism of the universe was somehow different.

3.3 The universe expansion in the matter era

Comparing (3,17) and (3,14), it has been already noted the similarity between the gravitational energy ε_p of one proton at the boundary distance Δr_u and the energy ε_{V_0} existing within each V_0 just because of the presence of the proton itself. (3,20) have been accordingly inferred. If the proton, or whatever else its mass might actually represent, would be ideally removed from any volume V_0 internal to the universe and displaced to the boundary of the universe, the energy lost by V_0 is balanced by that transferred to the boundary; within the limits of the present order of magnitude estimates, there is no net gain or loss of energy in this ideal process. This suggests that creating a vacancy in the universe after ideally moving its average amount of matter per unit cell just to the external

boundary of the universe occurs at zero energy cost. Strictly speaking ε_p should have been calculated in principle writing $M_u - m_p$, the numerical difference being however completely irrelevant for one proton only. Actually this reasoning is extensible to describe a relevant number of protons regarded at the boundary; as $M_u/m_p \approx 10^{80}$, for a large number n_p of protons such that $1 \ll n_p \ll M_u/m_p$ still holds (3,18) because $M_u \approx M_u - n_p m_p$. This means that large numbers of protons are expected to contribute to this ideal transfer process, i.e. large numbers of empty cells are to be expected in the universe. Of course the comparison between ε_{V_0} and ε_p has statistical meaning only, despite the actual structure of the visible mass in the universe and even regardless of the local element abundances in the universe, hidden within the global value of M_u and still undisclosed when reasoning about the mere average distribution of M_u. The following remarks are useful at this point.

- There is no actual flow of protons moving inwards or outwards throughout the universe; the uncertainty in the most agnostic form of (2,1) requires any quantum particle completely delocalized everywhere in the whole universe. The diameter $2\Delta r_u$ is a quantum delocalization range inside which no information is conceptually allowed about the local position and dynamical variables of any kind of particle, proton or else. So any particle could be in V_0 or at the boundary simply provided that there are available allowed states; (3,18) merely compares the energies of protons in two different places where they could in fact be, i.e. everywhere because V_0 could be itself everywhere in the universe.
- Two states of equal energy are allowed to the proton: the bulk state in V_0 and the boundary state at the rim of the universe. A proton at the boundary state leaves behind an empty cell V_0, i.e. a hole in one of the bulk allowed states. In general occupied and empty states are possible in the bulk and at the boundary of the universe. The global electroneutrality is ensured by the identical chance statistically allowed to antiprotons too.
- Both ideal chances are possible in principle despite the black hole character of the universe: the protons do not escape far from the boundary, they remain "glued" on the boundary like any electromagnetic radiation possibly arriving up there from the bulk of the universe. The Hawking entropy supports this idea.
- The chance of either alternative is consequence of the second law of thermodynamics; these bulk and boundary chances concurrently possible for the protons increase their number of allowed states and thus their configuration entropy. This crucial point, which will be further concerned later, agrees with the fact that (3,17) describes identically the total mass M_u at the ideal center of the universe and the mass m_p at the boundary Δr_u apart or, vice versa, the mass m_p at the ideal center of the universe and the total mass M_u concentrated on a point at the boundary Δr_u apart; indeed, according to the considerations of section 2, the local position of any particle is physically meaningless because of the quantum delocalization within an uncertainty range. Either extremal configuration, in principle possible for the universe, is however unlikely by entropy considerations.
- If V_0 scales as described by (3,20), which is admissible as no restraining hypothesis has been made on it, then (3,18) previously introduced for the proton at the time Δt_u is unchanged at any $\Delta t < \Delta t_u$; moreover the number of states N_{in} is expected constant, as in effect it has been found.

These ideas encourage regarding the proton in V_0 as a sort of template that symbolizes the average behavior of real matter in any bulk state and at the boundary state; as previously remarked, this is certainly the strongest form to affirm the large scale isotropy and homogeneity of the universe. Actually particles and antiparticles with the same m_p concurrently formed after the radiation era have statistically the same probability of being found in the boundary state; if so, the initial configuration of coexisting protons and antiprotons uniformly occupying all available bulk states generates subsequently a boundary halo of virtual couples plus possible annihilation photons along with corresponding vacuum states and matter states in the bulk universe. This configuration change increases the total entropy of the universe. In particular, the surface entropy at the boundary of the universe consists of the Hawking term σ_{H} plus a contribution related to the configuration of boundary states shared with that of the bulk universe. The entropy will be considered in some more detail in the next section. It will be shown that the way of thinking based on the degenerate quantum states of the universe rather than on the multiplicity of states describing its actual structure of matter, helps formulating a possible growth mechanism of the universe. Usually growth and expansion are synonyms; the next section emphasizes why actually it is not so in the present model, where growth does not merely mean swelling.

3.4 The universe growth in the matter era

Let the bulk universe at an arbitrary time after the big bang consist of a number N_{out} of V_0 empty cells and a corresponding number $N_{in} - N_{out}$ of filled V_0 cells; the external boundary is thus a layer formed by N_{out} glued protons and antiprotons missing in the bulk. So even this statistical picture of universe is consistent with the existence of an empty part of the real universe and its real matter structure: correspondingly to the further redistribution of $N_{out}V_0$ and $(N_{in} - N_{out})V_0$ volumes, in principle located randomly in the total volume $N_{in}V_0$ available, clusters of matter tend to coalesce together by gravitational interaction: the vacuum corresponds indeed to the N_{out} residual holes left in between. Anyway, if clusters

of empty cells and clusters of occupied cells are numerous enough, then their random distribution within V_u is still consistent with the assumption of overall statistical homogeneity and isotropy. This seems indeed the case, as the number N_{in} of V_0 volumes has been estimated of the order of the Eddington number 10^{80}. The chance of introducing arbitrary numbers N_{out} and $N_{in} - N_{out}$ of cells brings the universe towards a situation of dynamical equilibrium between the former and the latter; yet this final configuration, somehow attained, could be imagined as the conclusion of a gradual process consisting of a first redistribution step $N_{in} - N'_{out}$ and N'_{out} of filled and empty cells, which in turn generates progressively a subsequent redistribution $N_{in} - N'_{out} - N''_{out}$ and $N'_{out} + N''_{out}$ of new filled and empty cells along with possible coalescence of cells still filled, and so on. This idea stimulates considering the dimensionless entropy of a current configuration, $\sigma_b = N_{in}!/(N_{out}!(N_{in} - N_{out})!)$, due to the fact that all transient configurations compatible with zero energy balance are equiprobable; the subscript b stands for "bulk". As σ_b has a maximum as function of N_{out}, the formation of bulk holes fulfills the second law until this maximum is reached. Let σ_b describe a transient configuration at a given time and $\sigma'_b = N_{in}!/(N'_{out}!(N_{in} - N'_{out})!)$ that at a later time; the latter is allowed if N_{out} and the subsequent N'_{out} fulfill $\sigma'_b > \sigma_b$. Hence, after an arbitrary numbers of steps, are formed as a function of time multiple clusters of matter aggregates subsequently attained and thus differently configured, together with a progressive modification of the empty space between them. At the dynamical equilibrium no net state exchange occurs. Of course σ_b and σ'_b neglect, for simplicity and brevity, the further contributions σ_{arr} and σ'_{arr} due to the ways to arrange the respective clusters of matter into actual universe structures; yet σ_b and σ'_b symbolize qualitatively the first conceptual step to understand the actual configuration of the universe. Clearly, by virtue of (3,13), the σ_{arr} driven final arrangements of filled cells are nothing else but stars or galaxies or flows of elementary particles or any other observable object. The existence of P_{in} related to the matter energy density agrees with and justifies the universe expansion, which however at this point still seems like a mere bubble blowing up by internal pressure effect. But just this point poses a further question: does the universe in the matter era expand freely or is it constrained by an external pressure P_{out} opposing to its expansion? In principle the expansion requires $P_{in} > P_{out}$, not necessarily $P_{out} = 0$: the force that pushes forwards the unit surface of universe boundary must simply overcome that possibly tending to pull it backwards, i.e. to squeeze the universe size towards a big crunch. If the former position is correct, then P_{out} tends to decrease the acceleration with which the universe expands. Yet, what does originate P_{out}? A possible answer relies just on the presence of protons and antiprotons at the boundary states of the universe previously introduced. The boundary here introduced is not mere spherical rim; in effect the plain idea of geometrical margin would be unphysical itself. More sensibly, the mobile contour of the universe is defined by a crowd of N_{out} virtual protons and antiprotons along with electromagnetic radiation trapped on a fading shell, recall the Hawking entropy. In fact the previous considerations propose in a natural way that the boundary should be a physical layer of finite volume and finite thickness; so the chance of defining an energy density η_{out} due to these particles seems the most straightforward way to define P_{out}. In this respect, the further chance of demonstrating that $P_{out} \neq P_{in}$ is important not only to infer information about the acceleration of the boundary of the universe, controlled by the net force $P_{in} - P_{out}$ per unit surface of boundary, but also to infer that the physical nature of the outer layer must be different from that inside the universe. Before assessing the importance of this conclusion as concerns the matter/antimatter ratio, let us examine two points: the expansion equation and the physical meaning of η_{out}, to which is related the pressure P_{out} equivalently as in (3,19). This external pressure could be likewise regarded as external force acting towards the center of the universe or resistance of the universe to increase the total surface of its boundary. The latter idea is more easily viable to introduce the existence of a boundary layer, whose thickness surrounds the universe and characterizes $\eta_{in} \neq \eta_{out}$; if the layer would have the same physical nature of the bulk vacuum, then the boundary should be at rest or steadily moving rather than accelerating. Let $\rho_u V_u c^2$ be the energy stored inside the universe; since today's universe expands, according to the first law its total energy E must also include a PV_u-like term. Let $\delta E = c^2\delta(\rho_u V_u) + P_{net}\delta V_u$ be the change δE of total energy during the time interval δt, where $P_{net} = P_{in} - P_{out}$ describes the net force pushing forwards the boundary. As no energy escapes outside of a black hole universe $\dot{E} = \dot{\rho} V_u c^2 + \rho \dot{V}_u c^2 + (P_{in} - P_{out})\dot{V}_u = 0$; so $\dot{\rho} + \rho \dot{V}_u / V_u + (P_{in} - P_{out})\dot{V}_u/(V_u c^2) = 0$. According to (3,20), the size of the elementary volume V_0 scales as Δr^3, i.e. like $V_u = N_{in} V_0$; then $\dot{V}_u / V_u = 3\dot{a}/a$, whence the well known result

$$\dot{\rho} + 3\,\frac{\dot{a}}{a}\left(\rho + \frac{P_{net}}{c^2}\right) = 0; \qquad P_{net} = P_{in} - P_{out} \qquad (3,21)$$

The notation emphasizes that the time derivative of the radius defines the change rate of a co-moving length. The excess of internal pressure means that the layer outside the boundary is slightly different from the bulk. Note that also a negative pressure P_{out} counteracting P_{in} has been introduced in this reasoning.

Regard the boundary as if it would be a material layer characterized by a contractive energy per unit surface $\gamma = \varepsilon_\gamma / l^2$ that opposes to its stretching during the expansion; for instance, this effect can be guessed thinking to the opposite charges of the particles/antiparticles that crowd the boundary surface. Anyway the total contractive energy of a spherical bubble having internal radius Δr_u and volume V_u is $\varepsilon_\gamma = 4\pi\Delta r_u^2 \gamma$. Moreover the Young-Laplace equation of such sur-

face tension-like model of boundary reads $P_{in}-P_{out} = 2\gamma/\Delta r_u$ Suppose that $P_{out} = P_{in}/2$; then $P_{out} = \eta_{in}/3$, like that inside a universe with radiation only. This is equivalent to say that P_{in} is due to two contributions: one coming from its radiation density content and one due to the ability of the radiation to generate matter via quantum fluctuations. The former is counterbalanced by P_{out}, the latter is the active energy excess pushing outwards the boundary. Hence the expansion of the universe is controlled by the quantum contribution of radiation fluctuation extra energy that generates matter, without which the universe would still be a radiation volume. To check this idea note that (3,3) yields $M_u^2 G/\Delta r_u = M_u c^2/2$, i.e. one half of the universe energy is equal to the first (3,17) with the proton mass replaced by that of the whole universe. The same holds for the energy density, obtained dividing both sides by V_u. So if $P_{in}/2 = \eta_{in}/3$, then $P_{out} = \eta_{in}/3$ requires $\eta_{out} = \eta_{in}/2$. Hence the right hand side yields

$$\begin{aligned} \eta_{out} &= \frac{M_u^2 G}{V_u \Delta r_u} \approx 4.2 \times 10^{-11}\,\mathrm{J/m^3} \\ P_{out} &= 2.8 \times 10^{-11}\,\mathrm{Pa} \end{aligned} \qquad (3,22)$$

as it reasonably appears comparing with η_{in} of (3,12). This result implies interesting consequences. The total contractive energy of a spherical bubble of radius Δr_u and volume V_u is $\varepsilon_\gamma = 4\pi\Delta r_u^2\gamma$. Moreover the Young-Laplace equation reads $P_{in} - P_{out} = P_{in}/2 = 2\gamma/\Delta r_u$, so that $\gamma = P_{in}\Delta r_u/4$ yields $\varepsilon_\gamma = \pi\Delta r_u^3 P_{in} = M_u c^2/2$ thanks to (3,19). Hence the whole energy of the boundary layer generating its contractive surface tension is one half of the total bulk energy of the universe, i.e. that corresponding to the net pushing effect of the big-bang quantum fluctuation only. Also, this confirms that $P_{out} = P_{in}/2$ is an external pressure opposite to P_{in} and directed towards the universe center consistently with the curvature radius Δr_u. The numerical value of γ is $\approx 6 \times 10^{15}$ J/m^2, corresponding to $M_u c^2/2A_u$. It is interesting the fact that the boundary layer can be regarded as a real matter sheet curved by the pressure difference according to the Laplace equation. The initial black hole condition (3,3) is essential for this result. Note that it is possible to write

$$\eta_{out} = \frac{3}{16\pi\Delta r_u^2}\frac{c^4}{G} = \frac{3}{4}\frac{c^4}{A_u G}; \qquad \gamma = \frac{c^4\Delta r_u}{4A_u G} \qquad (3,23)$$

i.e. the compression force at the boundary of the universe is of the order of the Planck force acting on its total surface. It is interesting to note that replacing $A_u = 4l_P^2\sigma_{\mathrm{H}}$, it is possible to express γ as a function of the Hawking entropy. Moreover, once knowing η_{out} it is easy to find the thickness of the boundary layer. This energy density is that stored in a layer surrounding the universe δr_u thick. i.e. the boundary protons and antiprotons are actually contained in a shell of volume $(4\pi/3)[(\Delta r_u + \delta r_u)^3 - \Delta r_u^3]$; so

$$V_{out} = \zeta V_u; \qquad \zeta = (1 + \delta r_u/\Delta r_u)^3 - 1 \qquad (3,24)$$

which means that in fact the size of the universe is still described just by its radius Δr_u via a correction factor ζ. Having defined η_{out} at Δr_u, it is immediate to estimate also energy, mass and number of protons/antiprotons of the boundary layer through the following equations

$$\begin{aligned} \varepsilon_{out} &= V_{out}\eta_{out} = \zeta M_u^2 G/\Delta r_u = \zeta\,\frac{c^4}{4G}\,\Delta r_u \\ m_{out} &\approx \varepsilon_{out}/c^2 = \zeta\,\frac{c^2}{4G}\,\Delta r_u \\ n_{out} &\approx m_{out}/m_p = \zeta\,\frac{c^2}{4Gm_p}\,\Delta r_u. \end{aligned}$$

If $\delta r_u \gg \Delta r_u$, then $\zeta \approx (\delta r_u/\Delta r_u)^3$; if instead $\delta r_u \approx \Delta r_u$, then $\zeta \approx 7$. Moreover, trusting to the idea that $\delta r_u \ll \Delta r_u$ at the today time Δt_u, one finds $\zeta \approx 3\delta r_u/\Delta r_u$ and then $V_{out} \approx 4\pi\Delta r_u^2\delta r_u$. Suppose that $\delta r_u \approx 10^{-15}$ m, which corresponds to the size of the proton; then $V_{out} \approx 2 \times 10^{39}$ m^3 yields $\varepsilon_{out} \approx 10^{29}$ J; i.e. the boundary layer consists of a total mass $m_{out} \approx 10^{12}$ kg, to which correspond about $n_{out} \approx 6 \times 10^{38}$ protons and antiprotons. It would be also easy with the help of (3,20) to repeat the estimates also a different past times. Going beyond the raw numerical estimates, one concludes: (i) the number density n_{out}/V_{out} is of the order of 1/3 proton per cubic meter, a figure similar to that found in V_0 of the bulk universe; (ii) the number of boundary protons results $\ll N_{in}$, as it must be according to the previous considerations; (iii) the fact that the size of the proton is of the order of one fm means that the boundary layer is actually formed by a monolayer of protons and antiprotons; also this result seems in effect quite reasonable. The connection of these conclusions with the previous (3,1), (3,6) and (3,8) will appear shortly.

Now let us explain why the presence of the proton/antiproton couples at the boundary is important for the growth of the bulk universe. Assume that the empty V_0 cells of the universe, i.e. our core vacuum, actually includes couples of virtual particles and antiparticles that annihilate and then rematerialize: whatever their specific nature might be, a simple reasoning shows that the main effect of sharing these virtual couples between bulk states and boundary states is that of transferring to the aforesaid boundary layer the properties of the bulk universe. It is essential that both virtual particles and antiparticles have equal probability of being in either state, see the next section for more details; in this sense it is possible to regard them as a couple. These forerunner quantum couples are the precursors that generate a new boundary of the universe and activate its expansion. Indeed transferring the energy early contained in any V_0 towards the boundary means reproducing at the boundary the quantum states characterizing the bulk universe, i.e. not only that of protons and antiprotons but also the vacuum energy fluctuation generating them. This also means that the universe grows by replicating part of itself outside itself; the duplication concerns of course also the virtual couples of particles and antiparticles

characterizing the core vacuum, which once more confirms why (3,12) and (3,14) have been calculated with M_u and not with m_u. So in the present model expansion does not mean merely swelling: the chance that these couples annihilate and rematerialize at the external boundary of the universe likewise as they did inside the universe, means that even the external boundary assumes the feature of the core cells V_0. In effect the previous figures recalculated with a value of δr_u slightly larger than one proton monolayer yield a proton/antiproton density comparable to that within V_0 of the bulk universe; this clearly indicates that increasing δr_u means increasing the number of boundary states allowed to protons and antiprotons. Yet proton and antiproton density in the boundary layer equal to that existing in V_0 means that the bulk of the universe has been in fact expanded by a supplementary layer $\gtrsim \delta r_u$, i.e. the actual boundary is located a step δr_u beyond the previous one, and so on by successive steps consistent with a growth rate presently given by v_u of (2,6). The driving force of this "onion growth" process is the entropy increase required by the second law: all protons and antiprotons filling the bulk universe only, anyhow distributed and arranged, would define a degree of order greater than that where some of them have the additional chance of being further arranged in the only region furthermore conceivable, i.e. that glued to the external boundary of the black hole universe. Yet the key concept is clearly the quantum uncertainty, in its most agnostic form of (2,1): being completely delocalized everywhere in the universe, the particles can preferentially be in fact wherever they ensure the most advantageous entropy and growth conditions.

However, the question that then arises immediately is: does this chance expel to the boundary exactly equal amounts of particles and antiparticles or is there preferential transfer of either kind of them? From a statistical standpoint the answer is indeed that reasonably couples of virtual particles only should share this growth mechanism: drawing randomly from a multitude of particles and antiparticles, the realistic chance is that equal numbers of either kind are involved in the quantum state change. Despite this statistical equivalence, however, the next section will emphasize why the overall effect of the entropy increment is that of increasing the matter/antimatter ratio in the bulk universe.

3.5 The problem of matter and antimatter

This section describes a mechanism really possible soon after the end of the radiation era; the couples proton/antiproton just formed from the very hot radiation field have actual physical meaning, instead of being mere statistical entities suggested by (3,12). Is useful here a reasoning similar to that of the Dirac sea, which in the present context seems physically even more appropriate than the original one: are inherent here neither infinite states occupied by electrons with negative energy nor the doubtful concept of "neutrality" conventionally defined by the presence of infinite electrons in negative energy occupied states; the Pauli principle is no longer necessary to avert a weird radiation of negative energy.

In the original Dirac idea, a photon of energy $\geq 2m_ec^2$ excites an electron in the negative state above the forbidden gap; as a result, the electron just removed appears as a standard electron that leaves behind a related positive hole, the positron. Today we know that in fact two photons of sufficient energy are able to create a couple particle/antiparticle while fulfilling the conservation laws. Let us implement here this standpoint, emphasizing however that the driving energy has now entropic character: the energetic photons necessary to modify the Dirac sea of negative energy electron states is here replaced by the entropy increase $T\delta S$ that results from the combined configuration option, bulk state and boundary state, allowed for each proton and each antiproton. The number of proton and antiproton quantum states is the large but finite N_{in}. It has been already estimated that just after the radiation era T was of the order of $10^{32} \div 10^{33}$ K; this range of values seems high enough to account for a Dirac-like process. Discuss separately what happens when one proton and one antiproton pass from their own bulk states in V_0 to their respective boundary states; two V_0 states are involved in the process, the probability that this happens is equal for both.

One proton in the first V_0 has the same energy as in the boundary state; with the proton in this latter state a hole is left behind in this V_0, i.e. a neutral vacuum state forms in the bulk universe. No constrain is necessary about the energy $T\delta S$ to allow the change from bulk to boundary state, either configuration is allowed at zero energy cost; now one V_0 state is chargeless, whereas one boundary state is positively charged.

The Dirac reasoning for an antiproton in the second V_0 sounds as follows. A proton in the negative energy state in this V_0 is excited concurrently and with the same statistical probability of the previous process; now a constrain about the excitation energy is required and reads $T\delta S \geq 2m_pc^2 + m_ec^2$. This proton is thus excited, leaves unoccupied its initial state, overcomes the forbidden gap at the right hand side and appears as an ordinary proton; a negative hole, i.e. one antiproton, results by consequence. This hole is to be regarded in the boundary state, previously raised to a positive charge state by the first proton, to ensure the local electric neutrality; the ordinary proton co-generated in the second bulk state V_0 remains inside the bulk universe together with the negative charge of one electron; this latter, necessary for the total spin conservation and for the overall bulk neutrality at the minimum energy cost, occupies the former empty vacuum state V_0 left behind from the first proton.

Clearly this mechanism requires that both a proton and an antiproton change contextually and with the same probability their bulk states, in which case we have: (i) two boundary states altogether neutral occupied by one proton and one negative antiproton, which can yield by annihilation the electromagnetic radiation trapped at the boundary of the universe and concerned since the beginning by (3,1), as confirmed by

(3,6) and (3,8); (ii) a neutral bulk state formed by one proton and one electron occupying the two volumes V_0 left vacant. Also the electroneutrality in the bulk universe is thus fulfilled thanks to the electron energy included in the energy balance of $T\delta S$. On the one hand, therefore, the equal probability of exciting statistically one proton or one antiproton is essential to ensure the neutrality of both bulk and boundary states; on the other hand, by consequence of this mechanism a couple proton/antiproton is formed in the boundary state, whereas in the bulk one proton has replaced the antiproton with the help of one electron. In fact this process removes antimatter from the bulk universe, which appears as electromagnetic radiation surrounding the universe via entropy driven process; the holes of negative energy states, i.e. protons, concurrently generated along with electrons appear as bulk matter. Moreover just the annihilation electromagnetic halo ensures the growth of the universe, which therefore does not simply swell but replicates itself far at the boundary via annihilation energy. The separation boundary-antimatter from bulk-matter was likely allowed to occur just at the beginning of the matter era, when the matter started being generated from the extremely hot radiation field consistent with its $T\delta S$. It is reasonable to think that without this separation the bulk universe would have remained in the radiation era, because the two photon mechanism previously hypothesized would have continued to produce virtual matter that however endlessly annihilated with the virtual antimatter contextually generated. Since no energy escapes from the black hole universe, $T\delta S = \delta(TS) - S\delta T$ caused decrease of internal energy and cooling of the universe, until when the temperature decrease made impossible the radiation driven formation of virtual proton/antiproton couples and the consequent antimatter expulsion to the boundary along with the concurrent formation of low T matter. Begins just now the matter era. Of course all this is possible because of the total uncertainty of the quantum particles introduced in its most agnostic form of (2,1): these particles do not need any actual travel to go from bulk to boundary of the universe, being instead totally delocalized; they are simultaneously everywhere without any chance of specify their actual location. These ideas have been exploited to discuss the EPR paradox in the frame of a relativity model entirely based on the space-time uncertainty [12].

As concerns the point (i) above, (3,6) to (3,9) and related considerations about $\hbar\omega_{n=2}$ agree with the idea that both protons and antiprotons existing at the boundary of the universe contribute with their annihilation to form the halo of electromagnetic radiation surrounding the universe.

As concerns the point (ii), the presence of the electron is evidenced simply implementing the second (3,17): the electron energy ε_e early contributed by $T\delta S$ replaces ε_p in the empty V_0 left behind by the previous proton now occupying the boundary state, so the energy density in the bulk volume V_0 becomes ε_e/V_0. To confirm this mechanism, it is enough to estimate $T = (\varepsilon_e/V_0\mathrm{a})^{1/4}$ via the black body constant $\mathrm{a} = 5.67 \times 10^{-16}\ \mathrm{J/m^3K^4}$; today's $V_0 \approx 2\mathrm{m}^3$ yields $T \approx 2.63$ K. Of course in the past, when $V_0' \ll V_0$ according to (3,20), the energy density was higher and thus the background cosmic temperature accordingly higher; the low energy of the present cosmic radiation is due to the swelling of the early V_0', formerly of the order of the Planck volume, to the size of today's V_0 that decreases the electron energy density. This conclusion agrees with the condition $n\lambda = 2\Delta r$ previously introduced to describe the evolution of the radiation field as a function of the growing universe size during the radiation era. The mechanism that originates the CBMR dates back to the early beginning of the matter era when this mechanism took place, but is operating even presently: the today wavelength, due to the swelling of the early V_0' to the current V_0, is related to the virtual couples of particles/antiparticles that feed the growth of the universe keeping constant its black hole ratio $M_u/\Delta r_u$ according to (3,20) and the concept of vacuum. The small % discrepancy from the experimental value 2.72 K of today background cosmic radiation is due to having implemented the mere rest mass of the electron, whose kinetic energy instead is presumably not exactly zero; being the electron much lighter than the proton, a relativistic correction factor in the energy balance of $T\delta S$, corresponding to $\mathrm{v}_e \approx 0.5c$ and reasonably expected, increases slightly the energy density in V_0 and allows to fit exactly the experimental value. Yet this is not the main point: the most important aim of the model is to verify the sensibleness of estimated values with respect to the available experimental data and assess the conceptual consistency of the theoretical model with the current knowledge of the universe.

4 The dark mass

A crucial point that deserves a rational explanation, hitherto not yet concerned, regards the mass $m_?$. Some comments on this mass are here reported starting from (3,9) and (3,17) and comparing the energy $\hbar\omega_n$ with $\Delta\varepsilon_u = \hbar/\Delta t_u$. One finds

$$\frac{nc\Delta t_u}{2\pi\Delta r_u} \approx \frac{n}{20}. \tag{4,1}$$

In effect, with the help of (3,1) and (3,3) the ratio at left hand side is equal to about $n\xi/2\pi$ with $\xi = 0.3$ according to (2,5) and (2,6). In section 3.1 it has been highlighted that $n = 2$ means considering electromagnetic waves surrounding the universe whose energy corresponds to the annihilation of several protons with antiprotons; also, in agreement with (3,8), for $n = 2$ the right hand side of (4,1) becomes 10^{-1}. Recall now that just a factor ten has been already found in (3,4), when describing the ratio M_u/m_u. So it seems natural to introduce this ratio into (4,1) that becomes therefore

$$\frac{M_u}{m_u}\,\frac{c\Delta t_u}{\pi\Delta r_u} \approx 1. \tag{4,2}$$

Very large numbers that fit such a simple numerical value suggest a significant physical meaning hidden in the last equa-

tion: the fact that $M_u c\Delta t_u \approx \pi m_u \Delta r_u$ is interesting because it provides a new link between M_u and m_u, i.e. according to (3,4) $m_u c^2\hbar/\Delta t_u \approx m_u c^2\hbar\omega_{n=2} + m_? c^2\hbar\omega_{n=2}$ with $\omega_{n=2} = c/\pi\Delta r_u$. Going thus beyond the mere numerical result, let us generalize (4,2) to any Δt by replacing 1 with a number $q = q(\Delta t, \Delta r)$; so the subscript u characterizing today's quantities will be omitted, whereas different values are expected for $\omega_{n=2}$ and $m_?$. Multiply both sides of the resulting equation by c^2; recalling again (3,4), (4,2) turns into

$$qmc^2\,\frac{\hbar}{\Delta t} = mc^2\hbar\omega_{n=2} + m_? c^2\hbar\omega_{n=2};\quad \omega_{n=2} = \frac{c}{\pi\Delta r}. \qquad (4,3)$$

This equation is interesting because its terms are cross linked: a couple of terms shares mc^2, another couple $\hbar\omega_{n=2}$. This shows that m and $m_?$ are correlated. Moreover the fact that this equation contains squared energy terms, brings to mind an important equation inferred in the appendix, i.e.

$$\varepsilon^2 = (pc)^2 + \varepsilon^2_{rest}. \qquad (4,4)$$

Add $\zeta mc^2\hbar/\Delta t$ to both sides of (4,3); by comparison these equations suggest the following correspondences

$$\begin{aligned} &(q+\zeta)\,mc^2\,\frac{\hbar}{\Delta t} = \varepsilon^2 \\ &mc^2\left(\hbar\omega_{n=2} + \zeta\,\frac{\hbar}{\Delta t}\right) = (pc)^2 \\ &m_? c^2\,\hbar\omega_{n=2} = \varepsilon^2_{rest} \end{aligned} \qquad (4,5)$$

being $\zeta = \zeta(\Delta t, \Delta r)$ a function of Δr and Δt whose physical meaning will appear soon. In principle these correspondences, merely based on the one-to-one association between (4,3) and (4,4) having an analogous form, propose a possible explanation of the mass $m_?$.

The universe as a whole is to be regarded like a free spinless neutral macro-particle moving at uniform speed, whose kinetic and total energy are respectively related to the terms $(pc)^2$ and ε^2; accordingly $m_?$ accounts for the rest energy of the macro-particle universe. It seems surprising that this link, suggested by mere numerical analysis of the values of $\hbar\omega_{n=2}$ and $\hbar/\Delta t_u$ of (4,2), is provided by a formula of special relativity and not of general relativity. The energies of (4,3) concern the universe as a whole and not the interaction of its parts, galaxies and stars and so on, whose gravitational dynamics is governed by the general relativity. In effect, (3,3) regards the black-hole universe as a global object, a spinless macro-particle, whose properties are due to its total mass and total size only, regardless of its complex internal structure, mass composition and mass distribution assumed homogeneous at least on large scale. A valid support to propose a rectilinear uniform motion of the whole universe comes from the fact that indeed this idea cannot be excluded by any experiment: since Galileo it is known that such an inertial motion cannot be detected by any observer inside the universe. Perhaps a harder implication of this idea could concern the hypothetical reference system R_u able to describe this motion; however also this dilemma is actually a false problem in the present model, once thinking the size of the universe as an uncertainty range $\Delta r = r_1 - r_0$ in principle similar to that introduced in section 2 to describe energy levels and angular momentum of the quantum particles. It has been emphasized: (i) that neither r_0 nor r_1 must be specified to describe the quantum properties; (ii) that in fact both coordinates are not specifiable; (iii) that this conceptual lack of information prevents specifying the reference system R_u where is defined r_0 and the actual size of Δr defined by r_1. So it is conceptually impossible, but also inessential, to specify such R_u as regards the quantum properties of a particle within the range Δr_u during the time range Δt_u: if the properties of the quantum macro-particle we call universe do not depend on r_0 or r_1 but on Δr only, then the difficulty of defining R_u, e.g. its origin, becomes marginal. Anyway, since (4,1) and (4,3) come directly from the experimental values of Δr_u and Δt_u, there is no reason to reject them; in effect (4,3) and its relativistic free particle interpretation explain why one addend concerns the mass $m_?$ and its energy $m_? c^2$ additional to the visible mass m_u of stars. Now is justified the function ζ knowing that $\varepsilon = mc^2/\sqrt{1-(\mathrm{v}/c)^2}$ and $p = m\mathrm{v}/\sqrt{1-(\mathrm{v}/c)^2}$; also these formulas are shown in the appendix in the frame of the present model. Let us rewrite the three terms of (4,4) that define the relativistic energy of the free macro-particle universe of (4,5) as a function of its displacement constant velocity v_{mp} and mass M_{mp}; this means replacing v and m with v_{mp} and M_{mp}. Hence

$$\begin{aligned} &(q+\zeta)\,mc^2\,\frac{\hbar}{\Delta t} = \frac{M^2_{mp}c^4}{1-\mathrm{v}^2_{mp}/c^2} \\ &mc^2\left(\hbar\omega_{n=2} + \zeta\,\frac{\hbar}{\Delta t}\right) = \frac{M^2_{mp}\mathrm{v}^2_{mp}c^2}{1-\mathrm{v}^2_{mp}/c^2} \\ &m_? c^2\,\hbar\omega_{n=2} = M^2_{mp}c^4. \end{aligned} \qquad (4,6)$$

Taking the ratio side by side of the first two equations one finds with the help of (3,9)

$$\frac{\mathrm{v}^2_{mp}}{c^2} = \frac{\omega_{n=2}\Delta t + \zeta}{q+\zeta};\qquad \omega_{n=2}\Delta t = \frac{c}{\pi}\,\frac{\Delta t}{\Delta r} = \frac{\mathrm{v}}{\pi c} \qquad (4,7)$$

where v is the average expansion rate of the universe at Δt. Now we impose that v_{mp} is constant via the function ζ; so

$$\mathrm{v}_{mp} = \pm c\,\sqrt{\zeta_0};\ \ \zeta = \frac{\omega_{n=2}\Delta t - \zeta_0 q}{\zeta_0 - 1};\ \ q = \frac{M}{m}\,\omega_{n=2}\Delta t \qquad (4,8)$$

i.e. q generalizes (4,2). Note that M_{mp} does not appear in these equations; it is merely defined by the third (4,6) as a function of $m_?$, on which however no hypothesis has been made. So the definitions of ζ and q hold regardless of M_{mp}. An obvious condition is $0 < \zeta_0 < 1$; moreover $q + \zeta > 0$ and $\omega_{n=2}\Delta t + \zeta > 0$ are also evident because both sides of (4,6)

and (4,7) are positive. The former condition reads $q + \zeta = (\omega_{n=2}\Delta t - q)/(\zeta_0 - 1) > 0$, the latter reads $\omega_{n=2}\Delta t + \zeta = \zeta_0(\omega_{n=2}\Delta t - q)/(\zeta_0 - 1)$; owing to the expression of q both reduce to the unique condition $1 - M/m < 0$, which is indeed true as it has been introduced since the beginning in the present quantum model. Impose also $m_?\omega_{n=2} = const$, which yields $m_?c/\pi\Delta r = const$: this equation extends (3,20) that reads $M/\Delta r = const = m/\Delta r + m_?/\Delta r$ according to (3,4). In this way M_{mp} becomes a constant. Note that owing to (3,8) this result reads $m_?c^2\hbar\sqrt{\rho G} = \varepsilon^2_{rest}$; being by definition $\rho = (m_? + m)/V$, one concludes that ε_{rest} is defined even during the early the radiation era when the visible mass was $m = 0$ and the universe volume of the order of the Planck volume V_P. So, with obvious meaning of symbols, $\varepsilon^2_{rest} = m^{(0)}_?c^2\hbar\sqrt{m^{(0)}_?G/V_P}$ and remained constant since then; hence the third (4,5) reads $m_? = m^{(0)}_?\sqrt{\rho^{(0)}/\rho}$, with $\rho^{(0)} = m^{(0)}_?/V_P$. Of course, as already noted, $1/\rho$ is an increasing function of $m_?$ because the black hole condition $M/\Delta r = const$ requires M/V decreasing function of Δr^3. In conclusion (4,5) are appropriate to describe a free macro-particle of constant mass M_{mp} moving at constant rate v_{mp}. Eventually, note that the square energies of (4,5) are actually products of two different energies, as if they would come from geometrical averages like for instance $< \varepsilon > = \pm((q + \zeta)mc^2\hbar/\Delta t)^{1/2}$. So the black hole we call universe has, as a whole, the average energy $< \varepsilon >$ of a free particle that moves with average constant momentum $< pc > = \pm(mc^2(\hbar\omega_{n=2} + \zeta\hbar/\Delta t))^{1/2}$, whereas $m_?c^2$ and $\hbar\omega_{n=2}$ defining $< \varepsilon_{rest} > = \pm(m_?c^2\hbar\omega_{n=2})^{1/2}$ appear to be the ingredients of its average rest energy. Otherwise stated, the well defined mass balance between $m_?$ and m_u proposed here appears rationally motivated: m_u is due to the capability of the universe to create ordinary visible mass after the radiation era exploiting the available big-bang fluctuation energy; the additional mass $m_?$ ensures the existence of an efficient black hole universe that does not waste uselessly its valuable energy content. So it follows also the necessity of a displacing universe. Are unavoidable at this point at least three questions: does actually the equation $< \varepsilon > = \pm\sqrt{< pc >^2 + < \varepsilon_{rest} >^2}$ admit the minus sign? could an anti-universe actually exist with a matter/antimatter mechanism equal and opposite to that described in the previous section? is our whole universe a wave/corpuscle subjected itself to the uncertainty principle?

5 Discussion

The cosmology is probably the most difficult among the physical sciences because of both its multidisciplinary conceptual basis and scarcity of experimental data, besides inferred in a limited domain of time and space consistent with the light speed: past, present and future of the whole universe must be guessed despite the space-time horizon gives us access to a limited window of observable objects only. Just for this reason the theoretical models have a special role in cosmology. Usually the experimental data validate a theoretical model; here instead seems true the exact contrary, i.e. a sound self-consistent model highlights the physical meaning of the available experimental data. In this particular context is crucial the role of quantum mechanics. The correspondence principle states that the classical physics is the limit of quantum physics for high quantum numbers, which implicitly means that just the quantum principles are the true essence of physics and thus of cosmology as well. This explains the attempt of the present model, mostly based on quantum considerations rather than on relativistic considerations. Two important experimental values, the Hubble constant and the cosmic background radiation temperature, have been estimated with accuracy enough to conclude that the physical approach of the present quantum model of the universe is basically correct. (2,1) enable the most important equations of quantum mechanics and relativity to be inferred [12,13,14,18]; their generality is also proven in particular by the ability of describing quantum fluctuations of a relativistic free particle. For instance the appendix shows how to find the well known equation $p = \mathrm{v}\varepsilon/c^2$ via $\Delta p = \mathrm{v}\Delta\varepsilon/c^2$, whose importance for the present model has been already emphasized, e.g. (2,4) and (3,7); however Δp and $\Delta\varepsilon$ are not classical ranges but quantum uncertainty ranges. So a quantum particle whose local momentum and energy are included within the respective ranges, recall the explicative results of section 2, is subjected to quantum fluctuations of p and ε that expectedly alter also its propagation rate. This fact prospects new chances for the known equations of special relativity, which here appear in fact as quantum equations subjected to the weirdness of the quantum world. Further considerations on this topic are outside the purposes of the present paper. Yet it is worth mentioning that the EPR paradox, according which particles billions of light years apart can instantaneously exchange information via the so called quantum entanglement, is explained according to the agnostic physical meaning of (2,1); the concept of distance becomes itself undetermined once disregarding the local coordinates. Renouncing even to the concept of probability density for any particle to be somewhere, replaced by the mere idea of delocalization within an uncertainty range, the concept of distance is no longer definable. So it is unphysical to expect a different quantum behavior for particles definable very close or very far apart only classically. Certainly this odd conclusion is not the only weirdness of the quantum world: as it is shown in section 2, this agnostic standpoint has unexpectedly heuristic physical meaning. One kind of weird phenomenon is the quantum fluctuation, according which any macroscopic object at rest could suddenly excited to a self-perturbed state because of a transient excess of energy, justifiable via the uncertainty principle only. The behavior of a relativistic quantum particle during a quantum fluctuation is quoted here because it is in effect pertinent to the purposes of the paper. The considerations proposed in the appendix usefully contribute to explain cosmological problems like the inflationary era. In the paper [13] it was

shown that (2,1) only are enough to infer the following corollaries: (i) equivalence of all reference systems in describing the physical laws, (ii) existence of a maximum average displacement rate allowed for any particle in its delocalization range and (iii) invariance in all reference systems of such a maximum velocity. These corollaries are in fact the basic statements of special relativity. Moreover also the equivalence principle of general relativity and the coincidence of inertial and gravitational mass were also inferred [14] along with the concept of mass as corollaries of the space-time uncertainty.

6 Appendix

This appendix sketches shortly how the relativistic momentum and energy are obtained exploiting (2,1) only; it aims to make the present paper as self-contained as possible. Let the arbitrary delocalization ranges be defined in an arbitrary reference system R, where a photon travels at speed c through $\Delta x^{(c)}$; so ((2,1)) read $\Delta x^{(c)}\Delta p_x^{(c)} = n^{(c)}\hbar = \Delta t^{(c)}\Delta\varepsilon^{(c)}$. The superscripts emphasize that the ranges are sized to fulfil the delocalization condition during an appropriate time range $\Delta t^{(c)}$. Being by definition $\Delta x^{(c)}/\Delta t^{(c)} = c$, then $c\Delta p_x^{(c)} = \Delta\varepsilon^{(c)}$. To find how the momentum and energy ranges of a massive particle traveling at rate $\mathrm{v}_x < c$ through $\Delta x^{(c)}$ scale with respect to $\Delta p_x^{(c)}$ and $\Delta\varepsilon^{(c)}$, write $\Delta x^{(c)}\Delta p_x^{(\mathrm{v})} = n^{(\mathrm{v})}\hbar = \Delta t^{(\mathrm{v})}\Delta\varepsilon^{(\mathrm{v})}$. As neither v_x nor c appear explicitly in this equation, write $n^{(\mathrm{v})}\hbar = \Delta t^{(c)}\Delta\varepsilon^{(c)} = \Delta t^{(\mathrm{v})}\Delta\varepsilon^{(\mathrm{v})}$; this is true if $\Delta t^{(c)}$ and $\Delta\varepsilon^{(c)}$ scale respectively like $\Delta t^{(\mathrm{v})} = (c/\mathrm{v}_x)\Delta t^{(c)}$, as it is reasonable, and $\Delta\varepsilon^{(\mathrm{v})} = (\mathrm{v}_x/c)\Delta\varepsilon^{(c)}$, as a consequence. Replacing these positions in the former equation, $\Delta x^{(c)}\Delta p_x^{(\mathrm{v})} = \Delta t^{(c)}(\mathrm{v}_x/c)\Delta\varepsilon^{(c)}$ yields $c\Delta p_x^{(\mathrm{v})} = (\mathrm{v}_x/c)\Delta\varepsilon^{(c)}$. Actually the superscripts can be omitted because they have been introduced for clarity of exposition only, not to identify particular range sizes; both $\Delta p_x^{(\mathrm{v})}$ and $\Delta\varepsilon^{(c)}$ are indeed completely arbitrary like v_x itself; the superscripts are also irrelevant as concerns the functional relationship between the local values of the respective variables. Hence

$$p_x = \mathrm{v}_x\varepsilon/c^2; \qquad \Delta p_x = \mathrm{v}_x\Delta\varepsilon/c^2 \tag{A1}$$

regardless of how the respective uncertainty ranges are defined. Since an identical reasoning holds in any other reference system R', one concludes that $p'_x = \mathrm{v}'_x\varepsilon'/c^2$ is an invariant of special relativity. In principle the component of velocity defining the momentum component can be positive or negative; yet squaring this equation one surely handles positive terms. So write $\varepsilon^2(\mathrm{v}_\mathrm{x}/c)^2 = (p_xc)^2$; since $\mathrm{v}_\mathrm{x}/c < 1$ for a massive particle one finds $\varepsilon^2 > (p_xc)^2$, which compels writing $\varepsilon^2 = (p_xc)^2 + \varepsilon_o^2$. Calculate the limit $p_x/\mathrm{v}_\mathrm{x}$ for $\mathrm{v} \to 0$; denoting this limit as

$$\lim_{\mathrm{v}\to 0}\frac{p_x}{\mathrm{v}_x} = m \tag{A2}$$

the concept of mass m is introduced as a consequence of the uncertainty, whereas (A1) yields $\lim_{\mathrm{v}\to 0}\varepsilon = \varepsilon_{rest} = mc^2$ in agreement with the idea that the limit must be finite; indeed no reason requires $\varepsilon \to 0$ for $\mathrm{v}_\mathrm{x} \to 0$. Thus $p_x = m\mathrm{v}_x$ is the non-relativistic form of (A1). So the previous equation yields $mc^2 = \varepsilon_o^2$, i.e.

$$\varepsilon^2 = (pc)^2 + (mc^2)^2 \tag{A3}$$

as it is well known. Hence (2,1) define themselves without additional hypotheses the concept of mass and the relativistic and non-relativistic form of the respective local variables included in the ranges Δp and $\Delta\varepsilon$. Note that merging together both equations one finds the well known expressions consistent with the Lorentz transformations. Also note that the local values of p_x and ε are exactly definable in relativity, which is substantially classical physics subjected to the covariancy principle in a four dimensional space-time context; here instead, as shown in section 2, coordinates, momentum and energy are dynamical variables random, unknown and unknowable within the respective uncertainty ranges. This is the conceptual key to understand the further considerations of this appendix. In classical physics momentum and energy of a free particle are constants; yet it is not so in the quantum world, where quantum fluctuations are allowed to occur. The crucial point is that (A1) and (A3) are quantum results, despite their form agrees of course with that of special relativity; yet, being the particles completely delocalized, the local p and ε must be intended as random values within the respective uncertainty ranges. So these equations can be accordingly handled. Let us admit that during a short time range δt even the energy of a free particle is allowed to fluctuate randomly by $\delta\varepsilon$. Since during the time transient the particle is expectedly allowed to move in a arbitrary way, (A1) is now exploited to highlight the link between $\delta\varepsilon$ and the related changes δp and $\delta\mathrm{v}$. Differentiating (A1) one finds $\delta\varepsilon = c^2\delta p/\mathrm{v} - p(c/\mathrm{v})^2\delta\mathrm{v}$: with given p and v, this result defines the functional dependence of $\delta\varepsilon$ upon arbitrary δp and $\delta\mathrm{v}$. Sum $\delta\varepsilon$ and (A1) to find $\varepsilon + \delta\varepsilon = c^2(p + \delta p)/\mathrm{v} - \varepsilon\delta\mathrm{v}/\mathrm{v}$. In general $\delta p\delta x = n\hbar$ reads $(\delta p)^2 = n\hbar\delta p/\delta x$, whereas in an analogous way $(\delta\varepsilon)^2 = n\hbar\delta\varepsilon/\delta t$. Regard just in this way $\varepsilon + \delta\varepsilon$ and $p + \delta p$; putting $\delta x = \mathrm{v}\delta t$ and replacing in the last expression to calculate $\delta(\varepsilon + \delta\varepsilon)/\delta t$, one finds

$$\begin{aligned}&(n\hbar)^{-1}(\Delta\varepsilon)^2 = (n\hbar)^{-1}(\Delta pc)^2 - \varepsilon\delta\omega\\ &\Delta\varepsilon = \varepsilon + \delta\varepsilon; \qquad \Delta p = p + \delta p.\end{aligned} \tag{A4}$$

The term $\varepsilon\delta\omega$ results because $\mathrm{v}/\delta x$ has physical dimensions of a frequency ω, so that $\delta\mathrm{v}/\delta x = \delta\omega$. As $n\hbar\omega\delta\varepsilon = \delta(\varepsilon n\hbar\omega) - \varepsilon\delta(n\hbar\omega)$, replacing this identity in the last equation one finds $(\Delta\varepsilon)^2 = (\Delta pc)^2 + n\hbar\omega\delta\varepsilon - \delta(\varepsilon n\hbar\omega)$. Let us specify this result via the position

$$n\hbar\omega = \delta\varepsilon$$

which yields also $(\Delta\varepsilon)^2 - (\Delta pc)^2 = (\delta\varepsilon)^2 - \delta(\varepsilon\delta\varepsilon)$. At left hand side appear terms containing the ranges $\varepsilon + \delta\varepsilon$ and $p + \delta p$ only, at right hand side the ranges $\delta\varepsilon$ and δp only. These latter are both arbitrary; moreover ε and p are arbitrary as well. So it

is reasonable to expect that the last equation splits into two equations linked by a constant energy ε_o

$$(\Delta\varepsilon)^2 - (\Delta pc)^2 = \varepsilon_o^2 = (\delta\varepsilon)^2 - \delta(\varepsilon\delta\varepsilon). \qquad \text{(A5)}$$

Indeed ε_o agrees with both of them just because it does not depend upon neither of them. Trivial manipulations show that the first equation yields

$$\begin{aligned} p &= \pm\frac{\varepsilon_o \mathrm{v}/c^2}{\sqrt{r_\varepsilon^2 - r_p^2(\mathrm{v}/c)^2}}; \qquad & \varepsilon &= \pm\frac{\varepsilon_o}{\sqrt{r_\varepsilon^2 - r_p^2(\mathrm{v}/c)^2}} \\ r_p &= 1 + \frac{\delta p}{p} & r_\varepsilon &= 1 + \frac{\delta\varepsilon}{\varepsilon}. \end{aligned} \qquad \text{(A6)}$$

(A5) is fulfilled even during the transient. The value of the constant ε_o is immediately found as a consequence of (A2): in agreement with (A5) $\varepsilon_o^2 = \varepsilon_{rest}^2$, because A6 hold during the time transient allowing $\delta\varepsilon$; before and after that transient one must put $\delta\varepsilon = 0$ and $\delta p = 0$ in order to have the "standard" Einstein momentum and energy of the free particle, here inferred from A1 to A3. So

$$\varepsilon_{Ein}^2 = c^2 p_{Ein}^2 + \varepsilon_{rest}^2$$

$$p_{Ein} = \pm\frac{m\mathrm{v}}{\sqrt{1-(\mathrm{v}/c)^2}}; \qquad \varepsilon_{Ein} = \pm\frac{mc^2}{\sqrt{1-(\mathrm{v}/c)^2}}.$$

It is easy now to calculate the energy and momentum gaps during the time transient δt as a function of $\delta p/p$ and $\delta\varepsilon/\varepsilon$ as follows

$$\begin{aligned} \delta l\left(\frac{m\mathrm{v}}{\sqrt{r_\varepsilon^2 - r_p^2(\mathrm{v}/c)^2}} - \frac{m\mathrm{v}}{\sqrt{1-(\mathrm{v}/c)^2}}\right) &= n_{fl}\hbar \\ \delta t\left(\frac{mc^2}{\sqrt{r_\varepsilon^2 - r_p^2(\mathrm{v}/c)^2}} - \frac{mc^2}{\sqrt{1-(\mathrm{v}/c)^2}}\right) &= n_{fl}\hbar \end{aligned} \qquad \text{(A7)}$$

where δt is the time length of the fluctuation, δl the path traveled by the particle during δt and n_{fl} the number of states allowed to the particle during the energy transient. These equations are in effect nothing else but the uncertainty equations of the fluctuation gaps $\delta p_{fl} = p_{fl} - p_{Ein}$ and $\delta\varepsilon_{fl} = \varepsilon_{fl} - \varepsilon_{Ein}$. Of course $\delta p \to 0$ and $\delta\varepsilon \to 0$ after the transient, so the amounts within parenthesis vanish, while $n_{fl} = 0$ too; i.e. the fluctuation states are no longer accessible to the particle. Taking the ratio of these expressions, one finds

$$\frac{\delta l}{\delta t} = c\,\frac{c}{\mathrm{v}}. \qquad \text{(A8)}$$

According to (A8), during a quantum fluctuation of time length δt the uncertainty range δl allowed to any quantum particle corresponds to an average displacement rate $\delta l/\delta t = c^2/\mathrm{v} > c$, i.e. *as if* the particle would really propagate at superluminal rate. The reasoning to explain this result is similar to that explaining the recession motion of celestial objects mostly as a consequence of the expansion of the space-time itself. If the fluctuation modifies the size of the energy and momentum ranges, then according to (2,1) it must modify also the space and time range sizes. Yet the space range includes all local coordinates allowed to the particle: since this latter is anywhere in the space range because it is delocalized, and not because it really travels from point to point, modifying the space size means affecting the ability of the particle of being somewhere in the universe regardless of the velocity necessary to cover the path. This explains the apparent anomaly of superluminal velocity to figure out a fluctuation driven displacement. From a mathematical point of view, this is indeed possible provided that (A7) verify two inequalities: the first is $r_p\mathrm{v}/cr_\varepsilon < 1$, to avoid imaginary quantities, the second is $r_\varepsilon^2 - r_p^2(\mathrm{v}/c)^2 < 1 - (\mathrm{v}/c)^2$, in order that both left hand sides be positive. These inequalities merge into the unique $r_\varepsilon^2 - 1 < (r_p^2 - 1)(r_\varepsilon/r_p)^2$, which yields $1 - r_\varepsilon^{-2} < 1 - r_p^{-2}$ i.e. $r_\varepsilon^{-2} > r_p^{-2}$ and thus $r_\varepsilon^2 < r_p^2$. So, being $\delta p/p > \delta\varepsilon/\varepsilon$ according to (A6), $\varepsilon/p > \delta\varepsilon/\delta p$ reads thanks to (A1) and (2,1) $\mathrm{v}/c^2 > \delta t/\delta x$ and thus $\delta x/\delta t > c^2/\mathrm{v}$ even though $\mathrm{v} < c$. (A8) is confirmed noting that it could have been obtained more quickly and easily: rewrite (2,1) as $\Delta x/\Delta t = \Delta\varepsilon/\Delta p_x$ and recall (A1) $\Delta\varepsilon/\Delta p_x = c^2/\mathrm{v}_x$; replacing the latter into the former one finds $\Delta x/\Delta t = c^2/\mathrm{v}$. This result has the same form of (A8) and (3,7); without the steps (A4) to (A8) however the properties of the quantum fluctuation would not be evident. Owing to the arbitrariness of the range sizes, nothing in principle distinguishes Δx and Δt from δl and δt; yet (A7) emphasize the specific link between δl and δt and their conjugate momentum and energy just during the quantum fluctuation. For instance, (A7) admit $r_\varepsilon = 1$ and $r_p = 1$, i.e. $\delta\varepsilon = 0$ and $\delta p = 0$, in which case $n_{fl} = 0$ because of course there are no fluctuation states; instead $\Delta p_x = 0$ and $\Delta\varepsilon = 0$ are unphysical because they deny the concept of quantum uncertainty.

In conclusion the theoretical analysis describes the effect of the extra energy transient on the space-time uncertainty of the particle during the quantum fluctuation: a massive particle can displace more than allowed by its actual velocity. Transient displacement ranges $\delta l > c\delta t$ are possible for the boundary of the universe, even though forbidden in the early Einstein derivation of momentum and energy. Indeed the relativity is substantially classical physics; yet the beauty of the theory does not admit itself quantum phenomena like the fluctuations. These phenomena are instead allowed when deriving the Einstein formulas in the quantum frame of (2,1).

It is worth emphasizing however that in the particular case $\mathrm{v} = c$ even $\delta l/\delta t$ remains always and invariably equal to c.

It is clear now that also the universe expansion is interested by these results: the previous quantum considerations, unexpected in classical relativity, help to better understand and describe the so called "inflationary era". Regard the big

bang as a vacuum fluctuation that begins at the arbitrary time t_0 and expands the primordial sphere of radius r_0 according to the concepts introduced at the beginning of section 3. During δt the displacement δl of the boundary of the universe could overcome $c\delta t$, in agreement with $\delta\varepsilon \neq 0$ and $\delta p \neq 0$. Inflation did occur when the radiation density was such that the photons were allowed moving in a medium with refractive index $n_r > 1$ and matter particles, virtual or not, were generated in the radiation field during the early beginning of the later matter era. This idea agrees with the presence at the boundary of the primordial universe of the virtual couples of particles and antiparticles generating locally via their annihilation the halo of electromagnetic radiation introduced in (3,1).

As in the present approach the ranges sizes are unknown and conceptually unknowable, it is impossible to know exactly how long lasts δt. Yet it is possible to say that after a certain time range, when $\delta\varepsilon = 0$ and $\delta p = 0$ i.e. after the end of the fluctuation, the universe expansion continued at rate compliant with the usual condition v < c.

Consider an arbitrary number of particles, assumed for simplicity non-interacting; holds for i-th of them $p_i = \mathrm{v}_i\varepsilon_i/c^2$. Let Δp and $\Delta\varepsilon$ be the momentum and energy ranges including all p_i and ε_i; being the range sizes arbitrary, it is possible to write $\Delta p = \mathrm{v}\Delta\varepsilon/c^2$ with v defined in agreement with (A1). Suppose that a quantum fluctuation starts at an arbitrary time and modifies momenta and energies of some of the particles, so that the respective ranges are modified as well; then $(c^2/\mathrm{v})\Delta p = \Delta\varepsilon$ yields $(c^2/\mathrm{v})\delta\Delta p - (c/\mathrm{v})^2\delta\mathrm{v}\Delta p = \delta\Delta\varepsilon$. Moreover (2,1), which read $\Delta\varepsilon/2\pi = n\hbar\omega$ with $\omega = 2\pi/\Delta t$ and $\Delta p/2\pi = n\hbar k$ with $k = 2\pi/\Delta x$, yield $\delta\Delta\varepsilon/2\pi = n\hbar\delta\omega$ and $\delta\Delta p/2\pi = n\hbar\delta k$. The former is the Planck equation expressed as a function of $\Delta\varepsilon/2\pi$ instead of $\Delta\varepsilon$, the latter is the De Broglie equation also expressed as a function of $\Delta p/2\pi$ instead of Δp; however being the range sizes arbitrary, unknowable and inessential as concerns the eigenvalues of the physical observables, as shown in section 2, the factor $(2\pi)^{-1}$ is trivially irrelevant. It is remarkable instead that Δx and Δt of (2,1) are regarded here as wavelength and frequency of a wave, which is in fact possible in agreement with the general character of (2,1). One finds concurrently

$$\begin{aligned} &\frac{\delta\omega}{\delta k} = \frac{\omega'}{k}; \qquad \omega' = \omega - ku; \\ &u(\omega, k) = n_r^2\,\frac{\delta\mathrm{v}}{\delta\Delta p}\,\Delta p; \qquad n_r = \frac{c}{\mathrm{v}}. \end{aligned} \tag{A9}$$

Being v and δv arbitrary, it is evident that these equations hold whatever n_r might be. This conclusion is interesting because in effect the physical meaning of these equations depends just on the features of v. Call $\mathrm{v}_p = \omega/k$ and $\mathrm{v}_g = \omega'/k$, being thus $\omega' = \omega'(k)$. For $\mathrm{v} \equiv c$ (A1) reads $\Delta\varepsilon = c\Delta p$ and describes a set of electromagnetic waves propagating in the vacuum, whence $u = 0$ i.e. $\omega'/k \equiv \omega/k \equiv c$. If $\mathrm{v} < c$ is again constant, then these equations still describe a set of light waves propagating at the same rate v_p in non-dispersive medium with refractive index n_r; yet they are also compatible with a set of massive free particles displacing at the same rate. The case where $\mathrm{v} < c$ depends on k is more interesting. The equations describe light waves propagating with different velocities in a dispersive medium dependent on n_r; the first (A9) defines the group velocity $\mathrm{v}_g \neq \mathrm{v}_p$ of the whole packet formed in the dispersive medium. Analogous conclusion holds also for the matter waves: now the displacement of matter wave packet at rate v_g is related to the maximum probability to find somewhere the set of particles; indeed the first (A9) is also obtained from $\delta(\omega'/k)/\delta k = 0$, which suggests that ω'/k corresponds to the rate with which moves the maximum of the packet defined by the dispersion curve ω'/k vs k. Both electromagnetic waves and matter particles, despite their different physical nature, are thus compatible with a unique kind of equation: their common feature is the dual wave/corpuscle nature strictly connected with the quantization condition of (2,1).

The changes $\delta\omega$ and δk have been introduced as a consequence of quantum fluctuation; in effect it would be also possible to infer from $\delta\omega = \omega\delta k/k - u\delta k$ the Einstein formula for the energy fluctuations of blackbody radiation. For brevity this point is waived here; yet, is significant the ability of the quantum fluctuation to generate packets of particle waves and packets of electromagnetic waves having similar behavior. This conclusion helps to figure out the formation of matter in the radiation field during the radiation era as superposition of electromagnetic radiation and matter wave packets, both propagating with their characteristic group velocities $\mathrm{v}_g^{(r)}$ and $\mathrm{v}_g^{(m)}$. This supports the idea of fermion/antifermion pairs formed via photon fluctuations at appropriate energy fulfilling momentum and angular momentum conservation rules. The matter waves extended to all space time available justify the presence of matter throughout the universe. Indeed it is possible to write $\delta\omega/\delta k = \delta\omega^{(r)}/\delta k^{(r)} + \delta\omega^{(m)}/\delta k^{(m)}$; then, the addends at right hand side read $\delta\omega^{(r)}/\delta k^{(r)} = \mathrm{v}_g^{(r)}$ and $\delta\omega^{(m)}/\delta k^{(m)} = \mathrm{v}_g^{(m)}$. So the extra energy transient of the fluctuation of the radiation field (term at left hand side, because $\delta\omega$ is proportional to $\delta\Delta\varepsilon$) has generated a matter wave propagating at rate in general different from that of further radiation (terms at right hand side); the quantum fluctuation of this latter could generate in turn further matter and further radiation and so on, until the available energy is sufficient to repeat the process. The matter particle propagates with a group velocity $\mathrm{v}_g^{(m)}$ having finite space length; in principle the matter wave packet can also represent a chunk of matter having finite size and given probability of being found somewhere and moving in the universe. This supports the physical meaning of (3,12) as discussed in section 3.1.

Submitted on June 19, 2013 / Accepted on June 29, 2013

References

1. Burbidge E. M., Burbidge G. R., Fowler W. A., Hoyle F. Synthesis of the Elements in Stars. *Rev. Mod. Phys.*, 1957, v. 29, 547.

2. Kiefer C. Quantum Gravity, 2nd ed. Oxford University Press, Oxford, 2007.
3. Ashtekar A. and Geroch R. Quantum theory of gravitation. *Reports on Progress in Physics*, 1974, v. 37, 1211–56.
4. Polchinski J. String Theory. Cambridge University Press, 1998.
5. Green M. B., Schwarz J. H. and Witten E. Superstring Theory. Cambridge University Press, 1987.
6. Zlatev I., Wang L., Steinhardt P. J. Quintessence, Cosmic Coincidence, and the Cosmological Constant. *Phys. Rev. Lett.*, 1999, v. 82, 896–899.
7. Lidsey J. D., Wands D., Copeland E. J. Superstring Cosmology. *Physics Report*, 2000, v. 337 (4–5), 343.
8. Kachru S., Kumar J. and Silverstein E. *Phys. Rev. D*, 1999, v. 59, 106004.
9. Harvey J./,A. String Duality and Non-supersymmetric Strings. *Phys. Rev. D*, 1999, v. 59, 026002.
10. Leonhardt A. U., Paul H. Measuring the quantum state of light. *Progr. Quant. Electr.*, 1995, v. 19, 89–130.
11. Wigner E. P. On the quantum correction for thermodynamic equilibrium. *Phys. Rev.*, 1932, v. 40, 749–759.
12. Tosto S. Spooky Action at a Distance or Action at a Spooky Distance? *Progress in Physics*, 2012, v. 1, 11–26.
13. Tosto S. Quantum Uncertainty and Relativity. *Progress in Physics*, 2012, v. 2, 58–81.
14. Tosto S. Quantum Uncertainty and Fundamental Interactions. *Progress in Physics*, 2013, v. 2, 56–81.
15. Brans C. H., Dicke R. H. Mach's Principle and a Relativistic Theory of Gravitation. *Physical Review*, 1961, v. 124 (3), 925–935.
16. Wang Y., Wang Z. Time Variation of Newton's Gravitational Constant in Superstring Theories. *Phys. Rev. Lett.*, 1986, v. 57, 1978–1981.
17. Prigogine I., Geheniau J., Gunzig E., and Nardone P. *Proc Natl Acad Sci U S A*, 1988, v. 85 (20), 7428–7432.
18. Tosto S. An analysis of states in the phase space: from quantum mechanics to general relativity. arXiv gr-qc/0807.1011.
19. Seeger P. A., Fowler W. A., Clayton D. D. Nucleosynthesis of Heavy Elements by Neutron Capture. *Astrophysical Journal Supplement*, 1965, v. 11, 121.
20. Alpher R. A., Bethe H., Gamow G. The Origin of Chemical Elements. *Physical Review*, 1948, v. 73 (7), 803–804.
21. Moffat J. W. Superluminary Universe: A Possible Solution to the Initial Value Problem in Cosmology. *Intl. J. Mod. Phys. D*, (1993), v. 2 (3), 351–65. arXiv: gr-qc/9211020.

Dynamical 3-Space: Black Holes in an Expanding Universe

David P. Rothall* and Reginald T. Cahill†

School of Chemical and Physical Sciences (CaPS), Flinders University, SA 5042, Australia
E-mail: *david.rothall@flinders.edu.au †reg.cahill@flinders.edu.au

Black holes are usually studied without including effects of the expanding universe. However in some recent studies black holes have been embedded in an expanding universe, in order to determine the interplay, if any, of these two dynamical processes. Dynamical 3-space theory contains time independent solutions for black holes, which are spatial in-flows, and separately the time dependent Hubble expansion. This theory has explained numerous puzzles in observational astrophysics and contains 3 constants; G, α - which from experimental data turns out to be the fine structure constant, and δ - which is a small but nonzero distance, possibly a Planck-type length. The Hubble expansion in the dynamical 3-space theory cannot be "switched off", forcing the study, first, of isolated black holes coexisting with the expanding universe. It is shown that a time dependent black hole and expanding universe solution exists. The nature and implications of these solutions are discussed as they evolve over time. A dynamical network of black holes and induced linking cosmic filaments forming bubble structures is discussed, as a consequence of dynamical 3-space undergoing a dynamical breakdown of homogeneity and isotropy, even in the absence of baryonic matter.

1 Introduction

The motions of stars in galaxies are strongly affected by their central massive black holes, and that of galaxies in clusters are also affected by the expansion of the universe [13]. Then the need arises to analyse black holes in the expanding universe, with the view to checking if that expansion affects black hole characteristics. There is a long history of attempts to model this phenomenon analytically; early attempts include the Einstein-Strauss model through embedding Schwarzschild black holes in the background (FLRW) universe [10], and also the well known McVittie solution [16]. This gradually lead to models (see [12] or [8] for overviews) which include the cosmological constant. The currently accepted work is based on theories of gravitation by Newton, and then extended by Hilbert and Einstein. The use of these models has generated many questions about observational phenomena, such as "supermassive" galactic central black holes [11], bore hole anomalies [1, 23], flat spiral galaxy rotation curves [20] and cosmic filaments [24]. The "dark matter" and "dark energy" parameters introduced are required in order to fit the Friedmann universe expansion equation to the type 1a supernovae [19, 22] and CMB data [14]. A more recent account of space and time [2] models time as a non-geometrical process (keeping space and time as separate phenomena), which leads to the dynamical 3-space theory. This theory is a uniquely determined generalisation of Newtonian Gravity (NG) expressed in terms of a velocity field, defined relative to observers, rather than the original gravitational acceleration field. This velocity field corresponds to a space flow, which has been detected in numerous experiments. These include gas-mode Michelson interferometer, optical fibre interferometer and coaxial cable experiments, and spacecraft Earth-flyby Doppler shift data [5]. The observational phenomena mentioned above are now gradually becoming interpreted through understanding the dynamics of space, which appears to offer an explanation for "dark matter" and "dark energy" effects [6, 7]. A brief introduction to the dynamical 3-space theory along with experimental and observational tests is given in Sections 2-5. In Sections 6 and 7 we report the discovery of exact black hole solutions embedded in an expanding universe, and discuss the nature of their evolution over time, suggesting that primordial black holes develop linking filaments, which in turn form a cosmic network with bubble structures.

2 Dynamical 3–Space

Process Physics [2] is a theory of reality which models time as a non-geometric process, with space-geometry and quantum physics being emergent and unified phenomena. The emergent geometry is thought of as a structured quantum-foam "space" and is found to be dynamic and fractal in nature, with its 3 dimensionality only approximate at micro scales. If non-trivial topological aspects of the quantum foam are ignored, it may be coarse-grain embedded in a 3-dimensional geometrical manifold. This embedding ultimately allows us to describe the dynamics of the quantum foam, or space, using a classical velocity field $\boldsymbol{v}(\boldsymbol{r}, t)$, relative to an observer with coordinate system $\boldsymbol{r}$ and t [6], and here assuming zero vorticity, $\nabla \times \boldsymbol{v} = 0$:

$$\nabla\cdot\left(\frac{\partial \boldsymbol{v}}{\partial t} + (\boldsymbol{v}\cdot\nabla)\,\boldsymbol{v}\right) + \frac{5\alpha}{4}\left((trD)^2 - tr(D^2)\right) + \\ +\delta^2\nabla^2\left((trD)^2 - tr(D^2)\right) + ... = -4\pi G\rho; \quad D_{ij} = \frac{\partial v_i}{\partial x_j} \tag{1}$$

where $\rho = \rho(\boldsymbol{r}, t)$ is the usual matter density. *

The first term involves the Euler constituent acceleration, while the $\alpha-$ and $\delta-$ terms contain higher order derivative terms and describe the self interaction of space at different scales. Laboratory, geophysical and astronomical data suggest that α is the fine structure constant $\approx 1/137$, while δ appears to be a very small but non-zero Planck-like length. The emergence of gravity arises from the unique coupling of quantum theory to the 3-space [3], which determines the "gravitational" acceleration of quantum matter as a quantum wave refraction effect,

$$\boldsymbol{g} = \frac{\partial \boldsymbol{v}}{\partial t} + (\boldsymbol{v}\cdot\nabla)\boldsymbol{v} + (\nabla\times\boldsymbol{v})\times\boldsymbol{v}_R - \frac{\boldsymbol{v}_R}{1-\dfrac{\boldsymbol{v}_R^2}{c^2}}\frac{1}{2}\frac{d}{dt}\left(\frac{\boldsymbol{v}_R^2}{c^2}\right) + \ldots \quad (2)$$

where $\boldsymbol{v}_R = \boldsymbol{v}_0 - \boldsymbol{v}$ is the velocity of matter relative to the local space. The first two terms are the Euler space acceleration, the second term explains the Lense-Thirring effect when the vorticity is non-zero, and the last term explains the precession of planetary orbits.

Neglecting relativistic effects (1) and (2) give

$$\nabla\cdot\boldsymbol{g} = -4\pi G\rho - 4\pi G\rho_{DM}, \quad (3)$$

where

$$\rho_{DM}(\boldsymbol{r}, t) \equiv \frac{5\alpha}{16\pi G}\left((trD)^2 - tr(D^2)\right) + \\ + \frac{\delta^2}{32\pi G}\nabla^2\left((trD)^2 - tr(D^2)\right). \quad (4)$$

This is Newtonian gravity, but with the extra dynamical term which has been used to define an effective 'dark matter' density. Here ρ_{DM} is purely a space/quantum foam self interaction effect, and is the matter density needed within Newtonian gravity to explain dynamical effects caused by the α and δ effects in (1). This effect has been shown to offer an explanation for the 'dark matter' effect in spiral galaxies, anomalies in laboratory G measurements, bore hole g anomalies, and the systematics of galactic black hole masses, as noted below. When $\alpha = 0$ and $\delta = 0$, (3) reduces to Newtonian gravity. The $\alpha-$term has the same order derivatives as the Euler term, and so cannot be neglected *a priori*. It was, however, missed by Newton as its consequences are not easily observable in the solar system, because of the low mass of planets relative to the massive sun. However in galaxies this term plays a major role, and the Milky Way black hole data has given evidence for that term and as well for the next higher order derivative terms.

The spatial dynamics is non-local and instantaneous, which points to the universe being highly connected, consistent with the deeper pre-space process physics. Historically this was first noticed by Newton who called it action-at-a-distance. To see this, (1) can be written as a non-linear integro-differential equation

$$\frac{\partial \boldsymbol{v}}{\partial t} = -\nabla\left(\frac{\boldsymbol{v}^2}{2}\right) - G\int d^3r'\,\frac{\rho_{DM}(\boldsymbol{r}', t) + \rho(\boldsymbol{r}', t)}{|\boldsymbol{r} - \boldsymbol{r}'|^3}(\boldsymbol{r} - \boldsymbol{r}'). \quad (5)$$

This shows a high degree of non-locality and non-linearity, and in particular that the behaviour of both ρ_{DM} and ρ manifest at a distance irrespective of the dynamics of the intervening space. This non-local behaviour is analogous to that in quantum systems and may offer a resolution to the horizon problem.

3 Evidence for the α- and δ-dynamical terms

3.1 $\delta = 0$ – early studies of dynamical 3-Space

It has been shown that dynamical 3-space flows into matter [3]. External to a spherically symmetric matter density $\rho(r)$, (1) has a time-independent radial inflow solution $v(r) \sim 1/r^{\frac{1}{2}}$ leading to the matter inward acceleration $g(r) \sim 1/r^2$. This happens because the α- and δ-dynamical terms are identically zero for this inflow speed, and explains why these significant terms were missed by Newton in explaining Kepler's Planetary Laws. However, inside a spherically symmetric mass,

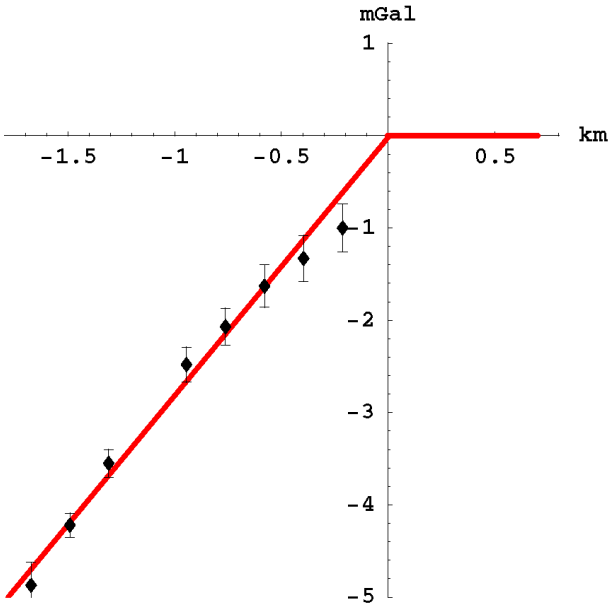

Fig. 1: The Greenland ice bore hole g anomaly data, giving $\alpha \approx 1/137$ from fitting the form in (6). The misfit at shallow depths arises from the ice not having reached the ice-shelf full density, which is a snow compactification effect. The Nevada rock bore hole data [23] also gives $\alpha \approx 1/137$. The bore hole anomaly is that gravity is stronger down a bore hole than predicted by Newtonian gravity.

*The α term in (1) has been changed by a factor of ten due to a numerical error found in the analysis of borehole data. All solutions are also altered by this factor.

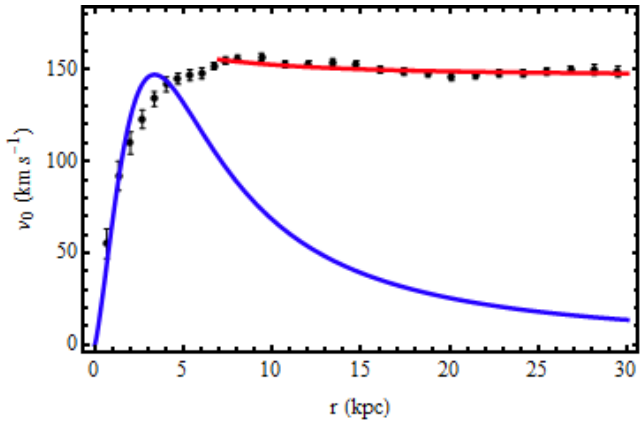

Fig. 2: The flat asymptotic star rotation speeds for the spiral galaxy NGC3198, with upper flat plot from the dynamical 3-space, while the lower form is from Newtonian gravity. The flat asymptotic form arises when $\alpha \neq 0$.

and in other circumstances, these terms play a significant dynamical role. Inside a spherically symmetric mass, such as the earth, Newtonian gravity and the new dynamics predict different matter accelerations,

$$\Delta g = g_{NG}(d) - g(d) = 20\pi\alpha G\rho d + O(\alpha^2) \qquad (6)$$

where $d < 0$ is the depth. The Greenland [1] (see Fig. 1) and Nevada bore hole data [23], reveal that $\alpha \approx 1/137$, the fine structure constant known from quantum theory. This suggests we are seeing a unification of gravity and the quantum theory.

In conventional theory black holes are required to have enormous quantities of actual in-fallen matter compressed into essentially a point-like region. Their $g \sim 1/r^2$ gravitational acceleration field is unable to explain flat spiral galaxy rotation curves, resulting in the invention of 'dark matter'. Dynamical 3-space theory however also predicts black holes in the absence of in-fallen matter, which produce a stronger acceleration field $g \sim 1/r$, as discussed below. They are spherically symmetric in-flows of space, with space not being conserved. In the absence of matter, $\rho = 0$, we set $(\boldsymbol{r}, t) = v(r)\hat{\boldsymbol{r}}$. Previous work considered solutions of (1) when $\delta = 0$, where the black hole solutions were found to have the form

$$v(r) = -\frac{\beta}{r^{\frac{5\alpha}{2}}} \qquad (7)$$

where β is an arbitrary parameter for the strength of the black hole. (1) also has straight-line filament solutions, with the form, when $\delta = 0$,

$$v(r) = -\frac{\mu}{r^{\frac{5\alpha}{4}}} \qquad (8)$$

where r is the perpendicular distance from the filament and μ is the arbitrary filament strength. The solutions (7) and (8) contain a singularity at $r = 0$ where the in-flow speed becomes infinite. Asymptotically, even when $\rho \neq 0$, these black hole solutions predict flat spiral galaxy rotation curves, for the inflow in (7) gives $g(r) = -5\alpha\beta^2/2r^{1+5\alpha} \sim -1/r$, giving the circular orbit speed $v_0(r) = (10\alpha\beta^2)^{1/2}/2r^{5\alpha/2}$, and illustrated in Fig. 2. This suggests that the 'dark matter' effect is caused by the α-dynamical term, a space self-interaction.

The Maxwell EM equations take account of the 3-space dynamics by making the change $\partial/\partial t \to \partial/\partial t + \boldsymbol{v}\cdot\nabla$. Then we obtain strong galactic light bending and lensing caused by the inflow speed in (7), or the solar light bending when $v \sim 1/r^{\frac{1}{2}}$. There are also recent direct experimental detections of the space flow velocity field by [5].

3.2 $\delta \neq 0$ – black holes and filaments

More recently the $\delta \neq 0$ scenario was considered. The form of (1) is expected as a semi-classical derivative expansion of an underlying quantum theory, where higher order derivatives are indicative of shorter length-scale physics. (1) when $\rho = 0$ has exact two-parameter, v_0 and $\kappa \geq 1$, black hole solutions

$$v(r)^2 = v_0^2(\kappa - 1)\frac{\delta}{r}\left(1 - {}_1F_1\left[-\frac{1}{2} + \frac{5\alpha}{2}, -\frac{1}{2}, -\frac{r^2}{\delta^2}\right]\right) - \\ - v_0^2\kappa\frac{8}{3}\frac{r^2}{\delta^2}\frac{\Gamma(\frac{3-5\alpha}{2})}{\Gamma(\frac{-5\alpha}{2})}\,{}_1F_1\left[1 + \frac{5\alpha}{2}, \frac{5}{2}, -\frac{r^2}{\delta^2}\right] \qquad (9)$$

where ${}_1F_1[a, b, w]$ is the confluent hypergeometric function. The parameters v_0 and κ set the strength and structure of the black hole, as discussed in [6]. (9) is a generalisation of (7), and for $r \gg \delta$ gives

$$v(r)^2 \approx A\frac{\delta}{r} + B\left(\frac{\delta}{r}\right)^{5\alpha} \qquad (10)$$

giving, from (2), $g(r) = GM(r)/r^2$, where $M(r)$ defines an "effective mass" contained within radius r, but which does not entail any actually matter,

$$M(r) = M_0 + M_0\left(\frac{r}{r_s}\right)^{1-5\alpha} \qquad (11)$$

and r_s is the distance where $M(r_s) = 2M_0$. This is shown in Fig. 3 for the Milky Way SgrA* black hole. At large r the in-flow speed becomes very slowly changing, thus predicting flat rotation curves given by [6]

$$v_{orb}(r)^2 = GM_0\left(\frac{r_s}{r}\right)^{5\alpha}\frac{1}{r_s}. \qquad (12)$$

Fig. 4 illustrates that for globular clusters and spherical galaxies the observational data implies the relationship $M_{BH} = \frac{\alpha}{2}M$. Again we see that the α-term dynamics appear to be the cause of this result, although this has yet to be derived from (1). Exact filament solutions for (1) also exist when $\delta \neq 0$, as a generalisation of (8):

$$v(r)^2 = v_0^2\frac{r^2}{\delta^2}\,{}_1F_1\left[1 + \frac{5\alpha}{4}, 2, -\frac{r^2}{2\delta^2}\right]. \qquad (13)$$

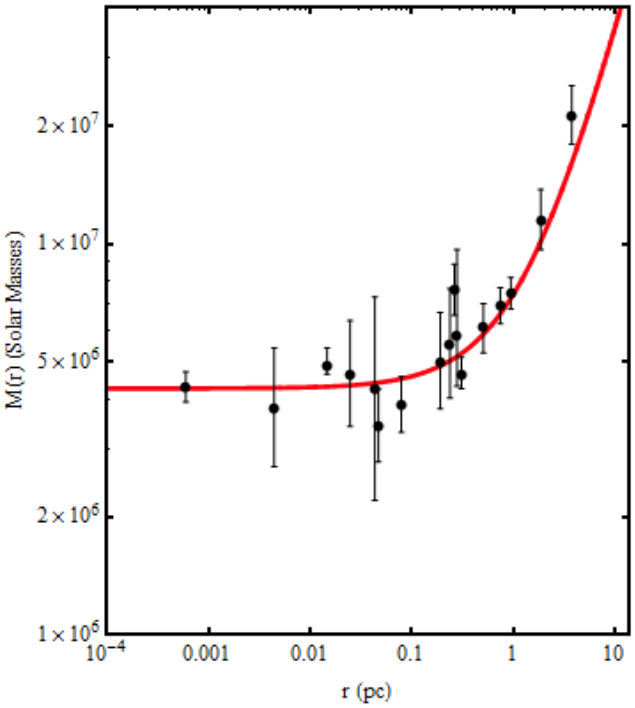

Fig. 3: Effective mass data $M(r)$ for the Milky Way SgrA* black hole, from star and gas cloud orbital data, showing the flat regime that mimics a point-like mass, but for which there is no actual matter contained within the black hole, and the linearly rising form beyond r_s =1.33pc, as predicted by (11), but which is usually attributed to a constant 'dark matter' density. This form is a direct consequence of the 3-space self-interactions in (1). The offset of the last two points indicate the presence of actual matter.

Here r is the distance perpendicular to the axis of the filament and $v(r)$ is the in-flow in that direction. The only known filament solution is for one that is infinitely long and straight. Both (9) and (13) are well behaved functions which converge to zero as $r \to 0$, i.e. the in-flow singularities are removed.

4 Expanding universe

(1) contains a time dependent expanding universe solution. Substituting the Hubble form $\boldsymbol{v}(\boldsymbol{r}, t) = H(t)\boldsymbol{r}$, and then $H(t) = \dot{a}/a$, where $a(t)$ is the universe scale factor and $\dot{a}(t) \equiv da(t)/dt$, we obtain

$$4a\ddot{a} + 10\alpha\dot{a}^2 = -\frac{16}{3}\pi G a^2 \rho \tag{14}$$

which is independent of δ. One of the key features in (14) is that even when $\rho = 0$, i.e. no matter, and $\alpha = 0$, $\ddot{a}(t) = 0$ and $a(t) = t/t_0$, and the universe is uniformly increasing in scale. Here $a(t_0) = 1$ and t_0 is the current age of the universe. This expansion of space is because the space itself is a dynamical system, and the (small) amount of actual baryonic matter merely slightly slows that expansion, as the matter dissipates space. Because of the small value of $\alpha = 1/137$, the α term only plays a significant role in extremely early epochs, but only if the space is completely homogeneous. In the limit $\rho \to 0$ we obtain the solution to (14)

$$\begin{aligned} a(t) &= \left(\frac{t}{t_0}\right)^{1/(1+5\alpha/2)} \\ H(t) &= \frac{1}{t(1+5\alpha/2)} \end{aligned} \tag{15}$$

which, as also reasoned by [17], predicts the emergence of a uniformly expanding universe after neglecting the α term. This allows a fit to the type 1a supernovae magnitude-redshift data (Fig. 5), as discussed in [7], and suggests that the dynamical 3-space theory also offers an explanation for the 'dark energy' effect. The ΛCDM parameters $\Omega_\Lambda = 0.73, \Omega_M = 0.27$, follow from either fitting to the supernovae data, or equally well, fitting to the uniformly expanding universe solution in (15) [7]. Via the dynamical 3-space solution the supernovae data gives an age for the universe of $t_0 = 13.7$ Gy.

5 Black hole – expanding universe

The Hubble solution (15) does not contain a free parameter, i.e. in the dynamical 3-space theory the universe necessarily expands, and hence it cannot be ignored when considering black holes and filaments. Since any radially flowing and time dependent $v(r, t)$ (i.e. containing both outflows and inflows) has spherical symmetry, (1) becomes, in the absence of matter

$$\begin{aligned} &\frac{\partial}{\partial t}\left(\frac{2v}{r} + v'\right) + vv'' + 2\frac{vv'}{r} + \\ &+ (v')^2 + \frac{5\alpha}{2}\left(\frac{v^2}{r^2} + \frac{2vv'}{r}\right) + \\ &+ \frac{\delta^2}{4r^4}\left(2v^2 + 2r^2(v')^2 + 6r^3v'v''\right) + \\ &+ \frac{\delta^2}{4r^4}\left(-4rvv' + 2r^2vv'' + 2r^3vv'''\right) = 0 \end{aligned} \tag{16}$$

where $v' \equiv \partial v/\partial r$. Now consider the black hole - expanding universe ansatz

$$\boldsymbol{v}(\boldsymbol{r}, t) = H(t)\boldsymbol{r} + w(r, t)\hat{\boldsymbol{r}} \tag{17}$$

where $w(r, t)$ is the spherically symmetric black hole inflow. After substituting this form we obtain a time dependent equation for $w(r, t)$. However by setting $w(r, t) = R(r)/t$ this time dependence is resolved, and (16) now may be solved for $R(r)$, implying that the Hubble outflow and black hole inflow are inseparable and compatible phenomena. Asymptotically, for $r \gg \delta$, the resulting equation for $R(r)$ has the solution

$$R(r) = -\frac{\nu}{r^{\frac{5\alpha}{2}}}, \quad \text{and so} \quad w(r, t) = -\frac{\nu}{r^{\frac{5\alpha}{2}}t} \tag{18}$$

which is the original black hole solution (7), but now with an inverse time dependence. (17) is for the black hole located at

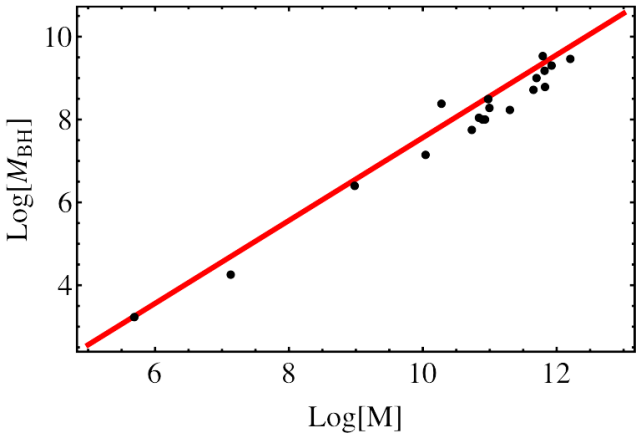

Fig. 4: Black hole masses M_{BH} vs mass M, in solar masses, for the globular clusters M15 and G1, and spherical galaxies [15]. The straight line is the relation $M_{BH} = \frac{\alpha}{2}M$, where α is the fine structure constant $\approx 1/137$. This demonstrates again the role of α in the dynamics of space and black holes.

$\boldsymbol{r} = \boldsymbol{0}$. For a black hole comoving with the local Hubble space flow the solution of (1) is

$$\boldsymbol{v}(\boldsymbol{r}, t) = H(t)\boldsymbol{r}' + w(r', t)\hat{\boldsymbol{r}}' \tag{19}$$

where $\boldsymbol{r}' = \boldsymbol{r} - a(t)\boldsymbol{r}_{BH}$ when the observer is at $\boldsymbol{r} = \boldsymbol{0}$, and the black hole is located at $a(t)\boldsymbol{r}_{BH}$. Macroscopic black holes are expected to form from coalescence of mini primordial black holes.

A consequence of (17) is that for any black hole there exists a critical radius r_c where the spatial inflow into the black hole is equal and opposite to the Hubble expansion (Fig. 6) so defining a sphere of influence. Test particles placed inside r_c are attracted to the black hole due to gravity, while those placed outside r_c, and at rest with respect to the local space, recede from it due to expansion. This critical radius is found to remain independent of time, i.e. r_c only depends on the black hole strength ν. r_c is expected to be sufficiently large that the black hole-star distance r in a galaxy today is negligible compared to r_c, i.e. $r \ll r_c$, therefore not affecting the size of the galaxies themselves. This effect would more likely be evident at a distance which galaxies are separated by, as suggested by the galaxy cluster data in [18]. For a Hubble constant $H_0 = 74$ km s^{-1} Mpc^{-1}, and using (12) for the in-flow speed, solving for $v_{orb}(r_c) = H_0 r_c$ for the Milky Way SgrA* black hole data (Fig. 3) yields $r_c = 1.6$ Mpc. For multiple black holes in the expanding space, (1) implies a more complex time evolution.

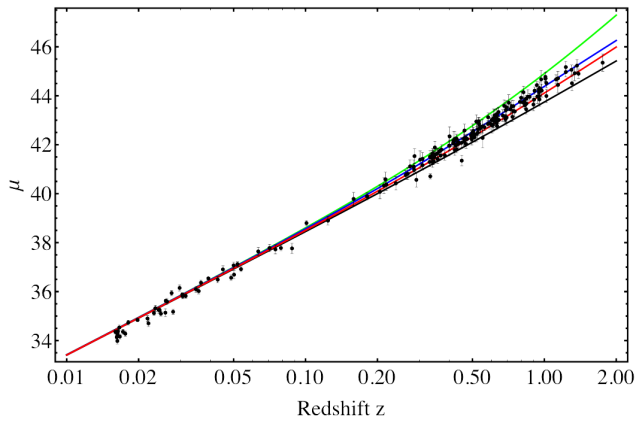

Fig. 5: Supernovae magnitude-redshift data. Upper curve (light blue) is 'dark energy' only $\Omega_\Lambda = 1$. Next curve (blue) is best fit of 'dark energy'-'dark-matter' $\Omega_\Lambda = 0.73$. Lowest curve (black) is 'dark matter' only $\Omega_\Lambda = 0$. Second lowest curve (red) is the uniformly expanding universe, and also predicted by dynamical 3-space (15).

6 Induced filaments and bubble networks

We have seen that the dynamical 3-space theory offers possible explanations for many phenomena, including that of an isolated black hole coexisting with the Hubble expansion. It also has filament solutions, in the absence of the Hubble expansion. However with multiple black holes a new feature appears to emerge, namely cosmic networks of black holes and induced filaments. First note that the black hole inflow speed in (10) is essentially very long range, resulting in the matter acceleration $g(r) \sim -1/r$, which is a key feature of these black holes, and may explain the "dark matter" effect. However this long range in-flow raises the question of how multiple black holes coexist when located within one another's sphere of influence? Fig. 7 shows the vector addition of the inflows for two black holes. This cannot be a solution of (1) as it is nonlinear and so does not have a superposition property. Whence this flow must evolve over time. Indeed the evolving flow

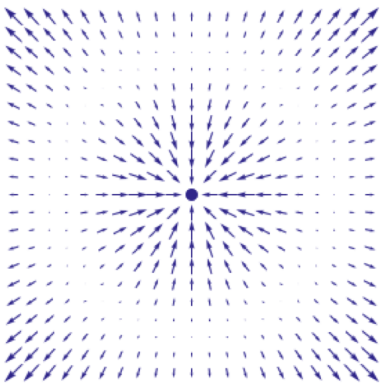

Fig. 6: Schematic 3-space velocity for an isolated black hole embedded in an expanding universe, see (17), showing radius at which flow reverses, defining the black holes sphere of influence.

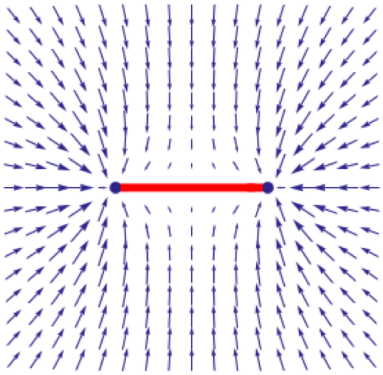

Fig. 7: 3-space in-flow velocity for two black holes located within their spheres of influence. Note the emergence of a filament forming between the black holes, indicative of a black-hole - filament network formation, see Fig. 8.

appears to form a filament connecting the two black holes. However even then there remains a long range inflow, which would lead to further filaments connecting black holes within their range of influence. These black holes are remnants of the early formation of space, and imply that (1) will undergo a dynamical breaking of symmetry, from an essentially homogeneous and isotropic 3-space, to a network of black holes and induced filaments. Note that the matter content of the universe is very small, and does not play a key role in this structure formation. A possible dynamically stable 3-space structure is shown in Fig. 8, which entails this network forming a bubble structure with the network defining a 'surface' for the bubbles. The stability of this is suggested by noting that the Hubble expansion within the interior of each bubble is now consistent with the inflow into the black holes and filaments, and so there is no longer a dynamical clash between the long range flows. Bubble structures like these are indeed found in the universe, where galaxies are observed to

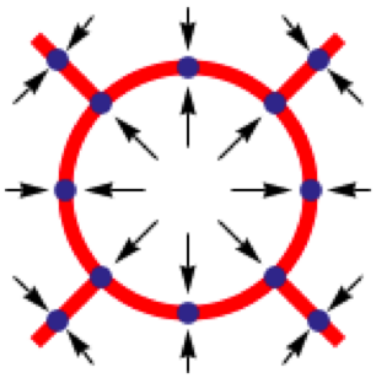

Fig. 8: 2D schematic section of a cosmic network of black holes and induced filaments. Vectors indicate 3-space flow, both within the bubble from the Hubble space expansion, and inwards to black holes (dots) and filaments (red lines). Only this bubble structure, shown here in cross-section, appears to be stable wrt the Hubble expansion.

be joined by filaments lying on spherical surfaces, filled with large voids [9, 21].

7 Conclusions

It is clear that instead of studying black-hole only cases, we need to model astrophysical and cosmological phenomena embedded in an expanding universe. The dynamical 3-space theory naturally forces us to do this, as there is no free parameter to switch off the emergent expanding universe solution, and so must be included. It has been shown that the long range black hole solutions found previously hold while embedded in an expanding universe. It is suggested that the time dependent nature of these new solutions explains in part the observed cosmic web. It appears that the dynamics of the 3-space, in the presence of primordial black holes, essentially defects in the space emerging from the quantum foam, renders a homogeneous and isotropic universe dynamically unstable, even without the presence of matter, resulting in a spatial bubble network. The long range $g \sim 1/r$ of both the black holes and induced filaments will cause matter to rapidly infall and concentrate around these spatial structures, resulting in the precocious formation of galaxies.

Submitted on July 1, 2013 / Accepted on July 6, 2013

References

1. Ander M. E. et al. *Phys. Rev. Lett.*, 1989, v. 62, 985.
2. Cahill R. T. Process physics: from information theory to quantum space and matter. Nova Science Publishers, New York, 2005.
3. Cahill R. T. Dynamical Fractal 3-Space and the Generalised Schrödinger Equation: Equivalence Principle and Vorticity Effects. *Progress in Physics*, 2006, v. 1, 27–34.
4. Cahill R. T. Dynamical 3-Space: Cosmic Filaments, Sheets and Voids. *Progress in Physics*, 2011, v. 2, 44–51.
5. Cahill R. T. Characterisation of Low Frequency Gravitational Waves from Dual RF Coaxial-Cable Detector: Fractal Textured Dynamical 3-Space. *Progress in Physics*, 2012, v. 3, 3–10.
6. Cahill R. T. and Kerrigan D. Dynamical Space: Supermassive Galactic Black Holes and Cosmic Filaments. *Progress in Physics*, 2011, v. 4, 50–64.
7. Cahill R. T., Rothall D. Discovery of Uniformly Expanding Universe. *Progress in Physics*, 2012, v. 4, 65–68.
8. Carr B. J. in Sanz J. L., Goicoechea L. J. (eds). Observational and Theoretical Aspects of Relativistic Astrophysics and Cosmology. World Scientific, Singapore, 1985.
9. De Lapparent V., Geller M. J., Huchra J. P. *ApJ*, 1986, v. 302, L1.
10. Einstein A., Straus E. G. *Rev. Mod. Phys.*, 1945, v. 17, 120.
11. Ghez A. M., Klein B. L., Morris M., Becklin E. E. *ApJ*, 1998, v. 509, 678.
12. Gibbons G. W., Maeda K. *Phys. Rev. Lett.*, 2010, v. 104, 131101.
13. Karachentsev D. et al. *A&A*, 2002, v. 383, 125.
14. Komatsu E. et al. *ApJS*, 2010, v. 192, 18.
15. Marconi A., Hunt L. K. *ApJL*, 2003, v. 589, L21.
16. McVittie G. C. *MNRAS*, 1933, v. 93, 325.
17. Melia F., Shevchuk A. S. H. *MNRAS*, 2012, v. 419, 2579.
18. Nandra R., Lasenby A. N., Hobson M. P. *MNRAS*, 2012, v. 422, 2945.

19. Perlmutter S., Aldering G., Goldhaber G., Knop R. A., Nugent P., Castro P. G., Deustua S., Fabbro S., Goobar A., Groom D. E., Hook I. M., Kim A. G., Kim M. Y., Lee J. C., Nunes N. J., Pain R., Pennypacker C. R., Quimby R., Lidman C., Ellis R. S., Irwin M., McMahon R. G., Ruiz-Lapuente P., Walton N., Schaefer B., Boyle B. J., Filippenko A. V., Matheson T., Fruchter A. S., Panagia N., Newberg H. J. M. and Couch W. J. Measurement of Ω and Λ from 42 High-Redshift Supernovae. *Astrophys.J.*, 1999, v. 517, 565–586.

20. Persic M., Salucci P., Stel F. *MNRAS*, 1996, v. 281, 27.

21. Ratcliffe A., Shanks T., Broadbent A., Parker Q. A., Watson F. G., Oates A. P., Fong R., Collins C. A. *MNRAS*, 1996, v. 281, L47

22. Riess A. G., Filippenko A. V., Challis P., Clocchiattia A., Diercks A., Garnavich P. M., Gilliland R. L., Hogan C. J., Jha S., Kirshne R. P., Leibundgut B., Phillips M. M., Reiss D., Schmidt B. P., Schommer R. A., Smith R. C., Spyromilio J., Stubbs C., Suntzeff N. B. and Tonry J. Observational Evidence from Supernovae for an Accelerating Universe and Cosmological Constant. *Astron.J.*, 1998, v. 116, 1009–1038.

23. Thomas J., Vogel P. *Phys. Rev. Lett.*, 1990, v. 65, 1173.

24. Vachaspati T. *Phys. Rev. Lett.*, 1986, v. 57, 1655.

Dilatation–Distortion Decomposition of the Ricci Tensor

Pierre A. Millette
E-mail: PierreAMillette@alumni.uottawa.ca, Ottawa, Canada

We apply a natural decomposition of tensor fields, in terms of dilatations and distortions, to the Ricci tensor. We show that this results in a separation of the field equations of General Relativity into a dilatation relation and a distortion relation. We evaluate these equations in the weak field approximation to show that the longitudinal dilatation mass relation leads to Poisson's equation for a newtonian gravitational potential, and that the transverse distortion wave relation leads to the linearized field equation of gravity in the Transverse Traceless gauge. The results obtained are in agreement with the Elastodynamics of the Spacetime Continuum.

1 Introduction

In a previous paper [1], we proposed a natural decomposition of spacetime continuum tensor fields, based on the continuum mechanical decomposition of tensors in terms of dilatations and distortions. In this paper, we apply this natural decomposition to the Ricci tensor $R^{\mu\nu}$ of General Relativity within the framework of the Elastodynamics of the Spacetime Continuum (*STCED*) [2].

2 Decomposition of the Ricci tensor

As shown in [1], the stress tensor $T^{\mu\nu}$ of General Relativity can be separated into a stress deviation tensor $t^{\mu\nu}$ and a scalar t_s according to

$$T^{\mu\nu} = t^{\mu\nu} + t_s\, g^{\mu\nu} \tag{1}$$

where

$$t^{\mu}{}_{\nu} = T^{\mu}{}_{\nu} - t_s\, \delta^{\mu}{}_{\nu} \tag{2}$$

$$t_s = \frac{1}{4}\, T^{\alpha}{}_{\alpha} = \frac{1}{4}\, T. \tag{3}$$

The Ricci curvature tensor $R^{\mu\nu}$ can also be separated into a curvature deviation tensor $r^{\mu\nu}$ (corresponding to a distortion) and a scalar r_s (corresponding to a dilatation) according to

$$R^{\mu\nu} = r^{\mu\nu} + r_s\, g^{\mu\nu} \tag{4}$$

where similarly

$$r^{\mu}{}_{\nu} = R^{\mu}{}_{\nu} - r_s\, \delta^{\mu}{}_{\nu} \tag{5}$$

$$r_s = \frac{1}{4}\, R^{\alpha}{}_{\alpha} = \frac{1}{4}\, R \tag{6}$$

where R is the contracted Ricci curvature tensor.

Using (1) to (6) into the field equations of General Relativity [3, see p. 72],

$$R^{\mu\nu} - \frac{1}{2}\, g^{\mu\nu} R = -\kappa T^{\mu\nu} \tag{7}$$

where $\kappa = 8\pi G/c^4$ and G is the gravitational constant, we obtain a separation of the field equations of General Relativity into dilatation and distortion relations respectively:

$$\begin{aligned} &\text{dilatation} : r_s = -\kappa t_s \\ &\text{distortion} : r^{\mu\nu} = \kappa t^{\mu\nu}. \end{aligned} \tag{8}$$

The dilatation relation of (8) can also be expressed as

$$R = -\kappa T. \tag{9}$$

The distortion-dilatation separation of tensor fields is thus also applicable to the field equations of General Relativity, resulting in separated dilatation and distortion relations. This result follows from the geometry of the spacetime continuum (*STC*) used in General Relativity being generated by the combination of all deformations present in the *STC* [2].

3 Weak field approximation

We evaluate these separated field equations (8) in the weak field approximation to show that these relations satisfy the massive longitudinal dilatation and massless transverse distortion results of *STCED* [2].

In the weak field approximation [4, see pp. 435–441], the metric tensor $g_{\mu\nu}$ is written as $g_{\mu\nu} = \eta_{\mu\nu} + h_{\mu\nu}$ where $\eta_{\mu\nu}$ is the flat spacetime diagonal metric with signature $(-\ +\ +\ +)$ and $|h_{\mu\nu}| \ll 1$. The connection coefficients are then given by

$$\Gamma^{\mu}{}_{\alpha\beta} = \frac{1}{2}\eta^{\mu\nu}(h_{\alpha\nu,\beta} + h_{\beta\nu,\alpha} - h_{\alpha\beta,\nu}) \tag{10}$$

or, after raising the indices,

$$\Gamma^{\mu}{}_{\alpha\beta} = \frac{1}{2}(h_{\alpha}{}^{\mu}{}_{,\beta} + h_{\beta}{}^{\mu}{}_{,\alpha} - h_{\alpha\beta}{}^{,\mu}). \tag{11}$$

The Ricci tensor is also linearized to give

$$R_{\mu\nu} = \Gamma^{\alpha}{}_{\mu\nu,\alpha} - \Gamma^{\alpha}{}_{\mu\alpha,\nu} \tag{12}$$

which becomes

$$R_{\mu\nu} = \frac{1}{2}(h_{\mu}{}^{\alpha}{}_{,\nu\alpha} + h_{\nu}{}^{\alpha}{}_{,\mu\alpha} - h_{\mu\nu,\alpha}{}^{\alpha} - h^{\alpha}{}_{\alpha,\mu\nu}). \tag{13}$$

The contracted Ricci tensor

$$R = g^{\mu\nu} R_{\mu\nu} \simeq \eta^{\mu\nu} R_{\mu\nu} \tag{14}$$

then becomes

$$R = \frac{1}{2}\eta^{\mu\nu}(h_{\mu}{}^{\alpha}{}_{,\nu\alpha} + h_{\nu}{}^{\alpha}{}_{,\mu\alpha} - h_{\mu\nu,\alpha}{}^{\alpha} - h^{\alpha}{}_{\alpha,\mu\nu}) \tag{15}$$

which, after raising the indices and re-arranging the dummy indices, simplifies to

$$R = h^{\alpha\beta}{}_{,\alpha\beta} - h^{\alpha}{}_{\alpha,\beta}{}^{\beta}. \tag{16}$$

4 Dilatation (mass) relation

Making use of (16) and (6) into the dilatation relation (9), we obtain the *longitudinal dilatation mass relation*

$$h^{\alpha}{}_{\alpha,\beta}{}^{\beta} - h^{\alpha\beta}{}_{,\alpha\beta} = \kappa T \tag{17}$$

and, substituting for κ from (7) and $T = \rho c^2$ from (30) of [2],

$$\nabla^2 h^{\alpha}{}_{\alpha} - \partial_\alpha \partial_\beta h^{\alpha\beta} = \frac{8\pi G}{c^2}\rho \tag{18}$$

where ρ is the rest-mass density. This equation is shown to lead to Poisson's equation for a newtonian gravitational potential in the next section.

The second term of (18) would typically be set equal to zero using a gauge condition analogous to the Lorentz gauge [4, see p. 438]. However, the second term is a divergence term, and it should not be set equal to zero in the general case where sources may be present.

4.1 Static newtonian gravitational field

We consider the metric perturbation [4, see pp. 412–416]

$$\begin{aligned} h_{00} &= -2\Phi/c^2 \\ h_{ii} &= 0, \quad \text{for } i = 1, 2, 3 \end{aligned} \tag{19}$$

where Φ is a static (i.e. time independent) newtonian gravitational field. Then the term

$$h^{\alpha\beta}{}_{,\alpha\beta} = h^{00}{}_{,00} = 0 \tag{20}$$

and (17) becomes

$$\nabla^2 h^{0}{}_{0} = \kappa T. \tag{21}$$

Using h_{00} from (19) and κ from (7), (21) becomes

$$\nabla^2 \Phi = \frac{4\pi G}{c^2} T. \tag{22}$$

Substituting for $T = \rho c^2$ from (30) of [2], we obtain

$$\nabla^2 \Phi = 4\pi G \rho \tag{23}$$

where ρ is the mass density. This equation is Poisson's equation for a newtonian gravitational potential.

5 Distortion (wave) relation

Combining (13) and (16) with (5) and (6) into the distortion relation of (8), we obtain the *transverse distortion wave relation*

$$\begin{aligned} &\frac{1}{2}\left(h_{\mu\alpha,\nu}{}^{\alpha} + h_{\nu\alpha,\mu}{}^{\alpha} - h_{\mu\nu,\alpha}{}^{\alpha} - h^{\alpha}{}_{\alpha,\mu\nu}\right) - \\ &-\frac{1}{4}\eta_{\mu\nu}\left(h^{\alpha\beta}{}_{,\alpha\beta} - h^{\alpha}{}_{\alpha,\beta}{}^{\beta}\right) = \kappa t_{\mu\nu} \end{aligned} \tag{24}$$

where $t_{\mu\nu}$ is obtained from (2) and (3). This equation can be shown to be equivalent to the equation derived by Misner *et al* [4, see their Eq.(18.5)] from which they derive their linearized field equation and transverse wave equation in the Transverse Traceless gauge [4, see pp. 946–950]. This shows that this equation of the linearized theory of gravity corresponds to a transverse wave equation.

This result highlights the importance of carefully selecting the gauge transformation used to simplify calculations. For example, the use of the Transverse Traceless gauge eliminates massive solutions which, as shown above and in [2], are longitudinal in nature, while yielding only non-massive (transverse) solutions for which the trace equals zero.

6 Discussion and conclusion

In this paper, we have applied a natural decomposition of tensor fields, in terms of dilatations and distortions, to the Ricci tensor. We have shown that this results in a separation of the field equations of General Relativity into a dilatation relation and a distortion relation. We have evaluated these equations in the weak field approximation to show that the longitudinal dilatation mass relation leads to Poisson's equation for a newtonian gravitational potential, and that the transverse distortion wave relation leads to the linearized field equation of gravity in the Transverse Traceless gauge. The results obtained are thus found to be in accord with the Elastodynamics of the Spacetime Continuum.

Acknowledgements

The author thanks Dr. Dmitri Rabounski for his editorial support of the *STCED* research.

Submitted on July 2, 2013 / Accepted on July 5, 2013

References

1. Millette P. A. On the Decomposition of the Spacetime Metric Tensor and of Tensor Fields in Strained Spacetime. *Progress in Physics*, 2012, v. 4, 5–8.
2. Millette P. A. Elastodynamics of the Spacetime Continuum. *The Abraham Zelmanov Journal*, 2012, v. 5, 221–277.
3. Wald R. M. General Relativity. The University of Chicago Press, Chicago, 1984.
4. Misner C. W., Thorne K. S., Wheeler J. A. Gravitation. W. H. Freeman and Co., San Francisco, 1973.

The Dark Side Revealed: A Complete Relativity Theory Predicts the Content of the Universe

Ramzi Suleiman

University of Haifa, Haifa 31509, Israel. E-mail: suleiman@psy.haifa.ac.il

Dark energy and dark matter constitute about 95% of the Universe. Nonetheless, not much is known about them. Existing theories, including General Relativity, fail to provide plausible definitions of the two entities, or to predict their amounts in the Universe. The present paper proposes a new special relativity theory, called *Complete Relativity theory (CR)* that is anchored in Galileo's relativity, but without the notion of a preferred frame. The theory results are consistent with Newtonian and Quantum mechanics. More importantly, the theory yields natural definitions of dark energy and dark matter and predicts the content of the Universe with high accuracy.

1 Introduction

1.1 Dark energy

The nature of dark energy ranks among the very most compelling of all outstanding problems in physical science [1, 2]. Conclusive evidence from supernovas and other observations show that, despite gravitation, the Universe is expanding with acceleration [3–6]. No existing theory is capable of explaining what dark energy is, but it is widely believed that it is some unknown substance with an enormous antigravitational force, which drives the galaxies of our Universe apart. It is also well established that at our time the Universe is comprised of $\approx 4.6\%$ atoms, $\approx 72\%$ dark energy and $\approx 23\%$ dark matter (see e.g., [1]). One explanation for dark energy is founded on Einstein's Cosmological Constant (λ), despite the fact that Einstein himself abandoned his constant, calling it his biggest mistake. According to this explanation the Universe is permeated by an energy density, constant in time and uniform in space. The big problem with this explanation is that for $\lambda \neq 0$ it requires that the magnitude of λ be $\approx 10^{120}$ (!) times the measured ratio of pressure to energy density [1].

An alternative explanation argues that dark energy is an unknown dynamical fluid, i.e., one with a state equation that is dynamic in time. This type of explanation is represented by theories and models which differ in their assumptions regarding the nature of the state equation dynamics [7–9]. This explanation is no less problematic since it entails the prediction of new particles with masses thirty-five orders of magnitude smaller than the electron mass, which might imply the existence of new forces in addition to gravity and electromagnetism [1]. At present there is no persuasive theoretical explanation for the existence, dynamics and magnitude of dark energy and its resulting acceleration of the Universe.

1.2 Dark matter

Dark matter is more of an enigma than dark energy. Scientists are more certain about what dark matter is not, than about what it is. Some contend that it could be Baryonic matter tied up in brown dwarfs or in chunks of massive compact halo objects "or MACHOs" [10, 11], but the common prejudice is that dark matter is not baryonic, and that it is comprised of particles that are not part of the "standard model" of particle physics. Candidates that were considered include very light axions and Weakly Interacting Massive Particles (WIMPs) which are believed to constitute a major fraction of the Universe's dark matter [2, 12–14].

Given the frustrating lack of knowledge about the nature of dark energy and dark matter, most experts contend that understanding the content of the Universe and its cosmic acceleration requires nothing less than "discovering a new physics" [14]. As example, the Dark Energy Task Force (DETF), summarized its 2006 comprehensive report on dark energy by stating that there is consensus among most physicists that "nothing short of a revolution in our understanding of fundamental physics will be required to achieve a full understanding of the cosmic acceleration" [1, see p. 6]. This statement includes the possibility of reconsidering Einstein's Special and General Relativity altogether.

The present paper meets the challenge by proposing a new relativity theory. The proposed theory, *which I term Complete Relativity Theory (or CR)*, is anchored in Galileo's relativity, but without the notion of a preferred frame. Alternatively, the theory could be seen as a generalization of the Doppler Formula [15, 16] to account for the relative dynamics of moving objects of mass. The theory's results are consistent with Newtonian mechanics and with Quantum mechanics. More importantly, the theory yields relativistic definitions of dark energy and dark matter, describes their dynamics and predicts the content of the Universe with impressive accuracy.

The following sections describe the theory for the special case of zero forces, resulting in constant relative velocities. I derive its time, distance, density, and energy transformations (sections 2.1–2.3) and compare the derived energy-term with Newton's and Einstein's *Special Relativity* terms. Section 3, which constitutes the core of this paper, puts forward a relativistic definition of dark energy and dark matter, describes

their dynamics as function of the relative velocity $\beta = \mathrm{v}/\mathrm{c}$, and calculates the present content of the Universe. Section 4 concludes with a brief discussion.

2 Complete Relativity (*CR*) theory postulates and transformations

CR theory rests on two postulates:

1. The magnitudes of ***all*** physical entities, as measured by an observer, depend on the relative motion of the observer with respect to the rest frame of the measured entities.
2. All translations of information from one frame of reference to another are carried by light or electromagnetic waves of equal velocity.

Note that postulate 1 applies to all measured entities, including the velocity of light. Thus, *CR* treats the velocity of light as a relativistic quantity and not as an invariant one as postulated by Einstein's *SR*.

2.1 Time transformation

The derivation of the time transformation of *CR* is similar to the derivation of the Doppler Formula, except that *CR* treats the relative time of a moving object with constant velocity, instead of the frequency of a traveling wave.

Consider the two frames of reference F and F' shown in Figure 1. Assume that the two frames are moving away from each other at a constant velocity v. Assume further that at time t_1 in F (and t'_1 in F') a body starts moving in the $+x$ direction from point x_1 (x'_1 in F') to point x_2 (x'_2 in F'), and that its arrival is signaled by a light pulse, which emits exactly when the body arrives at its destination. Denote the times of arrivals in F and F' by t_2 and t'_2, respectively. Finally, assume that the start times in F and F' are synchronized. Without loss of generality, we can set $t_1 = t' = 0$ and $x_1 = x'_1 = 0$.

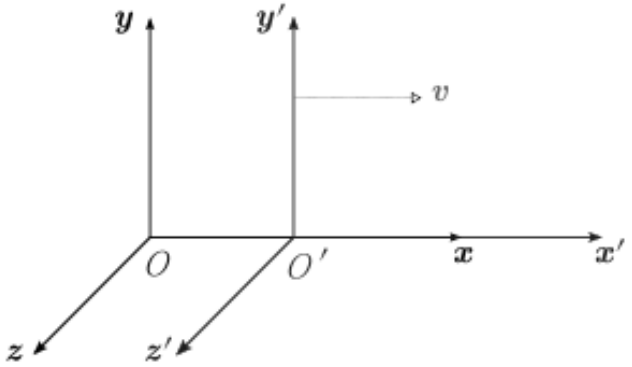

Fig. 1: Two observers in two reference frames moving with velocity v with respect to each other

The end time t_2, measured in F, equals the end time t'_2 plus the time δt which takes the light beam signaling the body's arrival at x_2 to reach the observer in F, or: $t_2 = t'_2 + \delta t$. But $\delta t = d/c$ where d is the distance (measured in F) travelled by F' relative to F, and ***c* is the velocity of light as measured in *F***. But $d = vt_2$, thus we can write:

$$t_2 = t'_2 + \frac{vt_2}{c} = t'_2 + \beta t_2 \,, \tag{1}$$

where $\beta = \frac{v}{c}$. Defining $t_2 = t$, $t_2 = t'$ and $\hat{t} = t/t'$, we get:

$$\hat{t} = \frac{t}{t'} = \frac{1}{1-\beta} \,. \tag{2}$$

Equation (2) is identical to the Doppler Formula, except that the Doppler Effect describes red- and blue-shifts of waves propagating from a departing or approaching wave source, whereas the result above describes the time transformation of moving objects. Note that $1/(1-\beta)$ is *positive* if F and F' *depart* from each other, and *negative* if they *approach* each other.

For the *round trip* from F and back, synchronization of the start time is not required. For this case the total relative time is given by (See Appendix, section1):

$$\hat{t} = \frac{t}{t'} = \frac{2}{1-\beta^2} \,. \tag{3}$$

For the one-way trip and a *departing* F' at velocity β ($0 \leqslant \beta \leqslant 1$), the proposed theory (*CR*) and Einstein's Special Relativity (*SR*) yield similar predictions, although the time dilation predicted by *CR* is larger than that predicted by *SR* (see Fig. 1Aa in the Appendix). Conversely, for an *approaching* F' ($\beta < 0$), *CR* predicts that the internal time measured at F will be *shorter* than that measured at F'. For the round trip the results of *CR* and *SR* (in $-1 \leqslant \beta \leqslant 1$) are qualitatively similar, except that the time dilation predicted by *CR* is larger than that predicted by *SR* (see Fig. 1Ab in the Appendix). For small β values the two theories yield almost identical results.

Note that the assumption that information is translated by light should not be considered a limitation of the theory, since its results are directly applicable to physical systems which use different transporters of information between two reference frames.

2.2 Distance transformation

The time duration, in frame F, of the event described above is equal to:

$$t_2 = \frac{x_2 - x_1}{c} = \frac{x_2}{c} \,, \tag{4}$$

where c is the velocity of light as measured in F. Similarly, the time duration of the event in F' could be written as:

$$t'_2 = \frac{x'_2 - x'_1}{c'} = \frac{x'_2}{c'} \,, \tag{5}$$

where c' is the velocity of light as measured in F'. From equations (4) and (5) we obtain:

$$\frac{x_2}{x'_2} = \frac{c'}{c}\frac{t_2}{t'_2} = \frac{c+v}{c}\frac{t_2}{t'_2} = \left(1 + \frac{v}{c}\right)\frac{t_2}{t'_2} = (1+\beta)\frac{t_2}{t'_2} \,. \tag{6}$$

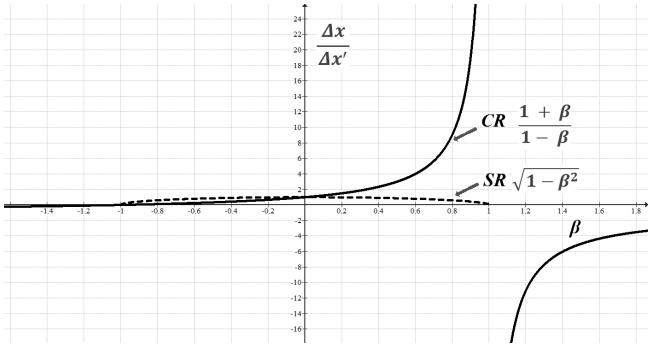

Fig. 2: Distance transformation.

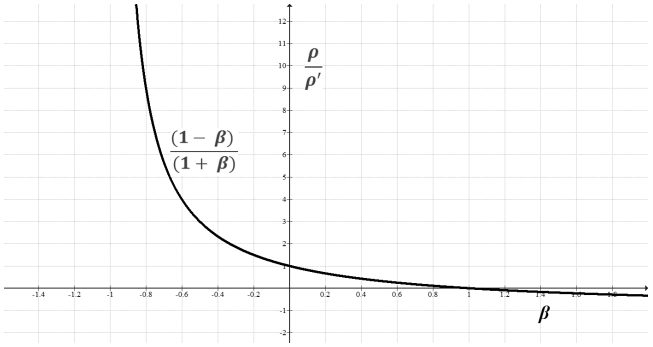

Fig. 3a: Density.

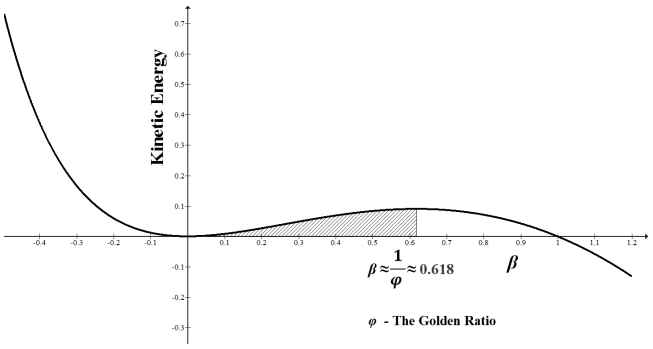

Fig. 3b: Energy.

Fig. 3: Density and energy as functions of velocity.

Substituting t_2/t_2' from (2) in (6) and denoting $x_2 = x$, $x_2' = x'$ and $\hat{x} = x_2/x_2'$ we get:

$$\hat{x} = \frac{x_2}{x_2'} = \frac{1+\beta}{1-\beta}. \tag{7}$$

The relative distance $\hat{x} = \Delta x \,/\, \Delta x' = (x_2 - x_1) \,/\, (x_2' - x_1')$ as a function of β, together with the respective relative distance according to *SR* (in dashed black) are shown in Figure 2. As shown by the figure, while *SR* prescribes that irrespective of direction, objects moving relative to an internal frame will contract, *CR* predicts that a moving object will contract or expand, depending on whether it approaches the internal frame or departs from it. For relative velocities exceeding the velocity of light ($\beta > 1$), *CR* predicts that $\hat{x}$ will become negative. Since $\Delta x'$ is positive, this implies that for bodies departing from an internal frame with a velocity higher than the velocity of light, the length of a rod of rest-length l_0, placed along the x axis, will be negative.

2.3 Density and energy transformations

Similar analyses for the density and kinetic energy (see Appendix, section 2) yield the following transformations:

Density:

$$\hat{\rho} = \frac{\rho}{\rho'} = \frac{(1-\beta)}{(1+\beta)} \tag{8}$$

and energy:

$$E = \frac{1}{2} m_0 c^2 \beta^2 \frac{(1-\beta)}{(1+\beta)}, \tag{9}$$

where m_0 is the rest mass in F'. Note that for $\beta \to 0$ (or $v \ll c$) *CR* reduces to Newton's mechanics ($\hat{t} = \hat{x} = \hat{\rho} = 1$, $E = \frac{1}{2} m v^2$). Figures 3 (a & b) depict the density and energy as functions of the velocity β. As shown by the figure the density of departing bodies relative to an observer in F is predicted to *decrease* with β, reaching zero for velocity equaling the speed of light. For bodies approaching the observer ($\beta < 1$) *CR*, similar to *SR*, predicts that the relative density will increase nonlinearly, from $\rho = \rho' = \rho_0$ at $\beta = 0$, to infinitely high values as β approaches -1. For $\beta < -1$ and $\beta > 1$, *CR* predicts that the relative density, as measured in F, will be negative.

The kinetic energy displays a non-monotonic behavior with two maxima: one at negative β values (approaching bodies) and the other at positive β values (departing bodies). The points of maxima (see Appendix, section 2) are $\beta_1 = \varphi - 1 \approx \approx 0.618$, and $\beta_2 = -\varphi \approx -1.618$, where φ is the Golden Ratio defined as $\varphi = \frac{\sqrt{5}+1}{2} \approx 1.618$ (see derivation in Appendix, section 2). The predicted decline in kinetic energy at velocities above $\beta \approx 0.618$ (see Fig. 3b), despite the decrease in velocity, suggests that mass and energy transform gradually from normal mass and energy to unobservable (dark) mass and energy.

The maximal kinetic energy at $\beta \approx 0.618$ is equal to:

$$\begin{aligned} E_{max} &= \frac{1}{2} m_0 c^2 (\varphi - 1)^2 \frac{1 - (\varphi - 1)}{1 + (\varphi - 1)} = \\ &= \frac{1}{2} m_0 c^2 (\varphi - 1)^2 \frac{(2 - \varphi)}{\varphi}. \end{aligned} \tag{10}$$

Since $\varphi - 1 = \frac{1}{\varphi}$ (See Appendix, section 2), Eq. 10 could be rewritten as:

$$E_{max} = \frac{1}{2} m_0 c^2 \frac{(2-\varphi)}{\varphi^3}. \tag{11}$$

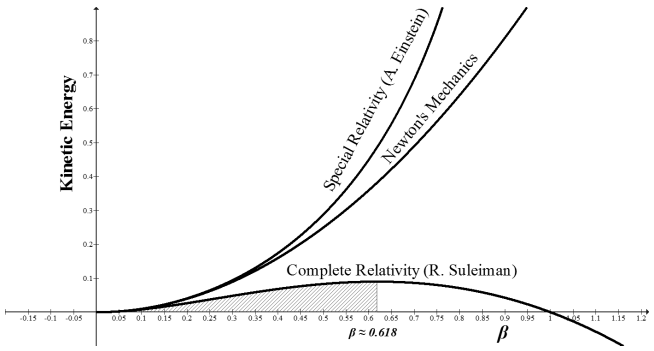

Fig. 4: Energy as a function of velocity according to three theories.

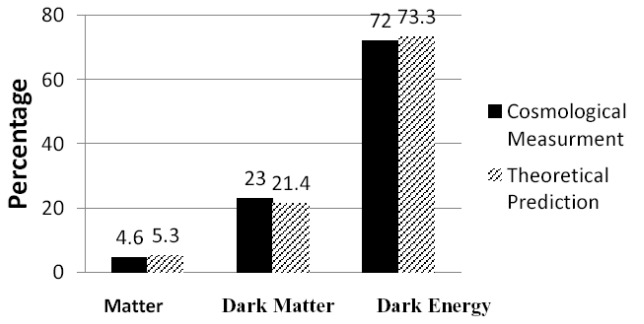

Fig. 5: Comparison between *CR*'s prediction of the content of the Universe and cosmological measurements

Substituting $\varphi = \frac{\sqrt{5}+1}{2}$ we obtain:

$$E_{max} \approx 0.04508497 m_0 c^2. \quad (12)$$

Notably, the energy-mass equivalent according to Eq. 12 is only $\approx 4.51\%$ of the amount predicted by the Einstein's famous equation $E = mc^2$. The above result is consistent with cosmological findings indicating that the percentage of Baryonic matter in the Universe is $\approx 4.6\%$. No less important the mass/energy conversion ratio (≈ 0.04508497) is precisely half of L. Hardy's probability of entanglement (0.09016994) [17–19]. This result confirms with a recent experimental finding [20], which demonstrated that applying a magnetic field at right angles to an aligned chain of cobalt niobate atoms, makes the cobalt enter a quantum critical state, in which the ratio between the frequencies of the first two notes of the resonance equals the Golden Ratio; the highest-order *E8* symmetry group discovered in mathematics [21].

For positive β values (departing objects) Figure 4 depicts *CR*'s energy function $E(\beta)$ together with the energy terms of Newton and Einstein's Special Relativity. As could be seen, while the latter theories predict that energy is strictly increasing with velocity, *CR* predicts a non-monotonic relationship with a maximum at $\beta \approx 0.618$ (the Golden ratio). As I shall show in the following section, this non-monotonic nature holds the key for explaining dark matter and dark energy.

3 The content of the Universe

The energy function Eq. 9 suggests that dark energy at a given velocity could be interpreted as the *difference between the energy measured at the internal frame and the energy measured at the external frame*. In other words, ***dark energy is defined as the energy loss due to relativity***. In formal terms, denote the energy at the internal and external frames by E' and E respectively, the kinetic energy measured at the internal and external frames could be expressed as: $E(\beta) = \frac{1}{2} m_0 c^2 \beta^2$ and $E'(\beta) = \frac{1}{2} m_0 c^2 \beta^2 \frac{(1-\beta)}{(1+\beta)}$, respectively, and the amount of dark energy, $DE(\beta)$, could be expressed as:

$$DE(\beta) = E'(\beta) - E(\beta) = \\ = \frac{1}{2} m_0 c^2 \beta^2 \left(1 - \frac{1-\beta}{1+\beta}\right) = m_0 c^2 \frac{\beta^3}{1+\beta}. \quad (13)$$

Similarly, ***dark matter, $m\_(\beta)$, at a given velocity is defined as the relativistic loss of matter at that velocity***. In other words, it equals the difference between the mass of normal matter measured at the internal and external frames. In formal notation: $m\_(\beta) = m_0 - m(\beta)$. Using the density transformation (Eq. 13), dark matter, $m(\beta)$, could be expressed as:

$$m\_(\beta) = m_0 - m(\beta) = m_0 \left(1 - \frac{1-\beta}{1+\beta}\right) = m_0 \left(\frac{2\beta}{1+\beta}\right). \quad (14)$$

The standard cosmological model of the Universe prescribes that it is comprised mainly of dark energy and dark matter (around 72% and 23%, respectively), with only less than 5% normal (Baryonic) matter. To compare matter with energy I use the matter-energy equivalence depicted in Eq. 12, according to which every unit of mass is equivalent to $\approx 0.045\, c^2$ energy units. Figure 5 depicts the dynamics of normal matter, dark matter, and dark energy as functions of β in the range $0 \leqslant \beta \leqslant 1$. Calculating the percentage of each component at $\beta = \varphi - 1 \approx 0.618$, or equivalently at redshift $z \approx 0.382$ (see Appendix, section 3) (yields $\approx 5.3\%$ Baryonic matter, $\approx 21.4\%$ dark matter, and $\approx 73.3\%$ dark energy, which is in excellent fit with current cosmological observations (See Fig. 6).

Statistical comparisons between the empirical and theoretical distributions of matter, dark matter, and dark energy, show that the difference is not significant ($p > 0.699$, Kolmogorov-Smirnov test). For velocities higher than $\beta = \frac{v}{c} \approx 0.618$ we get slightly different compositions. For example, for $\beta = 0.9$ (redshift $z \approx 0.474$) we get $\approx 89.4\%$ dark energy, $\approx 10\%$ dark matter and $\approx 0.6\%$ Baryonic matter. The average proportions in the range $0 \leqslant \beta \leqslant 1$ are about 85.80% dark energy, 12.35% dark matter and 1.85% Baryonic matter.

4 Concluding remarks

The biggest challenge of standard cosmology nowadays is to find a natural and more fundamental way to explain the detected presence of dark energy and dark matter. Most physicists agree that if this challenge is not met in the near future, then nothing less than "discovering a new physics" [14] and "a revolution in our understanding of fundamental physics" [2] will be required.

The present paper responds to the challenge by proposing a new relativity theory that is based on Galileo's relativity, but without the notion of a preferred frame. The analyses reveal that for low velocities the theory confirms with Newtonian mechanics and for high velocities it confirms with main predictions of quantum mechanics. More important for the present context, the proposed theory puts forward, for the first time, plausible definitions of dark matter and dark energy. The two entities are defined simply as the unobserved (dark) side of the matter-energy in the Universe. This definition yields formal expressions for the two entities which enable to predict the present content of the Universe with high accuracy. Two additional important results emerge from the analysis, each deserving a comprehensive treatment, are mentioned here very briefly:

1. For *departing* objects relative to the laboratory the mass-energy equivalence derived by the theory, is found to be $0.04508497 m_0 c^2$, which is exactly half Hardy's quantum coupling constant
2. The theory suggests a novel perspective of quantum phenomena, according to which the observed wave property of matter at high energies could be interpreted as a gradual transition of normal matter and normal energy to dark matter and dark energy. Such interpretation enables a long sought-after unification between Quantum Theory, and Newtonian mechanics, without leaving 95% of the Universe completely in the dark side of our knowledge.

References

1. Albrecht A. et al. Report of the Dark Energy Task Force. *Astro. Ph.*, 2006, 0609591.
2. Turner M. S. Dark matter: Theoretical perspectives. *PNAS*, 1993, v. 90, 4827–4834.
3. Riess A. G. et al. Observational evidence from supernovae for an accelerating Universe and a cosmological constant. *Astr. J.*, 1998, v. 116, 1009–1038.
4. Perlmutter S. et al. Discovery of a supernova explosion at half the age of the Universe. *Nature*, 1998, v. 391, 51–54.
5. Riess A. G. et al. The farthest known supernova: Support for an accelerating Universe and a glimpse of the epoch of deceleration. *Ap. J.*, 2001, v. 560 (1), 49–71.
6. Linder E. V. Exploring the expansion history of the Universe. *Phys. Rev. Lett.*, 2003, v. 90, 9 [4 pages].
7. Linder E. V. Probing gravitation, dark energy, and acceleration. *Phys. Rev. D*, 2004, v. 70 (2), 023511 [11 pages].
8. Sandvik H. B., Barrow J. D., Magueijo J. A Simple Cosmology with a Varying Fine Structure Constant. *Phys. Rev. Lett.*, 2002, v. 88, 031302 [4 pages].
9. Easson D. A. Framptona P. H., Smoota G. F. Entropic Accelerating Universe. *Physics Letters B*, 2011, v. 696 (3), 273–277.
10. Alcock C. EROS and MACHO combined limits on planetary-mass dark matter in the galactic halo. *The Astrophysical Journal*, 1998, v. 499, 9–12.
11. Alcock C. MACHO project limits on black hole dark matter in the 1-30 solar mass range. *The Astrophysical Journal Letters*, 2001, v. 550 (2), 169–172.
12. Steigman G., Turner M. S. Cosmological constraints on the properties of weakly interacting massive particles. *Nuclear Physics B*, 1985, v. 253, 375–386.
13. Sivertsson S., Gondolo P. The WIMP capture process for dark stars in the early Universe. *Astrophys. J.*, 2011, v. 729, 51 [11pages].
14. Aprile E. et al. Dark Matter Results from 100 Live Days of XENON100 Data. *Phys. Rev. Lett.*, 2011, v. 107, 131302 [6 pages].
15. O'Connor J. J., Roberston E. F. Christian Andreas Doppler- MacTutor History of Mathematics archive. University of St. Andrews, 1998.
16. Maulik D. Doppler Ultrasound in Obstetrics and Gynecology. Springer-Verlag, 2005.
17. Hardy L. Quantum mechanics, local realistic theories and Lorentz-invariant realistic theories. *Phys. Rev Lett.*, 1992, v. 68, 2981–2984.
18. Hardy L. Nonlocality of a single photon revisited. *Phys. Rev. Lett.*, 1994, v. 73, 2279–2283.
19. Penrose E. The Road to Reality. Jonathan Cape, London, 2004.
20. Coldea R., Tennant D. A., Wheeler E. M., Wawrzynska E., Prabhakaran D., Telling M., Habicht K., Smeibidl P., Kiefer K. Quantum criticality in an Ising chain: Experimental evidence for emergent E8 symmetry. *Science*, 2010, v. 327 (5962), 177–180.
21. Adams J. F. Lectures on exceptional Lie groups. Chicago Lectures in Mathematics, University of Chicago Press, 1996.

Appendix

1. The time transformation for the round-trip
2. Derivation of the density and energy transformations
3. The relationship between velocity (β) and redshift (z)
4. References

1 The time transformation for the round-trip

$$t = t_{Depart} + t_{Arrive} = \left(\frac{1}{1-\beta} + \frac{1}{1+\beta}\right)t' = \left(\frac{2}{1-\beta^2}\right)t', \quad (A1)$$

or,

$$\hat{t} = \frac{t}{t'} = \frac{2}{1-\beta^2}\,. \quad (A2)$$

Figure A1 depicts the relative time $\hat{t}$ as a function of β for the one-way and round trip. The dashed lines depict the corresponding predictions of *SR*.

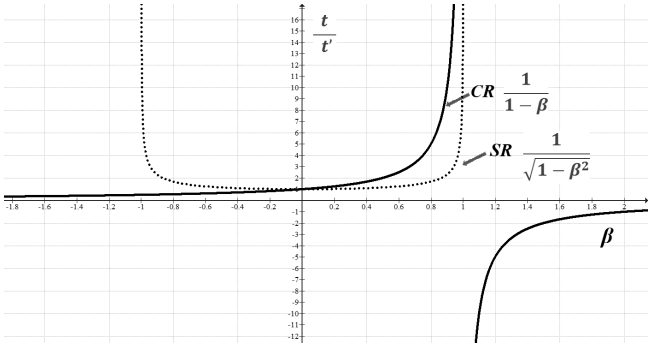

Fig. A1a

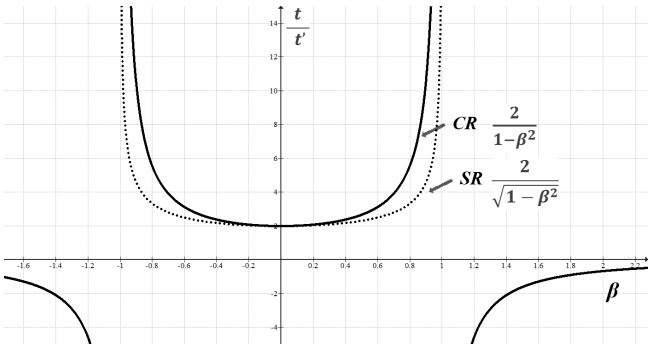

Fig. A1b

Fig. A1: Time transformations for the one-way (Fig. A1a) and round trip (Fig. A1b). The dashed lines depict the corresponding *SR* results.

2 Derivation of the density and energy transformations

To derive the density and kinetic energy transformation, consider the two frames of reference F and F' shown in Figure A2. Suppose that the two frames are moving relative to each other at a constant velocity v.

Consider a uniform cylindrical body of rest mass $m' = m_0$ and length $l' = l_0$ placed in F' along its travel direction. Suppose that at time t_1 the body leaves point x_1 (x'_1 in F') and moves with constant velocity v in the the $+x$ direction, until it reaches point x_2 (x'_2 in F') in time t_2 (t'_2 in F').

The body's density in the internal frame F' is given by:

$$\rho' = \frac{m_0}{Al_0}\,, \tag{A4}$$

where A is the area of the body's cross section, perpendicular to the direction of movement. In F the density is given by $\rho = \frac{m_0}{Al}$, where l is the object's length in F. Using the distance transformation l could be written as:

$$l = l_0\frac{1+\beta}{1-\beta}\,, \tag{A5}$$

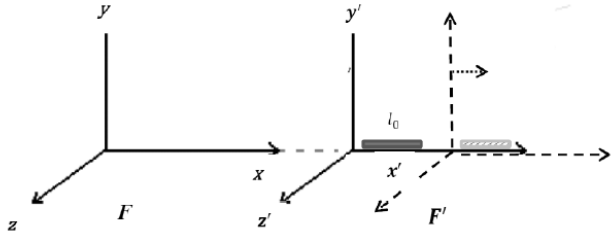

Fig. A2: Two observers in two reference frames, moving with velocity v with respect to each other

which yields:

$$\rho = \frac{m_0}{Al} = \frac{m_0}{Al_0}\frac{1-\beta}{1+\beta} = \rho'\frac{1-\beta}{1+\beta}\,,$$

or:

$$\frac{\rho}{\rho'} = \frac{1-\beta}{1+\beta}\,. \tag{A6}$$

Since the radius of the moving cylinder is perpendicular to the direction of motion, an observer at the internal frame F will measure a cylinder radius of $\Delta r = \Delta r_0$. The kinetic energy of a *unit of volume* is given by:

$$E = \frac{1}{2}\rho v^2 = \frac{1}{2}\rho_0\frac{1-\beta}{1+\beta}v^2,$$

or:

$$E = \frac{1}{2}\rho_0 c^2\beta^2\frac{1-\beta}{1+\beta}\,. \tag{A7}$$

And the energy for a departing particle of rest mass m_0 is given by:

$$E = \frac{1}{2}m_0 c^2\beta^2\frac{1-\beta}{1+\beta}\,. \tag{A8}$$

To calculate the value $\beta = \beta_{cr.}$ which satisfies $E = E_{max}$ we derive $\beta^2\frac{1-\beta}{1+\beta}$ with respect to β and equate the derivative to zero. This yields:

$$\begin{aligned}\frac{d}{d\beta}\left(\beta^2\frac{1-\beta}{1+\beta}\right) &= 2\beta\frac{1-\beta}{1+\beta} + \\ &+ \beta^2\frac{[(1+\beta)(-1)-(1-\beta)(1)]}{(1+\beta)^2} = \\ &= 2\beta\frac{(1-\beta^2-\beta)}{(1+\beta)^2} = 0\end{aligned} \tag{A9}$$

for $\beta \neq 0$ and we get:

$$\beta^2 + \beta - 1 = 0\,, \tag{A10}$$

which yields:

$$\beta_1 = -\varphi = -\frac{\sqrt{5}+1}{2} \approx -1.618 \tag{A11}$$

and

$$\beta_2 = \varphi - 1 = \frac{1}{\varphi} = \frac{\sqrt{5}-1}{2} \approx 0.618\,, \qquad (A12)$$

where φ is the Golden Ratio defined as: $\varphi = \frac{\sqrt{5}+1}{2}$ [A1-A3]. This is a striking result given the properties of this phenomenal number, due to its importance, together with the Fibonacci numbers, in mathematics, aesthetics, art, music, and more and its key role in nature, including the structure of plants, animals, the human body, human DNA [A1-A8] and brain waves [A9-A12] and in physics [A13]. The maximal kinetic energy at $\beta \approx 0.618$ is equal to:

$$E_{max} = \frac{1}{2} m_0 c^2 (\varphi - 1)^2 \frac{1-(\varphi-1)}{1+(\varphi-1)} = \\ = \frac{1}{2} m_0 c^2 (\varphi - 1)^2 \frac{2-\varphi}{\varphi}\,. \qquad (A13)$$

The term $\varphi - 1$ could be written as: $\varphi - 1 = \frac{\sqrt{5}+1}{2} - 1 = \\ = \frac{(\sqrt{5}+1)-2}{2} = \frac{\sqrt{5}-1}{2}$ Multiplying the numerator and denominator by $\frac{\sqrt{5}+1}{\sqrt{5}+1}$ yields:

$$\varphi - 1 = \frac{\sqrt{5}-1}{2}\frac{\sqrt{5}+1}{\sqrt{5}+1} = \frac{5-1}{2\sqrt{5}+1} = \\ = \frac{2}{\sqrt{5}+1} = \frac{1}{\frac{\sqrt{5}+1}{2}} = \frac{1}{\varphi}\,. \qquad (A14)$$

Eq. (A14) could be rewritten as:

$$E_{max} = \frac{1}{2} m_0 c^2 \frac{(2-\varphi)}{\varphi^3}\,. \qquad (A15)$$

Substituting $\varphi = \frac{\sqrt{5}+1}{2}$ we obtain:

$$E_{max} \approx 0.04508497 m_0 c^2. \qquad (A16)$$

3 The relationship between velocity and redshift

Redshift could be described as the relative difference between the observed and emitted wavelengths (or frequency). Let λ represents wavelength and f represents frequency ($\lambda f = c$ where c is the speed of light), then the redshift z is given by:

$$z = \frac{\lambda_r - \lambda_s}{\lambda_s} \qquad (\text{or} \quad z = \frac{f_s - f_r}{f_r})\,, \qquad (A17)$$

where $\lambda_s(f_s)$ is the wavelength (frequency) measured at the source and $\lambda_r(f_r)$ is the wavelength (frequency) measured at the receiver's laboratory.

Substituting $f_s = \frac{1}{t_s}$ and $f_r = \frac{1}{t_r}$ in (A17) above we obtain

$$z = \frac{f_s - f_r}{f_r} = \frac{\frac{1}{t_s} - \frac{1}{t_r}}{\frac{1}{t_r}} = \frac{t_r - t_s}{t_s} = \frac{t_r}{t_s} - 1. \qquad (A18)$$

But from Eq. 2 we have:

$$\frac{t_r}{t_s} = \frac{1}{1-\beta}\,. \qquad (A19)$$

Thus:

$$z = \frac{1}{1-\beta} - 1 = \frac{\beta}{1-\beta} \qquad (A20)$$

and

$$\beta = \frac{v}{c} = \frac{z}{1+z}\,. \qquad (A21)$$

4 References

A1. Olsen S. The Golden Section. New York, Walker & Co, 2006.

A2. Livio M. The Golden Ratio: The Story of Phi, the World's Most Astonishing Number. New York, Broadway Books, 2002.

A3. Huntley H. E. The Divine Proportion: a Study in Mathematical Beauty. New York, Dover, 1970.

A4. Stakhov A. Fundamentals of a new kind of mathematics based on the Golden Section. *Chaos, Solitions Fractals*, 2006, v. 27, 1124–1146.

A5. Pittard N., Ewing M., Jevons C. Aesthetic theory and logo design: examining consumer response to proportion across cultures. International Marketing Review, 2007, v. 24 (4), 457–73.

A6. Hammel G. T. Fascinating Fibonaccis: Mystery and Magic in Numbers. Dale Seymour Publications, 1987.

A7. Hammel G. T., Vaughan K. C. Math and Music: Harmonious Connections. Dale Seymour Publications, 1995.

A8. Klar A. J. S. Fibonacci's flowers. *Nature*, 2002, v. 417, 595.

A9. Weiss H., Weiss V. The golden mean as clock cycle of brain waves. *Chaos, Solitions Fractal*, 2003, v. 18 (4), 643–652.

A10. Conte E., Khrennikov A., Federici A., Zbilut J. P. Variability of brain waves: A new method based on a fractal variance function and Random Matrix Theory. *Chaos, Solitions Fractals*, 2009, v. 41 (5), 2790–2800.

A11. Weiss H., Weiss V. When frequencies never synchronize: the golden mean and the resting EEG. *Br. Res.*, 2010, v. 1335 (4), 91–102.

A12. Roopun A. K., Kramer M. A., Carracedo L. M., Kaiser M., Davies C. H., Traub R. D., Kopell N. J., Whittington M. A. Temporal interactions between cortical rhythms. *Front. Neuro.*, 2008, v. 2 (2), 145–154.

A13. Coldea R., Tennant D. A., Wheeler E. M., Wawrzynska E., Prabhakaran D., Telling M., Habicht K., Smeibidl P., Kiefer K. Quantum criticality in an Ising chain: Experimental evidence for emergent E8 symmetry. *Science*, 2010, v. 327 (5962), 177–180.

Submitted on: April 10, 2013 / Revised submission on: April 30, 2013
Accepted on May 01, 2013
After corrections: September 13, 2013

A New Model of Black Hole Formation

Gordon D. Thayer

1169 Carmella Circle, Sarasota, Florida 34243 U.S.A. E-mail: gdthayer@verizon.net

The formation of a black hole and its event horizon are described. Conclusions, which are the result of a thought experiment, show that Schwarzschild [1] was correct: A singularity develops at the event horizon of a newly-formed black hole. The intense gravitational field that forms near the event horizon results in the mass-energy of the black hole accumulating in a layer just inside the event horizon, rather than collapsing into a central singularity.

1 Introduction

This article describes the formation of a black hole and the physics of event horizon formation. In early 1916, a German physicist, Karl Schwarzschild, published a short paper in which he gave a solution to Einstein's general relativity field equations for spherically symmetric objects. Schwarzschild's solution "contains a coordinate singularity on a surface that is now named after him. In Schwarzschild coordinates, *this singularity lies on the sphere of points at a particular radius, called the Schwarzschild radius*" [1] (emphasis added). The significance of this paper has not been generally appreciated, although it led physicists eventually to accept black holes as real physical objects. Many black holes have been detected in recent years using astronomical techniques. But physicists in general have concluded that the singularity lies at the center of the black hole rather than on its event horizon. They have mostly ignored the results of Schwarzschild, who found that the singularity occurred at the event horizon itself rather than at the center of the spherical space enclosed by the event horizon. In this article I show by means of a suitably chosen thought experiment that Schwarzschild was correct.

2 A collapsing star

Following the occurrence of a Type 1a supernova, a neutron star is usually formed. For neutron stars with a mass greater than the Tolman-Oppenheimer-Volkoff limit (about 3 to 4 solar masses), the star will collapse to form a black hole. We need to follow the history of some points on and within the collapsing star in order to find out what really happens when a black hole is formed. To establish some boundary conditions, note that a point at the center of the collapsing star will not move with respect to a coordinate system centered on the star; the center of the system does not participate in the collapse. Of more interest is a point on the surface of the collapsing star. This point will have a velocity vector directed toward the center of the star with a speed that depends on the time from the initiation of collapse until the formation of the event horizon, at which time its speed is assumed to be the speed of light, c. Assume that a point halfway between the surface and the center will also have an inwardly directed velocity with half the speed of the surface point. In other words, the contraction is radially linear. Some departure from this linearity will not severely affect my conclusions.

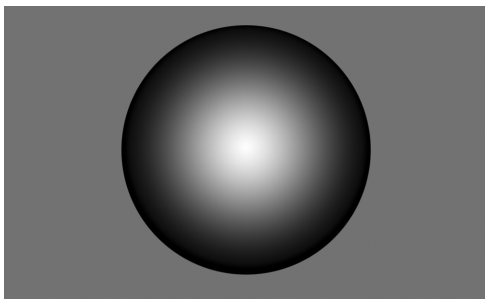

Fig. 1: Radial velocities in a collapsing star.

Figure 1 shows qualitatively what these radial velocities look like. The size of the star in the illustration is assumed to be approaching the Schwarzschild radius. The black colors indicate high radial velocity and white indicates small or zero velocities. The figure was constructed using the gradient tool in Photoshop and is linear in value from the center to the outer boundary. In reality, the darkest black should be confined to the very outer edges of the star and most of the interior should be either white or light gray. Nevertheless, the picture does give a good idea of the kind of radial velocities one would find in the cross-section of a collapsing star.

Figure 2 shows the situation at the moment when the event horizon forms. Note that the points at $0.995\,R_s$, where R_s is the Schwarzschild radius, have 10 times their normal, or rest, mass. The asymptote on the right goes to infinity at the Schwarzschild radius, $R = 1.0$ in the illustration. This is the singularity that Karl Schwarzschild discovered when he solved Einstein's field equations for a symmetrical, non-rotating body. The equation used to plot the points for the mass as a function of the radius is:

$$\frac{m}{m_0} = \frac{1}{\sqrt{1 - v^2/c^2}} \equiv \frac{1}{\sqrt{1 - R^2}}, \quad 0 \leqq R < 1. \qquad (1)$$

The validity of this special relativity equation under the conditions in the formation of an event horizon is unsure, but since a singularity is a singularity, and this equation defines one for $v = c$, it is likely as good as some other measure.

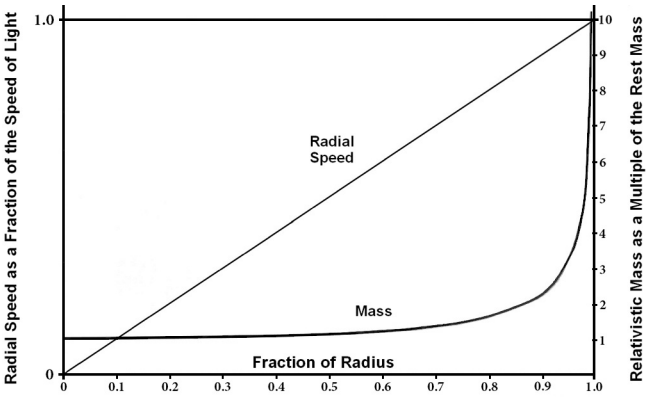

Fig. 2: Mass distribution in a newly-formed black hole. Drawing by the author.

The essential point is that most of the mass will be concentrated near the event horizon as soon as it forms. Thus the gravitational field will be quickly reversed, and with it, the velocity field inside the event horizon. Particles in the interior of the new black hole will be strongly attracted to the event horizon, since that is where most of the mass is located. This implies that the entire mass of the collapsed star could end up in a shallow region just inside the event horizon. There is no way to determine from the outside whether or not this happens.

In this scenario, the mass M is contained in a very thin layer at the radius R and the interior is empty. But how does it get there? According to Susskind [2, see p. 238] anything that impacts the event horizon of a black hole is absorbed by it, spreading over the entire extent of the event horizon the way a drop of ink dissolves rapidly in a basin of warm water. What if the event horizon itself comprises all of the mass contained in the black hole, held in a layer perhaps one Planck length in thickness? (Admittedly, that's a guess on my part.) From the outside, it would still behave like a black hole. All differences would be on the inside.

In my model the material of a collapsing star would, as soon as it has compacted enough to form a black hole, begin to migrate to the event horizon, like iron filings attracted to a magnet. The only place where the gravity of the material comprising the event horizon layer is neutral would be the exact, precise center of the black hole. But even so small a particle as a hadron would, sooner or later, wander off center — if for no other reason, because of the Heisenberg uncertainty principle. It would then be instantly attracted to the event horizon and would stick there like a bug on fly paper. Eventually the entire inside of the black hole would be empty. The layer comprising the event horizon layer may be extremely thin, but it is most definitely not a singularity, a mere mathematical point.

I recently discarded this possibility, but it appears that I may have been too hasty in doing so.

3 What happens to the matter in a black hole?

In this reconsidered theory, the singularity at the event horizon is only mathematical, not real. The mass of the collapsed star is contained in a thin layer just inside the event horizon, perhaps only a single Planck length thick. There is an external complement to this idea. Leonard Susskind [2, see pp. 233–234] writes:

> The only [solution] consistent with the laws of physics would be to assume that some kind of super-heated layer exists just above the horizon, perhaps no more than a Planck length thick... the layer must be composed of tiny objects, very likely no bigger than the Planck length. The hot layer would absorb anything that fell onto the horizon, just like drops of ink dissolving in water... This hot layer of stuff needed a name. Astrophysicists had already coined the name that I eventually settled on... They had used the idea of an imaginary membrane covering the black hole just above its horizon to analyze certain electrical properties of black holes. [They] had called this imaginary surface the stretched horizon, but I was proposing a real layer of stuff, located a Planck length above the horizon, not an imaginary surface.
>
> I liked the sound of "stretched horizon" and adopted it for my own purposes. Today the stretched horizon is a standard concept in black hole physics. It means the thin layer of hot microscopic "degrees of freedom" located about one Planck distance above the horizon.

I propose the name "Shell Theory" for my explanation of black hole formation.* This theory posits a one-to-one correspondence between the bits of entropy on the surface of the event horizon of a black hole and the particles of the collapsed star in the shell layer just inside the event horizon. The gravitational field and other external properties of the black hole will be exactly the same as if an infinite singularity existed at the center, because the amount of mass-energy in each case will be identical. All that is necessary for this condition to be true is that the distribution of mass inside the event horizon is spherically symmetrical. The shell theory has the same spherical symmetry as conventional theory with a singularity at the center of the black hole.

In the shell theory evolution of a black hole, the collapsing of the remnant star must stop as soon as the event horizon is formed. The reversal would start at a time somewhat prior to the formation of the event horizon. In figure 1 it is apparent that even before the outer layer of particles achieves a velocity magnitude equal to the speed of light, the distribution of

*For the purposes of this article, a "shell" is defined as the volume enclosed between concentric spheres of different radii.

mass within the collapsing object would favor the outer layers over the inner layers. This differential in the gravitational field would build up rapidly as the size of the collapsing star approached the Schwarzschild limit, so it would not be an instantaneous reversal.

The mass of a differential shell from the collapsing star as a function of the radius, assuming that the radial velocity of a point inside the object is a linear function of the radius up to the limit of $v = c$, at $R = R_s$, is:

$$d\frac{m}{m_0} = 4\pi R^2 \frac{m}{m_0}\, dR\,, \tag{2}$$

where

$$\frac{m}{m_0} = \frac{1}{\sqrt{1 - R^2}}\,. \tag{3}$$

Therefore the total relative mass of a spherical shell is given by the integral:

$$\frac{m}{m_0} = \int \frac{4\pi R^2 dR}{\sqrt{1 - R^2}} = 4\pi \left[\frac{1}{2}\sin^{-1}(R) - \frac{1}{2} R\sqrt{1 - R^2}\right]. \tag{4}$$

This result must be evaluated at three points: $R = 0$; $R = R$; and $R = R_s$. The result for $R = 0$ is simple: 0. For $R = R_s$ the term $(1 - R^2)$ becomes zero, and $\sin^{-1}(1)$ is $\frac{\pi}{2}$; so the result for $R = R_s$ is $\frac{\pi}{4}\,(\times 4\pi)$. Subtracting the two solutions from each other (ignoring the common factor of 4π) and setting the results equal to each other — so that we obtain the radius within which and without which there is equal mass — we have, after rearranging terms, the equation:

$$\sin^{-1}(R) = \frac{\pi}{4} + R\sqrt{1 - R^2}. \tag{5}$$

This equation, (5), is difficult to evaluate in closed form, but the result can be obtained easily through the process of successive iterations. The solution is approximately $R = 0.915$ (the difference between the two sides of the equation is 9×10^{-4} out of 1.155), meaning that the outer 8.5% of the sphere contains as much relativistic mass as the entire inner 91.5%.* This amply demonstrates that what was initially the inward implosion of a neutron star will now be a radially outward "explosion" within the confines of the event horizon — the surface implied by Schwarzschild's results.

4 Results and discussion

The likely end result will be that all of the mass-energy of a collapsed star ends up confined to a very thin layer — probably only one Planck length thick — just inside the event horizon. There may be a " black hole" there, but its matter will not be located in an infinitely dense singularity at the center point.

Also notice that for a solid body of uniform density, the gravitational field outside the surface is inversely proportional to the square of the distance from the center of the body, but for points inside the body the gravitational field is linear, diminishing to zero at the center. This reinforces the assumption that the collapse of the neutron star should be linear in nature. The effect as the radius of the shrinking star approaches and attains the Schwarzschild radius is to change this linear gravitational potential into a hyperbolic gravitational field, asymptotic to infinity at R_s.

The singularity at the Schwarzschild radius, or event horizon, is mathematical only and does not affect any real particles. The event horizon is described by a metric of points distributed over a spherical manifold, and the term "point mass" is an oxymoron since a point cannot have mass or any other physical property. It is nothing more than a mathematical position in space-time. In this context, note that the integration in equation (4) does not diverge at $R = R_s$, as it would if there were a true infinity at that point.

Where I have written the word "point" or "points", this term should not be taken literally. The reader should imagine a tiny amount of matter, perhaps a cubic Planck length (Planck volume) in size, located at a particular point in space-time. An actual point has no dimensions and therefore cannot have mass or any other physical property. The Planck volume is believed by many to be a quantum unit of space.

Submitted on July 8, 2013 / Accepted on July 14, 2013

References

1. Schwarzschild K. On the gravitational field of a sphere of incompressible fluid according to Einstein's theory. Communicated February 24th, 1916. *Sitzungsberichte der Königlich Preussischen Akademie der Wissenschaften zu Berlin, Phys.-Math. Klasse 1916*, 424–434. Translated from the German in 2008 by Larissa Borissova and Dmitri Rabounski. *The Abraham Zelmanov Journal*, 2008, volume 1, pages 20–32
2. Susskind L. The Black Hole War. New York, Little, Brown and Company, 2008.

*A more precise result is $0.914554 \pm 2 \times 10^{-6}$.

Dynamical 3-Space: Gravitational Wave Detection and the Shnoll Effect

David P. Rothall* and Reginald T. Cahill‡

School of Chemical and Physical Sciences, Flinders University, Adelaide 5001, Australia.
E-mail: *David.Rothall@flinders.edu.au, ‡Reg.Cahill@flinders.edu.au

Shnoll has investigated the non-Poisson scatter of rate measurements in various phenomena such as biological and chemical reactions, radioactive decay, photodiode current leakage and germanium semiconductor noise, and attributed the scatter to cosmophysical factors. While Shnoll didn't pinpoint the nature of the cosmophysical factors the Process Physics model of reality leads to a description of space, which is dynamic and fractal and exhibits reverberation effects, and which offers an explanation for the scattering anomaly. The work presented here shows a new way of generating the effects Shnoll discovered, through studying the phase difference of RF EM waves travelling through a dual coaxial cable Gravitational Wave Detector experiment.

1 Introduction – Shnoll effect

Over sixty years ago Simon Shnoll discovered a scatter anomaly in the measurements of the reaction rates of ATP-ase in actomyosin solutions over time that could not be explained [1]. Extensive research into this scatter anomaly lead to the conclusion that the reaction rates of the protein solution not only varied with time, but followed a distribution with preferred (discrete) values instead of a typical Poisson distribution. Over the following decades it was found that quite different phenomena also displayed similar scatter anomalies, ranging from chemical reactions to α-radiation activity in ^{239}Pu decay, photomultiplier dark noise and semiconductor noise fluctuations [2]. Shnoll's investigation of the scatter anomaly (referred to here as the Shnoll effect), between May 28 - June 01, 2004, produced 352,980 successive measurements of the α decay of a ^{239}Pu source [1]. Radioactive decay is considered to be a stochastic process, i.e. a random process with no preferred frequencies, and hence follows Poisson statistics. Fig. 1 is a layer histogram taken from Shnoll's data, with layer lines taken every 6000 measurements. The y-axis represents the frequency of decay rates and the x-axis is the number of decays per second - the decay rate. Over time the layer lines of the histogram exhibit a fine structure which become more prominent with more measurements, instead of canceling out as in the case of a typical Poisson distribution. This suggests that the radioactivity of ^{239}Pu takes on discrete values, and is not completely random.

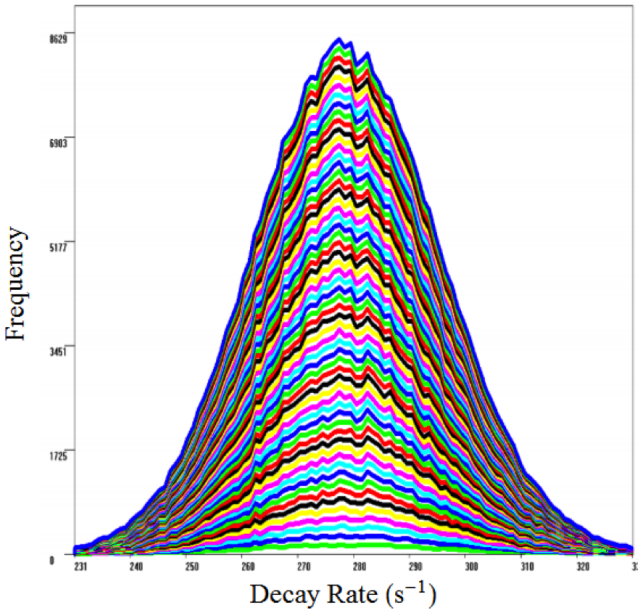

Fig. 1: Non-Poisson distribution of 352,980 measurements of ^{239}Pu α decay by Shnoll performed in 2004 (Fig. 2-2 of [1]). The layered histograms are taken every 6000 measurements. The x-axis denotes the number of decay events per second and the y-axis is the frequency of decay rate measurements.

Upon further study it was found that not only did the distribution (histogram) shapes vary over time, but the histogram shapes also correlated between different experiments run in parallel, regardless of whether they were located in the same laboratory or separated by thousands of kilometres. This was referred to as absolute time synchronism. Local-time synchronism was also observed, where histogram shapes of one experiment matched those of another with a time delay corresponding to the difference in longitudes of the two locations of the experiments (i.e. as the Earth rotates). A "near zone" effect was also discovered, where consecutive histograms in time of an individual experiment were found to be most similar in shape, regardless of the time scale used to generate the histograms, indicating the fractal nature of the scattering anomaly. The main conclusions drawn from Shnoll's research was that the consistency of the "scattering of results" of measurements in a time series arise due to inhomogeneities in the "space-time continuum" [1, 7]. These inhomogeneities are "caused by the movement of an object in the inhomogeneous gravitational field", e.g. as the Earth rotates/orbits the Sun, as the moon orbits the Earth, etc. While these inhomogeneities were not characterized by Shnoll there is a remark-

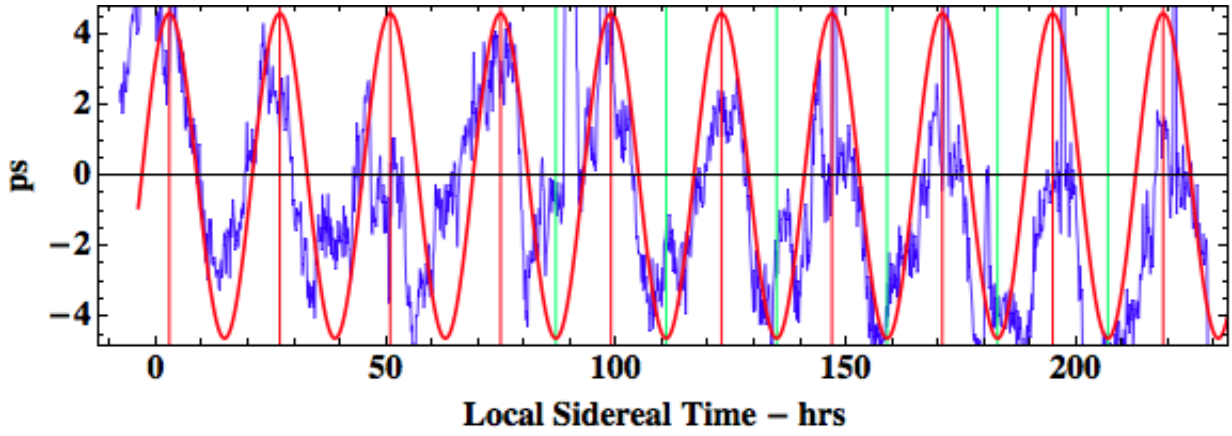

Fig. 2: Reproduction of Fig. 8 (top) from [5] showing the travel time differences (ps) between the two coaxial cable circuits in [5] plotted against local sidereal time, for the duration March 4 - 12, 2012. The smooth sine wave is a prediction made from the Dynamical 3-Space theory using NASA spacecraft Earth-flyby Doppler shift data.

able amount of evidence supporting this conclusion.

2 Dynamical 3-Space

An alternative explanation of the Shnoll effect has been proposed using an alternative theory known as dynamical 3-space theory; see Process Physics [3]. This arose from modeling time as a non-geometric process, i.e. keeping space and time as separate phenomena, and leads to a description of space which is itself dynamic and fractal in nature. It uses a uniquely determined generalisation of Newtonian Gravity expressed in terms of a velocity field $\boldsymbol{v}(\boldsymbol{r}, t)$, defined relative to an observer at space label coordinate $\boldsymbol{r}$, rather than the original gravitational acceleration field. The dynamics of space in the absence of vorticity, $\nabla \times \boldsymbol{v} = \boldsymbol{0}$, becomes*

$$\nabla\cdot\left(\frac{\partial \boldsymbol{v}}{\partial t} + (\boldsymbol{v}\cdot\nabla)\boldsymbol{v}\right) + \frac{5\alpha}{4}\left((trD)^2 - tr(D^2)\right) = -4\pi G\rho \qquad (1)$$

$$D_{ij} = \frac{\partial v_i}{\partial x_j} \qquad (2)$$

where $\rho(\boldsymbol{r}, t)$ is the usual matter density. The 1st term involves the Euler constituent acceleration, while the α-term describes a significant self interaction of space. Laboratory, geophysical and astronomical data suggest that α is the fine structure constant $\approx 1/137$. This velocity field corresponds to a space flow which has been detected in all of the experiments listed in section 3. In the spherically symmetric case and in the absence of matter $\rho = 0$, (2) contains solutions for black holes (spatial inflows) and an expanding universe (Hubble expansion) along with that for black holes embedded in an expanding universe [4]. (2) also contains solutions for the inflow of space into a matter density. Perturbing the spatial inflow into matter (i.e. simulating gravitational waves) was shown recently to produce reverberations in which the wave generates trailing copies of itself [8]. This reverberation effect is caused by the non-linear nature of the flow dynamics evident in (2) and will be shown in the coaxial cable data discussed in section 3.

*The α term in (2) has recently been changed due to a numerical error found in the analysis of borehole data. All solutions are also altered by these factors. (2) also contains higher order derivative terms - see [4] .

3 2012 Dual RF coaxial cable experiment

The Dynamical 3-Space theory was applied to an experiment which studied the radio frequency (RF) electromagnetic (EM) speed anisotropy, or ultimately the absolute motion of Earth through space. The effect of absolute motion has previously been studied using the results from Michelson - Morley, Miller, and DeWitte experiments [5]. These results are in remarkable agreement with the velocity of absolute motion of the Earth determined from NASA spacecraft Earth-flyby Doppler shift data all revealing a light/EM speed anisotropy of some 486 km/s in the direction RA=4.3^h, Dec = −75.0° [6]. The actual daily average velocity varies with days of the year because of the orbital motion of the Earth - the aberration effect discovered by Miller, but also shows fluctuations over time. The dual RF coaxial cable experiment, performed from March 4 - 12, 2012, measures the travel time difference of two RF signals propagating through dual coaxial cables [5]. The key effect in this 1st order in v/c experiment is the absence of the Fresnel drag effect in RF coaxial cables at a sufficiently low frequency. The experiment is designed such that one RF signal travels through one type of coaxial cable and returns via another type of cable, while the other signal does exactly the opposite. The cables are bound together such that any travel time effects due to temperature changes cancel as both cables are affected equally. Fig. 2 is a reproduction of the data obtained from the experiment in March 2012 where the travel time difference between the RF signals is plotted against sidereal time. The data is fitted, smooth curve, using

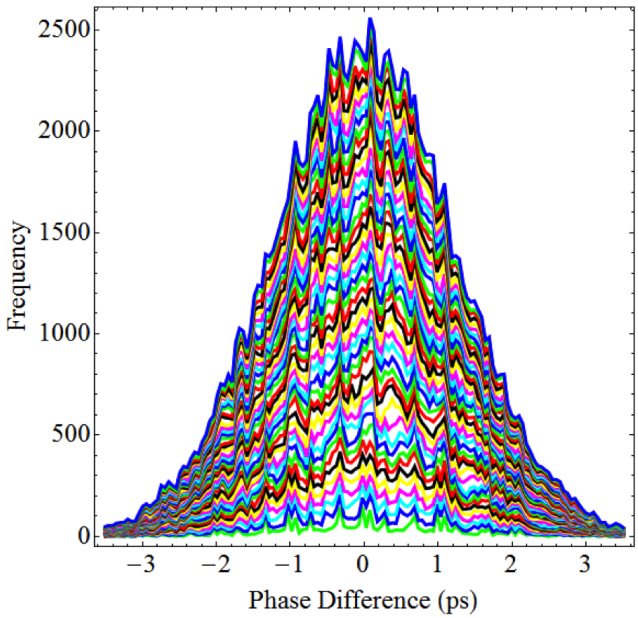

Fig. 3: Non-Poisson distribution of 155,520 measurements of the travel time difference (ps) observed between the two coaxial cable circuits of [5] from Mar 04, 2012 to Mar 12, 2012 in Adelaide. The layered histograms are taken every 3350 measurements to show a comparison with that of Fig. 1.

predictions from the NASA spacecraft Earth-flyby Doppler shift data, where a flow of space traveling at a speed of 499 km/s and direction RA=2.75^h, Dec = −77° predicts the overlaid sine wave, with dynamic range ∼8 ps. The Earth rotation effect, with respect to the galaxy, can be observed from the data, as well as turbulence effects. Turbulence effects are beginning to be characterized, and can be shown to correspond to what are, conventionally known as gravitational waves, although not those implied by General Relativity, but more precisely are revealing a fractal structure to dynamical 3-space, as illustrated in Fig. 4.

A Fast Fourier Transform of the data in Fig. 2 was taken to remove the Earth rotation effect (i.e. low frequency effects), and then a histogram taken of the resultant 155,520 measurements (after inverse FFT) to generate the layered histogram plot shown in Fig. 3. Layer lines are inserted every 3350 measurements to show a comparison with the Shnoll plot in Fig. 1. Fig. 3 is remarkably comparable to Fig. 1, thus suggesting that the Shnoll effect is also present in the coaxial cable EM anisotropy experiments. The structure observed appears to build up over time instead of cancelling out. It appears slightly noisier but this may be due to the fewer data points obtained than Shnoll (352,980 measurements). The structure observed is found to persist regardless of the time scale used for the phase difference, suggesting that the phenomenon causing this has a fractal nature as depicted in Fig.4. If this is indeed caused by a dynamical and fractal 3-space

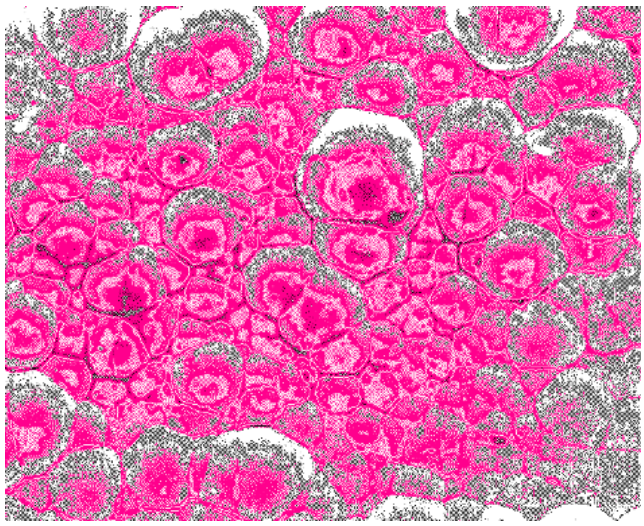

Fig. 4: Representation of the fractal wave data as revealing the fractal textured structure of the 3-space, with cells of space having slightly different velocities and continually changing, and moving with respect to the earth with a speed of ∼500 km/s.

then the persisting structure observed in Figures 1 and 3 correspond to regions of space passing the Earth that have preferred/discrete velocities, and not random ones, as randomly distributed velocities would result in a Poisson distribution, i.e. no features. A likely explanation for this is that the gravitational waves propagating in the 3-space inflow of the Earth or Sun could become phase locked due to the relative locations of massive objects. This would cause reverberation effects, i.e. regions of space which have the same speed and direction, which then repeat over time. The reverberations would be detectable in many experiments such as EM anisotropy, radiation decay, semiconductor noise generation, etc. and could in the future be used to further characterize the dynamics of space.

4 Conclusion

The data from a dual RF coaxial-cable / EM anisotropy - gravitatonal wave experiment displays the effect Shnoll observed previously in radioactivity experiments. It is suggested that these two experiments (along with other work by Shnoll) are caused by the fractal nature of space, together with the reverberation effect from gravitational waves, as predicted by the Dynamical 3-Space theory.

5 Acknowledgments

Special thanks to Professor Simon Shnoll for permission to use data from his work - see [1] for details. This report is from the Flinders University Gravitational Wave Detector Project, funded by an Australian Research Council Discovery Grant: *Development and Study of a New Theory of Gravity*.

Submitted on July 9, 2013 / Accepted on July 10, 2013

References

1. Shnoll S. E. Cosmophysical Factors in Stochastic Processes. American Research Press, Rehoboth, New Mexico, USA, 2012. Available from Progress in Physics website.
2. Shnoll S. E. Experimental investigations of local-time effect existence on laboratory scale and heterogeneity of space-time. *Progress in Physics*, 2007, v. 1, 64–69.
3. Cahill R. T. Process Physics: From Information Theory to Quantum Space and Matter. Nova Science Pub., New York, 2005.
4. Rothall D. P. and Cahill R. T. Dynamical 3-Space: Black Holes in an Expanding Universe. *Progress in Physics*, 2013, v. 4, 25–31.
5. Cahill R. T. Characterisation of Low Frequency Gravitational Waves from Dual RF Coaxial-Cable Detector: Fractal Textured Dynamical 3-Space. *Progress in Physics*, 2012, v. 3, 3–10.
6. Cahill R. T. Combining NASA/JPL One-Way Optical-Fiber Light-Speed Data with Spacecraft Earth-Flyby Doppler-Shift Data to Characterise 3-Space Flow. *Progress in Physics*, 2009, v. 4, 50–64.
7. Shnoll, S. E., Zenchenko T. A., Zenchenko K. I., Pozharskii E. V., Kolombet V. A. and Konradov A. A. Regular variation of the fine structure of statistical distributions as a consequence of cosmophysical agents. *Phys. Usp.*, 2000, v. 43 (2), 205–209.
8. Cahill R. T. and Deane S. T. Dynamical 3-Space Gravitational Waves: Reverberation Effects. *Progress in Physics*, 2013, v. 2, 9–11.

Potentialities of Revised Quantum Electrodynamics

Bo Lehnert

Alfvén Laboratory, Royal Institute of Technology, 10044 Stockholm, Sweden. E-mail: Bo.Lehnert@ee.kth.se

The potentialities of a revised quantum electrodynamic theory (RQED) earlier established by the author are reconsidered, also in respect to other fundamental theories such as those by Dirac and Higgs. The RQED theory is characterized by intrinsic linear symmetry breaking due to a nonzero divergence of the electric field strength in the vacuum state, as supported by the Zero Point Energy and the experimentally confirmed Casimir force. It includes the results of electron spin and antimatter by Dirac, as well as the rest mass of elementary particles predicted by Higgs in terms of spontaneous nonlinear symmetry breaking. It will here be put into doubt whether the approach by Higgs is the only theory which becomes necessary for explaining the particle rest masses. In addition, RQED theory leads to new results beyond those being available from the theories by Dirac, Higgs and the Standard Model, such as in applications to leptons and the photon.

1 Introduction and background

The vacuum state is not merely that of an empty space. Its energy has a nonzero ground level, the Zero Point Energy, being derived from the quantum mechanical energy states given e.g. by Schiff [1]. An example on the related vacuum fluctuations was provided by Casimir [2] who predicted that two closely spaced metal plates will attract each other. This is due to the fact that only small wavelengths can exist in the spacing, whereas the full spectrum of fluctuations exerts a net force on the outsides of the plates. The Casimir force was first demonstrated experimentally by Lamoreaux [3]. It implies that the vacuum fluctuations generate a real physical pressure and pressure gradient. Part of the quantum fluctuations also carry electric charges, as pointed out e.g. by Abbot [4]. The observed electron-positron pair formation from an energetic photon further indicates that electric charges can be created out of an electrically neutral state.

These established facts form the starting point of a revised quantum electrodynamic (RQED) theory by the author [5]. The theory is thus based on the hypothesis of a nonzero electric field divergence, $\operatorname{div}\mathbf{E} \neq 0$, in the vacuum. At the same time there is still a vanishing magnetic field divergence, $\operatorname{div}\mathbf{B} = 0$, due to the experimental fact that no magnetic monopoles have so far been observed. A nonzero electric field divergence has the following fundamental consequences [5]:

- The symmetry between the electric and magnetic fields **E** and **B** is *broken*.
- The nonzero electric charge density of a configuration with internal structure can both lead to a *net* integrated charge, and to *intrinsic charges* of both polarities.
- There exist *steady* electromagnetic states in the vacuum for which the energy density of the electromagnetic field gives rise to nonzero *rest masses* of corresponding particle models.

In the following treatise the basic field equations of RQED theory are first shortly described in Section 2. This is followed in Section 3 by a comparison to the related theories by Dirac as summarized by Morse and Feshbach [6], and that by Higgs [7]. The features and potentialities of RQED theory have earlier been described by the author [5, 8]. In Section 4 some complementary points will be presented, with special emphasis on results obtained beyond the Standard Model and not being deducible from other theories.

2 Basic field equations of Revised Quantum Electrodynamics

In four-dimensional representation the electromagnetic field equations have the general form

$$\left(\frac{1}{c^2}\frac{\partial^2}{\partial t^2} - \nabla^2\right) A_\mu = \mu_0 J_\mu \qquad \mu = 1, 2, 3, 4 \tag{1}$$

with the four-potentials $A_\mu = (\mathbf{A}, i\phi/c)$, **A** and ϕ as the magnetic vector potential and the electrostatic potential in three-space, and the four-current

$$J_\mu = (\mathbf{j}, ic\bar{\rho}) \tag{2}$$

with **j** and $\bar{\rho}$ as electric current density and electric charge density in three-space. The form (1) is obtained from the original set of equations through a gauge transformation in which the Lorentz condition

$$\operatorname{div}\mathbf{A} + \frac{1}{c^2}\frac{\partial\phi}{\partial t} = 0 \tag{3}$$

is imposed.

The source term due to the four-current (2) in the right-hand member of (1) has to satisfy the Lorentz invariance. This implies that

$$\mathbf{j}^2 - c^2\bar{\rho}^2 = const = 0 \tag{4}$$

when J_μ is required to vanish with the charge density $\bar{\rho}$. This finally results in a four-current

$$J_\mu = \bar{\rho}\,(\mathbf{C}, ic) \tag{5}$$

where

$$\mathbf{C}^2 = c^2 \tag{6}$$

and $\mathbf{C}$ is a velocity vector with a modulus equal to the velocity constant c of light. Concerning (6) two points should be observed [5]:

- The vector $\mathbf{C}$ both includes the case of a plane wave propagating at the scalar velocity c, and three-dimensional cases such as those of a cylindrical wave where $\mathbf{C}$ has at least two spatial components. In this way (6) can be considered as an *extension* of the Lorentz invariance to three dimensions.
- Equation (6) is quadratic and leads to two solutions. These represent the two resulting *spin* directions.

In a three-dimensional representation the field equations in the vacuum now become

$$\frac{\operatorname{curl}\mathbf{B}}{\mu_0} = \varepsilon_0\,(\operatorname{div}\mathbf{E})\,\mathbf{C} + \varepsilon_0\frac{\partial\mathbf{E}}{\partial t} \tag{7}$$

$$\operatorname{curl}\mathbf{E} = -\frac{\partial\mathbf{B}}{\partial t} \tag{8}$$

where

$$\mathbf{B} = \operatorname{curl}\mathbf{A} \qquad \operatorname{div}\mathbf{B} = 0 \tag{9}$$

$$\mathbf{E} = -\nabla\phi - \frac{\partial\mathbf{A}}{\partial t} \qquad \operatorname{div}\mathbf{E} = \frac{\bar{\rho}}{\varepsilon}. \tag{10}$$

These equations are gauge invariant, as in all cases where Maxwell's equations also include source terms.

The basic features of the RQED field equations are thus specified and summarized by the following points:

- The abolished symmetry between the electric and magnetic fields leads to equations having the character of *intrinsic linear* symmetry *breaking*.
- The equations are both Lorentz and gauge *invariant*.
- There is a *source* given by the "space-charge current density" of the first term in the right-hand member of (7). Through the nonzero electric field divergence this form introduces an additional degree of freedom, leading to new physical phenomena.
- Electromagnetic *steady* states with corresponding nonzero rest masses occur on account of (7).
- *New* and *modified* wave modes arise from the extended form (6) of Lorentz invariance.
- There is full symmetry between the solutions of positive and negative polarity, thereby realizing particle models for matter as well as for *antimatter*.

As described by Schiff [1] among others, Maxwell's equations are used as a guideline for proper interpretation of conventional quantum electrodynamical theory. Thereby Heitler [9] has shown that the quantized electrodynamic equations become identical with the original classical equations in which the electromagnetic potentials and currents merely become replaced by their quantum mechanical *expectation* values. In an analogous way, this also applies to the present RQED theory.

2.1 Steady electromagnetic states

As an example on steady electromagnetic states, a particle-shaped axisymmetric configuration is now considered in a spherical frame (r, θ, φ) with a current density $j = (0, 0, C\bar{\rho})$ and a magnetic vector potential $\mathbf{A} = (0, 0, A)$. Here $C = \pm c$ represents the two spin directions. From equations (7)–(10) with $\partial/\partial t = 0$, $\partial/\partial\varphi = 0$, $\rho = r/r_0$ and r_0 standing for a characteristic radial dimension, the result becomes [5]

$$CA = -\left(\sin^2\theta\right)DF \tag{11}$$

$$\phi = -\left[1 + \left(\sin^2\theta\right)D\right]F \tag{12}$$

$$\bar{\rho} = -\frac{\varepsilon_0}{r_0^2\rho^2}D\left[1 + \left(\sin^2\theta\right)D\right]F \tag{13}$$

where

$$\begin{gathered} D = D_\rho + D_\theta \\ D_\rho = -\frac{\partial}{\partial\rho}\left(\rho^2\frac{\partial}{\partial\rho}\right) \quad D_\theta = -\frac{\partial^2}{\partial\theta^2} - \frac{\cos\theta}{\sin\theta}\frac{\partial}{\partial\theta} \end{gathered} \tag{14}$$

and there is a separable generating function

$$\begin{gathered} F\,(r,\theta) = CA - \phi = G_0 \cdot G\,(\rho,\theta) \\ G\,(\rho,\theta) = R\,(\rho)\cdot T\,(\theta)\,. \end{gathered} \tag{15}$$

With equations (11)–(15) the net electric charge q_0, magnetic moment M_0, rest mass m_0, and integrated spin s_0 are then given by

$$q_0 = 2\pi\varepsilon_0 r_0 G_0 J_q \tag{16}$$

$$M_0 = \pi\varepsilon_0 C r_0^2 G_0 J_M \tag{17}$$

$$m_0 = \frac{\pi\varepsilon_0}{c^2} r_0 G_0^2 J_m \tag{18}$$

$$s_0 = \frac{\pi\varepsilon_0 C}{c^2} r_0^2 G_0^2 J_s \tag{19}$$

where

$$J_k = \int_{\rho_k}^{\infty}\int_0^{\pi} I_k\, d\rho\, d\theta \qquad k = q, M, m, s \tag{20}$$

and I_k are differential expressions given in terms of the quantities and operators of equations (11)–(15). In the integrals (20) the radii $\rho_k = 0$ when G is convergent at $\rho = 0$, and $\rho_k \neq 0$

are small radii of circles centered at $\rho = 0$ when G is divergent at $\rho = 0$ and a special renormalisation procedure has to be applied.

The form (15) of generating function has four alternatives. When $R(\rho)$ is divergent at $\rho = 0$ and $T(\theta)$ has top-bottom symmetry, there is a nonzero net charge q_0 and magnetic moment M_0, leading to models of charged leptons. In the remaining three cases both q_0 and M_0 vanish, thereby leading to neutral leptons such as massive neutrinos.

In addition to the quantization leading to expectation values of the field vectors, relevant second quantization conditions have to be imposed on the forms (16)–(19). These concern the spin, the magnetic moment, and the total magnetic flux [5].

2.2 New and modified wave modes

Due to experimental evidence, a model representing the wave packet of an individual photon in the vacuum has to satisfy the following general requirements:

- It should have a preserved and spatially limited geometrical shape of a wave packet propagating in an undamped way and in a defined direction, even at cosmical distances.
- To limit its geometrical shape, no artificial boundaries are to be imposed on the solutions of the field equations.
- The angular momentum in the direction of propagation, the spin, should be nonzero and have the constant value $h/2\pi$.

The field equations (7)–(10) have solutions satisfying these requirements. This applies e.g. to cylindrical waves in a frame (r, φ, z) with z along the direction of propagation. For these waves the velocity vector has the form

$$\mathbf{C} = c\,(0, \cos\alpha, \sin\alpha) \tag{21}$$

with a constant angle α. Normal modes varying as $f(r)\exp[i[-\omega t + kz)]$ in an axisymmetric case lead to the dispersion relation

$$\omega = kv \qquad v = c\,(\sin\alpha) \tag{22}$$

having phase and group velocities equal to v. Expressions for the components of $\mathbf{E}$ and $\mathbf{B}$ are then obtained from the separable generating function. A wave packet of narrow line width at a main wavelength λ_0 is further formed from a spectrum of these elementary modes. This finally leads to spatially integrated quantities such as net electric charge q, magnetic moment M, total mass m, and total spin s_z. The result is as follows:

- Both q and M vanish.
- There is a finite nonzero spin

$$\mathbf{s} = \mathbf{r} \times \frac{\mathbf{S}}{c^2} \qquad \mathbf{S} = \mathbf{E} \times \mathbf{B}/\mu_0 \tag{23}$$

  where $\mathbf{r}$ is the radius vector, $\mathbf{S}$ the Poynting vector, and $s_z = h/2\pi$ for the component of $\mathbf{s}$ in the z direction.
- A finite mass

$$m = m_0/\,(\cos\alpha) \tag{24}$$

  is obtained where m_0 stands for a nonzero but very small rest mass.

This solution leads to a characteristic radial dimension $\hat{r}$ for two modes given by

$$\hat{r} = \frac{\lambda_0}{2\pi\,(\cos\alpha)} \begin{cases} 1 & \text{(25a)} \\ \varepsilon & \text{(25b)} \end{cases}$$

where (25a) refers to a convergent generating function, and (25b) to a generating function which is divergent at $r = 0$ and where a special renormalisation procedure has to be applied.

The phase and group velocities of (22) are smaller than the velocity constant c. Still this difference from c can become small enough to be *hardly distinguishable*. An example can be given by $\sin\alpha = 1 - \delta$, $0 < \delta \ll 1$, $\varepsilon = \cos\alpha$, $0 < \varepsilon \ll 1$, and $\lambda_0 = 3 \times 10^{-7}$ m for a main wavelength in the visible range. When $\delta = 10^{-10}$ this yields characteristic radii of about 3×10^{-3} m and 5×10^{-7} m due to equations (25a) and (25b).

3 Relations to other fundamental theories

It has further to be established how the present RQED approach is related to such fundamental theories as that by Dirac [6] and by Higgs [7] with the associated Standard Model of elementary particles.

3.1 The theory by Dirac

To bring wave mechanical theory into harmony with the theory of relativity, Dirac adopted a new wave equation. Then it need not to be *assumed* that the electron is spinning or turning on its axis. According to the theory the electron will have an internal angular momentum (spin), and an associated magnetic moment. In fact there are four wave functions and corresponding matrices instead of one. These alternatives thus correspond to two spin directions, and to the two possibilities of matter and antimatter, such as in the form of the electron and the positron.

As seen from the previous sections, the present RQED theory is in full correspondence with that by Dirac, in including the two spin directions as well as particles and antiparticles. But the net elementary charge, e, and the finite electron rest mass, m_e, are only included as given and assumed parameters in the theory by Dirac, whereas these quantities are *deduced* from the field equations of RQED. The latter theory also leads to other new results beyond those being available from that by Dirac.

3.2 The theory by Higgs

The Standard Model of the theory on elementary particles is based on the source-free solutions of the field equations in

the vacuum as an empty space, i.e. (1) with a vanishing right-hand member. This leads to the Hertz equations having a vanishing electric field divergence, and it results in massless particles, in contradiction with their experimentally confirmed massive counterparts.

To resolve this contradiction, Higgs [7] proposed a *spontaneous nonlinear* mechanism of symmetry *breaking* by which an unstable boson of unspecified but large nonzero rest mass is formed, having vanishing spin and electric charge. The Higgs boson then decays into a whole succession of massive elementary particles.

During many years attempts have been made to find the Higgs boson. Finally the highly advanced and imposing experiments performed by the projects ATLAS [10] and CMS [11] at CERN have bebouched into the important confirmation of an existing unstable Higgs-like boson. The latter has been found to be characterized by vanishing electric charge and spin, combined with a rest mass of about 125 GeV. It was also observed to decay rapidly into successions of particles with smaller nonzero rest masses.

However, it could here be put into doubt whether this important experimental result provides a unique confirmation of the theory by Higgs, or if the theory described in Section 2 of this paper could as well explain the results without reference to the theory by Higgs. This question can be divided into two parts, i.e. the formation of a Higgs-like particle, and its decay. The first part thus concerns formation of a particle of mass in the range of 125 GeV, having vanishing charge and spin. Equations (11)–(15) imply that massive particles can be created already from the *beginning* by the intrinsic linear broken symmetry mechanism of RQED. Among the obtained solutions there is one which is expected to become unstable, having an unspecified but nonzero and large rest mass, as well as vanishing charge and spin [12]. Such a particle of mass 125 GeV can thus be predicted. Concerning the second part of the raised question, the resulting particle would, as in all earlier known cases, decay into several other massive particles in a way being independent of and not being unique for the Higgs mechanism. In this connection it might at a first sight be argued that the Higgs-like particle obtained from RQED is not identical with that considered by Higgs. This would, however, lead to the unlikely situation of two particles having the same basic and initial data of mass, charge and spin and resulting into the same decay processes, but still not being identical.

There may finally exist a certain similarity between the source of the Higgs field and that of the Zero Point Energy of RQED.

4 New results beyond other approaches

There are results from RQED which are not deducible from the Standard Model and other fundamental theories, as being demonstrated here by a number of examples.

4.1 Models of leptons

The field equations (7)–(10) in a steady state $\partial/\partial t = 0$ lead to new results and solutions:

- Charged lepton models arise from a divergent generating function and result in a point-charge-like geometry of *small* radial dimensions, such as that of the electron.
- A *deduced* elementary electric net charge is obtained. It is located within a *narrow* parameter channel situated around the experimental value, e, and having a width of only a few percent of e.
- Through a revised renormalisation process all relevant quantum conditions and all experimental values of charge, magnetic moment, rest mass, and spin can be reproduced by the choice of *only two* free scalar parameters, the so called counter-factors.
- The magnetic field contribution to equations (7)–(10) *prevents* charged leptons from "exploding" under the action of their electrostatic eigenforce.
- There are intrinsic electric charges of both polarities in leptons, each being about an order of magnitude larger than the net elementary charge e. It results in a Coulomb interaction force between these particles, being about two orders of magnitude larger than that due to the net charge. If these conditions would also hold for quarks, the total Coulomb force would become *comparable* and *similar* to the short-range interaction of the strong force [13]. This raises the question whether the intrinsic charge force will interfere with the strong force, or even become identical with it.

4.2 Model of the photon

In the time-dependent state of wave phenomena, equations (7)–(10) yield the following results:

- The Standard Model corresponds to a vanishing right-hand member of (1), and leads to the set of Hertz equations with a vanishing electric field divergence. In its turn, this gives rise to a vanishing photon spin as obtained from (23) and its quantized equivalent [5, 14]. Due to RQED theory there is on the other hand a photon model based on the extended relativistic forms of equations (6), (21) and (22), leading to a nonzero spin and an associated nonzero but very small rest mass [5, 14]. Thereby the spin of a photon wave packet does not merely have to be assumed in general terms, but becomes *deduced*. The spin occurs at the expense of a small reduction of the phase and group velocities in the direction of propagation.
- The needle-like photon model represented by equations (25a) and (25b) contributes to the *understanding* of the photoelectric effect and of two-slit experiments, with their wave-particle dualism.

- The RQED theory on screw-shaped wave modes is consistent with observed *hollow* geometry of corks-crew-shaped light beams [5].
- The nonzero electric field divergence and its intrinsic electric charges of alternating polarity also contributes to the understanding of electron-positron *pair formation* from an electrically neutral and energetic photon.

5 Conclusions

The present revised quantum electrodynamic theory includes the results of earlier fundamental theories, such as that by Dirac on electron spin and antimatter, and that by Higgs on massive elementary particles. It could thus be put into doubt whether the theory by Higgs becomes necessary for explaining the particle rest masses. In addition, the present theory leads to new results beyond those available from these and other so far established fundamental theories, as well as from the Standard Model in general.

Submitted on: July 29, 2013 / Accepted on: August 05, 2013

References

1. Schiff L. I. Quantum Mechanics. McGraw-Hill Book Comp.,Inc., New York-Toronto-London, 1949, Ch.IV, Sec.13; Ch.XIV.
2. Casimir H. B. G. On the attraction between two perfectly conducting plates. *Proc.K.Ned.Akad.Wet.*,1948, v. 51, 793–795.
3. Lamoreaux S. K. Demonstration of the Casimir force in the 0.6 to 6 μm range. *Phys.Rev.Letters*, 1997, v. 78 (1), 5–8.
4. Abbot L. The mystery of the cosmological constant. *Scientific American*, 1988, v. 258 (5), 106–113.
5. Lehnert B. Revised Quantum Electrodynamics. In Contemporary Fundamental Physics, Edited by V.V.Dvoeglazov. Nova Science Publishers, Inc., New York, 2013.
6. Morse P. M. and Feshbach H. Methods of Theoretical Physics. McGraw-Hill Book Comp., Inc., New York-Toronto-London, 1953, Part I, p.260.
7. Higgs P. W. Spontaneous symmetry breaking without massless bosons. *Physical Review*, 1966, v. 145, 1156–1168.
8. Lehnert B. A way to revised quantum electrodynamics. *Progress in Physics*, 2012, v. 2, April 2012, 21–27.
9. Heitler W. The Quantum Theory of Radiation. Third Edition, Oxford, Clarendon Press, 1954, Appendix, Sec.3, p.409.
10. Aad G. et al., ATLAS Collaboration, Observation of a new particle in the search for the Standard Model Higgs boson with the ATLAS detector at the LHC. *Phys.Lett*, 2012, v. B716, 1–29.
11. Chatrchyan S. et al., CMS Collaboration. Observation of a new boson at a mass of 125 GeV with the CMS experiment at the LHC. *Phys.Lett*, 2012, v. B716, 30–61.
12. Lehnert B. Higgs-like particle due to revised quantum electrodynamics. P*rogress in Physics*, 2013, v. 3, 31–32.
13. Lehnert B. Intrinsic charges and the strong force. *Progress in Physics*, 2013, v. 3, 17–20.
14. Lehnert B. Qn angular momentum and rest mass of the photon. *Journal of Plasma Physics*, Memorial volume dedicated to Padma K. Shukla, 2013(in press).

A Complete Relativity Theory Predicts with Precision the Neutrino Velocities Reported by OPERA, MINOS, and ICARUS

Ramzi Suleiman
University of Haifa, Haifa 31509, Israel. E-mail: suleiman@psy.haifa.ac.il

The present paper utilizes the recently proposed Complete Relativity Theory (CR) for the prediction of neutrino velocity in a prototypical neutrino velocity experiment. The derived expression for the relative difference of the neutrino velocity with respect to the velocity of light is a function of the anticipation time δt, the traveled distance D and the light velocity c, measured on Earth. It is independent neither on the traveling particle type nor on its energy level. With regard to fast neutrinos it is shown that the derived equation predicts with precision the results reported by OPERA, MINOS, and ICARUS. Since CR postulates that all physical entities, including the velocity of light, are relativistic entities, it follows that even though the results of the aforementioned experiments fail to support the neutrino superluminality claim, their precise prediction based on a theory that diametrically opposes SR, provides strong evidence for the inadequacy of SR in accounting for the dynamics of quasi-luminal particles. The aforementioned notwithstanding, a direct calculation of SR's predictions for the above mentioned studies yields grossly incorrect results.

1 Introduction

The findings of several high energy experiments conducted by MINOS, OPERA, ICARUS and other collaborations suggest that neutrinos travel at super-luminal or quasi-luminal velocities, e.g. [1–6]. The possibility of quasi-luminal neutrinos has been also confirmed by cosmological observations, see, e.g. [7, 8]. Among all experimental findings, the one that attracted most interest was the result reported in 2011 by OPERA [1], which (ostensibly) indicated that neutrinos have travelled faster than light. The reported anticipation time was $\delta t = 60.7 \pm 6.9\,(\text{stat.}) \pm 7.4\,(\text{sys.})$ ns and the relative neutrino velocity was $\frac{v_n - c}{c} = (5.1 \pm 2.9) \times 10^{-5}$. Many physicists have described the possibility that OPERA may have broken the limit of light-velocity as one of the greatest discoveries in particle physics, provided that it is replicated by an independent group, and CERN's Research Director announced in a press conference that "If this measurement is confirmed, it might change our view of physics" [9].

Within few months, numerous papers were written, proposing that OPERA's experimental design and/or measurements were flowed, or suggesting various explanations that accord with standard theories, see, e.g. [10–20]. Soon after, the ICARUS collaboration reported a null result, which contradicted OPERA's superluminal one [3]. The anticipation time measured by ICARUS was $0.3 \pm 4.0\,(\text{stat}) \pm 9.0$ (sys.) ns, which is one order of magnitude lower than the result reported by OPERA [1]. The following events witnessed the discovery of hardware malfunctions which resulted in measurement error and the publication of a corrected null result [5].

Theoretically, the possibility of superluminal particles has been treated within the framework of General Relativity by A. Zelmanov's theory of "physically observable quantities" [21, 22]. Other models which entertain the possibility to construct theories in which neutrinos travel faster than photons have recently been proposed, e.g. [20, 23].

Although many questions pertaining to the neutrino superluminality issue remain open to theoretical inquiry, the general stance among physicists contends that for the time being both superluminality and subluminality of neutrinos cannot be dismissed by existing data, and that more investigation of this issue is needed [23, 24]. The common view, which I shall refute hereafter, contends that the null result based on data aggregation from existing experiments, is consistent with Special Relativity and with the limits put on Lorentz violations, e.g. [12, 15, 24, 25].

Here I shall show that for three experiments conducted by MINUS, OPERA, and ICARUS, Special Relativity (SR) yields *grossly incorrect results* and that an expression for $\frac{v_n - c}{c}$ derived on basis of Complete Relativity Theory (CR), detailed in [26] in this volume, yields *precise predictions* for the three aforementioned experiments.

The reminder of the paper is organized as follows: Section 2 details a derivation of $\frac{v_n - c}{c}$ based on SR, and demonstrates that it yields grossly incorrect predictions for all the discussed experiments. Section 3 provides a brief description of CR, and utilizes the one-way time transformation for deriving an expression for $\frac{v_n - c}{c}$ in a typical quasi-luminal neutrino experiment. The derived expression is then used to make precise predictions for the results reported by the above mentioned studies. Section 4 ends with concluding remarks.

2 Special Relativity predictions

In general, all neutrino-velocity experiments utilized the same technology. Thus, for the sake of convenience and without loss of generality, I analyze the one implemented by OPERA shown schematically in Fig. 1.

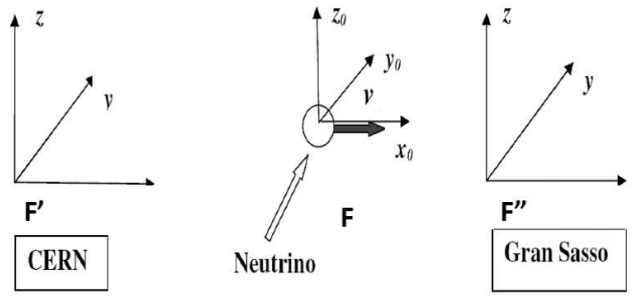

Fig. 1: The OPERA Setup.

From the perspective of Special Relativity (SR), the start and end laboratories F' and F'' are stationed in one frame of reference. The time dilation predicted by SR is given by:

$$\Delta_{SR} = T''_{G.Sasso} - T'_{CERN} = \frac{1}{\sqrt{1-\left(\frac{v_n}{c}\right)^2}}\, T. \qquad (1)$$

Where Δ_{SR} is the time difference between the start and end points, v_n is the neutrino's velocity, c is the velocity of light as it is measured on earth ($c = 299792.458$ km/sec) and T is the rest time at the neutrino's frame of reference F given by:

$$T = \frac{D}{v_n}. \qquad (2)$$

Where D is the distance between the source of the neutrino beam and the end point detector. Substituting the value of T in Eq. 1 we obtain:

$$\Delta_{SR} = \frac{1}{\sqrt{1-\left(\frac{v_n}{c}\right)^2}} \frac{D}{v_n}. \qquad (3)$$

For an early neutrino arrival time (δt) with respect to light photons we get:

$$\Delta_{SR} = \frac{D}{c} - \delta t. \qquad (4)$$

Substituting the value of Δ_{SR} from Eq. (3) in Eq. (4) and solving for $\frac{v_n}{c}$ we obtain:

$$\frac{v_n}{c} = \pm \sqrt{\frac{1}{2}\left(1 + \sqrt{1 - \frac{4}{1-\left(\frac{c\delta t}{D}\right)^2}}\right)}. \qquad (5)$$

For the result reported by ICARUS 2011: $\delta t = (0.3 \pm \pm 4.0\,(\text{stat}) \pm 9.0\,(\text{sys.})$ and $D = 674.385$ km. Substituting in Eq. 4 we get:

$$\frac{v_n}{c} \approx \pm(0.86603 + 0.5i) \qquad (6)$$

And,

$$\frac{c - v_n}{c} = \pm(-0.13397 + 0.5i). \qquad (7)$$

Calculations of SR's prediction of $\frac{c-v_n}{c}$ for the results reported by MINOS and OPERA (not reported here) yield similar (incorrect) results.

3 Complete Relativity predictions

Complete Relativity Theory (CR) rests on two postulates:

1. The magnitudes of all physical entities, as measured by an observer, depend on the relative motion of the observer with respect to the rest frame of the measured entities.
2. All translations of information from one frame of reference to another are carried by light or electromagnetic waves of equal velocity.

It should be stressed that the first postulate applies to all measured entities, *including the velocity of light*. CR treats the velocity of light as a relativistic quantity and not as an invariant one as postulated by SR. The derivations of CR's time, distance, mass-density and energy transformations are detailed elsewhere in this volume [26].

The derivation of a theoretical expression for $\frac{v_n - c}{c}$ in a typical superluminal neutrino experiment requires only the one-way time transformation. Viewed in the framework of CR, the experimental setup depicted in Fig. 1 includes *three* frames of reference: F' at CERN, F'' at Gran Sasso and F, the neutrino rest frame. F is *departing* from F' with velocity v_n and *approaching* F'' with velocity $-v_n$. F' and F'' are at rest relative to each other. According to CR [26], the time transformation for the one-way travel is given by:

$$\frac{t}{t_0} = \frac{1}{1 - \frac{v}{c}} \qquad (8)$$

Thus, we can write:

$$T'_{CERN} = \frac{1}{1 - \frac{v_n}{c}}\, T. \qquad (9)$$

Where v_n is the velocity of the neutrino relative to CERN's frame of reference F'.

Since the neutrino travelled *towards* Gran Sasso, applying the time transformation to F'' yields:

$$T''_{G.Sasso} = \frac{1}{1-\left(\frac{-v_n}{c}\right)}\, T = \frac{1}{1 + \frac{v_n}{c}}\, T. \qquad (10)$$

Experiment	Neutrino Anticipation Time (δt)	Experimental $\frac{v_n - c}{c}$	Theoretical $\frac{v_n - c}{c}$
MINOS $D = 734298.6$ m	$\left(126 \pm 32\,(\text{stat.}) \pm 6\,(\text{sys.})\right)$ ns	$(5.1 \pm 2.9)\,(\text{stat}) \times 10^{-5}$	$\mathbf{5.14 \times 10^{-5}}$
OPERA 2012 (corrected result) $D = 730085$ m	$\left(6.5 \pm 7.4\,(\text{stat.}) \begin{smallmatrix}+9.2\\-6.8\end{smallmatrix} (\text{sys.})\right)$ ns	$\left(2.7 \pm 3.1\,(\text{stat.}) \begin{smallmatrix}+3.8\\-2.8\end{smallmatrix} (\text{sys.})\right) \times 10^{-6}$	$\mathbf{2.67 \times 10^{-6}}$
ICARUS 2012 $D = 730478.56$ m	$\left(0.10 \pm 0.67\,(\text{stat.}) \pm 2.39\,(\text{sys.})\right)$ ns	$\left(0.4 \pm 2.8\,(\text{stat.}) \pm 9.8\,(\text{sys.})\right) \times 10^{-7}$	$\mathbf{0.41 \times 10^{-7}}$

Table 1: Experimental results and theoretical predictions for three superluminal neutrino experiments.

The time difference between CERN and Gran Sasso's could be written as:

$$D_t = T''_{G.Sasso} - T'_{CERN} = \\ = \left[\frac{1}{1+\frac{v_n}{c}} - \frac{1}{1-\frac{v_n}{c}}\right] T = -\frac{2\frac{v_n}{c}}{1-\left(\frac{v_n}{c}\right)^2} T. \quad (11)$$

Substituting the value of T in Eq. 11 we obtain:

$$D_t = -\frac{2\frac{v_n}{c}}{1-\left(\frac{v_n}{c}\right)^2} \frac{D}{v_n}. \quad (12)$$

For an early neutrino arrival time of δt with respect to the velocity of light we can write:

$$D_t = -\frac{2\frac{v_n}{c}}{1-\left(\frac{v_n}{c}\right)^2} \frac{D}{v_n} = \frac{D}{c} - \delta t. \quad (13)$$

Where $\frac{D}{c}$ is the light time arrival from CERN to Grand Sasso. Solving Eq. 13 for $\frac{v_n}{c}$ yields:

$$\frac{v_n}{c} = \sqrt{\frac{2}{1-\frac{c\delta t}{D}} - 1}\,. \quad (14)$$

Or,

$$\frac{v_n - c}{c} = \sqrt{\frac{2}{1-\frac{c\delta t}{D}} - 1} - 1. \quad (15)$$

Predictions

For the OPERA *corrected* result [2]

$$\delta t = \left(6.5 \pm 7.4\,(\text{stat.}) \begin{smallmatrix}+9.2\\-6.8\end{smallmatrix} (\text{sys.})\right) \text{ns}$$

and $D = 730.085$ km. Substituting in Eq. 15 we get:

$$\frac{v_n - c}{c} = \sqrt{\frac{2}{1-\frac{299792.458 \times 6.5 \times 10^{-9}}{730.085}} - 1} - 1 \approx \\ \approx \mathbf{2.67 \times 10^{-6}}. \quad (16)$$

Which is identical to the reported result of:

$$\frac{v_n - c}{c}\,(\text{Exp.}) = \left(2.7 \pm 3.1\,(\text{stat.}) \begin{smallmatrix}+3.8\\-2.8\end{smallmatrix} (\text{sys.})\right) \times 10^{-6}. \quad (17)$$

Equation 15 was also used to calculate theoretical predictions for the results reported by ICARUS [4] and MINOS [5]. The results are summarized in Table 1, which depicts all three experimental results against the corresponding theoretical predictions.

As could be seen in the table, *CR* yields accurate predictions for *all* three experimental results, *including the null ones*.

4 Concluding remarks

In this article I applied a recently proposed Complete Relativity Theory (CR) to analyze the neutrino travel in a typical neutrino-velocity experiment. CR treats all physical entities, including light velocity, as relativistic entities. Accordingly the measured velocity of light depends on the direction of the light propagation vector, relative to the laboratory. In terms of relative time, the start point laboratory (e.g., at CERN) will measure *time dilation*, whereas the end point laboratory (e.g., at Gran Sasso) will measure *time contraction*. It is important to note that the CR-based model presented in section 3 is independent of the particle type and its energy level. For the prediction of $\frac{v_n - c}{c}$ only the anticipation time δt and distance D between the start and end points are required [see Eq. 15].

The analysis brought above shows that CR predicts with near precision all the relative neutrino velocities $\frac{v_n - c}{c}$ obtained in recent neutrino-velocity experiments. In contrast, SR's predictions for all the discussed findings yields grossly incorrect results. What becomes clear from the analysis brought above

is that a breakdown of Einstein's SR does not require that the neutrino velocity exceeds the velocity of light.

Upon the announcement of the first null result, the leader of ICARUS collaboration leader was quoted by the press saying that had they found 60 nanoseconds, he would have sent a bottle of champagne to OPERA, and that instead, he suspects that he "will be toasting Einstein" [31]. The analysis presented in the present paper suggests that the news about rescuing SR were premature, and that it makes more sense to keep the champagne in the frigidaire.

Submitted on May 14, 2013 / Accepted on August 19, 2013

References

1. Adam T., et al. Measurement of the neutrino velocity with the OPERA detector in the CNGS beam. (OPERA Collaboration), 2011. arXiv:1109.4897.
2. Adam T., et al. Measurement of the neutrino velocity with the OPERA detector in the CNGS beam (OPERA Collaboration). *Journal of High Energy Physics*, 2012, v. 10, 093. arXiv:1109.4897.
3. Antonello M. et al. Measurement of the neutrino velocity with the ICARUS detector at the CNGS beam. *Physics Letters B*, 2012, v. 713 (1), 17–22.
4. Antonello M. et al. Precision measurement of the neutrino velocity with the ICARUS detector in the CNGS beam. *Journal of High Energy Physics*, 2012, 49. arXiv:1208.2629.
5. Adamson P. et al. Measurement of neutrino velocity with the MINOS detectors and NuMI neutrino beam. (MINOS Collaboration). *Physical Review D*, 2007, v. 76 (7), 2005–2012. arXiv:0706.0437.
6. Kalbfleisch G. R., Baggett N., Fowler C., Alspector J. Experimental comparison of neutrino, antineutrino, and muon velocities. *Physical Review Letters*, 1979, v. 43, 1361–1364.
7. Stodolsky L. The speed of light and the speed of neutrinos. *Physics Letters B*, 1988, v. 201 (3), 353–354.
8. Longo M. J. Tests of relativity from SN1987A. *Physical Review D*, 1987, v. 36, 3276–3277.
9. See announcement by said CERN Research Director, Prof. Sergio Bertolucci at: http://press.web.cern.ch/press/PressReleases/Releases 20 11/PR19.11E.html.
10. Garcia-Islas J. M. A very simple solution to the OPERA neutrino velocity problem. 2011. arXiv:1110.5866.
11. Mbelek J-P. Special relativity is consistent with the opera measurements of the neutrino "velocity". The Smithsonian/NASA Astrophysics Data System, 2011. arXiv:1110.4095.
12. Torrealba R. OPERA superluminal neutrinos explained by spontaneous emission and stimulated absorption, 2011. arXiv:1112.0815.
13. Cowsik R., Nussinov S., Sarkar U. Superluminal neutrinos at OPERA confront pion decay kinematics. *Physical Review Letters*, 2011, v. 107 (25), 251801.
14. Zichichi A. Time-shift in the OPERA set-up: Proof against superluminal neutrinos without the need of knowing the CERN-LNGS distance. *International Journal of Modern Physics*, 2012, v. 27 (18), 1230017. arXiv:1206.2840.
15. Schechter J., Shahid N. Neutrinos with velocities greater than c? *Physical Review D*, 2012, v. 85, 093008, 2012. arXiv:1201.4374.
16. Giudicea G. F., Sibiryakovb S., Strumiac A. Interpreting OPERA results on superluminal neutrino. *Nuclear Physics B*, 2012, v. 861 (1), 2012, 1–16.
17. Oda I. Subluminal OPERA neutrinos. *International Journal of Modern Physics A*, 2012, v. 27 (7), 1250033. arXiv:1112.5793.
18. Bo-Qiang, M. The phantom of the OPERA: superluminal neutrinos. *Modern Physics Letters A*, 2012, v. 27 (4). arXiv:1111.7050.
19. Hebecker A., Knochel A. The price of neutrino superluminality continues to rise. *Physics Letters B*, 2012, v. 715 (1-3), 116–120. arXiv:1111.6579.
20. Mu-Lin Y., Neng-Chao X., Huang W., Hu S. Superluminal neutrinos from special relativity with de sitter space-time symmetry. *Mod. Phys. Lett. A*, 2012, v. 27 (14), 1250076. arXiv:1111.4532.
21. Zelmanov A. On the relativistic theory of an anisotropic inhomogeneous universe (translated from the Russian manuscript, published in 1957). *The Abraham Zelmanov Journal*, 2008, v. 2008 (1), 33–63.
22. Rabounski D., Borissova L. Particles here and beyond the mirror. American Research Press, 2012.
23. Alexandre J., Ellis J., Mavromatos N. E. On the possibility of superluminal neutrino propagation. *Physics Letters B*, 2012, v. 706 (4-5), 456–461.
24. Linglia Z., Maa B-Q. Neutrino speed anomaly as signal of Lorentz violation. *Astroparticle Physics*, 2013, v. 44, 24–27.
25. Klinkhamer F. R. Superluminal neutrino, flavor, and relativity. *Physical Review D*, 2012, v. 85, 016011.
26. Suleiman R. The dark side revealed: a complete relativity theory predicts the content of the universe. *Progress in Physics*, 2013, v. 4, 34–40.
27. O'Connor J. J., Roberston E. F. Christian Andreas Doppler-MacTutor history of mathematics archive. University of St. Andrews, 1998.
28. Michelson A., Morley E. W. Relative motion of earth and luminiferous ether. *American Journal of Science*, 1887, v. 34, 333–345.
29. Piccard A., Stahel E. L'expérience de Michelson, réalisée en ballon libre. *Comptes Rendus*, 1926, v. 183 (7), 420–421.
30. Illingworth K. K. A Repetition of the Michelson-Morley experiment using Kennedy's refinement. *Physical Review*, 1927, v. 30 (5), 692–696.
31. Brumfiel G. Neutrinos not faster than light ICARUS experiment contradicts controversial claim. *Nature News*, 2012. http://www.nature.com/news/neutrinos-not-faster-than-light-1.10249.

Nanotechnology Quantum Detectors for Gravitational Waves: Adelaide to London Correlations Observed

Reginald T. Cahill

School of Chemical and Physical Sciences, Flinders University, Adelaide 5001, Australia. E-mail: reg.cahill@flinders.edu.au

The discovery of the nanotechnology zener diode quantum detector effect for gravitational waves is reported, based upon the quantum to classical transition being induced by dynamical 3-space fluctuations. Gravitational waves were detected by way of waveform correlations between time measurement in two Digital Storage Oscilloscopes, revealing time delays of 13 to 20 seconds over 24 hrs for Adelaide to London travel, varying as the earth rotates. The speed and direction were found, for January 1, 2013, to be 512 km/s, RA = 4.8 hrs, Dec = 83 deg S. This velocity agrees with previous detections using different techniques, such as the NASA spacecraft Earth-flyby Doppler shifts, which found 491 km/s, RA = 5.2 hrs, Dec = 80 deg S, for December 8, 1992. Consequently it was realised that nanotechnology zener diode quantum detectors have been operating, for different reasons, for some 15 years, and are known as RNGs (Random Number Generators) or REGs (Random Event Generators). The discovery herein reveals that they are not random. Correlations between data from a REG in Perth and a REG in London gave the speed and direction, for January 1, 2013, to be 528 km/s, RA = 5.3 hrs, Dec = 81 deg S. We also report highly correlated current fluctuations from collocated zener diode circuits. The GCP REG network constitutes an international gravitational wave detector network, with currently some 60 REGs operating, and with records going back to 1998. These detectors permit the study of dynamical 3-space structure, and also apparent anomalous scattering of the waves when passing deeper into the earth, solar flares, coronal mass ejections, earthquakes, and correlations with fluctuations in various rate processes such as nuclear decays. The quantum to classical transition is shown to be caused by 3-space dynamics, and so challenges the standard interpretation of probabilities in quantum theory.

1 Introduction

The speed and direction of gravitational waves have been directly measured via waveform time delays from detectors located in Adelaide and London, and separately from Perth and London. The Adelaide to London correlations were detected utilising the discovery that so-called "clock jitter" in two digital storage oscilloscopes (DSO) is actually correlated, with the London signal delayed relative to the Adelaide signal by 13 to 20 seconds, depending on sidereal time, so that at least part of the clock jitter is actually induced by passing gravitational waves. Subsequently similar correlations were discovered in Random Event Generator (REG) correlated data. These detect the quantum to classical transition for electrons tunnelling through a barrier in a tunnel diode, a nanotechnology device. According to the standard interpretation of quantum theory such electron current fluctuations should be completely random, which is why such devices are also known as hardware Random Number Generators (RNG), and have a variety of applications assuming such randomness.

These discoveries make the detection and study of gravitational waves particularly simple, and easily extend to a network of detectors, and for the REG technique an international network of such detectors has existed since 1998, and so that data is an extremely valuable to the characterisation of the gravitational wave effect, and also other phenomena which appear to be induced by more extreme fluctuations. Correlations of the gravitational wave forms permit determination of the speed and direction of space, which agrees with results from NASA Earth-flyby Doppler shift data, and with the 1925/26 Dayton Miller Mt.Wilson gas-mode Michelson interferometer data. The correlation data also reveals two new phenomena: a speed-up when the waves pass deeper into the earth, and a wave reverberation effect. For collocated zener diodes the current fluctuations are highly correlated, with no time delay effects, as expected. The quantum to classical transition is thus shown to be caused by 3-space dynamics, and so challenges the standard interpretation of probabilities in quantum theory.

2 Classical physics gravitational wave detectors

Classical gravitational wave detectors have employed a number of physical effects and designs: gas-mode Michelson interferometers, optical fibre Michelson interferometers, RF coaxial cable travel time differential measurements, and more compact RF coaxial cable – optical fibre measurements, spacecraft Earth-flyby Doppler effects, and dual RF coaxial cable travel time measurements [1,2]. All of these techniques utilise light or EMR anisotropy speed effect in a single device.

The key issue with such devices is that they are single-site devices, and require a calibration theory, which depends upon an assumed theory. For example the sensitivity of a Michelson interferometer, as indicated by the travel time difference between the two arms, and detected by means of fringe shifts as the detector is rotated, is given by

$$\Delta t = k^2 \frac{L v_p^2}{c^3} \cos(2(\theta - \psi)) \qquad (1)$$

where L is the arm length, v_P is the speed projected onto the plane of the interferometer, and the angles measure the rotation effect, see [1]. Eqn.(1) is applied to the data in conjunction with terms accounting for the inclined mirrors and temperature drift effects [1]. The critical factor k^2 is the calibration constant. With a gas present in the light path, with refractive index n, $k^2 \approx n^2 - 1$ to a good approximation. Results from two gas-mode Michelson interferometer experiments are shown in Fig. 1. The results reveal significant turbulence, which has been identified as gravitational waves, and much greater in magnitude than expected. Michelson and Morley in the 1st such experiment in 1887 assumed that $k^2 = 1$, whereas with air present, $n = 1.00029$, giving $k^2 \approx 0.0006$, and so much less sensitive than assumed. Note that a vacuum-mode Michelson interferometer has $k^2 = 0$, and so completely insensitive to gravitational waves.

A recent gravitational wave experiment used differential travel time measurements in a dual RF coaxial cable array [2]. This technique relies upon the absence of Fresnel drag in RF coaxial cables, at least for low RF frequencies (~10 MHz). The results agree with those form the Miller gas-mode Michelson interferometer, and from the NASA flyby Doppler shift data. The fluctuations were again observed to be a ~20% effect.

The interpretation of the magnitude of the detected effects in these classical detector experiments all rely upon some calibration theory, and there has always been confusion. Fortunately spacecraft flyby Doppler shift analysis does not suffer from such problems, and has indeed confirmed the results from the classical detectors. We now report the discovery that nanotechnology quantum detectors respond to the fluctuations of the passing space, and when the data from two well-separated detectors is subject to a correlation analysis of the two local waveforms the average speed and direction of the passing space is revealed, together with significant wave/turbulence effects. This technique gives an absolute measurement of travel times.

3 Quantum gravitational wave detectors

When extending the Dual RF Coaxial Cable Detector experiment to include one located in London, in addition to that located in Adelaide, an analysis of the measured DSO internal noise in each identically setup instrument was undertaken, when the extensive RF coaxial cable array was replaced by

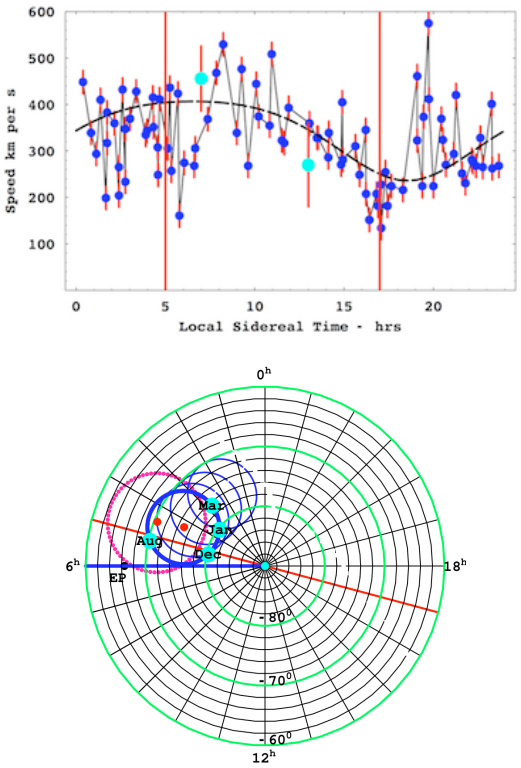

Fig. 1: Top: Speeds v_P, of the space velocity **v** projected onto the horizontal plane of the Miller gas-mode Michelson interferometer located atop Mt.Wilson, plotted against local sidereal, for a composite day, with data collected over a number of days in September 1925, see [1]. The data shows considerable fluctuations, from hour to hour, and also day to day, as this is a composite day. The dashed curve shows the non-fluctuating best-fit variation over one day, as the earth rotates, causing the projection onto the plane of the interferometer of the velocity of the average direction of the space flow to change. The maximum projected speed from the curve is 417 km/s, corresponding to a speed of 453 km/s, with a RA of ~5 hrs, which is very close to results reported herein. The Cassini flyby Doppler shift data in August 1999 gives a RA = 5.2 hrs [1]. The green data points, with error bars, at 7 hrs and 13 hrs, are from the Michelson-Morley 1887 data. The ~20% speed fluctuations are seen to be much larger than statistically determined errors, revealing the presence of turbulence in the space flow, i.e gravitational waves. Bottom: South celestial pole region. The dot (red) at RA = 4.3^h, Dec = 75°S, and with speed 486 km/s, is the direction of motion of the solar system through space determined from NASA spacecraft earth-flyby Doppler shifts [1], revealing the EM radiation speed anisotropy. The thick (blue) circle centred on this direction is the observed velocity direction for different days of the year, caused by earth orbital motion and sun 3-space inflow. The corresponding results from the Miller gas-mode interferometer are shown by 2nd dot (red) and its aberration circle (red dots). For December 8, 1992, the velocity is RA = 5.2^h, Dec = 80°S, speed 491 km/s, see Table 2 of [1]. The thinner blue aberration circles relate to determination of earth 3-space inflow speed, see [1].

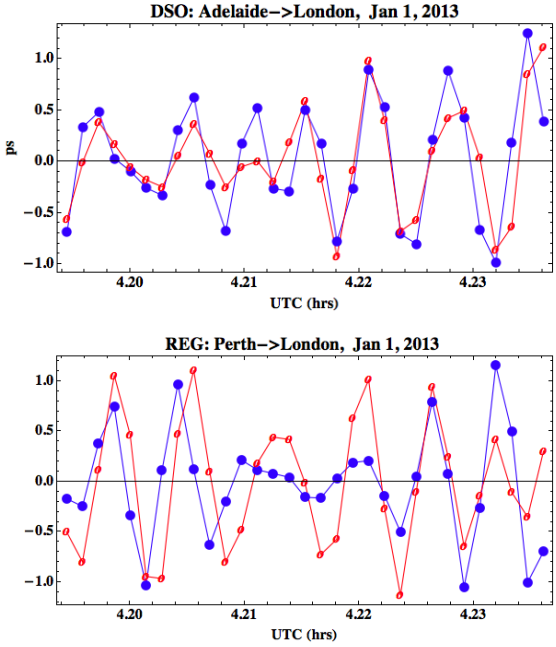

Fig. 2: Correlations in band-passed Adelaide-London DSO data (top) and Perth (Australia)-London REG data (bottom), for January 1, 2013, with London data (red, open dots) advanced by 15 s in both cases, over the same 200 s time interval. The data points are at 5 s intervals. In-phase correlations from collocated Zener Diode Detectors are shown in Fig. 7. The REG data was recorded every 1 s, and has been averaged to 5 s intervals for ease of comparison with DSO data. The data shows a quasi-periodicity of ~20 s, related to the reverberation effect [3]. The UTC time at all detectors was determined using internet timing applications, which have ms precision.

short leads. This was intended to determine the S/N ratio for the joint Adelaide-London experiment. Surprisingly the internal noise was found to be correlated, with the noise in the London DSO being some 13 to 20 seconds behind the Adelaide DSO* noise, see Fig. 2. The correlation data had a phase that tracked sidereal time, meaning that the average direction was approximately fixed wrt the galaxy, but with extensive fluctuations as well from the gravitational wave/turbulence effect, that had been seen in all previous experiments. The explanation for this DSO effect was not possible as the DSO is a complex instruments, and which component was responding to the passing space fluctuations could not be determined. But the correlation analysis did demonstrate that not all of the internal noise in the DSO was being caused solely by some random process intrinsic to the instrument. Subsequent experiments, below, now suggest that there are zener diodes within the time difference measurements hardware within the DSO.

The travel time delay $\tau(t)$ was determined by computing the correlation function

$$C(\tau,t) = \int_{t-T}^{t+T} dt' S_1(t'-\tau/2) S_2[t'+\tau/2) e^{-a(t'-t)^2} \qquad (2)$$

for the two detector signals $S_1(t)$ and $S_2(t)$. Here $2T = 200s$ is the time interval used, about UTC time t. The gaussian term ensures the absence of end-effects. Maximising $C(\tau,t)$ wrt τ gives $\tau(t)$ - the delay time vs UTC t, and plotted in Figs. 3 and 4, where the data has been binned into 1hr time intervals, and the rms also shown. The speed and direction, over a 24hr period, was determined by fitting the time delay data using

$$\tau = \frac{\mathbf{R}\cdot\mathbf{v}}{\mathbf{v}^2}, \qquad (3)$$

where $\mathbf{R}$ is the Adelaide-London spatial separation vector, and $\mathbf{v}(\theta,\delta)$ is the 3-space velocity vector, parametrised by a speed, RA and Declination. This expression assumes a plane wave form for the gravitational waves. The $\tau(t)$ delay times show large fluctuations, corresponding to fluctuations in speed and/or direction, as also seen in data in Fig. 1, and also a quasi-periodicity, as seen in Fig. 2. Then only minimal travel times, 10 s $< \tau <$ 22 s, were retained. Correlations, as shown in Fig. 2, are not always evident, and then the correlation function $C(\tau,t)$ has a low value. Only $\tau(t)$ data from high values of the correlation function were used. The absence of correlations at all times is expected as the London detector is not directly "downstream" of the Adelaide detector, and so a fractal structure to space, possessing a spatial inhomogeneity, bars continuous correlations, and as well the wave structure will evolve during the travel time. Fig. 2 shows examples of significant correlations in phase and amplitude between all four detectors, but with some mismatches. The approximate travel time of 15 s in Fig. 2 at ~4.2 hrs UTC is also apparent in Fig. 3, with the top figure showing the discovery of the correlations from the two DSO separated by a distance $R \approx 12160$ km. That the internal "noise" in these DSO is correlated is a major discovery.

There are much simpler devices that were discovered to also display time delayed correlations over large distances: these are the Random Number Generators (RNG) or Random Event Generators (REG). There are various designs available from manufacturers, and all claim that these devices manifest hardware random quantum processes, as they involve the quantum to classical transition when a measurements, say, of the quantum tunnelling of electrons through a nanotechnology potential barrier, ~10 nm thickness, is measured by a classical/macroscopic system. According to the standard interpretation of the quantum theory, the collapse of the electron wave function to one side or the other of the barrier, after the tunnelling produces a component on each side, is purely a random event, internal to the quantum system. However this interpretation had never been tested experimentally. Guided by the results from the DSO correlated-noise effect, the data

*LeCroy WaveRunner 6051A DSOs were used.

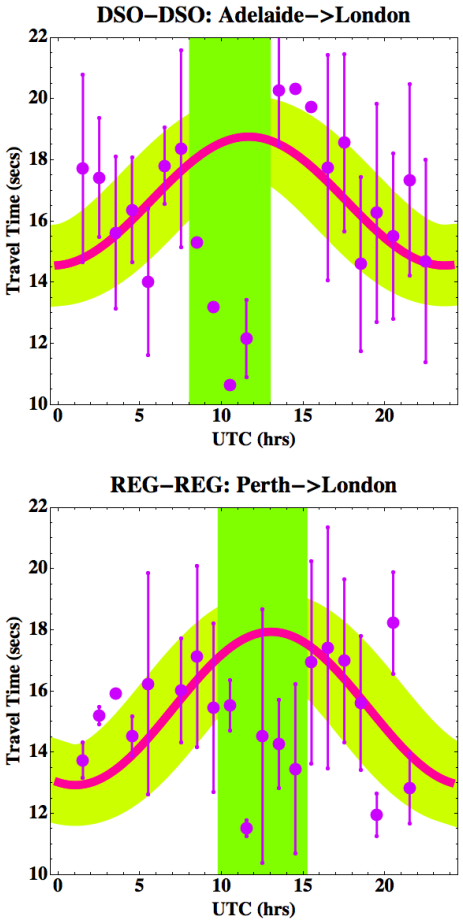

Fig. 3: Travel times from DSO-DSO Adelaide-London data (top), and REG-REG Perth-London data (bottom) from correlation analysis using (2). The data in each 1 hr interval has been binned, and the average and rms shown. The thick (red line) shows best fit to data using plane wave travel time predictor, (3), but after excluding those data points between 8 and 13 hrs UTC (top) and 10 and 15 hrs UTC (bottom), indicated by vertical band. Those data points are not consistent with the plane wave modelling, and suggest a scattering process when the waves pass deeper into the earth, see Fig. 5. The Perth-London phase is retarded wrt Adelaide-London phase by ~1.5 hrs, consistent with Perth being 1.5 hrs west of Adelaide. The Adelaide-London data gives speed = 512 km/s, RA = 4.8 hrs, Dec = 83°S, and the Perth-London data gives speed = 528 km/s, RA = 5.3 hrs, Dec = 81°S. The broad band tracking the best fit line is for ±1 sec fluctuations, corresponding to speed fluctuation of ±17 km/s. Actual fluctuations are larger than this, as 1st observed by Michelson-Morley and by Miller, see Fig. 1.

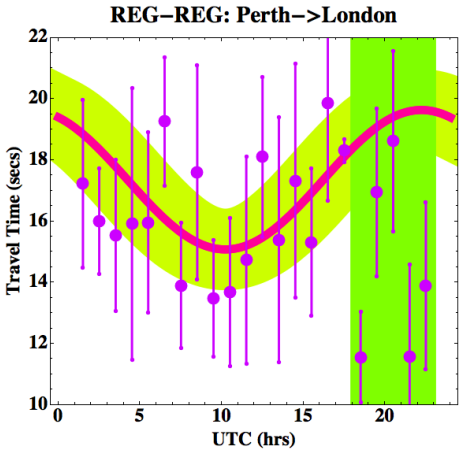

Fig. 4: Travel times from REG-REG Perth-London data for August 1, 2012. The data in each 1 hr interval has been binned, and the average and rms shown. The thick (red line) shows best fit to data using plane wave travel time predictor, (3), but after excluding those data points between 18 and 23 hrs UTC, indicated by vertical band. Those data points are not consistent with the plane wave modelling. This data gives speed = 471 km/s, RA = 4.4 hrs, Dec = 82°S. The change in phase of the maximum of the data, from UTC = 22±2 hr, for August 1, 2012, to UTC = 12±2 hr for January 2013 (Fig. 3), but with essentially the same RA, illustrates the sidereal effect: the average direction of the space flow is fixed wrt to the stars, apart from the earth-orbit aberration effect, Fig. 1.

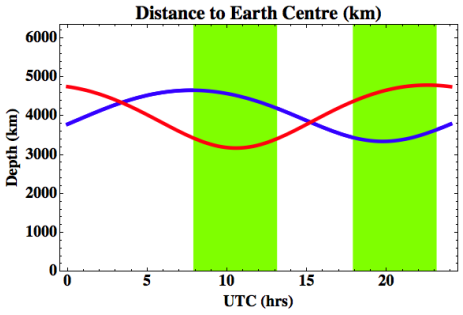

Fig. 5: Given measured space velocity, plots show maximum earth penetration depth of space detected by London detectors for Adelaide→London, Jan1, 2013 (red) and Perth→London, August 1, 2012 (blue), revealing that the anomalous scattering occurs when deeper depths are "traversed". The vertical shadings correspond to those in Fig. 3 (top) and Fig. 4.

from two REGs, located in Perth and London, was examined. The data* showed the same correlation effect as observed in the DSO experiments, see Figs. 2–4. However REGs typically employ a XOR gate that produces integer valued outputs with a predetermined statistical form. To study the zener diode tunnelling currents without XOR gate intervention two collocated zener diode circuits were used to detect highly correlated tunnelling currents, Figs. 6 and 7. When the detectors are separated by ~0.5 m, phase differences ~μs were observed and dependent on relative orientation. So this zener diode circuit forms a very simple and cheap nanotechnology quantum detector for gravitational waves.

*The data is from the GCP international network: `http://teilhard.global-mind.org/`

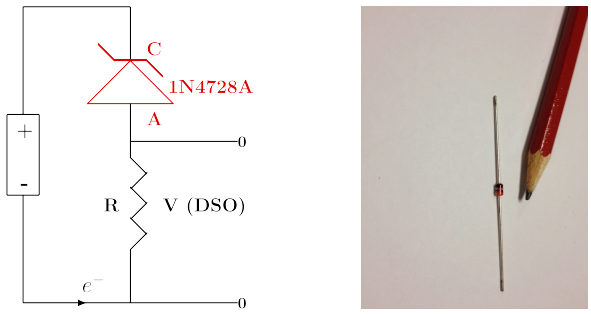

Fig. 6: Left: Circuit of Zener Diode Gravitational Wave Detector, showing 1.5 V AA battery, 1N4728A zener diode operating in reverse bias mode, and having a Zener voltage of 3.3 V, and resistor R = 10 kΩ. Voltage V across resistor is measured and used to determine the space driven fluctuating tunnelling current through the zener diode. Correlated currents from two collocated detectors are shown in Fig. 7. This design avoids data degradation from the XOR gate in commercial REGs. Right: Photo of zener diode showing size in comparison to pencil tip. The zener diode costs $0.5.

4 Dynamical 3-space gravitational waves

It is necessary to give some background to the interpretation of reported correlations as gravitational waves. Experiments and theory have suggested that space is a dynamical system:

$$\nabla\cdot\left(\frac{\partial \mathbf{v}}{\partial t}+(\mathbf{v}\cdot\nabla)\mathbf{v}\right)+\frac{5\alpha}{4}\left((trD)^2-tr(D^2)\right)+ \delta^2\nabla^2\left((trD)^2-tr(D^2)\right)+\ldots=-4\pi G\rho, \quad (4)$$

where $D_{ij}=\partial v_i/\partial x_j$ and $\rho(\mathbf{r},\mathbf{t})$ is the usual matter density. This entails a velocity field $\mathbf{v}(\mathbf{r},t)$ describing the motion of a structured 3-space relative to an observers frame of reference. This easily follows from writing Newtonian gravity in terms of a velocity field, which then permits additional terms, with coefficients α and δ. This field and its fluctuations has been repeatedly detected over some 125 years. The 1st term, the Newtonian gravity term, involves the Euler 3-space constituent acceleration, while the $\alpha-$ and $\delta-$ terms contain higher order derivative terms and describe the self interaction of space. Laboratory, geophysical and astronomical data suggest that α is the fine structure constant $\approx 1/137$, while δ appears to be a very small but non-zero Planck-like length. The emergence of gravity arises from the unique coupling of quantum theory to the 3-space, which determines the 'gravitational' acceleration of quantum matter as a quantum wave refraction effect,

$$\mathbf{g}=\frac{\partial \mathbf{v}}{\partial \mathbf{t}}+(\mathbf{v}\cdot\nabla)\mathbf{v}+(\nabla\times\mathbf{v})\mathbf{v}_\mathbf{R}-\frac{\mathbf{v}_\mathbf{R}}{1-\frac{\mathbf{v}_\mathbf{R}^2}{\mathbf{c}^2}}\frac{\mathbf{1}}{\mathbf{2}}\frac{\mathbf{d}}{\mathbf{dt}}\left(\frac{\mathbf{v}_\mathbf{R}^2}{\mathbf{c}^2}\right) \quad (5)$$

where $\mathbf{v_R}=\mathbf{v_0}-\mathbf{v}$ is the velocity of quantum matter relative to the local space. The 1st two terms are the Euler 3-space acceleration, the 2nd term explains the Lense-Thirring effect when the vorticity is non-zero, and the last term explains the precession of planetary orbits. Neglecting relativistic effects (4) and (5) give

$$\nabla\cdot\mathbf{g}=-4\pi\mathbf{G}\rho-4\pi\mathbf{G}\rho_\mathbf{DM}, \quad (6)$$

where ρ_{DM} is the α and δ term, describing a 3-space self-interaction effects, with the α term explaining the so-called 'dark matter' effects. The spatial dynamics is non-local and exhibits instantaneous effects, which points to the universe being highly connected, consistent with the deeper pre-space *Process Physics* [6]. Historically this was first noticed by Newton who called it action-at-a-distance. This shows a high degree of non-locality and non-linearity, and in particular that the behaviour of both ρ_{DM} and ρ manifest at a distance irrespective of the dynamics of the intervening space. A key implication of (6) is that observed fluctuations in $\mathbf{v}(\mathbf{r},t)$ can only generate gravitational effects via the ρ_{DM} processes. So the velocity field is more fundamental than the Newtonian gravitational acceleration field. Although not presented herein significant fluctuations in $\mathbf{v}(\mathbf{r},t)$ were observed to be correlated with solar flares, coronal mass ejections, and earthquakes. These effects suggest that the 11 year solar cycle is caused by galactic-scale larger than normal 3-space fluctuations. The delay of several days between major fluctuations and solar flares implies that the new 3-space/gravitational wave detectors may be used as an early warning system for such solar flares.

One consequence of the non-linearity of (4) is that fluctuations in $\mathbf{v}(\mathbf{r},t)$ develop reverberations [3], which are clearly apparent in the data in Fig. 2. Another implication suggested by the data is that when the 3-space fluctuations penetrate the earth the non-linearity cause the 3-space waveforms to manifest at a distance, without propagating through the intervening space, resulting in an apparent speed-up, as manifestly evident in the data – an effect that had to be taken into account in the analysis based upon a normal plane-wave like propagation, as indicated by the vertical bands in Figs. 3 and 4. The data from numerous experiments clearly shows that the so-called "gravitational waves" have observed properties very different from those commonly assumed.

5 Probability in Quantum Theory

The conventional quantum theories all have the generic form $i\hbar\partial\psi/\partial t=H\psi$, differing only by the configuration space on which ψ is based, and the Hamiltonian. The interpretation has been, as proposed by Born, that $|\psi|^2$ is the probability density for the location of a particle, which is assumed to exist apart from ψ. However missing from this generic unitary time evolution for ψ is (i) the existence of a dynamical 3-space, as distinct from the usual frame of reference, and which leads to gravity as am emergent phenomenon, and (ii) the existence of terms which model the localisation of ψ in space by a classical detector of quantum waves [5]. In [6, p. 40], it was

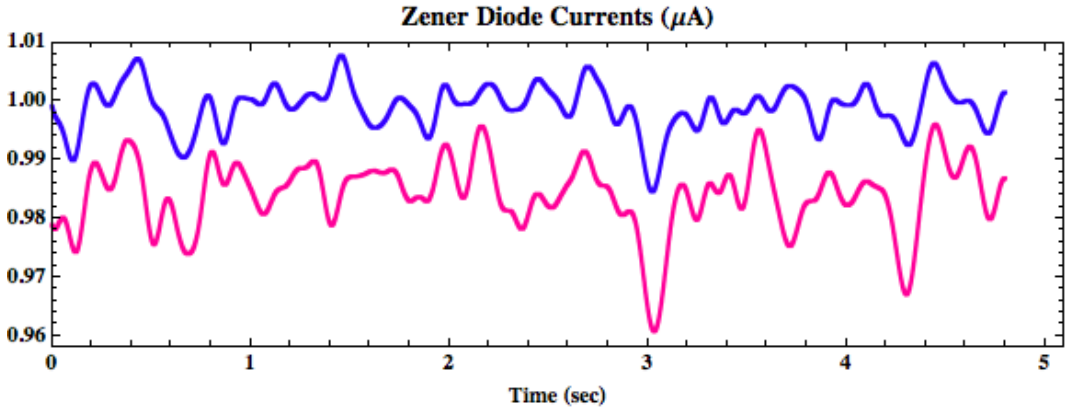

Fig. 7: Zener Diode tunnelling currents over 5 sec interval, showing higher time resolution than in Fig. 2. Band pass filter was used to remove higher frequencies. Plots have been displaced vertically for ease of viewing. The two zener diode circuits were collocated with the zener diodes separated by ~30 mm. Highly correlated currents are observed, demonstrating that the tunnelling currents are not random, as required by the conventional interpretation of quantum theory, and as 1st discovered in the Adelaide-London correlations.

argued that emergent classicality, including the ψ localisation effects, are caused by fluctuations in the 3-space. This and the present results would amount to the discovery that reality is fundamentally only quantum waves embedded in a quantum foam space, and that the classical world is an emergent macroscopic phenomenon: our reality is induced by the nature of 3-space fluctuations.

6 Conclusions

We have reported the discovery of the quantum detection of gravitational waves, showing correlations between well separated locations, that permitted the absolute determination of the 3-space velocity of some 500 km/s, in agreement with the speed and direction from a number of previous analyses, including in particular the NASA spacecraft earth-flyby Doppler shift effect. This discovery enables a very simple and cheap nanotechnology zener diode quantum gravitational wave detection technology, which will permit the study of various associated phenomena, such as solar flares, coronal mass ejections, earthquakes, eclipse effects, moon location effects, non-Poisson fluctuations in radioactivity [4], and other rate processes, and variations in radioactive decay rates related to distance of the earth from the Sun, as the 3-space fluctuations are enhanced by proximity to the sun.

Acknowledgements

This report is from the Flinders University Gravitational Wave Detector Project, funded by an Australian Research Council Discovery Grant: *Development and Study of a New Theory of Gravity*. Thanks to Professor Igor Bray for making this work possible. Thanks to GCP and its director Dr. Roger Nelson for the availability of extensive and valuable data from the REG international network:
`http://teilhard.global-mind.org/`
Thanks also to Dr. David Brotherton-Ratcliffe for providing the London DSO data and for several useful discussions.

Submitted on: September 01, 2013 / Accepted on: September 04, 2013

References

1. Cahill R.T. Combining NASA/JPL one-way optical-fiber light-speed data with spacecraft Earth-flyby Doppler-shift data to characterise 3-space flow. *Progress in Physics*, 2009, issue 4, 50–64.
2. Cahill R.T. Characterisation of low frequency gravitational waves from dual RF coaxial-cable detector: fractal textured dynamical 3-space. *Progress in Physics*, 2012, issue 3, 3–10.
3. Cahill R.T. and Deane S.T. Dynamical 3-space gravitational waves: reverberation effects. *Progress in Physics*, 2013, issue 2, 9–11.
4. Shnoll S.E. Cosmophysical Factors in Stochastic Processes. American Research Press, Rehoboth, New Mexico, USA, 2012.
5. Percival I. Quantum State Diffusion. Cambridge University Press, 1998.
6. Cahill R.T. Process Physics: From Information Theory to Quantum Space and Matter. Nova Science Pub., New York, 2005.

Atomic Weights Confirm Bipolar Model of Oscillations in a Chain System

Andreas Ries
Universidade Federal de Pernambuco, Centro de Tecnologia e Geociências, Laboratório de Dispositivos e Nanoestruturas,
Rua Acadêmico Hélio Ramos s/n, 50740-330 Recife – PE, Brazil
E-mail: andreasries@yahoo.com

We apply the bipolar model of oscillations in a chain system to the data set of standard atomic weights. 90% of these masses could be reproduced by this model and were expressed in continued fraction form, where all numerators are Euler's number and the sum of the free link and all partial denominators yields zero. All outliers were either radioactive or polynuclidic elements whose isotopic compositions as found in samples on Earth might not be fully representative for the mean values when considering samples from all parts of the universe.

1 Introduction

In several previous papers we applied the model of oscillations in a chain system to various systems such as the solar system [1], excited electronic states of atoms [2], the electron density in the Hydrogen atom [3], and more recently to the mass distribution of elementary particles [4].

Initially, this model was founded by Müller in three fundamental articles [5–7] and assumes that all protons in the universe are oscillators, coupled through the physical vacuum. As a consequence we can consider (in the most simplest case) a chain of equal harmonic proton oscillators with an associated logarithmic spectrum of eigenfrequencies which can be expressed through continued fractions. In that way, every mass is interpreted as a proton resonance state and expressed in continued fraction form.

Recently, a bipolar version of this model was proposed for the description of elementary particles [4], because the traditional version could not reproduce their masses in a fully satisfactory way. The idea of bipolarity postulates that the fundamental spectrum of proton resonances has an opposite, an anti-oscillation or inverted oscillation spectrum, and this is the spectrum of electron resonances.

Mathematically, two opposite oscillation states are characterized through equal continued fraction representations, but with the difference that in one case all denominators, the free link and the phase shift have been multiplied by (-1). From the analysis of elementary particle masses it was suggested to express the electron mass as a proton resonance and the proton mass as an electron resonance through the following equations (e is Euler's number):

$$\ln \frac{m_{electron}}{m_{proton}} = p_p + (-6) + \cfrac{e}{12 + \cfrac{e}{-6}}$$

and

$$\ln \frac{m_{proton}}{m_{electron}} = p_e + 6 + \cfrac{e}{(-12) + \cfrac{e}{6}}.$$

Numerically, p_p was found to be ≈ -1.75 [4]; for these phase shifts must hold p_p = -p_e.

In this article we show that the relative atomic masses can be reproduced by almost the same the bipolar model. The only parameter that must be adjusted is the phase shift (from $|p| \approx 1.75$ to $|p| \approx 1.79$) and this is a very minor change.

2 Data sources and computational details

The standard atomic weights, including the proton and electron reference masses were taken from the web-site of the National Institute of Standards (NIST) and were expressed in the atomic mass unit u. The following abbreviations and conventions for the numerical analysis hold:

The atomic masses are transformed into a continued fraction according to the equations

$$\ln \frac{m}{m_{electron}} = p_e + S, \qquad \ln \frac{m}{m_{proton}} = p_p + S,$$

where p is the phase shift (it must hold p_p = -p_e) and S is the continued fraction (e is Euler's number)

$$S = n_0 + \cfrac{e}{n_1 + \cfrac{e}{n_2 + \cfrac{e}{n_3 + ...}}}. \qquad (1)$$

The numerical value of the phase shift p is initially unknown and must be adjusted in such a way that the largest possible amount of atomic weights can be expressed through a continued fraction.

The continued fraction representation $p+S$ is abbreviated as $[p; n_0 \mid n_1, n_2, n_3, \dots]$, where the free link n_0 is allowed to be $0, \pm3, \pm6, \pm9 \dots$ and all partial denominators n_i can take the values $e+1, -e-1, \pm6, \pm9, \pm12 \dots$. In the tables these abbreviations were marked with P or E, in order to indicate proton or electron resonance states.

The absolute value of the difference between the atomic weight given by NIST and the atomic weight calculated from the associated continued fraction representation is defined as numerical error and listed in the tables.

An atomic weight is considered as an outlier when the corresponding continued fraction representation provides a mass value outside the interval "atomic mass ± standard deviation".

Table 1: Continued fraction representations of the 20 most accurately determined atomic weights (Helium and the set of 19 mononuclidic non-radioactive elements), x = 1.7918229 is the phase shift, SD = standard deviation.

Element symbol	Mass ± SD [u]	Continued fraction representation(s)	Numerical error [u]
He	$4.002602 \pm 2.0 \times 10^{-6}$	P [-x; 3 | 15, e+1, -6, e+1, 33, (6, -e-1, -e-1, -51)]	1.2×10^{-9}
Be	$9.0121822 \pm 4.0 \times 10^{-7}$	P [-x; 3 | e+1, -e-1, e+1, -e-1, -e-1, e+1, -6, -6, 12, (-9, 6)]	4.3×10^{-8}
F	$18.99840322 \pm 7.0 \times 10^{-8}$	E [x; 9 | -9, e+1, -e-1, e+1, -e-1, -1680, (1680)]	2.6×10^{-9}
Na	$22.9897692809 \pm 2.9 \times 10^{-9}$	E [x; 9 | -18, -9, -9, -e-1, e+1, -33, 12, (48)]	7.9×10^{-10}
Al	$26.98153863 \pm 1.2 \times 10^{-7}$	P [0; 3 | 9, 6, 18, -6, -6, e+1, 9, (-e-1, 33)]	1.2×10^{-9}
P	$30.97376163 \pm 2.0 \times 10^{-7}$	P [-x; 6 | -e-1, 12, -e-1, 6, -15, e+1, 6, (-15, e+1)] E [x; 9 | 18, 15, -18, 18, (-42)]	1.6×10^{-7} 1.1×10^{-7}
Sc	$44.9559119 \pm 9.0 \times 10^{-7}$	P [0; 3 | e+1, -9, 9, -e-1, e+1, -21, e+1, (-e-1, 18, -e-1)] E [0; 12 | -e-1, -12, e+1, -6, 126, e+1, -e-1, -120]	4.5×10^{-7} 9.1×10^{-8}
Mn	$54.9380451 \pm 7.0 \times 10^{-7}$	P [0; 3 | e+1, -e-1, e+1, -e-1, e+1, -e-1, 6, 18, e+1, -e-1, e+1, -e-1, (-27)] P [-x; 6 | -12, -e-1, e+1, -e-1, e+1, -6, 111, (-99)] E [0; 12 | -6, 6, e+1, -24, e+1, -e-1, e+1, -6, (18, -e-1, -e-1)] E [x; 9 | e+1, 63, -e-1, 6, -9, -18, (-51)]	2.2×10^{-7} 4.5×10^{-8} 1.2×10^{-8} 3.6×10^{-10}
Co	$58.9331950 \pm 7.0 \times 10^{-7}$	E [0; 12 | -6, -6, e+1, -e-1, e+1, -e-1, e+1, -e-1, 162, (-162)] E [x; 9 | e+1, -9, -6, -e-1, e+1, -24, -9, (-e-1, 39)]	5.7×10^{-8} 4.4×10^{-9}
As	$74.9215965 \pm 2.0 \times 10^{-6}$	P [-x; 6 | 27, -30, -27, (24)]	2.3×10^{-7}
Y	$88.9058483 \pm 2.7 \times 10^{-6}$	P [-x; 6 | 9, e+1, -e-1, e+1, -e-1, -102, -e-1, (87, e+1)]	5.1×10^{-7}
Nb	$92.9063781 \pm 2.6 \times 10^{-6}$	P [-x; 6 | 9, -6, -e-1, 21, e+1, -e-1, (27, e+1, -57)] E [0; 12 | 69, -e-1, -6, 18, -e-1, (-93, e+1, e+1)]	2.2×10^{-8} 6.9×10^{-7}
Rh	$102.905504 \pm 3.0 \times 10^{-6}$	P [-x; 6 | 6, 6, -6, e+1, -e-1, -6, -6, -e-1, (e+1)]	9.1×10^{-7}
I	$126.904473 \pm 4.0 \times 10^{-6}$	P [-x; 6 | e+1, e+1, e+1, -93, 6, -e-1, e+1, (-e-1, 81, -e-1, -e-1)]	3.6×10^{-7}
Cs	$132.905451933 \pm 2.4 \times 10^{-8}$	E [0; 12 | 6, e+1, -6, 99, e+1, 6, -6, (-111, -e-1, -e-1)]	1.7×10^{-8}
Pr	$140.9076528 \pm 2.6 \times 10^{-6}$	P [-x; 6 | e+1, -330, -e-1, 6, -e-1, e+1, (-12, 330)] E [0; 12 | 6, -63, -e-1, e+1, 9, -12, (48)]	4.4×10^{-8} 2.5×10^{-7}
Tb	$158.9253468 \pm 2.7 \times 10^{-6}$	P [-x; 6 | e+1, -6, e+1, -e-1, -6, 525, (-519, -e-1)]	5.8×10^{-8}
Ho	$164.9303221 \pm 2.7 \times 10^{-6}$	P [0; 6 | -e-1, e+1, 18, e+1, -6, 6, 75, (-99, -e-1)]	5.2×10^{-9}
Tm	$168.9342133 \pm 2.7 \times 10^{-6}$	P [0; 6 | -e-1, e+1, e+1, 6, 6, 6, 12, (15, -e-1, -51)]	3.2×10^{-9}
Au	$196.9665687 \pm 6.0 \times 10^{-7}$	P [0; 6 | -e-1, -78, e+1, e+1, 6, -e-1, e+1, (15, -e-1, 51)] E [0; 12 | e+1, -9, -e-1, -e-1, -15, e+1, 6, -e-1, e+1, -e-1, (e+1, 6)]	7.1×10^{-9} 4.6×10^{-7}

3 Results and discussion

It can be easily verified that the standard Müller model with the phase shifts p = 0 and p = 1.5 does not apply at all to the relative atomic weights, while the bipolar model with phase shifts of approximately ± 1.75 (as used in a previous study [4]) produces around 30% outliers. When working with the complete data set, varying the phase shift does not lead to a clear result. In that case we obtain a wealth of slightly different phase shifts, all providing a quite similar number of outliers and a similar sum of squared residuals (sum of squared numerical errors).

In order to arrive at a conclusion, the data set of 84 atomic masses was divided into two parts. The first part is composed of the element Helium (two stable isotopes, but still very low standard deviation) and the set of 19 non-radioactive mononuclidic elements. Here, the maximum measurement error is 2.7×10^{-6} u. The second part consists of the remaining elements; their standard deviations vary from $\sim 10^{-5}$ to 0.1 u (Pb) due to isotopic variations found in samples taken at different locations on Earth.

It is fact that the "mean atomic mass" of a mononuclidic element is everywhere in the universe exactly the same, while we would expect some variations in the atomic masses of polynuclidic elements when analyzing rock samples obtained from different galaxies. It is reasonable to assume that the conditions during the formation of the chemical elements were subjected to variations throughout the universe.

Therefore we give priority to the atomic masses of the mononuclidic chemical elements and only the first part of the data set has been analyzed thoroughly. The phase shift was adjusted in such a way that (a) the number of outliers, and (b) the sum of squared residuals are minimized. This leads to a phase shift of ≈ 1.79 (exact value is 1.7918229) which is close to ln(6). Table 1 lists these atomic masses together with

Table 2: Continued fraction representations of the atomic weights of polynuclidic elements, from H to Kr (except He), x = 1.7918229 is the phase shift, SD = standard deviation.

Element symbol	Mass ± SD [u]	Continued fraction representation(s)	Numerical error [u]
H	$1.00794 \pm 7 \times 10^{-5}$	P [0; 0 | 4128, (-4128)] E [x; 6 | -9, e+1, 6, -e-1, e+1, -e-1, e+1, (-e-1, 9, -12)]	2.5×10^{-8} 5.9×10^{-5}
Li	$6.941 \pm 2 \times 10^{-3}$	P [-x; 3 | e+1, 57, (e+1, -e-1, -e-1, -60)] E [0; 9 | 6, 27, (-42)]	5.5×10^{-4} 4.9×10^{-4}
B	$10.811 \pm 7 \times 10^{-3}$	P [0; 3 | -e-1, -e-1, -e-1, -9, (e+1, 6, e+1, e+1)] E [0; 9 | e+1, -e-1, -6, -e-1, (21, -24, e+1)] E [x; 9 | -e-1, e+1, 24, (-33)]	2.0×10^{-4} 5.5×10^{-5} 3.5×10^{-3}
C	$12.0107 \pm 8 \times 10^{-4}$	E [0; 9 | e+1, -e-1, e+1, -e-1, e+1, e+1, -6, (e+1, -9, 6, -e-1, -e-1, -e-1)] E [x; 9 | -e-1, 9, -9, -e-1, e+1, (-9, e+1)]	1.4×10^{-6} 6.8×10^{-4}
N	$14.0067 \pm 2 \times 10^{-4}$	E [x; 9 | -e-1, -6, e+1, e+1, -e-1, 9, (-12)]	6.2×10^{-5}
O	$15.9994 \pm 3 \times 10^{-4}$	P [0; 3 | -12, 6, 6, -e-1, (-e-1, 6, -9, e+1, e+1)]	9.0×10^{-7}
Ne	$20.1797 \pm 6 \times 10^{-4}$	P [0; 3 | -1056, (1053)] E [x; 9 | -9, -e-1, 42, (-42, e+1)]	2.3×10^{-5} 1.6×10^{-5}
Mg	$24.3050 \pm 6 \times 10^{-4}$	P [0; 3 | 15, -15, (-138, 135)] E [x; 9 | -30, e+1, -18, (-e-1, 39)]	8.4×10^{-9} 8.7×10^{-5}
Si	$28.0855 \pm 3 \times 10^{-4}$	P [0; 3 | 9, -e-1, -27, -e-1, e+1, (15, e+1)] P [-x; 6 | -e-1, e+1, e+1, e+1, -6, 18, (-e-1, -18, -e-1)]	2.7×10^{-4} 2.1×10^{-5}
S	$32.065 \pm 5 \times 10^{-3}$	P [0; 3 | 6, -27, -e-1, (e+1, 18)] P [-x; 6 | -e-1, 33, (-33, -6, e+1)] E [x; 9 | 15, -12, (6, -18)]	3.1×10^{-4} 1.4×10^{-5} 2.7×10^{-4}
Cl	$35.453 \pm 2 \times 10^{-3}$	E [0; 12 | -e-1, e+1, -12, -e-1, 6, (-6, e+1)]	9.1×10^{-5}
Ar	$39.948 \pm 1 \times 10^{-3}$	P [0; 3 | e+1, 9, e+1, -9, e+1, (-e-1, 6, -e-1, -e-1, -9)] P [-x; 6 | -6, e+1, -6, e+1, -12, (18, -e-1, -e-1)] E [0; 12 | -e-1, 9, -e-1, e+1, -e-1, (-21, e+1, e+1)] E [x; 9 | 6, e+1, 348, (-e-1, -363)]	4.3×10^{-7} 6.8×10^{-4} 3.9×10^{-4} 2.0×10^{-5}
K [Outlier]	$39.0983 \pm 1 \times 10^{-4}$	P [0; 3 | e+1, 6, e+1, 9, -e-1, e+1, -e-1, e+1, -e-1]	6.3×10^{-4}
Ca	$40.078 \pm 4 \times 10^{-3}$	P [-x; 6 | -6, e+1, -6, -e-1, 6] E [0; 12 | -e-1, 9, -e-1, -e-1, -e-1, (-21, e+1, e+1, e+1, e+1)] E [x; 9 | 6, e+1, 9, (-24, -e-1)]	1.1×10^{-3} 1.3×10^{-4} 8.0×10^{-4}
Ti	$40.078 \pm 1 \times 10^{-3}$	E [0; 12 | -e-1, -e-1, -6, e+1, 45, (-51, e+1)] E [x; 9 | e+1, e+1, -e-1, 9, (-23202, -e-1, 23184)]	1.2×10^{-5} 6.8×10^{-12}
V [Outlier]	$50.9415 \pm 1 \times 10^{-4}$	P [0; 3 | e+1, -e-1, 12, e+1, -e-1, e+1, -e-1, e+1, -e-1]	4.7×10^{-4}
Cr	$51.9961 \pm 6 \times 10^{-4}$	P [0; 3 | e+1, -e-1, 6, -9, -12, (12)] E [0; 12 | -6, e+1, -e-1, e+1, -15, e+1, (-e-1, 9, -e-1)]	1.8×10^{-5} 3.4×10^{-5}
Fe	$55.845 \pm 2 \times 10^{-3}$	P [-x; 6 | -15, e+1, -e-1, -30, (39)] E [0; 9 | e+1, -69, 6, (54, -e-1)]	1.6×10^{-4} 2.4×10^{-4}
Ni	$58.6934 \pm 4 \times 10^{-4}$	P [-x; 6 | -18, -e-1, e+1, -e-1, e+1, -e-1, (12, e+1)] E [0; 12 | -6, -6, 9, -e-1, e+1, (-9)]	2.9×10^{-4} 3.9×10^{-4}
Cu	$63.546 \pm 3 \times 10^{-3}$	P [-x; 6 | -42, -e-1, -15, (51, e+1)] E [x; 9 | e+1, -e-1, -e-1, e+1, -75, (66)]	8.5×10^{-5} 7.5×10^{-5}
Zn	$65.38 \pm 2 \times 10^{-2}$	P [-x; 6 | -78, e+1, (-e-1, 72)] E [0; 12 | -9, 9, e+1, (-e-1, -12)] E [x; 9 | e+1, -e-1, -12, e+1, (-21, 24, -e-1)]	3.4×10^{-3} 4.4×10^{-3} 9.8×10^{-5}
Ga	$69.723 \pm 1 \times 10^{-3}$	P [-x; 6 | 93, 6, e+1, (-105, -e-1)] E [x; 9 | e+1, -e-1, e+1, 6, e+1, -e-1, e+1, -e-1, (-e-1, -15)]	3.3×10^{-5} 4.5×10^{-6}
Ge	$72.64 \pm 1 \times 10^{-2}$	P [-x; 6 | 39, -12, (-33)]	1.1×10^{-3}
Se	$78.96 \pm 3 \times 10^{-2}$	P [-x; 6 | 18, -9, (-15)]	2.1×10^{-3}
Br	$79.904 \pm 1 \times 10^{-3}$	E [0; 12 | -24, -6, 6, (12)]	4.4×10^{-4}
Kr	$83.798 \pm 2 \times 10^{-3}$	P [-x; 6 | 12, e+1, -18, (6, -e-1, -6)] E [0; 12 | -42, -e-1, e+1, e+1, (-e-1, 30)]	3.4×10^{-5} 2.3×10^{-4}

Table 3: Continued fraction representations of the atomic weights of polynuclidic elements, from Rb to Os, x = 1.7918229 is the phase shift, SD = standard deviation.

Element symbol	Mass ± SD [u]	Continued fraction representation(s)	Numerical error [u]
Rb	$85.4678 \pm 3 \times 10^{-4}$	P [-x; 6 | 12, -9, 6, -6, -e-1, (-9, e+1)] E [0; 12 | -63, e+1, -15, (66, -e-1)]	2.3×10^{-4} 2.1×10^{-4}
Sr	$87.62 \pm 1 \times 10^{-2}$	E [0; 12 | -144, (132)]	5.8×10^{-3}
Zr	$91.224 \pm 2 \times 10^{-3}$	P [-x; 6 | 9, 21, e+1, (-36, -e-1)] E [0; 12 | 126, 6, (-144)]	2.8×10^{-4} 4.6×10^{-5}
Mo [Outlier]	$95.96 \pm 2 \times 10^{-2}$	E [0; 12 | 39, -e-1, e+1, -e-1, e+1]	5.7×10^{-2}
Ru	$101.07 \pm 2 \times 10^{-2}$	P [-x; 6 | 6, e+1, -9, -e-1, (6, -9)] E [0; 12 | 21, e+1, -e-1, (12, -45)]	3.5×10^{-3} 8.6×10^{-4}
Pd	$106.42 \pm 1 \times 10^{-2}$	P [-x; 6 | 6, 189, (6, -207)] E [0; 12 | 15, 6, -6, (-27)]	1.5×10^{-5} 8.2×10^{-3}
Ag [Outlier]	$107.8682 \pm 2 \times 10^{-4}$	E [0; 12 | 15, -e-1, -e-1, -6, e+1, -e-1, e+1, -e-1]	3.3×10^{-4}
Cd [Outlier]	$112.411 \pm 8 \times 10^{-3}$	E [0; 12 | 12, -15, e+1, -e-1, e+1, -e-1]	1.1×10^{-2}
In	$114.818 \pm 3 \times 10^{-3}$	P [-x; 6 | 6, -e-1, 6, -e-1, 6, e+1, (-24, e+1)]	2.5×10^{-3}
Sn	$118.710 \pm 7 \times 10^{-3}$	E [0; 12 | 9, 6, -e-1, e+1, -e-1, e+1, (-27)]	1.5×10^{-5}
Sb	$121.760 \pm 1 \times 10^{-3}$	P [-x; 6 | e+1, e+1, -e-1, 30, 6, (-42, -e-1)] E [0; 12 | 9, -12, e+1, e+1, -e-1, e+1, (-e-1, -9, -e-1)]	8.6×10^{-5} 6.3×10^{-4}
Te [Outlier]	$127.60 \pm 3 \times 10^{-2}$	P [-x; 6 | e+1, e+1, e+1, -e-1, e+1, -e-1, e+1]	7.2×10^{-2}
Xe [Outlier]	$131.293 \pm 6 \times 10^{-3}$	P [-x; 6 | e+1, 6, e+1, -e-1, e+1, -e-1, e+1, -e-1]	1.1×10^{-2}
Ba	$137.327 \pm 7 \times 10^{-3}$	P [-x; 6 | e+1, 21, 6, (-33, -e-1)] E [0; 12 | 6, 9, -9, e+1, (-18, -e-1)]	4.9×10^{-3} 8.9×10^{-4}
La	$138.90547 \pm 7 \times 10^{-5}$	P [-x; 6 | e+1, 42, -e-1, -e-1, -6, (-42, e+1)]	3.1×10^{-5}
Ce	$140.116 \pm 1 \times 10^{-3}$	P [-x; 6 | e+1, 132, 6, (-e-1, -144)] E [0; 12 | 6, 84, e+1, -e-1 (-102)]	5.8×10^{-4} 8.1×10^{-4}
Nd	$144.242 \pm 3 \times 10^{-3}$	E [0; 12 | 6, -9, e+1, -6, (9, -e-1, -12)]	8.9×10^{-4}
Sm	$150.36 \pm 2 \times 10^{-2}$	P [0; 6 | -e-1, e+1, -e-1, e+1, -e-1, -e-1, (-18, 12, e+1, e+1)] P [-x; 6 | e+1, -9, 12, (-e-1, -9)]	1.9×10^{-4} 2.8×10^{-3}
Eu	$151.964 \pm 1 \times 10^{-3}$	P [0; 6 | -e-1, e+1, -e-1, e+1, e+1, -6, (-69, -e-1, 69)] E [0; 12 | 6, -e-1, e+1, 6, e+1, -24, (-e-1)]	8.3×10^{-6} 8.7×10^{-5}
Gd	$157.25 \pm 3 \times 10^{-2}$	P [0; 6 | -e-1, e+1, -6, e+1, -e-1, e+1, (9, -e-1, -9)] P [-x; 6 | e+1, -6, 6, -12, (-e-1, 6)]	9.7×10^{-4} 1.2×10^{-3}
Dy	$162.500 \pm 1 \times 10^{-3}$	P [-x; 6 | e+1, -e-1, -e-1, -45, (e+1, 39)] E [0; 12 | e+1, e+1, -6, -e-1, -9, -e-1, e+1, (-e-1, 9, -6)]	5.0×10^{-4} 7.4×10^{-4}
Er	$167.259 \pm 3 \times 10^{-3}$	P [0; 6 | -e-1, e+1, 6, 6, e+1, (-18, -e-1)] P [-x; 6 | e+1, -e-1, -27, 30, (-9)] E [0; 12 | e+1, e+1, e+1, 63, (-e-1, -75, -e-1, -e-1)]	3.8×10^{-4} 1.3×10^{-4} 2.0×10^{-4}
Yb	$173.054 \pm 5 \times 10^{-3}$	P [0; 6 | -e-1, 6, -e-1, e+1, (222, e+1, -234)] P [-x; 6 | e+1, -e-1, 6, e+1, 9, e+1, (-e-1, -e-1, -21)] E [0; 12 | e+1, 6, e+1, -e-1, e+1, -e-1, -e-1, (-18)]	1.5×10^{-5} 8.6×10^{-4} 1.0×10^{-3}
Lu	$174.9668 \pm 1 \times 10^{-4}$	P [0; 6 | -e-1, 6, -6, 9, -e-1, e+1, e+1, (-15)] P [-x; 6 | e+1, -e-1, 6, -e-1, e+1, -6, -e-1, e+1, -e-1, (-6, e+1)]	1.4×10^{-5} 7.3×10^{-5}
Hf	$178.49 \pm 2 \times 10^{-2}$	P [-x; 6 | e+1, -e-1, e+1, -48, (-e-1, 42)]	1.9×10^{-3}
Ta	$180.94788 \pm 2 \times 10^{-5}$	E [0; 12 | e+1, 21, -39, -6, (-e-1, 12)]	1.1×10^{-5}
W	$183.84 \pm 1 \times 10^{-2}$	P [0; 6 | -e-1, 9, 9, -e-1, (e+1, -24, e+1)] P [-x; 6 | e+1, -e-1, e+1, -e-1, e+1, -e-1, 15, (-21)] E [0; 12 | e+1, 60, (-72, -e-1)]	3.4×10^{-3} 2.3×10^{-3} 1.8×10^{-3}
Re	$186.207 \pm 1 \times 10^{-3}$	P [0; 6 | -e-1, 12, -6, -12, (e+1)] E [0; 12 | e+1, -135, (123, -e-1)]	1.2×10^{-4} 5.8×10^{-4}
Os	$190.23 \pm 3 \times 10^{-2}$	E [0; 12 | e+1, -21, -e-1, (9)]	3.6×10^{-3}

Table 4: Continued fraction representations of the atomic weights of polynuclidic and radioactive elements, from Ir to U, x = 1.7918229 is the phase shift, SD = standard deviation.

Element symbol	Mass ± SD [u]	Continued fraction representation(s)	Numerical error [u]
Ir	$192.217 \pm 3 \times 10^{-3}$	E [0; 12 | e+1, -15, -e-1, -9, -e-1, (e+1, 12)]	1.1×10^{-3}
Pt	$195.084 \pm 9 \times 10^{-3}$	P [0; 6 | -e-1, 195, (-201, e+1)] E [0; 12 | e+1, -12, e+1, 15, (-e-1, -e-1, -15)]	1.9×10^{-3} 4.2×10^{-4}
Hg	$200.59 \pm 2 \times 10^{-2}$	P [0; 6 | -e-1, -21, 6, (e+1, 9)]	1.6×10^{-3}
Tl	$204.3833 \pm 2 \times 10^{-4}$	P [0; 6 | -e-1, -12, 6, -e-1, e+1, e+1] E [0; 12 | e+1, -6, -12, 6, e+1, -e-1, (-e-1)] E [x; 12 | -e-1, e+1, -e-1, -12, -27, (27, e+1)]	1.9×10^{-4} 5.4×10^{-5} 7.9×10^{-5}
Pb	207.2 ± 0.1	P [0; 6 | -e-1, -9, 6, (12, -15, e+1)] E [0; 12 | e+1, -6, 6, (27, -39, -e-1)] E [x; 12 | -e-1, e+1, -6, e+1, -e-1, e+1, -e-1 (-6)]	1.4×10^{-3} 8.4×10^{-5} 6.8×10^{-2}
Bi [Outlier]	$208.98040 \pm 1 \times 10^{-5}$	E [0; 12 | e+1, -6, e+1, -9, -e-1, -e-1, 6, e+1, -e-1, e+1, -e-1]	1.8×10^{-5}
Pa	$231.03588 \pm 2 \times 10^{-5}$	E [x; 12 | -e-1, 6, -6, -e-1, -e-1, -18, -6, (e+1, e+1, e+1, 12)]	1.2×10^{-6}
Th	$232.03806 \pm 2 \times 10^{-5}$	E [0; 12 | e+1, -e-1, e+1, e+1, -9, e+1, e+1, -9, e+1, -e-1 (6, -e-1, -e-1, -e-1, -e-1)] E [x; 12 | -e-1, 6, -12, -e-1, 6, 6, -e-1 (9, e+1, e+1, e+1, -27)]	1.7×10^{-5} 5.0×10^{-7}
U	$238.02891 \pm 3 \times 10^{-5}$	E [0; 12 | e+1, -e-1, e+1, -6, e+1, e+1, -e-1, -15, (-e-1, -e-1, 9)]	1.8×10^{-5}

the corresponding continued fraction representations and the numerical errors. As it can be seen, no outlier is present.

Moreover, many continued fractions show the effect of successively canceling denominators. For instance, the continued fraction representation for Be, as calculated by the computer is: P [-x; 3 | e+1, -e-1, e+1, -e-1, -e-1, e+1, -6, -6, 12, (-6, -360, ...)]. The denominators in brackets are not required to obtain a mass value inside the interval "atomic mass ± SD". Through a minimal manipulation, we obtain a zero sum of all denominators and the free link, without significantly changing the value of the fraction: P [-x; 3 | e+1, -e-1, e+1, -e-1, -e-1, e+1, -6, -6, 12, (-9, 6)]. As this procedure can be applied in a similar way to all elements, we demonstrate this and opted to express all continued fractions as a zero sum. Only redundant denominators (given in brackets) were manipulated to achieve the zero sums.

In a second step, the so-adjusted model was tested against the remaining 64 chemical elements. Only eight outliers were found (K, V, Mo, Ag, Cd, Te, Xe, Bi [radioactive]). Tables 2 to 4 show the results; for outliers, the best possible continued fraction is displayed (not as a zero sum), and it can be seen that in most cases the atomic mass is reproduced with a numerical error very little higher than the standard deviation.

4 Conclusions

The relative atomic masses are now the second data set that can be described by the bipolar model of oscillations in a chain system. In total, 10% outliers were found which might be attributed to the fact that the isotopic compositions of these outlier elements as found here on Earth are not good representatives for the true mean compositions when considering samples from distant parts of the universe.

Anyway, it is important to note that all mononuclidic elements can be described perfectly by this model.

Acknowledgments

The author greatly acknowledges the financial support from the Brazilian governmental funding agencies FACEPE and CNPq.

Submitted on September 11, 2013 / Accepted on September 15, 2013

References

1. Ries A. and Fook M.V.L. Application of the model of oscillations in a chain system to the solar system. *Progress in Physics*, 2011, v. 7(1), 103–111.
2. Ries A. and Fook M.V.L. Excited electronic states of atoms described by the model of oscillations in a chain system. *Progress in Physics*, 2011, v. 7(4), 20–24.
3. Ries A. The radial electron density in the Hydrogen atom and the model of oscillations in a chain system. *Progress in Physics*, 2012, v. 8(3), 29–34.
4. Ries A. A bipolar model of oscillations in a chain system for elementary particle masses. *Progress in Physics*, 2012, v. 8(4), 20–28.
5. Müller H. Fractal scaling Models of resonant oscillations in chain systems of harmonic oscillators. *Progress in Physics*, 2009, v. 5(2), 72–76.
6. Müller H. Fractal scaling models of natural oscillations in chain systems and the mass distribution of the celestial bodies in the solar system. *Progress in Physics*, 2010, v. 6(1), 62–66.
7. Müller H. Fractal scaling models of natural oscillations in chain systems and the mass distribution of particles. *Progress in Physics*, 2010, v. 6(3), 61–66.

Laboratory Instrument for Detecting the Earth's Time-Retarded Transverse Vector Potential

Joseph C. Hafele

Retired Physicist, Home Office: 618 S. 24th St., Laramie, WY, USA. E-mail: cahafele@bresnan.net

This article provides the basic design for a laboratory instrument that may detect the Earth's time-retarded transverse vector potential [Hafele J.C. *Zelm. Jour.*, 2012, v.5, 134]. The instrument is based on the compound pendulum used by N.A. Kozyrev to measure the change in weight of a suspended aircraft navigation gyroscope [Kozyrev N.A. *Zelm. Jour.*, 2012, v.5, 188]. If such an instrument is developed to measure the strength of the Earth's vector potential with a precision of about 1 part in 1000, the neoclassical causal theory can be worked backwards to calculate the speed of the Earth's gravitational field.

Introduction

A new causal version for Newtonian gravitational theory has been shown to explain exactly the six Earth flyby anomalies reported by NASA in 2008, and also explain exactly an overlooked lunar orbit anomaly [1, 2]. The new causal theory, which retains the traditional acausal radial component, requires in addition a small time-retarded transverse component for the Earth's gravitational field. The new transverse component is orthogonal to the traditional radial component and is directed along the east-west direction. It is well-known that the traditional radial component can be derived from the gradient of a scalar potential. However, the time-retarded transverse component can be derived only from the curl of a vector potential. The formula for the vector potential will be found by using Stoke's theorem. The resulting vector potential is directed along the north-south direction. The north-south component of the gravitational field is given by the time-derivative of the vector potential. By using an analogous Lorentz force law, it will be shown that a small time-dependent radial component is created by induction from the north-south gravitational field. This small induced radial component can slightly change the weight of a suspended gyroscope. By measuring the change in weight, the neoclassical causal theory can be worked backwards to deduce the strength of the vector potential, and thereby indirectly measure the speed of the Earth's gravitational field.

More than 60 years ago [3], N.A. Kozyrev used the causality principle to predict the need for a second universal velocity, one that is to be associated with rotational motion [4]. He designates c_2 as the speed for this second universal velocity. He developed a theory that suggests that the numerical value for c_2 should be related to the fine structure constant [5]. In electrostatic cgs units, the unit of electric charge is the statcoulomb.

The formula for the fine-structure constant, designated by α, in cgs electrostatic units, becomes [5]

$$\alpha = \frac{2\pi}{c}\frac{e^2}{h} \cong \frac{1}{137}, \qquad (1)$$

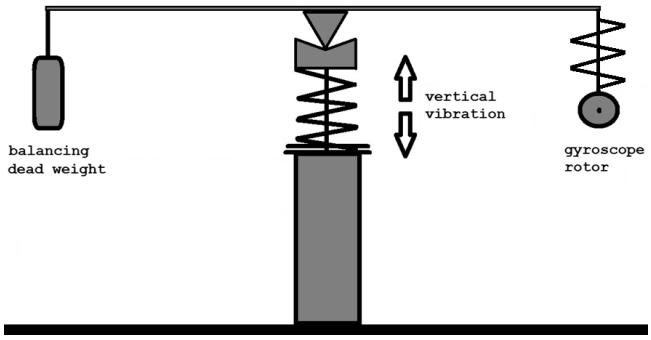

Fig. 1: Schematic of the compound pendulum developed by N.A. Kozyrev to measure a change in the weight of a gyroscope suspended from a balanced cross beam [6]. The preferred orientation of the cross beam appears to have been along the north/south direction, and that for the rotational axis of the gyroscope's rotor along the east/west direction. In some cases a weight change was detected by a small steady imbalance in the cross beam.

where c is the well-known speed of light in vacuum, e is the electronic charge in statcoulombs, and h is Plank's constant. The numerical value for the ratio e^2/h is 350 km/s. Kozyrev found by experiment that $c_2 \cong 700\,\text{km/s} = 2e^2/h = c/430 = \alpha c/\pi$.

A schematic for the compound pendulum developed by N.A. Kozyrev to measure c_2 is shown in Fig. 1 [6]. Kozyrev found that the weight of the gyroscope under certain conditions would change when there is a vertical vibration of the cross arm. Sometimes he observed a relative weight change on the order of 10^{-5}.

The objective of *this article* is to derive the effects of the neoclassical causal theory on a suspended gyroscope. We will find that the weight changes observed by N.A. Kozyrev may have been caused by the causal version of Newton's theory.

Parameter values and basis vectors

Numerical values for various parameters will be needed. Let m be the mass of the gyroscope's rotor, let R be its radius,

let ω_{rot} be its angular speed, let P_{rot} be the rotational period, let I_{rot} be the moment of inertia, let $\boldsymbol{J}_{rot}$ be the angular momentum vector, and let E_{rot} be the rotational energy. Typical numerical values for the parameters of an aircraft navigation gyroscope are [4]

$$\begin{aligned} &m = 0.1 \text{ kg},\\ &R = 2\times 10^{-2} \text{ m},\\ &\omega_{rot} = 2\pi 500 \text{ rad/s} = 3.14\times 10^{3} \text{ rad/s},\\ &P_{rot} = 2\pi/\omega_{rot} = 2\times 10^{-3} \text{ s},\\ &I_{rot} = mR^2 = 4\times 10^{-5} \text{ kg}\times\text{m}^2,\\ &J_{rot} = I_{rot}\omega_{rot} = 0.126 \text{ kg}\times\text{m}^2/s,\\ &E_{rot} = \frac{1}{2} I_{rot}\omega_{rot}^2 = 197 \text{ kg}\times m^2/s^2. \end{aligned} \tag{2}$$

Let the Earth be simulated by a spinning isotropic sphere of radius r_E, mass M_E, sidereal spin angular speed Ω_E, equatorial surface speed v_{eq}, moment of inertia I_E, surface gravitational scalar potential φ_E, surface gravitational field g_E, spin energy E_E, and spin angular momentum $\boldsymbol{J}_E$. Numerical values for the Earth's parameters are [1]

$$\begin{aligned} &G = 6.6732\times 10^{-11} \text{ N}\times\text{m}^2/\text{kg}^2,\\ &r_E = 6.37\times 10^{6} \text{ m},\\ &M_E = 5.98\times 10^{24} \text{ kg},\\ &\Omega_E = 7.29\times 10^{-5} \text{ rad/s},\\ &\mathrm{v}_{eq} = r_E\Omega_E = 4.65\times 10^{2} \text{ m/s},\\ &I_E = 8.02\times 10^{37} \text{ kg}\times\text{m}^2,\\ &\varphi_E = \frac{GM_E}{r_E} = 6.26\times 10^{7} \text{ m}^2/\text{s}^2,\\ &g_E = \frac{GM_E}{r_E^2} = 9.83 \text{ m/s}^2,\\ &E_E = \frac{1}{2} I_E\Omega_E^2 = 2.13\times 10^{29} \text{ kg}\times\text{m}^2/\text{s}^2,\\ &J_E = I_E\Omega_E = 5.85\times 10^{33} \text{ kg}\times\text{m}^2/\text{s}. \end{aligned} \tag{3}$$

Let (X, Y, Z) be the rectangular coordinates for an inertial frame-of-reference, let the Earth's center be at the origin, let the (X, Y) plane coincide with the equatorial plane, and let the axis of rotation coincide with the Z-axis. Let $\mathbf{e}_X$ be a unit vector directed outwardly along the X-axis, let $\mathbf{e}_Y$ be a unit vector directed outwardly along the Y-axis, and let $\mathbf{e}_Z$ be a unit vector directed outwardly along the Z-axis.

Let the spherical coordinates for an exterior field-point be (r,ϕ,λ), where r is the geocentric radial distance, ϕ is the azimuthal angle, and λ is the geocentric latitude. Let $\mathbf{e}_r$ be a unit vector directed upward along $\boldsymbol{r}$, let $\mathbf{e}_\phi$ be a unit vector directed towards the east, and let $\mathbf{e}_\lambda$ be a unit vector directed towards the north. The triad $(\mathbf{e}_r, \mathbf{e}_\phi, \mathbf{e}_\lambda)$ forms the basis for a right-handed system of orthogonal spherical coordinates.

Effects of a vertical vibration of a suspended gyroscope

Let the field-point be at the center of the rotor of an aircraft navigation gyroscope. Let λ be the geocentric latitude for the gyroscope. Let h be the rotor's height above the Earth's surface, let h_0 be a constant altitude, let h_1 be the vibration amplitude, and let ω_h be the angular speed for a vertical vibration. Then

$$h = h_0 + h_1\cos\omega_h t. \tag{4}$$

The time dependent geocentric radial distance becomes

$$r = r_E\left(1 + \frac{h_0}{r_E} + \frac{h_1}{r_E}\cos(\omega_h t)\right). \tag{5}$$

Let r_ϕ be the rotor's geocentric radius of gyration

$$r_\phi = r_E\cos\lambda\left(1 + \frac{h_0}{r_E} + \frac{h_1}{r_E}\cos(\omega_h t)\right). \tag{6}$$

Let $\mathbf{v}$ be the rotor's vector inertial velocity

$$\mathbf{v} = \mathbf{e}_r\mathrm{v}_r + \mathbf{e}_\phi\mathrm{v}_\phi + \mathbf{e}_\lambda\mathrm{v}_\lambda. \tag{7}$$

The formulas for v_r and v_ϕ are

$$\begin{aligned} &\mathrm{v}_r = \frac{dr}{dt} = -h_1\omega_h\sin(\omega_h t),\\ &\mathrm{v}_\phi = r_\phi\Omega_\phi = r_E\Omega_E\cos\lambda\left(1 + \frac{h_0}{r_E} + \frac{h_1}{r_E}\cos(\omega_h t)\right). \end{aligned} \tag{8}$$

Let E_r be the radial energy. If the radial energy is *constant*, then

$$\begin{aligned} constant = E_r &= \frac{1}{2} mv_r^2 - mg_E h =\\ &= \frac{1}{2} mh_1^2\omega_h^2\sin^2(\omega_h t) - mg_E(h_0 + h_1\cos(\omega_h t)). \end{aligned} \tag{9}$$

By using a trig identity for $\sin^2(\omega_h t)$, the time independent part of (9) becomes

$$constant = \frac{1}{4} mh_1^2\omega_h^2 - mg_E h_0. \tag{10}$$

Suppose a gyroscope is suspended by a spring of unstretched length ℓ_0 and spring constant k, as depicted in Fig. 2. Suppose the upper end of the spring is connected to a vibrator which can produce a time-dependent supporting force.

$$F_{up} = W + mh_{vib}\omega_{vib}^2\cos(\omega_{vib} t), \tag{11}$$

where W is the weight of the gyroscope. If the vibrator is turned off, $h_{vib} = 0$. In this case, the upper end of the spring is attached to a fixed solid point, and the system becomes a simple undriven harmonic oscillator.

Let $\delta\ell_0$ be the stretch of the spring when the gyroscope is attached. Then $k = W/\delta\ell_0 \cong mg_E/\delta\ell_0$, where g_E is the Earth's radial gravitational field at the surface. Let $\delta\ell_0 = h_0$. Then

$$k = \frac{mg_E}{h_0}. \tag{12}$$

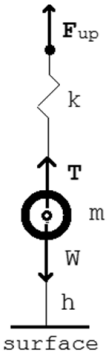

Fig. 2: Schematic for a forced harmonic oscillator; a rotor of mass m suspended by a spring of spring constant k with an upward supporting force F_{up}. Here T is the spring tension pulling up on the rotor, the weight W is the downward force of gravity on the rotor, and h is the height of the center of the rotor above the surface. Assume that the mass of the spring is negligible, and that the mass of the gyroscope approximately equals the mass of the rotor.

If the system is enclosed in a glass box, the damping of small amplitude free oscillations would be weak. The equation for an undamped harmonic oscillator is [7]

$$\frac{d^2h}{dt^2} + \omega_k^2 h = 0, \tag{13}$$

where

$$\omega_k^2 = \frac{k}{m} = \frac{g_E}{h_0}. \tag{14}$$

If $h_0 \cong 10^{-4}$ m, then $\omega_k \cong 313$ rad/s or 50 Hz. If $\omega_h = \omega_k$ and the constant of (10) is zero, the connection between h_1 and h_0 becomes

$$h_1 = 2h_0. \tag{15}$$

This shows that the constant h_0 is comparable with the amplitude h_1.

Now consider the forced harmonic oscillator. Suppose the vibrator is turned on and adjusted to an amplitude h_{vib} and angular speed ω_{vib}. In this case,

$$F_{up} = mg_E + mh_{vib}\omega_{vib}^2 \cos(\omega_{vib} t). \tag{16}$$

If $\omega_{vib} \cong \omega_k$, the system is at or near resonance [7]. At resonance, if the damping is small, the speed dh/dt is in phase with the driving force F_{up}, the average kinetic energy in the system is at a maximum, and the amplitude at the rotor h_1 can be many times greater than the driver amplitude h_{vib}.

The effects of vibration alone apply to any dead weight, because vibration alone does not depend on the rotation of the gyroscope's rotor. Gyroscopic forces do depend on the rotation of the rotor. Therefore, for a complete analysis, gyroscopic forces must be included.

Effects of gyroscopic forces

Gyroscopic forces cause precession and nutation [7, 8]. Precession is a steady revolution of the rotor around a vertical axis, and nutation is an up-down nodding motion of the rotor. The general problem for motions of a spinning rigid body can be quite complicated, but the problem is simplified for certain special cases. The case for "THE HEAVY SYMMETRICAL TOP WITH ONE POINT FIXED" is described in great detail by H. Goldstein [8, p. 213].

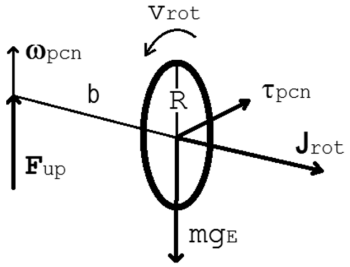

Fig. 3: Depiction of the gyroscopic forces acting on a rotor of mass m, radius R, and angular momentum vector $\mathbf{J}_{rot}$, which is supported by an upward force $\mathbf{F}_{up}$ at a distance b along the axel from the rotor's center to the support. Assume $\mathbf{J}_{rot}$ is in the horizontal plane. If $F_{up} = mg_E$, the precessional torque on the rotor $\tau_{pcn} = bmg_E$. In this case, the rotor precesses around the support with an angular speed $\omega_{pcn} = bmg_E/mR^2\omega_{rot}$.

Suppose the axel for a rotor is supported at a distance b from the center with an upward supporting force $\mathbf{F}_{up}$ and with the angular momentum vector $\mathbf{J}_{rot}$ released in the horizontal plane, as depicted in Fig. 3.

For a first case, suppose the supporting force is constant and equal to the weight, $F_{up} = mg_E$. Consider the case for slow precession without nutation.

Let ω_{pcn} be the precessional angular speed, and let v_{pcn} be the linear speed. Then the torque $\tau_{pcn} = bmg_E = J_{rot}\omega_{pcn}$. Solving for the angular speed gives $\omega_{pcn} = bg_E/R^2\omega_{rot}$.

If the distance $b = 0.1$ m, $R = 2\times10^{-2}$ m, and $\omega_{rot} = 3.14\times10^3$ rad/s, numerical values for ω_{pcn} and v_{pcn} are

$$\begin{aligned} \omega_{pcn} &= \frac{bg_E}{R^2\omega_{rot}} = 0.782 \quad \text{rad/s}, \\ \mathrm{v}_{pcn} &= b\omega_{pcn} = 7.82\times10^{-2} \quad \text{m/s}. \end{aligned} \tag{17}$$

Thus we find that the precessional speed for this case would be slow and constant at about 8 cm/s. Notice that this gyroscopic force supports the entire weight of the rotor.

Suppose the system is started with $\boldsymbol{J}_{rot}$ at a small initial angle $\delta\theta_0$ above the horizontal plane. Let h_{ntn} be the amplitude for nutation, which is the initial height above the horizontal plane. Then

$$h_{ntn} = b\tan\delta\theta_0. \tag{18}$$

When released, the rotor will precess with the angular speed ω_{pcn} of (17) and oscillate up and down with an upper maximum angle $\delta\theta_0$ and a lower minimum angle $\delta\theta_1$. Let ω_{ntn} be the angular speed for nutation. The formula for ω_{ntn} can be

found in [8, p. 221].

$$\omega_{ntn} = \frac{bg_E}{R^2\omega_{pcn}} = \omega_{rot} = 3.1\times10^3 \quad \text{rad/s}. \tag{19}$$

Thus we find that the frequency for nutation is the same as the frequency for the rotor, 500 Hz.

The formula for the difference $\sin\delta\theta_0 - \sin\delta\theta_1$ can be found in [7, p. 312].

$$\sin\delta\theta_0 - \sin\delta\theta_1 = \frac{2g_E b^3}{R^4\omega_{rot}^2}.$$

If $b = 0.1$ m, $R = 2\times10^{-2}$ m, and $\omega_{rot} = 3.14\times10^3$ rad/s, the numerical value for the difference becomes

$$\sin\delta\theta_0 - \sin\delta\theta_1 = 1.24\times10^{-2}, \tag{20}$$

the amplitude

$$h_{ntn} = 6.2\times10^{-4} \quad \text{m}, \tag{21}$$

and the linear speed for nutation becomes

$$\mathrm{v}_{ntn} = h_{ntn}\omega_{ntn}\sin(\omega_{ntn}t) \cong (1.9\ \text{m/s})\sin(\omega_{ntn}t). \tag{22}$$

Now let's change the length of the axel. Suppose the rotor's axel is extended on the other side of the support by the same distance b, and a dead weight that balances the cross beam is attached. If $\boldsymbol{J}_{rot}$ is directed outward from the supporting point, the dead weight would produce a torque equal in magnitude but opposite to the direction for τ_{pcn}, which would cancel the precessional motion. But such a balance would not cause any change in the nutational motion.

With the cross beam balanced in this manner, suppose the vibrator that supports the cross beam is turned on and adjusted to have an amplitude of h_{ntn} and an angular speed ω_{ntn}. This would induce an artificial nutation, but only if the gyroscope's rotor is spinning with an angular speed ω_{rot}. If the radial gravitational field contains a small time-dependent component with an angular speed near ω_{ntn}, there would be interesting interference effects and beat frequencies that could become visible in the balance of the cross beam.

The Earth's time-retarded transverse gravitational field

To satisfy the causality principle, the neoclassical causal theory postulates a new time-retarded transverse component for the Earth's gravitational field [1]. Let $\boldsymbol{g}_\phi$ be the Earth's time-retarded transverse component. The formula for the magnitude is [1]

$$g_\phi = C_\phi\left(1 - \frac{\Omega_\phi}{\Omega_E}\right)PS(r)\cos^2\lambda, \tag{23}$$

where the definition for the coefficient is

$$C_\phi = G\bar{\rho}r_E\frac{v_{eq}}{c_g}. \tag{24}$$

Here G is the gravity constant, r_E is the Earth's spherical radius, Ω_E is the Earth's sidereal angular speed, $\bar{\rho}$ is the Earth's mean mass density, c_g is the speed of propagation of the Earth's gravitational field, r is the geocentric radial distance to the field point, λ is the geocentric latitude for the field point, Ω_ϕ is the angular speed of the projection of the field point onto the equatorial plane, and $PS(r)$ is a power series representation for a triple integral over the Earth's volume.

The numerical value for C_ϕ with $c_g = c$ is

$$C_\phi = G\bar{\rho}r_E\frac{\mathrm{v}_{eq}}{c} = 3.635\times10^{-6} \quad \text{m/s}^2. \tag{25}$$

The formula for the power series is

$$PS(r) = \left(\frac{r_E}{r}\right)^3\left(C_0 + C_2\left(\frac{r_E}{r}\right)^2 + C_4\left(\frac{r_E}{r}\right)^4 + C_6\left(\frac{r_E}{r}\right)^6\right), \tag{26}$$

where the values for the coefficients are

$$\begin{aligned} C_0 &= 0.50889, \quad C_2 = 0.13931,\\ C_4 &= 0.01013, \quad C_6 = 0.14671. \end{aligned} \tag{27}$$

Let CPS_0 be the value for $PS(r_E)$. The definition and numerical value are

$$CPS_0 = C_0 + C_2 + C_4 + C_6 = 0.805. \tag{28}$$

Let $\boldsymbol{J}_Z$ be the geocentric angular momentum for the rotor, defined as

$$J_Z = mr_\phi^2\Omega_\phi \tag{29}$$

By conservation of angular momentum,

$$constant = \frac{J_z}{m} = r_\phi^2\Omega_\phi = r_E^2\Omega_E\cos^2\lambda \tag{30}$$

Solving (30) for Ω_ϕ gives

$$\Omega_\phi \cong \Omega_E\left(1 - 2\frac{h_0}{r_E} - 2\frac{h_1}{r_E}\cos(\omega_h t)\right) \tag{31}$$

Then the difference

$$1 - \frac{\Omega_\phi}{\Omega_E} = 2\frac{h_0}{r_E} + 2\frac{h_1}{r_E}\cos(\omega_h t). \tag{32}$$

Substituting (32) into (23) produces

$$g_\phi = C_\phi\left(2\frac{h_0}{r_E} + 2\frac{h_1}{r_E}\cos(\omega_h t)\right)PS(r)\cos^2\lambda. \tag{33}$$

The numerical value for g_ϕ with $c_g = c$, $r = r_E$, $h_0 = h_1 = 10^{-4}$ m, and $\lambda = 60^\circ$, is

$$g_\phi = \left(2.3\times10^{-17}\ \text{m/s}^2\right)\left(1 + \cos(\omega_h t)\right). \tag{34}$$

This result shows that the time-retarded transverse gravitational field for a suspended gyroscope is totally negligible.

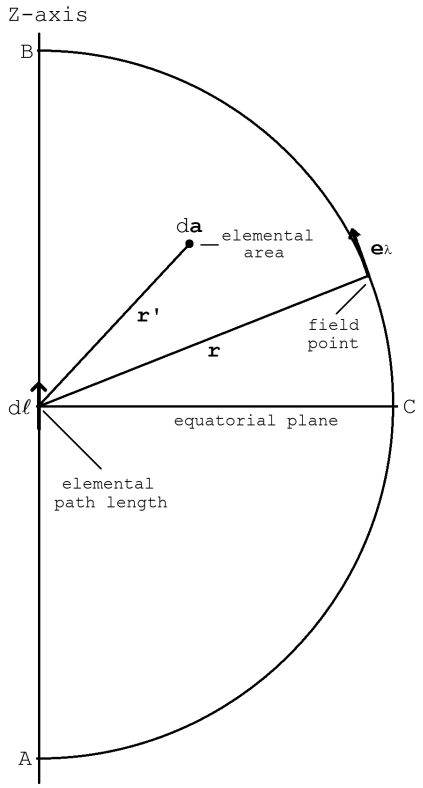

Fig. 4: Depiction of the semicircular area to be used for Stoke's theorem. The contour for the line integral is $A \to B \to C \to A$. Here $d\boldsymbol{\ell}$ is an elemental path length vector, d**a** is an elemental area vector, and $\mathbf{e}_\lambda$ is a unit vector for λ. The field-point is at **r** and the elemental area d**a** is at **r**′.

The Earth's time-retarded transverse vector potential

Let $\boldsymbol{A}$ be the vector potential for $\boldsymbol{g}_\phi$. Then by definition

$$\boldsymbol{g}_\phi = \boldsymbol{\nabla} \times \boldsymbol{A}. \tag{35}$$

Units for A are m^2/s^2, the same as the units for the scalar potential. Because the divergence of $\boldsymbol{g}_\phi$ is zero, the divergence of $\boldsymbol{A}$ must also be zero, which means that $\boldsymbol{A}$ cannot have a component directed along $\boldsymbol{e}_r$. Consequently, $\boldsymbol{A}$ must be directed along $\boldsymbol{e}_\lambda$.

The needed elemental vectors $d\boldsymbol{\ell}$ and d**a** for integration using Stoke's theorem are depicted in Fig. 4. Stoke's theorem states that the line integral of $\boldsymbol{A} \bullet d\boldsymbol{\ell}$ around a closed contour equals the surface integral of $\boldsymbol{\nabla} \times \boldsymbol{A} \bullet d\mathbf{a}$ over the surface bounded by the contour. It is symbolically written as

$$\oint \boldsymbol{A} \bullet \mathrm{d}\boldsymbol{\ell} = \iint \boldsymbol{\nabla} \times \boldsymbol{A} \bullet \mathrm{d}\mathbf{a}. \tag{36}$$

Consider the closed contour depicted in Fig. 4: $A \to B \to C \to A$. The left side of (36) becomes

$$\oint_{A \to B} \boldsymbol{A} \bullet d\boldsymbol{\ell} = 0, \qquad \oint_{B \to C \to A} \boldsymbol{A} \bullet d\boldsymbol{\ell} = A_\lambda \pi r. \tag{37}$$

The right side of (36) becomes

$$\iint \boldsymbol{\nabla} \times \boldsymbol{A} \bullet \mathrm{d}\mathbf{a} = g_\phi \iint r' dr' d\lambda' = g_\phi \frac{\pi}{2} r^2. \tag{38}$$

Next comes the solution

$$A_\lambda = \frac{1}{2} r g_\phi = A_0 \cos^2 \lambda \, PS'(r) \left(2\frac{h_0}{r_E} + 2\frac{h_1}{r_E} \cos(\omega_h t) \right) \tag{39}$$

where the definition for A_0 and its numerical value with $c_g = c$ and the definition for the power series for A_λ are

$$\begin{aligned} A_0 &= \frac{C_\phi r_E}{2} = 11.6 \quad \mathrm{m^2/s^2}, \\ PS'(r) &= \frac{r}{r_E} PS(r) = \\ &= C_0 \left(\frac{r_E}{r}\right)^2 + C_2 \left(\frac{r_E}{r}\right)^4 + C_4 \left(\frac{r_E}{r}\right)^6 + C_6 \left(\frac{r_E}{r}\right)^8. \end{aligned} \tag{40}$$

The formula that connects $\boldsymbol{g}_\lambda$ to the time-dependence of $\boldsymbol{A}_\lambda$ is [9, p. 219].

$$\begin{aligned} g_\lambda &= -\frac{1}{\mathrm{v}_k} \frac{dA_\lambda}{dt} = \\ &= 2\frac{A_0}{\mathrm{v}_k} \cos^2 \lambda \left(\frac{h_1 \omega_h}{r_E} PS'(r_E) \sin(\omega_h t) - \right. \\ &\quad \left. - \frac{dPS'}{dt} \left(\frac{h_0}{r_E} + \frac{h_1}{r_E} \cos(\omega_h t) \right) \right), \end{aligned} \tag{41}$$

where v_k is the "induction speed" for the neoclassical causal theory.

The numerical value for the average induction speed has been found to be [1]

$$\bar{\mathrm{v}}_k \cong 5 \times 10^3 \ \mathrm{m/s}. \tag{42}$$

The coefficient A_0 is inversely proportional to c_g. It is interesting to notice that A_0/v_k with $c_g = c$ is inversely proportional to $c\mathrm{v}_k$, and that

$$\sqrt{c\mathrm{v}_k} \cong 11 \times 10^5 \ \mathrm{m/s} = 1.7 c_2, \tag{43}$$

where c_2 is Kozyrev's secondary universal speed, the one that is to be associated with rotational motion [4].

Let CPS'_0 be the value for PS' at $r = r_E$.

$$CPS'_0 = PS'(r_E) = C_0 + C_2 + C_4 + C_6 = 0.805. \tag{44}$$

The value for dPS'/dt evaluated at $r = r_E$ is

$$\begin{aligned} \left.\frac{dPS'}{dt}\right|_{r=r_E} &= (2C_0 + 4C_2 + 6C_4 + 8C_6) \frac{h_1 \omega_h}{r_E} \sin(\omega_h t) = \\ &= 2.81 \frac{h_1 \omega_h}{r_E} \sin(\omega_h t). \end{aligned} \tag{45}$$

The formula for g_λ to first order in h_1/r_E reduces to

$$g_\lambda \cong C_\lambda \cos^2 \lambda \frac{h_1 \omega_h}{\mathrm{v}_k} \sin(\omega_h t), \tag{46}$$

where the definition and numerical value with $c_g = c$ for C_λ are

$$C_\lambda = 0.805 \times 2\frac{A_0}{r_E} = 0.805 C_\phi = 2.926 \times 10^{-6} \ \mathrm{m/s^2}, \quad (47)$$

and C_ϕ is given by (24).

If $h_1 = 10^{-4}$ m, $\omega_h = \omega_{rot}$, $\mathrm{v}_k = 5$ km/s, and $\lambda = 60^\circ$, the numerical value for g_λ reduces to

$$g_\lambda = (4.6 \times 10^{-11} \ \mathrm{m/s^2}) \sin(\omega_h t) \quad (48)$$

This result shows that the vector potential can produce a relatively large value for the north/south transverse gravitational field. The ratio for g_λ / g_ϕ, with g_ϕ from (34), is on the order of

$$\frac{g_\lambda}{g_\phi} \sim 2 \times 10^6. \quad (49)$$

Secondary radial induction field

The analogous Lorentz force law for gravity [1, 2] states that a north/south transverse gravitational field can induce a radial gravitational field. Let $\boldsymbol{g}_{ind}$ be the induced gravitational field. Then

$$\boldsymbol{g}_{ind} = \frac{\mathbf{v}}{\mathrm{v}_k} \times \boldsymbol{g} = \frac{1}{\mathrm{v}_k} \begin{vmatrix} \mathbf{e}_r & \mathbf{e}_\phi & \mathbf{e}_\lambda \\ \mathrm{v}_r & \mathrm{v}_\phi & \mathrm{v}_\lambda \\ g_r & g_\phi & g_\lambda \end{vmatrix}. \quad (50)$$

The induced gravitational field along $\mathbf{e}_r$ is the only one of the components that can change the weight of the rotor.

$$\mathbf{e}_r g_{ind} = \mathbf{e}_r \left(\frac{\mathrm{v}_\phi}{\mathrm{v}_k} g_\lambda - \frac{\mathrm{v}_\lambda}{\mathrm{v}_k} g_\phi \right) \cong \mathbf{e}_r \frac{\mathrm{v}_\phi}{\mathrm{v}_k} g_\lambda. \quad (51)$$

Substituting (8) and (42) into (51) gives

$$g_{ind} \cong C_{ind} \sin(\omega_h t), \quad (52)$$

where

$$C_{ind} = C_\lambda \frac{h_1 \omega_h}{\mathrm{v}_k} \frac{\mathrm{v}_{eq}}{\mathrm{v}_k} \cos^3 \lambda \quad (53)$$

If $\lambda = 60^\circ$, $h_1 = 10^{-4}$ m, $\omega_h = \omega_{rot}$, and $\mathrm{v}_k = 5$ km/s, the numerical value for C_{ind} reduces to

$$C_{ind} = 2.1 \times 10^{-12} \quad \mathrm{m/s^2}. \quad (54)$$

This result predicts a very small value for g_{ind}, but it is close to the order of magnitude for g_λ, which is predicted to be about 10^6 times g_ϕ. There may be some hidden effect that enhances g_{ind} by 10^6, in particular the nutation effects of (21) and (22). This question can be resolved only by experiment.

Conclusions and recommendations

It seems plausible but not proven that the weight changes observed by N.A. Kozyrev may have been caused by the neoclassical causal theory. Modern experimental techniques using digital electronics, sensitive strain gauges, sensitive accelerometers, and computer controls, can greatly increase the sensitivity and reliability of laboratory instruments. If an instrument that can detect the Earth's time-retarded transverse vector potential is developed with a precision of about 1 part in 1000, the theory can be worked backwards to provide a measured value for the speed of the Earth's gravitational field. To accomplish this end, a dedicated effort to develop an instrument, and comprehensive systematic studies using such an instrument, are highly recommended.

Acknowledgements

I thank Patrick L. Ivers for reviewing the manuscript for this article and suggesting improvements. I also thank Dr. Dmitri Rabounski for providing the schematic drawing for N. A. Kozyrev's compound pendulum.

Submitted on August 18, 2013 / Accepted on August 25, 2013
Updated with corrections on October 10, 2013

References

1. Hafele J.C. Earth Flyby Anomalies Explained by a Time-Retarded Causal Version of Newtonian Gravitational Theory. *The Abraham Zelmanov Journal*, 2012, v.5, 134–187.
2. Hafele J.C. Causal Version of Newtonian Theory by Time-Retardation of the Gravitational Field Explains the Flyby Anomalies. *Progress in Physics*, 2013, v.3, 3–8.
3. Hafele J.C. Comment on N.A. Kozyrev's "Possibility of Experimental Study of the Properties of Time". *Letters to Progress in Physics*, 2013, v.3, L1.
4. Kozyrev N.A. Possibility of Experimental Study of the Properties of Time. *The Abraham Zelmanov Journal*, 2012, v.5, 188–220.
5. Fine-structure constant. Wikipedia, http://en.wikipedia.org/wiki/Fine-structure_constant
6. Private communication from Dr. Dmitri Rabounski.
7. Becker R.A. Introduction to Theoretical Mechanics. McGraw-Hill, New York, 1954.
8. Goldstein H. Classical Mechanics. Addison-Wesley, Reading, Massachusetts, 1980.
9. Jackson J.D. Classical Electrodynamics. Wiley, New York, 1975.

Non-Linear Effects in Flow in Porous Duct

Hafeez Y. Hafeez*, Jean Bio-Chabi Orou† and Omololu A. Ojo‡

*Physics Department, Federal University Dutse, Nigeria. E-mail: hafeezyusufhafeez@yahoo.com
†University Abomey-Calavi, Republic of Benin. E-mail: Jchabi@yahoo.fr
‡African University of Science and Technology, Abuja – Nigeria. E-mail: prayerz@yahoo.com

In general, it is assumed in some non viscous flows that the flow velocity is constant at a cross-section. In this paper, we impose more realistic boundary conditions by, for example, introducing viscosity, and suction at walls, the net mass flow will change since the continuity equation must hold. The convective acceleration terms will be products of variables such that a non-linear behaviour will take place in the flow. The work will consist of deriving all the equations and parameters needed to described this kind of flow. An approximate analytic solution for the case of small Reynold number Re is discussed using perturbation techniques. Expression for the velocity components and pressure are obtained. The governing non-linear differential equation that cannot be solved analytically is solved numerically using Runge-Kutta Program and the graphs of axial and lateral velocity profiles are drawn.

1 Introduction

The problems of fluid flow through porous duct have arouse the interest of Engineers and Mathematicians, the problems have been studied for their possible applications in cases of membrane filtration, transpiration cooling, gaseous diffusions and drinking water treatment as well as biomedical engineering. Such flows are very sensitive to the Reynold number.

Berman was the first researcher who studied the problem of steady flow of an incompressible viscous fluid through a porous channel with rectangular cross section, when the Reynold number is low and the perturbation solution assuming normal wall velocity to be equal was obtained [1].

Sellars [2], extended the problem studied by Berman by using very high Reynold numbers.

Also wall suctions were recognize to stabilize the boundary layer and critical Reynold number for natural transition 46130 was obtained [3]. The stabilization effects of wall suction is due to the change of mean velocity profiles.

In the review of Joslin [4], it is also noticed that the uniform wall suction is not only a tool for laminar flow control but can also be used to damped out already existing turbulence.

The effects of Hall current on the steady Hartman flow subjected to a uniform suction and injection at the boundary plates has been studied [5].

Other reviews of flow in porous duct tend to focus only on one specific aspect of the subject at a time such as membrane filteration [8], the description of boundary conditions [6] and the existence of exact solutions [7].

In this paper, we consider the steady two-dimensional laminar flow of an incompressible viscous fluid between two parallel porous plates with equal suction and assume that the wall velocity is non uniform.

2 Formulation of the problem

The steady laminar flow of an incompressible viscous fluid between two parallel porous plates with an equal suction at walls and non uniform cross flow velocity is considered. The well known governing equations of the flow are:

Continuity equation

$$\frac{\partial u}{\partial x}+\frac{\partial v}{\partial y}=0. \tag{1}$$

Momentum equations (without body force)

$$u\frac{\partial u}{\partial x}+v\frac{\partial u}{\partial y}=-\frac{1}{\rho}\frac{\partial p}{\partial x}+\nu\left(\frac{\partial^2 u}{\partial x^2}+\frac{\partial^2 u}{\partial y^2}\right), \tag{2}$$

$$u\frac{\partial v}{\partial x}+v\frac{\partial v}{\partial y}=-\frac{1}{\rho}\frac{\partial p}{\partial y}+\nu\left(\frac{\partial^2 v}{\partial x^2}+\frac{\partial^2 v}{\partial y^2}\right). \tag{3}$$

Let us consider channel flow between uniformly parallel plates with equal suction. Assuming that we are far downstream of the entrance, the boundary conditions can be defined as

$$y=h, u=0, v=v_w, \tag{4}$$

$$y=-h, u=0, v=-v_w. \tag{5}$$

Let $\overline{u}(0)$ denote the average axial velocity at an initial section ($x=0$). Then it is clear from a gross mass balance that $\overline{u}(x)$ will differ from $\overline{u}(0)$ by the amount $\frac{v_w}{h}x$. This observation led Berman(1953) to formulate the following relation for the stream in the channel [9].

$$\psi(x,y)=(h\overline{u}(0)-v_w x)\,f(y^*). \tag{6}$$

Where $y^*=\frac{y}{h}$, $\psi(x,y)$ is a stream function,$\overline{u}(0)$ is initial average axial velocity and f is dimensionless function to be determined. The velocity components follow immediately from

the definition of ψ:

$$u(x,y^*)=\frac{\partial\psi}{\partial y}=\left(\overline{u}(0)-\frac{v_w x}{h}\right)f'(y^*)=\overline{u}(x)f'(y^*), \quad (7)$$

$$v(x,y^*)=-\frac{\partial\psi}{\partial x}=v_w f(y^*)=v(y). \quad (8)$$

The stream function must now be made to satisfy the momentum equations (2) and (3) for steady flow (2) and (3) will now become

$$u\frac{\partial u}{\partial x}+\frac{v}{h}\frac{\partial u}{\partial y^*}=-\frac{1}{\rho}\frac{\partial p}{\partial x}+\nu\left(\frac{\partial^2 u}{\partial x^2}+\frac{1}{h^2}\frac{\partial^2 u}{\partial y^{*2}}\right), \quad (9)$$

$$u\frac{\partial v}{\partial x}+\frac{v}{h}\frac{\partial v}{\partial y^*}=-\frac{1}{\rho h}\frac{\partial p}{\partial y^*}+\nu\left(\frac{\partial^2 v}{\partial x^2}+\frac{1}{h^2}\frac{\partial^2 v}{\partial y^{*2}}\right). \quad (10)$$

Using (7) and (8) in (9) and (10), the momentum equations reduces to,

$$-\frac{1}{\rho}\frac{\partial p}{\partial x}=\left(\overline{u}(0)-\frac{v_w x}{h}\right)\left(\frac{v_w}{h}\left(ff''-f'^2\right)-\frac{\nu}{h^2}f'''\right), \quad (11)$$

$$-\frac{1}{\rho h}\frac{\partial p}{\partial y^*}=\frac{v_w^2}{h}ff'-\frac{\nu v_w}{h^2}f''. \quad (12)$$

Now differentiating (12) w.r.t x, we get

$$\frac{\partial^2 p}{\partial x\partial y^*}=\frac{\partial^2 p}{\partial x\partial y}=0. \quad (13)$$

Differentiating (11) w.r.t y^*, we get

$$\frac{\partial^2 p}{\partial x\partial y^*}=\left(\overline{u}(0)-\frac{v_w x}{h}\right)\frac{d}{dy^*}\left(\frac{v_w}{h}\left(ff''-f'^2\right)-\frac{\nu}{h^2}f'''\right). \quad (14)$$

From (13), (14) can be written as

$$\frac{d}{dy^*}\left(\frac{v_w}{h}\left(ff''-f'^2\right)-\frac{\nu}{h^2}f'''\right)=0, \quad (15)$$

$$\frac{v_w}{h}\left(ff'''-f'f''\right)-\frac{\nu}{h^2}f''''=0.$$

Let the suction Reynold number be $Re=\frac{hv_w}{\nu}$ and substitute into above expression, we get

$$f''''+Re\left(f'f''-ff'''\right)=0. \quad (16)$$

(16) has no known analytic-closed form solution, but it can be integrated once i.e integrate (16) w.r.t y^*, we get

$$f'''+Re\left(f'^2-ff''\right)=K=const. \quad (17)$$

The boundary conditions on $f(y^*)$ 0f (4) and (5) can now be written as,

$$f(1)=1, f(-1)=-1, f'(1)=0, f'(-1)=0. \quad (18)$$

Hence, the solution of the equations of motion and continuity is given by non-linear fourth order differential equation (16) subject to the boundary condition (18).

3 Results

3.1 Approximate analytic solution (perturbation)

The non-linear ordinary differential equation (16) subject to condition (18) must in general be integrated numerically. However for special case when "Re" is small, approximate analytic results can be obtained by the use of a regular perturbation approach. Note that perturbation method has been used because the equations (16 and 18) are non-linear by using that technique, we get a linear approximated version of the true equations. The solution of $f(y^*)$ may be expanded in power of Re [10]

$$f(y^*)=\sum_{n=0}^{\infty}Re^n f_n(y^*) \quad (19)$$

where $f_n(y^*)$ satisfies the symmetric boundary conditions

$$f_0(0)=f_0'(1)=f_0''(0)=0, \quad f_0(1)=1 \quad (20)$$

and

$$f_n(0)=f_n'(1)=f_n''(0)=0, \quad f_n(1)=1. \quad (21)$$

Here f_n are independent of Re. Substituting (19) in (16), we get

$$\left(f_0''''+Ref_1''''+Re^2f_2''''\right)+Re\Big[\left(f_0'+Ref_1'+Re^2f_2'\right)\left(f_0''+Ref_1''+Re^2f_2''\right)-\left(f_0+Ref_1+Re^2f_2\right)\left(f_0'''+Ref_1'''+Re^2f_2'''\right)\Big]=0.$$

Equating coefficients of Re, we get

$$f_o''''=0, \quad (22)$$

$$f_1''''+f_o'f_o''-f_of_o'''=0, \quad (23)$$

$$f_2''''+f_o'f_1''+f_1'f_o''-f_of_1'''-f_1f_o'''=0. \quad (24)$$

The solution of (22) is of the form

$$f_o(y^*)=\frac{Ay^{*3}}{6}+\frac{By^{*2}}{2}+Cy^*+D,$$

where A,B,C and D are constants.

Applying the boundary condition (20) to the above equation, we get

$$f_o(y^*)=\frac{1}{2}\left(3y^*-y^{*3}\right). \quad (25)$$

The solutions of Eq (23) and (24) subject to the boundary condition (21), are:

$$f_1(y^*)=-\frac{1}{280}\left(y^{*7}-3y^{*3}-2y^*\right), \quad (26)$$

$$f_2(y^*)=\frac{1}{1293600}\times\left(14y^{*11}-385y^{*9}+198y^{*7}+876y^{*3}-703y^*\right). \quad (27)$$

Hence, the first order perturbation solution for $f(y^*)$ is

$$f'(y^*) = f_o(y^*) + Ref_1(y^*),$$
$$f^1(y^*) = \frac{1}{2}\left(3y^* - y^{*3}\right) - \frac{Re}{280}\left(y^{*7} - 3y^{*3} - 2y^*\right). \quad (28)$$

The second order perturbation of solution for $f(y^*)$ is

$$f^2(y^*) = f_o(y^*) + Ref_1(y^*) + Re^2 f_2(y^*),$$

$$f^2(y^*) = \frac{1}{2}\left(3y^* - y^{*3}\right) - \frac{Re}{280}\left(y^{*7} - 3y^{*3} - 2y^*\right) + \frac{Re^2}{1293600}\left(14y^{*11} - 385y^{*9} + 198y^{*7} + 876y^{*3} - 703y^*\right). \quad (29)$$

Hence, the first order expression for the velocity components are:

$$u(x, y^*) = \left[\overline{u}(0) - \frac{v_w x}{h}\right] f'(y^*) = \left[\overline{u}(0) - \frac{v_w x}{h}\right]\frac{3}{2}\left(1 - y^{*2}\right)\left(1 - \frac{Re}{420}\left(2 - 7y^{*2} - 7y^{*4}\right)\right), \quad (30)$$

$$v(x, y^*) = v_w f(y^*) = v_w\left[\frac{1}{2}\left(3y^* - y^{*3}\right) - \frac{Re}{280}\left(y^{*7} - 3y^{*3} - 2y^*\right)\right]. \quad (31)$$

For pressure distribution, from Eq. (11) we get

$$\frac{h^2}{\rho\nu}\frac{\partial p}{\partial x} = \left[\overline{u}(0) - \frac{v_w x}{h}\right]\left[f'''(y^*) + Re\left(f'^2(y^*) - f(y^*)f''(y^*)\right)\right],$$

and since $f'''(y^*) + Re\left(f'^2(y^*) - f(y^*)\right)f''(y^*)) = K$, from (17), we have:

$$\frac{\partial p}{\partial x} = \frac{K\rho\nu}{h^2}\left[\overline{u}(0) - \frac{v_w x}{h}\right] = \frac{K\mu}{h^2}\left[\overline{u}(0) - \frac{v_w x}{h}\right]. \quad (32)$$

Now, from Eq. (12), we have

$$\frac{\partial p}{\partial y^*} = \frac{\mu v_w}{h} f''(y^*) - \rho\nu^2 f(y^*)f'(y^*). \quad (33)$$

Since $dp = \frac{\partial p}{\partial x}dx + \frac{\partial p}{\partial y^*}dy^*$, then

$$dp = \frac{K\mu}{h^2}\left[\overline{u}(0) - \frac{v_w x}{h}\right]dx + \left[\frac{\mu v_w}{h} f''(y^*) - \rho\nu^2 f(y^*)f'(y^*)\right]dy^*. \quad (34)$$

Integrating (34), we get

$$p(x, y^*) = p(0, 0) - \frac{\rho\nu^2}{2} f^2(y^*) + \frac{K\mu}{h^2}\left[\overline{u}(0)x - \frac{v_w x^2}{2h}\right] + \frac{\mu v_w}{h}\left[f'(y^*) - f'(0)\right]. \quad (35)$$

The pressure drop in the major flow direction is given by

$$p(x, 0) - p(x, y^*) = \frac{K\mu}{h^2}\left[\frac{v_w x^2}{2h} - \overline{u}(0)x\right]. \quad (36)$$

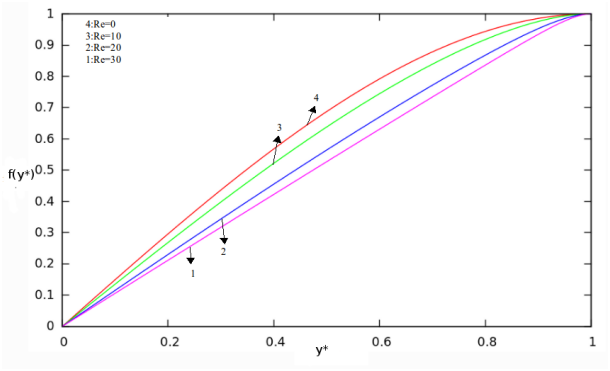

Fig. 1: Lateral velocity profiles for flow between parallel plates with equal suctions for different values of Re.

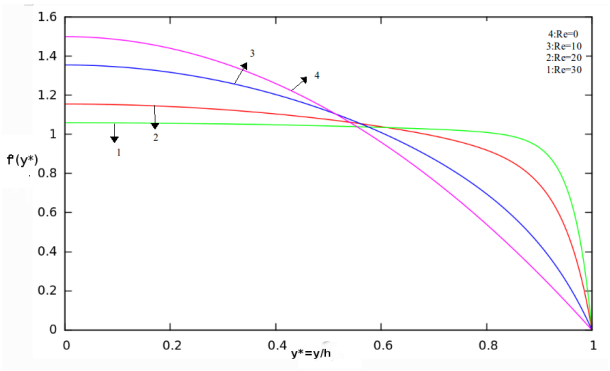

Fig. 2: Axial velocity profiles for flow between parallel plates with equal suctions for different values of Re.

3.2 Numerical solution

The approximate results of the previous section are not reliable when the Reynold number is not small. To obtain the detail information on the nature of the flow for different values of Reynold number (i.e. $Re = 0, 10, 20, 30$), a numerical solution to the governing equations is necessary. The Runge-Kutta program App.C is used to solve Eq. (17) numerically. One initial condition and constant (K) are unknown; i.e. starting at $y^* = 1$, then $f''(1)$ and K were guessed and the solution double-iterated until $f(-1) = -1$ and $f'(-1) = 0$. The most complete sets of profiles are shown in the figs. 1 and 2.

4 Discussion

The velocity profiles have been drawn for different values of Reynold number (i.e. $Re = 0, 10, 20, 30$). The shapes change smoothly with Reynold number and show no odd or unstable behaviour. Suction tends to draw the profiles toward the wall. From fig. (1), it is observed that for $Re > 0$ in the region $0 \le y^* \le 1$, $f(y^*)$ decreases with the increase of Reynold number Re. Also from fig. (2), it is observed that, for $Re > 0$,

then $f'(y^*)$ decreases with an increase of the Reynold number in the range of $0 \leq y^* \leq 1$.

5 Conclusion

In this paper, a class of solutions of laminar flow through porous duct has been presented. Numerical approach is necessary for arbitrary values of Re. Also, when a cross flow velocity along the boundary is not uniform, a numerical technique is necessary to solve Eq. (2) and (3). Also, from the results obtained in this article, we can now conclude that, the non-linear effects of a flow of the porous duct is due to non uniform cross flow velocity and non vanishing terms of convective acceleration of momentum equations. The perturbation solution obtained for this problem reduces to the results of Berman [1].

Acknowledgement

The authors wish to thank Dr. Chifu E. Ndikilar for his time, useful discussions and help in preparing the numerical solution to this problem.

Nomenclature

A,B,C,D: Constants
K: Arbitrary Constant
f: Dimensionless function representing lateral velocity profile
h: Height of the channel
P: Pressure
x: Axial distance
y: Lateral distance
v_w: Lateral wall velocity
u(x,y): Axial velocity component
v(x,y): Lateral velocity component
$y^* = \frac{y}{h}$: Dimensionless lateral distance
$Re = \frac{v_w h}{\nu}$: Wall Reynold number

Greek Symbols

μ: Shear viscosity
ν: Kinematic viscosity
ρ: Fluid density
$\psi(x, y)$: Stream function.

Submitted on: August 23, 2013 / Accepted on: September 03, 2013

References

1. Berman A.S. Laminar flow in channels with porous walls. *Journal of Applied Physics* 1953, v. 24, 1232–1235.
2. Sellars J.R. Laminar flow in channels with porous walls at high suction Reynold number. *Journal of Applied Physics* 1955, v. 26, 489.
3. Drazin P.G. and Reid W.H. Hydrodynamic stability, Cambridge University Press, (1981).
4. Joslin R.D. Aircraft laminar flow control. *Annual Review of Fluid Mechanics* 1998, v. 30, 1–29.
5. Abu-El-Dhat E. Hartman flow with uniform suction and injection at the boundary plate. M.Sc. Thesis, Helwan University, Egypt, (1993).
6. Sahraoui M. and Kaviany M. Slip and no-slip velocity boundary-conditions at interface of porous, plain media. *International Journal of Heat and Mass Transfer*, 1992, v. 35(4), 927–943.
7. Wang C.Y. Exact solutions of the steady-state Navier-Stokes equations. *Annual Review of Fluid Mechanics*, 1991, v. 23, 159–178.
8. Belfort G. Fluid-mechanics in membrane filtration – recent developments. *Journal fo Membrane Science*, 1989, v. 40, 123–147.
9. Frank White. Viscous fluid flow, 2nd edition, McGraw-Hill company New York, (1991).
10. Ganesh S. and Krishnambal S. Magnetohydrodynamics flow of viscous fluid between two parallel plates. *Journal of Applied Science* 2006, v. 6(11), 2420–2425.

Understanding the Dirac Equation and the Electron-Vacuum System

William C. Daywitt

National Institute for Standards and Technology (retired), Boulder, Colorado. E-mail: wcdaywitt@me.com

It has been close to a century since the Dirac equation first appeared, but it has yet to be understood on an intuitive, fundamental level. The reason for this lack of understanding is twofold: the equation is expressed in terms of the *secondary* constant $\hbar$; and the vacuum state and its coupling to the electron particle have not been developed as part of the electron model. What follows briefly reviews the vacuum coupling and illustrates it by deriving the Schrödinger and Pauli equations as derivatives of the Dirac equation, and by explaining the zitterbewegung response that is a vacuum dynamic associated with the coupling force. It is argued that the fields of quantum electrodynamics have as their origin the degenerate vacuum state.

1 Introduction

The Dirac electron defined here is a massive "point" charge $(-e_*, m)$ that obeys the Dirac equation and is coupled to the negative-energy Planck vacuum (PV) continuum via the two-term coupling force [1]

$$\frac{e_*^2}{r^2} - \frac{mc^2}{r} \tag{1}$$

the massive charge exerts on the PV. The electron Compton radius $r_c\,(= e_*^2/mc^2)$ is that radius from the center of the massive charge (in its rest frame) to the radius r_c where the coupling force vanishes. The bare charge $(-e_*)$ itself is massless, while the electron mass m results from the bare charge being driven by the zero-point electromagnetic field [2] [3]; corresponding to which is a vanishingly small sphere containing the driven charge whose center defines the center of both the driven charge and its derived mass. It is from the center of this small sphere that the position operator $\mathbf{r}$ for the massive charge and the electron-vacuum complex is defined and from which the radius r in (1) emerges.

The PV model of the complete electron consists of two interdependent dynamics, the dynamics of the massive charge in the previous paragraph and the dynamics of the PV continuum to which the massive charge is coupled. An example of the latter dynamic is the (properly interpreted) zitterbewegung [4] [1] that represents a harmonic-oscillator-type excitation taking place at the $r = r_c$ sphere surrounding the massive point charge, an oscillation resulting from the vacuum response to the vanishing of (1) at r_c. The point-like nature of the massive charge, in conjunction with the continuum nature of the PV, are what give the electron its so-called wave-particle-duality. Mathematically, the electron's wave nature is apparent from the fact that the spinor solutions to the Dirac equation are spinor *fields*, and it is upon these fields that the covariant gradient operator

$$\partial_\mu = \frac{\partial}{\partial x^\mu} = \left(\frac{\partial}{c\partial t}, \nabla\right) \tag{2}$$

operates. Thus the spinors are associated with PV distortion — with no distortion the gradients vanish, resulting in null spinors and the dissolution of (3).

The free-particle Dirac equation can be expressed in the form (from (A10) in Appendix A)

$$ir_c \frac{\partial}{c\partial t}\begin{pmatrix}\phi\\ \chi\end{pmatrix} + \begin{pmatrix}\vec{\sigma}\cdot ir_c\nabla\chi\\ \vec{\sigma}\cdot ir_c\nabla\phi\end{pmatrix} = \begin{pmatrix}\phi\\ -\chi\end{pmatrix} \tag{3}$$

in terms of the single constant r_c, a constant that normalizes the operator in (2). The free-space particle solution ϕ, and the negative-energy vacuum solution χ, for this electron-vacuum system are 2×1 spinors and $\vec{\sigma}$ is the Pauli 2×2 vector matrix. The spinor solutions from the two simultaneous equations in (3) are strongly coupled by the inverted χ-ϕ spinor configuration of the second term, showing the vacuum state to be an integral part of the electron phenomenon. (It will be seen that this coupling is even present in the nonrelativistic Schrödinger equation.) The negative spinor $(-\chi)$ on the right is a manifestation of the negative-energy nature of the vacuum. Equation (3) expresses the Dirac equation in terms of the normalized PV gradients on the left of the equal sign.

What follows illustrates the previous ideas by reiterating the standard development of the free-particle Schrödinger equation and the minimal coupling substitution leading to the Pauli equation.

2 Schrödinger equation

The Dirac-to-Schrödinger reduction [5, p. 79] begins with eliminating the high-frequency components from (3) by assuming

$$\begin{pmatrix}\phi\\ \chi\end{pmatrix} = \begin{pmatrix}\phi_0\\ \chi_0\end{pmatrix} e^{-imc^2t/\hbar} = \begin{pmatrix}\phi_0\\ \chi_0\end{pmatrix} e^{-ict/r_c} \tag{4}$$

where ϕ_0 and χ_0 are slowly varying functions of time compared to the exponentials. Inserting (4) into (3) gives

$$ir_c \frac{\partial}{c\partial t}\begin{pmatrix}\phi_0\\ \chi_0\end{pmatrix} + \begin{pmatrix}\vec{\sigma}\cdot ir_c\nabla\chi_0\\ \vec{\sigma}\cdot ir_c\nabla\phi_0\end{pmatrix} = \begin{pmatrix}0\\ -2\chi_0\end{pmatrix} \tag{5}$$

where the 0 on the right is a 2×1 null spinor. This zero spinor indicates that the mass energy of the free particle is being ignored, while the effective negative-mass energy of the "vacuum particle" has been doubled. In effect, mass energy for the particle-vacuum system has been conserved by shifting the mass energy of the free particle to the vacuum particle.

The lower of the two simultaneous equations in (5) can be reduced from three to two terms by the assumption

$$\left| ir_c \frac{\partial \chi_0}{c\partial t} \right| \ll |-2\chi_0| \tag{6}$$

if the kinetic energy (from the first equation in (A2)) of the vacuum particle is significantly less than its effective mass energy. Inserting (6) into (5) yields

$$ir_c \frac{\partial}{c\partial t}\begin{pmatrix}\phi_0\\0\end{pmatrix} + \begin{pmatrix}\vec{\sigma}\cdot ir_c\nabla\chi_0\\ \vec{\sigma}\cdot ir_c\nabla\phi_0\end{pmatrix} = \begin{pmatrix}0\\-2\chi_0\end{pmatrix} \tag{7}$$

as the nonrelativistic version of (3). The mass energy of the free particle, and the kinetic energy of the vacuum particle (associated with the lower-left null spinor), are discarded in the Schrödinger approximation.

Separating the two equations in (7) produces

$$ir_c \frac{\partial \phi_0}{c\partial t} + \vec{\sigma}\cdot ir_c\nabla\chi_0 = 0 \tag{8}$$

and

$$\vec{\sigma}\cdot ir_c\nabla\phi_0 = -2\chi_0 \tag{9}$$

and inserting (9) into (8) leads to

$$ir_c \frac{\partial \phi_0}{c\partial t} - \frac{(\vec{\sigma}\cdot ir_c\nabla)^2}{2}\phi_0 = 0\,. \tag{10}$$

Finally, inserting the Pauli-matrix identity (A12)

$$(\vec{\sigma}\cdot ir_c\nabla)^2 = I\,(ir_c\nabla)^2 \tag{11}$$

into (10) yields the free-particle Schrödinger equation

$$ir_c \frac{\partial \phi_0}{c\partial t} = \frac{(ir_c\nabla)^2}{2}\,\phi_0 \quad \text{or} \quad i\hbar\frac{\partial \phi_0}{\partial t} = \frac{(i\hbar\nabla)^2}{2m}\,\phi_0 \tag{12}$$

where the two spin components in ϕ_0 are ignored in this approximation. The scalar harmonic function

$$\phi_0 \longrightarrow \exp\left[-i(Et - \mathbf{p}\cdot\mathbf{r})/\hbar\right] \tag{13}$$

satisfies both equations as it should, and leads to the nonrelativistic energy-momentum relation $E = p^2/2m$, where $\mathbf{p} = m\mathbf{v}$. The equation on the left in (12) expresses the Schrödinger equation in terms of PV gradients.

The vacuum property implied by (11), and the fact that ϕ_0 is a spinor field, show that the vacuum state is a significant (but hidden) part of the nonrelativistic Schrödinger equation. The Dirac-to-Pauli reduction leads to the same conclusion.

3 Minimal coupling

By itself the coupling force (1) is insufficient to split the twofold degeneracy of the spinors in the free-particle Dirac (3) and Schrödinger (12) equations. It takes an external field to effect the split and create the well-known 1/2-spin electron states. The following illustrates this conclusion for the case of the minimal coupling substitution.

The minimal coupling substitution [5, p.78] is

$$p^\mu \longrightarrow p^\mu - eA^\mu/c \tag{14}$$

where e is the magnitude of the observed electron charge, $p^\mu = (E/c, \mathbf{p})$ is the 4-momentum, and $A^\mu = (A_0, \mathbf{A})$ is the electromagnetic 4-potential. Inserting (14) with (A1) and (A2) into the Dirac equation (A3) leads to

$$\left(i\hbar\frac{\partial}{\partial t} - eA_0\right)\psi - c\boldsymbol{\alpha}\cdot\left(\widehat{\mathbf{p}} - \frac{e\mathbf{A}}{c}\right)\psi = mc^2\beta\psi \tag{15}$$

which can be expressed as

$$ir_c \frac{\partial}{c\partial t}\begin{pmatrix}\phi\\\chi\end{pmatrix} + \begin{pmatrix}\vec{\sigma}\cdot(ir_c\nabla + \mathbf{a})\chi\\ \vec{\sigma}\cdot(ir_c\nabla + \mathbf{a})\phi\end{pmatrix} = a_0\begin{pmatrix}\phi\\\chi\end{pmatrix} + \begin{pmatrix}\phi\\-\chi\end{pmatrix} \tag{16}$$

in the 2×1 spinor formulation, where $a_0 \equiv eA_0/mc^2$ and $\mathbf{a} \equiv e\mathbf{A}/mc^2$. Then proceeding as in Section 2 produces

$$ir_c \frac{\partial}{c\partial t}\begin{pmatrix}\phi_0\\0\end{pmatrix} + \begin{pmatrix}\vec{\sigma}\cdot(ir_c\nabla + \mathbf{a})\chi_0\\ \vec{\sigma}\cdot(ir_c\nabla + \mathbf{a})\phi_0\end{pmatrix} = a_0\begin{pmatrix}\phi_0\\\chi_0\end{pmatrix} + \begin{pmatrix}0\\-2\chi_0\end{pmatrix}. \tag{17}$$

The Compton radius in (16) and (17) has been accounted for as a gradient normalizer. The remaining constants (e and m) appear only in association with the 4-potential A^μ — if the external potential vanishes, the electron charge and mass are removed ($a_0 = 0$ and $\mathbf{a} = \mathbf{0}$) from the equations, and (16) and (17) reduce to (3) and (7) respectively. Furthermore, the energy eA_0 appears to increase the energy level of the negative-energy PV continuum. This latter conclusion can be appreciated by combining the two terms on the right side of (17):

$$\begin{pmatrix}\left(eA_0/mc^2\right)\phi_0\\ (eA_0/mc^2 - 2)\chi_0\end{pmatrix} \tag{18}$$

where a_0 has been replaced by its definition. With a constant potential energy $eA_0 = 2mc^2$, the lower parenthesis vanishes and the free-space electron energy and the vacuum-energy spectrum just begin to overlap [1]. This latter result is the phenomenon that leads to the relativistic Klein paradox [5, p. 127].

If it is further assumed that

$$|a_0\chi_0| \ll |-2\chi_0| \tag{19}$$

then (17) becomes

$$ir_c \frac{\partial}{c\partial t}\begin{pmatrix}\phi_0\\0\end{pmatrix} + \begin{pmatrix}\vec{\sigma}\cdot(ir_c\nabla + \mathbf{a})\chi_0\\ \vec{\sigma}\cdot(ir_c\nabla + \mathbf{a})\phi_0\end{pmatrix} = a_0\begin{pmatrix}\phi_0\\0\end{pmatrix} + \begin{pmatrix}0\\-2\chi_0\end{pmatrix} \tag{20}$$

which is the nonrelativistic version of (16). Then eliminating χ_0 from the two simultaneous equations in (20) leads to the equation

$$ir_c\frac{\partial\phi_0}{c\partial t} = \frac{\overrightarrow{\sigma}\cdot(ir_c\nabla+\mathbf{a})\overrightarrow{\sigma}\cdot(ir_c\nabla+\mathbf{a})}{2}\phi_0 + a_0\phi_0 \qquad (21)$$

for the spinor ϕ_0. Equation (21) then leads to the Pauli equation [5, p.81].

Using (A11) to calculate the square of the numerator in the first term on the right of the equal sign in (21) yields

$$ir_c\frac{\partial\phi_0}{c\partial t} = \frac{(ir_c\nabla+\mathbf{a})^2}{2}\phi_0 + \frac{i\overrightarrow{\sigma}\cdot(ir_c\nabla\times\mathbf{a})}{2}\phi_0 + a_0\phi_0 \qquad (22)$$

remembering that ϕ_0 post-multiplies the square before calculation. The first term in (22) contains the electron's orbital angular momentum; and the second its spin, as manifested in the scaler product of $\overrightarrow{\sigma}$ and the curl of the vector potential $\mathbf{A}$. Using (A1), the corresponding spin operator can be expressed as

$$\widehat{s} = \frac{\hbar\overrightarrow{\sigma}}{2} = \frac{e_*^2\overrightarrow{\sigma}}{2c} = \frac{(-e_*)(-e_*)\overrightarrow{\sigma}}{2c} \qquad (23)$$

where one of the charges $(-e_*)$ in (23) belongs to the massive point charge $(-e_*, m)$ and the other to the separate Planck particles $(-e_*, m_*)$ within the PV. The product e_*^2 suggests that the spin may be related to the interaction of the massive point charge with the PV charges when the vacuum is under the influence of a magnetic field $\mathbf{B}\,(=\nabla\times\mathbf{A})$.

4 Conclusions and comments

The physics of the PV state [1, 6] has provided a simple intuitive explanation for the Dirac, Schrödinger, and Pauli equations in terms of the massive point charge $(-e_*, m)$ and its interaction (1) with the PV. It is the ignorance of this coupling force that has obscured the meaning of the Dirac equation since its inception and, as seen in the next paragraph, the meaning of the zitterbewegung frequency.

The electron Compton relation $r_c m = e_*^2$ in (A1) holds for both combinations $(\mp e_*, \pm m)$; so the vacuum hole $(e_*, -m)$ exerts a coupling force on the vacuum state that is the negative of (1). The combination of the two forces explain why the zitterbewegung frequency $(2c/r_c$ [1] [4]) is twice the angular frequency $(mc^2/\hbar = c/r_c)$ associated with the electron mass (from Appendix B).

The purpose of this paper is to illustrate the massive-charge-PV nature of the electron phenomenon; and to reestablish the vacuum state as an essential and necessary part of a complete electron theory, that part that has been superseded by the idea of the quantum field. While the quantum field formalism, like the Green function formalism, is an important tool [5, p. 143] [7], the present author believes that the corresponding quantum field does not constitute an essential physical phenomenon apart from the dynamics of vacuum state (from Appendix C).

Appendix A: Dirac equation

The PV is characterized in part by the two Compton relations [1]

$$r_c mc^2 = r_* m_* c^2 = e_*^2 \quad (= c\hbar) \qquad (A1)$$

connecting the massive point charge $(-e_*, m)$ of the electron to the individual Planck particles $(-e_*, m_*)$ within the degenerate PV, where r_c and m, and r_* and m_* are the Compton radius and mass of the electron and Planck particles respectively. The bare charge $(-e_*)$ is massless and is related to the observed electronic charge $(-e)$ via the fine structure constant $\alpha = e^2/e_*^2$. From (A1), the energy and momentum operators can be expressed as

$$\widehat{E} = i\hbar\frac{\partial}{\partial t} = mc^2\left(ir_c\frac{\partial}{c\partial t}\right) \text{ and } \widehat{\mathbf{p}} = -i\hbar\nabla = mc(-ir_c\nabla) \qquad (A2)$$

the parenthetical factors implying that the operators, operating on the Dirac spinors, provide a measure of the gradients within the PV continuum. In the present free-electron case, these gradients are caused solely by the coupling force (1) and its negative (Appendix B).

The upper and lower limits to the PV negative-energy spectrum are $-mc^2$ and $-m_*c^2$ respectively, where m_* is the Planck mass. The continuum nature of the vacuum is an approximation that applies down to length intervals as small as ten Planck lengths $(10\,r_*)$ or so; that is, as small as $\sim 10^{-32}$cm.

Using (A1) and (A2), the Dirac equation [5, p.74]

$$ie_*^2\frac{\partial\psi}{c\partial t} + \boldsymbol{\alpha}\cdot ie_*^2\nabla\psi = mc^2\beta\psi \qquad (A3)$$

can be expressed as

$$ir_c\frac{\partial\psi}{c\partial t} + \boldsymbol{\alpha}\cdot ir_c\nabla\psi = \beta\psi \qquad (A4)$$

where the 4×4 vector-matrix operator

$$\boldsymbol{\alpha} = \begin{pmatrix} 0 & \overrightarrow{\sigma} \\ \overrightarrow{\sigma} & 0 \end{pmatrix} \qquad (A5)$$

where $\overrightarrow{\sigma} = (\sigma_1, \sigma_2, \sigma_3)$ and

$$\sigma_1 = \begin{pmatrix} 0 & 1 \\ 1 & 0 \end{pmatrix} \quad \sigma_2 = \begin{pmatrix} 0 & -i \\ i & 0 \end{pmatrix} \quad \sigma_3 = \begin{pmatrix} 1 & 0 \\ 0 & -1 \end{pmatrix} \qquad (A6)$$

are the three 2×2 Pauli matrices. The 4×4 matrix operator

$$\beta = \begin{pmatrix} I & 0 \\ 0 & -I \end{pmatrix} \qquad (A7)$$

where I represents the 2×2 unit matrix and the zeros here and in (A5) are 2×2 null matrices. The covariant gradient operator

$$\frac{\partial}{\partial x^\mu} = \left(\frac{\partial}{\partial x^0}, \frac{\partial}{\partial x^1}, \frac{\partial}{\partial x^2}, \frac{\partial}{\partial x^3}\right) = \left(\frac{\partial}{c\partial t}, \nabla\right) \qquad (A8)$$

is seen in (A2) and (A4) to have its differential coordinates normalized $(\partial x^\mu/r_c)$ by the electron Compton radius.

The 4×1 spinor wavefunction ψ can be expressed as [5, p. 79]

$$\psi = \begin{pmatrix} \phi \\ \chi \end{pmatrix} \tag{A9}$$

where ϕ and χ are the usual 2×1 spinors, and where the two components in each represent two possible spin states. The spinor ϕ is the free-space particle solution and χ is the negative-energy hole solution. Inserting (A9) into (A4), and carrying out the indicated matrix operations, yields the Dirac equation

$$ir_c \frac{\partial}{c\partial t}\begin{pmatrix} \phi \\ \chi \end{pmatrix} + \begin{pmatrix} \overrightarrow{\sigma} \cdot ir_c\nabla\chi \\ \overrightarrow{\sigma} \cdot ir_c\nabla\phi \end{pmatrix} = \begin{pmatrix} \phi \\ -\chi \end{pmatrix} \tag{A10}$$

in terms of the 2×1 spinors.

The following is an important property of the Pauli matrices, and the PV state (because of $\overrightarrow{\sigma}$): the vector Pauli matrix $\overrightarrow{\sigma}$ obeys the identity [5, p.12]

$$(\overrightarrow{\sigma} \cdot \mathbf{a})(\overrightarrow{\sigma} \cdot \mathbf{b}) = I\,\mathbf{a} \cdot \mathbf{b} + i\overrightarrow{\sigma} \cdot \mathbf{a} \times \mathbf{b} \tag{A11}$$

where $\mathbf{a}$ and $\mathbf{b}$ both commute with $\overrightarrow{\sigma}$, but are otherwise arbitrary three-vectors. Using (A11) (with $\mathbf{a} = \mathbf{b} = r_c\nabla$) leads to

$$(\overrightarrow{\sigma} \cdot r_c\nabla)^2 = I\,(r_c\nabla)^2 \tag{A12}$$

which connects the normalized ∇ operator in the relativistic Dirac equation to the same operator in the nonrelativistic Schrödinger equation.

Inserting the operators from (A2) into (A10) and rearranging the result leads to the two simultaneous equations

$$\left(\widehat{E} - mc^2\right)\phi = c\overrightarrow{\sigma} \cdot \widehat{p}\chi \tag{A13}$$

and

$$\left(\widehat{E} + mc^2\right)\chi = c\overrightarrow{\sigma} \cdot \widehat{p}\phi\,. \tag{A14}$$

Then, pre-multiplying (A13) by $(\widehat{E} + mc^2)$ and using (A14) and (A11) leads to

$$\left(\widehat{E^2} - m^2c^4\right)\phi = c^2\widehat{p^2}\,\phi \tag{A15}$$

and, after reversing the process, to an identical equation for χ. Thus both ϕ and χ separately obey the Klein-Gordon equation [5, p.31].

Appendix B: Zitterbewegung frequency

The following rough heuristic argument identifies the two coupling forces that explain why the zitterbewegung frequency [1, 4] is twice the angular frequency ($mc^2/\hbar = c/r_c$) associated with the electron mass energy.

The force the massive point charge $(-e_*, m)$ exerts on the PV is given by equation (1) which, using $r = r_c + \Delta r$ and $r_c = e_*^2/mc^2$, leads to

$$\frac{e_*^2}{(r_c + \Delta r)^2} - \frac{mc^2}{r_c + \Delta r} = -\frac{(e_*^2/r_c^3)\Delta r}{(1 + \Delta r/r_c)^2} \approx -\left(\frac{e_*^2}{r_c^3}\right)\Delta r \tag{B1}$$

for small $\Delta r/r_c$. This yields the harmonic oscillator motion from Newton's second law

$$\frac{d^2\Delta r}{dt^2} = -\left(\frac{e_*^2}{mr_c^3}\right)\Delta r = -\left(\frac{c}{r_c}\right)^2\Delta r \tag{B2}$$

with the "spring constant" (e_*^2/r_c^3) and oscillator frequency c/r_c. The corresponding motion that is due to the vacuum hole $(e_*, -m)$ (whose charge and mass fields exert a force that is the negative of (1)) is

$$-\frac{d^2\Delta r}{dt^2} = +\left(\frac{c}{r_c}\right)^2\Delta r \tag{B3}$$

showing that the massive free charge and the vacuum hole cause identical accelerations within the PV continuum.

The total vacuum acceleration is the sum of (B2) and (B3)

$$\frac{d^2\Delta r}{dt^2} = -2\left(\frac{e_*^2}{mr_c^3}\right)\Delta r = -2\left(\frac{c}{r_c}\right)^2\Delta r \tag{B4}$$

with the corresponding harmonic oscillator frequency

$$\sqrt{\frac{2e_*^2}{mr_c^3}} = \sqrt{2}\,\frac{c}{r_c} \tag{B5}$$

which is $\sqrt{2}$ times the angular frequency associated with the electron mass energy. Given the roughness of the calculations, this result implies that the combined massive-charge forces, acting simultaneously on the PV continuum, are the source of the zitterbewegung with its $2c/r_c$ frequency.

Appendix C: Quantum field

The PV is envisioned as a *degenerate* negative-energy sea of fermionic Planck particles. Because of this degeneracy, the vacuum experiences only small displacements from equilibrium when stressed. Thus the displacements due to the coupling force (1) are small, and so the potential energy corresponding to the stress can be approximated as a quadratic in those displacements. This important result enables the vacuum to support normal mode coordinates and their assumed quantum fields, as explained in the simple demonstration to follow.

The normal mode connection [8, pp. 109–119] to the quantum field can be easily understood by examining a string, stretched between two fixed points in a stationary reference frame, that exhibits small transverse displacements from equilibrium. In this case, the corresponding potential energy can be expressed in terms of quadratic displacements. If the displacements are represented by the function $\phi(t, x)$ at time t and position x along the string, then the quadratic assumption implies that the displacements must obey the wave equation

$$\frac{1}{c^2}\frac{\partial^2\phi}{\partial t^2} = \frac{\partial^2\phi}{\partial x^2} \tag{C1}$$

where c is a propagation velocity. The string geometry leads to the Fourier series representation

$$\phi(t, x) = \sum_{n=1}^{N} a_n(t) \sin(n\pi x/L) \tag{C2}$$

for the standing wave on the string, where L is the string length. Inserting (C2) into (C1) produces

$$\ddot{a}_n(t) = -\omega_n^2 a_n(t) \qquad \text{where} \qquad \omega_n = n\pi c/L \tag{C3}$$

and where the amplitude $a_n(t)$ is that of a harmonic oscillator.

The constant characterizing the Dirac equation is the Compton radius r_c. So it is reasonable to set the string length $L \sim r_c$ to determine the fundamental frequency $\omega_1 = \pi c/L$ in (C3). Furthermore, the harmonics of ω_1 can have wavelengths of the order of the Planck length r_* (antiparticle excitation is, of course, ignored in this rough argument); so the length L can be subdivided

$$N = \frac{L}{\text{minimum length division of string}} \sim \frac{r_c}{r_*}$$

$$= \frac{3.86 \times 10^{-11}}{1.62 \times 10^{-33}} \sim 10^{22} \tag{C4}$$

times, and ϕ in (C2) can be expressed as an integral if convenient since $r_* \ll r_c$.

The total energy of the vibrating string can thus be expressed as

$$E = \int_0^L \left[\frac{\rho}{2} \left(\frac{\partial \phi}{\partial t} \right)^2 + \frac{\rho}{2} c^2 \left(\frac{\partial \phi}{\partial x} \right)^2 \right] dx \tag{C5}$$

which, inserting (C2) into (C5), results in [8, p.117]

$$E = \frac{L}{2} \sum_{n=1}^{N} \left[\frac{\rho \dot{a}_n^2}{2} + \frac{\rho \omega_n^2 a_n^2}{2} \right] \tag{C6}$$

where the first and second terms in (C5) and (C6) are the kinetic and potential string energies respectively (ρ is the string density).

The crucial significance of (C6) is that it is a sum of independent normal-mode energies, where the $a_n(t)$ are the normal mode coordinates. From this normal mode setting, the quantum field energy

$$E = \sum_{n=1}^{N} \left(n_n + \frac{1}{2} \right) \hbar \omega_n = mc^2 \sum_{n=1}^{N} \left(n_n + \frac{1}{2} \right) r_c k_n \tag{C7}$$

is defined, where n_n is the number of normal modes associated with the wavenumber $k_n = \omega_n/c$. In effect, the integers $n_n (\geqslant 0)$ determine the quantized energy level of each normal mode oscillator $a_n(t)$. The $1/2$ component in (C7) is the zero-point energy of the string-vacuum system.

At this point the quantum-field formalism discards the preceding foundation upon which the fields are derived, and assumes that the fields themselves are the primary reality [8, p. 119]. Part of the reason for this assumption is that, in the past, no obvious foundation was available. However, the demonstration here provides such a foundation on the simple, but far-reaching assumption that the vacuum is a degenerate state which can sustain a large stress without a correspondingly large strain.

Submitted on September 11, 2013 / Accepted on September 21, 2013

References

1. Daywitt W.C. The Electron-Vacuum Coupling Force in the Dirac Electron Theory and its Relation to the Zitterbewegung. *Progress in Physics*, 2013, v. 3, 25.
2. Puthoff H.E. Gravity as a Zero-Point-Fluctuation Force. *Physical Review A*, 1989, v. 39, no. 5, 2333–2342.
3. Daywitt W.C. The Source of the Quantum Vacuum. *Progress in Physics*, 2009, v. 1, 27.
4. Barut A.O. and Bracken A.J. *Zitterbewegung* and the Internal Geometry of the Electron. *Physical Review D*, 1981, v. 23, no. 10, 2454–2463.
5. Gingrich D.M. Practical Quantum Electrodynamics. CRC, The Taylor & Francis Group, Boca Raton, London, New York, 2006.
6. Daywitt W.C. The Planck Vacuum. *Progress in Physics*, 2009, v. 1, 20. See also www.planckvacuum.com.
7. Milonni P.W. The Quantum Vacuum—an Introduction to Quantum Electrodynamics. Academic Press, New York, 1994.
8. Aitchison I.J.R., Hey A.J.G. Gauge Theories in Particle Physics Vol. 1. Taylor & Francis, New York, London, 2003.

Geometric Distribution of Path and Fine Structure

Janez Špringer

Cankarjeva Cesta 2, 9250 Gornja Radgona, Slovenia, EU. E-mail: info@lekarna-springer.si

Previously (*Progr. Phys.*, v.2, 105–106) one predicted the exact value of the inverse fine structure constant respecting the double surface concept on Bohr orbit. In this paper one extends the same principle on the geometric distribution of the frequencies of the path of the electron in the ground state of Hydrogen atom. The inverse fine structure constant reflects the kind of the distribution and the later increases the constant in the range of the fifth decimal from $\alpha^{-1}_{0-sided} > 137.036006$ to $\alpha^{-1}_{\infty-sided} < 137.036018$.

1 Theoretical background

The number 137 expresses the translation component n of the path s of the electron on Bohr orbit [1]. Let us consider other translations n around this value are also possible. Each of them has its own frequency:

$$f_z = f(z), \text{ where } z = n - 137,\ n \in \mathbb{Z}. \tag{1}$$

It is also reasonable to assume the sum of the frequencies of all translations equals the unit which is the frequency of the whole translation of the path:

$$F_z = \sum f_z = 1. \tag{2}$$

The two-sided distribution ranges from the translation $n = -\infty$ to $n = 137$ on Bohr orbit and further from there to $n = \infty$. Overall interval is opened since the frequencies at the infinite ends $f_{\pm\infty}$ equal zero and can be ignored. There are also possible even-sided distributions provided on the arbitrary number of two-sided dimensions. From this point of view the non-distribution at $n = 137$ is regarded as zero-sided.

Each translation n belongs to its path s_n so the frequency of the former is identical to the frequency of the later. Product of the given frequency of the path f_z and the path s_n itself is the pondered partial path $f_z \cdot s_n$ inside the whole distribution of the path:

$$s_{whole} \cdot F_z = s_{whole} = \sum f_z \cdot s_n\,. \tag{3}$$

The inverse fine structure constant reflecting the whole distribution of the path [2] can be then expressed as:

$$\alpha^{-1}_{distributed} = \sum f_z \cdot s_n. \tag{4}$$

According to the double-surface concept [2] the value of the path s_n depends on the translation n:

$$s_n = n\left(2 - 1\Big/\sqrt{1 + \pi^2/n^2}\right), \text{ where } n \in \mathbb{Z}. \tag{5}$$

Knowing the type of the distribution function of frequencies $f(z)$ the inverse fine structure constant $\alpha^{-1}_{distributed}$ can be calculated. And vice versa, knowing the inverse fine structure constant $\alpha^{-1}_{distributed}$ the type of the distribution function of frequencies $f(z)$ can be speculated.

Our subject of interest in this paper is the geometric distribution of the frequencies of the path with ratio $1/2$ where the jumping of the electron to the non-adjacent positions is not allowed.

2 The two-sided geometric distribution

This is the symmetric distribution of the frequencies of the path provided on and around the zero numbered position z at $n = 137$:

$$f_z = \frac{1}{3}\frac{1}{2^{|z|}}, \text{ where } z \in \mathbb{Z}. \tag{6}$$

The sum of the frequencies f_z of all translations n from $-\infty$ to $+\infty$ equals the unit:

$$F_z = \sum_{z=-\infty}^{z=\infty} f_z = 1,$$

since

$$\sum_{z=-\infty}^{z=\infty} \frac{1}{3}\frac{1}{2^{|z|}} = \frac{1}{3}\sum_{z=-\infty}^{z=-1}\frac{1}{2^{|z|}} + \frac{1}{3}\sum_{z=0}^{z=0}\frac{1}{2^z} + \frac{1}{3}\sum_{z=1}^{z=\infty}\frac{1}{2^z} = \\ = \frac{1}{3} + \frac{1}{3} + \frac{1}{3} = 1. \tag{7}$$

The value of the inverse fine structure constant reflecting the 2-sided geometric distribution of the frequencies of the path of the electron in the ground state of Hydrogen atom can be calculated with the help of equations (1), (4), (5) and (6):

$$\alpha^{-1}_{2-sided} = \frac{1}{3}\sum_{n=-\infty}^{n=\infty} \frac{n\left(2 - 1\Big/\sqrt{1 + \pi^2/n^2}\right)}{2^{|n-137|}}\,. \tag{8}$$

The values of the frequencies of the path f_z rapidly lessen in the negative as well as positive direction from the zero numbered position z on Bohr orbit so the enough accurate value of the constant can be calculated numerically on the appropriate finite interval, for instance $n = [104, 170]$:

$$\alpha^{-1}_{2-sided} \approx 137.036014. \tag{9}$$

3 The even-sided geometric distribution

On the arbitrary number of sides generalized distribution of the frequencies of the path makes sense to be taken into account when some extra two-sided dimensions are proposed to be involved. The distribution on the even number of k sides is then expressed as:

$$f_z = \frac{1}{k+1}\frac{1}{2^{|z|}}, \text{ where } z \in \mathbb{Z} \text{ and } k = 2m,\ m \in \mathbb{N}_0. \quad (10)$$

The sum of the frequencies f_z of the infinite number of translations n on all k-sides and one zero position equals the unit:

$$F_z = \sum_{z=-\infty}^{z=\infty} f_z = 1,$$

since

$$\sum_{z=-\infty}^{z=\infty}\frac{1}{k+1}\frac{1}{2^{|z|}} = \frac{k}{2}\sum_{z=-\infty}^{z=-1}\frac{1}{k+1}\frac{1}{2^{|z|}} + \sum_{z=0}^{z=0}\frac{1}{k+1}\frac{1}{2^{z}} + \\ + \frac{k}{2}\sum_{z=1}^{z=\infty}\frac{1}{k+1}\frac{1}{2^{z}} = \frac{k}{2}\frac{1}{k+1} + \frac{1}{k+1} + \frac{k}{2}\frac{1}{k+1} = 1. \quad (11)$$

The value of the inverse fine structure constant reflecting the k-sided geometric distribution of the path of the electron in the ground state of Hydrogen atom is found with the help of equations (1), (4), (5), (10) and (11):

$$\alpha^{-1}_{k-sided} = \frac{k}{2(k+1)}\sum_{n=-\infty}^{n=136}\frac{n\left(2-1\Big/\sqrt{1+\pi^2/n^2}\right)}{2^{|n-137|}} + \\ + \frac{137\left(2-1\Big/\sqrt{1+\pi^2/137^2}\right)}{k+1} + \\ + \frac{k}{2(k+1)}\sum_{n=138}^{n=\infty}\frac{n\left(2-1\Big/\sqrt{1+\pi^2/n^2}\right)}{2^{n-137}}, \quad (12)$$

where $n \in \mathbb{Z}$ and $k = 2m$, $m \in \mathbb{N}_0$.

The enough accurate value of the constant can be calculated numerically on the appropriate finite interval. For the acceptable results rounded on the six decimals can be used the finite intervals $n = 137 \pm 33$ instead of the infinite ones $n = 137 \pm \infty$. There is the infinite number of the even-sided distributions available from $k = 0$ to $k = \infty$. The 2-sided distribution at $k = 2$ is only one of them.

4 The non-distribution

Such special distribution of the frequencies of the path of the electron is considered on the zero position and zero sides on Bohr orbit. At $k = 0$ the equation (10) and (11) are simplified to $f_z = F_z = 1$ so the equation (12) takes the known form useful for the calculation of the theoretical inverse fine structure constant[2],(5):

$$\alpha^{-1}_{0-sided} = 137\left(2-1\Big/\sqrt{1+\pi^2/137^2}\right) > 137.036006. \quad (13)$$

5 The infinite-sided geometric distribution

Such special distribution of the frequencies of the path of the electron takes place on the infinite sides around Bohr orbit. At $k = \infty$ the equation (12) is shortened for the vanished middle term and transformed into the next simplified form useful for the finding the theoretical inverse fine structure constant:

$$\alpha^{-1}_{\infty-sided} = \sum_{n=-\infty}^{n=136}\frac{n\left(2-1\Big/\sqrt{1+\pi^2/n^2}\right)}{2^{|n-137|+1}} + \\ + \sum_{138}^{n=\infty}\frac{n\left(2-1\Big/\sqrt{1+\pi^2/n^2}\right)}{2^{n-137+1}} < 137.036018. \quad (14)$$

6 The inverse fine structure reflecting the geometric distribution

The distributed value of the inverse fine structure constant seems to be greater than the non-distributed one since:

$$\alpha^{-1}_{\infty-sided} \approx 137.036018 > \alpha^{-1}_{2-sided} \approx \\ \approx 137.036014 > \alpha^{-1}_{0-sided} \approx 137.036006. \quad (15)$$

The answer doesn't lie in the frequency of the path f_z which otherwise equally decreases on both sides of the number 137 but depends on the factor $\left(2-1\Big/\sqrt{1+\pi^2/n^2}\right)$ which increases more with $n < 137$ than decreases with $n > 137$. The overall effect is thus the increasing value of the distributed inverse fine structure constant inside the range of the fifth decimal.

7 Conclusions

According to the double surface concept the exact inverse fine structure constant reflects the kind of the distribution of the frequencies of the path of the electron in the ground state of Hydrogen atom. The factor $\left(2-1\Big/\sqrt{1+\pi^2/n^2}\right)$ asymmetrically changes partial values of the constant what results the increasing value of the whole constant. The number of sides of the distribution influences the above change in the range of the fifth decimal. The zero-, two- and infinite-sided geometric distribution of the frequencies of the path yields on the six decimal rounded inverse fine structure constant of 137.036006, 137.036014 and 137.036018, respectively.

Dedication

This fragment is dedicated to my daughters Alenka, Manica and Natalija.

Submitted on September 17, 2013 / Accepted on September 22, 2013

References

1. Špringer J. Fine structure constant as a mirror of sphere geometry. *Progress in Physics*, 2013, v. 1, 12–14.
2. Špringer J. Double surface and fine structure. *Progress in Physics*, 2013, v. 2, 105–106.

A Prediction of an Additional Planet of the Extrasolar Planetary System Kepler-62 Based on the Planetary Distances' Long-Range Order

Felix Scholkmann

Bellariarain 10, 8038 Zürich, Switzerland. E-mail: felix.scholkmann@gmail.com

Recently, the discovery of the extrasolar planetary system Kepler-62 comprising five planets was reported. The present paper explores whether (i) the sequence of semi-major axis values of the planets shows a long-range order, and whether (ii) it is possible to predict any additional planets of this system. The analysis showed that the semi-major axis values of the planets are indeed characterized by a long-range order, i.e. the logarithmic positions of the planets are correlated. Based on this characteristic, an additional planet at 0.22 AU in the Kepler-62 system is predicted.

1 Introduction

In April 2013, NASA's Kepler Mission reported [1] the detection of an extrasolar planetary system comprising five planets (Kepler-62b, c, d, e and f) orbiting a star (Kepler-62) of spectral type K2, luminosity class V, 69 ± 0.02% the mass and 63 ± 0.02% the radius of the Sun. The Kepler-62 extrasolar planetary system is located in the constellation Lyra, ∼1200 light years away from Earth. The five planets have a size of 1.31, 0.54, 1.95, 1.61 and 1.41 Earth radii ($R_\oplus$). The two outermost planets (e, f) are likely to be solid planets possibly with liquid water on their surfaces since their position is within Kepler-62's Habitable Zone. The five planets were detected by analyzing the brightness variations of Kepler-62 based on images obtained by the Kepler spacecraft.

In an analysis of distances between planets of our solar system (including the dwarf planet Pluto and the asteroid Ceres) it was shown by Bohr and Olsen [2] that the sequence of distances show a long-range order on a logarithmic scale, i.e. the logarithmic positions of the planets are correlated and follow a periodic pattern; they seem to obey a "quantization". The authors tested the statistical significance of the obtained long-range order by using a permutation test, which revealed that the regularity of the distances between the planets in our solar system is very unlikely to have originated by chance.

In a subsequent study by the same authors [3], they applied their analysis to the extrasolar planetary system HD 10180 and determined that (i) the logarithmic position of the six planets show also a long-range order, and (ii) that this property is enhanced when including a seventh (hypothetically existing) planet at a position of 0.92 ± 0.05 AU, i.e. between the planets HD 10180f and HD 10180g. Based on this analysis, they postulated a possible additional planet in the HD 10180 system at a distance of 0.92 AU.

The goal of the present analysis was to apply the same data analysis approach [2, 3] to the recently discovered extrasolar planetary system Kepler-62 and thus to analyze whether (i) the semi-major axis values of the planets show a long-range order, and whether (ii) the analysis predicts additional planets of this system.

2 Materials and methods

2.1 Data

The parameter values of the Kepler-62's exoplanets were obtained from the listing in Borucki et al. [1]. In particular, two parameters were selected for the present analysis: the semi-major axis (a) and the radius (r) of each planet. For the values, see Table 1.

Planet	i	a [AU]	a [km]	r [$R_\oplus$]	r [km]	$\hat{a}$
62b	1	0.0553	8.2728×10^6	1.31	8355	2.1130
62c	2	0.0929	1.3898×10^7	0.54	3444	2.6317
62d	3	0.120	1.7952×10^7	1.95	12437	2.8877
62e	4	0.427	6.3878×10^7	1.61	10269	4.1570
62f	5	0.718	1.0741×10^8	1.41	8993	4.6767

Table 1: Kepler-62 system parameters according to [1]. i: planet number counting outwardly from the star Kepler-62, a: semi-major axis, r: radius of the planet, ($\hat{a}_i = \ln(a_i/10^6\,\mathrm{km})$), a and r are given in two different units ([AU], [km]) and ([$R_\oplus$], [km]), respectively.

2.2 Data analysis

For the analysis, the semi-major axis value (given in units of 10^6 km) of each exoplanet was first divided by 10^6 km, then logarithmized ($\hat{a}_i = \ln(a_i/10^6\,\mathrm{km})$) and according to these values a multimodal probability distribution function (PDF) $p(\hat{a})$, as introduced by Bohr and Olsen [2], was calculated by

$$p(\hat{a}) = \sum_{i=1}^{N} \alpha_i \, e^{-\beta}, \tag{1}$$

with $N = 5$ (i.e. the maximum number of planets of Kepler-62) and β given as

$$\beta = \frac{j - \hat{a}_i}{w_p / 2\sqrt{2\ln(2)}}, \tag{2}$$

for $j = 1, 1.01, 1.02, \ldots, 10$, with w_p the width (i.e. the full-width-at-half-maximum) of each Gaussian peak of the PDF, and α_i a scale factor. The scale factor defined the magnitude

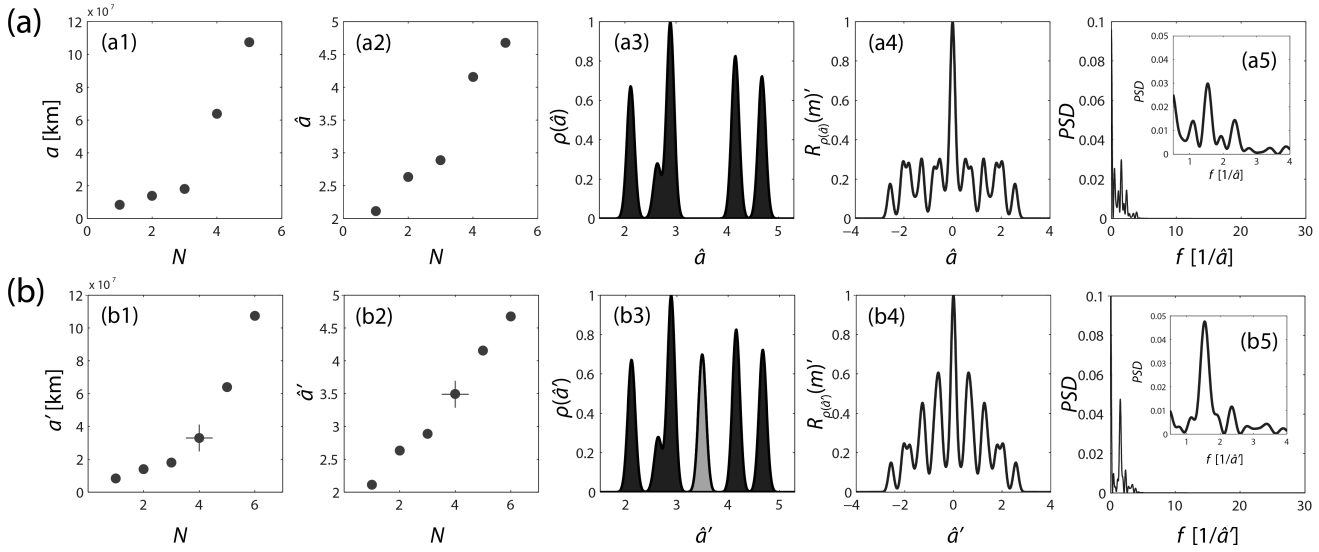

Fig. 1: Results of the analysis of the multimodal PDF $\rho(\hat{a})$ (a1-a5) and the new one $\rho(\hat{a}')$ with the additional hypothetical exoplanet (marked with a cross in Fig. (b1) and (b2), and marked with a black are of the Gaussian peak in Fig. (b3)) found using the optimization approach visualized in Fig. 2.

of each peak. For the present analysis, the scale factor was assigned to the radius of the specific planet, i.e. $\alpha_i = r_i$. The rationale for this definition is that larger planets should be contribute more to the overall multimodal PDF than smaller planets. A linear relationship was chosen rather than the non-linear one used by Bohr and Olsen [2, 3] in order to circumvent the definition of the specific type of non-linear relationship which is unknown per se. For the width of each peak, $w_p = 0.25$ was used which ensures an optimum compromise between a too strong overlap of the Gaussian peaks on the one side and to small peaks on the other. Thus, $\rho(\hat{a})$ represents a sum of Gaussian peaks located at the logarithmized planets semi-major axis values ($\hat{a}$) and weighted by (α_i), the individual radius value of the planet.

In the next step, the autocorrelation sequence of the multimodal PDF was calculated according to

$$R_{\rho(\hat{a})}(m) = \sum_{n=0}^{N-m-1} \rho(\hat{a}_{n+m})\,\rho(\hat{a}_n), \qquad (3)$$

for $m = 1, 2, \ldots, 2N-1$, with N the number of samples of $\rho(\hat{a})$. Then, the autocorrelation function (ACF) was determined by

$$R_{\rho(\hat{a})}(m)' = \frac{1}{R_{\rho(\hat{a})}(1)}\, R_{\rho(\hat{a})}(m), \qquad (4)$$

i.e. $R_{\rho(\hat{a})}(m)$ was normalized by its maximum value given by $R_{\rho(\hat{a})}(1)$ so that $R_{\rho(\hat{a})}(1)' = 1$. The type and grade of the order (short- or long-range) of the input sequence can be determined using the ACF characteristics.

In order to quantify the periodicity in the ACF (i.e. the long-range order of the input sequence), in the next step the frequency-dependent power spectral density (PSD), i.e. the power spectrum (PS), of the multimodal PDF $\rho(\hat{a})$ was calculated by the periodogram method, which is the windowed discrete Fourier transform (DFT) of the biased estimate of autocorrelation sequence. For the calculation, 2^{12} points in the DFT were used by zero-padding $\rho(\hat{a})$ to a length of 2^{12} enabling a proper frequency resolution.

In order to analyze whether an additional hypothetical planet increases the long-range order, the above-mentioned signal processing steps (i.e. calculation of the multimodal PDF, the ACF and the PS) were repeated with the input signal $\rho(\hat{a})$ in which an additional Gaussian peak was inserted, corresponding to the hypothetical exoplanet's position. The high of the peak was set to the mean values of the radius of the five exoplanets. The new peak was introduced between the peaks associated with values of Kepler-62e and Kepler-62f since visual inspection reveals a gap in the multimodal PDF in this region. The semi-major axis value was varied between 0.15-0.38 AU and the corresponding ACF and PS were calculated. For each PS, the maximum PSD value of the fundamental frequency of $\rho(\hat{a})$ (i.e. the first peak after the global maximum at position 0) was calculated. From the obtained values, the maximum was determined which indicate the strongest long-range order of the corresponding sequence with the added new exoplanet. This new multimodal PDF was denoted as $\rho(\hat{a}')$, with $\hat{a}'$ the vector with the new semi-major axis values.

3 Results

The analysis of the semi-major axis values of Kepler-62's planets b-f revealed an exponential like function (Fig. 1(a1))

or a quasi linear one when logarithmized values were used (Fig. 1(a2)).

The calculated multimodal PDF is shown in Fig. 1(a3). The ACF and the PS are shown in Fig. 1(a3) and 1(a4), respectively. The search of the optimal semi-axis value of the additional (hypothetical) planet revealed that a global maximum of the PSD value in the frequency range of 1.1538 $1/\hat{a}$ (≈ 0.6502 units of $\hat{a}$) can be clearly determined, as depicted in Fig. 2. Thus, the analysis predicts an additional planet at a distance of 0.22 AU from the star Kelper-62. The characteristics of the resulting new multimodal PDF $\rho(\hat{a}')$ with all six planets are shown in Fig. 1(b1-b5).

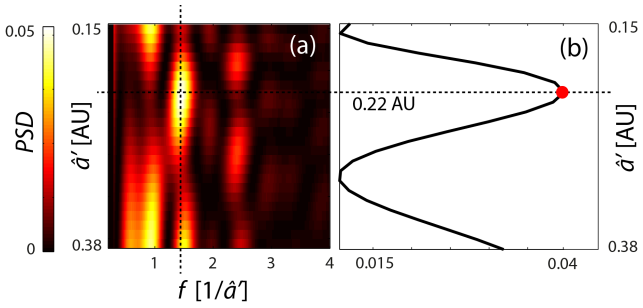

Fig. 2: (a) Color-coded visualization of the PSD values for the $\rho(\hat{a})$ function with the added hypothetical exoplanet at different positions. (b) Function of the PSD values for the frequency of 1.1538 $1/\hat{a}$. The global maximum indicates the value which corresponds to the strongest increase in the long-range order.

4 Discussion and conclusion

From the analysis conducted in the present study, the following conclusions can be drawn:

(i) The positions of the exoplanets Kepler-62a–f show a long-range order inferred from the peak-like structure (four peaks) in the ACF which is captured by the power spectrum as one single peak, corresponding to linear periodicity of the logarithmized distances between the planets.

(ii) The strength of the long-range order increases when an additional planet with a distance of 0.22 AU from the star is added to the five observed ones. This result was obtained by an optimization procedure testing all possible positions for this planet in the gap between Kepler-62e and Kepler-62f.

A prediction of possible additional planets in the Kepler-62 extrasolar system was put forward also recently by Bovaird and Lineweaver [4]. They applied a two-parameter fit to 68 different extrasolar planetary systems in total and predicted 141 additional planets. For the fitting they used a function (denoted by them as a modified Titius-Bode relation) of the form $a_n = \alpha C^n$, with a_n an the semi-major axis, two free parameters (α, C), and n a variable with the quantized values $n = 1, 2, 3, \ldots$. Based on their approach, they predicted for the Kelpler-62 system 7 additional planets with semi-major distance values of 0.07, 0.15, 0.20, 0.26, 0.33, 0.55 and 0.92 AU. Thus, the approach of Bovaird and Lineweaver predicts a finer periodicity compared to the prediction (0.22 AU) described by the present paper. Only the future will tell which approach is better in modeling the exoplanetary characteristics, i.e. the next discovery of an exoplanet of Kepler-62.

By the best of my knowledge, the two predictions (by Bovaird and Lineweave, and the present one), are the only ones published at the present concerning the extrasolar planetary system Kepler-62.

For other extrasolar planetary systems, various authors have reported a periodicity/quantization of the planetary positions and predicted additional orbits/planets based on this.

For example, Naficy et al. [5], recently compared two approaches for modelling and predicting by using either a squared model of the form $r_n = GM\, n^2/(v_0^2\, k^2)$ (with r_n the orbital radius of the n-th planet, G the gravitational constant, M the mass of a central body of the system, and the free parameters v_0^2, k, and n) or an exponential one given by $r_n = a\, e^{bn}$ (with a, b, n free parameters). In both cases, the parameter values of n are integers. The authors concluded that the "exponential model has a better coincidence to observational data" [5]. In addition they observed a relation between the values of the b parameter and the mass of the central star of the system, indicating a possible physical mechanism underlying the exponential model. The squared model was also used in a study analyzing extrasolar planetary systems conducted by Rubčić and Rubčić [11].

Another study based on an exponential model was conducted by Poveda and Lara [24] to examine the extrasolar planetary system 55 Cancri. However, problems with this study were pointed out later [23].

In another study, Panov [6] applied an exponential model of the type $a_n = C\, e^{2n/k}$ to extrasolar planetary systems and reported a good fit as well as predictions of additional planets.

As early as 1996, Nottale found that "the distribution of the semi-major axis of the firstly discovered exoplanets was clustered around quantized values according to the law $a/GM = (n/w_0)^2$, in the same manner and in terms of the same constant $w_0 = 144$ km/s as in our own inner Solar System" [7, 8]. This approach is a result of the "scale relativity" theory developed by Nottale [9, 10, 32, 33]. In 2008, an updated analysis involving 300 exoplanets was published [10] which confirmed and extended the validity of the initial analysis of 1996.*

An analysis with 443 exoplanets (i.e. all known in 2011) was conducted by Zoghbi [26]. This revealed a quantization of the planet's angular momentum which was shown to have a probability of $p < 0.024$ being due to pure chance.

*It would be worthwhile and interesting to repeat the analysis with the presently 732 confirmed exoplanets (September 2013, http://exoplanets.org).

In another study, using the equation $r_n = GM/(c\,\alpha\,e^n)$, with α the dimensionless fine structure constant of $\sim 1/137$ and c the speed of light, Pintr et al. [12] reported a strong agreement between the orbital data of the two analyzed extrasolar planetary system and the expected values. The interesting thing about this work is that the equation is derived from a physical theory describing the effects of electric and magnetic effects on the evolution of a solar system.

Finally, as mentioned earlier, employing a similar method to the one used in this paper (i.e. analysis of correlation property of the logarithmized planetary positions), Olsen and Bohr [3] analysed the extrasolar planetary HD 10180 and predicted an additional planet at 0.92 ± 0.05 AU.

Apart from analyzing extrasolar planetary systems, empirical relationships for the distances of the planets of our solar system started to be published centuries ago when J. D. Titius (1729–1796) and E. Bode (1744–1826) described an apparent regularity of the planetary radii, later known as the Titius-Bode law (expressed in 1787 in its more modern mathematical form by Wurm: $r_n = 0.4 + 0.3 \times 2^n$, $n = -\infty$ (Mercury), $0, 1, 2, \ldots$) [13]. This equation predicted the position of Uranus, but failed to fit for the planetary positions of Neptune and Pluto. Based on the many studies about regularities in planetary distances/radii conducted until now, the Titius-Bode law can be regarded as a first phenomenological description of a possible fundamental law of planetary spacing. The work of Bohr and Olsen [2, 3] in particular strongly suggests that the orbital spacing of planetary systems obey a long-range order and not a simple short-range one, supporting the notion that the quantization is not down to chance.

Concerning the physical mechanism involved in creating a long-range order in planetary systems, this issue is not resolved yet. However, important approaches have been put forward over the last decades. For example, Wells showed that the planetary distances can be "accurately predicted by the eigenvalues of the Euler-Lagrange equations resulting from the variation of the free energy of the generic plasma that formed the Sun and planets" [14, 15]. Further research of the author led him to conclude that "a unification of the morphology of the solar system" and other astrophysical phenomena "can be accomplished by a basic consideration of the minimum-action states of cosmic and/or virtual vacuum field plasmas" [16]. Finally he came to the conclusion that a unification of all physical forces can be derived based on the assumption that they are regarded "as 'fluid' or 'Magnus' forces generated by vortex structures (particles) in the virtual plasma gas" [15–17]. The work of Wells should be carefully reconsidered since it might be a key to understanding regular patterns, long-range orders and quantization of astronomical systems and structures. In addition, analysis based on the theoretical framework of stochastic electrodynamics (SED) that shed new light on the origin of the solar system [18], and also the finding of Graner and Dubrulle [19, 20] that Titius-Bode-like laws appear when assuming a scale and rotational invariance of the protoplanetary system, might also be important for an understanding of the observed patterns.

Other approaches worth exploring for further research are that based on large-scale quantization in space plasmas [22], modelling celestial mechanics using the Schrödinger equation [21, 27, 29, 39–41, 43], resonance effects [25, 28], orbital angular momentum quantization per unit mass [30, 37], fractal scaling modeling using the continued fraction method [31], conservation of mass and momentum, and stability of the angular momentum deficit [35, 36], the stochastisation hypothesis [34], macroscopic quantization due to finite gravitational propagation speed [38], and the Weyl-Dirac approach to gravity [42].

One significant difficulty in explaining the observed regularities of distances is the fact that planets can migrate large distances after their formation (e.g. [44–48]). A model that gives an explanation of the regularities must include this observed fact. One possible explanation might be to regard the quantization pattern as an attractor in a phase-space of the planet's migration movements.

In conclusion, the present analysis of the extrasolar planetary system Kepler-62 reveals that (i) the semi-major axis values of the planets show a long-range order, and (ii) that there might be an additional planet at the distance of 0.22 AU between Kepler-62e and Kepler-62f.

Submitted on September 18, 2013 / Accepted on September 29, 2013

References

1. Borucki W. J., Agol E., Fressin F., Kaltenegger L., Rowe J., et al. Kepler-62: A five-planet system with planets of 1.4 and 1.6 Earth radii in the Habitable Zone. *Science*, 2013, v. 340 (6132), 587–590.
2. Bohr J., and Olsen K. Long-range order between the planets in the Solar system. *Monthly Notices of the Royal Astronomical Society*, 2010, v. 403, L59–L63.
3. Olsen K. and Bohr J. Pair-correlation analysis of HD 10180 reveals a possible planetary orbit at about 0.92 AU. 2010, arXiv: astro-ph.EP/1009.5507.
4. Bovaird T. and Lineweaver, C.H. Exoplanet predictions based on the generalised Titius-Bode relation. 2013, arXiv: astro-ph.EP/1304.3341.
5. Naficy K., Ayubinia A. and Saeedi M. Exponential law as a more comp atible model to describe orbits of planetary systems. *Iranian Journal of Physics Research*, 2012, v. 12 (3), 25–31.
6. Panov K. P. The orbital distances law in planetary systems. *The Open Astronomy Journal*, 2009, v. 2, 92–94.
7. Nottale L., Schumacher G. and Lefévre E.T. Scale-relativity and quantization of exoplanet orbital semi-major axes. *Astronomy and Astrophysics*, 2000, v. 361, 379–387.
8. Nottale L. Scale-relativity and quantization of extra-solar planetary systems. *Astronomy and Astrophysics*, 1996, v. 315, L9–L12.
9. Nottale L. Fractal Space-Time and Microphysics: Towards a Theory of Scale Relativity. World Scientific, 1993.
10. Nottale L. Scale relativity and fractal space-time: theory and applications. 2008, arXiv: physics.gen-ph/0812.3857.
11. Rubčić A. and Rubčić, J. Planetary orbits on solar and extrasolar systems. *Fizika A*, 2010, v. 19 (3), 133–144
12. Pintr P., Peřinová V., and Lukš A. Allowed planetary orbits in the solar system. *Chaos, Solitons & Fractals*, 2008, v. 36, 1273–1282.

13. Jaki S. L. The Early History of the Titius-Bode Law. *American Journal of Physics*, 1972, v. 40 (7), 1014–1023
14. Wells D. R. Was the Titius-Bode series dictated by the minimum energy states of the generic solar plasma? *IEEE Transactions on Plasma Science*, 1990, v. 19 (1), 73–76.
15. Wells D. R. Titius-Bode and the helicity connection: a quantized field theory of protostar formation. *IEEE Transactions on Plasma Science*, 1989, v. 14 (6), 865–873.
16. Wells D. R. Quantization effects in the plasma universe. *IEEE Transactions on Plasma Science*, 1989, v. 17 (2), 270–281.
17. Wells D. R. Unification of gravitational, electrical, and strong forces by a virtual plasma theory. *IEEE Transactions on Plasma Science*, 1992, v. 20 (6), 939–943.
18. Surdin M. The origin of the solar system and stochastic electrodynamics. *Il Nuovo Cimento C*, 1980, v. 3 (6), 626–634.
19. Graner F. and Dubrulle B. Titius-Bode laws in the solar system. I. Scale invariance explains everything. *Astronomy and Astrophysics*, 1994, v. 282, 262–268.
20. Graner F. and Dubrulle B. Titius-Bode laws in the solar system. II. Build your own law from disk models. *Astronomy and Astrophysics*, 1994, v. 282, 269–276.
21. Nie Q. Comprehensive research on the origin of the solar system structure by quantum-like model. *International Journal of Astronomy and Astrophysics*, 2010, v. 1. 52–61.
22. Livadiotis G., McComas D.J. Evidence of large-scale quantization in space plasmas. *Entropy*, 2013, v. 15, 1118–1134.
23. Kotliarov I. The Titius-Bode law revisited but not revived. 2008, arXiv: physics.space-ph/0806.3532.
24. Poveda A. and Lara P. The exo-planetary system of 55 Cancri and the Titius-Bode law. *Revista Mexicana de Astronomía y Astrofísica*, 2008, v. 44, 243–246.
25. Patterson C. W. Resonance capture and the evolution of the planets. 1987, *Icarus*, v. 70, 319–333.
26. Zoghbi J.-P. A. Quantization of planetary systems and its dependency on stellar rotation. *Publications of the Astronomical Society of Australia*, 2011, v. 28 (3), 177-201.
27. Peřinová V, Lukš A. and Pintr P. Distribution of distances in the solar system. *Chaos, Solitons & Fractals*, 2007, v. 34 (3), 669–676.
28. Torbett M., Greenberg R., Smoluchowski R. Orbital resonances and planetary formation sites. *Icarus*, v. 49 (3), 313–326.
29. Smarandache F. and Christianto V. Schrödinger Equation and the Quantization of Celestial Systems. *Progress in Physics*, 2006, v. 2, 63–67.
30. Potter F. Multi-planet exosystems all obey orbital angular momentum quantization per unit mass predicted by quantum celestial mechanics (QCM). *Progress in Physics*, 2013, v. 3, 60–61.
31. Müller H. Fractal scaling models of natural oscillations in chain systems and the mass distribution of the celestial bodies in the solar system. *Progress in Physics*, 2010, v. 1, 62–66.
32. Nottale L. Scale-relativity and quantization of the universe. I. Theoretical framework. *Astronomy and Astrophysics*, 1997, v. 327, 867–889.
33. Hermann R., Schumacher G., and Guyard R. Scale relativity and quantization of the solar system. *Astronomy and Astrophysics*, 1998, v. 335, 281–286.
34. Cresson J. The stochastisation hypothesis and the spacing of planetary systems. *Journal of Mathematical Physics*, 2011, v. 52 (11), 113502.
35. Laskar J. On the spacing of planetary systems. *Physical Review Letters*, 2000, v. 84 (15), 3240–3243.
36. Hernández-Mena C. and Benet L. Statistics and universality in simplified models of planetary formation. *Monthly Notes of the Royal Astronomical Society*, 2010, v. 412 (1), 95–106.
37. Rafie F. Quasi-quantization of the orbits in the Solar System. *Astronomical and Astrophysical Transactions*, 2005, v. 24 (2), 81–92.
38. Giné J. On the origin of the gravitational quantization: The Titius–Bode law. *Chaos, Solitons & Fractals*, 2007, v. 32 (2), 362–369.
39. De Neto M., Maia L. A., Carneiro S. An alternative theoretical approach to describe planetary systems through a Schrödinger-type diffusion equation. *Chaos, Solitons & Fractals*, 2004, v. 21 (1), 21–28.
40. Scardigli F. A quantum-like description of the planetary systems. *Foundations of Physics*, 2007, v. 37, 1278–1295.
41. De Neto M. Pythagoras' celestial spheres in the context of a simple model for quantization of planetary orbits. *Chaos, Solitons & Fractals*, 2006, v. 30 (2), 399–406.
42. Moyassari P., and Jalalzadeh S. Weyl geometry approach to describe planetary systems. 2004, arXiv: gr-qc/0410073.
43. Chang Y.-F. Quantized phenomena in astronomy and astronomic quantum theory. *International Journal of Sciences*, 2013, v. 2, 58–73.
44. Minton D. A. and Malhotra R. A record of planet migration in the main asteroid belt. *Science*, 2009, v. 457, 1109–1111.
45. Rein H. Period ratios in multiplanetary systems discovered by Kepler are consistent with planet migration. *Monthly Notices Letters of the Royal Astronomical Society*, 2012, v. 427 (1), L21–L24.
46. Fernández J. A., and W.-H. Ip. Some dynamical aspects of the accretion of Uranus and Neptune - The exchange of orbital angular momentum with planetesimals. *Icarus*, 1984, v. 58, 109–120.
47. Ipatov S. I. Migration of bodies in the accretion of planets. *Solar System Research*, 1993, v. 27, 65–79.
48. Lin D. N. C., Bodenheimer P., and Richardson D.C. Orbital migration of the planetary companion of 51 Pegasi to its present location. *Nature*, 1996, v. 380, 606–607.

SPECIAL REPORT

Forty Lines of Evidence for Condensed Matter — The Sun on Trial: Liquid Metallic Hydrogen as a Solar Building Block

Pierre-Marie Robitaille

Department of Radiology, The Ohio State University, 395 W. 12th Ave, Columbus, Ohio 43210, USA.
robitaille.1@osu.edu

Our Sun has confronted humanity with overwhelming evidence that it is comprised of condensed matter. Dismissing this reality, the standard solar models continue to be anchored on the gaseous plasma. In large measure, the endurance of these theories can be attributed to 1) the mathematical elegance of the equations for the gaseous state, 2) the apparent success of the mass-luminosity relationship, and 3) the long-lasting influence of leading proponents of these models. Unfortunately, no direct physical finding supports the notion that the solar body is gaseous. Without exception, all observations are most easily explained by recognizing that the Sun is primarily comprised of condensed matter. However, when a physical characteristic points to condensed matter, *a postori* arguments are invoked to account for the behavior using the gaseous state. In isolation, many of these treatments appear plausible. As a result, the gaseous models continue to be accepted. There seems to be an overarching belief in solar science that the problems with the gaseous models are few and inconsequential. In reality, they are numerous and, while often subtle, they are sometimes daunting. The gaseous equations of state have introduced far more dilemmas than they have solved. Many of the conclusions derived from these approaches are likely to have led solar physics down unproductive avenues, as deductions have been accepted which bear little or no relationship to the actual nature of the Sun. It could be argued that, for more than 100 years, the gaseous models have prevented mankind from making real progress relative to understanding the Sun and the universe. Hence, the Sun is now placed on trial. Forty lines of evidence will be presented that the solar body is comprised of, and surrounded by, condensed matter. These 'proofs' can be divided into seven broad categories: 1) Planckian, 2) spectroscopic, 3) structural, 4) dynamic, 5) helioseismic, 6) elemental, and 7) earthly. Collectively, these lines of evidence provide a systematic challenge to the gaseous models of the Sun and expose the many hurdles faced by modern approaches. Observational astronomy and laboratory physics have remained unable to properly justify claims that the solar body must be gaseous. At the same time, clear signs of condensed matter interspersed with gaseous plasma in the chromosphere and corona have been regrettably dismissed. As such, it is hoped that this exposition will serve as an invitation to consider condensed matter, especially metallic hydrogen, when pondering the phase of the Sun.

The Sun is a world so different from our own . . . However [relative to understanding its structure], *one must not lose heart; over the past few years science has made a lot of progress, and those who come after us will not fail to make even more.*

Father Angelo Secchi, S.J., 1875 [1, p. 300, V. I][*]

1 Introduction

A long time ago, men like Gustav Kirchhoff, Johann Zöllner, William Thomson (Lord Kelvin), and James Jeans viewed the photosphere (or the solar body) as existing in the liquid state [2, 3]. Despite their stature, scientists, since the days of Herbert Spencer and Angelo Secchi, slowly drifted towards the concept that the Sun was a ball of gas surrounded by condensed matter [2, 3].[†]

Others, of equal or greater prominence, including August Ritter, Jonathan Lane, Franz Schuster, Karl Schwarzschild, Arthur Eddington, Subrahmanyan Chandrashekhar, and John Bahcall, would have their chance to speak [2, 3]. The Sun became a fully gaseous plasma.

As a consequence, the gaseous Sun has imbedded itself at the very foundation of astronomy. Few would dispute that

[*]Translations from French were executed by the author.

[†]In the mid-1800s, five great pillars had given birth to the gaseous Sun: 1) Laplace's Nebular Hypothesis, 2) Helmholtz' contraction theory, 3) Cagniard de la Tour's critical phenomena and Andrew's critical temperatures, 4) Kirchhoff's formulation of his law of thermal emission, and 5) the discovery of pressure broadening in gases. Each of these has previously been addressed in detail [2].

the Sun is a gas and that our understanding of all other stars and the entire universe, is inherently linked to this reality. Therefore, any endeavor to touch the phase of the Sun must be viewed as an attempt to reformulate all of astronomy.

Yet, when astrophysics remained a young science, observational astronomers, such as James Keeler, Edwin Frost, and Charles Abbot [4], objected to the theoretical basis for a gaseous Sun. August Schmidt was the first to mathematically dismiss the solar surface as illusion. Speaking of him, Charles Abbot, the director of the Smithsonian Observatory would write, *"Schmidt's views have obtained considerable acceptance, but not from observers of solar phenomena"* [5, p. 232]. In 1913, Charles Maunder made the point even more forcefully, *"But under ordinary conditions, we do not see the chromosphere itself, but look down through it on the photosphere, or general radiating surface. This, to the eye, certainly looks like a definite shell, but some theorists have been so impressed with the difficulty of conceiving that a gaseous body like the Sun could, under the conditions of such stupendous temperatures as there exist, have any defined limit at all, that they deny that what we see on the Sun is a real boundary, and argue that it only appears so to us through the effects of the anomalous refraction or dispersion of light. Such theories introduce difficulties greater and more numerous than those that they clear away, and they are not generally accepted by the practical observers of the Sun"* [6, p. 28]. Alfred Fowler, the first Secretary of the International Astronomical Union, shared these views, *"The photosphere is thus regarded as an optical illusion, and remarkable consequences in relation to spots and other phenomena are involved. The hypothesis appears to take no account of absorption, and, while of a certain mathematical interest, it seems to have but little application to the actual Sun"* [7].

With time, however, the voices of the observational astronomers were silenced by the power and elegance of the mathematical arguments [2, 3]. Those who could not follow sophisticated theory could no longer become professional astronomers. At Cambridge, the Mathematical Tripos became and remained an accepted path to a Ph.D. degree in astronomy [8]. Theory [9–14],* rather than observation, came to dictate the phase of the Sun and all solar phenomena were explained in terms of a gaseous entity.

As gases are unable to support structure, additional means were adopted to explain solar observations. Magnetic fields became the solution to every puzzle [12], even though gases are incapable of their generation.† Over time, theoretical approaches claimed one victory after the next, until it seemed as if the Standard Solar Models [11, 13, 14] were unshakable. Gases were inappropriately endowed with all of the properties of condensed matter.

In reality, a closer examination would have revealed that many theoretical achievements were inapplicable. Some of the difficulties stemmed from improper experimental conclusions. The universality of several laws [15–20], on which the entire solar framework rested [9, p. 27–58], was the product of faulty assumptions [21–24]. These errors were introduced when theoretical physics remained in its infancy. But now, they were governed by other branches of physics (i.e. blackbody radiation and condensed matter physics [15–20, 25]), not by astronomy. The most pressing problems were never properly solved by the physics community [21–24].

Solar theory was replete with oversights and invalid assumptions, but the shortcomings would be extremely difficult to detect. Problems which were 'solved 100 years ago' still lurked in the background [19,20]. Too much forward progress was desired with too little attention paid to the road traveled. Most viewed that only a few minor problems remained with gaseous equations of state [13,14]. Evidence that the Sun was not a gas was dismissed with complex schemes often requiring the suspension of objectivity.

Nonetheless, many lines of evidence had revealed that the body of the Sun must be comprised of condensed matter (see Table I). Slowly, arguments initially advanced by men like Gustav Kirchhoff [26] and James Jeans [27, 28] began to reemerge. Moreover, they were joined by an arsenal of new observations. Today, at least forty proofs can be found disputing the gaseous nature of the Sun. There are surely more to be discovered.‡ Conversely, not one direct proof exists that the body of the Sun must be considered a gaseous plasma.

It is clear that the lines of evidence for condensed matter which are contained herein§ are worthy of a cohesive discussion. For the purpose of this presentation, they are subdivided and reorganized into seven broad categories: 1) Planckian, 2) spectroscopic, 3) structural, 4) dynamic, 5) helioseismic, 6) elemental, and 7) earthly. Each proof will be discussed relative to the liquid metallic hydrogen (LMH) model [36, 39, 47, 48] wherein condensed hydrogen, pressurized in the solar interior, assumes a graphite-like lattice on the photosphere [39, 40, 45, 48], a more metallic nature in sunspots and faculae [40,45,52], a diffuse presence in a somewhat cool

*Eddington's mass-luminosity relationship [9, p. 145–179] stands as one of the great triumphs of the gaseous models. Today, this finding is well established in observational astronomy and Eddington's derivation is worthy of a detailed treatment. Due to space limitations, the topic will not be addressed herein. Suffice it to state that Eddington's derivation was dependent on the validity of Kirchhoff's law and no effort has been made to account for the relationship if the stars were made of condensed matter. At the same time, it must be noted that through the mass-luminosity relationship, an observation linked to distant objects, came to dictate the phase of the Sun. The relationship is not contingent on the behavior of the Sun itself, although the latter does lie on the main sequence of the stars.

†Magnetic fields are the product of underlying microscopic structure in condensed matter. As such, whenever a magnetic field is generated on Earth, condensed matter must be involved, either to directly generate it, or to cause the ordered flow of charge.

‡Solar astronomers, upon further consideration, will recognize that their own subject areas might also provide additional lines of evidence. With time, these complimentary proofs will eventually surface.

§The author presents a complete list of his relevant works [2–4, 29–62] in order to facilitate the study of these problems.

Table 1: Forty Lines of Evidence for Condensed Matter — The Sun on Trial.

corona [57, 58, 60], and a solid character in the core [50].*

Of these lines of evidence, the thermal proofs will always remain central to understanding the condensed nature of solar material. They are tied to the most important questions relative to light emission [15–20] and have the ability to directly link physical observation to the presence of a vibrational lattice, a key aspect of all matter in the condensed phase [21–24]. Hence, the discussion begins with the thermal lines of evidence, as inherently related to blackbody radiation [15–25, 63] and to the earliest scientific history of the Sun [2, 3].

*The model adopts a liquid state for the surface of the Sun, as this is in keeping with macroscopic observations. However, an extended structural lattice, not simply a random assembly of degenerate atoms, is required, as demonstrated in §2. Of course, on the scale of solar dimensions, even a material with the rigidity of a solid on Earth (i.e. with a high elastic modulus), might well appear and behave macroscopically as a liquid on the photosphere.

2 Planckian (or Thermal) Lines of Evidence

The Sun emits a spectrum in the visible and infrared region of the electromagnetic spectrum (see Fig. 1) whose detailed analysis provides a total of eight lines of evidence relative to the presence of condensed matter.† For gaseous models, solar emission must be explained using the most complex of schemes, resting both on the validity of Kirchhoff's law of thermal emission [15, 16] and on the *'solar opacity problem'* [42].

Agassi reminds us that *"Browsing through the literature, one may find an occasional use of Kirchhoff's law in some*

†These proofs require the longest descriptions, as they touch many concepts in physics. Since they deal with thermal phenomena, they can also be referred to as the *'Planckian'* lines of evidence, in recognition of Max Planck's contribution to this area of physics [19, 20]. Beyond physics, Max Planck's philosophical writings (see references in [64]) and personal conduct [65], despite the evil of his times, have much to offer to modern society.

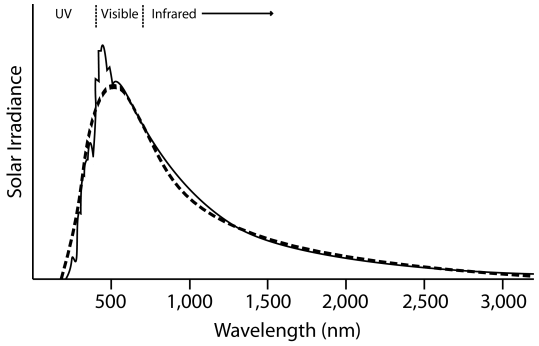

Fig. 1: Schematic representation of the visible spectrum of the Sun (adapted from Fig. 1–3 in [66]). To a first approximation, the solar spectrum is very nearly identical to that of a blackbody with a temperature of ∼5,800 K (dashed line).

experimental physics, but the only place where it is treated at all seriously today is in the astrophysical literature" [63]. In reality, it would not be an overstatement to argue that Kirchhoff's law [15, 16] constitutes the very core of accepted solar theory. Any problems with its formulation would send shock waves not only throughout stellar astrophysics, but to every corner of modern astronomy. Hence, the discussion with respect to the thermal lines of evidence commences with a review of Kirchhoff's law [15, 16] and of blackbody radiation [17–25]. This will be followed by an overview of these principles, as applied to the Sun and the resulting solar opacity problem [42].

2.1 Blackbody Radiation and Kirchhoff's Law

The author has previously stated that, *"Kirchhoff's law is one of the simplest and most misunderstood in thermodynamics"* [24].* Formulated in 1860 [15,16], the law was advanced to account for the light emitted from objects in response to changes in temperature. Typically, in the mid-1800s, the objects were black, as they were covered with soot, or black paint, for best experimental results [21, 23, 24]. Thus, this field of research became known as the study of *'blackbody radiation'* [21, 23, 24]. Kirchhoff attempted to synthesize an overarching law into this area of physics in order to bring a certain unification to laboratory findings. At the time, physics was in its infancy and theorists hoped to formulate laws with *'universal'* consequences. Such was Kirchhoff's goal when his law of thermal emission was devised.

The heart of Kirchhoff's law states that, *"If a space be entirely surrounded by bodies of the same temperature, so that no rays can penetrate through them, every pencil in the interior of the space must be so constituted, in regard to its quality and intensity, as if it had proceeded from a perfectly black body of the same temperature, and must therefore be independent of the form and nature of the bodies, being determined by the temperature alone . . . In the interior therefore of an opake red-hot body of any temperature, the illumination is always the same, whatever be the constitution of the body in other respects"* [16, §16].†

Blackbody radiation was governed strictly by the temperature and the frequency of interest. *The nature of the walls was irrelevant.* Kirchhoff introduced the idea that blackbody radiation somehow possessed a *'universal'* significance and was a property of all cavities [15, 16].

Eventually, Max Planck [19, 20] provided a mathematical form for the spectral shape of blackbody emission sought by Kirchhoff [15, 16]. Kirchhoff's law became ingrained in Planck's formulation [20, §24–§62]. By extension, it also became an integral part of the laws of Wien [17] and Stefan [18], as these could be simply derived from Planck's equation [20, §31–§60]. In turn, the laws of radiation, came to form the very foundation of the gaseous models (see e.g. [9, p. 27–58]).

Since blackbody radiation was thought to be of a *'universal'* nature and *independent of the nature of the walls*, Max Planck, was never able to link his equation to a direct physical cause [21, 23, 24].‡ He spoke of any such attempt as a *'hopeless undertaking'* [20, §41]. In this respect, blackbody radiation became unique in physics. Planck's equation was not linked to anything in the material world, as Kirchhoff's law [15, 16] had dictated that the process was detached from physical causality [20, 21].

With his law, Gustav Kirchhoff was informing the physics community that the light emitted by an object will always correspond to the same *'universal'* spectrum at a given temperature, provided that the object be enclosed and the entire system remain at thermal equilibrium. Any enclosure contained the same blackbody radiation. The nature of the enclosure was not relevant to the solution, given that it was truly opaque. Perfectly reflecting enclosures, such as those made from silver, should function as well as perfectly absorbing enclosures made from graphite or coated with carbon black.

In reality, Kirchhoff erred in believing that the nature of

*A detailed series of publications related to the analysis of Kirchhoff's law has previously appeared. These can be consulted by those who seek a more extensive discussion of the subject matter (see [21–24]).

†Note how this last sentence immediately implied that, if the solar interior could be viewed as enclosed, then the radiation existing within it must be of the same form (intensity versus frequency) as that emitted by a blackbody at the temperature in question.

‡In processes where light is emitted, there are five aspects to consider: 1) the physical setting, 2) separate energy levels created in this setting, 3) a transition species which will make use of these energy levels, 4) the production of a photon, and 5) an equation. For instance, for Lyman-α radiation these correspond to 1) the hydrogen atom, 2) the two electronic orbitals involved in the transition — principle quantum numbers N=2 and N=1, 3) the electron as the transition species, 4) the Lyman-α emission at 1216Å, and 5) the Rydberg formula. Alternatively, in speaking of the proton nuclear magnetic resonance line from water, these correspond to 1) the hydrogen atoms of the water molecules placed in a magnetic field, 2) the hydrogen nuclear spin up or spin down states, 3) the hydrogen nuclear spin as a transition species, 4) the hydrogen line at 4.85 ppm, and 5) the Larmor equation. Analogous entries can be made for any spectroscopic process in physics, with the exception of blackbody radiation. In that case, only the 4th and 5th entries are known: 4) the nature of the light and 5) Planck's equation [21].

the enclosure did not matter [21–24]. Perfectly reflecting enclosures manifest the radiation of the objects they contain, not blackbody radiation (see [22] for a proof). To argue otherwise constitutes a violation of the First Law of Thermodynamics. Furthermore, if Kirchhoff's law was correct, any enclosed material could serve as an experimental blackbody. But, laboratory blackbodies are known to be extremely complex devices, typically involving the use of specialized *'nearly perfectly absorbing'* materials over the frequencies of interest.*

Max Planck believed that *"...in a vacuum bounded by totally reflecting walls any state of radiation may persist"* [20, §61]. In itself, this was contrary to what Kirchhoff had stated, as noted above, *"...In the interior therefore of an opake red-hot body of any temperature, the illumination is always the same, whatever be the constitution of the body in other respects"* [16, §16]. Throughout his text on thermal radiation [20], Max Planck repeatedly introduces a *'small carbon particle'* to ensure that the radiation he was treating was truly black [21, 23]. He viewed the particle as a *catalyst* and believed that it simply accelerated the move towards black radiation. In reality, he had introduced a perfect absorber/emitter and thereby filled the cavity with the radiation desired (see [22] for a proof). If Kirchhoff's law was correct, this should not be necessary. The carbon particle was much more than a simple catalyst [21, 23].

Another repercussion to Kirchhoff's statement was the belief that objects could radiate internally. In fact, Planck would use this approach in attempting to derive Kirchhoff's law (see [20, p. 1–45]).† Yet, conduction and/or convection properly govern heat transfer within objects, not internal radiation. Thermal radiation constitutes an attempt to achieve equilibrium with the outside world.

The idea that all opaque enclosures contain blackbody radiation was demonstrably false in the laboratory and Kirchhoff's law of thermal emission, invalid [21–24].‡ Rather, the best that could be said was that, at thermal equilibrium and in the absence of conduction or convection, the absorption of radiation by an object was equal to its emission. This was properly formulated by Balfour Stewart in 1858, one year before Kirchhoff developed his own law [22, 25].

The universality which Kirchhoff sought was not present. Regrettably, Max Planck had embraced this concept and, as a direct consequence, blackbody radiation was never linked to a direct physical cause. Tragically, the astrophysical community would come to believe that blackbody radiation could be produced without the presence of condensed matter. Upon this *ex nihilo* generation, it built the foundations of a gaseous Sun [9, p. 27–58] and the framework of the universe.

2.2 Kirchhoff's Law, Solar Opacity, and the Gaseous Models of the Sun

Given thermal equilibrium, Kirchhoff's belief that all opaque enclosures contained blackbody radiation had profound consequences for astronomy. If the Sun was considered to be an enclosure operating under thermal equilibrium, then by Kirchhoff's law, it was filled with blackbody radiation (e.g. [9, p. 27–58]). Nothing was required to produce the radiation, other than adherence to Kirchhoff's condition. Even so, use of the laws of thermal emission [15–20] explicitly required the presence of thermal equilibrium in the subject of interest (i.e. conduction and convection must not be present [21–24]).

As for the Sun, it operates far out of equilibrium by every measure, emitting a large amount of radiation, but absorbing essentially none. Furthermore, it sustains clear differential convection currents on its surface, as reported long ago by Carrington [67, 68]. Consequently, how could the proponents of the gaseous models justify the use of the laws of thermal emission to treat the interior of the Sun [9, 13, 14]? How could an object like the Sun be considered enclosed?

Arthur Eddington viewed the Sun as filled with radiation which was essentially black. For him, the Sun acted like a slowly leaking sieve [9, p. 18]. In speaking of the application of Stefan's law [18] to the solar interior, Eddington argued, *"To a very high degree of approximation the last two results are immediately applicable to the interior of a star. It is true that the radiation is not in an ideal enclosure with opaque walls at constant temperature; but the stellar conditions approach the ideal far more closely than any laboratory experiments can do"* [9, p. 99–100]. He justified these statements based on the *very opaque* nature of stellar material which he inferred by considering a distant star, Capella [9, p. 100].

Stefan's law codified a fourth power dependence on temperature (T^4) [18]. At the same time, the gaseous Sun was thought to sustain a core temperature of roughly 1.6×10^7 K [13, p. 9] while displaying an apparent surface temperature of only 6,000 K. Therefore, application of Stefan's law [18] to imaginary concentric spheres [13, p. 2] located in the interior of the Sun would result in a great deal more photons produced in the core than ever emitted by its surface. Through the application of such logic, the Sun could be viewed as a slowly leaking sieve and essentially perfectly enclosed. Eddington inferred that the opacity, or ability to absorb a photon, within the Sun was extremely elevated. Under these circumstances,

*For an extensive list of references on laboratory blackbodies and the materials used in their preparation, see [23].

†In his derivation, Planck did not permit his volume-elements to reflect light [20, p. 1–45]. As a result, all these elements became perfectly absorbing and he was able to obtain Kirchhoff's law. However, had he properly included reflection, he would have convinced himself that Kirchhoff's law was invalid (see [21–24] for a complete discussion).

‡One cannot expect scientists to revisit the validity of every law upon which they shall base their work. As such, if 20th century astronomers committed a misstep in applying Kirchhoff's law to the Sun, it is not at all clear how this could have been prevented. Indeed, when the author was first considering these problems, he actually believed that Kirchhoff's law was valid (i.e. [29]), but that the Sun simply failed to meet the requirements set forth by enclosure. It was only later, following an extensive review of blackbody radiation [21–24], that he came to realize that there was an error in the law itself.

light produced in the solar interior could not travel very far before being absorbed (see [9, p. 100] and [14, p. 185–232]).*

Arthur Milne argued that the interior of a star could be viewed as being in *local thermal equilibrium*, thereby insisting that Kirchhoff's law could be applied within the Sun. Speaking of the solar interior, he stated, *"If the atoms are sufficiently battered about by colliding with one another, they assume a state (distribution of stationary states) characteristic of thermodynamic equilibrium at temperature T"* [69, p. 81–83]. Unfortunately, these words describe the conditions required for the onset of conduction [70]. Thermal equilibrium could never exist at the center of the Sun, as the setting prevailing at the core would facilitate a non-radiative process [21–24].†

Max Planck has clearly stated that thermal equilibrium can only exist in the absence of all conduction, *"Now the condition of thermodynamic equilibrium requires that the temperature shall be everywhere the same and shall not vary with time . . . For the heat of a body depends only on the heat radiation, since on account of the uniformity in temperature, no conduction of heat takes place."* [20, §24]. That is why he insisted that the walls of the enclosure be rigid (e.g. [20, §24–25]), as no energy must be carried away through the action of the momentum transfer which accompanies collisions. Accordingly, Milne's arguments, though they rest at the heart of the gaseous solar models, are fallacious. It is inappropriate to apply Stefan's law to the interior of the Sun, as conductive forces violate the conditions for enclosure and the requirements for purely radiative heat transfer.‡

In his treatise on heat radiation, Planck warned against applying the laws of thermal emission directly to the Sun, *"Now the apparent temperature of the Sun is obviously nothing but the temperature of the solar rays, depending entirely on the nature of the rays, and hence a property of the rays and not a property of the Sun itself. Therefore it would be not only more convenient, but also more correct, to apply this notation directly, instead of speaking of a fictitious temperature of the Sun, which can be made to have meaning only by the introduction of an assumption that does not hold in reality"* [20, §51]. Planck must have recognized that the Sun possessed convection currents on its surface [41], as Carrington's discovery [67] would have been well-established throughout scientifically educated society.

To further complicate matters, astrophysics must create sufficient opacity in the Sun. Opacity acts to contain and shift the internal radiation essential to the gaseous models. It has been said that absorption of radiation in the solar interior takes place through the summation of innumerable processes (including bound-bound, bound-free, free-free, and scattering reactions [14, p. 185–232]). Such a hypothesis constitutes the *'stellar opacity problem'*.§ The blackbody spectrum which could be produced in the laboratory using simple materials like graphite, soot, or metal-blacks [21–24], at once required the summation of a large set of processes which were not known to contribute to the production of the blackbody spectrum on Earth [41, 42]. The central problem for gas models is not that the Sun sustains clear convection at the level of the photosphere, nor that inferred conduction exists at its core. Rather, it was that Kirchhoff's law was not valid and that Planck's equation had not been linked to the physical world [21–24]. The laws of thermal emission could not be applied to the Sun. It was not reasonable to account for the production of a blackbody spectrum using opacity calculations which depended on processes unrelated to thermal emission [42]. The production of blackbody radiation required much more than imaginary enclosures. It required the presence of nearly perfectly absorbing condensed matter, as well-demonstrated by all laboratory experiments over the course of more than 200 years (see [21–24] and references therein).

2.3 The Eight Planckian Lines of Evidence

The eight Planckian (or thermal) lines of evidence, on their own, provide sufficient proof that the Sun is comprised of condensed matter. Each of these proofs includes two components 1) a discussion of some aspect of thermal radiation, and 2) the associated structural implications. It has been well-established in experimental physics that the thermal emissivity of a material is directly linked to its structure [71]. Furthermore, condensed matter is known to possess varying directional emissivities which play a key role in understanding the structures associated with the Sun, including the degree to which one might infer that they are metallic [66, 72, 73].

2.3.1 Solar Spectrum #1

The blackbody lineshape of the solar spectrum (see Fig. 1) has been known since the days of Samuel Langley (see [74, Plate 12 and 21] and [75, Plate IV]).¶ Still, though astrophysics

*Eddington concluded that *"the stars on the main series possess nearly the same internal temperature distribution"* and inferred core temperatures in the millions of degrees [9, p. 177–178]. Given his belief that the laws of thermal emission [15–20] could be applied to the core of the stars, the temperatures he inferred would result in the production of photons with X-ray energies. Over thousands of years, these photons would slowly work their way out to escape at the photosphere. But as they traveled to the surface, they would slowly lose energy and become shifted to ever lower frequencies. Finally, upon reaching the surface, they would emit in the visible region of the electromagnetic spectrum. To accomplish the feat, the gas models required that perfect and gradual changes in opacity enabled a blackbody spectrum produced at X-ray frequencies to be slowly converted to one existing in white light. The issue has previously been addressed by the author [3, 36, 42] and provides an example where accepted science required the suspension of disbelief.

†The density at the center of the Sun is believed to approach 150 g/cm^3 [14, p. 483], a value compatible with conductive solids on Earth.

‡The Sun is known to possess powerful magnetic fields and a solar dynamo. Their existence strongly argues for conduction within condensed matter (see [35, 39] and §5.3).

§The author has previously addressed the stellar opacity problem [42].

¶The first Planckian proof [45] was initially treated in [29, 35, 36, 42, 43].

has tried to explain the production of this light for nearly 150 years [2, 3], little real progress has been made in this direction. As demonstrated in Section 2.2, the gaseous models fail to properly account for the occurrence of the solar spectrum. Gases are unable to emit a continuous spectrum. Rather, they emit in bands (see [21,70] and references therein). Even when pressure broadened, these bands cannot produce the blackbody lineshape. Moreover, when gases are heated, their emissivity can actually drop [21,70], in direct contradiction of Stefan's law [18]. Under these circumstances, the answer cannot be found in the gaseous state. One must turn to condensed matter.

Throughout history, the production of a blackbody spectrum [21, 23, 24] has been facilitated by the use of graphite [76–84] or soot. For this reason, even after the formulation of Kirchhoff's law, astronomers envisioned that graphite particles floated on the surface of the Sun [2, 3]. Hastings recognized that the solar surface was too hot to permit the existence of carbon in the condensed state [85]. He noted that *"Granting this, we perceive that the photosphere contains solid or liquid particles hotter than carbon vapor, and consequently not carbon"* [85]. As a result, in 1881, he suggested that *"... the substance in question, so far as we know it, has properties similar to those of the carbon group"* [85]. Hastings wanted something which had the physical characteristics of graphite, especially related to emissivity. Yet, the only aspect of graphite which could contribute to its emissive characteristics was its lattice structure. He was indirectly searching for a material which might share the lattice arrangement known to exist in graphite (see Fig. 2), but which might likewise be reasonably expected to exist on the surface of the Sun.

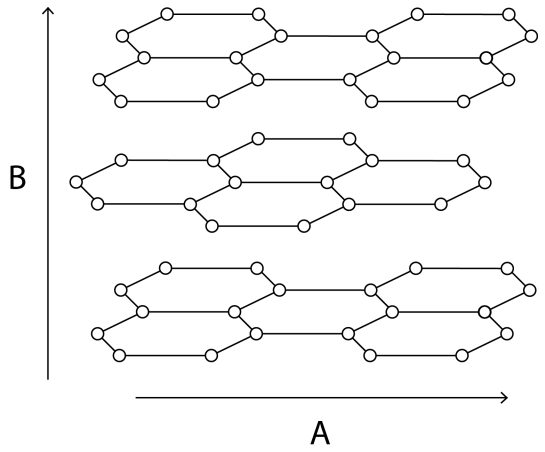

Fig. 2: Schematic representation of the layered hexagonal lattice found in graphite (adapted from Fig. 1 in [48]).

Eventually, Cecilia Payne determined that the stars were largely made of hydrogen [86] and Henry Norris Russell [87] extended the conclusion to the Sun.* Whatever was responsible for the thermal spectrum had to be composed of hydrogen.

Then, in 1935, a seminal work appeared which had the potential to completely alter our understanding of the stars [36, 39]. Eugene Wigner (Nobel Prize, Physics, 1963) and H.B. Huntington [88], proposed that at sufficient pressures, hydrogen could become metallic. More importantly, they would make a direct link between the structure of metallic hydrogen and that of graphite itself, *"The objection comes up naturally that we have calculated the energy of a body-centered metallic lattice only, and that another metallic lattice may be much more stable. We feel that the objection is justified. Of course it is not to be expected that another simple lattice, like the face-centered one, have a much lower energy, — the energy differences between forms are always very small. It is possible, however, that a layer-like lattice has a much greater heat of formation, and is obtainable under high pressure. This is suggested by the fact that in most cases of Table I of allotropic modifications, one of the lattices is layer-like*[1]*..."* [88]. The footnote in the text began, *"Diamond is a valence lattice, but graphite is a layer lattice ..."* [88].

With time, Brovman et al. [89] would propose that metallic hydrogen might be metastable. Like diamonds, it would require elevated pressures for formation, but remain stable at low pressures once synthesized. Neil Ashcroft and his group hypothesized that metallic hydrogen might be metastable between its solid and liquid forms [90, 91].

Metallic hydrogen remains elusive in our laboratories (see [39, 92] for recent reviews). Nonetheless, this has not prevented astrophysics from invoking its existence within brown dwarfs and giant planets [93–95], or even in neutron stars [96]. In fact, based on expected densities, temperatures, and elemental abundances obtained using the gaseous models for the solar core, metallic hydrogen has been said to exist at the center of the Sun [97–99].†

In previous astrophysical studies [93–99], thermal emission has not guided the selection of the form which metallic hydrogen would adopt. As a result, they have sidestepped the layered graphite-like structure first suggested by Wigner and Huntington [88]. Nonetheless, it seems clear that metallic hydrogen, based on the inferred solar abundance of hydrogen [86, 87] and extensive theoretical support (see [39, 92] for

*See [47] for a detailed discussion on the composition of the Sun.

†Setsuo Ichimaru was primarily concerned with nuclear reactions in high density plasmas [97–99]. His work on the solar core is based on assumptions for the composition of the solar interior [97, p. 2] which are derived from the gaseous models, *"In the Sun ... the mass density and the temperature are estimated to be 156 g/cm^3 and 1.55x10^7, respectively. The mass fraction of hydrogen near the core is said to be 0.36 and thus the mass density of metallic hydrogen there is 56.2 g/cm^3"* [98, p. 2660]. Ichimaru places specific emphasis on the One-Component Plasma (OCP) [97, pp. 103 & 209]. He assumed that the lattice points were those of a body-centered cubic [97]. The body-centered cubic is a solid structure. Its existence within the Sun had not been justified beyond inferred densities. Ichimaru's assumptions would have been easily supported by recent seismological evidence which demonstrates that the solar core experiences solid body rotation (see [50] and §6.5 in this work). His supposition has important consequences for driving nuclear reactions within the Sun (see [44, 48] and §7.1 in this work).

reviews), constitutes an ideal building material for the entire Sun which is appropriate for 21st century thought.

Thus, theoretical condensed matter physics unknowingly provided astronomy with everything needed to explain the origin of the thermal spectrum (see Fig. 1). Payne and Russell had determined that the Sun was composed of hydrogen [86, 87]. Under the enormous pressures which existed in the solar interior, Wigner and Huntington [88] allowed that this hydrogen could be converted to the metallic state and adopt the lattice structure of graphite. Work by Brovman et al. [89] enabled metallic hydrogen, formed under high pressure conditions within the solar interior, to be metastable at the surface. Thermal emission could then result from lattice vibrations [21], occurring within layered metallic hydrogen, much like what occurs with graphite on Earth.

In contrast to the gaseous models, where photons take millions of years to escape from the solar core [9], in a liquid metallic hydrogen (LMH) Sun, light can be instantly produced at the level of the photosphere, using mechanisms identical to those found within graphite. Complex changes in internal solar opacities are not required [42]. The solar spectrum can be explained without recourse to unsuited gases [21, 70], imaginary enclosures [9], dismissal of observed conduction [69] and convection [67, 68], the need for local thermal equilibrium [69], or Kirchhoff's erroneous law [15, 16]. The conjecture that solar thermal emission is produced by hydrogen in the condensed state on the surface of the Sun is simpler than any scheme brought forth by the gaseous models. Furthermore, it unifies our understanding of thermal emission in the stars with that of laboratory models on Earth. But most importantly, it results in the incorporation of a structural lattice directly onto the photosphere, providing thereby a basis upon which every other physical aspect of the Sun can be directly explained — from the presence of a true surface to the nature of all solar structures. Hydrogen's ability to exist as condensed matter within the solar body, photosphere, chromosphere, and corona, appears all but certain. The remainder of this work should help to further cement this conclusion.

Fig. 3: Image of the Sun displaying how the intensity of the disk decreases towards the limb [100]. Note this image was described as follows, *"Sunspot group in context. The diameter of the Sun is 100 times larger than the diameter of the Earth. This image was recorded with our finder telescope at about the same time as the 15 July images and movies. Target: The Sun; Date: 15 Jul 2002"*. It is reproduced herein thanks to the generosity of the Royal Swedish Academy of Sciences (www.solarphysics.kva.se/NatureNov2002/press_images_eng.html — accessed online 9/15/2013). The SST is operated on the island of La Palma by the Institute for Solar Physics of the Royal Swedish Academy of Sciences in the Spanish Observatorio del Roque de los Muchachos of the Instituto de Astrofísica de Canarias.

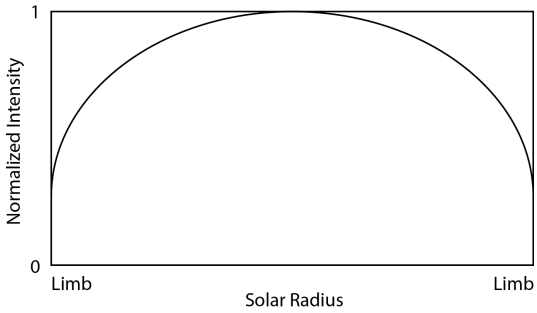

Fig. 4: Schematic representation of the white light intensity variation across the solar disk which is responsible for visible limb darkening. The extent of intensity variation is frequency dependent [101].

2.3.2 Limb Darkening #2

According to Father Angelo Secchi, while Galileo denied the existence of limb darkening (see Figs. 3, 4), the phenomenon had been well established by Lucas Valérius of the Lincei Academy, *"...the image of the Sun is brighter in the center than on the edges."* [1, p. 196, V. I].*

In 1902, Frank Very demonstrated that limb darkening was a frequency dependent phenomenon [101] which he attributed to scattering in the solar atmosphere and reflection with carbon particles.†

Very's study of solar emission [101] eventually led to the *law of darkening* initially developed by Karl Schwarzschild [102], whereby the observed phenomenon could be explained by relying on the assumption that radiative equilibrium existed within the stars. Once again, this was viewed as a great triumph for gaseous models (see [3] for additional details).

Arthur Eddington would come to adopt Milne's treatment [103] of the *law of darkening* [9, p. 320–324]. However, all of these approaches shared a common flaw: they were based on the validity of Kirchhoff's law [15, 16]. Karl Schwarzschild's derivation began with the words, *"If E is the emission of a black body at the temperature of this layer and one assumes that Kirchhoff's law applies, it follows that the layer will radiate the energy Eadh in every direction"* [102, p. 280 — in Meadows].

Beyond the validity of Kirchhoff's law, these derivations sidestepped the reality that clear convection currents existed

*The second Planckian proof [45] was initially treated in [3, 35, 40, 42].

†As nearly perfect absorbers, carbon particles make for poor reflectors.

on the exterior of the Sun [67, 68]. Remarkably, just a few years after publishing his classic derivation of the law of darkening [103], Milne himself argued that local thermal equilibrium did not apply in the outer layers of the stars [69]. Arthur Eddington also recognized that the laws of emission could not be used to treat the photosphere, *"The argument cannot apply to any part of the star which we can see; for the fact that we see it shows that its radiation is not 'enclosed' "* [9, p. 101]. As such, how could Kirchhoff's law be invoked to explain limb darkening?

To further complicate the situation, any explanation of limb darkening for gaseous models would once again resurrect the solar opacity problem [42]. How could the exterior of the Sun generate a perfect blackbody spectrum using an assembly of processes not seen within graphite?

Gas models accounted for limb darkening by insisting that the observer was sampling different depths within the Sun (see Fig. 5). When viewing the center of the disk, our eye was observing radiation originating further in the interior. This radiation was being released from a layer which was at a higher temperature. Hence, by the Wien's law [17] it appeared brighter. As for limb radiation, it was being produced at shallower depths, thereby appearing cooler and darker.

These ideas were reliant on the belief that the surface of the Sun was merely an illusion,* a conjecture which will be refuted in §3.1, §3.2, §3.7, §4.3, §4.5, §5.1, §5.2, §5.5, §5.7, §6.1, §6.2, and §6.3.

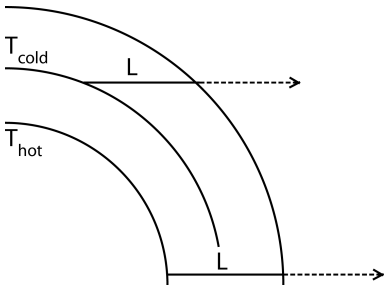

Fig. 5: Schematic representation of how limb darkening is explained in the gas models. When viewing the center of the solar disk, the line of sight travels to a greater depth (L), where it reaches a hotter layer in the solar body. Conversely, when the limb is visualized, the line of sight (L) is restricted to a cooler upper layer. One of the fallacies of this explanation is that the outer layers of the photosphere cannot be considered enclosed (i.e. we can see through them when we visualized the center of the disk). So, photospheric radiation could not be blackbody, even assuming that Kirchhoff's law was valid. Eddington himself had reached this conclusion [9, p. 101].

In the end, the simplest explanation for limb darkening lies in the recognition that directional spectral emissivity occurs naturally within condensed matter [66, 71–73]. Poor conductors tend to have elevated normal emissivities which gradually fall as the angle of observation is decreased (see Fig. 6). This is precisely what is being observed across the solar disk. Good conductors often display lower normal emissivities, which can gradually increase as the angle of observation is decreased, prior to decreasing rapidly as the viewing angle becomes parallel to the surface (see Fig. 6).

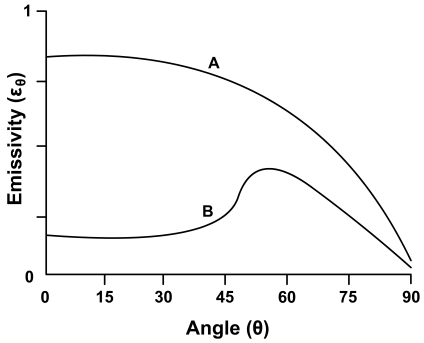

Fig. 6: Schematic representation of directional spectral emissivities for non-conductors (A) and conductors (B). Note that in non-metals, the spectral emissivity decreases monotonically with viewing angle. Conversely, in metals, while the normal emissivity can be substantially reduced, the emissivity can rise with increasing angle before precipitously dropping (adapted from [72]).

Limb darkening revealed that the solar photosphere was condensed, but not highly metallic.† Graphite itself behaves as an excellent emitter, but only a modest conductor. It can be concluded, based on Figs. 4 & 6, that the liquid metallic hydrogen which comprises the solar surface is not highly metallic. The inter-atomic distances in this graphite-like layered material (a Type-I lattice) would be slightly larger than those found in the more metallic sunspots (a Type II lattice), as previously described by the author [35, 39, 40].

2.3.3 Sunspot Emissivity #3

Galileo viewed sunspots (see Fig. 7) as clouds floating very near the solar surface [105].‡ His great detractor, Christoph Scheiner, initially saw them as extrasolar material [2], but eventually became perhaps the first to view them as cavities [1, p. 15, V. I]. This apparent depression of sunspots was confirmed by Alexander Wilson [2] who, in 1774 [106], used precise geometric arguments to establish the effect which now bears his name [1, p. 70–74]. In 1908, George Ellery Hale discovered that sunspots were characterized by intense magnetic fields [107]. This remains one of the most far reaching findings in solar science.

*To this day, astronomy continues to maintain that the Sun's surface is an illusion, as seen in this text produced by the National Solar Observatory, *"The density decreases with distance from the surface until light at last can travel freely and thus gives the illusion of a visible surface"* [104, p. 4].

†As a side note, Frank Very had suggested [101] that the limb darkening of the Sun might be associated with the solar granulations [3, 101]. As will be seen in §2.3.4, the thought was not without merit.

‡The third Planckian proof [45] was initially the 13th line of evidence [35]. It has been presented, in greater detail, within [4, 40, 45].

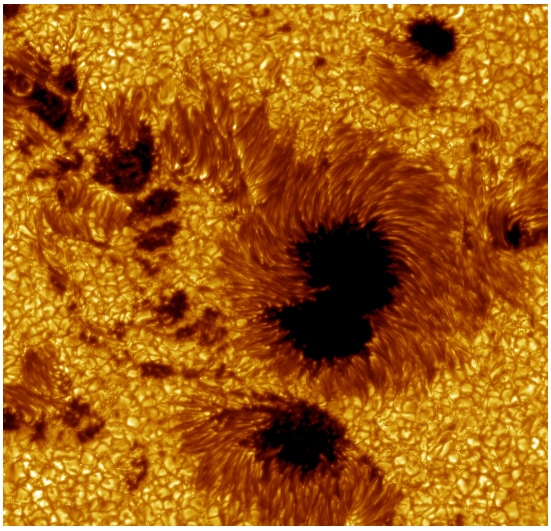

Fig. 7: Part of a sunspot group near the disk center acquired with the Swedish 1-m Solar Telescope [100]. This image has been described as follows by the Institute for Solar Research of the Royal Swedish Academy of Sciences, *"Large field-of-view image of sunspots in Active Region 10030 observed on 15 July 2002. The image has been colored yellow for aesthetic reasons ... Dark penumbral cores — Observations: Göran Scharmer, ISP; Image processing: Mats Löfdahl, ISP; Wavelength: 487.7 nm; Target: AR10030; Date: 15 Jul 2002"*. This image is available for publication thanks to the generosity of the Royal Swedish Academy of Sciences (www.solarphysics.kva.se/NatureNov2002/press_images_eng.html — accessed online 9/15/2013). The SST is operated on the island of La Palma by the Institute for Solar Physics of the Royal Swedish Academy of Sciences in the Spanish Observatorio del Roque de los Muchachos of the Instituto de Astrofísica de Canarias.

In addition to the Wilson effect, sunspot emissivity has been found to drop significantly with increasing magnetic field strength [108, 109]. The magnetic fields within sunspot umbra are known to have a vertical orientation. Their intensity increases in the darkest regions of the umbra (e.g. [110, p. 75] and [111, p. 80]). Sunspot emissivity has also been hypothesized to be directional, with increasing emissivity towards the limb [111, p. 75–77]. In this regard, Samuel Langley had observed, *"With larger images and an improved instrument, I found that, in a complete ring of the solar surface, the photosphere, still brilliant, gave near the limb absolutely less heat than the umbra of the spots"* [112, p. 748]. Edwin Frost echoed Langley, *"A rather surprising result of these observations was that spots are occasionally relatively warmer than the surrounding photosphere"* [113]. Today, the apparent directional changes in the emissivity of sunspots has been dismissed as due to *'stray light'* [111, p. 75–77].

Since a gaseous Sun is devoid of a real surface, the *'Wilson Effect'* cannot be easily explained within these bounds. Once again, optical depth arguments must be made (e.g. see [110, p. 46] and [114, p. 189-190]). In order to account for the emissivity of sunspots, gaseous models propose that magnetic fields prevent the rising of hot gases from the solar interior [104]. Hence, the spot appears cool. But sunspots can possess light bridges (see Secchi's amazing Fig. 33 in [1, p. 69, V. I]). These are characterized by higher emissivities and lower magnetic fields [111, p. 85–86]. The problem for the gaseous models is that light bridges seem to *'float'* above the sunspot. How could these objects be warmer than the material below? Must a mechanism immediately be found to heat light bridges? Sunspots are filled with substructure, including that which arises from Evershed flow. Such substructure is well visible in Fig. 7. However, gases are unable to support structure. How can a gaseous solar model properly account for Evershed flow, while dismissing the surface as an illusion? The problem, of course, remains that all these illusions actually are behaving in systematic fashion (see §5.1). Furthermore, in modern astronomy, the apparent change in sunspot emissivity towards the limb must be dismissed as a *'stray light'* effect. But the most pressing complication lies in the reality that gases are unable to generate powerful magnetic fields (see §5.3). They can respond to fields, but have no inherent mechanism to produce these phenomena. Along these lines, how can magnetic fields be simultaneously produced by gases while at the same time prevent them from rising into the sunspot umbra? On Earth, the production of powerful magnets involves the use of condensed matter and the flow of electrons within conduction bands, not isolated gaseous ions or atoms (see §5.3).

In contrast to the gaseous models, the idea that the Sun is comprised of condensed matter can address all of these complications. The *'Wilson Effect'*, one of the oldest and simplest of solar observations, can continue to be explained without difficulty by using elementary geometry [106], precisely because a true surface can be invoked [45]. The lowered emissivity of sunspot umbra, in association with increased magnetic field strengths, strongly suggests that sunspots are metallic in nature. Langley's observation that sunspots display increased limb emissivity relative to the photosphere can be explained as related to metallic effects.* The increased emissivity and lower magnetic field strength observed within light bridges could be explained by assuming that they, like the photosphere, are endowed with a Type I lattice [35, 39, 40] with lowered metallic properties. Conversely, the decreased normal emissivity of sunspot umbra along with their increased magnetic field strength suggests a more metallic Type II lattice [35, 39, 40] in these structures.

In sunspots, the electrons responsible for generating magnetic fields can be viewed as flowing freely within the conduction bands available in metallic hydrogen. This implies

*This is not to say that stray light cannot present problems. However, these effects should make faculae even less apparent towards the limb, further highlighting the importance of the increase in emissivity which those structures display (see §2.3.5). Definitive answers may come eventually by examining large sunspots.

that the lattice within sunspot umbrae are positioned so that the hexagonal hydrogen planes (see direction A in Fig. 2) are nearly orthogonal to the solar surface (see Fig. 8). In the penumbra, they would be oriented more horizontally, as demonstrated by the magnetic field lines in this region. The accompanying emissivity would be slightly stronger, resulting in the penumbra appearing brighter. As such, the emissivity in layered metallic hydrogen appears to be highly dependent on the orientation of the hexagonal hydrogen planes.

Likewise, it has been observed that sound waves travel faster within sunspots than within the photosphere [116, 117]. These findings are supportive of the idea that sunspots are denser and more metallic than the photosphere itself. The use of condensed matter brings with it both structure and function.

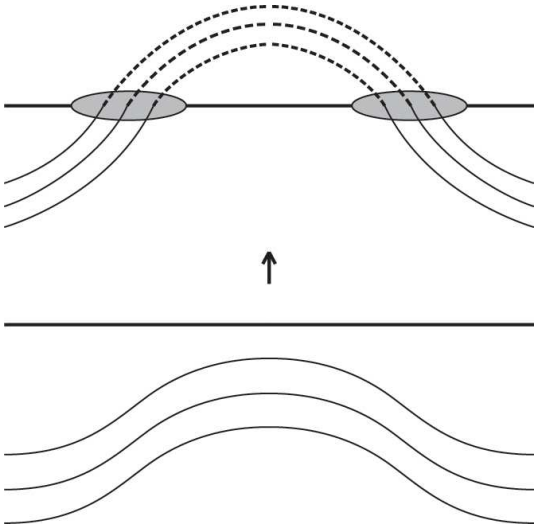

Fig. 8: Schematic representation of the appearance of a pair of sunspots on an active solar surface. The horizontal thick line illustrates the location of the photosphere, the thin lines the layers of metallic hydrogen, and the dashed lines the magnetic field. The two shaded circles outline the position of sunspots. In the lower portion of the figure, the layers of metallic hydrogen are below the level of the photosphere, but are being pushed up by intercalate elements which have entered the gas phase (see §5.1 in [48]). In the upper portion of the figure, the layers of metallic hydrogen have now broken through the photospheric level. The two sunspots are being linked solely by magnetic field lines, as the metallic hydrogen which once contained them has vaporized into the solar atmosphere. This figure is an adaptation based on Fig. 22 in [115]. Along with this legend, it previously appeared in [52].

2.3.4 Granular Emissivity #4

When observed at modest resolution, the surface of the Sun is covered with granules (see Fig. 9).* The appearance of these structures caused considerable controversy within astronomy in the mid-1800s [40], but they have been well described and illustrated [118–122] since the days of Father Secchi [1, p. 48–59, V. I]. Individual granules have limited lifetimes, can be arranged in mesogranules, supergranules, or giant cell [40, 118–122], and seem to represent a convective process.†

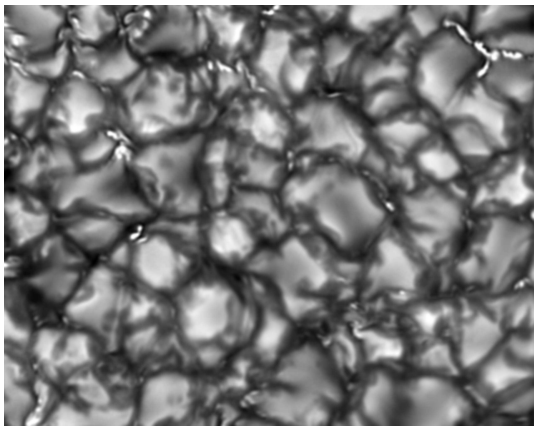

Fig. 9: High resolution image of solar granules acquired by Vasco Henriques on May 23, 2010 using the Swedish 1-m Solar Telescope (SST). Bright granules are surrounded by dark intergranular lanes which can contain magnetic bright points (see §2.3.5). This image has been described as follows, *"The SST is operated on the island of La Palma by the Institute for Solar Physics of the Royal Swedish Academy of Sciences in the Spanish Observatorio del Roque de los Muchachos of the Instituto de Astrofísica de Canarias — High resolution granulation — Observer: Vasco Henriques; Image processing: Vasco Henriques Date: 23 May 2010"*. http://www.solarphysics.kva.se (accessed online 9/15/2013).

Though granules are dynamic convective entities which are constantly forming and dying on the surface of the Sun, they have been found to observe the laws of Aboav-Weaire and of Lewis [123–125], along with the perimeter law, for space filling structures in two dimensions [126]. That granules can be viewed as crystals was first hypothesized by Chacornac in 1865 [127]. Clearly, the laws of space filling cannot be applied to gases which expand to fill the space of containers. They cannot, on their own, restrict the spatial extent which they occupy. The laws of space filling can solely be observed by materials which exist in the condensed state. Adherence to these laws by granules [126] constitutes important evidence that these structures are comprised of condensed matter.

Studies reveal that granules can contain *'dark dots'* at their center, linked to *'explosive'* structural decay. Rast [128] has stated that this decay *"can be better understood if granu-*

*The fourth Planckian proof [45] was initially part of the 14th line of evidence [45]. It has been presented, in greater detail, within [40] which contains an extensive list of references on the subject.

†This aspect of solar granules will be discussed in §5.1 as it is linked to activity on the solar surface. For the time being, the focus will remain on the structural and emissive aspects.

lation is viewed as downflow-dominated-surface-driven convection rather than as a collection of more deeply driven upflowing thermal plumes". These arguments depend on the presence of a true solar surface. Noever has linked the decay of granules associated with the appearance of *'dark dots'* to the perimeter law alone [126], once again implying that structure determines dynamic evolution.

Granules are characterized by important emissive characteristics. These structure tend to be brighter at their center and surrounded by dark intergranular lanes (see Fig. 9) whose existence has been recognized by the mid-1800s [40].

In order to account for the emissive properties of granules, the gaseous models maintain that these structures represent convective elements. Hot gases, rising from deep within the Sun, emerge near the center of these formations, while cooler material, held in the dark intergranular lanes, slowly migrates towards the solar interior. In this case, emissivity is linked to temperature changes alone, as dictated by Wien's law [17]. This hypothesis rests on the validity of Kirchhoff's law [15, 16, 20–24] and depends upon subtle changes in solar opacity [42] in adjacent regions of the solar surface. As seen in §2.1 and §2.2, these arguments are invalid.

Within the context of the LMH model [35, 39], granules are viewed as an integral portion of the true undulating surface of the Sun. Their complex radiative properties can be fully explained by considering directional spectral emissivity. As sub-components of the photosphere, the same mechanism invoked to understand limb darkening §2.3.2 can be used to explain granular emissivity.

The normal emissivity of these bubble-like structures remains somewhat elevated. As the viewing angle moves away from the normal,* emissivity progressively drops in accordance with the known behavior of non-metals (see Fig. 6). Intergranular lanes appear dark, not because they are cooler (an unlikely scenario in the same region of the Sun), but rather, because less photons are observed when the surface being visualized becomes increasingly coincident with the direction of emission. In a sense, with respect to thermal emission, each granule constitutes a mini-representation of the macroscopic limb darkening observed across the disk of the Sun (see §2.3.2), an idea first expressed by Very [101].

In the LMH model, granules therefore possess a Type I lattice [35, 39], which is somewhat less metallic than the Type-II lattice found in sunspots. This is revealed by the lack of strong magnetic fields associated with granules and by the slowly decaying center-to-limb variation in directional emissivity observed on the solar surface (see §2.3.2). In a manner analogous to what is observed in sunspots, the emissivity of layered metallic hydrogen would imply that the hexagonal hydrogen planes are oriented parallel to the solar surface at the center of a granules providing higher emissivity, or brighter appearance, in this instance. The orientation should become more vertical in the intergranular lanes, thereby accounting for their darker appearance. The LMH model [35, 39] dispenses with optical depth and variable temperature arguments. It elegantly accounts for solar emission using a single phenomenon (directional spectral emissivity in condensed matter) applicable across the full range of solar observations.

2.3.5 Facular Emissivity #5

In visible light, faculae are difficult to observe at the center of the solar disk, but often become quite apparent towards the limb.† Father Secchi noted the difficulty of observing faculae at the center of the disk [1, p. 49, V. I] and George Ellery Hale commented on the enhanced emissivity of faculae towards the limb, *"The bright faculae, which rise above the photosphere, are conspicuous when near the edge of the Sun, but practically invisible when they happen to lie near the center of the disk . . . "* [129, p. 85–86]. Solar faculae appear to float on the photosphere itself. The structures have long been associated with sunspots [130]. Wang et al. recently postulated that these objects could result from the conversion of sunspots, wherein the horizontal magnetic field contained within penumbrae makes a transition to a vertical field in faculae [131]. Faculae are known to possess strong magnetic fields [132–134].

The emissivity of faculae as they approach the solar limb [135] cannot be reasonably explained within the context of the gaseous models. The accepted scheme, Spruit's *'hot wall'* [136, 137] model is illustrated in Fig. 10. When the faculae are at the center of the disk, the observer is able to see deeper into the Wilson depression to the flux tube *'floor'* [137, p. 926]. This floor is thought to be at a lower temperature and, according to the laws of blackbody emission [15–20], appears relatively dark. As for the *'walls'* of the flux tube, they are said to sustain elevated temperatures and appear bright when compared to the deeper *'floor'*. As the flux tube moves towards the limb, the observer can no longer observe the *'floor'* and one of the *'hot walls'* becomes increasingly visible. With time, even that *'hot wall'* disappears. This agrees with observation: facular emissivity is initially indistinguishable from that of the photosphere at disk center. It then increases and becomes bright with respect to the rest of the solar surface, as theses objects move towards the limb. Finally, the emissivity decreases precipitously at the limb.

To help explain the emissivity of faculae, the gas models suggest macroscopic structures, *'cool floors'* and *'hot walls'*. Gases are incapable of generating such features. In faculae, flux tubes are said to be permitting heat from the solar interior to rise into the *'hot walls'*. Yet, to account for the darkness

*Normal viewing occurs when the line of sight is perpendicular to the surface.

†The fifth Planckian proof, as related to facular emissivity, was initially presented as the 15th line of evidence [45].

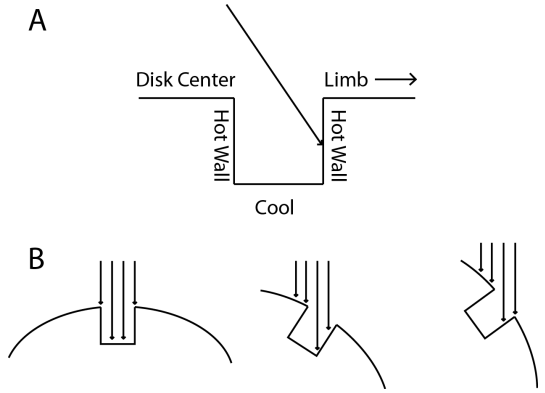

Fig. 10: Schematic representation of Spruit's *'hot wall'* model [136, 137]. A) Faculae are represented as depressions in the solar surface. Depending on the line of sight, the observer will sample either a *'cool floor'*, or a *'hot wall'*. B) When sampling at the center of the solar disk, he/she will only be able to visualize a *'cool floor'* whose temperature approaches that of the granules on the surface. Under the circumstances, the faculae are not visible. However, as these objects move towards the limb, the line of sight will initially sample more of the *'hot wall'* and the faculae appear brighter. When the edge of the Sun is approached, the hot walls can no longer be readily sampled and the emissivity of the faculae are perceived to drop rapidly.

within sunspots, the models had required that field lines inhibited the upward flow of hot gases beneath the umbra (see §2.2.3).

It is immediately apparent that the emissive behavior just described within faculae exactly parallels the known radiative properties of metals, as previously illustrated in Fig. 6. Faculae possess strong magnetic fields [132–134]. In combination with their directional emissivity, this all but confirms that they are metallic in nature.

In addition to faculae, an extension of Spruit's hot wall model has been invoked to explain the presence of magnetic bright points found within the dark intergranular lanes of the granules [138]. As the name implies, magnetic bright points are also believed to possess strong magnetic fields [12, 138, 139]. Moreover, they display powerful center-to-limb variations in their emissivity [138], being most visible at the center of the solar disk within the dark intergranular lanes. In the case of magnetic bright points, it is the *'floor'* which is viewed as bright, as light is said to originate from *"deeper photospheric layers that are usually hotter"* [138].*

The problem rests in the realization that magnetic bright points are located within the dark intergranular lanes. As a result, in order to explain the presence of locally strong magnetic fields within these objects, it is hypothesized that an *"efficient turbulent dynamo transforms into magnetic fields part of the kinetic energy of the granular convection"* [138]. This serves to emphasize the problems faced by the gas models.

Within the context of the LMH model [35, 36, 39], the presence of faculae and magnetic bright points on the solar surface are elegantly explained by invoking lattice structure. Since faculae are associated with sunspots [130] and even thought to be ejected from these structures [131], it is reasonable to propose that they can be metallic in nature (see Fig. 6), that their structural lattice mimics the type II lattice found in sunspots, and that they have not yet relaxed back to the Type-I lattice found in granules. In this case, the brightness of faculae implies that their hexagonal hydrogen planes lie parallel to the solar surface. This should account for both emissivity and the presence of associated magnetic fields in these structures.

In the end, the simplest explanation for the origin for magnetic bright points may be that they are nothing more than facular elements. Rising from internal solar regions, they have not fully relaxed from a Type II to a Type I lattice, but have been transported through granular flow to deeper intergranular lanes. Their center-to-limb emissivity variations may well rest in the realization that they are hidden from view by the granules themselves as the limb is approached. Hence, their numbers appear to fall towards the edge of the solar disk [138].

2.3.6 Chromospheric Emissivity #6

While hydrogen-α emissions are responsible for the red glow of the chromosphere visible during an eclipse, this region of the Sun also emits a weak continuous spectrum [56] which has drawn the attention of solar observers for more than 100 years [140–147].† Relative to this emission, Donald Menzel noted, *"...we assumed that the distribution in the continuous chromospheric spectrum is the same as that of a black body at 5700°, and that the continuous spectrum from the extreme edge is that of a black body at 4700°. There is evidence in favor of a lower temperature at the extreme limb in the observations by Abbot, Fowle, and Aldrich of the darkening towards the limb of the Sun"* [142].

The gaseous models infer that the chromosphere has an average density of $\sim 10^{-12}$ g/cm^3 [115, p. 32].‡ Despite a 10^5 drop in density with respect to the photosphere, these treatments continue to advance that the continuous emission in the chromosphere is being produced by neutral H, H$^-$, Rayleigh scattering, and electron scattering (see [145, 146] and [150, p. 151–157]). But, none of these processes can be found in graphite (see §2.1 and §2.2).

*These layers were not hotter in Spruit's model [136, 137].

†The sixth Plankian proof [45] was initially presented as the 26th line of evidence [56].

‡In these models, the photosphere is assumed to have a density of $\sim 10^{-7}$ g/cm^3, while the outer chromosphere has a density of $\sim 10^{-15}$ g/cm^3 [148]. This constitutes an 8 order of magnitude decrease in just a few thousand kilometers. As a point of reference, the density of the Earth's atmosphere at sea level is $\sim 1.2 \times 10^{-3}$ g/cm^3 [149] or ~10,000 greater than calculated photospheric densities for the gas models.

Alternatively, within the context of the LMH model, the chromospheric continuous emission provides evidence that condensed matter exists in this region of the solar atmosphere [56]. This is in keeping with the understanding that continuous spectra, which can be described using blackbody behavior, must be produced by condensed matter [21–24]. In this regard, the chromosphere may be viewed as a region of hydrogen condensation and recapture within the Sun. Though generating condensed matter, the chromosphere is not comprised of metallic hydrogen.*

2.3.7 K-Coronal Emissivity #7

The white light emitted by the K-corona is readily visualized during solar eclipses.† Observing from Iowa in 1869, William Harkness *"obtained a coronal spectrum that was continuous except for a single bright green line, later known as coronal line K1474"* on the Kirchhoff scale [151, p. 199]. Eventually, it became clear that the continuous spectrum of the K-corona was essentially identical to photospheric emission [152–156], with the important distinction that the former was devoid of Fraunhofer lines. In addition, the spectrum of the K-corona appeared to redden slightly with increasing distance from the solar surface, *"microphotograms for solar distances varying from R=1.2s to R=2.6s show that the coronal radiation reddens slightly as the distance from the Sun is increased"* [156]. The reddening of the K-coronal emission suggested that the corona was cooling with increased distance from the solar surface.‡

Within the context of the gas models, the corona is extremely hot and thus, cannot be self-luminous in the visible spectrum. Rather, these models maintain that coronal white light must represent photospheric radiation. But as the thermal spectrum from the photosphere is punctuated with Fraunhofer absorption lines (see §3.7), some mechanism must be devised to explain their absence in coronal light. As such, proponents of the gaseous models have proposed that coronal light is being scattered by highly relativistic electrons [115, 148, 157, 158]. The Fraunhofer absorption lines are hypothesized to become highly broadened and unobservable. Relativistic electrons require temperatures in the millions of degrees. These temperatures are inferred from the line emissions of highly ionized ions in this region of the Sun (see §3.8). Unfortunately, such a scheme fails to account for the reddening of the coronal spectrum [156].

In contrast, the LMH model [35, 39] states that the solar corona contains photospheric-like condensed matter (Type I) and is, accordingly, *self-luminous* [57]. It is well-known that the Sun expels material into its corona in the form of flares and coronal mass ejections. It is reasonable to conclude that this material continues to emit (see §2.3.8) and may eventually disperse into finely distributed condensed matter in this region of the Sun. The reddening of the coronal spectrum implies that the apparent temperatures of the corona are no greater than those within the photosphere.§ The apparent temperature slowly decreases, as expected, with increased distance from the solar surface. The production of highly ionized ions in the corona reflects condensed matter in the outer solar atmosphere (see §2.3.8, §3.8, and §5.5). As for the Fraunhofer lines, they do not appear on the spectrum of the K-corona owing to insufficient concentrations of absorbing species exist in this region of the Sun. There is no need to invoke scattering by relativistic electrons.

2.3.8 Coronal Structure Emissivity #8

The corona of the active Sun is filled with structures easily observed using white-light coronographs [154, 155].¶ Flares [159–162], prominences and coronal mass ejections [163–171], streamers [172–174], plumes [175], and loops [176–178], can all be visualized in white light.

The mechanism for generating white-light in this wide array of structures remains elusive for the gaseous models, in part because the densities, in which they are hypothesize to exist, are lower than $\sim 10^{-15}$ g/cm^3 [148]. Moreover, the release of white-light by these structures tends to be explosive in nature, particularly when flares are involved [179–186]. These phenomena cannot be adequately explained by relying on gradual changes in opacity [42] or the action of rela-

*Metallic hydrogen requires extreme pressures for formation [39, 92] which can only exist within the solar body. As a result, though condensation is occurring within the chromosphere and corona, the resulting products are not metallic. Rather, it is likely that chromospheric material is comprised of dense hydrogen wherein molecular interactions between hydrogen atoms still persists [92]. Conversely, condensed matter which has been ejected from the solar body can be metallic in character and has been proposed to become distributed throughout the corona [60]. The solar atmosphere can simultaneously support the existence of two forms of hydrogen: chromospheric non-metallic material, like as coronal rain or spicules (see §5.4, §5.6 and [53, 59]) and coronal material which resembles photospheric Type-I metallic hydrogen (see §2.3.7 and §2.3.8) and [57, 58, 60]) and which can be found in the corona and its associated structures (see §3.8, §4.6, §5.5, §5.7 and §6.6 for complimentary evidence).

†The seventh Plankian proof [45] was initially presented as the 27th line of evidence [57, 60].

‡Yet, the *"single bright green line"* which had been observed by Harkness would eventually be identified as originating from highly ionized iron (i.e. FeXIV). Within the gaseous context, the only means of generating these ions would involve the presence of extreme temperatures in the corona. Conversely, the ions could be produced if condensed matter can be postulated to exist in this region of the Sun. The origin of highly ionized ions in the corona constitutes one of the most elegant lines of evidence for the presence of condensed matter in this region of the Sun, supporting the idea that the corona is, in fact, cool (see [60] and §3.8 for a complete discussion).

§The author has stated that the true energy content of the photosphere would correspond to real temperatures in the millions of degrees. The vast majority of this energy is trapped within the translational degrees of freedom associated with the differential convection currents. The conduction bands responsible for the solar magnetic fields likewise harness some of the solar surface energy. The apparent temperature of ~6,000K corresponds to the energy contained within the photospheric vibrational degrees of freedom [41].

¶The eighth Plankian proof [45] was initially presented as the 28th line of evidence [58].

tivistic electrons to scatter photospheric light [160, 161, 164, 187, 188]. Currently, many of these structures are believed to derive their energy from coronal magnetic sources overlying active regions [12]. That is a result having no other means of accounting for this extensive and abrupt release of energy in the gaseous Sun [179].

Within the context of the LMH model [35, 39], the white-light emitted by coronal structures is associated with their condensed nature. Since many of these formations originate from eruptions taking place at the level of the photosphere, such a postulate appears reasonable. As a result, coronal structures should be regarded as *self-luminous*. The explosive increase in white-light is related to powerful lattice vibrations associated with their formation [21]. Long ago, Zöllner [189] had insisted that flares involved the release of pressurized material from within the Sun [3]. These mechanisms remain the most likely, as they properly transfer energy out of the solar body, not back to the surface from the corona (see §5.1).

3 Spectroscopic Lines of Evidence

Though Gustav Kirchhoff erred [21–24] relative to his law of thermal emission [15, 16], his contributions to solar science remain unchallenged. Not only was he amongst the first to properly recognize that the Sun existed in liquid state [2, 26], but as the father of spectral analysis, along with Robert Bunsen, he gave birth to the entire spectroscopic branch of solar science [190, 191]. Using spectroscopic methods, Kirchhoff successfully identified the lines from sodium on the Sun and this led to an avalanche of related discoveries, spanning more than a century [190, 191]. Indeed, all of the thermal proofs discussed in §2, are the result of spectroscopic analysis, centered on the blackbody spectrum observable in visible and infrared light. It is fitting that the next series of proofs are spectroscopic, this time centering on line emission of individual atoms or ions. These eight lines of evidence highlight anew the power of Kirchhoff's spectroscopic approaches.

3.1 UV/X-ray Line Intensity #9

The Sun is difficult to study in the ultraviolet (UV) and X-ray bands due to the absorption of this light by the Earth's atmosphere.* As a consequence, instruments like the AIA aboard NASA's Solar Dynamic Observatory (see Fig. 11) are being used for these observations [192, p. ix]. When the Sun is observed at these frequencies, striking evidence is produced on the existence of a real solar surface. Harold Zirin describes the findings as follows, *"The case in the UV is different, because the spectrum lines are optically thin. Therefore one would expect limb brightening even in the absence of temperature increase, simply due to the secant increase of path length. Although the intensity doubles at the limb, where we see the back side, the limb brightening inside the limb is minimal . . . Similarly, X-ray images show limb brightening simply due to increased path length."* [193]. Fig. 11 presents this phenomenon in X-Ray at 94Å, for a somewhat active Sun.†

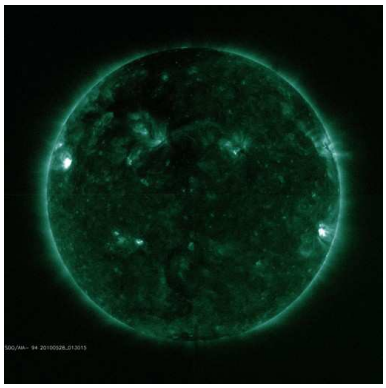

Fig. 11: AIA X-Ray image of an active Sun obtained on 5/28/2010 at 94Å displaying limb brightening and surface activity. This image (20100528_013015_512_0094.jpg) has been provided Courtesy of NASA/SDO and the AIA, EVE, and HMI science teams using data retrieval (http://sdo.gsfc.nasa.gov/data/aiahmi).

When the observer is directly examining the center of the opaque solar disk, weak spectral lines are obtained at these frequencies. The lines brighten slightly as observation moves towards the limb, owing to a slightly larger fraction of the solar atmosphere being sampled (line of sight 2 versus 1 in Fig. 12). However, immediately upon crossing the solar limb, a pronounced increase in spectroscopic intensity can be recorded. In fact, it approximately doubles, because a nearly two-fold greater line of sight is being viewed in the solar atmosphere. This can be understood if one would compare a line of sight very near line 3 in Fig. 12 (but still striking the solar disk) with line 3 itself.

In this manner, UV and X-ray line intensities can provide strong evidence that the Sun possesses an opaque surface at these frequencies which is independent of viewing angle. Limb darkening is not observed, as was manifested in the visible spectrum (see §2.3.2), in that condensed matter is not being sampled. Rather, the behavior reflects that gases are being monitored above a distinct surface through which UV and X-ray photons cannot penetrate.‡

3.2 Gamma-Ray Emission #10

Occasionally, powerful gamma-ray flares are visible on the surface of the Sun and Rieger [194] has provided evidence that those with emissions >10 MeV are primarily visualized

*This proof was first presented as the 25th line of evidence [55].

†A 171Å UV image from the quite Sun has been published [192, p. 38]. The Solar Dynamic Observatory website can be accessed for images at other frequencies in the ultra-violet (http://sdo.gsfc.nasa.gov/data/aiahmi).

‡Note that these findings further bring into question the optical depth arguments that had been brought forth to explain limb darkening within the gaseous models in §2.3.3. Should the Sun truly possess a vacuum-like photospheric density of only 10^{-7} g/cm^3 [148], then the limb should not act as such a dramatic boundary relative to the intensity of UV and X-ray emissions.

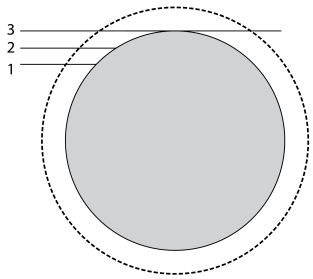

Fig. 12: Schematic representation of path lengths present when the outer atmosphere (area outlined by dashes) of the Sun (body in gray) is viewed from the Earth. Paths 1 and 2 terminate on the solar surface. Just beyond the limb, path 3 samples the front and back side of the solar atmosphere, resulting in a two fold increase in line intensity. This figure is an adaptation based on Fig. 2.4 in [192] and, along with this legend, was previously published [55].

near the solar limb (see Fig. 13).* Speaking of Rieger's findings, Ramaty and Simnett noted that "*Gamma-ray emitting flares are observed from sites located predominantly near the limb of the Sun ... This effect was observed for flares detected at energies >0.3 MeV, but it is at energies >10 MeV that the effect is particularly pronounced ... Since in both of these cases the bulk of the emission is bremsstrahlung from primary electrons, these results imply that the radiating electrons* (are) *strongly anisotropic, with more emission in the directions tangential to the photosphere than in directions away from the Sun*" [195, p. 237].

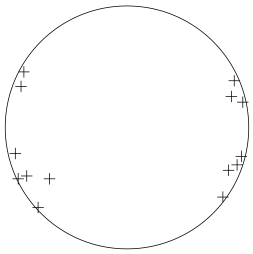

Fig. 13: Schematic representation of approximate flare positions with >10 MeV of energy on the solar disk displaying their predominance near the limb. This figure is meant only for illustrative purposes and is an adaptation based on Fig. 9 in [194] which should be examined for exact flare locations. This figure was previously published in [49].

The production of anisotropic emission would typically imply that structural constraints are involved in flare production. Since the gaseous Sun cannot sustain structure, another means must be used to generate this anisotropy. Based on theoretical arguments, Ramaty and Simnett consequently advance that: "*... the anisotropy could result from the mirroring of the charged particles in the convergent chromospheric magnetic fields*" [195, p. 237]. The anisotropy of gamma-ray emission from high energy solar flares is thought to be generated by electron transport in the coronal region and magnetic mirroring of converging magnetic flux tubes beneath the transition region [195]. The energy required for flare generation could thereby be channeled down towards the solar surface from the corona itself. Conveniently, the chromosphere instantly behaves as an *'electron mirror'*. Devoid of a real surface, another mechanism was created to *act* as a surface.

The inability to generate flare anisotropy using the most obvious means — the presence of a true photospheric surface — has resulted in a convoluted viewpoint. Rather than obtain the energy to drive the flare from within the solar body, the gaseous models must extract it from the solar atmosphere and channel it down towards the surface using an unlikely mechanism. It remains simpler to postulate that the anisotropy observed in high energy solar flares is a manifestation that the Sun has a true surface. The energy involved in flare generation can thereby arise from the solar interior, as postulated long ago by Zöllner [189]. In this respect, the LMH model [35, 39] retains distinct advantages when compared to the gaseous models of the Sun.

3.3 Lithium Abundances #11

Kirchhoff's spectroscopic approaches [190, 191] have enabled astronomers to estimate the concentrations of many elements in the solar atmosphere.† Application of these methods have led to the realization that lithium was approximately 140-fold less abundant in the solar atmosphere than in meteors [196, 197].

In order to explain this discrepancy, proponents of the gaseous stars have advanced that lithium must be transported deep within the interior of the Sun where temperatures $>2.6\times10^6$ K are sufficient to destroy the element by converting it into helium [^{7}Li $(p,\alpha)^4$He] [198]. To help achieve this goal, lithium must be constantly mixed [198–200] into the solar interior, a process recently believed to be facilitated by orbiting planets [201, 202]. Though these ideas have been refuted [203], they highlight the difficulty presented by lithium abundances in the gaseous models.

As for the condensed model of the Sun [35, 39], it benefits from a proposal [54], brought forth by Eva Zurek, Neil Ashcroft, and others [204], that lithium can act to stabilize metallic hydrogen [88, 92]. Hence, lithium levels could appear to be decreased on the solar surface, as a metallic hydrogen Sun retains the element in its interior. At the same time, lithium might be coordinated by metallic hydrogen in the corona, therefore becoming sequestered and unavailable for emission as an isolated atom.

*This proof was first presented as the eighteenth line of evidence [49].

†This proof was initially discussed in [54]. See [47], for a detailed discussion of how elemental abundances have been estimated.

In this manner, lithium might be unlike the other elements, as these, including helium, are likely to be expelled from the solar interior (see §5.1) as a result of exfoliative forces [48]. Lithium appears to have a low abundance, but, in reality, it is not being destroyed. This would better reconcile the abundances of lithium observed in the solar atmosphere with that present in extrasolar objects. Clearly, if lithium is being destroyed within the stars, it becomes difficult to explain its abundance in meteors. This problem does not arise when abundances are explained using a LMH model, as metallic hydrogen can sequester lithium into its lattice.

3.4 Hydrogen Emission #12

The *'flash spectrum'* associated with solar eclipses characterizes the chromosphere.* The strongest features within this spectrum correspond to line emissions originating from excited hydrogen atoms. As far back as 1931, the outstanding chromospheric observer, Donald H. Menzel, listed more than twenty-three hydrogen emission lines originating from this region of the Sun (see Table 3 in [205, p. 28]). It is the cause of these emissions which must now be elucidated. The most likely scenario takes advantage of the condensation appearing to occur in the chromospheric layer (see §5.4 §5.6 and [56, 59]).

By modern standards, the nature of the chromosphere remains a mystery, as Harold Zirin reminds us, *"The chromosphere is the least-well understood layer of the Sun's atmosphere...Part of the problem is that it is so dynamic and transient. At this height an ill-defined magnetic field dominates the gas and determines the structure. Since we do not know the physical mechanisms, it is impossible to produce a realistic model. Since most of the models ignored much of the data, they generally contradict the observational data. Typical models ignore other constraints and just match only the XUV data; this is not enough for a unique solution. It reminds one of the discovery of the sunspot cycle. While most of the great 18th century astronomers agreed that the sunspot occurrence was random, only Schwabe, an amateur, took the trouble to track the number of sunspots, thereby discovering the 11-year cycle"* [193]. But if mystery remains, it is resultant of the denial that condensed matter exists in this layer of the Sun.

The chromosphere is characterized by numerous structural features, the most important of which are spicules (see Fig. 14) [59, 150]. Even in the mid-1800s, Secchi would provide outstanding illustrations of these objects (see Plate A in [1, V. II]). He would discuss their great variability in both size and orientation, *"In general, the chromosphere is poorly terminated and its external surface is garnished with fringes ... It is almost always covered with little nets terminated in a point and entirely similar to hair ... it often happens, especially in the region of sunspots, that the chromosphere presents an aspect of a very active network whose surface, unequal and rough, seems composed of brilliant clouds analogous to our cumulus; the disposition of which resembles the beads of our rosary; a few of which dilate in order to form little diffuse elevations on the sides"* [1, p. 31–36, V. II].

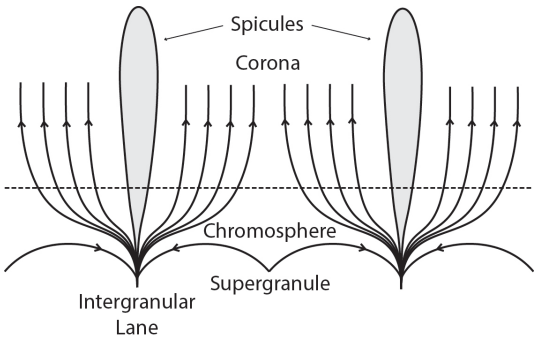

Fig. 14: Schematic representation of spicules overlying the intergranular lane on the outer boundary of a supergranule and surrounded by magnetic field lines emanating from the solar surface. While simplistic, this illustration conveys the basic structural elements needed for discussion. This figure was previously published in [59] and is an adaptation based on Fig. IV-13 in [206, p. 162].

At first glance, spicules are thought to have a magnetic origin, as these fields seem to flood the chromosphere [148, 150, 206–215]. In reality, matter within the chromosphere seems to form and dissipate quickly and over large spatial extent, with spicules reaching well into the corona [148, 150, 206–215]. The random orientation which spicules display, as noted long ago by Secchi [1, p. 31–36, V. II], along with their velocity profiles (see §5.6), should have dispelled the belief that these structures are magnetic in origin. Rather, they appear to be products of condensation (§5.6).†

If spicules and chromospheric matter are genuinely the product of condensation reactions, then their mechanism of formation might shed great light into the emissive nature of this solar layer.

3.4.1 The Liquid Metallic Hydrogen Solar Model

The search for answers begins by considering condensation processes known to occur on Earth [59].

In this respect, while studying the agglomeration of silver clusters, Gerhart Ertl's (Nobel Prize, Chemistry, 2007) laboratory noted that *"Exothermic chemical reactions may be accompanied by chemiluminescence. In these reactions, the released energy is not adiabatically damped into the heat bath of the surrounding medium but rather is stored in an ex-*

*This proof was first presented as the seventeenth line of evidence [47, 59].

†While non-magnetic, spicules might nonetheless be confined by magnetic fields present in the charged plasmas or coronal metallic hydrogen that surrounds them, much as illustrated in Fig. 14.

cited state of the product; decay from this excited state to the ground state is associated with light emission" [216].

The reactions of interest are seldom studied. Those which must arouse attention involve the condensation of two silver fragments and the formation of an activated cluster species: $Ag_n + Ag_m \rightarrow Ag^*_{m+n}$ [216]. With respect to the chromosphere, the important features of these reactions involve the realization that condensation processes are exothermic.

When silver clusters condense, energy must be dissipated through light emission. This constitutes a vital clue in explaining why the chromosphere is rich in hydrogen emission lines [59, 205]. Once an activated cluster is formed, it can relax by ejecting an excited atom: $Ag^*_{m+n} \rightarrow Ag_{m+n-1} + Ag^*$. The reactions are completed when the ejected excited species emits light to reenter the ground state: $Ag^* \rightarrow Ag + h\nu$.

Taking guidance from the work in metal clusters [216], hydrogen emission lines in the chromosphere might be seen as produced through the condensation of hydrogen fragments, $H_n + H_m \rightarrow H^*_{m+n}$. The resultant condensation product could then relax through the ejection of an excited hydrogen atom, $H^*_{m+n} \rightarrow H_{m+n-1} + H^*$, which finally returns to a lower energy state with light emission, $H^* \rightarrow H + h\nu$. This could give rise to all the Lyman lines ($N_2 > 1 \rightarrow N_1 = 1$). If one postulates that the excited hydrogen atom can hold its electron in any excited orbital $N_2 > 2$, H^{**}, then the remaining complement of hydrogen emission lines could be produced $H^{**} \rightarrow H^* + h\nu$ (Balmer $N_2 > 2 \rightarrow N_1 = 2$, Paschen series $N_2 > 3 \rightarrow N_1 = 3$, and Brackett series $N_2 > 4 \rightarrow N_1 = 4$).

But since the chromosphere is known to possess spicules and mottles [148, 150, 206–215], it is more likely that hydrogen is condensing, not onto a small cluster, but rather, onto very large condensed hydrogen structures, CHS [59].* The most logical depositing species in these reactions would be molecular hydrogen, as it has been directly observed in sunspots [217, 218], on the limb [219], and in flares [218]. Importantly, the emission from molecular hydrogen is particularly strong in chromospheric plages [220], providing further evidence that the species might be the most appropriate to consider.

As a result, it is reasonable to postulate that molecular hydrogen could directly interact with large condensed hydrogen structures, CHS, in the chromosphere [59]. The reaction involved would be as follows: $CHS + H_2 \rightarrow CHS\text{–}H^*_2$. This would lead to the addition of one hydrogen at a time to large condensed structures and subsequent line emission from the ejected excited species, $H^* \rightarrow H + h\nu$. Numerous reactions could simultaneously occur, giving rise to the rapid growth of chromospheric structures, accompanied with significant light emission in all spectral series (i.e. Lyman, Balmer, Paschen, and Brackett).

*Chromospheric condensed hydrogen structures, CHS, are likely to be composed of extremely dense condensed matter wherein molecular hydrogen interactions linger [92].

3.4.2 The Gaseous Solar Models

The situation being promoted in §3.4.1, concerning hydrogen line emission in the chromosphere, is completely unlike that currently postulated to exist within the gaseous Sun [59]. In the gas models, line emission relies on the accidental excitation of hydrogen through bombardment with either photons or electrons [206, p. 2]. The process has no purpose or reason. Atoms are randomly excited, and then, they randomly emit.

Przybilla and Butler have studied the production of hydrogen emission lines and the associated lineshapes in the gaseous models. They reached the conclusion that some of the hydrogen emission lines *"collisionally couple tightly to the continuum"* [221]. Their key source of opacity rests with the H^- ion, which has previously been demonstrated to be incapable of providing the desired continuous emission [42]. Of course, it is impossible to *"collisionally couple tightly to the continuum"* [221] in the gaseous models, as the continuum originates solely from opacity changes produced by an array of processes [42]. In the chromosphere, where average densities are postulated to be extremely low ($\sim 10^{-15}$ g/cm^3 [148]), continuous emission is thought to be produced by neutral H, H^-, Rayleigh scattering, and electron scattering (see [145, 146] and [150, p. 151–157]). Clearly, it is not possible to tightly couple to all of these mechanisms at once.

Przybilla's and Butler's computations [221] involve consideration of line blocking mechanisms and associated opacity distribution functions [222]. Stark line broadening mechanisms must additionally be invoked [223].

Beyond the inability of gases to account for the continuous spectrum and the shortcomings of solar opacity calculations [42], the central problem faced in trying to explain hydrogen emission and the associated line shapes rests in the Stark mechanisms themselves. Stark line broadening relies upon the generation of local electric fields near the emitting hydrogen atom. These fields are believed to be produced by ions or electrons which come into short term contact with the emitting species [223]. On the surface at least, the approach seems reasonable, but in the end, it relies on far too many parameters to be useful in understanding the Sun.

In the laboratory, Stark broadening studies usually center upon *extremely dense plasmas*, with electron numbers approaching 10^{17} cm^{-3} [224]. Stehlé, one of the world's preeminent scientists relative to Stark linewidth calculations [223, 225, 226], has analyzed lineshapes to infer electron numbers ranging from 10^{10} to 10^{17} cm^{-3} [227].† She initially assumes that plasmas existing within the chromosphere (T=10,000 K) have electron numbers in the 10^{13} cm^{-3} range [223]. Other

†While the vast majority of plasma studies report electron densities in the 10^{17} cm^{-3} range, the He I studies range from 10^{15} cm^{-3} to 10^{17} cm^{-3} [224]. The lowest electron numbers, 10^{15} cm^{-3}, are produced using arc discharge low density plasma settings. However, these could have little relevance in the Sun, as arc experiments rely on the capacitive discharge of large voltages. They do not depend on fluctuating electromagnetic fields [228].

sources call for much lower values. For instance, electron numbers of $\sim 10^{16}$ m^{-3} (or $\sim 10^{10}$ cm^{-3}) are obtained from radio measurements by Cairns et al. [229] and of no more than $\sim 10^{15}$ m^{-3} (or $\sim 10^{9}$ cm^{-3}) are illustrated in Dwivedi Fig. 3 [157, p. 285]. Stark experiments on Earth typically utilize electron numbers which are approximately 1–100 million times greater than anything thought to exist in the chromosphere.

A minor objection to the use of Stark broadening to explain the width of the hydrogen lines in the gaseous models rests on the fact that the appropriate experiments on hydrogen plasma do not exist. The plasma form of hydrogen (H II) is made of protons in a sea of electrons. It lacks the valence electron required for line emission. The closest analogue to excited hydrogen in the Sun would be ionized helium in the laboratory [224], although ionized Argon has been used for the Hβ profile [227].*

However, the most serious problem rests in the realization that these methods are fundamentally based on the presence of electric or electromagnetic fields in the laboratory. For instance, the inductively produced plasmas analyzed by Stehlé [227] utilize discharges on the order of 5.8 kV [227]. Inductively produced plasmas involve directionally-oscillating electromagnetic fields. Spark or arc experiments utilize static electric fields to induce capacitive discharges across charged plates. In every case, the applied electric field has *a distinct orientation*. Such conditions are difficult to visualize in a gaseous Sun, particularly within the spicules (see §3.4 and §5.7), given their arbitrary orientations. Random field orientations are incapable of line broadening, as well understood in liquid state nuclear magnetic resonance.

Stark broadening requires constraints on the electric field. In the gaseous models, these must take the form of a charged particle which approaches, precisely at the correct moment, an emitting species. The use of such mechanisms to account for chromospheric line profiles is far from justified. But, as the gaseous models cannot propose another explanation, everything must rest on Stark mechanisms, however unlikely these are to be valid in this setting.

In the end, it is not reasonable that matter existing at the concentration of an incredible vacuum ($\sim 10^{-15}$ g/cm^3 [148]) could be Stark broadened, given the extremely low electron numbers associated with the chromosphere [157, 229]. Computations have merely extended our *'observational range'* to electron numbers never sampled in the laboratory. According to the gas models, the chromosphere is a region of extremely low density, but high density plasmas must be studied to enable Stark analysis. Then, while the results of Stark broadening calculations appear rigorous on the surface, they contain experimental shortcomings. Spatially aligned electric fields cannot exist throughout the spicular region of a fully gaseous solar atmosphere, lone electrons are unlikely to produce the desired electric fields, and atoms such as argon have little relevance to hydrogen. In any case, given enough computational flexibility, any lineshape can be obtained, but opacity considerations remain [42].

3.4.3 Summary

As just mentioned in §3.4.2, Stark experiments involve electron densities far in excess of anything applicable to the solar chromosphere. Using the same reasoning, it could be argued that metallic hydrogen has not been created on Earth [39, 92]. The criticism would be justified, but this may be simply a matter of time. Astrophysics has already adopted these materials in other settings [93–96] and experimentalists are getting ever closer to synthesizing metallic hydrogen [39, 92]. The Sun itself appears to be making an excellent case that it is comprised of condensed matter.

Unlike the situation in the gaseous solar models, where hydrogen emission becomes the illogical result of random reactions, within the context of the liquid hydrogen model, it can be viewed as the byproduct of systematic and organized processes (see §3.4.1). An underlying cause is associated with line emission, dissipation of the energy liberated during condensation reactions. The driving force is the recapture of hydrogen through condensation, leading ultimately to its re-entry into the solar interior. This tremendous advantage cannot be claimed by the gaseous models.

Pressure (or collisional) broadening can be viewed as the most common mechanism to explain line broadening in spectroscopy. This mechanism can be invoked in the condensed model, because the atmosphere therein is not devoid of matter (see §2.3.6, §5.4, §5.5, §5.6, §6.6 and [56, 58, 59]).

It is possible that line broadening is occurring due to direct interaction between the emitting species and condensed hydrogen structures in the chromosphere. In this case, emission would be occurring simultaneously with the ejection of hydrogen. Under the circumstances, hydrogen line shapes may be providing important clues with respect to the interaction between molecular hydrogen and larger condensed structures in the chromosphere. If Stark broadening mechanisms play any role in the Sun, it will only be in the context of condensed matter generating the associated electric field.

3.5 Elemental Emission #13

Beyond hydrogen, the solar chromosphere is the site of emission for many other species, particularly the metals of the main group and transition elements.† For gaseous models, these emissions continue to be viewed as the product of random events (see §3.4.2). However, for the LMH model, con-

*The use of argon to represent hydrogen immediately suggests that these methods are not relevant to the Sun. Unlike hydrogen, argon has valence shells containing up to 18 electrons. This many electrons, when either ionized or polarized, presents an analogue with little or no resemblance to hydrogen and its lone electron.

†This proof was first presented as the thirtieth line of evidence [59].

densation remains the focus (§3.4.1), but this time with the assistance of the hydrides.

The solar disk and the sunspots are rich in hydrides including CaH, MgH, CH, OH, H_2O, NH, SH, SiH, AlH, CoH, CuH, and NiH [230, 231]. CaH and MgH have been known to exist in the Sun for more than 100 years [232]. Hydrogen appears to have a great disposition to form hydrides and this is important for understanding the role which they play in the chromosphere.

At the same time, the emission lines from CaII and MgII are particularly strong in the chromosphere [206, p. 361-369]. These represent emissions from the Ca^+ and Mg^+ ions. Yet, the inert gas configurations for these atoms would lead one to believe that the Ca^{+2} (CaIII) and Mg^{+2} (MgIII) lines should have been most intense in the chromosphere. As such, why is the Sun amplifying the CaII and MgII lines? Surely, this cannot be a random phenomenon (§3.4.2),* as these should have led to the buildup of the most stable electronic configuration.

The answer may well lie in reconsidering the condensation reactions presented in §3.4.1, but this time substituting CaH for molecular hydrogen. It should be possible for CaH and a condensed hydrogen structure, CHS, to interact, thereby forming an activated complex, CHS + CaH → CHS-HCa*. This complex could then emit a CaII ion in activated state, Ca^{+*}, and capture the hydrogen atom: CHS–HCa* → CHS–H + Ca^{+*}. Finally, the emission lines from CaII would be produced, as Ca^{+*} (CaII*) returns to the ground state: $Ca^{+*} \rightarrow Ca^+ + h\nu$. As was the case when discussing the condensation of molecular hydrogen (§3.4.1), if one permits the electrons within the excited state of CaII to initially occupy any electronic orbital, CaII**, then all possible emission lines from CaII could be produced: $Ca^{+**} \rightarrow Ca^{+*} + h\nu$. A similar scheme could be proposed for MgH and the other metal hydrides, depending on their relative affinity for CHS.

There is an important distinction between this scenario and that observed with molecular hydrogen (§3.4.1). When metal hydrides are utilized in this scheme, the condensation reactions are delivering both a proton and *two* electrons to the condensed hydrogen structure. The reactions involving molecular hydrogen delivered a single electron. This interesting difference can help to explain the varying vertical extent of the chromosphere when viewed in Hα, CaII, or HeII (see §3.6 and §4.7).

When sampling the solar atmosphere, electron densities appear to rise substantially as one approaches the photosphere (see [229] and [157, p. 285]). Hence, the lower chromosphere is somewhat electron rich with respect to the upper regions of this layer. Thus, in the lower chromosphere, condensation reactions involving the ejection of atomic hydrogen and neutral atoms can abound. As the altitude increases, a greater affinity for electrons arises and condensation can now be facilitated by species like as the metal hydrides, which can deliver two electrons per hydrogen atom.† This explains why CaII lines in the chromosphere can be observed to rise to great heights [193].

At the same time, lines from neutral metals, M, are more prevalent in the lower chromosphere [193]. Since this area is electron rich, a two electron delivery system is unnecessary and reactions of the following form can readily occur: 1) MH + CHS → CHS-HM*, 2) CHS–HM* → CHS–H + M*, and 3) M* → M + $h\nu$. In this case, only a single electron has been transferred during hydrogen condensation.

Perhaps, it is through the examination of linewidths that the most interesting conclusions can be reached. The emission lines of Hα, Ca, and Mg from spicules are very broad, suggesting a strong interaction between CHS and the ejected atoms, in association with ejection and light emission [234–236]. In contrast, spicule emission linewidths from Hβ, Hγ, Hϵ, the D3 line from He, and the neutral line from oxygen are all sharp [234]. One could surmise that the interaction between these species and condensed hydrogen structures are weaker upon ejection.

It is reasonable to conclude that the hydrides play an important role in facilitating condensation within the chromosphere [59]. Hydrides enable the delivery of hydrogen in a systematic manner and, most importantly, either one or two electrons, depending on the electron densities present on the local level. Such an elegant mechanism to account for the prevalence of CaII and MgII in the chromosphere cannot be achieved by other models. Moreover, unlike the LMH model, the gaseous models take no advantage of the chemical species known to exist in the solar atmosphere.

3.6 Helium Emission #14

The analysis of helium emission in the chromosphere may well provide the most fascinating adventure with regard to the spectroscopic lines of evidence.‡ This stands as fitting tribute to helium [47], as it was first observed to exist on the Sun [237, 238]. These seminal discoveries exploited the presence of helium within prominences and the disturbed chromosphere [239, 240]. Astronomers would come to view solar helium as extremely abundant [241, 242], but these con-

Here is a brief list of interesting ions and the ionization energies required for their production: HII = 13.6 eV; HeII = 24.6 eV; HeIII = 54.4 eV; MgII = 7.6 eV; MgIII = 15.0 eV; CaII = 6.1 eV; CaIII = 11.8 eV and FeXIV = 361 eV [233]. In this respect, note how the first ionized form of helium, HeII, requires 24.6 eV for its production. The generation of many triplet forms of orthohelium HeI will demand energies of ~20 eV. To remove two electrons from calcium yielding CaIII (the stable Ca^{+2} ion) only requires 11.8 eV. As a result, how can the gas models account for the presence of CaII lines at high altitude on the Sun (5-10,000 km), when this ion only requires 6.1 eV for production? If such powerful HeII and HeI* can be observed, why is CaIII, which requires only 11.8 eV for its generation and has the inert gas, [Ar], configuration, not the preferred form of calcium? This provides a powerful clue that the presence (or absence) of an individual ion on the Sun is related to chemistry and not to temperature.

†As will be seen in §3.8, it is envisioned that the corona of the Sun is harvesting electrons.

‡This proof was first presented as the 32nd line of evidence [61].

clusions have been challenged and may need to be revisited [47, 48, 61]. There is considerable reason to conclude that the solar body is actively ejecting He from its interior [47, 48].

Though helium can be found in spicules [193] and prominences, it is difficult to observe on the solar disk. It can be readily visualized in the chromosphere where the spatial extent of the 30.4 nm HeII emission lines can greatly exceed those from Hα (see the wonderful Fig. 1 in [243]). With increased solar activity, helium emission can become pronounced in the solar atmosphere (see Fig. 15 and [244]).

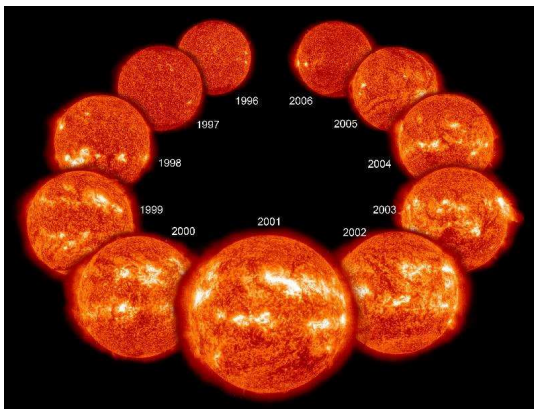

Fig. 15: Image of consecutive years in the solar cycle taken in the HeII line at 30.4 nm. NASA describes this image as follows, *"An EIT image in the 304 Angstrom wavelength of extreme UV light from each year of nearly an entire solar cycle"*. Courtesy of SOHO/[EIT] consortium. SOHO is a project of international cooperation between ESA and NASA. (http://sohowww.nascom.nasa.gov/gallery/images/cycle002.html — Accessed on 9/20/2013).

In the chromosphere, the helium which gives rise to emission lines can possess both of its electrons (HeI) or lose an electron to produce an ion (HeII). HeII resembles the hydrogen atom in its electronic configuration. However, the situation concerning HeI can be more complex. When this species exists in the ground state, both of its electrons lie in the 1S orbital (N=1) with their spins antiparallel, as dictated by Pauli's exclusion principle. In the excited state (i.e. 1 electron in the N=1 shell, and the second electron in any of the N>1 shells), helium can exist either as a singlet (parahelium — spins remaining antiparallel to one another) or as a triplet (orthohelium — spins assume a parallel configuration). Interestingly, the line emissions from the triplet states of orthohelium can be quite strong on the limb of the Sun.

For instance, a well-known triplet HeI transition occurs at 1083 nm (10830Å) which is barely visible on the disk, but it is nearly as intense as Hα on the limb [245, p. 199–200]. At the same time, the HeI triplet D3 line at 588 nm can be enhanced 20 fold when visualization moves from the disk to the limb [245, p. 199-200].*

During the eclipse of March 29, 2006, the triplet D3 line was carefully examined. It appeared to have a binodal altitude distribution with a small maximum at ~250 km and a stronger maximum between 1300-1800 km (see Fig. 6 in [244]). This bimodal distribution was not always observed (see Fig. 7 in [244]). But generally, the D3 line is most intense at an altitude of ~2,000 km, with an emission width of approximately 1,600 km. The triplet D3 lines show no emission near the photosphere.

Within the context of gaseous models, it is extremely difficult to account for the presence of excited HeI triplet states in the chromosphere. Helium requires ~20 eV† to raise an electron from the N=1 shell to the N=2 shell. How can excitation temperatures in excess of 200,000 K be associated with a chromosphere displaying apparent temperatures of 5,000-10,000K, values not much greater than those existing on the photosphere?

Therefore, since proponents of gaseous models are unable to easily account for the powerful D3 line emission, they have no choice but to state that helium is being excited by coronal radiation which has descended into the chromosphere [244, 246]. In a sense, helium must be *'selectively heated'* by the corona. These proposals strongly suggest that the gaseous models are inadequate. It is not reasonable to advance that an element can be selectively excited by coronal radiation, and this over its many triplet states. At the extreme, these schemes would imply that coronal photons could strip away all electrons from chromospheric atoms. Yet, even lines from neutral atoms are observed.‡

On the other hand, helium emissions can be easily understood in the LMH model [35, 36, 39], if attention is turned toward condensation reactions believed to occur within the chromosphere (see §3.4, §3.5 and [59, 61]).

In this respect, it must be recognized that the famous helium hydride cation (HeH^+) *"is ubiquitous in discharges containing hydrogen and helium"* [247].

First discovered in 1925 [248], HeH^+ has been extensively studied [249, 250] and thought to play a key role in certain astrophysical settings [251–253]. In the laboratory, its spectral lines were first observed by Wolfgang Ketterle (Nobel Prize, Physics, 2001) [254, 255]. The author has previously noted, *"Although it exists only in the gas phase, its Brønsted acidity should be extremely powerful. As a result, the hydrogen hydride cation should have a strong tendency to donate a proton, without the concerted transfer of an electron"* [61].

Turning to Fig. 16, it appears that the action of the helium hydride cation, HeH^+, can lead to a wide array of reactions within the chromosphere. These processes are initiated with

*Lines from neutral helium can be enhanced 50 fold on the limb relative to the disk [245, p. 199-200].

†1 eV = 11,600 K ; 20 eV = 232,000 K.

‡Selective excitation was also used to account for the emission lines from molecular hydrogen [220]. But it is more likely that these reflect the delivery of a hydrogen cluster (see §3.4.1) with H_2^* rather than H^* expulsion.

its transfer to condensed hydrogen structures, CHS, believed to be be forming (see §2.3.6, §3.4, §3.5, §3.7, §5.4, §5.6, §6.6) in this region of the solar atmosphere. As was the case with hydrogen (§3.4) and elemental (§3.5) emission lines, everything hinges on the careful consideration of condensation.

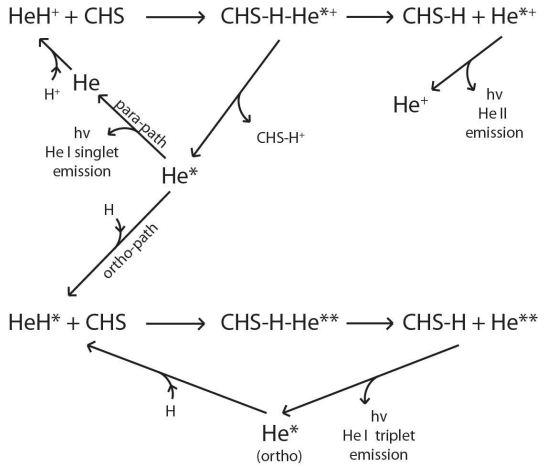

Fig. 16: Schematic representation of possible pathways involved when the helium hydride ion, HeH^+, or the excited helium hydride molecule, HeH^*, react with condensed hydrogen structures, CHS, in the chromosphere of the Sun. The pathways presented can account for all emission lines observed from He I and He II. Note in this scheme that excited helium, He^*, is being produced initially through the interaction of HeH^+ with CHS. This excited helium, He^*, if it assumes the triplet state (orthohelium — electrons in the same orientation: spin up/up or down/down), will become trapped in excited state. This triplet helium can then be used repeatedly, in cyclic fashion, to condense hydrogen atoms onto chromospheric structures, CHS (as shown in the lower half of the figure). Alternatively, if excited helium He^* is initially produced in the singlet state (parahelium — electrons in different orientation: spin up/down), emission can immediately occur generating the singlet lines from He I. This scheme accounts for the strong triplet He I transition at 10830 Å observed in the flash spectrum of the chromosphere. Unlike the situation in the gas models, random collisional or photon excitations are not invoked to excite the helium atoms. De-excitation processes would also be absent, helping to ensure the buildup of triplet state orthohelium in this model. This figure, along with its legend, was previously published in [61].

First, HeH^+ and CHS react to form an activated complex: CHS + HeH^+ → CHS-H-He^{+*}. If the expulsion of an excited helium ion (He^{+*}) follows, full transfer of a proton and an electron to CHS will have occurred (top line in Fig. 16). The resulting He^{+*} would be able to relax back to a lower energy state through emission, leading to the well known He II lines in the chromosphere (top right in Fig. 16).

Alternatively, when HeH^+ reacts with CHS, the expulsion of an excited helium atom (He^*) could follow (see Fig. 16) involving the transfer of a proton — but no electron — to the CHS. As a strong Brønsted acid, HeH^+ should permit these reactions (namely: CHS–HHe^{+*} → CHS–H^+ + He^*). Expulsion of an activated helium atom (He^*) can lead to two conditions, depending on whether the electrons within this species are antiparallel (parahelium) or parallel (orthohelium). Within helium, the excited electron is allowed by selection rules to return to the ground state, if and only if, its spin is opposed to that of the ground state electron. As a result, only parahelium can relax back to the ground state: $He^* \rightarrow He + h\nu$. This leads to the HeI lines from singlet helium.

As for the excited orthohelium, it is unable to relax, as its two electrons have the same spin (either both spin up or both spin down). *Trapped* in the excited state, this species can at once react with hydrogen, forming the excited helium hydride molecule, which, like the helium hydride cation, is known to exist [256, 257]: $He^* + H \rightarrow HeH^*$.

Excited helium hydride can react with CHS in the chromosphere, but now resulting in a doubly activated complex: CHS + $HeH^* \rightarrow$ CHS-H-He^{**}, wherein one electron remains in the ground state and the other electron is promoted beyond the 2S shell.* To relax, the doubly excited He^{**} atom, must permit an electron currently in the 2P or higher orbital, to return to the 2S or 2P orbitals.

The helium D_3 line would be produced by a $3^3D \rightarrow 2^3P$ transition [245, p. 95]. The $2^3P \rightarrow 2^3S$ transition is associated with the strong triplet He I line at 10830 Å [245, p. 95]. Alternatively, a $3^3P \rightarrow 2^3S$ transition produces the triplet He I line at 3890 Å [245, p. 95].

Importantly, since excited orthohelium cannot fully relax back to the ground state, it remains available to recondense with atomic hydrogen in the chromosphere. This results in its continual availability in the harvest of hydrogen. A cyclic process has been created using orthohelium (He^*). The priming of this cycle had required but a single instance where hydrogen was transferred to CHS by HeH^+, without the complementary transfer of an electron (top line in Fig. 16).† In this manner, much like what occurred in the case of molecular hydrogen (§3.4) and the metal hydrides (§3.5), the body of the Sun has been permitted to recapture atomic hydrogen lost to its atmosphere. It does not simply lose these atoms without any hope of recovery [59, 61, 62].

Within the LMH model, the prominence of the helium triplet lines can be elegantly explained. They result from the systematic excitation of helium, first delivered to condensed hydrogen structures by the helium hydride cation (HeH^+), a well-known molecule [247–254] and strong Brønsted acid. The generation of triplet state excited helium can be explained in a systematic fashion and does not require unrealistic temperatures in the corona. It is not an incidental artifact produced by improbably selective excitations generated using

*The possibility that He^{**} could have no electrons in the ground state is not considered.

†The production of Ca II emission lines from CaH had resulted in the transfer of two electrons per hydrogen atom (see §3.5). This can help keep charge neutrality in condensation reactions involving HeH^+.

coronal photons. Organized chemical reactions govern the behavior of helium in the Sun, not random events.

3.7 Fraunhofer Absorption #15

When examined under high spectral resolution, the visible spectrum of the Sun is punctuated by numerous absorption lines, which appear as dark streaks against a brighter background.* These lines were first observed by William Hyde Wollaston in 1802 [258]. They would eventually become known as *Fraunhofer lines* after the German scientist who most ably described their presence [259]. Fraunhofer lines can be produced by many different elements. They manifest the absorption of photospheric light by electrons, contained within gaseous atomic or ionic species above the photosphere, which are being promoted from a lower to a higher energy level.

In 1862, Kirchhoff was the first to argue that the Fraunhofer lines provided evidence for a condensed solar body, *"In order to explain the occurrence of the dark lines in the solar spectrum, we must assume that the solar atmosphere incloses a luminous nucleus, producing a continuous spectrum, the brightness of which exceeds a certain limit. The most probable supposition which can be made respecting the Sun's constitution is, that it consists of a solid or liquid nucleus, heated to a temperature of the brightest whiteness, surrounded by an atmosphere of somewhat lower temperature."* [190, p. 23].

Amongst the most prominent of the Fraunhofer lines are those associated with the absorption of photospheric light by the hydrogen atoms. The preeminent Fraunhofer lines are generated by the Balmer series. These lines are produced when an excited hydrogen electron (N=2) absorbs sufficient energy to be promoted to yet higher levels ($H\alpha$ $N=2\rightarrow N=3$ 656.3 nm; $H\beta$ $N=2\rightarrow N=4$ 486.1 nm; $H\gamma$ $N=2\rightarrow N=5$ 434.1 nm; $H\delta$ $N=2\rightarrow N=6$ 410.2 nm; etc). They can be readily produced in the laboratory by placing hydrogen gas in front of a continuous light source.

In 1925, Albrecht Unsöld reported that the solar Fraunhofer lines associated with hydrogen did not decrease as expected [260]. He noted intensities across the Balmer series ($H_\alpha = 1$; $H_\beta = 0.73$; $H_\gamma = 0.91$; $H_\delta = 1$) which where highly distorted compared to those expected in a hydrogen gas, as predicted using quantum mechanical considerations ($H_\alpha = 1$; $H_\beta = 0.19$; $H_\gamma = 0.07$; $H_\delta = 0.03$) [260].

Hydrogen lines were known to be extremely broad from the days of Henry Norris Russell and Donald H. Menzel, who had observed them in association with solar abundance [87] and chromospheric studies [205], respectively. Commenting on the strength of the hydrogen Balmer series, Henry Norris Russell would write, *"It must further be born in mind that even at solar temperatures the great majority of the atoms of any given kind, whether ionized or neutral, will be in the state of lowest energy... One non-metal, however, presents a real and glaring exception to the general rule. The hydrogen lines of the Balmer series, and, as Babcock has recently shown, of the Paschen series as well, are very strong in the Sun, though the energy required to put an atom into condition to absorb these series is, respectively, 10.16 and 12.04 volts — higher than for any other solar absorption lines. The obvious explanation — that hydrogen is far more abundant than the other elements — appears to be the only one"* [87, p. 21–22].

In the photospheric spectrum, the hydrogen absorption lines are so intense that the observer can readily garner data from the Lyman (N=1 → N=2 or higher), Balmer (N=2 → N=3 or higher), Paschen (N=3 → N=4 or higher), and Brackett (N=4 → N=6 or higher) series [87, 205, 260–264].

The central questions are three fold: 1) Why are the hydrogen lines broad? 2) Why does hydrogen exist in excited state as reflected by the Balmer, Paschen, and Brackett lines? and 3) Why is the normal quantum mechanical distribution of the Balmer series distorted as first reported by Unsöld [260]?

In the gaseous models, different layers of the solar atmosphere have to be invoked to account for the simultaneous presence of Lyman, Balmer, Paschen and Brackett line profiles in the solar spectrum [261–264]. Once again, as when addressing limb darkening (see §2.3.2), the models have recourse to optical depth [261–264]. These approaches fail to adequately account for the production of the excited hydrogen absorption.

As noted in §3.4, in the setting of the LMH model, excited hydrogen atoms can be produced through condensation reactions occurring in the solar chromosphere. These atoms could be immediately available for the absorption of photons arising from photospheric emission. Hence, condensation reactions provide an indirect mechanism to support the generation of many hydrogen Fraunhofer line. Since these lines are being produced in close proximity to condensed matter, it is reasonable to conclude that their linewidths are determined by their interaction with such materials and not from optical depth and Stark mechanisms (see §3.4). This may help to explain why the intensity of the Balmer lines, as first reported by Unsöld [260], do not vary as expected in gases from quantum mechanical considerations. Unsöld's findings [260] strongly suggest that the population of excited hydrogen atoms is being distorted by forces not known to exist within gases. Once again, this calls attention to condensed matter.

3.8 Coronal Emission #16

As was discussed in §2.3.7, the K-corona is the site of continuous emission which reddens slightly with altitude, but whose general appearance closely resembles the photospheric spectrum [57].† This leads to the conclusion that condensed matter must be present within this region of the Sun [57]. Still, the nature of the corona is more complicated, as the same region which gives rise to condensed matter in the K-

*This proof was first presented as the sixteenth line of evidence [47, 59].

†This proof was first presented as the 31st line of evidence [60, 62].

corona is also responsible for the production of numerous emission lines from highly ionized elements (e.g. FeXII-FeXXV [192]) in the E-corona [60].*

When examined in light of the gaseous solar models, the production of highly ionized species requires temperatures in the million of degrees [192]. Temperatures as high as 30 MK have been inferred to exist in the corona [192, p. 26], even if the solar core has a value of only 16 MK [13, p. 9]. Flares have been associated with temperatures reaching 10^8 K [273], and radio sampling has called for values between 10^8 and 10^{10} K [245, p. 128].

Given the temperatures inferred in attempting to explain the presence of highly ionized atoms in the K-corona, proponents of the gaseous models deny that this region can be comprised of condensed matter. Harold Zirin summarizes the situation best, *"... there is something erroneous in our basic concept of how ionization takes place"* [245, p. 183].

Rather than cause a dismissal of condensed matter, such extreme temperature requirements should lead to the realization that the gaseous models are fundamentally unsound [62]. It is not reasonable to assume that the corona harbors temperatures which exceed those found in the core. Furthermore, to arrive at these extreme values, the corona must somehow be heated. The *"zoo"* [148, p. 278] of possible heating mechanisms is substantial [148, p. 239–251]. According to E.R. Priest, the hypothesized mechanisms are fundamentally magnetic in nature as *"all the other possible sources are completely inadequate"* [273]. The problem for gaseous models can be found in the realization that their only means of producing highly ionized atoms must involve violent bombardment and the removal of electrons to infinity. These schemes demand impossible temperatures.†

It is more reasonable to postulate that elements within the corona are being stripped of their electrons when they come into contact with condensed matter. The production of highly ionized atoms involves electron affinity, not temperature. The belief that the corona is a region characterized by extremely elevated temperatures is erroneous. The cool K-coronal spectrum is genuine. The associated photons are directly produced by the corona itself, not by the photosphere (see §2.3.7).

Moreover, condensed matter can have tremendous electron affinities. This is readily apparent to anyone studying lightning on Earth. Thunderhead clouds have been associated with the generation of 100 keV X-rays [274, p. 493-495], but no-one would argue that the atmosphere of the Earth sustains temperatures of 10^9 K. Lightning can form *"above volcanoes, in sandstorms, and nuclear explosions"* [274, p. 67]. It represents the longest standing example of the power of electron affinity, as electrons are transferred from condensed matter in the clouds to the Earth's surface, or vise versa [274–276].

Metallic hydrogen should exist in the K-corona, as Type-I material has been ejected into this region (see §2.3.8) by activity on the photosphere [58]. Electrical conductivity in this region is thought to be very high [277, p. 174]. Thus, the production of highly ionized elements can be explained if gaseous atoms come into contact with this condensed matter. For example, iron (Fe) could interact with metallic hydrogen (MH) forming an activated complex: MH + Fe $\rightarrow$ MH–Fe*. Excited Fe could then be ejected with an accompanying transfer of electrons to metallic hydrogen: MH–Fe* $\rightarrow$ MH–$n\bar{e}$ + Fe^{+n*}. The emission lines observed in the corona are then produced when the excited iron relaxes back to the ground state through photon emission, Fe^{+n*} $\rightarrow$ Fe^{+n} + $h\nu$. Depending on the local electron affinity of the condensed metallic hydrogen, the number of electrons transferred, n, could range from single digits to ~25 [192] in the case of iron.‡

The scheme formulated with iron can be extended to all the other elements,§ resulting in the production of all coronal emission lines. The governing force in each case would be the electron affinity of metallic hydrogen which may increase with altitude. Highly ionized species are not produced through the summation of multiple electron ejecting bombardments. Rather, multiple electrons are being stripped simultaneously, in single action, by transfer to condensed matter. In this manner, the *electron starved* corona becomes endowed with function, *the harvesting of electrons from elements in the solar atmosphere, thereby helping to maintain the neutrality of the solar body* [60].

In this sense, the chromosphere and corona have complimentary action. The chromosphere harvests hydrogen atoms and protons. The corona harvests electrons.¶

As for the transition zone (see Fig. 1.1 in [192]), it does not exist. This region was created by the gaseous models in order to permit a rapid transition in apparent temperatures between the cool chromosphere and hot corona (see [62] for a complete discussion). In the metallic hydrogen model, the apparent temperatures in both of these regions are cool, there-

*The story which accompanies the mystical element coronium (or FeXIV) in the corona and its discovery by the likes of Harkness, Young, Grotian, and Edlén [151–153] has been recalled [265–268]. Wonderful images of the corona have recently been produced from highly ionized iron (e.g. FeX-FeXIV) [269–272].

†It will be noted in §5.5, that the gaseous solar models infer widely varying temperatures within the *same* regions of the corona when analyzing coronal loops (see Fig. 22). How could it be possible to sustain vastly differing values in the *same* region of the solar atmosphere? These findings are indicative that we are not sampling temperature, but rather substructures with distinct electron affinities. These substructures take advantage of a wide array of species to transfer electrons. Evidence for such a solution can be found in Fig. 1.10 of [192] which describes flare substructure and the associated variations in emitting species (arcade emitting in FeXII — spine emitting in FeXXIV and Ca XVII).

‡In this regard, it is important to note that most of the ions present in the *"XUV spectrum are principally those with one or two valence electrons"* [245, p. 173]. This observation is highly suggestive that systematic processes are taking place, not random bombardments.

§A least one electron must remain for line emission.

¶While the corona is primarily composed of metallic hydrogen, as will be seen in §5.4, it can provide a framework to allow for the condensation of hydrogen in non-metallic form.

fore a transition zone serves no purpose [62]. The changes in atomic and ionic compositions observed in the solar atmosphere can be accounted for by 1) the varying ability of molecular species to deliver hydrogen and protons to condensed hydrogen structures in the chromosphere as a function of altitude, and 2) to changes in the electron affinity of metallic hydrogen in the corona.

This scenario resolves, at long last, the apparent violation of the Second Law of Thermodynamics which existed in the gaseous model of the Sun. It is not realistic that the center of the Sun exists at 16 MK [13, p. 9], the photosphere at 6,000 K, and the corona at millions of degrees. A solution, of course, would involve the recognition that most of the energy of the photosphere is maintained in its convection currents and conduction bands [37], not in the vibrational modes responsible for its thermal spectrum and associated apparent temperature. But now, the situation is further clarified. The corona is not being heated — it is cool. No violation of the Second Law of Thermodynamics exists, even if photospheric convection and conduction are not considered.

4 Structural Lines of Evidence

The structural lines of evidence are perhaps the most physically evident to address, as they require only elementary mechanical principles to understand.

4.1 Solar Collapse #17

Should stars truly be of gaseous origin, then they are confronted with the problem of solar collapse.* Somehow, they must prevent the forces of gravity from causing the entire structure to implode upon itself.

Arthur Eddington believed that stellar collapse could be prevented by radiation pressure [9]. Photons could transfer their momentum to stellar particles and thereby support structure. These ideas depend on the existence of radiation within objects, a proposal which is counter to all laboratory understanding of heat transfer. Conduction and convection are responsible for the transfer of energy within objects [70]. It is only if one wishes to view the Sun as an assembly of separate objects that radiation can be invoked.

Eventually, the concept that the Sun was supported exclusively by radiation pressure was abandoned. Radiation pressure became primarily reserved for super-massive stars [13, p. 180-186]. Solar collapse was prevented using *'electron gas pressure'* [13, p. 132], with radiation pressure contributing little to the solution [13, p. 212].

But the idea that *'electron gas pressure'* can prevent a star from collapsing is not reasonable [3, 35, 43, 48]. The generation of gas pressure (see Fig. 17) requires the existence of true surfaces, and none can exist within a gaseous Sun.† When a particle travels towards the solar interior, it can simply undergo an elastic collision, propelling a stationary particle beneath it even further towards the core. Without a surface, no net force can be generated to reverse this process: the gaseous Sun is destined to collapse under the effect of its own gravity [48].

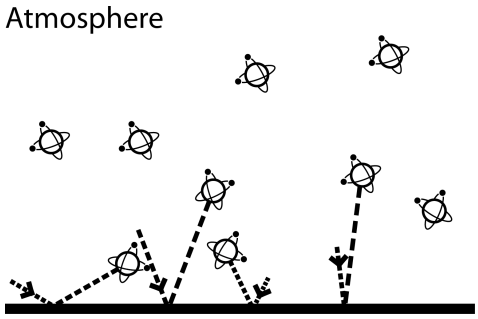

Fig. 17: Schematic representation of the generation of gas pressure. As particles travel towards a real surface, they eventually undergo a change in direction resulting in the creation of a net upwards force.

Donald Clayton, a proponent of the gaseous models, describes the situation as follows, *"The microscopic source of pressure in a perfect gas is particle bombardment. The reflection (or absorption) of these particles from a real (or imagined) surface in the gas results in a transfer of momentum to that surface. By Newton's second law* ($F = dp/dt$)*, that momentum transfer exerts a force on the surface. The average force per unit area is called the pressure. It is the same mechanical quantity appearing in the statement that the quantity of work performed by the infinitesimal expansion of a contained gas is* $dW = PdV$*. In thermal equilibrium in stellar interiors, the angular distribution of particle momenta is isotropic; i.e., particles are moving with equal probabilities in all directions. When reflected from a surface, those moving normal to the surface will transfer larger amounts of momentum than those that glance off at grazing angles*" [14, p. 79]. The problem is that real surfaces do not exist within gaseous stars and *'imagined'* surfaces are unable to be involved in a *real* change in momentum. *'Electron gas pressure'* cannot prevent solar collapse.

Unlike the scenario faced by Eddington with respect to solar collapse, James Jeans had argued that liquid stars were immune to these complications, *"And mathematical analysis shews that if the centre of a star is either liquid, or partially so, there is no danger of collapse; the liquid center provides so firm a basis for the star as to render collapse impossible"* [278, p. 287]. By their very nature, liquids are essentially incompressible. Therefore, liquid stars are self-supporting and a LMH Sun faces no danger of collapse.

*This proof was first presented as the third line of evidence [3, 35, 43, 48].

†Conversely, the extended nature of our atmosphere is being maintained through gas pressure precisely because our planet possesses a real surface. When gas particles strike the Earth's surface, they undergo an immediate change in direction with upward directed velocities. Without the presence of a true surface, a net change in particle velocity cannot occur.

4.2 Density #18

Hot gases do not *self-assemble*.* Rather, they are well-known to rapidly diffuse, filling the volume in which they are contained. As a result, hot gaseous *'objects'* should be tenuous in nature, with extremely low densities. In this respect, hot gases offer little evidence that they can ever meet the requirements for building stars.

In an apparent contradiction to the densities expected in gaseous *'objects'*, the solar body has a substantial average density on the order of 1.4 g/cm^3 [279]. In gaseous models, the Sun is believed to have a density approaching 150 g/cm^3 in its core, but only $\sim 10^{-7}$ g/cm^3 at the level of the photosphere [148]. In this way, a gaseous star can be calculated with an average density of 1.4 g/cm^3. But gaseous models would be in a much stronger position if the average density of the Sun was consistent with that in a sparse gas, i.e. $\sim 10^{-4}$ g/cm^3, for instance. It is also concerning that the average density of the Sun is very much coincident with that observed in the outer planets, even though these objects have much smaller total masses.† The giant planets are no longer believed to be fully gaseous, but rather composed of metallic hydrogen [93–95], suggestions which are contrary to the existence of a gaseous Sun.

The Sun has a density entirely consistent with condensed matter. If the solar body is assembled from metallic hydrogen [35, 39], it is reasonable to presume that it has a somewhat uniform distribution throughout its interior.‡ This would be in keeping with the known, essentially incompressible, nature of liquids.

4.3 Radius #19

Within gaseous models, the Sun's surface cannot be real and remains the product of optical illusions [2, 4, 51].§ These conjectures were initially contrived by the French astronomer, Hervé Faye. In 1865, Faye [280] had proposed that the Sun was gaseous [2, 4] and would write, *"This limit is in any case only apparent: the general milieu where the photosphere is incessantly forming surpasses without doubt, more or less, the highest crests or summits of the incandescent clouds, but we do not know the effective limit; the only thing that one is permitted to affirm, is that these invisible layers, to which the name atmosphere does not seem to me applicable, would not be able to attain a height of 3', the excess of the perihelion distance of the great comet of 1843 on the radius of the photosphere"* [280]. With those words, the Sun lost its true surface. Everything was only *'apparent'* (see §1). Real dimensions, like diameter or radius, no longer held any validity. Nonetheless, Father Secchi considered the dimensions of the Sun to be a question of significant observational importance, despite problems related to their accurate measure [1, p. 200–202, V. I].

Today, the radius of the Sun (~696,342±65 km) continues to be measured [51] and with tremendous accuracy — errors on the order of one part in 10,000 or even 2 parts in 100,000 (see [281] for a table). Such accurate measurements of spatial dimensions typify condensed matter and can never characterize a gaseous object.¶ They serve as powerful evidence that the Sun cannot be a gas, but must be composed of condensed matter.

The situation relative to solar dimensions is further complicated by the realization that the solar diameter may well be variable [282]. Investigations along these lines are only quietly pursued [283], as the gas models are unable to easily address brief fluctuations in solar dimensions. The stability of gaseous stars depends on hydrostatic equilibrium and relies on a perfect mechanical and thermal balance [13, p. 6–67]. Failing to maintain equilibrium, gaseous stars would cease to exist.

Conversely, fluctuating solar dimensions can be readily addressed by a liquid metallic hydrogen Sun, since this entity enables localized liquid/gas (or solid/gas) transitions in its interior (see [48, 51, 52] and §5.1).

4.4 Oblateness #20

James Jeans regarded the high prevalence of binaries as one of the strongest lines of evidence that the stars were liquids [27, 28].‖ Indeed, it could be stated that most of his thesis rested upon this observation. As a spinning star became oblate, it eventually split into two distinct parts [27, 28]. Oblateness can be considered as a sign of internal cohesive forces within an object and these are absent within a gaseous star. As a result, any oblateness constitutes a solid line of evidence that a rotating mass is comprised of condensed matter.

The physics of rotating fluid masses has occupied some of the greatest minds in science, including Newton, Maclaurin, Jacobi, Meyer, Liouville, Dirichlet, Dedekind, Riemann, Poincaré, Cartan, Roche, and Darwin [3]. The problem also captivated Chandrashekhar (Nobel Prize, Physics, 1983) for nine years of his life [284].

Modern studies placed the oblateness of the Sun at 8.77×10^{-6} [287]. Though the Sun appears almost perfectly

*This proof was first presented as the fourth line of evidence [35, 36].

†The Earth has a density of 5.5 g/cm^3; Jupiter 1.326 g/cm^3; Saturn 0.687 g/cm^3; Neptune 1.638 g/cm^3; Uranus 1.271 g/cm^3 [279].

‡Setsuo Ichimaru had assumed, based on the gaseous models, that the core of the Sun had a density of 150 g/cm^3 when he considered that it could be composed of metallic hydrogen [97–99]. He did not address the composition of the solar body or atmosphere.

§This proof was first presented as the 21st line of evidence [51].

¶As a point of reference relative to the accuracy of measurements, machinists typically work to tolerances of a few thousands of an inch. According to a young machinist (Luke Ball, Boggs and Associates, Columbus, Ohio), a *"standard dial caliper is accurate to ± 0.001", and a micrometer provides greater accuracy to ± 0.0001". The Mitutoyo metrology company was founded in 1934, and they produce a digital high-accuracy sub-micron micrometer that is accurate to .00002."*

‖This proof was first presented as the eighth line of evidence [3, 35, 36, 50].

round, it is actually oblate [50].* To explain this behavior, astrophysicists invoked that the Sun possessed a constant solar density as a function of radial position [287]. This proposal is in direct conflict with the gaseous solar models [13, 14] which conclude that most of the solar mass remains within the central core. An essentially constant internal density is precisely what would be required within the context of a liquid metallic Sun [35, 39].

At present, helioseismic measurements (see §6) indicate that the degree of solar oblateness may be slightly smaller [288, 289], but the general feature remains. The degree of solar oblateness may well vary with the solar cycle [290]. As was the case for variations in solar radius (§4.3), these changes pose difficulties for the gaseous models. That the Sun is slightly oblate provides excellent evidence for internal cohesive forces, as seen in condensed matter.

4.5 Surface Imaging #21

With the advent of the 1-m Swedish Solar Telescope (SST), the solar surface has been imaged with unprecedented resolution [100, 291].† This resolution will increase dramatically in a few years when the construction of the Advanced Technology Solar Telescope is completed in Hawaii [104].

Using the SST, scientists report, *"In these pictures we see the Sun's surface at a low, slanting angle, affording a three-dimensional look at solar hills, valleys, and canyons"* [291]. . . *"A notable feature in our best images of sunspots is that many penumbral filaments, which are isolated from the bulk of the penumbra and surrounded by dark umbra, show dark cores"*. . . *"Inspection of our images shows numerous varieties of other very thin dark lines in magnetic regions"* . . . *"'hairs' that are seemingly emanating from pores into the closest neighbouring granules, 'canals' in the granulation near spots and pores, and running dark streaks crossing penumbral filaments diagonally"* [100].

Since antiquity, solar observers have been fascinated with structure on the surface of the Sun. Now, as telescopic resolution continues to increase, they are documenting, *almost in 3D*, the existence of structure on the solar surface with increased certainty. They resort to words like *'hills'*, *'valleys'*, and *'canyons'* to describe the surface of the Sun and they focus increasingly on substructures, like the dark cores of the penumbra. How can this structural detail be compatible with gases? Structure remains a property of condensed matter and gases can support none. Moreover, if the solar surface is but an *'illusion'*, what point can there be in documenting the nature of these structures? But the problem is even more vexing for the gaseous models, as films are currently being taken of the Sun in high resolution (see Supplementary Materials for [100] on the Nature website), and our *'illusions'* are *behaving* as condensed matter (see §5.1) [292, 293].

Father Secchi, perhaps the most able solar observer of the 19th century, drew with painstaking attention numerous details on the solar surface which he viewed as real [1]. He emphasized that *"there is thus no illusion to worry about, the phenomena that we have just exposed to the reader are not simple optical findings, but objects which really exist, faithfully represented to our eyes using instruments employed to observe them"* [1, p. 35–36, V. II]. The authors of the wonderful SST Nature paper [100] seem to discard illusions, *"We are, however, confident that the dark cores shown here are real"* [100]. Nonetheless, they maintain the language associated with the gaseous models, *"A dark-cored filament could be produced by an optically thin cylindrical tube with hot walls—perhaps a magnetic flux tube heated on the surface by the dissipation of electrical currents"* [100].

Commenting on [100] in light of accepted theory, John H. Thomas states, *"Computer simulations of photospheric magnetoconvection show very small structures, but the simulations have not yet achieved sufficient resolution to determine the limiting size. The horizontal mean free path — in other words, the average distance traveled without interacting — of a photon in the solar photosphere is about 50 km, and so this might be expected to be the smallest observable length scale, because of the smoothing effect of radiative energy transfer. But sophisticated radiative-transfer calculations show that fine structures as small as a few kilometers should in principle be directly observable"* [294].

The problem for the gas models rests in their prediction that the photosphere has a density ($\sim 10^{-7}$ g/cm^3 [148]) which is 10,000 times lower than that of the Earth's atmosphere at sea level — surpassing some of the best vacuums on Earth. Structure cannot be claimed to exist in a vacuum and has never been demonstrated to be associated with the equations of radiation transfer (see [292, 294] and references therein). It is inherently a property of condensed matter, without any need for internal photons. As a result, modeling associated with the analysis of structural entities on the solar surface, which is fundamentally based on ideas of a gaseous Sun [292, 294], are unlikely to be of any lasting value with respect to understanding the complexities of the photosphere. The most elegant solution rests in accepting that these structures are real and comprised of condensed matter.

4.6 Coronal Holes/Rotation #22

Coronal holes (see Fig. 18) are believed to be regions of low-density plasma that open freely into interplanetary space [52,

*As a point of interest, the Southern star Achernar, has a tremendous oblateness which approaches 1.5 [285]. This value cannot be explained using the standard gaseous models wherein most of a star's mass is restricted to the core. As such, scientists have sought to find alternative means to account for this oblateness [286].

†This proof was first presented as the eleventh line of evidence [4, 35, 36, 42]. Solar surface imaging can include frequencies outside visible light. It continues to reveal the presence of new structures, not described in §2. These, and those to come, are included herein as a separate line of evidence as solar surface imaging exposes more structural complexity and temporal evolution.

295, 296].* They are associated with the presence of fast solar winds (see §5.8).

When the Sun becomes active, coronal holes can appear anywhere on the solar surface [52, 295, 296]. In contrast, when it is quiet, coronal holes are viewed as *'anchored'* onto the polar regions of the solar surface [297, p. 10]. This *'anchoring'* constitutes a powerful sign that the Sun is comprised of condensed matter, as this behavior directly implies both long-term structure within the corona and the existence of a true solar surface. *'Anchoring'* requires two distinct regions in the Sun which cooperate with each other to produce *structural restriction*.

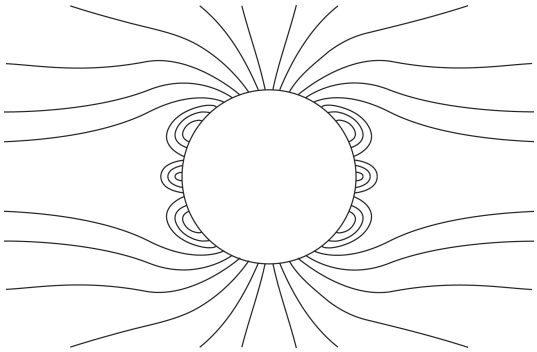

Fig. 18: Schematic representation of coronal holes over the polar caps of a quiet Sun. This figure is an adaptation based on Fig. 2 in [295]. Along with its legend, it was previously published in [52].

The corona possesses *"... a radially rigid rotation of 27.5 days synodic period from 2.5 $R_\odot$ to >15$R_\odot$"* [277, p. 116] as established by the LASCO instrument aboard the SOHO satellite [298]. Rigid rotation of the entire corona strongly suggests that the solar body and the corona possess condensed matter.

Coronal material† contains magnetic fields lines which, in turn, are anchored at the level of the photosphere [62]. *'Anchoring'*, once again, requires structure both within the solar body and within the solar atmosphere. The condensed nature of the corona and coronal structures has already been discussed in §2.3.7, §2.3.8, and §3.8. It will be treated once again in §5.5, and §6.6. The relevant structure of the solar interior will be discussed in §5.1. The presence of *'anchoring'* within coronal holes and the rigid rotation of the corona is best explained by condensed matter.

4.7 Chromospheric Extent #23

Eddington recognized the great spatial extent of the chromosphere and pondered on how this material was supported [9, p. 362].‡ At the time, he knew that chromospheric emission lines (see §3.4, §3.5, and §3.6) could extend up to 14,000 km [9, p. 362]. For Eddington, the answer to chromosphere chromospheric extent rested upon radiation pressure, but the solution would prove insufficient [62].

Bhatnagar and Livingston provide a lucid presentation of the chromospheric scale height problem within the context of the gaseous models [277, p. 140–145]. They recall how initial *'hydrostatic equilibrium'* arguments could only account for a density scale height of 150 km [277, p. 141]. In order to further increase this scale height to the levels observed, it was hypothesized that the chromosphere had to be heated, either through turbulent motion, wave motion, magnetic fields, or 5-minute oscillations [277, p. 140–145]. The entire exercise demonstrated that the spatial extent of the chromosphere represented a significant problem for the gaseous models. The great solar physicist Harold Zirin has placed these difficulties in perspective, *"Years ago the journals were filled with discussions of 'the height of the chromosphere'. It was clear that the apparent scale height of 1000 km far exceeded that in hydrostatic equilibrium. In modern times, a convenient solution has been found — denial. Although anyone can measure its height with a ruler and find it extending to 5000 km, most publications state that it becomes the corona at 2000 km above the surface. We cannot explain the great height or the erroneous models... While models say 2000 km, the data say 5000"* [193].

Obviously, a gas cannot support itself [62]. Hence, the spatial extent of the chromosphere constitutes one of the most elegant observations relative to the existence of a condensed solar photosphere. Within the context of the LMH model [35, 39], the Sun possesses a condensed surface. This surface provides a mechanism to support the chromosphere: gas pressure (see Fig. 17) — the same phenomenon responsible for the support of the Earth's atmosphere [48].

It was demonstrated in §4.1, that electron gas pressure cannot prevent a gaseous star from collapsing onto itself, being that these objects lack real surfaces. However, a liquid metallic hydrogen Sun has a real surface, at the level of the photosphere. When a gaseous atom within the solar atmosphere begins to move towards the Sun, it will eventually strike the surface. Here, it will experience a change in direction, reversing its downward vertical component and thereby placing upward pressure on the solar atmosphere, as displayed in Fig. 17. Gas pressure can simply account for the spatial extend of the chromosphere in condensed solar models [35, 39]. Moreover, under this scenario, the chromosphere might be supported by the escape of gaseous atoms from the solar interior as manifested in solar activity (see §5.1). This provides an acceptable mechanism in the condensed models, as they do not need to maintain the hydrostatic equilibrium essential to the gaseous Sun. In any event, chromospheric heat-

*The anchoring of coronal holes was first presented as the 22nd line of evidence [52], while the rigid rotation of the corona was once treated as the 33rd [62]. These two proofs, being closely related to one another, have now been combined.

†See the wonderful Fig. 106 in [1, p. 310, V. I] relaying the corona during the eclipse of July 8, 1842

‡This proof was first presented as the 34th line of evidence [62].

ing, from turbulent motion, wave motion, magnetic fields, or 5-minute oscillations [277], is not required to support the great spatial extent of the chromosphere in the LMH model.

4.8 Chromospheric Shape #24

Secchi had observed that the diameter of the observable Sun varied with filter selection (blue or red) during a solar eclipse [1, p. 320, V. I]. Currently, it is well established that the dimensions of the chromosphere are perceived as vastly different, whether it is studied in Hα, or using the HeII line at 30.4 nm [243, Fig. 1]. The chromosphere also appears to be prolate [243]. This prolateness has been estimated as $\Delta D/D = 5.5\times10^{-3}$ in HeII and 1.2×10^{-3} in Hα — more extended in polar regions than near the equator [243]. The shape of this layer has been demonstrated to be extremely stable, with no significant variation over a two year period [243].*

The prolate nature of the chromosphere and the extended structure which the Sun manifests above the polar axis cannot be easily explained by the gaseous models. A gaseous Sun should be a uniform object existing under equilibrium conditions, with no means of generating preferential growth in one dimension versus another. When the Sun is quiet, the greater extent of the chromosphere above the poles is associated with the presence of large anchored coronal holes in this region §(4.6). Coronal holes, in turn, manifest the presence of fast solar winds (see §5.8). A link to the fast solar winds is made in the gaseous Sun [243], despite the recognition that the origins of these winds (§5.8), and of the coronal holes with which they are associated (§4.6), remains an area of concern within these models [48, 52].

Even the oblate nature of the solar body had provided complications for the gaseous Sun (§4.4). This oblateness could be explained solely on internal cohesive forces and rotational motion in the LMH model (§4.4). But, the prolate nature of the chromosphere reflects something more complex.

According to the LMH model, fast solar winds (§5.8) are produced when intercalate atoms (see §5.1 Fig. 19) are actively being expelled from the lattice of the solar body [48, 52]. During this processes, some hydrogen is ejected, but unlike the other elements, it is often recaptured to help maintain the solar mass. In this respect, the solar chromosphere has been advanced as a site of hydrogen recondensation in the solar atmosphere (see §5.4, §5.6 and [59,61]). It appears prolate because, at the poles, more hydrogen is being expelled. Thus, more is recaptured over a greater spatial area. In analogous fashion, the corona has been designated as a site of electron recapture within the Sun [60]. With increasing distance from the solar surface, coronal atoms are increasingly stripped of their electrons. This is an electron affinity problem, wherein metallic hydrogen in the solar atmosphere scavenges for electrons and strips them from adjacent atoms [60]. Therefore, the chromosphere [59] and corona [60] act in concert to recapture protons and electrons, bringing them back onto the solar surface.

In §3.4, it was proposed [59] that the Hα emission is the direct result of the recondensation of atomic hydrogen, delivered by molecular hydrogen, onto larger condensed hydrogen structures, CHS, within the chromosphere. HeII emission results from the recondensation of atomic hydrogen, delivered by the helium hydride molecular cation [61], onto these structures (see §3.6).

In the lower chromosphere, neutral molecular hydrogen exists and can deliver atomic hydrogen with ease, resulting in Hα emission. However, with increasing height, it becomes more scarce, as the corona captures electrons. Once deprived of its sole electron, hydrogen cannot emit.

In contrast, with increased elevation, the helium hydride cation can become more abundant, as atomic helium can now harvest lone protons. Of course, neutral helium hydride in the ground state is not stable [256, 257]. Helium must first capture a lone proton (or first lose an electron to become He^+ and capture neutral hydrogen) to form the stable molecule. This readily occurs with increased height. Thus, HeII emissions are seen at the greatest chromospheric elevations. Since the helium hydride cation produced at these elevations can migrate towards the solar surface, one is able to observed HeII lines all the way down to the level of the photosphere.

Such an elegant account, exploiting chemical principles to understand line emission, cannot be framed by the gaseous models relative to the prolate nature for the chromosphere. This includes the possible causes for the differential spatial extent of Hα versus HeII lines (see Fig. 1 in [243]).

5 Dynamic Lines of Evidence

The dynamic lines of evidence involve time or orientation related changes in solar structure, emission, flow, or magnetic field. Along with many of the structural (§4) and helioseismic (§6) lines of evidence, they are amongst the simplest to visualize.

5.1 Surface Activity #25

The surface of the Sun is characterized by extensive activity.† The solar surface is often viewed as *'boiling'*, or as a *'boiling gas'*. But, gases and a gaseous Sun are unable to *'boil'*. Gases are the result of such actions. Only liquids can boil, while

*To fully understand this proof, it is necessary to simultaneously consider the origins of surface activity (§5.1), coronal holes (§4.6), solar winds (§5.8), Hα emission (§3.4) and HeII emission (§3.6). If the reader believes it difficult to follow, he/she may wish to move to other lines of evidence and return to this section once a more complete picture has been gained. This proof is listed as a structural proof (§3), even though it results from dynamic (§5) and spectroscopic (§3) processes, because it is expressed as the steady state appearance of the chromosphere when the Sun is quiet. In 1997, the sunspot number was near minimum and the data presented in [243] was acquired at that time.

†This proof was first presented as the ninth line of evidence [35, 36].

solids sublime.*

Since gases cannot boil, in order to explain activity on the solar surface, the gaseous models must have recourse to magnetic fields and flux tubes. In the case of sunspots (§2.3.3 [4, 40, 45]), faculae (§2.3.5 [45]), and magnetic bright points (§2.3.5), these fields are located within the solar body. In the case of the chromosphere (§5.6), flares (§2.3.8), and coronal mass ejections (§2.3.8), they arise from the corona. The arguments are fallacious, as magnetic fields themselves depend on structure for formation. Unable to account for their own existence (see §5.3), they cannot be responsible for creating such features within a gaseous medium.

The only prominent active features of the Sun, whose formation appears not to be inherently tied to magnetic fields, are granules (§2.3.4 [40, 45]). These are thought to be generated by subsurface heat which is being transported to the upper visible layers [40, 118–122]. A change in *'gas density'* is required within the photospheric vacuum.

In actuality, those who model granules in the laboratory (see [40] for a detailed review) understand that they are best represented as the products of Bénard convection [314–318], a process dominated by surface tension, not buoyancy [118, p. 116]. The gaseous models, unable to provide for a real surface on the Sun, must reject Bénard convection. The problem is further complicated with the realization that granules obey the 2D laws of structure (see §2.3.4) and that explosive phenomena, associated with *'dark dot'* formation, can be explained solely on the basis of structural considerations [126] (see §2.3.4). To add to the suspension of disbelief, proponents of the gaseous models maintain that the photosphere exists at the density of an ultra-low pressure vacuum ($\sim 10^{-7}$ g/cm^3 [148]). With respect to surface activity, all efforts by the gaseous models to understand the observed phenomena can be seen to collapse, when faced with the simple challenge that their solar surface is only an *'illusion'* [4]. Scientists are confronted with the intellectual denial of objective reality.

The LMH model [35, 36] can account for solar activity, since it allows for structure and takes advantage of the consequences. Granular convection can be explained with ease, as a LMH Sun possesses a true surface and the associated tension required for Bénard convection [314–318].

The emissive behavior of the Sun (see §2.3) strongly argues that the photosphere is comprised of a layered structure much like that found in graphite (see Fig. 2) and first proposed in metallic hydrogen [39] by Wigner and Huntington [88]. Layered materials like graphite are known to form intercalation compounds [48, 79–83] when mixed with other elements (see Fig. 19). In the case of metallic hydrogen, this implies that the non-hydrogen elements occupy interlayer lattice points [48], while the hexagonal hydrogen framework remains intact. It is the science of intercalation compounds which is most closely linked to the understanding of solar activity [48].

Within graphite, the diffusion of elements across hexagonal planes is hindered (see [48] for references), while diffusion within an intercalate layer is facilitated. The same principles are being invoked within the layered metallic hydrogen layers thought to exist in the Sun. Graphite intercalation compounds [79–83] are known to undergo exfoliation, an often violent process (see [79, p. 9] and [83, p. 406], where sudden phase transitions in the intercalation region from condensed to gaseous results in the expulsion of the intercalate atoms. In the laboratory, exfoliation can be associated with a tremendous expansion of lattice dimensions, as the gaseous expansion of the intercalate layers acts to greatly increase the separation between groups of hexagonal planes [79–83].

It is the process of exfoliation which can guide our understanding of solar activity. Exfoliation can be seen to result in the active degassing of the intercalation regions existing within the Sun. When the Sun is quiet, it is degassing primarily at the poles. This results in the fast solar winds (see §5.8) and coronal holes (see §4.6 [52]) in this region. It leads to the conclusion that the hydrogen hexagonal planes in the polar convection zones† tend to be arranged in a direction which is orthogonal to the solar surface.

However, in the equatorial convection zones, the hexago-

*Descriptions of a Sun which is *'boiling'* can be found throughout the printed word. Examples occur in 1) children's books [299], 2) popular writings [300, 301], 3) university level communications [302–305], 4) scientific news articles [306, 307], or 5) scholarly publications [115, 308–313]: 1) *"The sun is a boiling mass of hot gasses"* [299, p. 21], 2) *"It shows rather clearly that the Sun is a boiling mass of energy, vastly violent and constantly changing"* [300]; *"Convection is also at work transferring energy from the radiative zone to the photosphere, with a vertical boiling motion"* [301], 3) *"The surface of the Sun shows us a pattern of boiling gas arranged in a distinctive cellular pattern known as granulation"* [302]; *"Solar plasma emitted from the Sun is a boiling off of the Sun's atmosphere"* [303]; *"It is easy to think of the sun as benign and unchanging, but in reality the sun is a dynamic ball of boiling gases that scientists are only beginning to understand"* [304]; *"Our Sun is an extremely large ball of bubbling hot gas, mostly hydrogen gas"* [305], 4) *"We don't yet have a model that explains these hills"* [Jeffrey R.] *Kuhn said, although he suspects that they are caused by the interaction of boiling gas and the sun's powerful magnetic field"* [306]; *"The researchers found that, as expected, this tumultuous region resembles a pot of boiling water: hot material rises through it, and cooler gases sink"* [307], 5) *"Under poor to fair seeing conditions, sometimes the solar limb appears boiling, this gives some idea about the degree of air turbulence"* [115, p. 54]; *"The surface of the Sun boils in an active manner as the result of the continuous production of energy inside the Sun"* [308]; *"The hot corona boiling off the surface of the Sun toward the cold void of interplanetary space constitutes the solar wind"* [309]; *"The current general idea on the global balance ... is that energy conducted down from the low corona must 'boil off' mass from the chromosphere ..."* [310]; *"Near its surface, the Sun is like a pot of boiling water, with bubbles of hot, electrified gas — actually electrons and protons in the forth state of matter known as "plasma" — circulating up from the interior, rising to the surface, and bursting out into space"* [311]; *"The sun is a churning mass of hot ionized gas with magnetic fields threading their way through every pore and core, driven by energies boiling out from the interior where the fusion of hydrogen into helium at a temperature of 15 million K liberates the nuclear energy that keeps the cauldron boiling"* [312]; *"The magnetic field guides these flows, thus influencing on the average the radial distribution in the 'boiling' layer"* [313].

†A solar layer beneath the photosphere.

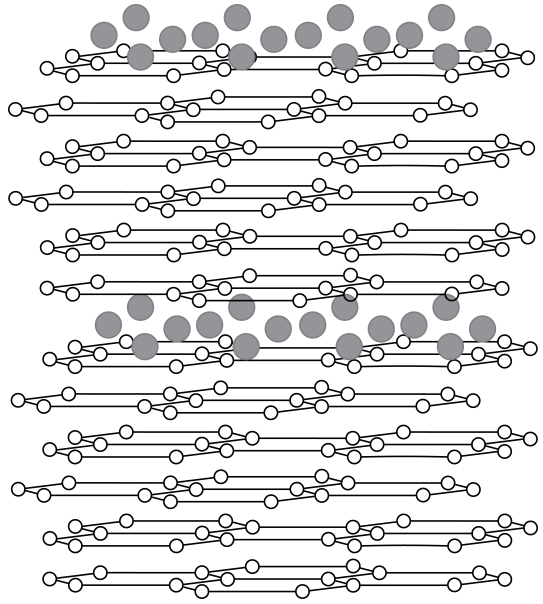

Fig. 19: Schematic representation of a proposed metallic hydrogen intercalation compound, wherein protons occupy the hexagonal lattice planes and non-hydrogen elements are located in the intercalation region. Intercalation compounds are characterized by a *'stage index'*, n, which accounts for the number of hexagonal planes between intercalate layers. In this case, n=6. This figure was previously published as Fig. 3 in [48].

nal hydrogen planes are hypothesized to be oriented parallel to the solar surface. Under the circumstances, atoms in the intercalation regions cannot freely diffuse into the solar atmosphere. They remain essentially *trapped within the Sun*, as reflected by the presence of slow solar winds above the equator. Over half the course of the eleven year solar cycle, intercalate elements slowly increase in number until, finally, the Sun becomes active (see Fig. 15) and exfoliative processes begin. The intercalate atoms begin to break and displace the hexagonal hydrogen planes, as they work their way beyond the confines of the photosphere. Coronal holes become visible at random locations throughout the Sun, indicating the reorientation of hydrogen planes in the interior. With time, the Sun degasses its equatorial region and returns to the quiet state.

In this regard, the series of images displayed in Fig. 15 are particularly telling, as they illustrate that helium levels in the lower solar atmosphere increase significantly with solar activity (examine carefully the periphery of the central image obtained in 2001 compared with images obtained in 1996 or 2005).* The Sun appears to be degassing helium, as previously concluded [48]. This further strengthens the argument that it does not, as popularly believed, possess large amounts of helium in its interior (see [47] for a detailed discussion). Rather, careful observation of the solar cycle reveals that the Sun must be comprised primarily of hydrogen, as it constantly expels other elements from its interior. The notable exception, as was seen is §3.3, relates to lithium [54].†

Relative to solar activity, the liquid metallic Sun allows for the buildup of true pressure in its interior, as intercalate elements enter the gas phase. This could account for changes in solar dimension (§4.3) and shape (§4.4, §6.3) across the cycle. It also explains the production of solar flares in accordance with ideas coined long ago by Zöllner [3, 189]. In a robust physical setting, mechanical pressure is all that is required, not energy from the corona. The same can be said of prominences, whose layered appearance (Fig. 20) highly suggests that they are the product of exfoliative forces within the Sun. Prominences reflect the separation of entire sheets of material from the Sun, exactly as found to occur when exfoliative forces act within graphite [48].

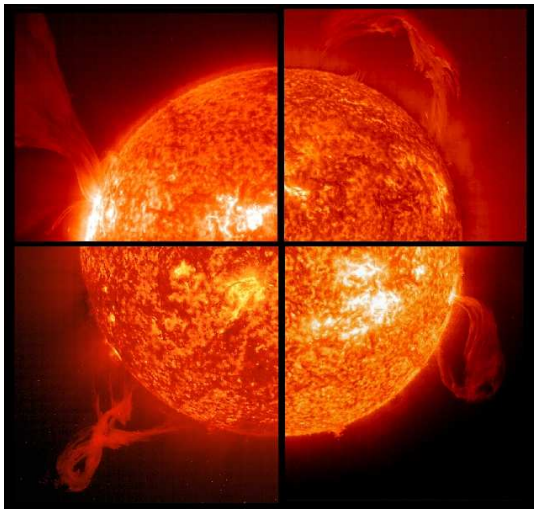

Fig. 20: An assembly of solar images obtained in the HeII line at 30.4 nm displaying the layered appearance of prominences. NASA describes this image as follows, *"A collage of prominences, which are huge clouds of relatively cool dense plasma suspended in the Sun's hot, thin corona. At times, they can erupt, escaping the Sun's atmosphere. For all four images, emission in this spectral line of EIT 304Å shows the upper chromosphere at a temperature of about 60,000 degrees K. The hottest areas appear almost white, while the darker red areas indicate cooler temperatures. Going clockwise from the upper left, the images are from: 15 May 2001; 28 March 2000; 18 January 2000, and 2 February 2001."*. Courtesy of SOHO/[EIT] consortium. SOHO is a project of international cooperation between ESA and NASA. (http://sohowww.nascom.nasa.gov/gallery/images/promquad.html — Accessed on 9/20/2013).

*Best performed using the high resolution image on the NASA SOHO website: http://sohowww.nascom.nasa.gov/gallery/images/large/304cycle.jpg.

†Deuterium and tritium, as hydrogen isotopes, should remain in the hexagonal proton planes. Like lithium, within a LMH model of the Sun, they should be retained within the solar body, with only small numbers escaping in the solar winds.

5.2 Orthogonal Flows #26

The orthogonal nature of material flow in the photosphere and corona (see Fig. 21) provides one of the simplest and most elegant lines of evidence that the Sun is comprised of condensed matter.* In 1863, Carrington established the differential rotation of the photosphere [67, 68]. His studies revealed that solar matter, at the level of the photosphere, experiences a net displacement in a direction parallel to the solar surface. Yet, solar winds (§5.8) are moving radially away from the Sun. This orthogonal flow of matter at the interface of the photosphere and the atmosphere just above it demands the presence of a physical boundary. Such a surface is unavailable in the gaseous models, but self-evident in a liquid metallic hydrogen setting.

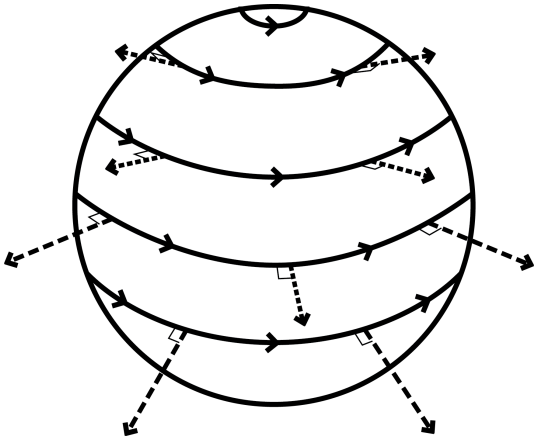

Fig. 21: Schematic representation of the orthogonal photospheric and coronal flows associated with Carrington's differential rotations [67] and the solar winds.

5.3 Solar Dynamo #27

As first noted by George Ellery Hale [107], the Sun possesses strong magnetic fields which can undergo complex windings and protrusions [12].† Magnetic fields are ubiquitous on the solar surface and within the corona. They are not manifested solely in sunspots (§2.3.3). As seen in §2.3.5, strong fields can be observed in faculae and magnetic bright points, while weak fields are present above the granules (§2.3.4) and in coronal structures (§2.3.8).

Within the context of the gaseous models, solar magnetic fields are believed to be produced by the action of a powerful solar dynamo [319, 320] generated at the base of the convection zone near the tachocline layer, well beneath the solar photosphere [12]. A dynamo represents a self-sustained amplification of magnetic fields, produced in conjunction with flow in conducting fluids. In the laboratory, they are studied using liquid metals, typically molten sodium [321–324]. Dynamo behavior must always involve the flow of conductive fluids across magnetic fields. This, in turn, *"induces electrical currents, which, under appropriate flow and magnetic field configurations, can sustain the field against dissipation"* [319].

Perhaps the greatest driving force for understanding the behavior of dynamos in the laboratory has been the presence of planetary and stellar magnetic fields [319–324]. It is not reasonable to apply these studies to a gaseous Sun.

All dynamo laboratories rely on the use of molten sodium. This substance acts as an incompressible conductive liquid metal [321–324].‡ To generate dynamo effects under experimental conditions, flow is typically induced into the metal using mechanical devices like pumps or turbines [321–324]. External induction coils are present which can provide initial magnetic fields to help either "seed" or "drive" the studies [321–324].

It is important to note that macroscopic structure is being imposed in these systems. In every case, the flow of liquid metallic sodium is being confined and directed by structure (tubes, vats, canisters) [321–324]. Insulating materials are always present, whether provided by the presence of pressurizing argon at 80 p.s.i. in a vat [321, 322] or by the inability of molten sodium to direct its own flow when propelled through pipes [323, 324]. Experimental geometries are carefully selected (see e.g. [323, Fig. 1]), including the location of induction coils [321, 322]. Mechanical devices are providing energy to drive these systems and external static magnetic fields supplement the sampling.§

In this respect, Lowe and Wilkinson constructed the first working model of a geomagnetic dynamo [328]. It was composed of solid iron alloy cylinders, rotating within a casting of the same material, wherein a small amount of mercury maintained the required electrical contact [328]. In relaying this design, Lowe and Wilkinson insisted that, *"Self-exciting dynamos are very common on the surface of the Earth, but these rely on the insulation between wires to direct the induced currents into an appropriate path; they are multiply connected"* [328].

These conditions are unlike those in gaseous stars which, by their very nature, are devoid of structure, have no ability to *"direct the induced currents into an appropriate path"* [328], and are incapable of acting as insulators. The situation has been summarized as follows, *"Whereas technical dynamos consist of a number of well-separated electrically conducting parts, a cosmic dynamo operates, without any ferromagnetism, in a nearly homogeneous medium"* [324]. With these

*This proof was first presented as the tenth line of evidence [35, 36].

†This proof was first presented as the twelfth line of evidence [35].

‡Conveniently, the density of liquid metallic sodium (ρ ~0.927 g/cm^3 [325, p. 4–128]) approaches that hypothesized to exist at the tachocline layer in the gaseous models of the Sun (ρ ~0.2 g/cm^3 [326]).

§Much like in medicine, where MRI can be performed using only the Earth's magnetic field (~0.5 gauss) [327], it is impossible to perform dynamo experiments within the laboratory in the absence of an initial ambient static field magnetic field, as has been recognized (e.g. [323]).

words, astrophysical dynamos fell outside the realm of experimental science, precisely because they are thought to exist in objects, like gaseous stars, unable to impart a physical architecture.

Astrophysics cannot hope that magnetic fields impart *'illusionary'* details and emissive properties to photospheric objects (e.g. sunspots and faculae), while at the same time requiring that real structure exists in a gaseous Sun. This structure must somehow enable the formation of powerful magnetic fields and the buildup of a solar dynamo. The fact remains that the generation of strong magnetic fields on Earth always requires the action of condensed matter. As they have no structure, gases are unable to generate magnetic fields on a macroscopic level. They are simply subject to their action. It is improper to confer upon gases behavior which cannot even be approached in the laboratory.

It is hard to envision that hydrogen in non-metallic form, as is currently hypothesized to exist in the gaseous stars, will be able to match the conductivity observed in a real metal (see Fig. 2 in [329]). Gases obviously cannot possess conduction bands and, therefore, lack the central element required to generate powerful magnetic fields on Earth. At the melting point, liquid sodium has a conductivity ($\sim 10^7\,\Omega^{-1}\,\mathrm{m}^{-1}$ [321–324]) which very much approaches that observed in the solid [321–324]. Near this point and in the solid state, conduction bands are responsible for the conductivity measured in sodium.* Hence, it should not be surprising that, just as the metal melts, some quantum mechanical conditions involved in forming these conduction bands remains (i.e. there remains some interatomic order). Otherwise, a substantial change in conductivity would be evident.

With all these factors in mind, it is reasonable to suggest that the structural lattice present in liquid metallic hydrogen provides a superior setting to account for dynamo action in the Sun. Metallic hydrogen should be able to support real structure. Protons would occupy the hexagonal planes (see Fig. 2) and electrons flow in the conduction bands necessary to generate magnetic fields. A LMH Sun should display a density, throughout its interior, similar to molten sodium. Conductive paths could be set up in the hexagonal hydrogen (i.e. proton) planes which can benefit from the insulating action of intercalate elements (see Fig. 19). As a direct consequence, changes in the dynamo and in the magnetic field intensity, in association with the solar cycle, can be accounted for as a byproduct of exfoliative forces (see §5.8). When the intercalate elements are expelled from the Sun, conductive shorts are created between hexagonal hydrogen planes which were once insulated from one another. This provides a mechanism to both build and destroy the solar dynamo. Furthermore, by turning to this substance as a solar building block, laboratory dynamo experiments become linked to a substance which may come to have great importance on Earth [92, 98], not only in the distant stars.

*Thermal vibrations can lower conductivity as temperatures are increased, but this effect is neglected in this case since both solid and liquid phases can exist at the melting point. Thus, any effect of thermal vibrations should be similar at this temperature in both phases.

5.4 Coronal Rain #28

Innocuous findings can lead to the greatest discoveries.† In this respect, coronal rain [330–333] will not present an exception. This subtle effect consists of *"cool and dense matter"* which is *"ubiquitous"* within the solar atmosphere and which is constantly falling towards the solar surface [330–333]. It is said to be composed of a *"a myriad of small blobs, with sizes that are, on average 300 km in width and 700 km in length"* [333]. When these aggregate, they produce *showers* [333]. Coronal rain has been associated with coronal loops and attempts have been made to link its existence to loop substructure [334].

As coronal rain falls towards the surface, its rate of descent does not match that expected from gravity considerations alone [333]. From the standpoint of the gaseous solar models, it appears that coronal rains and showers are retarded by the effects of gas pressure in the solar atmosphere [333]. These models rely on cycles of heating and condensation to explain coronal rain [332, 333]. But these arguments are not consistent with the belief that the lower chromosphere has a density of only $\sim 10^{-12}$ g/cm^3 [115, p. 32] and that gas pressure cannot exist (§4.1) in these models. How can condensation take place within a hot corona (see §3.7) while maintaining a gaseous state, which even at photospheric densities, would only be $\sim 10^{-7}$ g/cm^3 [148]? How can a vacuum retard the rate of descent of these particles? With respect to the existence of coronal rain, the gaseous models of the Sun simply lack the necessary flexibility to provide a reasonable account of this phenomenon.

Alternatively, the LMH model [35, 39], has advanced that condensed matter populates the outer solar atmosphere (see §2.3.6, §2.3.7, §2.3.8, §3.4, §3.5, §3.6, §3.8, §4.6, §4.7, §4.8, §5.5, §5.6, §5.7, and §6.6). Cool/dense coronal and chromospheric layers consequently stand as pillars of this model [56–60]. In this regard, the presence of coronal rain can be more readily explained if one permits true condensation to occur within the solar atmosphere.

As highlighted in §2.3.7 and §2.3.8, the K-corona should be viewed as a region containing diffuse metallic hydrogen [57, 60]. However, given the lack of pressure which exists in the K-corona, this metallic hydrogen cannot regenerate itself. Rather, coronal metallic hydrogen has entered the solar atmosphere after being expelled from the solar body during active periods (see §2.3.8, §5.5, §6.6 and [57, 58, 60]).

Though coronal LMH would be unable to self-regenerate, it should be able to provide a surface upon which other materials could condense. This appears to be what is happening with coronal rain.

†This proof was first presented as the 23rd line of evidence [53].

In this regard, it is important to note that coronal rain is usually visualized in Hα and CaII [334]. These emission lines are chromospheric in nature (see §3.4 and §3.5). Their use in detecting coronal rain strongly suggests that this material, unlike the coronal loops (§5.5) with which it is often associated [334], is actually condensing chromospheric material.*

Thus, much like water vapor on Earth condenses in the morning on the grass, hydrogen, in non-metallic form, appears to generate a dense condensate onto the coronal metallic hydrogen framework. This could explain why coronal rain can been seen flowing down coronal loops [334]. As the two substances are distinct, the hydrogen condensate slowly drifts back down to rejoin the solar surface. Since coronal rain remains attracted to the metallic hydrogen surfaces of the corona, it is unable to simply respond to the forces of gravity and its descent appears to be retarded.

Consequently, the analysis of coronal rain and its behavior appears to provide wonderful examples of the interplay between structure and function within the solar atmosphere. It strongly suggests that two distinct forms of condensed hydrogen are present in this region: 1) dense molecular hydrogen in the chromosphere [92] and 2) metallic hydrogen in the corona. Coronal rain is assisting in the harvest of hydrogen atoms from the corona. In unison, the metallic hydrogen framework, upon which it is condensing, acts to scavenge electrons from non-hydrogen atoms [56–60], which it could channel either to the solar body, or directly to coronal rain. In this manner, the corona functions to help preserve both the mass and charge balance of the Sun.

5.5 Coronal Loops #29

Coronal loops can be readily observed, both in the continuum [178–180] (see §2.3.8) and using distinct atomic emission lines (see §3.5 and §3.6), as shown in see Fig. 22. They represent *"inhomogeneous structures"*, which appear to be attached to the solar surface and which can extend well into the outer atmosphere [335, p. 83–84]. They can be relatively small (1 Mm in length and 200 km thick) or have great physical extent (several million meters to *"a substantial fraction of the solar radius"* with diameters of 1.5 Mm) [336]. While loops do not seem to possess substructure at the resolutions currently available [336], they may display such features on scales of about 15 km [336], a value well beyond current resolutions. Based on the analysis of coronal rain, it has been suggested that coronal loops have substructures smaller than 300 km [334].

As discussed in §5.4, coronal loops are associated with the presence of coronal rain. In this regard, the former may well represent a metallic hydrogen framework within the solar atmosphere unto which chromospheric matter, like coronal rain, can condense. This would appear to be confirmed

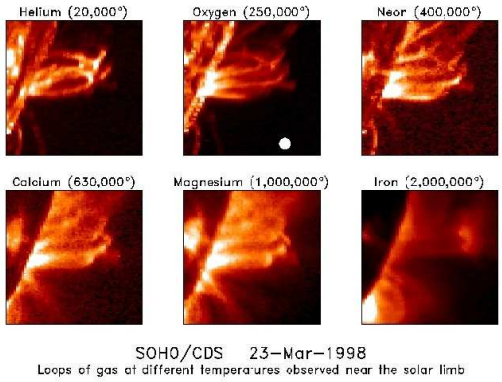

Fig. 22: Coronal loops visualized in helium, oxygen, neon, calcium, magnesium, or iron. Temperatures associated with each image have been inferred from the gaseous solar models. They correspond to 20,000 K, 250,000 K, 400,000 K, 630,000 K, 1,000,000 K, and 2,000,000 K, respectively. NASA describes this image as follows, *"CDS can produce images of the Sun at many wavelengths. In addition to hydrogen, the Sun's atmosphere contains atoms of common elements like helium, oxygen and magnesium. In the high temperature conditions of the Sun's atmosphere, these atoms emit light at different wavelengths depending on the temperature of the gas containing them. Therefore by tuning into different wavelengths we can make images of material which is at different temperatures. This capability is illustrated in the picture above, where CDS has taken images of magnetic loops of material which extend high into the Sun's atmosphere. These loops have been rendered more easily visible by observing them when they occur near the limb of the Sun, and hence they are highlighted against the dark background of space. The elements and their characteristic temperatures are indicated on the individual images. One of the surprises that the new SOHO/CDS data have produced is to show that loops at different temperatures can co-exist in the same regions of the Sun's atmosphere. The white disk plotted on the oxygen image shows the Earth to the same scale."* Courtesy of SOHO/[CDS] consortium. SOHO is a project of international cooperation between ESA and NASA. (http://sohowww.nascom.nasa.gov/gallery/SolarCorona/cds015.html — Accessed on 9/29/2013).

in Fig. 22, as both chromospheric lines (see §3.4, §3.5, §3.6) and coronal lines (see §3.8) can be detected within coronal loops.

Coronal loops hold an interesting line of evidence for condensed matter. It has been observed that *"the hydrostatic scale height. . . has always the same vertical extent, regardless of how much the loop is inclined, similar to the water level in communicating water tubes with different slopes"* [335, p. 84] (see Fig. 23).

The vertical height to which some coronal loops appear filled with matter does not change depending on inclination. The loop is containing matter which behaves as a liquid. Conversely, if the loop was merely plasma, the effects of vertical extent on loop appearance would be difficult to justify.

In this regard, it may well be that the manner in which

*Chromospheric matter is likely to be comprised of condensed matter where molecular interactions between hydrogen atoms persist [92].

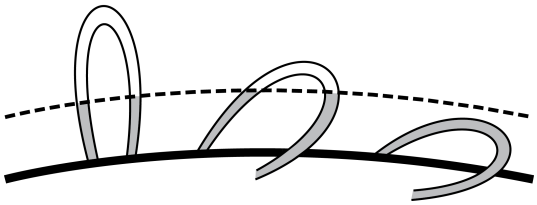

Fig. 23: Schematic representation of the vertical extent of scale height (dashed line) in coronal loops. Material fills the loop up to the scale height. If the loop is significantly inclined from the vertical axis, then it can be somewhat evenly filled with matter. The analogy can be made with water filling a tube which is more or less inclined [335, p. 84].

coronal loops appear to *'fill'* with height might represent a build up of condensed hydrogen onto these structures. As the loops assume an increasingly vertical position, material of a chromospheric nature should slowly settle towards the base of these structures, as it makes its descent down to re-enter the solar interior (see §3.4, §3.5, §3.6). Gaseous solar models are unable to rival this explanation.

5.6 Chromospheric Condensation #30

As discussed briefly in §3.4, the chromosphere is filled with spicules [337] which seem to extend as disoriented hair beyond the surface of the Sun.* As demonstrated in Fig. 24, spicules can be observed in Hα. They can also be seen in other chromospheric emission lines, including those from calcium and helium (see §3.5, §3.6 and [150, p. 8]).

The gaseous models of the Sun have no simple means to account for the formation of these structures.† Proponents of these models have expressed that two classes of spicules exist. Type II spicules are short-lived (10-150s), thin (<200 km), and said to fade [338]. Type I spicules have a 3–7 minute lifetime and move up and down [338]. It has been stated that Type II spicules might be responsible for heating the corona [338], but this claim, along with the very existence of Type II spicules, has been challenged [339]. Nonetheless, despite the densities brought forth, spicules are still believed to be propelling matter into the corona.

Counter to these ideas, the metallic hydrogen model holds that spicules are the product of condensation reactions (see §3.4, §3.5, §3.6 and [59, 61]). They enable hydrogen atoms, gathered in the solar atmosphere, to rejoin the solar body. The greatest clues for such a scenario come from the analysis of spicular velocities which appear to be essentially independent of gravitational forces [209–215].‡

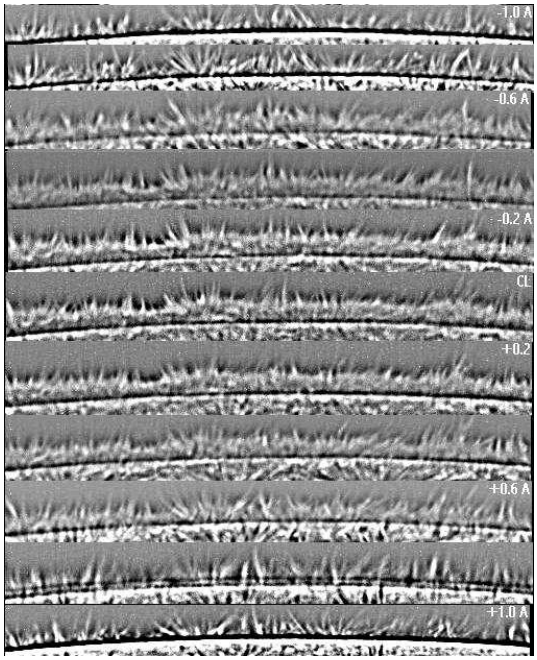

Fig. 24: A series of images displaying spicules in Hα on the solar limb. These images are displayed through the courtesy of the Big Bear Solar Observatory which have described the series as follows, *Limb Spicules: The Figure shows the limb of the Sun at different wavelengths within the H-alpha spectral line (from 0.1 nm bluewards to 0.1 nm redwards of the line center). Some of the spicules (jets) extend above height of 7000 km. The images have been processed with a high pass filter.*" http://www.bbso. njit. edu/images.html — Accessed on 9/30/2013.

Spicules seem to move up with nearly uniform speeds [206, p. 61]. These speeds can actually increase with elevation [150, p. 45–60]. Spicules can rise in jerky fashion or stop quite suddenly [150, p. 45–60]. They can *"expand laterally or split into two or more strands after being ejected"* [337].

All of this behavior, and the ability to document it, suggests that spicules are not devoid of density against an even sparser background. Rather, they seem to be the product of condensation. It is almost as if much of the material in the chromosphere exists in a state of critical opalescence, that strange state wherein matter is not quite liquid and not fully gaseous [35].§ Just a slight disturbance can cause the entire substance to rapidly condense. Such a process would be essentially independent of direction (vertical or horizontal), but

*This proof was first presented as the seventh line of evidence [35, 56, 59, 61].

†Spicules extend well into the lower corona where densities, according to the gaseous models, could be no greater than $\sim 10^{-15}$ g/cm^3, i.e. the density of the upper chromosphere [148]. The associated densities are $\sim 10^{-12}$ of the Earth's atmospheric density at sea level ($\sim$1.2x10^{-3} g/cm^3 [149]).

‡Some authors have attempted, although not very convincingly, to establish a relationship between spicular velocities and gravitational forces (e.g. [337]).

§The author has previously described the situation as follows, *"Critical opalescence occurs when a material is placed at the critical point, that combination of temperature, pressure, magnetic field, and gravity wherein the gas/liquid interface disappears. At the critical point, a transparent liquid becomes cloudy due to light scattering, hence the term critical opalescence. The gas is regaining order as it prepares to re-enter the condensed phase"* [35].

would be guided by local fluctuations in material concentrations. This would explain the erratic behavior and orientation of spicules.

The formation of spicular material suggests processes that are being observed near the critical point of a dense form of hydrogen [92] in the chromosphere. In moving from the corona to the photosphere, the effect of gravity becomes more important and, though temperatures might not be changing much (see §2.3.7), material in the chromosphere could be falling sufficiently below the critical point to allow for rapid condensation [35].*

Whether or not critical phenomena are being expressed in the chromosphere [35], it remains relatively certain that spicules themselves represent sites of condensation in the solar atmosphere, as manifested both by their dynamic behavior and by the emission lines with which they are associated (§3.4, §3.5, §3.6 and [59, 61]). It is highly likely that spicules are not propelling matter into the corona, but rather, that they are enabling hydrogen, present in the solar atmosphere, to reassume a condensed state and return to the solar body. In this case, they act to harvest hydrogen and return it to the photospheric intergranular lanes [59], as illustrated above in Fig. 14.

As with coronal rain, the chromospheric matter which makes up spicules should be comprised of dense hydrogen which is non-metallic, as it retains some hydrogen-hydrogen molecular interactions within its lattice [92]. This dense form of hydrogen, upon entering the pressurized environment of the solar interior, could then be transformed back to the metallic state [59].

5.7 Splashdown Events #31

Following violent flares, matter can be seen falling, in large fragments, back onto the solar surface.† The phenomenon resembles a huge mass of liquid projected into the air and then crashing back to the ground. A particularly impressive event was witnessed on June 7, 2011 [340, 341]. Solar material was ejected, as a great, almost volcanic appearing event, occurred on the photosphere. Solar matter was projected far into the corona, reaching heights well in excess of 500,000 km. Upon reaching a certain impressive altitude, the ejected photospheric matter was seen to fall back onto the solar body. Striking the surface, the descending material produced strong brightening at the impact points.

These events elegantly support the contention that flares and CMEs are driven by the buildup of pressure within the solar interior, not by transferring energy from the corona [189]. Most importantly, following the ejection of material from a flare, the return of mass towards the solar surface can be distinctly visualized. The associated impact points provide clear evidence that the ejected material and the surface upon which it splashes are comprised of condensed matter.

5.8 Solar Winds and the Solar Cycle #32

Solar winds have presented astronomy with a wealth of information, especially when addressing variations in helium abundances [342–351].‡ Two kinds of solar winds can be monitored. They are known as slow (<400 km/s) and fast (400–800 km/s) winds [349]. They differ only slightly in their particles fluxes (2.7×10^8 cm^{-2} s^{-1} versus 1.9×10^8 cm^{-2} s^{-1}, respectively), though they can have significant variations in their proton densities (8.3 cm^{-3} versus 2.5 cm^{-3}, respectively) [349]. Fast solar winds are typically associated with coronal holes [52, 349].

For the gaseous solar models, the origin of solar winds depends on the presence of a hot corona, which thermally expands as gravitational forces decrease with distance [352]. The body of the Sun is not involved, as a gaseous Sun must remain in perfect hydrostatic equilibrium, i.e. the forces of gravity must be exactly balanced with electron gas and radiation pressure [13, p. 6–7].

In bringing forth a solution for the origin of solar winds, Parker [352] would carefully consider earlier findings [353, 354]. Biermann had studied the orientation of comet tails and concluded that coronal particles were flowing away from the solar body [353]. At the same time, Unsöld and Chapman deduced that the Sun was expelling charged particles responsible for geomagnetic storms and computed the associated densities [354]. Parker would make the logical link between these events, but required for his solution that the space occupied by coronal matter expanded as it moved away from the Sun [352]. In order to permit this expansion, he postulated that the corona must exist at millions of degrees [352]. He believed that the outer corona could remain very hot, since Chapman had calculated, a few years before [355], that ionized gases could possess tremendous conductivities. Therefore, heat could be channeled from the lower corona to the outer solar atmosphere, to drive the solar winds.

As a result, the gaseous models have required the impossible from the corona. The latter must be heated to temperatures well beyond those of the solar core (see §3.8) using processes based on magnetic fields [148, p. 239–251]. Then, it must transfer this energy in two directions. First, the corona must be able to drive all violent activity on the solar surface [12], like flares and coronal mass ejections (see §5.1 and [179]). Second, it must allow energy, through its elevated conductivity [355], to reach the outermost layers of the solar atmosphere. In this manner, the corona itself can provide the thermal energy required to drive the solar winds [352].

But, if energy can dissipate into the outer corona through elevated conductivity, how can it be available to drive surface activity? How does the directionally opposite flow of heat in a

*There could be substantial opposition to the idea that critical phenomena are being observed in the chromosphere. However, spicule formation seems to reflect the scale length effects which characterize these processes.

†This proof was first presented as the 24th line of evidence [53].

‡This proof was first presented in [47, 48, 52].

conductive material, like the corona, not constitute a violation of the Second Law of Thermodynamics?* Furthermore, why require that heat be transferred into the corona from the solar interior prior to its application elsewhere in the Sun? Why not simply let the solar body do the work?

In any event, to maintain the requirements of hydrostatic equilibrium [13, p. 6–7], the Sun must let its ultra-low density vacuum-like corona maintain every unexplained process. It does so by transferring energy from the solar interior using magnetic fields, even though gases are unable to generate such phenomena §5.3.

The requirements that the corona is hot also introduces the problem of the cool K-coronal spectrum (see §2.3.7), which must, in turn, be explained with relativistic electrons. How could relativistic electrons survive in a conductive medium? Resorting to this proposal hampers the search for the underlying causes of the solar cycle.

Conversely, Christophe Robitaille has theorized that the Sun is expelling non-hydrogen elements synthesized within its interior (private communication and [48]).† In the LMH model, the Sun possesses a true graphite-like layered lattice (see Fig. 2) over much of its volume, except perhaps, in the core.‡ It is known in graphite, that layered lattices can accommodate the intercalation of atoms [18], as has been illustrated in Fig. 19. In this case, protons occupy the hexagonal planes, electrons are flowing in conduction bands, and non-hydrogen atoms are found in the intercalation regions. These atoms can freely diffuse in the intercalation zones, but would experience restricted diffusion across hexagonal hydrogen planes (see Fig. 19). Such simple considerations, within the context of intercalate structures, can readily account for the solar winds [47, 48, 52].

In this model, the tremendous pressures within the solar interior provide the driving forces for the solar wind. Non-hydrogen atoms in intercalation regions are being expelled from the solar body by simple mechanical action, in accordance with known exfoliative processes in graphite [48]. For instance, an atom traveling at 800 km/s could leave the center of the Sun and escape at the surface in only fifteen minutes [52].§

During quiet solar periods, the known presence of fast solar winds over coronal holes [52, 349] could be readily explained. It requires that the intraplanar axis (A in Fig. 2) of metallic hydrogen, in the polar convection zone, be positioned orthogonally to the solar surface [52]. This would enable the rapid ejection of intercalate atoms from the solar interior at the poles when the Sun is quiet.¶ In the convection zone below the solar equator, the intraplanar axis (A in Fig. 2) would be rotated by 90°, becoming parallel to the solar surface. This would act to restrict the degassing of intercalate atoms, resulting in slow solar winds above the equator.

A clearer understanding of solar winds provides new insight into helium abundances [47]. It has been argued that current estimates of solar helium levels are largely overestimated [47]. Evidence suggests that, during active periods, the Sun is expelling helium from its equatorial region, not retaining it (see Fig. 15) [47].

Helium levels in the solar wind can vary substantially with activity. When the Sun is quiet, the average He/H ratio in the slow solar wind is much less than 2%, often approaching <0.5 % (see Fig. 1 in [348]). However, when the Sun is active, the ratio approaches 4.5% [348]. Relative helium abundances can rise substantially with solar activity, like flares [347], and the He/H ratio increases dramatically during geomagnetic storms [343]. Extremely low He/H ratio values of 0.01, rising to 0.08, with an average of 0.037 have been reported, when the Sun was quiet [343]. He/H ratios can vary greatly, especially in slow solar winds [343, 346]. Therefore, astronomers have assumed that solar winds cannot be used to assay this element [347]. However, it is more likely that what is being observed has not been correctly interpreted.

Extremely low He/H ratios challenge the premise that the Sun has an elevated helium abundance [47, 241, 242], sending shock waves throughout cosmology (see [47] for more detail). As helium can be essentially absent from the solar wind, astronomers, rather than infer that the Sun has a low helium abundance, assume that the elements must not be properly sampled. Helium must be gravitationally settling in the Sun (see [48] for a detailed discussion) or is being destroyed on the way to the detectors by processes occurring in the corona [347, p. 298].

The fast solar wind is thought to represent a less biased appraisal of elemental abundances [347, p.295], precisely because helium is being ejected from the Sun and subsequently appears abundant. Aellig et al. report that the fast solar wind has a helium abundance of 4–5% throughout the course of their five year observation (see Fig. 2 in [348]).

These results can be readily explained when considering that the Sun is condensed matter. When the Sun is quiet, it is degassing its intercalation regions, primarily from the poles. Large amounts of helium can accordingly populate the fast solar wind. When solar activity is initiated, the Sun begins to degas its equatorial regions. Much of this helium then travels along with slow solar winds to our detectors, and those concentrations are likewise elevated. However, when the Sun is

*It is already difficult to accept that a low density vacuum could transfer its energy to the solar surface. This scheme becomes even more strained when coronal energy is permitted to flow freely, using conductive paths, away from the Sun. The only solution implies a violation of the First Law of Thermodynamics, i.e. energy is being created in the middle of the corona.

†Lithium provides one notable exception, as seen in §3.3 and [54].

‡A body center cubic structure, as proposed in computational studies of dense plasmas by Setsuo Ichimaru [97], would be appropriate for the solar core (see §6.5).

§This compares to thousands, perhaps millions, of years for a photon to leave the core of the gaseous Sun (see §2.3.1 and [42]).

¶Coronal holes persist above the poles during periods of reduced solar activity (see §4.6).

quiet, virtually no helium reaches our detectors in the slow solar winds, as this element is now trapped in the equatorial intercalation regions. This scenario provides strong motivation for concluding that the Sun is actively degassing helium and that the true internal abundances of this element must be much lower than currently estimated [47, 241, 242].*

Not only can the LMH model account for the production of solar winds, but it advances an underlying cause of the solar cycle: degassing of the solar body [48, 52]. When the Sun is quiet, fast solar winds are able to degas the convection zones below the poles. This helps to explain why sunspots are never seen at these latitudes. However, during this period, the equatorial regions are experiencing restricted degassing. This is due to the parallel orientation of the hexagonal hydrogen planes in layered metallic hydrogen lattice, with respect to the solar surface. Such an orientation prevails in the underlying convection zone when the Sun is quiet. Solar activity is initiated when active degassing of the equatorial planes begins. This occurs in association with a rotation or partial breakdown of the hydrogen planes, as was seen when discussing sunspots (§2.3.3). This is the reason why coronal holes can appear anywhere on the solar surface when the Sun is active, as discussed in §4.6. When accounting for solar winds, coronal holes, and solar activity, the LMH model far surpasses in insight anything offered by the gaseous models.

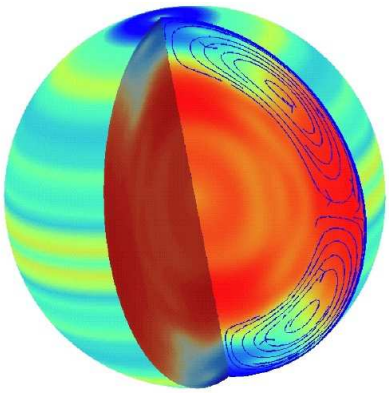

Fig. 25: Variations in sound speed within the Sun. Red regions are hotter than the standard solar models, while blue regions are cooler. This image has been provided courtesy of SOHO/[Michelson Doppler Imager] consortium. SOHO is a project of international cooperation between ESA and NASA. (http://sohowww.nascom.nasa.gov/gallery/images/mdi025.html — Accessed on 10/1/2013).

6 Helioseismic Lines of Evidence

Seismology remains a science of the condensed state. Even so, proponents of the gaseous models adhere to the belief that helioseismology can claim otherwise. In this section, a group of six helioseismic conclusions will be briefly examined. Each provides compelling evidence that the Sun is comprised of condensed matter. It might be argued that other helioseismic lines of evidence could be extracted. Only six have been selected for their scientific impact.

6.1 Solar Body Oscillations #33

The Sun acts as a resonant cavity.† It sustains oscillations, as sound waves travel (see Fig. 25), within its interior [356–360]. The most prevalent solar oscillation has a period of 5 minutes, but many more modes exist [356–360]. Thus, the solar surface is reflecting internal audio waves and this causes the entire solar body to *'ring'*, as it succumbs to seismic activity.

Though scientists currently utilize helioseismology to justify the gaseous models [356–360], the conclusions would be better suited to a condensed Sun. It is not reasonable that a photosphere, with a density of only $\sim 10^{-7}$ g/cm^3 [148], can act as a resonant cavity. Within the gaseous models, the Sun has no distinct surface, hence it cannot provide a physical boundary to sustain solar oscillations.

Fig. 25 displays slight differences in sound speed with the standard gaseous model. A detailed analysis of such studies can be profitable. Bahcall et al. [361] have also compared theoretical results with experimental helioseismic findings for standard gaseous models. Absolutely amazing fits are obtained throughout the solar interior, but the authors fail to provide comparisons for the outer 5% of the Sun (see Figs. 12 and 13 in [361]). Yet, all observational data is being acquired precisely from this region. Therefore, any perceived experimental/theoretical agreement has little validity.

As was concluded in §3.1, the Sun presents the observer with a distinct surface in the UV and X-Ray bands. This surface is covered by low-frequency 3 mHz oscillations [362]. Evidence for a distinct surface has also been presented by gamma-ray flares (see §3.2). The Sun behaves as a resonant cavity in the audio bands, implying a true surface. But the gaseous models must maintain that the solar surface is but an *'illusion'*, to somewhat poorly account for limb darkening (see §2.3.2). Unfortunately, illusions make for poor resonant cavities. It is more logical to infer that the Sun has a distinct surface over the entire span of relevant wavelengths (audio to X-ray), as provided by condensed matter.

Despite denial that the Sun is either liquid or solid, astronomers refer to solar seismic events as *"similar to earthquakes"* [362]. Such analogies are in keeping with the known truth that seismology is a science of condensed matter. The same can be said for the Sun.

*In this regard, it should be remembered that the chromosphere and the corona are working to actively recapture hydrogen, protons, and electrons. This would act to elevate the He/H ratio detected in any solar wind. In addition, since the Sun is degassing intercalate regions and its average stage index (see Fig. 19) may be quite large, the solar body might best be viewed as composed almost entirely of hydrogen.

†This proof was first presented as the fifth line of evidence [35, 36, 42].

6.2 Mass displacement #34

On July 9, 1996 a powerful X-ray flare disrupted the solar surface, as illustrated in Fig. 26 [362, 363].* This image was obtained through Doppler methods. Consequently, material moving towards the observer appeared brighter, while matter propagating away from the detector seemed darker. Therefore, the flare itself was bright.

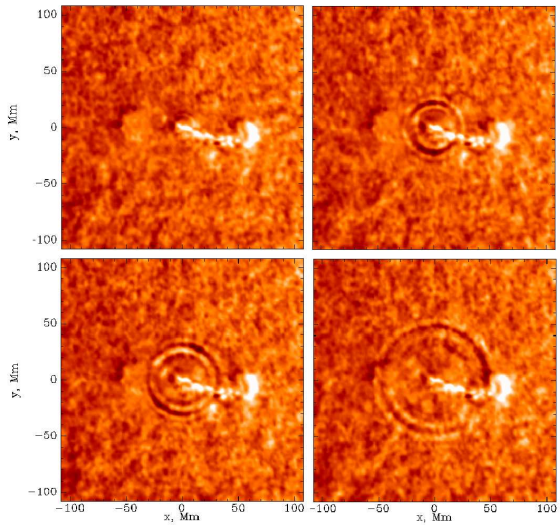

Fig. 26: Doppler image of a solar flare and the associated disturbance on the solar surface acquired by the NASA/ESA SOHO satellite [362]. Courtesy of SOHO/[Michelson Doppler Imager] consortium. SOHO is a project of international cooperation between ESA and NASA.

Kosovichev and Zharkova [362] support the notion, central to the gaseous models, that flares are being excited with coronal energy. They suggest that *"a high-energy electron beam* (is) *heating the cool chromospheric 'target' "*. Surface activity is driven, not from the interior of the Sun, but from the coronal vacuum. Nonetheless, the displacement of material observed in Fig. 25 strongly supports Zöllner's ideas regarding the nature of solar flares, as previously discussed in §5.1 and §5.7. It appears that the flare was produced when pressurized material was ejected from the solar body beyond the photospheric surface.

But, when the flare emerged, it produced enormous transverse waves on the surface of the Sun. The crest to crest distances are on the order of 10 Mm. Kosovichev and Zharkova [362] describe these transverse waves as *"resembling ripples from a pebble, thrown into a pond"* and maintain that the behavior can be explained with computations involving gas models. Still, they visualize *"ripples on a pond"*, a direct reference to behavior which can only be observed in condensed matter. Gases can sustain longitudinal, not transverse waves. Attempts to generate these waves, not only in a gas, but in an ultra-low-density vacuum, challenges scientific reason.

6.3 Higher Order Shape #35

Seismological studies have revealed that the Sun is not perfectly oblate (§4.4) but rather, is characterized by higher order quadrupolar and hexadecapolar shape terms which appear dependent on the solar cycle [364].† Higher order shape terms involve forces beyond those produced with simple rotation of a homogeneous liquid mass. They imply *internal structure within the Sun*. Hence, they stand as a sublime indication that the solar body possesses real structure beyond the core.

It would be extremely difficult to justify that fully gaseous objects could ever sustain observable internal structural effects. Yet, the higher order quadrupolar and hexadecapolar shape terms must arise from internal structure. Conversely, within the context of the LMH model, higher order shape terms would be expected. It has already been mentioned that the hexagonal hydrogen plane orientation (see Fig. 19), at the level of the convection zone, could account for coronal holes, solar winds, and the solar cycle (see §5.8). Hexagonal hydrogen planes could give rise to large layers, moving over one another, whose orientation relative to the solar surface could slowly vary from equatorial to polar regions (i.e. parallel versus orthogonal).‡ This would give rise to true underlying structure in the convection zone, as expressed in higher order shape terms.

6.4 Tachocline and Convective Zones #36

The Sun possesses a convection zone characterized by differential rotation [356–360].§ While a gas can easily be thought to undergo differential rotation, the Sun is characterized by another region: a tachocline layer separates the convection zone from the solid solar core (see §6.5).

The tachocline region acts as a shear layer within the Sun. This layer is known to be prolate in nature [360, 365–367]. The tachocline is generally thicker and shallower at the higher latitudes [360, 366]. It seems to display some temporal variability across the solar cycle [366], strongly suggesting, once again, that structural changes are taking place within the solar body (see §5.8 and §6.3).

When considering the tachocline layer, it is important to recall that shear stresses require the presence of a physical plane. For instance, the equation for shear stress, τ, states that τ=F/A, where F=force and A=Area. It is not possible

*This proof was one of the earliest [4, 29] and was presented, at one time, as the sixth line of evidence [35].

†This proof was first presented in [50], as supportive of §4.4. However, solar oblateness does not depend on the use of helioseismology for its determination (§4.4) and has been invoked by Jeans [27, 28] as providing a mechanism to generate binaries [3]. As for higher order shape, it is indicative of forces which differ from those involved in creating oblateness. Upon reconsideration, higher order shape now stands on its own as a separate line of evidence.

‡This resembles tectonic shifts on Earth. Such a parallel was drawn by Luc Robitaille (personal communication).

§This proof was first presented as the nineteenth line of evidence [50].

to have a shear stress without acting on a surface, or an organized lattice plane of atoms, as provided by condensed matter. Imaginary planes cannot experience shear forces.

Consequently, the shear nature of the tachocline, and the fact that it displays a prolate nature, provides clear evidence that the solar body is physically structured. Furthermore, it appears that this is an area of the Sun which can undergo changes with the solar cycle. These results are most gracefully explained by the LMH model.

6.5 Solar Core #37

As was suggested in §6.4, the core of the Sun undergoes solid body rotation [368].* This conclusion, has been reached by a virtual *who's who* of authority in helioseismology [368]. In the central portion of the Sun, *"...the rotation rate appears to be very little, if at all. Its value is 430 nHz"* [368].

Solid body rotation in the solar interior directly implies that the body of the Sun cannot be gaseous. This rotation requires the presence of powerful cohesive forces within the Sun. None can exist in a gaseous object.

The observation is more in line with Setsuo Ichimaru's conjecture (§2.3.1 and §5.8) that the central portion of the Sun can be considered to exist as a one-component plasma of metallic hydrogen [97, pp. 103 & 209]. Ichimaru adopted the body-centered cubic structure in his studies [97–99] and this lattice configuration would make sense at the center of the Sun.

In this respect, Ichimaru based the density of metallic hydrogen in the core on conclusions derived from gaseous models. If the photosphere of the Sun is truly condensed, then the values he adopted (56.2 g/cm^3 [98, p. 2660]) would be much too elevated. In a liquid model, the density cannot vary much throughout the solar body, remaining near 1.4 g/cm^3 (i.e. slightly lower at the photosphere and slightly higher in the core). At the center of the Sun, we are merely witnessing a change in lattice structure from a layered Type-I lattice over most of the photosphere, to a more metallic layered Type II lattice in the convection zone, and finally to a body-centered cubic lattice in the core. Intercalate atoms would be present within Type I and Type II layered lattices. If they change from the condensed to the gaseous phase, these intercalate atoms could slightly reduce the average densities of these layers.

The LMH model is more in keeping with physical observations within the Sun. It is not reasonable to advance that gases rotate as solid bodies. Condensed matter enables the formation of a solid core which can account for the observed rotations.

6.6 Atmospheric Seismology #38

Helioseismology has been extended to the outer solar atmosphere [214, 369–372].† Coronal and chromospheric studies [214, 369–372] have successfully detected seismic waves in this region of the Sun and the presence of both incompressible and compressible waves is now well-established. These are viewed as magnetohydrodynamic waves (MHD) in nature.‡

The existence of incompressible transverse waves in the solar atmosphere [214, 369–372] suggests, once again, that this region of the Sun contains condensed matter. These have been observed in spicules [214] and within the chromospheric level [372]. Their detection implies that the densities of these solar layers are well in excess of those which typify Earthly vacuums.

As a point of interest, it is known that comets can send shock waves throughout the solar corona and chromosphere. On January 29, 2013 (see [373]), a comet begins to disrupt the solar atmosphere when it is more than $1R_{\odot}$ away from the solar surface. At this location, the corona has no density ($<10^{-15}$ g/cm^3, the density of the upper chromosphere [148]), according to the gaseous models. It is unfeasible that an ultra-low-pressure vacuum could be able to respond to the entry of a comet in this manner. The ability of comets to trigger shock wave propagation throughout the solar atmosphere indicates that this is a region of elevated density. This conclusion is in keeping with the LMH model of the Sun.

7 Elemental Lines of Evidence

7.1 Nucleosynthesis #39

It has been gloriously stated that the elements were formed in the stars.§ In this, there appears to be much truth [374–388]. From its inception, stellar nucleosynthesis has always been closely linked to stellar evolution [129, 374–378].

The idea that the Sun could synthesize helium was first proposed by men such as Gamow [377, 378], Bethe [379–381], von Weisäcker [382] and Hoyle [383, 384]. The p-p reaction, wherein two protons combine to make a deuteron, while relying on positron and neutrino emission, would come to play a vital role in ^{4}He synthesis within low mass stars [374, p. 118]. For stars with a greater mass than the Sun, Bethe and von Weisäcker, in 1938 and 1939 [380–382], advanced that ^{4}He was being formed in a simple cycle involving nitrogen, carbon, and oxygen (CNO).

Early on, Hans Bethe had argued that *"no element heavier than ^{4}He can be built up in ordinary stars"* [381]. With those words, the Sun was crippled and stripped of its ability to make any element beyond helium.

Bethe had reached his conclusion based on the probability of nuclear reactions in the gas phase and at the temperatures of ordinary stellar cores [381, p. 435]. If this was true, how did the Sun come to acquire the other elements? For Bethe, the answer appeared straightforward, *"The heavier elements found in stars must therefore have existed already when the*

*This proof was first presented as the twentieth line of evidence [50].
†This proof was first presented as the 29th line of evidence [58].
‡See [372] for a brief, but well compiled, literature review.
§This proof was first presented in [44, 48].

star was formed" [381]. Extremely large and hot, first generation stars, had, soon after the Big Bang, created the heavy elements [389]. These elements merely represented contamination in the Sun, a product of objects extinguished long ago.

At the time that the CNO cycle was outlined [380–382], the discovery of metabolic cycles was creating a fury in biology. Just a few years before, in 1932, Hans Krebs (Nobel Prize, Medicine and Physiology, 1953) had discovered the urea cycle [390]. He would go on to outline the tricarboxylic acid (TCA or Krebs) cycle in 1937 [391], the discovery for which he gained international acclaim. It cannot be doubted that these great pathways in biology influenced astrophysical thought. Cycles seemed all powerful.

Biological cycles initially concealed their many lessons. It would take years to fully understand that they were highly regulated entities. Biological cycles required a complement of reactions and cofactors (small activator molecules or ions) which could either sustain the levels of intermediates or activate key enzymatic reactions. Similar regulation would be difficult to envision in the case of the CNO cycle. As a result, can this cycle truly occupy central positions in the synthesis of ^{4}He in the stars? Why confound the process by resorting to a cycle, when simple reactions between hydrogen atoms should be sufficient for all stars?

It would seem fortuitous that precisely the proper amounts of carbon, nitrogen, and oxygen has been distributed within stellar interiors, to permit these reactions to take place. If stars are truly gaseous, how do they ensure that these elements are not destroyed, or used up, by competing nuclear reactions — something which can be prevented or exploited to advantage in biology? Unlike a biological cell, with its intricate means of forming, separating, and transferring metabolites, the gaseous star cannot control the course of a single reaction. Everything must occur by chance. This complication is directly opposed to the subsistence of cycles.*

Concerning nucleosynthesis, proponents of the gaseous models require the improbable. Hobbled by theory, they must claim that first generation stars created the heavy elements. Moreover, they advance that, while mankind has successfully synthesized many elements, the Sun is unable to build anything beyond helium. First generation stars which no longer exist had done all the work [389]. These conclusions, once again, call for the suspension of disbelief. It is much more reasonable to assume that the Sun has the ability to synthesize all the naturally occurring elements, based on their presence in the solar atmosphere.

In turning his attention to dense plasmas, Ichimaru recognized that they could provide additional freedom in elemental synthesis [97–99]. These ideas have merit. In the LMH model, dense structures enable the synthesis of heavy elements which is not restricted to the solar core, but expressed in the convection zone where the intercalation regions can be found.

A metallic hydrogen framework can restrict protons to lattice points in the hexagonal plane and confine other atoms to the intercalate layer [48]. Solar pressure and lattice vibrations could act in concert to enhance the probability of nuclear reactions. Two adjacent protons, in the hexagonal hydrogen plane, could give rise to a deuterium atom, with the associated positron and neutrino emission [388]. This deuterium could then react with another, leading directly to the synthesis of ^{4}He. Alternatively, it could fuse with a proton, leading to the formation of ^{3}He. Both ^{4}He and the light helium isotope, ^{3}He, would be immediately ejected into the intercalation region [48].† Over time, the intercalation region could sustain other nuclear reactions and become the birthplace of all naturally occurring heavy isotopes. The Sun and the stars gain the ability to synthesize all of the elements [44, 48].

In this regard, it is well-known that solar flares can give tremendous ^{3}He abundance enhancements [180]. Eruptive flares have been known to produce ^{3}He/^{4}He ratios approaching 1 [186], and thousand-fold enhancements of this ratio have been observed [392]. These findings can be better understood in a solar model wherein ^{3}He is being preferably channeled into intercalation regions over ^{4}He. ^{3}He could then display an enhancement over ^{4}He when released into the solar atmosphere during activity.‡ It would be difficult to account for the finding for the gaseous models, but the result can be reasonably explained using the LMH model.§

8 Earthly Lines of Evidence

The earthly lines of evidence may be the most powerful. They are certainly the most far reaching. Climate dictates our future and the survival of humanity.

Thus, it is fitting to close this discussion with the climatic line of evidence. This acts to highlight that there is much more to studying the Sun than intellectual curiosity. As such, the *'Young Sun Problem'* and the great Maunder minimum of the middle ages are briefly discussed.¶

*Note that the author has proposed a cycle in §3.6. In this case however, the formation of triplet He has not been left to chance. It is the direct product of a systematic chemical reaction. The other reactant in the cycle, hydrogen, is present in excess.

†^{3}He could also emit a positron to make tritium, ^{3}H. Remaining in the hexagonal plane, this hydrogen isotope could then react with a single proton to make ^{4}He, which could then be expelled into the intercalate region.

‡This requires simply that the reaction of a deuterium atom with a proton is preferred over its reaction with another deuterium atom. This would be expected in a hyrogen based Sun.

§The solar neutrino problem has not been addressed in this work as a full exposition would involve too much discussion. Suffice it to state that difficulties involved in obtaining proper neutrino counts highly suggest that the Sun is sustaining other nuclear reactions beyond the simple synthesis of ^{4}He.

¶These constitute a single line of evidence as they are both related to climatic changes on Earth.

8.1 Climatic #40

8.1.1 The Young Sun Problem

The gaseous models infer that, when the Sun was young, it was much cooler than it is at present [393–395]. Once thought to be faint and dissipating much less heat onto the surface of the Earth, a gaseous Sun became increasingly warm over time. Thus, the Sun was once thought to be faint, dissipating little energy onto the Earth. Two billion years ago, the mean temperature of the Earth's surface would have been below the freezing point of water [393]. A paradox arises, since geological studies have revealed that water existed on Earth in liquid state as early as 3.8 billion years ago [393–395].

In order to resolve this problem, Carl Sagan was one of the first to advance that the answer could be found in the Earth's atmosphere [395]. If the young atmosphere was rich in CO_2, then the greenhouse effect and global warming [396] provided an explanation [393–395]. Everything appeared to be resolved [393].

Still, some remained unsatisfied with the greenhouse solution. Several stated that a young Sun was more massive and accordingly, hotter [393, p. 457]. In this scenario our Sun lost enormous amounts of material over the years through *"a vigourous, pulsation driven, solar wind"* [393, p. 457]. The young Sun could have been fifteen times more luminous than now, simply as a consequence of these changes in mass [393, p. 458].

But, it is difficult to conceive how a gaseous star, violently expelling mass despite great gravity, will cease to do so as gravitational forces decrease. Nonetheless, these basic ideas have survived, although with less dramatic changes in mass loss [397]. In this approach, the gaseous young Sun was not faint, but bright [397]. This was more in keeping with warm temperatures both on the Earth and on Mars [397]. Greenhouse effects could not simultaneously explain these findings.

In the end, the LMH model has a distinct advantage relative to the young Sun problem. Only the gaseous equations of state demand that a star like the Sun must become increasingly luminous as it evolves.* But over time, a Sun based on condensed matter, should cool from the most luminous (Class O) to the coolest star type (i.e. Class M).

Some may highlight that, if our Sun was once an O class star, there should be no water on Earth. The supposition is not valid. When the Earth was young, scientific consensus states that it was molten (see e.g. [399]). This can be easily explained if the Sun was once an O Class star, but not if it was a faint gaseous object. The Earth, like our Sun, cooled over time. The LMH model is much more in accordance with observational facts in this regard.†

8.1.2 The Maunder Minimum

A great minimum appeared in the Sunspot cycle during the middle ages. This minimum was first recognized by Spörer and Maunder [400–404]. It is known today as the *Maunder minimum* [403]. Many believe that the Maunder minimum was associated with a *'little ice age'* on Earth [403]. The conclusion is particularly timely, since the Sun may be entering another minimum in 2013, as solar activity apparently drops to a 100 year low [405].

What causes these minimae? In gaseous models, the answers will be difficult to ascertain, as these ideas have difficulty accounting for any solar activity. As for the LMH model, it is based on the tenant that solar activity must be fundamentally related to degassing of intercalate atoms. Perhaps the Maunder minimum arises because the Sun has been thoroughly degassed, either through an unknown internal mechanism or an external force.

In this regard, it may be important to recall that comets appear to send shock waves through the solar atmosphere as they come near the Sun [373]. These shock waves could be degassing our star beyond normal, hence reducing the need for future solar activity. *Shock degassing* may seem unlikely. However, comets do have periodic motions around the Sun. One or more could cyclically return to cause such effects. In this respect, the comet ISON is arriving in just a few days [406]. It will be interesting to note the shock wave it commands as it orbits the Sun.‡

8.2 Conclusion

Throughout these pages, a trial has unfolded relative to the constitution of the Sun. Prudent consideration of the question requires the objective analysis of solar data. Observations must be gathered and rigorously considered in light of known laboratory findings. Such were the lessons imparted long ago when Gustav Kirchhoff first contemplated the nature of the Sun [26].

Kirchhoff's approach has now been repeated. A wealth of information has been categorized and meticulously evaluated. Data spanning every aspect of the solar science has been included. Not a single fact was deliberately omitted or ignored. Rather, the full complement of available evidence has been weighed and described. The Sun itself was permitted to offer full testimony. In completing this exercise, a total

*The author has previously addressed Lane's law and the increased luminosity gained by the gaseous stars as they evolve [3]. With respect to stellar evolution, the LMH model will advance that stars cool as they evolve and do not increase in luminosity. The brightest stars (Classes O and A) are actually the youngest, while the faintest are the oldest (Class M). This is completely contrary to current beliefs in astronomy. Stellar evolution will be addressed in considerable in detail in an upcoming work [398].

†The mystery of the appearance of water on a planet that was once molten has not been properly addressed by anyone to the author's knowledge.

‡Shock related degassing of the Sun should be viewed as something positive. A star unable to properly degas might well exfoliate, as discussed in [48], and become a red giant or a supernova. Therefore, shock degassing may well be necessary, even if Earthly temperatures subsequently fall for rather long periods of time.

of forty lines of evidence have been addressed in seven broad categories. Each has spoken in favor of condensed matter.

Of these, the Planckian lines of evidence, as outlined in §2, will always merit the preeminent positions, since they directly reveal true lattice structure at the atomic level. The solar spectrum, limb darkening, and the directional emissivity of many structures (sunspots, granules, faculae, magnetic bright points, spicules, the K-corona, and coronal structures) highlight that metallic and non-metallic material can be found within the Sun.

The spectroscopic lines of evidence may well be the most elegant. It is not only that they provide obvious clues for a solar surface, but that they finally expose the underlying cause of line emission within the chromosphere and corona. In this regard, molecular hydrogen and the metal hydrides strongly suggest that the chromospheric flash spectrum reflects the presence of condensation reactions in the solar atmosphere. Yet, it is triplet helium which has rendered the most definitive declaration. It appears that an activated helium cycle does indeed exist in the chromosphere, harvesting hydrogen atoms and enabling them to rejoin the solar surface. In concert, the cool-LMH-containing K-corona scavenges electrons, thus helping to preserve solar neutrality. The associated light emission from highly ionized ions speaks to the power of spectroscopic observation.

The structural lines of evidence remain the simplest to understand. The many arguments concerning solar collapse, density, dimension, shape, appearance, and extent, are simultaneously straightforward and disarming.

Perhaps the most intriguing lines of evidence are dynamic manifestations of solar activity. Surface activity, the boiling action of the Sun, and the orthogonal arrangement of its photospheric/coronal flows leave no opportunity for a gaseous Sun. The existence of a solar dynamo, with its requirement for the interplay between conductors and insulators, offers no more. Coronal rain and loops, along with spicular velocities and splashdown events, require the presence of condensed matter. Slow and fast solar winds point to an object constantly striving to expel material, emphasizing the dynamic aspects of a condensed Sun.

Few sciences are more tied to condensed matter than seismology. The Sun with its oscillations, mass displacements, shape, internal layers (convection zone, tachocline, and core), and atmospheric waves, has highlighted that it belongs in the company of solids and liquids.

Elemental lines of evidence call for a complete revision of scientific thought relative to how the Sun derives its energy. First generation stars must join the company of other untenable theories, as an unchained Sun is finally permitted to synthesize all of the elements.

The sole earthly line of evidence was climatic. In ages past, the Earth was molten. The Sun must have been much more luminous than it is today, leading to the conclusion that it was born as an O-class star. Its temporal variations across the ages, might be best understood as an ever-present need to eject elements from its interior.

Finally, a conclusion must inevitably be drawn. Can a gaseous Sun truly survive, based solely on mathematical arguments, when not a single observational line of evidence lends it support? In the end, such an arsenal of observational proofs has been supplied that there can be little doubt in the answer. Formulas can never supersede observational findings. Hence, only a single verdict can be logically rendered. The Sun must be comprised of condensed matter.

The consequences are far reaching. They call for a new beginning in astronomy. Nonetheless, there is hope that a reformulation of astrophysics can bring with it a wealth of knowledge and discovery. As scientists turn their thoughts to a condensed Sun, may they renew their fervor in the pursuit and understanding of stellar observations.

Epilogue

No more appropriate closing words can be uttered than those of Cecilia Payne, she who established that we live in a hydrogen based universe [86]: "*The future of a subject is the product of its past, and the hopes of astrophysics should be implicit in what the science has already achieved. Astrophysics is a young science, however, and is still, to some extent, in a position of choosing its route; it is very much to be desired that present effort should be so directed that the chosen path may lead in a permanently productive direction. The direction in which progress lies will depend on the material available, on the development of theory, and on the trend of thought . . . The future progress of theory is a harder subject for prediction, than the future progress of observation. But one thing is certain: observation must make the way for theory, and only if it does can the science have its greatest productivity . . . There is hope that the high promise of astrophysics may be brought to fruition.*" Cecilia Payne-Gaposchkin [407, p. 199–201].

Acknowledgment

The Swedish 1-m Solar Telescope science team is recognized for Figs. 3, 7, and 9. The SST is operated on the island of La Palma by the Institute for Solar Physics of the Royal Swedish Academy of Sciences in the Spanish Observatorio del Roque de los Muchachos of the Instituto de Astrofísica de Canarias.

NASA/SDO and the AIA science team acquired the data displayed in Fig. 11. NASA/SOHO and the EIT, CDS, and MDI science teams, were responsible for Figs. 15, 20, 22, and 26. The Big Bear Solar Observatory is recognized for Fig. 24.*

Luc Robitaille is acknowledged for the preparation of all other figures.

*Agency URLs — http://www.isf.astro.su.se; http://sdo.gsfc.nasa.gov; http://sohowww.nascom.nasa.gov; http://www.bbso.njit.edu.

Not enough can be said of Dmitri Rabounski and Larissa Borissova with respect to their lifelong love of science and their immediate interest in the problem of liquid stars [408].

Dedication

This work is dedicated to those who, through their support, sacrifice, compassion, and understanding, permitted that my life be dedicated to science — my wife Patricia Anne* and our sons: Jacob,† Christophe,‡ and Luc.§

Submitted on: October 7, 2013
Accepted in revised form on: October 13, 2013
First published online on: October 13, 2013

References

1. Secchi A. Le Soleil (Vol. I/II). Gauthier-Villars, Paris, 1875/1877. (Available online: Vol. I — http://archive.org/details/lesoleil01secc; Vol. II — http://archive.org/details/lesoleil02secc).
2. Robitaille P.M. A thermodynamic history of the solar constitution — I: The journey to a gaseous Sun. *Progr. Phys.*, 2011, v. 3, 3–25.
3. Robitaille P.M. A thermodynamic history of the solar constitution — II: The theory of a gaseous Sun and Jeans' failed liquid alternative. *Progr. Phys.*, 2011, v. 3, 41–59.
4. Robitaille P.-M. On the presence of a distinct solar surface: A reply to Hervé Faye. *Progr. Phys.*, 2011, v. 3, 75–78.
5. Abbot C.G. The Sun. D. Appleton and Company. New York, 1911.
6. Maunder E.W. Are the planets inhabited? Harper & Brothers, London, 1913.
7. Fowler A. Some problems in astronomy IV. Solar and stellar photospheres. *The Observatory*, 1913, v. 36, 182–185.
8. University of Cambridge, Institute of Astronomy, Ph.D. Program, Requirements for Admission to Postgraduate Study (accessed online on 8/29/2013: http://www.ast.cam.ac.uk/admissions/phd).
9. Eddington A.S. The internal constitution of the stars. Cambridge University Press, Cambridge, U.K., 1926.
10. Fowler R.H. On dense matter. *Mon. Not. Roy. Astron. Soc.*, 1926, v. 87, 114–122.
11. Bahcall J.N. and Pinsonneault M.H. Standard solar models, with and without helium diffusion, and the solar neutrino problem. *Rev. Mod. Phys.*, 1992, v. 64, no.4, 885–926.
12. Hassan S.S. Magnetic flux tubes and activity on the Sun. In, *Lectures on Solar Physics* (H.M. Antia, A. Bhatnagar and R. Ulmschneider, Eds.), Springer, Berlin, 2003, p. 173–201.
13. Kippenhahn R. and Weigert A. Stellar structure and evolution. Springer-Verlag, Berlin, 1990.
14. Clayton D.D. Principles of stellar evolution and nucleosynthesis. MgGraw-Hill, New York, 1968.
15. Kirchhoff G. Über den Zusammenhang zwischen Emission und Absorption von Licht und. Wärme. *Monatsberichte der Akademie der Wissenschaften zu Berlin*, sessions of Dec. 1859, 1860, 783–787.
16. Kirchhoff G. Über das Verhältnis zwischen dem Emissionsvermögen und dem Absorptionsvermogen. der Körper fur Wärme und Licht. *Poggendorfs Annalen der Physik und Chemie*, 1860, v. 109, 275–301. (English translation by F. Guthrie: Kirchhoff G. On the relation between the radiating and the absorbing powers of different bodies for light and heat. *Phil. Mag.*, 1860, ser. 4, v. 20, 1–21).
17. Wien W. Über die Energieverteilung in Emissionspektrum eines schwarzen Körpers. *Ann. Phys.*, 1896, v. 58, 662–669.
18. Stefan J. Über die Beziehung zwischen der Warmestrahlung und der Temperature. *Sitzungsberichte der mathematischnatur wissenschaftlichen Classe der kaiserlichen Akademie der Wissenschaften*, Wien 1879, v. 79, 391–428.
19. Planck M. Über das Gesetz der Energieverteilung im Normalspektrum. *Annalen der Physik*, 1901, v. 4, 553–563 (English translation by ter Haar D.: Planck M. On the theory of the energy distribution law in the normal spectrum. The old quantum theory. Pergamon Press, 1967, 82–90; also Planck's December 14, 1900 lecture *Zur Theorie des Gesetzes der Energieverteilung in Normalspectrum*, which stems from this paper, can be found in either German, or English, in: Kangro H. Classic papers in physics: Planck's original papers in quantum physics. Taylor & Francis, London, 1972, 6–14 or 38–45).
20. Planck M. The theory of heat radiation. P. Blakiston's Son & Co., Philadelphia, PA, 1914.
21. Robitaille P-M. On the validity of Kirchhoff's law of thermal emission. *IEEE Trans. Plasma Sci.*, 2003, v. 31, no. 6, 1263–1267.
22. Robitaille P.-M. A critical analysis of universality and Kirchhoff's Law: A return to Stewart's Law of Thermal Emission. *Progr. Phys.*, 2008, v. 3, 30–35.
23. Robitaille P.-M. Blackbody radiation and the carbon particle. *Progr. Phys.*, 2008, v. 3, 36–55.
24. Robitaille P.-M. Kirchhoff's law of thermal emission: 150 Years. *Progr. Phys.*, 2009, v. 4, 3–13.
25. Stewart B. An account of some experiments on radiant heat, involving an extension of Prévost's theory of exchanges. *Trans. Royal Soc. Edinburgh*, 1858, v. 22, no. 1, 1–20 (also found in Harper's Scientific Memoirs, edited by J.S. Ames: The Laws of Radiation and Absorption: Memoirs of Prévost, Stewart, Kirchhoff, and Kirchhoff and Bunsen, translated and edited by D.B. Brace, American Book Company, New York, 1901, 21–50).
26. Kirchhoff G. The physical constitution of the Sun. In *Researches on the solar spectrum and the spectra of the chemical elements*. Translated by H.E. Roscoe, Macmillan and Co., Cambridge, 1862, 23–31.
27. Jeans J.H. Problems of Cosmogony and Stellar Dynamics — Being an Essay to which the Adams Prize of the University of Cambridge for the year 1917 was Adjudged. Cambridge University Press, 1919.
28. Jeans J.H. Astronomy and Cosmogony. Cambridge University Press, 1928.
29. Robitaille P.M. The collapse of the Big Bang and the gaseous Sun. *New York Times*, March 17, 2002, p. A10 (available online: http://thermalphysics.org/pdf/times.pdf).
30. Robitaille P.M. Evidence for a liquid plasma model of the Sun. *Am. Phys. Soc. Meeting — April*, 2004, S280002.
31. Robitaille P.M. The Sun as a hot liquid plasma: additional evidence. *Am. Phys. Soc. Meeting — Ohio Spring*, 2004, S50002.
32. Robitaille P.M. The photosphere as condensed matter. *Am. Phys. Soc. Meeting — Ohio Fall*, 2004, S60005.
33. Robitaille P.M. The Sun as a hot liquid plasma: more evidence. *Am. Phys. Soc. Meeting — NE Fall*, 2004, S10004.
34. Robitaille P.M. The Sun as a high energy/high density liquid metallic hydrogen plasma. *The 33rd IEEE International Conference on Plasma Science*, June 4-8, 2006, Traverse City, Michigan, p. 461, DOI:10.1109/PLASMA.2006.1707334.

*She insisted that this work be produced and that the proofs be gathered in one treatise.

†Jacob was the first to state that someday forty proofs would be published.

‡Chrisophe provided several of these lines of evidence in a paper we jointly authored based on the behavior of the solar winds and the structure of the Sun [48]. At the time, I had failed to recognize that these constituted additional proofs for condensed matter.

§Ever creative, Luc generated many of the figures in my relavent papers and has been a careful and just critic of both style and scientific presentation.

35. Robitaille P.M. The solar photosphere: Evidence for condensed matter. *Progr. Phys.*, 2006, v. 2, 17–21 (also found in slightly modified form within *Research Disclosure*, 2006, v. 501, 31–34; title #501019).
36. Robitaille P.M. A high temperature liquid plasma model of the Sun. *Progr. Phys.*, 2007, v. 1, 70–81 (also in arXiv: astro-ph/0410075v2, Oct. 4, 2004).
37. Robitaille P.M. A radically different point of view on the CMB. In, *Questions of Modern Cosmology — Galileo's Legacy*, ed. by M. D'Onofrio and C. Burigana, Springer, New York, 2009, p. 93–108.
38. Robitaille P.M. Liquid metallic hydrogen: Building block of a liquid Sun. *Am. Phys. Soc. Meeting — Ohio Spring*, 2011, D4.00005.
39. Robitaille P.M. Liquid metallic hydrogen: A Building block for the liquid Sun. *Progr. Phys.*, 2011, v. 3, 69–74.
40. Robitaille P.M. On solar granulations, limb darkening, and sunspots: Brief insights in remembrance of Father Angelo Secchi. *Progr. Phys.*, 2011, v. 3, 79–88.
41. Robitaille P.M. On the temperature of the photosphere: Energy partition in the Sun. *Progr. Phys.*, 2011, v. 3, 89–92.
42. Robitaille P.M. Stellar opacity: The Achilles heel of the gaseous Sun. *Progr. Phys.*, 2011, v. 3, 93–99.
43. Robitaille P.M. Lessons from the Sun. *Progr. Phys.*, 2011, v. 3, 100–102.
44. Robitaille P.M. Nucleosynthesis of the elements and the LMH model of the Sun. *Am. Phys. Soc. Meeting — Four Corners Annual*, 2012, D1.00026.
45. Robitaille P.M. Magnetic fields and directional spectral emissivity in sunspots and faculae: Complimentary evidence of metallic behavior on the surface of the Sun. *Progr. Phys.*, 2013, v. 1, 19–24.
46. Robitaille P.M. On the nature of the chromosphere: Condensation and line emission. *Am. Phys. Soc. Meeting — Ohio Spring*, 2013, E2.00007.
47. Robitaille P.-M. Liquid metallic hydrogen II. A critical assessment of current and primordial helium levels in the Sun. *Progr. Phys.*, 2013, v. 2, 35–47.
48. Robitaille J.C. and Robitaille P.-M. Liquid metallic hydrogen III. Intercalation and lattice exclusion versus gravitational settling and their consequences relative to internal structure, surface activity, and solar winds in the Sun. *Progr. Phys.*, 2013, v. 2, 87–97.
49. Robitaille P.-M. Commentary relative to the distribution of gamma-ray flares on the Sun: Further evidence for a distinct solar surface. *Progr. Phys.*, 2013, v. 2, L1–L2.
50. Robitaille P.-M. Commentary relative to the seismic structure of the Sun: Internal rotation, oblateness, and solar shape. *Progr. Phys.*, 2013, v. 2, L3–L4.
51. Robitaille P.-M. Commentary on the radius of the Sun: Optical illusion or manifestation of a real surface? *Progr. Phys.*, 2013, v. 2, L5–L6.
52. Robitaille P.-M. Commentary on the LMH model of the Sun: Insight relative to coronal holes, sunspots, and solar activity. *Progr. Phys.*, 2013, v. 2, L7–L9.
53. Robitaille P.-M. Commentary on the LMH model of the Sun II. Insight relative to coronal rain and splashdown events. *Progr. Phys.*, 2013, v. 2, L10–L11.
54. Robitaille P.M. Commentary on the LMH model of the Sun III. Insight into solar lithium abundances. *Progr. Phys.*, 2013, v. 2, L12–L13.
55. Robitaille P.-M. Commentary relative to the emission spectrum of the solar atmosphere: Further evidence for a distinct solar surface. *Progr. Phys.*, 2013, v. 3, L2–L4.
56. Robitaille P.-M. The LMH model of the Sun and the solar atmosphere I. Continuous emission and condensed matter within the chromosphere. *Progr. Phys.*, 2013, v. 3, L5–L7.
57. Robitaille P.-M. The LMH model of the Sun and the solar atmosphere II. Continuous emission and condensed matter within the corona. *Progr. Phys.*, 2013, v. 3, L8–L10.
58. Robitaille P.-M. The LMH model of the Sun and the solar atmosphere III. Importance of continuous emission spectra from flares, coronal mass ejections, prominences, and other coronal structures. *Progr. Phys.*, 2013, v. 3, L11–L14.
59. Robitaille P.-M. The LMH model of the Sun and the solar atmosphere IV. On the nature of the chromosphere. *Progr. Phys.*, 2013, v. 3, L15–L21.
60. Robitaille P.-M. The LMH model of the Sun and the solar atmosphere V. On the nature of the corona. *Progr. Phys.*, 2013, v. 3, L22–L25.
61. Robitaille P-M. The LMH model of the Sun and the solar atmosphere VI. Helium in the chromosphere. *Progr. Phys.*, 2013, v. 3, L26–L29.
62. Robitaille P.M. The LMH model of the Sun and the solar atmosphere VII. Further insights into the chromosphere and corona. *Progr. Phys.*, 2013, v. 3, L30–L36.
63. Agassi J. The Kirchhoff-Planck radiation law. *Science*, 1967, v. 156, no. 3771, 30–37.
64. Robitaille P.M. Max Karl Ernst Ludwig Planck (1858-1947). *Progr. Phys.*, 2007, v. 4, 117–120.
65. Heilbron J.L. The Dilemmas of an Upright Man — Max Planck and the Fortunes of German Science. Harvard University Press, Cambridge, MA, 1996.
66. Modest M.F. Radiative heat transfer. McGraw-Hill, New York, 1993, p. 92–108.
67. Carrington R.C. Observations on the Spots of the Sun, from November, 9, 1853, to March 24, 1861, Made at Redhill. Williams and Norgate, London, 1863.
68. Kitchatinov L.L. Solar differential rotation: Origin, models, and implications for dynamo. *ASI Conference Series — 1st Asia Pacific Solar Physics Meeting*, 2011, v. 2, 71–80 (also available online: arXiv:1108.1604v2 [astro-ph.SR] 9/4/2013).
69. Milne E.A. Thermodynamics of the stars. *Handbuch der Astrophysik*, 1930, v. 3, Part 1, 65–255 (also in Menzel D.H. Selected Papers on the Transfer of Radiation: 6 papers by Arthur Schuster, K. Schwarzschild, A.S. Eddington, S. Rosseland, E.A. Milne. Dover Publications, Inc., New York, 1966, p. 77–269).
70. Robitaille P.M. The little heat engine: Heat transfer in solids, liquids, and gases. *Progr. Phys.*, 2007, v. 4, 25–33.
71. Touloukian Y.S., DeWitt D.P. Thermophysical Properties of Matter (Vols. 1-8), IFI/Plenum, New York, 1972.
72. Thirumaleshwar M. Fundamentals of Heat and Mass Transfer, Dorling Kindersley, Dehli, 2009, p. 652.
73. Incropera F.P., DeWitt D.P., Bergman T.L. and Lavine A.S. Fundamentals of Heat and Mass Transfer, 6th Edition. John Wiley & Sons, Hoboken, NJ, 2007.
74. Langley S. P. Experimental determination of wave-lengths in the invisible prismatic spectrum. *Mem. Natl. Acad. Sci.*, 1883, v. 2, 147–162; Plate 12 and 21.
75. Langley S. P. On hitherto unrecognized wavelengths. *Phil. Mag.*, 1886, v. 22, 149–173; Plate IV–VI.
76. Kelly B.T. Physics of graphite. Applied Science Publishers, London, U.K., 1981, p. 34–61.
77. Delhaès P. World of carbon — vol. 1: Graphite and precursors. Gordon and Breach Science Publishers, Amsterdam, The Netherlands, 2001.
78. Pierson H.O. Handbook of carbon, graphite, diamond and fullerenes: Properties, processing and applications. Noyes Publications, Park Ridge, N.J., 1993.
79. Dresselhaus M.S. and Dresselhaus G. Intercalation compounds of graphite. *Adv. Phys.*, 2002, v. 1, no. 1, 1–186 (reprinted from *Adv. Phys.*, 1981, v. 30(2), 139–326).
80. Pietronero L. and Tosatti E. Physics of intercalation compounds. Springer-Verlag, Berlin, 1981.

81. Zabel H. and Solin S.A. Graphite intercalation compounds I: Structure and dynamics. Springer-Verlag, Berlin, 1990.
82. Dresselhaus M.S. and Kalish R. Ion implantation in diamond, graphite and related materials. Springer-Verlag, Berlin, 1992.
83. Enoki T., Suzuki M. and Endo M. Graphite intercalation compounds and applications. Oxford University Press, Oxford, U.K., 2003.
84. Martin W.H. and Brocklehurst J.E. The thermal expansion behavior of pyrolytic graphite-bromine residue compounds. *Carbon*, 1964, v. 1, no. 2, 133–141.
85. Hastings C.S. A theory of the constitution of the Sun, founded upon spectroscopic observations, original and other. *Am. J. Science*, 1881, v. 21, no. 121, 33–44.
86. Payne C.H. The relative abundances of the elements. Stellar Atmospheres. Harvard Observatory Monograph no. 1 (Harlow Shapley, Editor), Harvard University Press, Cambridge, MA, 1925 (reprinted in part in Lang K.R. and Gingerich O. A source book in astronomy and astrophysics, 1900–1975, Harvard University Press, Cambridge, MA, 1979, p. 245–248).
87. Russell H.N. On the composition of the Sun's atmosphere. *Astrophys. J.*, 1929, v. 70, 11–82.
88. Wigner E. and Huntington H.B. On the possibility of a metallic modification of hydrogen. *J. Chem. Phys.*, 1935, v. 3, 764–70.
89. Brovman E.G., Kagan Yu.M. and Kholas A. Properties of metallic hydrogen under pressure. *Sov. Phys. JETP*, 1972, v. 35, no. 4, 783–787.
90. Chakravarty S. and Ashcroft N.W. Ground state of metallic hydrogen. *Phys. Rev. B*, 1978, v. 18, 4588–4597.
91. Mon K.K., Chester G.V. and Ashcroft N.W. Simulation studies of a model of high-density metallic hydrogen. *Phys. Rev. B*, 1980, v. 21, 2641–2646.
92. McMahon J.M., Morales M.A., Pierleoni C. and Ceperley D.M. The properties of hydrogen and helium under extreme conditions. *Rev. Mod. Phys.*, 2012, v. 84, no. 4, 1607–1653.
93. Hubbard W.B., Guillot T., Lunime J.I., Burrows A., Saumon D., Marley M.S., Freedman R.S. Liquid metallic hydrogen and the structure of brown dwarfts and giant planets. *Phys. Plasmas*, 1997, v. 4, no. 5, 2011–2015 (also arXiv:astro-ph/9703007v1).
94. Nellis W.J., Ross M. and Holmes N.C. Temperature measurements of shock-compressed hydrogen: Implications for the interior of Jupiter. *Science*, 1995, v. 269, no. 5228, 1249–1252.
95. Nellis W.J., Weir S.T. and Mitchell A.C. Metallization and electrical conductivity of hydrogen in Jupiter. *Science*, 1996, v. 273, no. 5277, 936–938.
96. Lai D. and Salpeter E.E. Hydrogen phases on the surfaces of a strongly magnetized neutron star. *Astrophys. J.*, 1997, v. 491, 270–285.
97. Ichimaru S. Statistical Plasma Physics — Volume II: Condensed Plasmas, Addison-Westly, Redwood, CA, 1991 (reprinted by Westview Press, Boulder, CO, 2004).
98. Ichimaru S. and Kitamura H. Pycnonuclear reactions in dense astrophysical and fusion plasmas. *Phys. Plasmas*, 1999, v. 6, no. 7, 2649–2671.
99. Ichimaru S. Radiative proton-capture of high-Z nuclei in the sun and in liquid-metallic hydrogen. *Phys. Let. A*, 2000, v. 266, 167–172.
100. Scharmer G. B., Gudiksen B.V., Kiselman D., Löfdahl M.G., Rouppe van der Voort L.H.M. Dark cores in sunspot penumbral filaments. *Nature*, 2002, v. 420, 151–153.
101. Very F. The absorptive power of the solar atmosphere. *Astrophys. J.*, 1902, v. 16, 73–91.
102. Schwarzschild K. Über das Gleichgewicht der Sonnenamospäre. *Nachrichten von der Königlichen Gesellschaft der Wissenschaften zu Göttigen, Göttinger Nachrichten*, 1906, v. 195, 41–53 (English translation: Concerning the equilibrium of the solar atmosphere, found in: Menzel D.H. Selected Papers on the Transfer of Radiation: 6 papers by Arthur Schuster, K. Schwarzschild, A.S. Eddington, S. Rosseland, E.A. Milne. Dover Publications, Inc., New York, 1966, p. 25–34 and Meadows A.J. Early Solar Physics. Pergamon Press, Oxford, 1970, 277–290).
103. Milne E.A. Radiative equilibrium in the outer layers of a star: The temperature distribution and the law of darkening. *Mon. Not. Roy. Astron. Soc.*, 1921, v. 81, 361–375.
104. National Solar Observatory. Advanced Technology Solar Telescope — ATST. http://atst.nso.edu/sites/atst.nso.edu/files/press/ATST_book.pdf (accessed online on 9/10/2013).
105. Galilei G. and Scheiner C. On sunspots (translated by Eileen Reeves and Albert Van Helden), The University of Chicago Press, Chicago, IL, 2010.
106. Wilson A. Observations on the solar spots. *Phil. Trans. Roy. Soc.*, 1774, v. 64, 1–30.
107. Hale G.E. On the probable existence of a magnetic field in Sun-spots. *Astrophys. J.*, 1908, v. 28, 315–343.
108. Leonard T. and Choudhary D.P. Intensity and magnetic field distribution of sunspots. *Solar Physics*, 2008, v. 252, 33–41.
109. Martinez Pillet V. and Vázquez M. The continuum intensity-magnetic field relation in sunspot umbrae. *Astron. Astrophys.*, 1993, v. 270, 494–508.
110. Thomas J.H. and Weiss N.O. Sunspots and starspots. Cambridge University Press, Cambridge, U.K., 2008.
111. Sobotka M. Fine structure in sunspots. In, *Motions in the solar atmosphere* (A. Hanslmeier and M. Messerotti, eds.), Astrophysics and Space Science Library, v./,239, Kluwer Academic Publishers, Dordrecht, 1999, p. 71–97.
112. Langley S. Sur la température des diverses régions du soleil. Les noyaux noirs des taches. *Comptes Rendus*, 1875, v. 80, 746–749.
113. Frost E.B. Observations on the thermal absorption in the solar atmosphere made at Potsdam. *Astronnomische Nachrichten*, 1892, v. 130(3105–3106), 129–146.
114. Tandberg-Hanssen E. Solar Activity. Blaisdell Publishing Co., Waltham, M.A., 1967.
115. Bhatnagar A. Instrumentation and observational techniques in solar astronomy. In, *Lectures on Solar Physics* (H.M. Antia, A. Bhatnagar and R. Ulmschneider, Eds.), Springer, Berlin, 2003, p. 27–79.
116. Moradi H. and Cally P.S. Time-distance modeling in a simulated sunspot. *Solar Physics*, 2008, v. 251, 309–327.
117. Ilonidis S. and Zhao J. Determining absorption, emissivity reduction, and local suppression coeffcients inside sunspots. *Solar Physics*, 2011, v. 268, 377–388.
118. Bray R.J., Loughhead R.E., Durrant C.J. The solar granulation. Cambridge University Press, Cambridge, 1984.
119. Muller R. The solar granulation. In, *Motions in the solar atmosphere* (A. Hanslmeier and M. Messerotti, eds.), Astrophysics and Space Science Library, Kluwer Academic Publishers Dordrecht, 1999, v. 239, 35–70
120. Hirzberger J. Granulation and waves. *Astron. Nachr.*, 2003, v. 324, no. 4, 344–348.
121. Roudier Th. and Muller R. Structure of the solar granulation. *Solar Physics*, 1986, v. 107, 11–26.
122. Hirzberger J. On the brightness and velocity structure of solar granulation. *Astron. Astrophys.*, 2002, v. 392, 1105–1118.
123. Weaire D. and Rivier N. Soap, cells and statistics random patterns in two dimensions. *Contemp. Phys.*, 1984, v. 25, 59–99.
124. Rivier N. Structure of random cellular networks.*Science on Form: Proc. First Int. Symp. Sci. Form*, KTK Scientific Publishers, Tokyo, 1986, 451–458.

125. Chiu S.N. Aboav-Weaire's and Lewis' Law A review. *Mater. Charact.*, 1995, v. 34, 149–165.

126. Noever D.A. Solar granulation and statistical crystallography: a modeling approach using size-shape relations. *Astron. Astrophys.*, 1994, v. 282, 252–261.

127. Chacornac, On the physical constitution of the Sun. (25/12/1864). *The Reader*, 1865, v. 5, 16–17.

128. Rast M.P. On the nature of "exploding" granules and granule fragmentation. *Astrophys. J.*, 1995, v. 443, 863–868.

129. Hale G.E. The study of stellar evolution: An account of some recent methods of astrophysical research, The decennial publications of the University of Chicago — Second Series, Vol. X. University of Chicago Press, Chicago, 1908.

130. de la Rue W., Stewart B. and Loewy B. Researches on solar physics — Series II: On the behaviour of sun-spots with regard to increase and diminution (abstract). *Proc. Roy. Soc. London*, 1865, v. 14, 59–63.

131. Wang H., Deng N. and Liu C. Rapid transition of uncombed penumbrae to faculae during large flares. *Astrophys. J.*, 2012, v. 748, no. 2, 76(9 pp).

132. Chapman G.A. Facular line profiles and facular models. *Astrophys. J. Supp. Ser.*, 1977, v. 33, 35–54.

133. Tarbell T.D. and Title A.M. Measurements of magnetic fluxes and field strengths in the photospheric network. *Solar Physics*, 1977, v. 52, 13–25.

134. Ortiz A., Solanki S.K., Domingo V., Fligge M. and Sanahuja B. On the intensity contrast of solar photospheric faculae and network elements. *Astron. &Astrophys.*, 2002, v. 388, 1036–1047.

135. Libbrecht K.G. and Kuhn J.R. On the facular contrast near the solar limb. *Astrophys. J.*, 1985, v. 299, 1047–1050.

136. Spruit H.C. Pressure equilibrium and energy balance of small photospheric fluxtubes. *Solar Physics*, 1976, v. 50, 269–295.

137. Walton S.R. Flux tube models of solar plages. *Astrophys. J.*, 1987, v. 312, 909–929.

138. Bonet J.A., Cabello I. and Almeida S. Center-to-limb variation of the area covered by magnetic bright points in the quiet Sun. *Astron. & Astrophys.*, 2012, v. 539, A6.

139. Sanchez Almeida J., Bonet J.A., Viticchie B. and Del Moro D. Magnetic bright points in the quiet Sun. *Astrophys. J. Letters*, 2010, v. 715, no. 1, L26–L29.

140. Evershed J. Wave-length determinations and general results obtained from a detailed examination of spectra photographed at the solar eclipse of January 22, 1898. *Phil. Trans. Roy. Soc. London*, 1901, v. 197, 381–413.

141. Evershed J. Preliminary report of the expedition to the south limit of totality to obtain photographs of the flash spectrum in high solar latitudes. *Proc. Roy. Soc. London*, 1900, v. 67, 370–385.

142. Menzel D.H. and Cillié G.G. Hydrogen emission in the chromosphere. *Astrophys. J.*, 1937, v. 5, 88–106.

143. Athay R.G., Billings D.E., Evans J.W. and Roberts W.O. Emission in hydrogen Balmer lines and continuum in flash spectrum of 1952 total solar eclipse at Karthoum, Sudan. *Astrophys. J.*, 1954, v. 120, 94–111.

144. Athay R.G., Menzel D.H., Pecker J.C. and Thomas R.N. The thermo dynamic state of the outer solar atmosphere V. A model of the chromosphere from the continuous emission. *Astrophys. J. Suppl. Ser.*, 1955, v. 1, 505–519.

145. Hiei E. Continuous spectrum in the chromosphere. *Publ. Astron. Soc. Japan*, 1963, v. 15, 277–300.

146. Weart S.R. and Faller J.E. Photoelectric eclipse observation of the continuum at the extreme solar limb. *Astrophys. J.*, 1969, v. 157, 887–901.

147. Gingerich O. and de Jager C. The Bilderberg model of the photosphere and low chromosphere. *Solar Phys.*, 1968, v. 3, 5–25.

148. Ulmschneider P. The physics of the chromospheres and coronae. In, *Lectures on Solar Physics* (H.M. Antia, A. Bhatnagar and R. Ulmschneider, Eds.), Springer, Berlin, 2003, p. 232–280.

149. NASA. Air properties definitions. (Accessed online on 2/13/2013) www.grc.nasa.gov/WWW/k-12/airplane/airprop.html www.grc.nasa.gov/WWW/k-12/airplane/airprop.html (accessed online on 9/10/2013).

150. Bray R.J. and Loughhead R.E. The Solar Chromosphere, Chapman and Hall, London, U.K., 1974.

151. Dick S. Sky and Ocean Joined: The U.S. Naval Observatory 1830–2000. Cambridge University Press, Cambridge, 2003, p. 196–205.

152. Evershed J. Wave-length determinations and general results obtained from a detailed examination of spectra photographed at the solar eclipse of January 22, 1898. *Phil. Trans. Roy. Soc. London*, 1901, v. 197, 381–413.

153. Grotian W. Über die intensitätsverteilung des kontinuierlichen spektrums der inneren korona. *Zeitschrift fur Astrophysik*, 1931, v. 3, 199–226.

154. Lyot B. La couronne solaire étudiée en dehors des éclipses. *Comptes Rendus*, 1930, v. 191, 834–837.

155. Lyot B. A study of the solar corona and prominences without eclipses — George Darwin Lecture. *Mon. Not. Roy. Astron. Soc.*, 1939, 580-=594 (22 pages with plates).

156. Allen C.W. The spectrum of the corona at the eclipse of 1940 October 1. *Mon. Not. Roy. Astron. Soc.*, 1946, v. 106, 137–150.

157. Dwivedi B.N. The solar corona. In, *Lectures on Solar Physics* (H.M. Antia, A. Bhatnagar and R. Ulmschneider, Eds.), Springer, Berlin, 2003, p. 281–298.

158. van de Hulst H.C. The electron density of the corona. *Bull. Astronom. Inst. Netherlands*, 1950, v. 11, no. 410., 135–149.

159. Carrington R.C. Description of a singular appearance seen in the Sun on September 1, 1859. Mon. Not. Roy. Astron. Soc., 1859, v. 20, 13–15.

160. Machado M.E., Emslie A.G., Avrett E.H. Radiative backwarming in white-light flares. *Solar Phys.*, 1989, v. 124, 303–317.

161. Hiei E. A continuous spectrum of a white-light flare. *Solar Phys.*, 1982, v. 80, 113–127.

162. Wang H. Study of white-light flares observed by Hinode. *Res. Astron. Astrophys.*, 2009, v. 9, no. 2, 127–132.

163. Tandberg-Hanssen E. Solar prominences — An intriguing phenomenon. *Solar Phys.*, 2011, v. 269, 237–251.

164. Tandberg-Hanssen E. A spectroscopic study of quiescent prominences. *Astrophysica Novegica*, 1964, v. 9, no. 3, 13–32.

165. Yakovkin N.A. and Zeldina M.Yu. The prominence radiation theory. *Solar Phys.*, 1975, v. 45, 319–338.

166. Gopalswamy N. and Hanaoka Y. Coronal dimming associated with a giant prominence eruption. *Astrophys. J. Lett.*, 1998, v. 498, L179–L182.

167. Gopalswamy N., Shimojo M., Lu W., Yashiro S., Shibasaki K. and Howard R.A. Prominence eruptions and coronal mass ejections: A statistical study using microwave observations. *Astrophys. J.*, 2003, v. 586, 562–578.

168. Sheeley N.R., Walters J.H., Wang Y.M. and Howard R.A. Continuous tracking of coronal outflows: Two kinds of coronal mass ejections. *J. Geophys. Res.*, 1999, v. 104, no. A11, 24739–24767.

169. St. Cyr O.C., Howard R.A., Sheeley N.R., Plunkett S.P., Michels D.J., Paswaters S.E., Koomen M.J., Simnett G.M., Thompson B.J., Gurman J.B., Schwenn R., Webb D.F., Hildner E. and Lamy P.L. Properties of coronal mass ejections: SOHO LASCO observations from January 1996 to June 1998. *J. Geophys. Res.*, 2000, v. 105, no. A8, 18169–18185.

170. Hudson H.S. and Cliver E.W. Observing coronal mass ejections without coronagraphs. *J. Geophys. Res.*, 2001, v. 106, no. A11, 25199–25213.

171. Yashiro S., Gopalswamy N. Michaelek G, St. Cyr O.C., Plunkett S.P., Rich N.B. and Howard R.A. A catalog of white-light coronal mass ejections observed by the SOHO spacecraft. *J. Geophys. Res.*, 2004, v. 109, A07105(11 pages).

172. Wang Y.M. Nonradial coronal streamers. *Astrophys. J.*, 1996, v. 456, L119–L121.

173. Wang Y.M., Sheeley N.R., Walters J.H., Brueckner G.E., Howard R.A., Michels D.J., Lamy P.L., Schwenn R. and Simnett G.M. Origin of streamer material in the outer corona. *Astrophys. J.*, 1998, v. 498, L165–L168.

174. Vourlidas A. A review of white-light streamers at the end of cycle 23. *Proc. IAU: Solar Activity and its Magnetic Origin*, 2006, v. 233, 197–204.

175. Del Zanna G., Bromage B.J.I. and Mason H.E. Spectroscopic characteristics of polar plumes. *Astron. Astrophys.*, 2003, v. 398, 743–763.

176. Mouschovias T.Ch. and Poland A.I. Expansion and broadening of coronal loop transients: A theoretical explanation. *Astrophys. J.*, 1978, v. 220, 675–682.

177. Kjeldseth-Moe O. and Brekke P. Time variability of active region loops observed with the coronal diagnostic spectrometer (CDS) on SOHO. *Solar Phys.*, 1998, v. 182, 73–95.

178. Landi E., Miralles M.P., Curdt W. and Hara H. Physical properties of cooling plasma in quiescent active region loops. *Astrophys. J.*, 2009, v. 695, 221-237.

179. Ambstha A. The active and explosive Sun. In, *Lectures on Solar Physics* (H.M. Antia, A. Bhatnagar and R. Ulmschneider, Eds.), Springer, Berlin, 2003, p. 127–172.

180. Kahler S.W. Solar flares and coronal mass ejections. *Ann. Rev. Astron. Astrophys.*, 1992, v. 30, 113–141.

181. Priest E.R. Solar flare theory and the status of flare understanding. In *High Energy Solar Physics: Anticipating HESSI. ASP Conf. Ser.*, 2000, v. 206, 13–26.

182. Priest E.R. and Forbes T.G. The magnetic nature of solar flares. *Astron. Astrophys. Rev.*, 2002, v. 10, 313–377.

183. Hudson H.S. Global properties of solar flares. *Space Sci. Rev.*, 2011, v. 158, 5–41.

184. Holman G.D. The mysterious origin of solar flares. *Sci. Am.*, 2006, v. 294, no. 4, 38–45.

185. Forbes T.G. Magnetic reconnection in solar flares. *Geophys. Astrophys. Fluid Dynam.*, 1991, v. 62, 15–36.

186. Ramaty R., Mandzhavidze N., Kozlovsky B. and Murphy R.J. Solar atmospheric abundances and energy content in flare-accelerated ions from gamma-ray spectroscopy. *Astrophys. J.*, 1995, v. 455, L193–L196.

187. Watanabe K., Krucker S., Hudson H., Shimizu T., Masuda S., and Ichimoto K. G-band and hard X-ray emissions of the 2006 December 14 flares observed by HINODE/SOT and RHESSI. *Astrophys. J.*, 2010, v. 715, 651–655.

188. Anderson J.L. Hinode discovers origin of white-light flares. NASA–Marshall Space Flight Center. Accessed online on 4/17/2013: http://www.nasa.gov/centers/marshall/news/news/releases/2010/10-052.html

189. Zöllner F. On the temperature and physical constitution of the Sun. *Phil. Mag. 4th Series*, 1870, v. 40, 313–327 (essentially reprinted in: Zöllner F. On the Sun's temperature and physical constitution. *Nature*, 1870, v. 2(52), 522–526).

190. Kirchhoff G. Researches on the Solar Spectrum, and the Spectra of the Chemical Elements (Translated by H.E. Roscoe), Macmillan and Co., Cambridge, U.K., 1862.

191. Kirchhoff G. and Bunsen R. Chemical analysis by spectral observations. (Reprinted from *Poggendorf's Annalen der Physik*, 1860, v. 110, In, *The laws of Radiation and Absorption — Memoirs by Prévost, Stewart, Kirchhoff, and Kirchhoff and Bunsen.* (D.B. Brace, Ed.), American Book Company, N.Y., 1901, p. 99–126).

192. Phillips K.J.H., Feldman U. and Landi E. Ultraviolet and X-Ray Spectroscopy of the Solar Atmosphere: Cambridge Astrophysics Series — Vol. 44, Cambridge University Press, Cambridge, U.K., 2008.

193. Zirin H. The mystery of the chromosphere. *Solar Phys.*, 1996, v. 169, 313–326.

194. Rieger E. Solar flares: High-energy radiation and particles. *Solar Phys.*, 1989, v. 121, 323–345.

195. Ramaty R. and Simnett G.M. Accelerated particles in solar flares. In, *The Sun in Time* (C.P. Sonett, M.S. Giampapa and M.S. Matthews, Eds.), The University of Arizona Press, Tuscon, AZ, 1991, p. 232–259.

196. Grevesse N. Solar abundances of lithium, beryllium, and boron. *Solar Phys.*, 1968, v. 5, 159–180.

197. Wiens R.C., Bochsler P., Burnett D.S. and Wimmer-Schweingruber R.F. Solar and solar-wind isotopic compositions. *Earth Plan. Sci. Let.*, 2004, v. 222, 697–712.

198. Uitenbroek H. The effect of photospheric granulation on the determination of the lithium abundance in solar-type stars. *Astrophys. J.*, 1998, v. 498, 427–440.

199. Schatzman E. Turbulent transport and lithium destruction in main sequence stars. *Astron. Astrophys.*, 1977, v. 56, 211–218.

200. Pinsonneault M.H. Rotational mixing and lithium depletion. In, *Light Elements in the Universe: Proc. IAU Symposium*, 2009, v. 268, 375-380.

201. Pinsonneault M.H. A fossil record for exoplanets. *Nature*, 2009, v. 462, no. 7270, 168–169.

202. Israelian G., Delgado Mena E., Santos N.C., Sousa S.G., Mayor M., Udry S., Dominguez Cerdena C., Rebolo R. and Randich S. Enhanced lithium depletion in Sun-like stars with orbiting planets. *Nature*, 2009, v. 462, no. 7270, 189–191.

203. Baumann P., Ramirez I., Melendez J., Aslund M. and Lind K. Lithium depletion in solar-like stars: no planet connection. *Astron. Astrophys.*, 2010, v. 519, A87(11 pages).

204. Zurek E., Hoffmann R., Ashcroft N.W., Oganov A.R., Lyakhov A.O. A little bit of lithium does a lot for hydrogen. *Proc. Nat. Acad. Sci. USA* USA, 2009, v. 106, no. 42, 17640—17643.

205. Menzel D.H. A Study of the Solar Chromosphere. *Publications of the Lick Observatory*, University of California Press, Berkeley, CA, v. 17, 1931.

206. Athay R.G. The Solar Chromosphere and Corona: Quiet Sun. D. Reidel Publishing Co., Boston, M.A., 1976.

207. Thomas R.N. and Athay R.G. Physics of the Solar Chromosphere. Interscience Publishers, New York, N.Y., 1961.

208. Heinzel P. Understanding the solar chromosphere. In, *"Exploring the Solar System and the Universe"*, (V. Mioc, C. Dumitrache, N.A. Popescu, Eds.), American Institute of Physics, 2008, 238–244.

209. Woltjer L. A photometric investigation of the spicules and the structure of the chromosphere. *Bull. Astron. Inst. Netherlands*, 1954, v. 12, no. 454, 165–176.

210. Rush J.H. and Roberts W.O. Recent studies of chromospheric spicules. *Australian J. Phys.*, 1954, v. 7, 230–243.

211. Beckers J.M. Solar spicules. *Ann. Rev. Astron. Astrophys.*, 1972, v. 10, 73–100.

212. Lorrain P. and Koutchmy S. Two dynamical models for solar spicules. *Solar Phys.*, 1996, v. 165, 115–137.

213. Sterling A. Solar spicules: A review of recent models and targets for future observations. *Solar Phys.*, 2000, v. 196, 79–111.

214. Zaqarashvili T.V. and Erdélyi R. Oscillations and waves in solar spicules. *Space Sci. Rev.*, 2009, v. 149, 355–388.

215. Pasachoff J.M., Jacobson W.A. and Sterling A.C. Limb spicules from ground and from space. *Solar Phys.*, 2009, v. 260, 59–82.

216. Konig L., Rabin I, Schultze W. and Ertl G. Chemiluminescence in the agglomeration of metal clusters. *Science*, 1996, v. 274, no. 5291, 1353–1355.

217. Jordan C., Bueckner G.E., Bartoe J.D.F., Sandlin G.D. and Vanhoosier M.E. Emission lines of H2 in the extreme-ultraviolet solar spectrum. *Astrophys. J.*, 1978, v. 226, 687–697.

218. Bartoe J.D.F., Brueckner G.E., Nicolas K.R., Sandlin G.D., Vanhoosier M.E. and Jordan C. H2 emission in the solar atmosphere. *Mon. Not. Roy. Astron. Soc.*, 1979, v. 187, 463–471.

219. Sandlin G.D., Bartoe J.D.F., Brueckner G.E., Tousey R. and Vanhoosier M.E. The high-resolution solar spectrum, 1175-1770Å. *Astrophys. J. Suppl. Ser.*, 1986, v. 61, 801–898.

220. Innes D.E. SUMER-Hinode observations of microflares: excitation of molecular hydrogen. *Astron. Astrophys.*, 2008, v. 481, no. 1, L41–L44.

221. Przybilla N. and Butler K. The solar hydrogen spectrum in non-local thermodynamic equilibrium. *Astrophys. J.*, 2004, v. 610, L61–L64.

222. Kurucz R. ATLAS9 Stellar Atmosphere Programs and 2 km/s grid — CD-ROM No. 13, *Smithsonian Astrophysical Observatory*, 1993.

223. Stehlé C. and Hutcheon R. Extensive tabulations of Stark broadened hydrogen line profiles. *Astro. & Astrophys. Suppl. Ser.*, 1999, v. 140, 93–97.

224. Konjević N., Lesage A., Fuhr J.R. and Wiese W.L. Experimental Stark widths and shifts for spectral lines of neutral and ionized atoms (A critical review of selected data for the period 1989 through 2000). *J. Phys. Chem. Ref. Data*, 2002, v. 31, no. 3, 819–927.

225. Stehlé C. Stark broadening of hydrogen Lyman and Balmer lines in the conditions of stellar envelopes. *Astron. Astrophys. Suppl. Series*, 1994, v. 104, 509–527.

226. Stehlé C. and Jacquemot S. Line shapes in hydrogen opacities. *Astron. Astrophys.*, 1993, v. 271, 348–359.

227. Acon B.W., Stehlé C., Zhang H. and Montaser A. Stark-broadened hydrogen line profiles predicted by the model microfield method for calculating electron densities. *Spectrochimica Acta B: Atomic Spectros.*, 2001, v. 56, 527–539.

228. Mijatović Z., Konjević N., Ivković M. and Kobilarov R. Influence of ion dynamics on the width and shift of isolated He I lines in plasmas — II. *Phys. Rev. E*, 1995, v. 51, no. 5, 4891–4896.

229. Cairns I.H., Lobzin V.V., Warmuth A., Li B., Robinson P.A., and Mann G. Direct radio probing and interpretation of the Sun's plasma density profile. *Astrophys. J. Letters*, 2009, v. 706, L265–L269.

230. Wöhl H. On molecules in sunspots. *Solar Phys.*, 1971, v. 16, 362–372.

231. Sinha K. Molecules in the Sun. *Proc. Astron. Soc. Australia*, 1991, v. 9, 32–36.

232. Olmsted C.M. Sun-spot bands which appear in the spectrum of a calcium arc burning in the presence of hydrogen. *Astrophys. J.*, 1908, v. 27, 66–69.

233. Ionization Potentials. — Accessed on 10/5/2013. http://www.physics.ohio-state.edu/~lvw/handyinfo/ips.html.

234. Athay R.G. Line broadening in chromospheric spicules. *Astrophys. J.*, 1961, v. 134, 756–765.

235. Zirker J.B. The solar H and K lines of ionized calcium. *Solar Phys.*, 1968, v. 3, 164–180.

236. Gulyaev R.A. and Livshits M.A. Width of Ca^+H line in spicules. *Soviet Astron.*, 1966, v. 9, no. 4, 661–663.

237. Janssen J. Indications de quelques-uns des résultats obténus à Guntoor, pendant l' éclipse du mois d'août dernier. *Comptes Rendus*, 1868, v. 67, 838–39.

238. Lockyer J.N. Notice of an observation of the spectrum of a solar prominence. *Proc. Roy. Soc. London*, 1868, v. 17, 91–92.

239. Kragh H. The solar element: A reconsideration of helium's early history. *Ann. Science*, 2009, v. 66, no. 2, 157–182.

240. Taylor R.J. The helium problem. *Quart. J. Roy. Astron. Soc.*, 1967, v. 8, 313–333.

241. Grevesse N. and Sauval A.J. Standard solar composition. *Space Science Reviews*, 1998, v. 85, 161–174.

242. Asplund M., Grevesse N., Sauval A.J. and Scott P. The chemical composition of the Sun. *Ann. Rev. Astron. Astrophys.*, 2009, v. 47, 481–522.

243. Auchère F., Boulade S., Koutchmy S, Smartt R.N., Delaboudinière J.P., Georgakilas A., Gurman J.B. and Artzner G.E. The prolate solar chromosphere. *Astron. & Astrophys.*, 1998, v. 336, L57–L60.

244. Marchenko G.P., Akimov L.A., Belkina I.L. and Velikodsky Y.I. Solar chromosphere in the D_3 helium line from spectra of the eclipse of March 29, 2006. *Kinematics Phys. Celestial Bodies*, 2011, v. 27, no. 4, 183–190.

245. Zirin H. The Solar Atmosphere. Cambridge University Press, Cambridge, U.K., 1998.

246. Centeno R., Bueno J.T., Uitenbroek H. and Collados M. The influence of coronal EUV irradiance on the emission in the HeI 10830Å and D_3 multiplets. *Astrophys. J.*, 2008, v. 677, 742–750.

247. Grandinetti F. Helium chemistry: A survey of the role of the ionic species. *Inter. J. Mass Spectrom.*, 2004, v. 237, 243–267.

248. Hogness T.R. and Lunn E.G. The ionization of hydrogen by electron impact as interpreted by positive ray analysis. *Phys. Rev.*, 1925, v. 26, 44–55.

249. Tolliver D.E., Kyrala G.A and Wing W. H. Observation of the infrared spectrum of helium-hydride molecular ion $^4HeH^+$. *Phys. Rev. Let.*, 1979, v. 43, no. 23, 1719–1722.

250. Crofton M.W., Altman R.S., Haese N.N. and Oka T. Infrared spectra of $^4HeH^+$, $^4HeD^+$, $^3HeH^+$, and $^3HeD^+$. *J. Chem. Phys.*, 1989, v. 91, 5882-5886.

251. Roberge W. and Dalgarno A. The formation and destruction of HeH^+ in astrophysical plasmas. *Astrophys. J.*, 1982, v. 255, 489–496.

252. Engel E.A., Doss N., Harris G.J. and Tennyson J. Calculated spectra for HeH^+ and its effect on the opacity of cool metal-poor stars. *Mon. Not. Roy. Astron. Soc.*, 2005, v. 357, 471–477.

253. Galli D. and Palla F. The chemistry of the early universe. *Astron. Astrophys.*, 1998, v. 335, 403–420.

254. Ketterle W., Figger H. and Walther H. Emission spectra of bound helium hydride. *Phys. Rev. Lett.*, 1985, v. 55, no. 27, 2941–2944.

255. www.nobelprize.org/nobel_prizes/physics/laureates/2001/ketterle.html

256. Ketterle W., Figger H. and Walther H. Emission spectra of bound helium hydride. *Phys. Rev. Lett*, 1985, v. 55, 2941–2944.

257. Ketterle W., Dodhy A. and Walther H. Bound-free emission of the helium hydride molecule. *Chem. Phys. Let.*, 1986, v. 129, no. 1, 76–78.

258. Wollaston W.H. A method of examining refractive and dispersive powers, by prismatic reflection. *Phil. Trans. Roy. Soc. London*, 1802, v. 92, 365–380.

259. Fraunhofer J. Bestimmung des Brechungs-und des Farbenzerstreuungs-Vermögens verschiedener Glasarten, in Bezug auf die Vervollkommnung achromatischer Fernröhre. *Denkschriften der Königlichen Akademie der Wissenschaften zu München*, 1814/1815, v. 5, 193–226.

260. Unsöld A. Über die Struktur der Fraunhofersehen Linien und die quantitative Spektralanalyse der Sonnenatmosphäre. Zeitschrift für Physik, 1928, v. 46, no. 11–12, 765–781.

261. Kuli-Zade D.M. Profiles of the stronger Fraunhofer lines in the solar spectrum. I. Hydrogen lines. *Sov. Astron.*, 1965, v. 8, no. 5, 736–743.

262. Bondal K.R. and Gaur V.P. On some visible and infrared atomic hydrogen lines in three photospheric models. *Bull. Astron. Soc. India*, 1986, v. 14, 73–78.

263. de Jager C., Migeotte M. and Neven L. The profile of the Brackett alpha line in the solar spectrum. *Ann. Astrophys.*, 1956, v. 19, 9–18.

264. Cowley C.R. and Castelli F. Some aspects of the calculation of Balmer lines in the Sun and stars. *Astron. & Astrophys.*, 2002, v. 387, 595–604.

265. Hufbauer K. Exploring the Sun: Solar Science since Galileo. The Johns Hopkins University Press, Baltimore, 1991, p. 112–114.

266. Claridge G.C. Coronium. *J. Roy. Astron. Soc. Canada*, 1937, v. 31, no. 8, 337–346.

267. Unsigned. Origin of the coronium lines. *Nature*, 1942, v. 150, no. 3817, 756–759.

268. Milne A.E. Presidential Address — Award of the Gold Medal to Professor Bengt Edlén. *Mon. Not. Roy. Astron. Soc.*, 1945, v. 105, 138–145.

269. Wood B.E., Karovska M., Cook J.W., Brueckner G.E., Howard R.A., Korendyke C.M. and Socker D.G. Search for brightness variations in FeXIV coronagraph observations of the quiescent solar corona. *Astrophys. J.*, 1998, v. 505, 432–442.

270. Habbal S.R., Druckmüller M., Morgan H., Daw A., Johnson J., Ding A., Arndt M., Esser R., Rušin V. and Scholl I. Mapping the distribution of electron temperature and Fe charge states in the corona with total solar eclipse observations. *Astrophys. J.*, 2010, v. 708, 1650–1662.

271. Habbal S.R., Druckmüller M., Morgan H., Scholl I., Rušin V., Daw A., Johnson J. and Arndt M. Total solar eclipse observations of hot prominence shrouds. *Astrophys. J.*, 2010, v. 719, 1362–1369.

272. Habbal S.R., Morgan H. and Druckmüller M. A new view of coronal structures: Implications for the source and acceleration of the solar wind — First Asia-Pacific Solar Physics Meeting. *ASI Conf. Ser.*, 2011, v. 2, 259–269.

273. Priest E.R. Solar flare theory and the status of flare understanding. *High Energy Solar Physics: Anticipating HESSI (R. Ramaty and N. Mandzhavidze, Eds.), ASP Conf. Ser.*, 2000, v. 206, 13–26.

274. Rakov V.A. and Uman M.A. Lightning: Physics and Effects. Cambridge University Press, Cambridge, U.K., 2003.

275. Uman M.A. Lightning. Dover Publicatons. New York, N.Y., 1984.

276. Uman M.A. The Lightning Discharge (International Geophysics Series — Vol. 39), Academic Press, Inc., New York, N.Y., 1987.

277. Bhatnagar A. and Livingston W. Fundamentals of Solar Astronomy (World Scientific Series in Astronomy and Astrophysics — Vol. 6), World Scientific, New Jersey, 2005.

278. Jeans J.H. The Universe Around Us. 1st Edition, Cambridge University Press, 1933.

279. NASA. Factsheets. (Accessed online on 9/14/13)
http://nssdc.gsfc.nasa.gov/planetary/factsheet/earthfact.html
http://nssdc.gsfc.nasa.gov/planetary/factsheet/jupiterfact.html
http://nssdc.gsfc.nasa.gov/planetary/factsheet/saturnfact.html
http://nssdc.gsfc.nasa.gov/planetary/factsheet/neptunefact.html
http://nssdc.gsfc.nasa.gov/planetary/factsheet/uranusfact.html

280. Faye H. Sur la constitution physique du Soleil. Les Mondes, 1865, v. 7, 293–306 (translated into English by Patrice Robitaille: On the physical constitution of the Sun — Part I. *Progr. Phys.*, 2011, v. 3, 35–40.

281. Emilio M., Kuhn J.R., Bush R.I, and Scholl I.F. Measuring the solar radius from space during the 2003 and 2006 Mercury transits. *Astrophys. J.*, 2012, v. 750, 135(8 pages).

282. Chapman G.A., Dobias J.J., and Walton S.R. On the variability of the apparent solar radius. *Astrophys. J.*, 2008, v. 681, no. 2, 1698–1702.

283. Rozelot J.P. and Damiani C. Rights and wrongs of the temporal solar radius variability. *Eur. Physical J. H*, 2012, v. 37, no. 5, 709–743.

284. Chandrasekhar S. Ellipsoidal Figures of Equilibrium. Yale Univerity Press, New Haven, 1969.

285. Domiciano de Souza A., Kervella P., Jankov S., Abe L., Vakili F., di Folco E. and Paresce F. The spinning-top Be star Achernar from VLTI-VINCI. *Astron. & Astrophys.*, 2003, v. 407, L47–L50.

286. Carciofi A.C., Domiciano de Souza A., Magalhães A.M., Bjorkman J.E. and Vakili F. On the Determination of the Rotational Oblateness of Achernar. *Astrophys. J.*, v. 676, no. 1, L41–L44.

287. Godier S and Rozelot J.P. The solar oblateness and its relationship with the structure of the tacholine and the Sun's subsurface. *Astron. & Astrophys.*, 2000, v. 355, 365–374.

288. Gough D. How oblate is the Sun? *Science*, 2012, v. 337, 1611–1612.

289. Kuhn J.R., Bush R., Emilio M. and Scholi I.F. The precise solar shape and its variability. *Science*, 2012, v. 337, 1638–1640.

290. Rozelot J.P., Damiani C. and Lefebvre S. Variability of the solar shape (before space dedicated missions). *J. Atmospher. Solar-Terrestrial Phys.*, 2009, v. 71, 1683–1694.

291. Roberts A.M. Solar faculae stand exposed. *Sky & Telescope*, 2003, v. 106, no. 4, 26.

292. Scharmer G.B., Henriques V.M.J., Kiselman D. and de la Cruz Rodríguez. Detection of convective downflows in a sunspot umbra. *Science*, 2011, v. 333, no. 6040, 316–319.

293. AAAS. AAAS News Release — "SCIENCE: Pinpointing the Nature of Filaments in Sunspots." www.aaas.org, 7 Sept 2011

294. Thomas J.H. Solar physics: The Sun under a microscope. *Nature*, 2002, v. 420, 134–135.

295. Cranmer S.R. Coronal holes. In, *Encyclopedia of Astronomy and Astrophysics*, (Paul Murdin, Ed.), Institute of Physics Publishing, Bristol, 2001, v. 1, p. 496–501.

296. Cranmer S.R. Coronal holes. *Living Rev. Solar Phys.*, 2009, v. 6, 3–66.

297. Chitre S.M. Overview of solar physics. In, *Lectures on Solar Physics* (H.M. Antia, A. Bhatnagar and R. Ulmschneider, Eds.), Springer, Berlin, 2003, p. 1–26.

298. Lewis D.J., Simnett G.M., Brueckner G.E., Howard R.A., Lamy P.L. and Schwenn R. LASCO observations of the coronal rotation. *Solar Phys.*, 1999, v. 184, no. 2, 297–315.

299. Shevick E. Science Action Labs: Astronomy (Illustrated by Rojas M.G.), Teaching & Learning Company, Dayton, OH, 2002.

300. Moore P. and Watson J. Observing the Solar System. In *Astronomy with a Budget Telescope, Patrick Moore's Practical Astronomy Series*, 2012, p. 31-64.

301. Jenkins J.L. The Sun, Yesterday and Today in *The Sun and How to Observe it: Astronomers' Observing Guides*, Springer, New York, 2009, p. 1–15.

302. University Corporation for Atmospheric Research. A closer look. Approved by Peter Fox Last revised: Mon Apr 10 15:08:11 MDT 2000. http://www.ucar.edu/communications/lasers/sun/closer.html (accessed on 9/10/2013)

303. NASA, Release No. 67-124, Mariner E/Venus 67, 1967 p. 20. http://ntrs.nasa.gov/archive/nasa/casi.ntrs.nasa.gov/19670017987_1967017987.pdf (accessed on 9/10/2013)

304. Saarman E. Sun seeker, Stanford Report, May 10, 2006. http://news.stanford.edu/news/2006/may10/hoeksema-051006.html (accessed on 9/10/2013)

305. NASA, Astronomy Picture of the Day, January 10, 2000. http://apod.nasa.gov/apod/ap000110.html (accessed on 9/16/2013)

306. L.A. Times. New images show Sun is covered by wide mountains of hot gases. December 16, 1996. http://articles.latimes.com/1996-12-19/local/me-10771_1_hot-gases (accessed on 9/10/2013)

307. Lang K. SOHO reveals the secrets of the Sun, *Scientific Am.*, 1997, v. 276(3), p. 40(8 pages).

308. Ludwig G.H. Particles and fields in space research. *Geophys. Astron. Space Exploration NASA SP-13*, 1962, p.21–29.

309. Baker D.N. Critical issues in space plasma physics. *Phys. Plasmas* 1999, 6(5), 1700–1708.

310. Jordan S.D. The solar optical telescope (SOT), *Space Science Rev.*, 1981, v. 29(4), 333-340.

311. Marhavilas P.K. The space as a natural laboratory of electrotechnics. *J. Eng. Science Tech. Rev.*, 2008, v. 1, 9–18.

312. Verschuur G. The Radio Sun and Planets in *The Invisible Universe: The Story of Radio Astronomy*, Springer, New York, 2007, p. 23–32.

313. Filipov B. and Koutchmy S. On the origin of the prolate solar chromosphere. *Solar Phys.*, 2000, v.196, 311–320.

314. Bénard H. Les tourbillons céllulaires dans une nappe liquide. *Rev. Gen. Sci. Pures Appl.*, 1900, v. 11, 1261–1271; 1309–1328.

315. Bénard H. Les toubillons céllulaires dans une nappe liquid transportant de la chaleur par convection en régime permanent. *Ann. Chim.Phys.*, 1901, v. 23, 62–144.

316. Ozbelge H.O. On the surface structure and the hydrodynamics of the Bénard Cells. *Experiment. Fluids*, 1989, v. 8, 238–240.

317. Cerisier P., Rahal S., Rivier N. Topological correlations in Bénard-Marangoni convective structures. *Phys. Rev. E.*, 1996, v. 54, no. 5, 5086–5094.

318. Thiele U. and Eckert K. Stochastic geometry of polygonal networks an alternative approach to the hexagon-square-transition in Bénard convection. *Phys. Rev. E*, 1998, v. 58, 3458–3468

319. Charbonneau P. and Smolarkiewicz P.K. Modeling the Solar Dynamo. *Science*, 2013, v. 340, no. 6128, 42–43.

320. Tobias S.M. The Solar Dynamo. *Phil. Trans. Roy. Soc. A*, 2002, v. 360, no. 1801, 2741–2756.

321. Nornberg M.D., Spence E.J., Kendrick R.D., Jacobson C.M. and Forest C.B. Measurements of the magnetic field induced by a turbulent flow of liquid metal. *Phys. Plasmas*, 2006, v. 13, 055901(8 pages); also arXiv:physics/0510265v3 [physics.plasm-ph].

322. Nornberg M.D., Spence E.J., Kendrick R.D., Jacobson C.M. and Forest C.B. Intermittent Magnetic Field Excitation by a Turbulent Flow of Liquid Sodium. *Phys. Rev. Let.*, 2006, v. 97, no.4, 044503(4 pages).

323. Stieglitz R. and Müller U. Experimental demonstration of a homogeneous two-scale dynamo. *Phys. Fluids*, 2001, v. 13, no. 3, 561–564.

324. Gailitis A., Lielausis O., Dement'ev S., Platacis E., Cifersons A., Gerbeth G., Gundrum T., Stefani F., Christen M., Hänel H. and Will G. Detection of a Flow Induced Magnetic Field Eigenmode in the Riga Dynamo Facility. *Phys. Rev. Let.*, 2000, v. 84, no. 19, 4365–4368.

325. Density of molten elements and representative salts. In, *CRC Handbook of Chemistry and Physics*, 2013–2014, CRC Press, Baca Raton, FL, p. 4-128.

326. Schecter D.A., Boyd J.F. and Gilman P.A. "Shallow-Water" Magnetohydrodynamic Waves in the Solar Tachocline. *Astrophys. J.*, v. 551, L185–L188.

327. Mohorič A., Planinšič G., Kos M., Duh A. and Stepišnik J. Magnetic Resonance Imaging System Based on Earth's Magnetic Field. *Inst. Science Tech.*, 2004, v./,32, no. 6, 655–667.

328. Lowes F.J. and Wilkinson I. Geomagnetic dynamo: A laboratory model. *Nature*, 1963, v. 198, no. 4886, 1158–1160.

329. Asinovskii E.I. and Markovets V.V. The limiting electric conductivity of plasma. *Phys. Letters A*, 2003, v. 319, 510–513.

330. De Groof A., Berghmans D., van Driel-Gesztelyi L. and Poedts S. Intensity variations in EIT shutterless mode: Waves or Flows? *Astron. Astrophys.*, 2004, v. 415, no. 3, 1141–1151.

331. De Groof A., Bastiaensen C., Müller D.A.N., Berghmans D., and Poedts S. Detailed comparison of downflows seen both in EIT 30.4 nm and Big Bear Hα movies. *Astron. Astrophys.*, 2005, v. 443, no. 1, 319–328.

332. Müller D.A.N., De Groof A., Hansteen V.H. and Peter H. High-speed coronal rain. *Astron. Astrophys.*, 2005, v. 436, no. 3, 1067–1074.

333. Antolin R., Vissers G. and van der Voort L.R. On-Disk coronal rain. *Solar Phys.*, 2012, v. 280, no. 2, 457–474.

334. Antolin R. and van der Voort L.R. Observing the fine structure of loops through high-resolution spectroscopic observations of coronal rain with the CRISP instrument at the Swedish Solar Telescope. *Astrophys. J.*, 2012, v. 745, no. 2, 152(21 pages).

335. Aschwanden M. Physics of the Solar Corona: An Introduction with Problems and Solutions. Springer in association with Praxis Publishing, Chichester, U.K., 2005.

336. Peter H., Bingert S., Klimchuk J.A., de Forest C., Cirtain J.W., Golub L., Winebarger A.R., Kobayashi K. and Korreck K.E. Structure of solar coronal loops: From miniature to large-scale. *Astron. & Astrophys.*, 2013, v. 556, A104(12 pages).

337. Tsiropoula G., Tziotsious K., Kontogiannis I., Madjarska M.S., Doyle J.G. and Suematsu Y. Solar fine-scale structures I. Spicules and other small-scale, jet-like events at the chromospheric level: Observations and physical parameters. *Space Sci. Rev.*, 2012, v. 169, 181–244.

338. De Pontieu B., McIntosh S.W., Hansteen V.H., Carlsson M., Schrijver C.J., Tarbell T.D., Title A.M., Shine R.A., Suematsu Y., Tsuneta S., Katsukawa Y., Ichimoto K., Shimizu T. and Nagata S. A tale of two spicules: The impact of spicules on the magnetic chromosphere. *Publ. Astron. Soc. Japan*, 2007, v. 59, 655–660.

339. Zhang Y.Z., Shirata K, Wang J.X., Mao X.J., Matsumoto T., Liu Y. and Su T.T. Revision of spicule classification. *Astrophys. J.*, 2012, v. 750, 16(9 pages).

340. Moskowitz C. Gargantuan Sun explosion rocks astronomers. *SPACE.com* (created June 9, 2011 at 12:34 PM ET — accessed online on January 29, 2011).

341. NASA/SDO/Helioviewer.org [2011/06/07 04:00:00 to 11:00:00 UTC]. Observed well using 5 min frames SDO AIA 304. These events have been captured in video format and posted numerous times online: e.g. Newsflash *Skywatch Media* YouTube Channel; Phil Plait *Bad Astronomy Blog* on YouTube. (Accessed online on January 29, 2013).

342. Formisano V. and Moreno G. Helium and heavy ions in the solar winds. *Revista del Nuovo Cimento*, 1971, v. 1, no. 3, 365–422.

343. Robbins D.E., Hundhausen A.J. and Bame S.J. Helium in the solar-wind. *J. Geophys. Res.*, 1970, v. 75, no. 7, 1178–1187.

344. Ogilvie K.W. and Hirshberg J. The solar cycle variation of the solar wind helium abundance. *J. Geophys. Res.*, 1974, v. 79, no. 31, 4595–4602.

345. Bame S.J., Asbridge J.R., Feldman W.C. and Gosling J.T. Evidence for a structure-free state at high solar wind speeds. *J. Geophys. Res.*, 1977,v. 82, no. 10, 1487–1492.

346. Borrini G., Gosling J.T., Bame S.J., and Feldman W.C. Helium abundance enhancements in the solar wind. *J. Geophys. Res.*, 1982, v. 87, no. A9, 7370–7378.

347. Bochsler P. Structure of the solar wind and compositional variations. *Space Sci. Rev.*, 1998, v. 85, 291–302.

348. Aellig M.R., Lazarus A.J. and Steinberg J.T. The solar wind helium abundance: Variations with wind speed and solar cycle. *Geophys. Res. Let.*, 2001, v. 28, no. 14, 2767–2770.

349. Wurz P. Solar Wind Composition. In: The Dynamic Sun: Challenges for Theory and Observations, *ESA SP-600*, 2005, v. 5.2, 1–9.

350. Kasper J.C., Stevens M.L., Lazarus A.J. and Ogilvie K.W. Solar wind and helium abundance as a function of speed and heliographic latitude: Variation through a solar cycle. *Astrophys. J.*, 2007, v. 660, 901–910.

351. Wang Y.M. Relating the solar wind helium abundance to the coronal magnetic field. *Astrophys. J.*, 2008, v. 683, 499–509.

352. Parker E.N. Dynamics of the interplanetary gas and magnetic fields. *Astrophys. J.*, 1958, v. 128, 664–675.

353. Biermann L. Über die Ursache der chromosphärischen Turbulenz und des UV-Exzesses der Sonnenstrahlung. *Zeitshrift für Physik*, 1948, v. 25, 161–177.

354. Unsöld A. and Chapman S. Optical and radiofrequency ansorption by solar corpuscular burts. *The Observatory*, 1949, v. 69, 219–221.

355. Chapman S. The Viscosity and Thermal Conductivity of a Completely Ionized Gas. *Astrophys. J.*, 1954, v. 120, 151–155.

356. Gough D.O., Leibacher J.W., Scherrer P.H., Toomre J. Perspectives in Helioseismology. *Science*, 1996, v. 272, no. 5266, 1281–4.

357. Gough D.O. Seismology of the Sun and distant stars. D. Riedel Publishing Company. Dordrecht, 1986.

358. Kosovichev A.G. Solar Oscillations. In: Stellar Pulsation — Challenges for Theory and Observation. *AIP Int. Conf. Series.*, 2009, v. 1170, 547–559 (also in arXiv:1001.5283 [astro-ph.SR])

359. Christensen-Dalsgaard J. Helioseismology. *Rev. Mod. Phys.*, 2003, v. 74, 1073–1129 (also in arXiv:astro-ph/0207403).

360. Antia H.M. Solar interior and helioseismology. In, *Lectures on Solar Physics* (H.M. Antia, A. Bhatnagar and R. Ulmschneider, Eds.), Springer, Berlin, 2003, p. 80–126.

361. Bahcall J.N., Pinsonneault M.H. and Basu S. Solar models: Current epoch and time dependences, neutrinos, and helioseismological properties. *Astrophys. J.*, 2001, v. 555, 990–1012.

362. Kosovichev A.G. and Zharkova V.V. X-ray flare sparks quake inside the Sun. *Nature*, 1998, v. 393, 317–318.

363. Fleck B., Brekke P., Haugan S., Duarte L.S., Domingo V., Gurman J.B. and Poland A.I. Four years of SOHO discoveries — Some highlights. *ESA Bulletin*, 2000, v. 102, 68–86.

364. Kuhn J.R., Bush R.I., Schench X., and Scherrer P. The Sun's shape and brightness. *Nature*, 1998, v. 392, no. 6672, 155-157.

365. Charbonneau P., Christensen-Dalsgaard, Henning R., Larsen R.M., Schou J., Thompson M.J. and Tomczyk S. Helioseismic constraints on the structure of the solar tachocline. *Astrophys. J.*, 1999, v. 557, no. 1, 445–460.

366. Antia H.M. and Basu S. Revisiting the solar tachocline: Average properties and temporal variations. *Astrophys. J. Lett.*, 2011, v. 735, no. 2, L45(6 pages).

367. Miesch M.S. Large-scale dynamics of the convection zone and tachocline. *Living Rev. Solar Phys.*, 2005, v. 2, (URL 2, (2005), 1. URL http://www.livingreviews.org/lrsp-2005-1 — Accessed 10/1/2013.

368. Schou J., Antia H.M., Basu S., Bogart R.S., Bush R.I., Chitre S.M., Christensen-Dalsgaard J., di Mauro M.P., Dziembowski W.A., Eff-Darwich A., Gough D.O., Haber D.A., Hoeksema J.T., Howe R., Korzennik S.G, Kosovichev A.G., Larsen R.M., Pijpers F.P., Scherrer P.H., Sekii T., Tarbell T.D., Title A.M., Thompson M.J. and Toomre J.Helioseismic Studies of Differential Rotation in the Solar Envelope by the Solar Oscillations Investigation Using the Michelson Doppler Imager. *Astrophys. J.*, 1998, v. 505, no. 1, 390–417.

369. Nakariakov V.M. and Verwichte E. Coronal waves and oscillations. *Living Rev. Solar Phys.*, 2005, v. 2, 3–65.

370. Roberts B. Progress in coronal seismology. *Proc. IAU: Waves and Oscillations in Solar Atmosphere*, 2007, v. 247, 3–19.

371. De Moortel I. An overview of coronal seismology. *Phil. Trans. R. Soc. A*, 2005, v. 363, 2743–2760.

372. Morton R.J., Verth G., Fedun V., Shelyag S. and Erdélyi R. Evidence for the photospheric excitation of incompressible chromospheric waves. *Astrphys. J.*, 2013, v. 768, no. 1, 17(11 pages).

373. SOHO/LASCO C2 NASA/ESA [2011/05/10 20:00:00 to 2011/05/11 08:00:00 UTC]. These events have been captured in video format and displayed online: e.g. youtube.com/watch?v=igeBrSGk5FA; *Russia Today* youtube.com/watch?NR=1&v=Mat4dWpszoQ&feature=fvwp. (Accessed online on January 29, 2013: Examine beginning at 2011/05/10 2:48:00 to 2011/05/10 4:00:00). NASA provides a tool to generate such films: http://lasco-www.nrl.navy.mil/index.php?p=js_lasco1.

374. Gamow G. The birth and death of the sun: A lucid explanation of stellar evolution and atomic energy. New American Library, New York, N.Y., 1952.

375. Arnett D. Supernovae and nucleosynthesis: An investigation of the history of matter, from the Big Bang to the present. Princeton University Press, Princeton, N.J., 1996.

376. Pagel B. E. J. Nucleosythesis and the chemical evolution of galaxies (2nd Edition), Cambridge University Press, Cambridge, U.K., 2009.

377. Gamow G. Nuclear energy sources and stellar evolution. *Phys. Rev.*, 1938, v. 53, 595–604.

378. Gamow G. Nuclear reactions in stellar evolution. *Nature*, 1939, v. 144, 620–622.

379. Bethe H.A. and Critchfield C.L. The Formation of Deuterons by Proton Combination. *Phys. Rev.*, 1938, v. 54, no. 4, 248–254.

380. Bethe H. A. Energy Production in Stars. *Phys. Rev.*, 1939, v. 55, no. 1, 103.

381. Bethe H.A. Energy Production in Stars. *Phys. Rev.*, 1939, v. 55, no. 5, 434–456.

382. von Weizsäcker C. F. Über Elementumwandlungen in Innern der Sterne II. *Physikalische Zeitschrift*, 1938, v. 39, 633–646.

383. Hoyle F. The synthesis of the elements from hydrogen. *Mon. Not. Roy. Astron. Soc.*, 1946, v. 106, 343–383.

384. Hoyle F. On nuclear reactions occurring in very hot stars. I. The synthesis of elements from carbon to nickel. *Astrophys. J. Suppl. Ser.*, 1954, v. 1, 121–146.

385. Burbidge M., Burbidge G.R., Fowler W.A. and Hoyle F. Synthesis of the elements in stars. *Rev. Mod. Phys.*, 1957, v. 29, no. 4, 547–654.

386. Wallerstein G., Iben I., Parker P., Boesgaard A.M., Hale G.M., Champagne A.E., Barnes C.A., Käppeler F., Smith V.V., Hoffman R.D., Timmes F.X., Sneden C., Boyd R.N., Meyer B.S. and Lambert D.L. Synthesis of the elements in stars: Forty years of progress. *Rev. Mod. Phys.*, 1997, v. 9, no. 4, 995–1084.

387. Bahcall J.N. Neutrinos from the Sun. *Sci. Am.*, 1969, v. 221, no. 1, 28–37.

388. Bahcall J.N. How the Sun shines. http://www.nobelprize.org/nobel_prizes/themes/physics/fusion/.

389. Beers T.C. The first generation stars. *Science*, 2005, v. 309, no. 5733, 390–391.

390. Nickelsen K. and Graβhoff G. Concepts from the Bench: Hans Krebs, Kurt Henseleit and the Urea Cycle. In: "Going Amiss in Experimental Research" (G. Hon, J. Schickore, F. Steinle, Eds.), *Boston Stud. Phil. Science*, 2009, v. 267, 91–117.

391. Krebs H.A., Salvin E. and Johnson A. XX. The formation of citric and α-ketoglutaric acid in the mamalian body. *Biochem. J.*, 1938, v. 32, no. 1, 113-117.

392. Reames D.V. and Ng C.K. Heavy-element abundances in solar energetic particle events. *Astrophys. J.*, 2004, v. 610, 510–522.

393. Kasting J.F. and Grinspoon D.H. The faint young Sun problem: In "The Sun in Time" (C.P. Sonett, M.S. Giampapa, and M.S. Matthews, Eds.), The University of Arizona, Tuscon, 1991, pp. 447–462.

394. Zahnle K., Arndt N., Cockell C., Halliday A., Nisbet E., Selsis F. and Sleep N.H. Emergence of a habitable planet. *Space Sci. Rev.*, 2007, v. 129, 35–78.

395. Solanski S.K. Solar variability and climate change: Is there a link. *Astron. & Geophys.*, 2002, v. 43, no. 5, 5.9–5.13.

396. Lacis A.A., Schmidt G.A., Rind D. and Ruedy R.A. Atmospheric CO_2: Principal control knob governing the Earth's temperature. *Science*, 2010, v. 330, 356–359.

397. Sackmann I.-J. and Boothboyd A. Our Sun V. A bright young Sun consistent with helioseismology and warm temperatures on ancient Earth and Mars. *Astrophys. J.*, 2003, v. 583, 1024–1039.

398. Robitaille P.M. Class-O Wolf-Rayet stars and the birth of the Sun. A new look at stellar evolution. (manuscript in preparation)

399. Murthy V.R. Geochemical evidence for an initially molten Earth. *Phys. Earth Planetary Interiors*, 1992, v. 71, no. 1-2, 46–51.

400. Maunder E.W. Spoerer's Researches on Sun-Spots. *Mon. Not. Roy. Astron. Soc.*, 1890, v. 50, 251–252.

401. Spörer G. Über die Periodicität Sonnenflecken seit dem Jahre 1618, vornehmlich in Bezug auf die heliographische Breite derselben, und Nachweis einer erheblichen Störung dieser Periodicität während eines langen Zeitraumes. la. 4°. *Nova Acta der Ksl. Leopold-Caroline Deutschen Akademie der Natuifoischei*, v. 53, no. 2, 283–324.

402. Spörer. Sur les différences que présentent l'hémisphère nord et l'hémisphère sud du Soleil. *Bull. Astronomique*, 1889, Ser. 1, v. 6, 60–63.

403. Eddy J.A. The Mauder Minimum. *Science*, v. 192, no. 4245, 1189–1202

404. Beckman J.E. and Mahoney T.J. The Mauder minimum and climate change: Have historical records aided current research? *ASP Conf. Ser.*, 1998, v. 153, 212–217.

405. Times of India. Solar Activity Drops to 100 Year Low, Puzzling Scientists. Sept. 18, 2013. http://timesofindia.indiatimes.com/topic/Solar-activity-drops-to-100-year-low.

406. NASA. Big Sun-diving comet discovered. http://solarsystem.nasa.gov/scitech/display.cfm?ST_ID=2504.

407. Haramundanis K. Cecilia Payne-Gaposchkin: An autobiography and other recollections (2nd Edition), Cambridge University Press, Cambridge, U.K., 1996.

408. Rabounski D. and Borissova L. Inside Stars. American Research Press, Rehoboth, NM, 2013. (available online: http://ptep-online.com/index_files/books_files/stars2013.pdf).

n-Valued Refined Neutrosophic Logic and Its Applications to Physics

Florentin Smarandache
University of New Mexico, Math and Sciences Division, 705 Gurley Ave., Gallup, NM 87301, USA.
E-mail:smarand@unm.edu

In this paper we present a short history of logics: from particular cases of 2-symbol or numerical valued logic to the general case of n-symbol or numerical valued logic. We show generalizations of 2-valued Boolean logic to fuzzy logic, also from the Kleene's and Lukasiewicz' 3-symbol valued logics or Belnap's *4*-symbol valued logic to the most general *n-symbol or numerical valued refined neutrosophic logic*. Two classes of neutrosophic norm (*n-norm*) and neutrosophic conorm (*n-conorm*) are defined. Examples of applications of neutrosophic logic to physics are listed in the last section. Similar generalizations can be done for *n-Valued Refined Neutrosophic Set*, and respectively *n-Valued Refined Neutrosopjhic Probability*.

1 Two-Valued Logic

1.1 The Two Symbol-Valued Logic

It is the Chinese philosophy: *Yin and Yang* (or Femininity and Masculinity) as contraries:

Fig. 1: Ying and Yang

It is also the Classical or *Boolean Logic*, which has two symbol-values: truth T and falsity F.

1.2 The Two Numerical-Valued Logic

It is also the Classical or *Boolean Logic*, which has two numerical-values: truth *1* and falsity *0*. More general it is the *Fuzzy Logic*, where the truth (*T*) and the falsity (*F*) can be any numbers in *[0,1]* such that $T + F = 1$.

Even more general, *T* and *F* can be subsets of *[0,1]*.

2 Three-Valued Logic

2.1 The Three Symbol-Valued Logics

1. *Lukasiewicz 's Logic*: True, False, and Possible.
2. *Kleene's Logic*: True, False, Unknown (or Undefined).
3. Chinese philosophy extended to: *Yin*, *Yang*, and *Neuter* (or Femininity, Masculinity, and Neutrality) - as in Neutrosophy. Neutrosophy philosophy was born from neutrality between various philosophies. *Connected with Extenics* (Prof. Cai Wen, 1983), and Paradoxism (F. Smarandache, 1980). *Neutrosophy* is a new branch of philosophy that studies the origin, nature, and scope of neutralities, as well as their interactions with different ideational spectra. This theory considers every notion or idea <A> together with its opposite or negation <antiA> and with their spectrum of neutralities <neutA> in between them (i.e. notions or ideas supporting neither <A> nor <antiA>). The <neutA> and <antiA> ideas together are referred to as <nonA>. Neutrosophy is a generalization of Hegel's dialectics (the last one is based on <A> and <antiA> only). According to this theory every idea <A> tends to be neutralized and balanced by <antiA> and <nonA> ideas - as a state of equilibrium. In a classical way <A>, <neutA>, <antiA> are disjoint two by two. But, since in many cases the borders between notions are vague, imprecise, Sorites, it is possible that <A>, <neutA>, <antiA> (and <nonA> of course) have common parts two by two, or even all three of them as well. *Such contradictions involves Extenics*. Neutrosophy is the base of all neutrosophics and it is used in engineering applications (especially for software and information fusion), medicine, military, airspace, cybernetics, physics.

2.2 The Three Numerical-Valued Logic

1. *Kleene's Logic*: True (*1*), False (*0*), Unknown (or Undefined) (*1/2*), and uses "min" for $\wedge$, "max" for $\vee$, and "1-" for negation.
2. More general is the *Neutrosophic Logic* [Smarandache, 1995], where the truth (*T*) and the falsity (*F*) and the indeterminacy (*I*) can be any numbers in *[0, 1]*, then $0 \leq T + I + F \leq 3$. More general: Truth (*T*), Falsity (*F*), and Indeterminacy (*I*) are standard or nonstandard subsets of the nonstandard interval $]^{-}0, 1^{+}[$.

3 Four-Valued Logic

3.1 The Four Symbol-Valued Logic

1. It is *Belnap's Logic*: True (*T*), False (*F*), Unknown (*U*), and Contradiction (*C*), where *T*, *F*, *U*, *C* are symbols,

not numbers. Below is the Belnap's conjunction operator table:

∩	F	U	C	T
F	F	F	F	F
U	F	U	F	U
C	F	F	C	C
T	F	U	C	T

Restricted to *T,F,U*, and to *T,F,C*, the Belnap connectives coincide with the connectives in Kleene's logic.

2. Let *G* = Ignorance. We can also propose the following two 4-Symbol Valued Logics: *(T, F, U, G)*, and *(T, F, C, G)*.
3. *Absolute-Relative 2-, 3-, 4-, 5-, or 6-Symbol Valued Logics* [Smarandache, 1995]. Let T_A be truth in all possible worlds (according to Leibniz's definition); T_R be truth in at last one world but not in all worlds; and similarly let I_A be indeterminacy in all possible worlds; I_R be indeterminacy in at last one world but not in all worlds; also let F_A be falsity in all possible worlds; F_R be falsity in at last one world but not in all worlds; Then we can form several Absolute-Relative 2-, 3-, 4-, 5-, or 6-Symbol Valued Logics just taking combinations of the symbols T_A, T_R, I_A, I_R, F_A, and F_R. As particular cases, very interesting would be to study the Absolute-Relative 4-Symbol Valued Logic (T_A, T_R, F_A, F_R), as well as the Absolute-Relative 6-Symbol Valued Logic (T_A, T_R, I_A, I_R, F_A, F_R).

3.2 Four Numerical-Valued Neutrosophic Logic

Indeterminacy I is refined (split) as U = Unknown, and C = contradiction. T, F, U, C are subsets of [0, 1], instead of symbols; This logic generalizes Belnap's logic since one gets a degree of truth, a degree of falsity, a degree of unknown, and a degree of contradiction. Since $C = T \wedge F$, this logic involves the Extenics.

4 Five-Valued Logic

1. Five Symbol-Valued Neutrosophic Logic [Smarandache, 1995]: Indeterminacy I is refined (split) as U = Unknown, C = contradiction, and G = ignorance; where the symbols represent:
   T = truth;
   F = falsity;
   U = neither T nor F (undefined);
   $C = T \wedge F$, which involves the Extenics;
   $G = T \vee F$.
2. If *T, F, U, C,* G are subsets of *[0, 1]* then we get:a *Five Numerical-Valued Neutrosophic Logic*.

5 Seven-Valued Logic

1. *Seven Symbol-Valued Neutrosophic Logic* [Smarandache, 1995]:
   I is refined (split) as *U, C, G*, but *T* also is refined as T_A = absolute truth and T_R = relative truth, and *F* is refined as F_A = absolute falsity and F_R = relative falsity. Where: U = neither (T_A or T_R) nor (F_A or F_R) (i.e. undefined); $C = (T_A or T_R) \wedge (F_A or F_R)$ (i.e. Contradiction), which involves the Extenics;
   $G = (T_A or T_R) \vee (F_A or F_R)$ (i.e. Ignorance). All are symbols.
2. But if T_A, T_R, F_A, F_R, *U, C, G* are subsets of *[0, 1]*, then we get a *Seven Numerical-Valued Neutrosophic Logic*.

6 n-Valued Logic

1. *The n-Symbol-Valued Refined Neutrosophic Logic* [Smarandache, 1995]. In general:
   T can be split into many types of truths: $T_1, T_2, ..., T_p$, and *I* into many types of indeterminacies: $I_1, I_2, ..., I_r$, and *F* into many types of falsities: $F_1, F_2, ..., F_s$, where all $p, r, s \geq 1$ are integers, and $p + r + s = n$.
   All subcomponents T_j, I_k, F_l are symbols for $j \in \{1, 2..., p\}$, $k \in \{1, 2..., r\}$, and $l \in \{1, 2..., s\}$.
   If at least one $I_k = T_j \wedge F_l$ =contradiction, we get again the Extenics.
2. *The n-Numerical-Valued Refined Neutrosophic Logic.* In the same way, but all subcomponents T_j, I_k, F_l are not symbols, but subsets of *[0,1]*, for all $j \in \{1, 2..., p\}$, all $k \in \{1, 2..., r\}$, and all $l \in \{1, 2..., s\}$. If all sources of information that separately provide neutrosophic values for a specific subcomponent are independent sources, then in the general case we consider that each of the subcomponents T_j, I_k, F_l is independent with respect to the others and it is in the non-standard set $]^-0, 1^+[$. Therefore per total we have for crisp neutrosophic value subcomponents T_j, I_k, F_l that:

$$^-0 \leq \sum_{j=1}^{p} T_j + \sum_{k=1}^{r} I_k + \sum_{l=1}^{s} F_l \leq n^+ \qquad (1)$$

   where of course $n = p + r + s$ as above. If there are some dependent sources (or respectively some dependent subcomponents), we can treat those dependent subcomponents together. For example, if T_2 and I_3 are dependent, we put them together as $^-0 \leq T_2 + I_3 \leq 1^+$. The non-standard unit interval $]^-0, 1^+[$, used to make a distinction between absolute and relative truth/ indeterminacy /falsehood in philosophical applications, is replace for simplicity with the standard (classical) unit interval $[0, 1]$ for technical applications.
   For at least one $I_k = T_j \wedge F_l$ = contradiction, we get again the Extenics.

7 n-Valued Neutrosophic Logic Connectors

1. **n-Norm and n-Conorm defined on combinations of t-Norm and t-Conorm**
   The n-norm is actually the neutrosophic conjunction operator, NEUTROSOPHIC AND ($\wedge_n$); while the n-conorm is the neutrosophic disjunction operator, NEUTROSOPHIC OR ($\vee_n$).
   One can use the t-norm and t-conorm operators from the fuzzy logic in order to define the **n-norm** and respectively **n-conorm** in neutrosophic logic:

$$\begin{aligned} &n-norm((T_j)_{j=\{1,2,...,p\}},\\ &(I_k)_{k=\{1,2,...,r\}},(F_l)_{l=\{1,2,...,s\}})\\ &=([t-norm(T_j)]_{j=\{1,2,...,p\}},\\ &\quad [t-conorm(I_k)]_{k=\{1,2,...,r\}},\\ &\quad [t-conorm(F_l)]_{l=\{1,2,...,s\}}) \end{aligned} \tag{2}$$

   and

$$\begin{aligned} &n-conorm((T_j)_{j=\{1,2,...,p\}},(I_k)_{k=\{1,2,...,r\}},\\ &(F_l)_{l=\{1,2,...,s\}})\\ &=([t-conorm(T_j)]_{j=\{1,2,...,p\}},\\ &\quad [t-norm(I_k)]_{k=1,2,...,r},\\ &\quad [t-norm(F_l)]_{l=1,2,...,s}) \end{aligned} \tag{3}$$

   and then one normalizes if needed.
   Since the n-norms/n-conorms, alike t-norms/t-conorms, can only approximate the inter-connectivity between two n-Valued Neutrosophic Propositions, there are many versions of these approximations.
   For example, for the n-norm: the indeterminate (sub)components I_k alone can be combined with the t-conorm in a pessimistic way [i.e. lower bound], or with the t-norm in an optimistic way [upper bound]; while for the n-conorm: the indeterminate (sub)components I_k alone can be combined with the t-norm in a pessimistic way [i.e. lower bound], or with the t-conorm in an optimistic way [upper bound].
   In general, if one uses in defining an n-norm/n-conorm for example the t-norm $min\{x, y\}$ then it is indicated that the corresponding t-conorm used be $max\{x, y\}$; or if the t-norm used is the product $x\dot{y}$ then the corresponding t-conorm should be $x+y-x\dot{y}$; and similarly if the t-norm used is $max\{0,\ x+y-1\}$ then the corresponding t-conorm should be $min\{x+y,\ 1\}$; and so on.
   Yet, it is still possible to define the n-norm and n-conorm using different types of t-norms and t-conorms.
2. **N-norm and n-conorm based on priorities**
   For the *n-norm* we can consider the priority: T<I<F, where the subcomponents are supposed to conform with similar priorities, i.e.

$$\begin{aligned} &T_1<T_2<...<T_p<I_1<I_2<...\\ &<I_r<F_1<F_2<...<F_s. \end{aligned} \tag{4}$$

   While for the **n-conorm** one has the opposite priorities: T>I>F, or for the refined case:

$$\begin{aligned} &T_1>T_2>...>T_p>I_1>I_2>...\\ &>I_r>F_1>F_2>...>F_s. \end{aligned} \tag{5}$$

   By definition A<B means that all products between A and B go to B (the bigger).
   Let's say, one has two neutrosophic values in simple (non-refined case):

$$(T_x, I_x, F_x) \tag{6}$$

   and

$$(T_y, I_y, F_y) \tag{7}$$

   Applying the n-norm to both of them, with priorities T < I < F, we get:

$$\begin{aligned} &(T_x, I_x, F_x)\wedge_n(T_y, I_y, F_y)\\ &=(T_xT_y, T_xI_y+T_yI_x+I_xI_y,\\ &\quad T_xF_y+T_yF_x+I_xF_y+I_yF_x+F_xF_y). \end{aligned} \tag{8}$$

   Applying the n-conorm to both of them, with priorities T > I > F, we get:

$$\begin{aligned} &(T_x, I_x, F_x)\vee_n(T_y, I_y, F_y)\\ &=(T_xT_y+T_xI_y+T_yI_x+T_xF_y+T_yF_x,\\ &\quad I_xI_y+I_xF_y+I_yF_x, F_xF_y). \end{aligned} \tag{9}$$

   In a lower bound (pessimistic) n-norm one considers the priorities T < I < F, while in an upper bound (optimistic) n-norm one considers the priorities I < T < F.
   Whereas, in an upper bound (optimistic) n-conorm one considers T > I > F, while in a lower bound (pessimistic) n-conorm one considers the priorities T>F>I.
   Various priorities can be employed by other researchers depending on each particular application.

8 Particular Cases

If in *6 a)* and *b)* one has all $I_k = 0, k = \{1, 2, ..., r\}$, we get the **n-Valued Refined Fuzzy Logic**.

If in *6 a)* and *b)* one has only one type of indeterminacy, i.e. k=1, hence $I_1 = I > 0$, we get the **n-Valued Refined Intuitionistic Fuzzy Logic**.

9 Distinction between Neutrosophic Physics and Paradoxist Physics

Firstly, we make a distinction between Neutrosophic Physics and Paradoxist Physics.

1. **Neutrosophic Physics**
   Let <A> be a physical entity (i.e. concept, notion, object, space, field, idea, law, property, state, attribute, theorem, theory, etc.), <antiA> be the opposite of <A>, and <neutA> be their neutral (i.e. neither <A> nor <antiA>, but in between).

Neutrosophic Physics is a mixture of two or three of these entities <A>, <antiA>, and <neutA> that hold together.

Therefore, we can have neutrosophic fields, and neutrosophic objects, neutrosophic states, etc.

2. **Paradoxist Physics**
Neutrosophic Physics is an extension of Paradoxist Physics, since Paradoxist Physics is a combination of physical contradictories <A> and <antiA> only that hold together, without referring to their neutrality <neutA>. Paradoxist Physics describes collections of objects or states that are individually characterized by contradictory properties, or are characterized neither by a property nor by the opposite of that property, or are composed of contradictory sub-elements. Such objects or states are called paradoxist entities.

These domains of research were set up in the *1995* within the frame of neutrosophy, neutrosophic logic/ set/probability/statistics.

10 n-Valued Refined Neutrosophic Logic Applied to Physics

There are many cases in the scientific (and also in humanistic) fields that two or three of these items <A>, <antiA>, and <neutA> simultaneously coexist.

Several **Examples** of paradoxist and neutrosophic entities:

- anions in two spatial dimensions are arbitrary spin particles that are neither bosons (integer spin) nor fermions (half integer spin);
- among possible Dark Matter candidates there may be exotic particles that are neither Dirac nor Majorana fermions;
- mercury (Hg) is a state that is neither liquid nor solid under normal conditions at room temperature;
- non-magnetic materials are neither ferromagnetic nor anti-ferromagnetic;
- quark gluon plasma (QGP) is a phase formed by quasi-free quarks and gluons that behaves neither like a conventional plasma nor as an ordinary liquid;
- unmatter, which is formed by matter and antimatter that bind together (F. Smarandache, 2004);
- neutral kaon, which is a pion and anti-pion composite (R. M. Santilli, 1978) and thus a form of unmatter;
- neutrosophic methods in General Relativity (D. Rabounski, F. Smarandache, L. Borissova, 2005);
- neutrosophic cosmological model (D. Rabounski, L. Borissova, 2011);
- neutrosophic gravitation (D. Rabounski);
- qubit and generally quantum superposition of states;
- semiconductors are neither conductors nor isolators;
- semi-transparent optical components are neither opaque nor perfectly transparent to light;
- quantum states are metastable (neither perfectly stable, nor unstable);
- neutrino-photon doublet (E. Goldfain);
- the "multiplet" of elementary particles is a kind of "neutrosophic field" with two or more values (E. Goldfain, 2011);
- A "neutrosophic field" can be generalized to that of operators whose action is selective. The effect of the neutrosophic field is somehow equivalent with the "tunneling" from the solid physics, or with the "spontaneous symmetry breaking" (SSB) where there is an internal symmetry which is broken by a particular selection of the vacuum state (E. Goldfain). Etc.

Many types of logics have been presented above. For the most general logic, the n-valued refined neutrosophic logic, we presented two classes of neutrosophic operators to be used in combinations of neutrosophic valued propositions in physics.

Similar generalizations are done for **n-Valued Refined Neutrosophic Set, and respectively n-Valued Refined Neutrosophic Probability**.

Submitted on October 24, 2013 / Accepted on October 26, 2013

References

1. Dubois D. Uncertainty Theories, Degrees of Truth and Epistemic States, http://www.icaart.org/Documents/Previous-Invited-Speakers/2011/ICAART2011-Dubois.pdf
2. Smarandache F. (Editor). Proceedings of the Introduction to Neutrosophic Physics: Unmatter and Unparticle — International Conference, Zip Publ., Columbus, 2011.
3. Rabounski D., Smarandache F., Borisova L. Neutrosophic Methods in General Relativity. Neutrosophic Book Series, 10. *Hexis, Phoenix*, AZ, 2005. (Re-printed in Russian as: Netrosofskie Metody v Obshchey Teorii Otnositelnosti. *Hexis, Phoenix*, AZ, 2005.)
4. Smarandache F. Neutrosophic Logic and Set, mss., http://fs.gallup.unm.edu/neutrosophy.htm, 1995.
5. Smarandache F. A Unifying Field in Logics: Neutrosophic Field. *Multiple-Valued Logic / An International Journal*, 2002, v.8, no.3, 385–438. (This issue of the journal is dedicated to Neutrosophy and Neutrosophic Logic.)
6. Rivieccio U. Neutrosophic logics: Prospects and problems. *Fuzzy Sets and Systems*, 2008, v. 159, issue 14, 1860–1868.
7. Smarandache F. An Introduction to the Neutrosophic Probability Applied in Quantum Statistics. *Bulletin of Pure and Applied Sciences, Physics* 2003, v. 22D, no. 1, 13–25.
8. Smarandache F. Neutrosophic Set-A Generalization of the Intuitionistic Fuzzy Set. *Intern. Journal of Pure and Applied Mathematics*, 2005, v. 24, no. 3, 287–297.
9. Dezert J. Open questions on neutrosophic inference. Neutrosophy and neutrosophic logic. *Multiple-Valued Logic / An International Journal*, 2002, v. 8, no. 3, 439–472.
10. Webster's Online Dictionary, Paraconsistent probability (neutrosophic probability). http://www.websters-online-dictionary.org

Path Distribution Energy and Possible Consequences

Janez Špringer

Cankarjeva Cesta 2, 9250 Gornja Radgona, Slovenia, EU. E-mail: info@lekarna-springer.si

Previously (*Progress in Physics, 2013, v. 4, 83–84*) one investigated the geometric distribution of the frequencies of the path of the electron in the ground state of Hydrogen atom. In this paper one shows that the resulting difference detected on the fifth decimal of the inverse fine structure constant is accompanied by the difference in the quantized energy up to 0.04 eV. The difference in charge as well as energy of the distributed and non-distributed electrons could explain the origin of van der Waals intermolecular interactions.

1 Theoretical background

The distribution of the path of the electron changes the inverse fine structure constant [1]. Let us see what is accompanied to that change. The inverse fine structure constant can be expressed as:

$$\alpha^{-1} = \frac{2\varepsilon_0 hc}{e^2}\,. \tag{1}$$

The energy equivalent of the mass of the electron E_e can be expressed as [2]:

$$E_e = m_e c^2 = \frac{e^2}{4\pi\varepsilon_0 r_e}\,. \tag{2}$$

The inverse fine structure constant α^{-1} and the energy equivalent of the mass of the electron E_e are in inverse proportion since combining (1) and (2) the next relation is given:

$$\alpha^{-1} = \frac{hc}{2\pi E_e r_e}\,. \tag{3}$$

Other parameters staying untouched the inverse fine structure constant α^{-1} is changed due to the change of the electron charge e and consequently the energy equivalent of the mass E_e. Energetically more favorable is the greater inverse fine structure constant α^{-1} since it belongs to the smaller charge e and energy equivalent E_e. Therefore the proposed distributed path of the electron in the ground state of Hydrogen atom [1] is more favorable than non-distributed one. Having greater α^{-1} possesses lower E_e. The most favorable is the infinite-sided distribution with the largest α^{-1} and the lowest E_e. Energies of the discrete distributions are quantized. The difference in energy between the non-distributed electron E_0 and on the arbitrary number of the even-sides k distributed electron E_k is given by:

$$\Delta E_k = E_0 - E_k. \tag{4}$$

Because of the inverse proportion of α^{-1} and E_e holds:

$$\frac{\alpha^{-1}_{k-sided}}{\alpha^{-1}_{0-sided}} = \frac{E_0}{E_k}\,. \tag{5}$$

The difference in energy is then expressed as:

$$\Delta E_k = \left(\frac{\alpha^{-1}_{k-sided}}{\alpha^{-1}_{0-sided}} - 1\right) E_0\,. \tag{6}$$

The difference in energy between the energy equivalents of the mass of the electron at the different number of sides of distribution ΔE_k (4) is also the difference of the distribution energies ΔE_d:

$$\Delta E_k = \Delta E_d = \Delta E_{0-distribution} - E_{k-distribution}\,. \tag{7}$$

The distribution energy of the non-distribution is assumed to be zero:

$$E_{0-distribution} = 0. \tag{8}$$

So the distribution energy of the path of the electron of the arbitrary *k-sided* distribution is given by:

$$E_{k-distribution} = -\Delta E_d = -\Delta E_k. \tag{9}$$

The negative distribution energy means that energy is released in the case when the electron path becomes distributed, and on the contrary, the energy is spent in the case when the electron path becomes non-distributed. The distribution of the path of the electron does not need to be atom-radius dependent (it is distribution-radius dependent) [1] so what applies for Hydrogen atom could hold true also for other atoms.

2 Calculation of the Distribution Energy

The non-distribution energy $E_{0-distribution}$ is zero by definition (8).

On the two decimals rounded energy of the two-sided distribution can be calculated with the help of equations (6) and (9) knowing the CODATA value of the energy equivalent of the mass of the electron $E_e = 510998.91$ eV, and the appropriate distributed inverse fine structure constants $\alpha^{-1}_{0-sided} = 137.036006$ and $\alpha^{-1}_{2-sided} = 137.036014$ [1]:

$$E_{2-distribution} = -0.03 \text{ eV}. \tag{10}$$

On the two decimals rounded energy of the infinite-sided distribution can be calculated in the same way knowing the inverse fine structure constant $\alpha^{-1}_{\infty-sided} = 137.036018$ [1]:

$$E_{\infty-distribution} = -0.04 \text{ eV}. \quad (11)$$

The infinite number of the quantized distribution energies in the range of 0.04 eV can be calculated on all *k*-sides of the ground state of Hydrogen atom. Of course this paper brings no statement of how many of them are physically true.

3 Instead of conclusion

The proposed quantized distribution energies of the electron seem to have physico-chemical consequences. Ranged up to 0.04 eV (10), (11) are of the same order of magnitude as the typical energies from 0.4 kJ/mol to 4 kJ/mol of the van der Waals interaction between atoms [3]. Indeed:

$$\frac{4 \text{ kJ}}{\text{mol}} \approx \frac{0.04 \text{ eV}}{\text{molecule}}. \quad (12)$$

The different energy and charge of the distributed and non-distributed electrons could explain the origin of the mentioned intermolecular interactions.

Dedication

This fragment is dedicated to my wife Ivka.

Submitted on October 7, 2013 / Accepted on October 23, 2013

References

1. Špringer J. Geometric Distribution of Path and Fine Structure. *Progress in Physics*, 2013, v. 4, 83–84.
2. Haken H., Wolf H.C., Brewer W.D. The Physics of Atoms and Quanta: Introduction to Experiments and Theory. 2005, Springer. p. 70.
3. http://chemwiki.ucdavis.edu/Physical_Chemistry/Quantum_Mechanics/Atomic_Theory/Intermolecular_Forces/Van_Der_Waals_Interactions. Retrieved October 2013.

LETTERS TO PROGRESS IN PHYSICS

Open Letter by the Editor-in-Chief:
Declaration of Academic Freedom (Scientific Human Rights)
The Slovene Translation

Deklaracija akademske svobode
(Človekove pravice na znanstvenem področju)

Original text published in English: *Progress in Physics*, 2006, v.1, 57–60. Izvirno angleško besedilo: Dmitri Rabounski, glavni urednik revije *Progress in Physics*. E-mail: rabounski@yahoo.com. V slovenščino prevedla Janez Špringer in Darinka Špringer (Slovenija, EU), E-mail: info@lekarna-springer.si.

1 člen: Preambula

Začetek 21. stoletja bolj kot katero koli drugo obdobje v zgodovini človeštva odseva globino in pomembnost vloge znanosti in tehnologije pri stvareh, ki nas kot ljudi zadevajo.

Nadvse prevladujoča narava moderne znanosti in tehnologije je privedla do splošnega prepričanja, da je bodoča pomembnejša odkritja mogoče doseči v glavnem ali zgolj v velikih vladnih ali korporativno financiranih raziskovalnih skupinah, ki imajo na voljo nezaslišano drag instrumentarij in nebroj pomožnega osebja.

Običajna predstava pa je vendarle izmišljena in lažno zrcali dejansko naravo, kako se do znanstvenih odkritij v resnici pride. Veliki in dragi tehnološki projekti, kakor koli že so zapleteni, niso nič drugega kot izid uporabe poglobljenih znanstvenih uvidov manjših skupin predanih raziskovalcev ali samostojnih znanstvenikov, ki pogosto delajo v odmaknjenosti. Znanstvenik, ki dela sam, je sedaj in bo v prihodnje, kakor je bil že v preteklosti, sposoben priti do odkritja, ki lahko bistveno vpliva na usodo človeštva in spremeni obličje celotnega planeta, kjer tako nepomembno prebivamo.

Do velikih odkritij se po navadi dokopljejo posamezniki, ki delajo na podrejenih delovnih mestih znotraj vladnih agencij, raziskovalnih in izobraževalnih ustanov ali komercialnih podjetij. Posledično direktorji podjetij in institucij raziskovalca pogosto omejujejo in zatirajo, saj stremijo k drugim ciljem in želijo znanstveno raziskavo nadzorovati, odkritje pa uporabiti organizaciji ali sebi v prid ter sami sebe poveličati.

Zgodovina znanstvenih odkritij je prepolna zatiranja in posmehovanja, ki ju je izvajala sprevrnjena elita; šele v poznejših letih so bili primeri razkriti v pravi luči zaradi nezadržnega pohoda praktične nujnosti in intelektualnega razsvetljenja. Takisto je znanost omadeževana in oskrunjena s plagiatorstvom in namernim popačenjem, ki so ju zaradi zavisti in pohlepa izvajali brezobzirneži. In tako je tudi danes.

Namen te deklaracije je ohraniti in nadaljevati temeljno doktrino, da mora znanstveno raziskovanje potekati tako brez prikritega kot odkritega represivnega vpliva birokratskih, političnih, religioznih in kapitalskih smernic in da znanstveno ustvarjanje ni nič manjša človekova pravica kot druge takšne pravice in silni upi, zapisani v mednarodnih sporazumih in mednarodnem pravu.

Vsi znanstveniki naj spoštujejo to deklaracijo v znak solidarnosti z mednarodno znanstveno skupnostjo in z namenom, da bi se prebivalcem sveta omogočile pravice za neovirano znanstveno ustvarjanje na podlagi individualnih sposobnosti in naravnanosti. Za napredek v znanosti gre, za to naj si kot spodobni državljani prizadevajo po svojih najboljših močeh v tem nespodobnem svetu, in za blagor človeštva. Znanost in tehnologija sta bili že predolgo žrtvi zatiranja.

2 člen: Kdo je znanstvenik

Znanstvenik je oseba, ki se ukvarja z znanostjo. Vsakdo, ki sodeluje z znanstvenikom pri razvijanju in predlaganju idej in podatkov pri raziskavi ali njeni uporabi, je tudi znanstvenik. Formalna izobrazba ni predpogoj za to, da kdo postane znanstvenik.

3 člen: Kje nastaja znanost

Znanstveno raziskavo je mogoče izvajati na sploh kjerkoli, denimo v službi, med potekom formalnega izobraževanja in med sponzoriranim akademskim programom, tako v skupinah ali kot posameznik, ki neodvisno raziskuje doma.

4 člen: Svobodna izbira raziskovalne teme

Mnogim znanstvenikom, ki se potegujejo za višje strokovne nazive ali so udeleženi pri drugih raziskovalnih programih v akademskih ustanovah, kot so na primer univerze in šole za izpopolnjevalni študij, starejši akademiki in/ali administratorji preprečujejo delo na raziskovalni temi po lastni izbiri. Ne sicer zaradi primanjkljaja ustrezne opreme in prostorov, pač pa iz razloga, da akademska hierarhija in/ali drugi uradniki enostavno ne odobravajo takšnih raziskav, saj bi lahko prevrnile prevladujočo dogmo in favorizirane teorije ali celo ogrozile financiranje drugih projektov, ki jim predlagana

raziskava nemara odvzame veljavo. Avtoriteta ortodoksne večine pogosto onemogoči moteč raziskovalni projekt, tako da niti avtoriteta niti proračun nista prizadeta. Ta vsakdanja praksa je namerna ovira za svobodno znanstveno misel. Ker je povsem neznanstvena in zločinska, ji ne moremo gledati skozi prste.

Znanstvenik, ki dela za katero koli akademsko ustanovo, avtoriteto ali agencijo, mora biti pri izbiri raziskovalne teme popolnoma svoboden, omejen sme biti le z materialno podporo in intelektualnimi sposobnostmi, ki jih zmore nuditi izobraževalna ustanova, agencija ali avtoriteta. Če znanstvenik raziskuje kot član raziskovalne skupine, naj bodo vloge direktorjev raziskav in vodij skupin le svetovalne in posvetovalne narave glede na izbiro ustrezne raziskovalne teme znanstvenikov v skupini.

5 člen: Svobodna izbira raziskovalnih metod

Pri izvedbi raziskovalnega programa znotraj akademskega okolja administrativno osebje ali starejši akademiki pogosto silijo k uporabi drugačnih raziskovalnih metod od tistih, ki jih je znanstvenik sam izbral. Razlogov za to ni mogoče poiskati drugje kot v osebnih preferencah, pristranskosti, institucionalni politiki, uredniških zapovedih ali kolektivni avtoriteti. Takšna precej razširjena praksa je namerno zanikanje miselne svobode in ni dopustna.

Nekomercialni ali akademski znanstvenik ima pravico obdelati raziskovalno temo na kateri koli razumen način in s kakršnimi koli razumnimi sredstvi, za katera sam meni, da so najučinkovitejša. Končna odločitev o načinu poteka raziskave je le znanstvenikova.

Če nekomercialni ali akademski znanstvenik deluje kot član nekomercialne ali akademske skupine znanstvenikov, naj imajo vodje projektov in direktorji raziskav zgolj svetovalne in posvetovalne pravice in naj ne slabijo, omejujejo in na kakršen koli drug način posegajo v uporabo raziskovalne metode in obdelavo raziskovalne teme znanstvenika znotraj skupine.

6 člen: Svobodna udeležba in sodelovanje pri raziskovanju

Prakso moderne znanosti bremeni značilno institucionalno rivalstvo, ki ga spremljata osebna zavist in ohranjanje ugleda za vsako ceno brez upoštevanja raziskovalne resničnosti. To dejstvo znanstvenikom pogosto preprečuje sodelovanje s kompetentnimi kolegi, tako nameščenimi v rivalskih ustanovah kot drugimi brez sleherne akademske pripadnosti. Tudi takšna praksa je namerna ovira znanstvenemu napredku.

V primeru, da nekomercialni znanstvenik potrebuje pomoč drugega znanstvenika in slednji vanjo privoli, se ga sme brez zadržka prositi za kakršno koli in vsakršno pomoč pod pogojem, da nudenje pomoči ne presega okvira raziskovalnega proračuna. Če pomoč ni vezana na proračun, se sme znanstvenik svobodno odločiti zanjo in pritegniti k sodelovanju pomočnika povsem po lastni presoji brez kakršnega koli vmešavanja kogar koli.

7 člen: Svobodno nestrinjanje pri znanstveni razpravi

Zaradi skrivnega ljubosumja in pridobitniškega interesa moderna znanost prezira odprto razpravo in odločno preganja tiste znanstvenike, ki dvomijo o ortodoksnih stališčih. Znanstveniki z izrednimi sposobnostmi, ki opozorijo na pomanjkljivosti v trenutni teoriji ali interpretaciji podatkov, so zelo pogosto označeni za čudake, saj je tako mogoče njihova stališča z lahkoto ignorirati. Javno in zasebno so zasmehovani, sistematično pa se jim onemogoča tudi udeležba na znanstvenih kongresih, seminarjih in kolokvijih, tako da njihove ideje ostanejo brez poti do občinstva. Načrtno ponarejanje podatkov in napačno interpretiranje teorij današnje dni brezobzirnežem pogosto služita kot orodje za prikrivanje tako tehničnih kot znanstvenih dejstev. Izoblikovali so se mednarodni odbori znanstvenih nastopačev, ki prirejajo in usmerjajo mednarodne kongrese, kjer smejo svoje referate ne glede na vsebinsko kakovost predstavljati le njihovi privrženci. Ti odbori z zatekanjem k prevaram in lažem iz javne blagajne izvlečejo velikanske vsote denarja za financiranje svojih sponzoriranih projektov. Da se denar lahko še naprej nemoteno steka na račune za njihove projekte in jim tako zagotavlja dobro plačane službe, se vsakršno znanstveno utemeljeno nasprotovanje njihovim predlogom utiša z vsemi njim razpoložljivimi sredstvi. Oporečnim znanstvenikom se na podlagi njihovih ukazov vročajo odpovedi; drugim se s pomočjo mreže skorumpiranih pajdašev prepreči dostop do akademskih imenovanj. V spet drugih okoliščinah se onemogočijo kandidature pri programih za pridobitev višje stopnje strokovnosti, na primer doktorskega naziva, in to zaradi izražanja idej, ki spodkopavajo moderno teorijo, ne glede na to, za kakšno staro ortodoksno teorijo že gre. Temeljno dejstvo, ki pravi, da nobena znanstvena teorija ni dokončna in nedotakljiva, in je zategadelj odprta za razpravo in ponovno preverbo, popolnoma ignorirajo. Prav tako ignorirajo dejstvo, da ima nek pojav več mogočih razlag, in se škodoželjno obregnejo ob vsako, ki ni v skladu z ortodoksnim mnenjem; da pa bi opravičili svoja pristranska mnenja, se brez obotavljanja poslužujejo neznanstvene argumentacije.

Vsi znanstveniki naj imajo pravico do svobodne razprave o svojih raziskavah in raziskavah drugih. Naj bodo brez strahu pred javnim ali zasebnim objektivno neutemeljenim posmehom oziroma brez bojazni, da bodo na podlagi neupravičenih navedb postali tarče obtoževanja, omalovaževanja, poniževanja in siceršnjega zaničevanja. Nihče naj ne bo postavljen v položaj, kjer bi bila zaradi izražanja znanstvenih stališč ogrožena njegovo preživljanje in ugled. Svoboda znanstvenega izražanja naj bo najpomembnejša. Uporaba avtoritete za ovržbo znanstvenih dokazov ni znanstvena in naj se je ne uporablja za zavezovanje ust, zatiranje, ustrahovanje, preganjanje ali kakršno koli drugo

priganjanje oziroma ustvarjanje pritiska na znanstvenika. Namerno zamolčanje znanstvenih dejstev ali dokazov z dejanjem ali opustitvijo dejanja in namerno prirejanje podatkov v podporo dokazom ali za diskreditiranje nasprotnega stališča je znanstvena prevara, ki velja za znanstveni zločin. Načelo dokazov naj vodi vso znanstveno razpravo, najsi bodo ti dokazi praktični, teoretični ali preplet obojega.

8 člen: Svobodno objavljanje znanstvenih dognanj

Obžalovanja vredna cenzura znanstvenih člankov je postala današnje dni stalna praksa uredniških odborov pomembnejših revij in elektronskih arhivov ter navez njihovih domnevnih strokovnih razsodnikov. Razsodnike zvečine varuje anonimnost, tako da avtor ne more preveriti njihove domnevne strokovnosti. Objava znanstvenega dela se današnje dni rutinsko zavrne v primeru, ko se avtor ne strinja s preferenčno teorijo in večinsko pravovernostjo ali jima celo nasprotuje. Brez vsebinskih razlogov se marsikateri članek samodejno zavrne, zgolj če je njegov avtor na seznamu nečislanih pri urednikih, razsodnikih ali drugih strokovnih cenzorjih. Obstaja črni seznam disidentskih znanstvenikov, s katerega vsebino so seznanjeni povezani uredniški odbori. Vse to je velikanska pristranskost in graje vredno zatiranje svobodnega mišljenja ter si zasluži obsodbo mednarodne znanstvene skupnosti.

Vsi znanstveniki naj imajo pravico predstaviti dognanja svojih znanstvenih raziskav ali v celoti ali delno na ustreznih znanstvenih konferencah ter jih objaviti v tiskanih znanstvenih revijah, elektronskih arhivih in drugih medijih. Nobenemu znanstveniku naj se ne zavrne objava članka ali poročila, predloženega za objavo v znanstveni reviji, elektronskem arhivu ali drugem mediju zgolj zato, ker njegovo delo zaseje dvom o trenutnem večinskem prepričanju, je v nasprotju s pogledi uredniškega odbora, spodkopava temelje trenutnih ali bodočih raziskovalnih projektov drugih znanstvenikov ali je v nasprotju s kakršno koli politično dogmo, verskim prepričanjem in osebnim mnenjem drugega. Prav tako naj ne bo noben znanstvenik uvrščen na črno listo ali kako drugače cenzuriran, nihče pa mu tudi naj ne preprečuje objavljanja.

Noben znanstvenik naj zaradi obljube prejemanja daril ali kakršnih koli podkupnin ne ovira, spreminja ali se kako drugače vpleta v objavljanje del drugega znanstvenika.

9 člen: Soavtorstvo znanstvenih del

V znanstvenih krogih je komaj še skrito dejstvo, da ima veliko soavtorjev raziskovalnih člankov malo ali skoraj nič opraviti z objavljeno raziskavo. Veliko nadzornikov podiplomskih študentov, denimo, se ne brani pripisa za soavtorstvo člankov, ki so jih pod njihovim formalnim nadzorom napisali podrejeni znanstveniki. V veliko takšnih primerih je dejanski pisec inteligentnejši od formalnega nadzornika. V drugih primerih, spet zaradi slave, slovesa, denarja, ugleda ali česar podobnega, si tretje osebe pripisujejo soavtorstvo člankov. Pravim avtorjem takšnih člankov preostane le ugovor, z njim pa tvegajo, da bodo na nek način kaznovani, celo v obliki zavrnitve pri kandidiranju za višji raziskovalni naziv ali sodelovanje v raziskovalni skupini, kot se pogosto dogaja. Veliko jih je bilo v takšnih okoliščinah v resnici zavrnjenih. Te pretresljive prakse ne moremo več dopustiti. Avtorstvo naj se pripiše le za raziskavo odgovornim osebam.

Noben znanstvenik naj ne predlaga drugemu, ki ni sodeloval pri raziskavi, da bi postal soavtor članka, in noben znanstvenik naj ne dovoli soavtorstva sebi, če ni pomembneje prispeval k raziskavi, o kateri govori članek. Noben znanstvenik ali znanstvenica naj ne privoli v prisilo predstavnikov akademske ustanove, podjetja, vladne agencije ali katere koli druge osebe, da bi si prisvojili soavtorstvo za raziskavo, kjer nimajo pomembnih zaslug; prav tako naj noben znanstvenik ne dovoli uporabe neupravičenega soavtorstva v zameno za kakršno koli darilo ali drugo podkupnino. Nihče naj kakor koli ne sili znanstvenika, da bi bil kot soavtor pripisan kdor koli, ki ni pomembno prispeval k raziskavi v članku.

10 člen: Neodvisnost pripadnosti

Danes je veliko znanstvenikov zaposlenih na podlagi kratkoročnih pogodb. S prekinitvijo pogodbe o zaposlitvi ugasne tudi akademska pripadnost. Med uredniškimi odbori pogosto prevladuje politika, da se člankov tistih brez akademske ali komercialne pripadnosti ne objavlja. Zaradi takšne izključenosti znanstvenik nima dostopa do mnogih virov, zmanjšajo se mu tudi možnosti za predstavitev govorov in razprav na konferencah. To nečedno prakso je treba ustaviti. Znanost se ne prepoznava po pripadnosti.

Zaradi umanjkanja pripadnosti akademski ustanovi, znanstvenemu inštitutu, vladnemu ali komercialnemu laboratoriju ali kateri koli drugi organizaciji naj noben znanstvenik ne bo prikrajšan za možnost predstavitve svojih člankov na konferencah, kolokvijih in seminarjih, za objavljanje v katerem koli mediju, za dostop do knjižnic ali znanstvenih publikacij, za udeležbo na znanstvenih simpozijih in za izvajanje predavanj.

11 člen: Prost dostop do znanstvenih informacij

Večina specializiranih znanstvenih knjig in veliko znanstvenih revij ustvarja malo ali nič dobička, tako da jih komercialni založniki niso pripravljeni izdajati brez denarnih prispevkov, ki jih nudijo akademske ustanove, vladne agencije, človekoljubni skladi in podobni. V takšnih okoliščinah bi morali komercialni založniki dovoliti prost dostop do elektronskih različic publikacij in si prizadevati za čim nižjo ceno tiskovin.

Vsi znanstveniki naj si prizadevajo, da bi bili njihovi raziskovalni članki brezplačno dostopni za mednarodno znanstveno skupnost; če ne gre drugače, pa vsaj za minimalno

ceno. Vsi znanstveniki naj se lotijo oprijemljivih ukrepov in ponudijo svoje strokovne knjige po najnižji mogoči ceni, saj bodo znanstvene informacije le na tak način na voljo širši mednarodni znanstveni skupnosti.

12 člen: Etična odgovornost znanstvenikov

Zgodovina priča, da so znanstvena odkritja lahko v rabi tako za dobre kot zle namene: za blagor enih in v pogubo drugih. Ker se napredka znanosti in tehnologije ne da ustaviti, je treba zagotoviti razmere za omejitev zlonamerne rabe. Le demokratično izvoljena vlada brez verskih, rasnih in drugih predsodkov lahko obvaruje civilizacijo. Le demokratično izvoljena vlada, sodišča in odbori lahko obvarujejo pravico do svobodnega znanstvenega ustvarjanja. Danes različne nedemokratične države in totalitarni režimi izvajajo dejavne raziskave na področju jedrske fizike, kemije, virologije, genetskega inženiringa in še kje, z namenom, da bi naredili jedrsko, kemijsko in biološko orožje. Noben znanstvenik naj prostovoljno ne sodeluje z nedemokratičnimi državami in totalitarnimi režimi. Vsak znanstvenik, ki je prisiljen sodelovati pri razvoju orožja za takšne države, mora najti način in sredstva za upočasnitev napredovanja raziskovalnih programov in zmanjšati znanstveni učinek, tako da lahko civilizacija in demokracija na koncu prevladata.

Vsi znanstveniki so moralno odgovorni za svoje znanstvene stvaritve in odkritja. Noben znanstvenik naj samovoljno ne sodeluje pri načrtovanju in izdelavi orožja kakršne koli vrste za kakršno koli nedemokratično državo ali totalitarni režim ali dovoli uporabe svojih znanstvenih veščin in znanja za razvoj česar koli takšnega, kar bi lahko na kakršen koli način ogrožalo človeštvo. Znanstvenik naj živi, kakor veli naslednje reklo: ⟩⟩Sleherna nedemokratična vladavina in kršitev človekovih pravic sta zločin!⟨⟨

Posvetilo (Dedication)

Ta prevod je posvečen Manici, prevajalčevi drugi hčeri in prevajalkini nečakinji, ter ekipi dvigalcev uteži Plamen.

This translation is dedicated to Manica, Translators' second daughter and niece, respectively, and to the weightlifting team Plamen.

V Gornji Radgoni, 14. julija 2013

LETTERS TO PROGRESS IN PHYSICS

On Meta-Epistemic Determination of Quality and Reality in Scientific Creation

(An Address to Those Against Real Science, Scientific Creation, Intellectual Freedom, and Epistemic Culture)

Indranu Suhendro

The Zelmanov Cosmophysical Group
http://www.zelmanov.org

This is an open letter entitled as "On Meta-Epistemic Determination of Quality and Reality in Scientific Creation". An address to those against real science, scientific creation, intellectual freedom, and epistemic culture. Inspired by the Declaration of Academic Freedom.

Suffice it to say once and for all that you — and so many others like you — are not epistemically qualified to assess and categorize in any way my person, my work, nor any of my highly dignified and most devoted colleagues (as profoundly silent and understanding as they are), nor our scientific-philosophical group as a whole, both positively and negatively, whether in whole or in part. Such an attempt — particularly such a smug, narrow, shallow, pseudo-intellectual vacuity, which has foamed and mushroomed throughout certain loose forums, online and offline — is essentially epistemically superficial, hollow, arbitrary, and inauthentic, no matter how much pompous sophistication it displays (by this, I simply mean sophisticated solipsism, verbal and mental, stemming from the widespread, persistent epistemic problem of solipsistic syllogism and syllogistic solipsism). It has nothing whatsoever to do with the determination of Quality (quality-in-itself) and Reality (reality-in-itself) in the realmost sense.

The real tragedy of this world, at large (including academia), consists in the lack of epistemic character; of insight and creation (especially scientific creation); of independence and freedom; of objectivity and universality; of honesty and integrity; of solitude and originality; of "qualic" ideation, imagination, intellection, and identity; of a true sense of epistemicity and existentialism; of the ontic-epistemic unity of sight and sense — in other words, of Quality and Reality. These profound characteristics, throughout history, have never been, and will never be, embodied in the collective majority, let alone the very imitators (in contrast to real creators) and their stooges. These belong only to the truly solitary, independent, authentic few among intellectuals capable of not just filibustering and pan-handling raw fragments of knowledge, but also of critically and figuratively substantiating all types of knowledge and understanding. Such an individual is very, very rare.

If you have never heard, nor comprehended, notorious affairs in science such as the Erasmus affair, the Abel affair, the Galois affair, the Bolyai affair, the Wagener affair, the Dewey affair, the Alfven affair, the Sidis affair, the Pirsig affair, and, most recently, the Arp affair, the Wolfram affair, and the Perelman affair (alongside other such affairs in the annals of art and philosophy); whether you deem yourself a scientist or a lay person, you would better not assert anything potentially misleading in this category, especially publicly. As Michael Crichton once lamented, science is not the same, and should never be equal to, "consensus science" — with consensus (often very falsely, abusively masquarading as "democracy" and "objectivity") often being the first and last hiding place (refuge) for scoundrels, mere biased opportunists and affiliates, and pseudo-scientists —; science is simply about one person (or a few), one thinker, one scientist, being correct (in the sense of expanding horizons), no matter how much public opposition and alienation (e.g. Faustian and Kierkegaardian epistemic alienation) he faces, thus contributing not only to the discovery of new facts, but also to the discovery of new ways of thinking and new landscapes of ideation.

That is why in this passage, I shall very militantly emphasize upon the sublime adjective "epistemic" repeatedly (though I generally do not repeat myself): a truly revolutionary science not only contains a new methodology and a new phenomenology, but also a new epistemology and epistemicity, a new ontology and onticity — it introduces new, vaster, more profound "paint", "brush", "canvas", and "dimension", along with a whole new sketch.

Thus, for instance, using the word "fringe" oversimplifyingly and over-homogenizingly when describing a very peculiar scientist or a scientific group, without ever bothering to base it on correct epistemic qualifications, is slanderous, non-scientific, and non-sensical, far removed from real scientific attitude (whether it is perpetrated by academics and politicians first-hand or by lay people). It is a latent trait of characterless pan-academic memesis and mimicry (e.g. as contrasted with the "mnemonist sense" of the Soviet scientist A. Luria) and of pseudo-objectivity, pseudo-science, and pseudo-skepticism (e.g. in the sense of the sociologist of science M. Truzzi).

Besides, basically there are two kinds of "fringes" (referring to both "mere outsiders" and "those who are self-conscious on the boundary") with respect to the majority ("mob consciousness") in any given domain of thought: 1) the utterly wrong "crackpot" one, which is just basic, quickly self-dispersing non-sense without any significance, and 2) the subtle, mercurial "vortical" one — frontier science laden with extreme originality, creativity, synthesis, and daringness –, which DOES have true, profound, substantial epistemic qualification, novelty, merit, and life (i.e. space and direction) in the sublime heart and vein of science, philosophy, and art.

Without this in the very life of the sciences, all good human endeavors, speculations, and ideas are as good as being suffocated, dwarfened, and nullified, and thus organically dead, instead of epistemically, creatively breathing, living, and winging. It is this cross-roads, frontier-type, revolutionary, vortical kind of science that matters the most in the penultimate, genuine progress of science, let alone all of humanity, a merit to be most fairly appreciated in its own universal time, not simply in a temporary "age" dominated by some contemporaneous power-structures and political interests.

To paraphrase Schopenhauer, every genuine — truly epistemically original and weighty — truth, along with its markedly lone proponents (included are the geniuses and mavericks concerned not with merely "adding color and ice to a pre-existing drink and cup", but with opening new frontiers, dimensions, and grounds entirely), is effervescently conscious of three stages pertaining to the reactionary, abusive behavior of the crowd, the majority, whether practically in power or not: first, it is ignored; second, it is ridiculed, rejected, slandered, and violently opposed; third, it is accepted as "self-evident" — and yet this last phase is often only in conjunction with Oppenheimer's (and Kuhn's) warning, "they (the proponents of fortress status-quo) do not get convinced ever, they simply die first".

In this sense, and only in this sense, there is no such a thing as a "single scientific method". Serious paradigms coexist at the frontiers not as mere parallels and alternatives with respect to each other, but already as profound alternating paradigms.

Genius, one with genuine academic freedom, is the very faculty responsible for novelty in individual scientific creation and collective scientific production, including, inevitably at a very fundamental level, new scientific theories, syntheses, and results as well as new ways of managing science altogether. This is because the structure of scientific revolution takes place simultaneously at methodological, phenomenological, axiological-ethical, epistemological, and even ontological levels. One cannot separate individual scientific creation and collective scientific production from the underlying philosophy and sociology of science. This way, self-aware epistemology serves as the very gradient on the slope of knowledge all the way to the mountain peak of scientific progress and revolution.

Suppression, abuse, slander, and any other kind of ill-treatment done by the majority towards anything intellectually new and blossoming by a minority in this category can truly be likened to child abuse: for here we are dealing with the infancy and growth — as well as the very ground, seeds, roots — of future scientific clarity, superstructures, and foundations.

Science evolves, revolves, snarls, twists, and surmounts on tensed — indeed epistemically intense and maudlin — edges and ridges, on suave pavements and narrow lanes, on lone fulcrums and horizons, as well as in broad day-light and in long stringent evenings, in the silent wet limits of the world, in poignant cracks and labyrinths; and the spirit of scientific revolution, let alone dialectics, is embodied this way, through critical, paradoxical, synthetic, epistemic, universal free thinking. Any form of dogmatic suppression and stymie in science in any epoch (i.e. in antiquity, modernism, post-modernism, and "post-post-modernism") is intolerable, a cumbersome instance which usually easily shows itself perfidiously in cases of epistemically hideous over-funding, over-politicization, over-elitism, over-sycophancy, over-patronizing, and over-establishment.

If one is not uniquely, naturally well-versed in these logico-dialectical strands of thinking, one is simply not a real scientist and creator capable of any profound insight and zenith. Such an attitude should also underlie a real, truly enlightened scientific enterprise and editorship: irrespective of the individual views of the editors and reviewers of a scientific guild, one must allow diverse new ideas to flourish and co-exist (as long as they are true new ideas, and not obvious "pieces of crackpottery", in the minimum epistemic sense). This should naturally, winnowingly manifest spontaneous scientific-epistemic certainty and solidity, far removed from the prevalent type of superficial insecurity, fear, and suppression.

While a scientist, I am also an acutely epistemic artist, independent philosophical mind, keen observer-participant, and free thinker, and this indelible quality wholly underlies my scientific path. Insight, originality, creativity, and solitude are the things that matter the most to me — not mere conformity, suitability, respectability, and normalcy. If I display my work of art (e.g. painting, sculpture, and musical score), and if it is indeed my very own authentic creation and self-conscious novel expression of profundity and eccentricity, I need not list any so-called "references": the object — the work — is ALREADY there in its entirety, and it is lone, universal, and transparent as it is, possessing both a verizon and a horizon. True originality shines through effortlessly, especially as regards scientific creation (and not mere "review" or "documentation"). There is no difference in this matter, whether I create scientifically, artistically, or philosophically: when I create something, I create it in a most comprehensive scientific, artistic, and philosophical sense. This ensures

real quality. Reality alone — and the Universe — is the parameter, not fallible and unqualified observers. It goes without saying that my "predecessors" in this drive naturally include Einstein, who did not bother to do the "administrative non-essentials" (listing so-called "references") in his 1905 and subsequent revolutionary papers, and Wittgenstein, who hardly referred to some other work in his 1918 masterpiece *Tractatus Logico-Philosophicus*.

Pueril, arbitrary comments such as the ones you and the many often perpetrate in a popular forum, and in certain other forums, are but mere psychological detours, infinitely away from real objectivity, verging on typical character assassination and individual abuse. Given a Rembrandt painting, or at least a Modigliani one, or indeed the work of any pan-Renaissance artist, one should not speak of the "person" of the artist in such a cowardly, biased, envious way or hastily resort to ill-chatter, but, first and foremost, one should behold and withhold, witness and withstand, his very art, ALREADY laid bare and transparent for all its mystery and mastery. If one still does not know what one is trying to comprehend or appreciate here, one should at least possess silent humility before the horizon and verizon of things: the qualitative distance between substantial ideas and mere opinions is infinite and asymmetric. It is ethically, universally very lame to form mere borrowed opinions, to downplay certain contributions, and to resort to ad hominem attack, as is often the case. Opinions are mere opinions, not real ideas, let alone absolute truths. I repeat: "Doxa" is never the same as "Eidos". One is here speaking of the determination and qualification of Reality and Quality, i.e. of "unicity" and "qualicity".

Again, certain such popular treatments verging on the immoral and the ethically ill are epistemically very trivial, categorically replete with misleading logical error (non-sequitur), ad hominem attack, individual abuse, hyper-semiotics, hypernarration, oxymornonism, pseudo-science, pseudo-skepticism, pseudo-philosophy, pseudo-objectivity, solipsism, and epistemic shallowness.

You know nothing about us first-hand, absolutely nothing. You have only seen shadows and facades, and have only heard petty rumors, slander, and gossip (while we never seek enemies and pettiness in any case). We protect our individuality and wish to advance common scientific freedom and objectivity so universally much, perhaps "too much", that we rarely enlist "who we are", other than simply delivering our objectives. An objective of ours is not mere "inter-subjectivity", but truly epistemically qualified.

As regards "who we are", we are simply peculiar general relativists and cosmologists as well as core theoreticians and experimentalists. Also, we have never enlisted all our helpers/supporters one by one as well as our real "address" at length — only a decoy tertiary one for mere administrative and convenience purposes, not scientific purposes — for it matters not whether we reveal such things or not. What matters is the science. We are a core body of just a few acutely epistemic- progressive science creators throughout the world. That said, our group has more than one headquarters in the world. What essentially matters is the real scope, puissance, renaissance, and dimension of our scientific productivity and guardianship. We, a unique combination of the "very young" and "very old", epistemically and experientally, are serving science, philosophy, artistry, and humanity with all our strength, in necessary absolute freedom.

Indeed, some of us have had core scientific experiences as far back as the two world wars and the cold war along the contours of history, scientific creation, existential alienation, political turbulence, and cultural-scientific administration. A lot of us have synthesized first-hand the landscapes of both core Soviet and American science, East and West, and beyond. We are neither "big" nor "small"; we are infinite and infinitesimal. We know the world within and without, within-the-within and without-the-without. We alone know who we are. We know history and the human tendencies very well. We truly know where we have come from and where we are heading. We are quintessentially scientific and humanistic.

We do not populate typical non-scientific forums (especially countless on the internet), where mere bipolar, biased opinions are inevitably found in abundance: we are scientists in the most extreme sense of epistemic integrity and predisposition. We do not have time for trinkets, no matter how popular or trendy. We cherish creative solitude, universality, objectivity, independence, and democracy, so uniquely, so intensely, in a single, most variegated meta-epistemic framework, in order to be able to fully, impartially contribute to the betterment of our world in the way we know the most.

Do not bother to respond to this letter: you and so many others are not qualified to do so properly. Doing so shall only reveal, again and again, the very epistemic limitations you have at your core, and hence the very lack of substance lingering therein. Besides, this address is not a mere intellectual rambling or raving, it is simply meant to be a celestial sonnet akin to an ocean symphony and a contrapuntal melody, with "all the secret knowledge of harmony and counterpoint". Now, we shall withdraw into infinite silence, as usual, ever-pugnaciously dwelling in the realm of pure scientific creation.

Thus I hereby declare, once again, all-time individual and collective academic freedom in science, from science, to science, for science.

* * *

Dedicated in the name of truth, beauty, science, creativity, freedom, and genius to Grisha Perelman. And to a much better world rid of the rigid and frigid excess of characterless politics, solipsism, suppression, tyranny, and conformity; a most tranquil, vivid, living world-organism genuinely fond of self-growth and of ideation, individuation, character, liberty, and honesty.

Appendix: Overture on Character and Independence*

Talent warms-up the given (as they say in cookery) and makes it apparent; genius brings something new. But our time lets talent pass for genius. They want to abolish the genius, deify the genius, and let talent forge ahead.

Kierkegaard

Philosophy becomes poetry and science imagination, in the enthusiasm of genius.

Disraeli

In every work of genius, we recognize our own rejected thoughts; they come back to us with a certain alienated majesty.

R. W. Emerson

Genius is the ability to act rightly without precedent — the power to do the right thing the first time.

Elbert Hubbard

Society expresses its sympathy for the geniuses of the past to distract attention from the fact that it has no intention of being sympathetic to the geniuses of the present.

Celia Green

There is in every [such] madman a misunderstood genius whose idea, shining in his head, frightened people, and for whom delirium was the only solution to the strangulation that life had prepared for him.

Antonin Artaud, of Van Gogh

The case with most men is that they go out into life with one or another accidental characteristic of personality of which they say: "Well, this is the way I am. I cannot do otherwise". Then the world gets to work on them and thus the majority of men are ground into conformity. In each generation a small part cling to their "I cannot do otherwise" and lose their minds. Finally there are a very few in each generation who in spite of all life's terrors cling with more and more inwardness to this "I cannot do otherwise". They are the geniuses. Their "I cannot do otherwise" is an infinite thought, for if one were to cling firmly to a finite thought, he would lose his mind.

Kierkegaard

It is easy to live after the world's opinion; it is easy in solitude to live after your own; but the great man is he who, in the midst of the crowd, keeps with perfect sweetness the independence of solitude.

R. W. Emerson

I call that mind free which protects itself against the usurpations of society, which does not cower to human opinion, which feels itself accountable to a higher tribunal than man's, which respects itself too much to be the slave of the many or the few.

Channing

The genius differs from us men in being able to endure isolation, his rank as a genius is proportionate to his strength for enduring isolation, whereas we men are constantly in need of "the others", the herd; we die, or despair, if we are not reassured by being in the herd, of the same opinion as the herd.

Kierkegaard

Talent is hereditary; it may be the common possession of a whole family (e.g. the Bach family); genius is not transmitted; it is never diffused, but is strictly individual.

Otto Weininger

The age does not create the genius it requires. The genius is not the product of his age, is not to be explained by it, and we do him no honour if we attempt to account for him by it ... And as the causes of its appearance do not lie in any one age, so also the consequences are not limited by time. The achievements of genius live for ever, and time cannot change them. By his works a man of genius is granted immortality on the earth, and thus in a threefold manner he has transcended time. His universal comprehension and memory forbid the annihilation of his experiences with the passing of the moment in which each occurred; his birth is independent of his age, and his work never dies.

Otto Weininger

It is the genius in reality and not the other who is the creator of history, for it is only the genius who is outside and unconditioned by history. The great man has a history, the emperor is only a part of history. The great man transcends time; time creates and time destroys the emperor.

Otto Weininger

Genius is the ability to escape the human condition; Humanity is the need to escape.

Q. Uim

Some superior minds are unrecognized because there is no standard by which to weigh them.

Joseph Joubert

Thousands of geniuses live and die undiscovered — either by themselves or by others.

Mark Twain

Geniuses are like thunderstorms. They go against the wind, terrify people, cleanse the air.

Kierkegaard

A genius is one who can do anything except make a living.

Joey Adams

Could we teach taste or genius by rules, they would be no longer taste and genius.

Joshua Reynolds

*Courtesy: Kevin Solway's extensive philosophical library.

Genius is the highest morality, and, therefore, it is every one's duty. Genius is to be attained by a supreme act of the will, in which the whole universe is affirmed in the individual. Genius is something which "men of genius" take upon themselves; it is the greatest exertion and the greatest pride, the greatest misery and the greatest ecstasy to a man. A man may become a genius if he wishes to. But at once it will certainly be said: "Very many men would like very much to be *original geniuses*", and their wish has no effect. But if these men who "would like very much" had a livelier sense of what is signified by their wish, if they were aware that genius is identical with universal responsibility — and until that is grasped it will only be a wish and not a determination — it is highly probable that a very large number of these men would cease to wish to become geniuses.

Otto Weininger

Universality is the distinguishing mark of genius. There is no such thing as a special genius, a genius for mathematics, or for music, or even for chess, but only a universal genius. The genius is a man who knows everything without having learned it.

Otto Weininger

Genius is the capacity for productive reaction against one's training.

Bernard Berenson

It is frequently the tragedy of the great artist, as it is of the great scientist, that he frightens the ordinary man. If he is more than a popular story-teller it may take humanity a generation to absorb and grow accustomed to the new geography with which the scientist or artist presents us. Even then, perhaps only the more imaginative and literate may accept him. Subconsciously the genius is feared as an image breaker; frequently he does not accept the opinions of the mass, or man's opinion of himself.

Loren Eiseley, in "The Mind as Nature"

I swear to you, sirs, that excessive consciousness is a disease — a genuine, absolute disease. For everyday human existence it would more than suffice to have the ordinary share of human consciousness; that is to say, one half, one quarter that that which falls to the lot of a cultivated man in our wretched nineteenth century [...] It would, for instance, be quite enough to have the amount of consciousness by which all the so-called simple, direct people and men of action live.

Fyodor Dostoevsky

Great geniuses have the shortest biographies. Their cousins can tell you nothing about them.

R. W. Emerson

The genius is not a critic of language, but its creator, as he is the creator of all the mental achievements which are the material of culture and which make up the objective mind, the spirit of the peoples. The "timeless" men are those who make history, for history can be made only by those who are not floating with the stream. It is only those who are unconditioned by time who have real value, and whose productions have an enduring force. And the events that become forces of culture become so only because they have an enduring value.

Otto Weininger

Talent, lying in the understanding, is often inherited; genius, being the action of reason or imagination, rarely or never.

Samuel T. Coleridge

When a true genius appears in this world, you may know him by this sign, that the dunces are all in confederacy against him.

Jonathan Swift

Precisely because the tyranny of opinion is such as to make eccentricity a reproach, it is desirable, in order to break through that tyranny, that people should be eccentric. Eccentricity has always abounded when and where strength of character has abounded; and the amount of eccentricity in a society has generally been proportional to the amount of genius, mental vigor, and moral courage it contained. That so few dare to be eccentric marks the chief danger of the time.

John Stuart Mill

Genius is its own reward; for the best that one is, one must necessarily be for oneself... Further, genius consists in the working of the free intellect., and as a consequence the productions of genius serve no useful purpose. The work of genius may be music, philosophy, painting, or poetry; it is nothing for use or profit. To be useless and unprofitable is one of the characteristics of genius; it is their patent of nobility.

Schopenhauer

Great passions are for the great of souls. Great events can only be seen by people who are on a level with them. We think we can have our visions for nothing. We cannot. Even the finest and most self-sacrificing visions have to be paid for. Strangely enough, that is what makes them fine.

Oscar Wilde

Fortunately for us, there have been traitors and there have been heretics, blasphemers, thinkers, investigators, lovers of liberty, men of genius who have given their lives to better the condition of their fellow-men. It may be well enough here to ask the question: What is greatness? A great man adds to the sum of knowledge, extends the horizon of thought, releases souls from the Bastille of fear, crosses unknown and mysterious seas, gives new islands and new continents to the domain of thought, new constellations to the firmament of mind. A great man does not seek applause or place; he seeks for truth; he seeks the road to happiness, and what he ascertains he gives to others. A great man throws pearls before swine, and the swine are sometimes changed to men. If the great had always kept their pearls, vast multitudes would be barbarians now. A great man is a torch in the darkness, a beacon: in

superstition's night, an inspiration and a prophecy. Greatness is not the gift of majorities; it cannot be thrust upon any man; men cannot give it to another; they can give place and power, but not greatness. The place does not make the man, nor the scepter the king. Greatness is from within.

Robert Ingersoll

No one suffers so much as he [the genius] with the people, and, therefore, for the people, with whom he lives. For, in a certain sense, it is certainly only "by suffering" that a man knows. If compassion is not itself clear, abstractly conceivable or visibly symbolic knowledge, it is, at any rate, the strongest impulse for the acquisition of knowledge. It is only by suffering that the genius understands men. And the genius suffers most because he suffers with and in each and all; but he suffers most through his understanding...

Otto Weininger

He is a man of *capacity* who possesses considerable intellectual riches: while he is a man of *genius* who finds out a vein of new ore. Originality is the seeing nature differently from others, and yet as it is in itself. It is not singularity or affectation, but the discovery of new and valuable truth. All the world do not see the whole meaning of any object they have been looking at. Habit blinds them to some things: shortsightedness to others. Every mind is not a gauge and measure of truth. Nature has her surface and her dark recesses. She is deep, obscure, and infinite. It is only minds on whom she makes her fullest impressions that can penetrate her shrine or unveil her Holy of Holies. It is only those whom she has filled with her spirit that have the boldness or the power to reveal her mysteries to others.

William Hazlitt

Genius is present in every age, but the men carrying it within them remain benumbed unless extraordinary events occur to heat up and melt the mass so that it flows forth.

Denis Diderot

The ego of the genius accordingly is simply itself universal comprehension, the center of infinite space; the great man contains the whole universe within himself; genius is the living microcosm. He is not an intricate mosaic, a chemical combination of an infinite number of elements; [...] as to his relation to other men and things must not be taken in that sense; he is everything. In him and through him all psychical manifestations cohere and are real experiences, not an elaborate piece-work, a whole put together from parts in the fashion of science. For the genius the ego is the all, lives as the all; the genius sees nature and all existences as whole; the relations of things flash on him intuitively; he has not to build bridges of stones between them.

Otto Weininger

I made art a philosophy, and philosophy an art: I altered the minds of men and the colour of things: there was nothing I said or did that did not make people wonder... I treated Art as the supreme reality, and life as a mere mode of fiction: I awoke the imagination of my century so that it created myth and legend around me: I summed up all systems in a phrase, and all existence in an epigram.

Oscar Wilde, in *De Profundis*

Submitted on: May 16, 2013 / Accepted on: July 21, 2013

LETTERS TO PROGRESS IN PHYSICS

Simple Explanation for why Parallel-Propagating Photons do not Gravitationally Attract

Raymond Jensen

Dept. of Mathematics and Science, Northern State University, Aberdeen SD, 57401 USA. E-mail: rwjst4@alumni.nd.edu

In this article it is shown that photons of light, when traveling in parallel, do not attract one another gravitationally. This has been shown previously using general relativity, however here it is only assumed a Newtonian approximation to the gravitational attraction between photons. The explanation for the lack of gravitational attraction is simple: as co-moving objects accelerate in parallel, the flow of time is retarded, as observed by a stationary observer, according to special relativity. Hence so is the tendency for the objects to move toward one another. As the velocity of the objects approach c, the time required for the objects to approach one another approaches infinity, and so there is no gravitational attraction between objects which move parallel at the speed of light.

1 Introduction

In 1931 Tolman, Ehrenfest and Podolsky [1] were first to publish studies on how light interacts with light gravitationally. Among other things, they found that when photons move in parallel beams, there is no gravitational attraction between them. The authors did not give a physical explanation for this peculiarity. In 1999, Faraoni and Dumse [2] studied the problem of gravitational attraction between photons and concluded that for photons moving in parallel, the reason for the lack of gravitational attraction is due to an exact cancellation of the gravitomagnetic and gravitoelectric forces between them. Both sets of authors used a linear approximation to the metric to come to their conclusions. Here, we come to the same conclusion, but it is argued that the lack of gravitation can be entirely explained in Minkowski spacetime with assumption of the Newtonian approximation for gravity. This is reasonable, since the gravitational fields between photons can be expected to be very weak.

2 No attraction between parallel photons

Consider two free particles separated by distance x initially at rest in empty space with respect to an observer. The observer will find that after a time interval t, the objects will come together due to their mutual gravitational attraction. Since the objects are regarded to be small, it is sufficient to assume Newtonian mechanics in the calculation of t, however calculation of the exact value is not necessary for the purpose of the argument here.

Next, consider what happens when the two objects are returned to a distance x apart from one another, accelerated to some terminal velocity v perpendicular to x, and then released. Upon release, the objects initially move parallel to one another, with distance x between, but as before, begin to attract, and eventually come together. However, in this instance, the time required for the two objects to come together, in accordance with special relativity, is $t' = t/\sqrt{1 - v^2/c^2} > t$. Thus, according to a stationary observer, it takes longer for the two objects to approach one another, when their center-of-mass frame is moving at some non-zero velocity. Since the factor $1/\sqrt{1 - v^2/c^2} \to \infty$ as $v \to c$, the time required for the two particles to come together as $v \to c$, approaches infinity. The time required for the objects to deviate from their parallel trajectories is hence also infinite. The conclusion here is that for two particles moving at the speed of light, since time propagation in their center-of-mass frame is nonexistent, their gravitational attraction is also nonexistent. Although x was taken to be perpendicular to the direction of propagation, this condition can be relaxed without changing the conclusion of no gravitational attraction.

3 Attraction between coplanar non-parallel photons

In both of the references, the authors found that for non-parallel propagation, the gravitational attraction between photons is non-zero. This can be reasoned, for some simple cases, as follows: suppose the two particles, in this case photons, are returned to their original positions, but upon release, propagate away from one another at a relative angle $2\theta > 0$, according to a stationary observer. Then, the center of mass frame propagates at a velocity $v = c\cos\theta < c$ and so gravitational attraction between photons is retarded by a factor of $1/\sin\theta$, according to a stationary observer. For example, at $2\theta = 180^\circ$, the photons trajectories are antiparallel to one another, and there is no retardation since the center of mass frame is stationary. The same applies for photons converging at these nonzero angles.

Submitted on: September 10, 2013 / Accepted on September 15, 2013

References

1. Tolman R. C., Ehrenfest P., Podolsky B. On the gravitational field produced by light. *Physical Review*, 1931, v. 37, 602–615.
2. Faraoni V., Dumse R. M. The gravitational interaction of light: from weak to strong fields. *General Relativity and Gravitation*, 1999, v. 31 (1), 91–105.

Progress in Physics is an American scientific journal on advanced studies in physics, registered with the Library of Congress (DC, USA): ISSN 1555-5534 (print version) and ISSN 1555-5615 (online version). The journal is peer reviewed and listed in the abstracting and indexing coverage of: Mathematical Reviews of the AMS (USA), DOAJ of Lund University (Sweden), Zentralblatt MATH (Germany), Scientific Commons of the University of St.Gallen (Switzerland), Open-J-Gate (India), Referential Journal of VINITI (Russia), etc. Progress in Physics is an open-access journal published and distributed in accordance with the Budapest Open Initiative: this means that the electronic copies of both full-size version of the journal and the individual papers published therein will always be acessed for reading, download, and copying for any user free of charge. The journal is issued quarterly (four volumes per year).

Electronic version of this journal: http://www.ptep-online.com

Postal address:
Department of Mathematics and Science,
University of New Mexico, 705 Gurley Avenue, Gallup, NM 87301, USA

Printed in the United States of America